ISSN 0110-3326

RESEARCH REPORT

Retrofitting of Reinforced Concrete Moment Resisting Frames

Shigeru Hakuto

Supervised by R. Park and H. Tanaka

August 1995 **95-4**

Department of Civil Engineering

University of Canterbury
Christchurch New Zealand

RETROFITTING OF REINFORCED CONCRETE MOMENT RESISTING FRAMES

A Thesis
Submitted in Partial Fulfilment
of
the Requirements for the Degree
of
Doctor of Philosophy in Civil Engineering
at the
University of Canterbury
Christchurch
New Zealand

by

Shigeru Hakuto

1995

To
Masako and Lisa

ABSTRACT

A seismic assessment of a reinforced concrete building designed in the late 1950's in New Zealand has revealed several possible problems of behaviour during future severe earthquakes. Typical problems are (1)columns with inadequate flexural strength to prevent column sidesway mechanisms(soft stories), (2)large diameter longitudinal beam bars passing through interior columns with small depth, (3)poor anchorage of longitudinal beam reinforcement in exterior columns, (4)small quantities of transverse reinforcement for shear, confinement of compressed concrete and restraint against premature buckling of longitudinal compression reinforcement in beams and columns, and (5)small quantities of shear reinforcement in beam-column joint cores.

An experimental programme was carried out to investigate seismic assessment procedures of existing reinforced concrete frames with poorly detailed reinforcement, and retrofit techniques by jacketing with new reinforcement. Three full-scale beam-interior column joint subassemblages with reinforcement details typical of reinforced concrete building designed in the 1950's were constructed. The beam-column joint core lacked shear reinforcement and the longitudinal beam bars were poorly anchored in the joint core. One of the beam-column joint replicas was tested as-built subjected to simulated severe seismic loading. The test results indicated that beam-interior column joints of early building frames would suffer severe diagonal tension cracking in the event of a major earthquake. The damaged(tested) beam-column joint replica, and the two undamaged(not tested) beam-column joint replicas, were then retrofitted by jacketing with new reinforced concrete and tested under simulated seismic loading. It was found that concrete jacketing was a useful technique for enhancing the stiffness, strength and ductility.

Four full-scale beam-column joint subassemblages with reinforcing details of early reinforced concrete frames were also constructed and tested subjected to severe seismic loading. Two of the subassemblages were beam-interior column joint specimens which lacked shear reinforcement. These two subassemblages had different column depth to beam bar diameter ratios and were tested mainly to investigate the effect of the bond conditions along the beam bars passing through the joint core on the seismic behaviour of beam-column joints without shear reinforcement. The other two subassemblages were beam-exterior column joints with limited shear reinforcement and with different arrangements of beam bar hooks in the joint core. In one specimen the beam bar hooks were bent away from the joint core(the tails of the top bars were bent up and the tails of the bottom beam bars were bent down), as was the case in many early frames. In the other specimen the tails of the beam bars were bent into the joint core, as is current practice. Seismic load tests showed that the performance of the beam-exterior column joints with very little shear reinforcement was significantly

influenced by the directions in which the tails of the beam bar hooks in the joint core were bent. Beam-exterior column joints of early building frames in which the tails of the hooks of the beam bars are bent out of the joint core would behave unsatisfactory during future severe earthquakes.

A theoretical study was conducted to investigate the seismic behaviour of the joints without shear reinforcement. The shear mechanisms of such joints were postulated based on the test results in this study. One approach to assess the seismic performance of the beam-column joints without shear reinforcement is proposed. The approach was based on a limiting nominal horizontal joint shear stress which is a function of the displacement ductility factor imposed on the frame. The seismic behaviour of beams with small quantities of transverse reinforcement was also studied in terms of available curvature ductility factors and shear strengths.

ACKNOWLEDGEMENTS

The research work reported in this thesis was carried out in the Department of Civil Engineering, University of Canterbury, New Zealand.

I wish to express my deepest gratitude to Professor R. Park and Dr. H. Tanaka, supervisors of this project, for their invaluable advice, encouragement and patience. Special thanks are given to Emeritus Professor T. Paulay for his fruitful discussions and Dr. A.J. Carr for the helpful advice. I would like to sincerely thank Professors S. Otani, University of Tokyo, and K. Kusakabe, Kobe University, for their assistance to enable me to study in New Zealand.

Thanks are extended to the technical staff of the Civil Engineering Department under the management of Mr. G.E. Hill, for their assistance and advice in the experimental programme. In particular, Mr. N.J. Hickey is thanked for his valuable contributions to the experimental work, friendship and intelligence to understand my Japanese English. Thanks are also given to Messrs. R.N. Allen, G.H. Clarke, G.P. Hill, M. Stuart-Jones and P.A. Murphy for their construction of the test frames and test specimens, and Mr M.R. Griffin for his computer work. Also acknowledged are Mr. H.H. Crowther, now retired, for the purchase of the materials, Mr. M. Roestenburg for his photographic work and Mrs. V. Grey for her drawing work.

I also wish to thank my fellow postgraduate students and visitors, in particular, Dr. J. I. Restrepo-Posada for his constructive discussions and Mr. J. Maffey for his invaluable suggestion of the test specimen. Also thanks are due to Drs. P.C. Cheung, B. Li, A. Mori and X. Li, and Messrs. X.A. Xin, J. Lai, H.K. Kung, I. Satyarno and K. Munyao for their friendship during this research. The fruitful discussions(in Japanese) with the structural engineers of Japan, Messrs M. Tabuchi, Y. Sato and T. Komuro are appreciated.

Thanks are given to Mr. M. Teraoka, Fujita Kogyo Company of Japan, for providing the invaluable test data.

The financial assistance provided by the Earthquake Commission of New Zealand is gratefully acknowledged. Tokyu Construction Company of Japan is also thanked for their financial support and for accepting my study in New Zealand.

Finally, I would like to thank my wife, Masako and our parents for their understanding, encouragement and support during the past years.

TABLE OF CONTENTS

NOTATION

a	= shear span
A_e	= effective shear area
A_g	= gross area of column section
A_s	= area of tension reinforcement
A'_s	= area of compression reinforcement
A_{st}	= total area of longitudinal reinforcement of column
A_v	= area of shear reinforcement
A_1	= cross section area of the existing member
A_2	= cross section area of jacket around the existing member
b	= width of compression face of beam
b_c	= overall width of column
b_j	= effective width of joint
b_w	= web width of beam
BI	= bond index
c	= neutral axis depth measured from extreme compression fibre
C	= basic seismic coefficient in NZS 4203 : 1984
	= lateral force coefficient in NZS 4203 : 1992
	= strength index in Section 2.2.2
	= basic seismic index in Section 2.3.5.2
C_c	= concrete compression force of beam
C'_c	= concrete compression force of column
C_{cu}	= compression force of column
C_d	= seismic design coefficient
C_h	= basic seismic hazard acceleration coefficient
C_s	= compression force of beam bar
C'_s	= compression force of column bar
C_{Bl}, C_{Br}	= compression force of beam
d	= distance from extreme compression fibre to centroid of tension reinforcement
d_b	= nominal diameter of bar
d_c	= effective depth of column
D	= gross column diameter
D'	= diameter of confined concrete core
D_c, D_s	= diagonal compression force
DF	= displacement ductility factor
E_c	= modulus of elasticity of concrete
E_o	= basic seismic index
E_s	= modulus of elasticity of reinforcement

f	= shape factor
f_c	= diagonal compressive stress
f'_c	= compressive strength of concrete
	= probable compressive strength of concrete in Chapter 2
$f'_c{}^*$	= weighted average compressive strength of concrete
f'_{cr}	= principal tensile stress of concrete at the onset of joint diagonal cracking
f_{ct}	= principal tensile stress of concrete
f'_{c1}	= compressive strength of existing concrete
f'_{c2}	= compressive strength of jacket concrete
f_r	= modulus of rapture of concrete
f_t	= diagonal tension strength of concrete
	= splitting tensile strength of concrete in Chapter 3
	= diagonal tensile stress in Chapter 8
f_u	= ultimate strength of reinforcement
f_y	= yield strength of reinforcement
f_{yv}	= yield strength of shear reinforcement
f_1	= stress in compression reinforcement
F	= ductility index
F_i	= horizontal static load at level i of a structure
G	= geological index
h	= storey height or vertical distance between the column end pins
	= section depth in Section 8.5.3.3
h_b	= beam depth
h_c	= column depth
h_i	= distance between top and bottom linear potentiometers in the region i of the beam
	= storey height at level i of a structure in Chapter 2
h'_i	= distance between left and right linear potentiometers in the region i of the column
h_j	= effective depth of joint
h_s	= horizontal distance of the region estimating the average shear distortion in the beam
I_e	= effective moment of inertia
I_g	= moment of inertia of gross concrete section about the centroidal axis, neglecting the reinforcement
I_s	= seismic index
j_t	= distance between the upper and lower stringers
k	= coefficient of concrete contribution to shear strength
K_e	= measured initial stiffness of the test specimen
$K_{theoretical}$	= theoretical initial stiffness of the test specimen

l	= beam span or horizontal distance between the beam end pins
l'_b	= distance from the column face to the centre of the beam end pin
l'_c	= distance from the beam face to the centre of the column end pin
l_j	= initial length of the diagonal in the joint
l_{jh}	= horizontal distance of the diagonal in the joint
l_{jv}	= vertical distance of the diagonal in the joint
l_s	= initial length of the diagonal in the beam
L	= clear span
L_u	= limit state factor for the ultimate limit state
M	= structural material factor
M_b	= flexural strength of beam section
	= beam moment at the column centreline in Section 2.3.3.2
	= beam face moment in Chapter 8
M_c	= flexural strength of column section
	= column face moment in Section 2.2.4.3
	= column moment at the beam centreline in Section 2.3.3.2
M_{cu}	= column face moment
M_f	= probable flexural strength of section
M_i	= ideal flexural strength
M_{p1}, M_{p2}	= probable flexural strength of section
M_{Bl}, M_{Br}	= beam face moment
M_{Bn}	= beam probable flexural strength
M_{Cn}	= column probable flexural strength
N	= axial load applied to the bottom column of Specimen O1
p_w	= web reinforcement ratio
P	= applied horizontal load
	= axial load on column in Section 8.5.3.3
P_b	= balanced failure load
P_e	= column load in compression due to the design gravity and seismic loading
P_i	= theoretical ideal horizontal load strength of the test specimen
P_u	= axial load on column
P_{EP}	= probable axial load on column due to earthquake load
R	= risk factor
R_b	= clear rib spacing of deformed bar
R_p	= inelastic hinge rotation angle
R_s	= drift requirement for serviceability limit state
R_u	= drift requirement for ultimate limit state
R_v	= axial load reduction factor
s	= spacing of shear reinforcement
s_i	= gauge length of region i in the beam

s'_i	= gauge length of region i in the column
S	= structural type factor
$S_a(e)$	= equivalent elastic response strength
S_d	= structural design index
S_{min}	= minimum requirement for horizontal load strength of a structure
S_p	= structural performance factor
	= sway potential index in Section 2.2.4.4
T	= tension force in the beam bar
	= natural period of vibration in Section 2.3.4
	= time index in Section 2.2.2
T'	= tension force in the column bar
T'_b, T'_{b1}, T'_{b2}	= additional tension force in the beam bar
T'_c, T'_{c1}, T'_{c2}	= additional tension force in the column bar
T_{cr}	= critical period of a structure
T_{cu}	= tension force in the column bar
T_s	= period of structure required for serviceability limit state
T_u	= period of structure required for ultimate limit state
T_{Bl}, T_{Br}	= tension force in the beam bar
T1	= fundamental translational period of vibration
u_b	= average bond stress
v_b	= nominal beam shear stress
	= basic shear stress in Chapter 2
v_c	= shear stress carried by concrete
	= nominal horizontal joint shear stress in Section 2.2.4.3
${}_dv_c$	= ductile shear stress carried by concrete
${}_{nd}v_c$	= non-ductile shear stress carried by concrete
v_d	= ductile shear stress
v_{jh}	= nominal horizontal shear stress in joint core(=V_{jh}/b_jh_j)
$v_{j,cr}$	= nominal horizontal joint shear stress at the onset of diagonal cracking
v'_{jh}	= nominal horizontal shear stress in joint core(=V_{jh}/b_jd_c)
v_{nd}	= non-ductile shear stress
v_s	= shear stress carried by stirrups or hoops
V	= total horizontal seismic force at the base of a structure
V_b, V_{Bl}, V_{Br}	= beam shear force
V_c	= column shear force
	= shear force carried by concrete in Section 8.5.3
V_{cf}	= final shear strength carried by concrete
V_{ci}	= initial shear strength carried by concrete
V_{cu}	= column shear force
V_d	= maximum shear force demand

V_f, V_{fp}	= shear force when the beam or column flexural strength is reached at column or beam face
	= final shear strength in Chapter 8
V_i	= initial shear strength
V_{if}	= shear corresponding to ideal flexural strength
V_{jh}	= horizontal shear force across a joint
V_{max}	= maximum shear strength of the beam
V_n	= nominal shear strength
V_p	= probable non-ductile shear strength(= $v_{nd}bd$)
	= axial load component of the column shear strength in Section 8.5.3.3
V'_p	= minimum probable non-ductile shear strength
V_{pd}	= probable ductile shear strength(= $v_n bd$)
V_s	= shear force carried by shear reinforcement
V_{sf}	= final shear strength carried by shear reinforcement
V_{si}	= initial shear strength carried by shear reinforcement
V_E	= beam shear force at the development of probable beam flexural strength due to earthquake load
W_i	= seismic weight at level i of a structure
x_i	= distance from the column face to the centre of the region i in the beam
y_i	= distance from the beam face to the centre of the region i in the column
Z	= zone factor
α	= inclination of the diagonal compression force to the beam axis
α, α_j	= angle of the diagonal in the joint to the beam axis
α_s	= angle of the diagonal in the beam to the beam axis
β	= $((1+\cot^2\theta)p_w f_{yv})/(\nu_o f'_c)$
γ_j	= average shear distortion of the joint
γ_s	= average shear distortion of the beam
γ_1, γ_2	= shear distortion
δ_b	= beam deformation
$\delta_{b,f}$	= beam deformation due to flexure
$\delta_{b,fe}$	= beam deformation due to fixed-end rotation
$\delta_{b,s}$	= beam deformation due to shear
δ_c	= column deformation
$\delta_{c,f}$	= column deformation due to flexure
$\delta_{c,fe}$	= column deformation due to fixed-end rotation
$\delta_{c,s}$	= column deformation due to shear
δ_i	= displacement measured over the region i
${}_b\delta_i$	= bottom displacement measured over the region i of the beam
${}_l\delta_i$	= left displacement measured over the region i of the column
${}_r\delta_i$	= right displacement measured over the region i of the column

${}_{t}\delta_i$	= top displacement measured over the region i of the beam
δ_j, δ'_j	= changes in the length of the diagonals in the joint
δ_s, δ'_s	= changes in the length of the diagonals in the beam
Δ	= horizontal displacement of the test specimen
Δ_b	= horizontal displacement due to beam deformation
$\Delta_{b,f}$	= horizontal displacement due to beam flexural deformation
$\Delta_{b,fe}$	= horizontal displacement due to beam fixed-end rotation
$\Delta_{b,s}$	= horizontal displacement due to beam shear deformation
Δ_c	= horizontal displacement due to column deformation
$\Delta_{c,f}$	= horizontal displacement due to column flexural deformation
$\Delta_{c,fe}$	= horizontal displacement due to column fixed-end rotation
Δ_j	= horizontal displacement due to joint shear distortion
Δ_y	= yield displacement
$\Delta_{y,\ theoretical}$	= theoretical yield displacement
Δ_1 to Δ_6	= displacements measured at points 1 to 6
ΔT_c	= bond force of beam bar resisted by diagonal concrete strut
$\Delta T'_c$	= bond force of column bar resisted by diagonal concrete strut
ΔT_s	= bond force of beam bar resisted by tension force in column bar in the joint core
$\Delta T'_s$	= bond force of column bar resisted by tension force in beam bar in the joint core
ε_{cu}	= maximum compressive strain in concrete
${}_{ave}\varepsilon_i$	= average strain measured over the region i
ε_l	= tensile strain in longitudinal direction of column
ε_{sh}	= strain at commencing strain hardening of steel in tension
ε_t	= tensile strain in transverse direction of column
ε_y	= yield strain of steel
$\theta_{b,ife}$	= fixed-end rotation of the beam
$\theta_{b,i}$	= rotation estimated over the region i of the beam
$\theta_{c,ife}$	= fixed-end rotation of the column
$\theta_{c,i}$	= rotation estimated over the region i of the column
θ_{st}	= inclination of the strut by arch action
θ_t	= inclination of the strut by truss action
μ	= structural ductility factor
	= displacement ductility factor in Section 8.5.3.3
μ_{min}	= minimum requirement for structural ductility factor
ν, ν_o	= factor for reduced effective compressive strength of diagonal strut
ρ	= ratio of tension reinforcement(=A_s/bd)
ρ'	= ratio of compression reinforcement(=A'_s/bd)
ρ_s	= ratio of volume of hoop or spiral reinforcement to total volume of concrete core
ρ_t	= ratio of total longitudinal reinforcement of column(=A_{st}/A_g)
ρ_w	= ratio of tension reinforcement(=A_s/bd)

Φ	= storey index
$\Phi_{b,i}$	= curvature estimated over the region i of the beam
$\Phi_{c,i}$	= curvature estimated over the region i of the column
Φ_u	= beam curvature at ultimate
Φ_y	= beam curvature at first yield
φ	= mechanical reinforcement ratio

CHAPTER 1

INTRODUCTION

1.1 THE NEED FOR RETROFITTING

Rapid growth in the understanding of the behaviour of structures during severe earthquakes has enabled new buildings to be designed to be more capable of earthquake resistance. At the same time, the development of seismic design methods has left some doubts concerning the available seismic resistance of existing buildings. In addition to very old buildings for which seismic design was not considered, the behaviour of many buildings, designed according to older building codes, is questioned whenever a revision is enforced to meet more stringent design requirements. It is obvious that a certain portion of the stock of existing buildings may be inadequate according to more recent seismic design standards.

Recent earthquakes in many different countries of the world have emphasized the problems of early reinforced concrete structures, which were not designed according to current design codes. The 1985 Mexico earthquake and recent Californian earthquakes(the 1987 Whittier Narrows, the 1989 Loma Prieta and the 1994 Nothridge) demonstrated the disastrous behaviour of many existing structures and the need for repair and strengthening. The 1985 Mexican earthquake with unique ground motions caused unprecedented damage to reinforced concrete structures in Mexico city : 210 buildings collapsed and thousands were damaged, and thousands of lives were lost[Rosenblueth and Meli 1986]. The damage due to Californian earthquakes can be characterised by the dramatic structural collapse of several major highway bridges[Priestley 1988, Benuska 1990 and Moehle 1994]. The greatest damage occurred in older structures on soft ground.

Analyses of existing typical early reinforced concrete structures and observations of damage by recent earthquakes have indicated that members and joints may have inadequate strength, and/or ductility[Park 1992]. This means that many of those old reinforced concrete structures may need to be retrofitted to survive future earthquakes. The possible need for strengthening is of particular concern in the case of reinforced concrete structures constructed before the 1970's in New Zealand.

The experience in Mexico City following the 1985 earthquake increased the world-wide interest in the need for reducing the risk posed by hazardous structures. With the increasing cost of new construction, repair and/or strengthening of existing structures has become an attractive way to provide safety to building occupants and to protect the owner's investments. In the aftermath of the 1985 Mexico earthquake, more than a thousand buildings were retrofitted[Jirsa 1987, Mitchell et al 1988 and Jara et al 1989] , many of which had columns and joints with inadequate reinforcing details[Rosenblueth and Meli 1986]. Also, in the United States and New Zealand, there has been increased activity on retrofitting existing buildings and bridges to improve their seismic performance.

However, seismic assessment and retrofit procedures for existing reinforced concrete structures have yet to be fully established. The design and construction procedures used for repair and strengthening of existing concrete structures have been based on mainly experience, engineering judgement and limited experimental evidence. The decision to retrofit has also relied on engineering judgement due to the scarcity of information concerning the seismic performance of beams, columns and joints with deficiencies typical of those old structures. Current building codes only address new construction. It is a matter of urgency that further experimental and analytical research on the seismic behaviour of such members and subassemblages be conducted to further establish seismic assessment procedures. Also, several retrofit techniques are available to correct the deficiencies of existing reinforced concrete structures, and the effectiveness of some those techniques has already been examined experimentally. Further research is required to develop more economic retrofit methods. This will result in the further development of procedures for the seismic retrofitting of existing reinforced concrete structures.

In this chapter, a literature review on the seismic retrofitting of reinforced concrete structures is presented. The objectives and organization of this study are also described.

1.2 METHODS OF RETROFITTING CONCRETE STRUCTURES

1.2.1 Background

Typically, reinforced concrete structures have been retrofitted by one or a combination of the following basic methods :

1) a local repair scheme, which includes epoxy resin injection or replacement of damaged concrete and steel
2) infilling techniques
3) steel bracing techniques
4) steel jacketing techniques
5) concrete jacketing techniques

Recently, base isolation techniques were also used for retrofit measures[Gates et al 1992].

In this section, a brief literature review of the experimental and analytical studies related to repair and strengthening techniques of reinforced concrete structures in seismic active regions is presented.

1.2.2 Local Repair Scheme

Two techniques, epoxy injection and replacement techniques, have been commonly used for a local repair scheme. The epoxy injection technique is used for the restoration of concrete elements with low levels of damage. That is, no crushed or spalled concrete, no fracture or buckling of steel and small crack widths. Pressure injection of the resin is the method most commonly used. Vacuum may also be applied for injection. When crack widths are larger than 5.0 mm, and concrete crushing or steel buckling is observed, the damaged portions of the element should be repaired using the removal and replacement technique. This technique consists of removing the loose concrete and/or damaged steel bars, and replacing with new materials to restore the strength and stiffness of the damaged element. It is important to use new materials with higher strength.

Most of the research reported on the repair of concrete structural members and frame connections has involved the epoxy injection technique. In general, epoxy injection is successful in restoring the tensile strength of the concrete of the damaged members. Properly repaired structural members could possess approximately the same shear and flexural strengths as those before they were damaged[Popov and Bertero 1975, Gyoten et al 1977 and Owen et al 1984]. In all tests, the energy dissipation and stiffness of the repaired structure were somewhat reduced due to microcracks which are difficult to inject. Some test results[Popov and Bertero 1975 and Lee et al 1977] showed that an epoxy injection technique does not restore the bond between steel bars and surrounding concrete once destroyed. This is because the epoxy cannot penetrate through the small clearance around the reinforcement. Moreover, the pulverized material around the reinforcement prevent the improvement of bond by epoxy injection techniques.

The results tested on the original and repaired beam-interior column joint subassemblages indicated that both pressure injection and vacuum impregnation technique restored the bond between concrete and steel reinforcement effectively[French et al 1990]. It was found that epoxy injection into bond splitting cracks along deformed bars of a reinforced concrete member was an effective repair method to improve bond stiffness and strength[Tasai 1992].

Lee et al investigated the effectiveness of the epoxy injection technique, and the removal and replacement technique on the seismic behaviour of the beam-exterior column joints[Lee et al 1977]. Only the beams of the damaged test specimens were repaired using high early strength materials. It was found that the strengths of the beams retrofitted were increased effectively. However, the beam-column joint, not retrofitted, became a critical region since the shear force transmitted into the joint was increased due to an increase in the beam strength.

1.2.3 Infilling Techniques

One of the most common methods used in Japan after the 1968 Tokachi-Oki and 1978 Miyagiken-Oki earthquakes was the infilling wall technique[Endo et al 1984]. This method was also used in Mexico City, as seen in Fig.1.1, but to less extent, for strengthening structures after the 1985 earthquake[Jirsa 1987 and Jara et al 1989]. The aim of this technique is to increase the lateral load strength and stiffness of existing reinforced concrete buildings. It is an effective approach to the strengthening of low- to medium-rise buildings. Enhancement of strength permits extensive inelastic displacement under a severe earthquake to be avoided. One of the disadvantages of infilling wall techniques is that new foundations and/or strengthening of the existing foundations are often required to resist the increased forces transferred from the superstructure as well as the increased mass associated with the strengthening[Mitchell et al 1988].

Experimental studies of strengthening methods using various types of infilling techniques have been conducted extensively in Japan[Higashi et al 1977, 1980, 1984, Hayashi et al 1980, Sugano and Fujimura 1980 and Aoyama et al 1984], as mentioned in the following paragraphs.

In the first test on the infilling wall techniques[Higashi et al 1977], the effect of small precast walls placed separately in the frames was studied on one storey, one bay, one-fourth scale specimens. The effect of side-walls placed adjacent to existing columns on the lateral load capacity was also investigated. In frames strengthened by precast panels, the stiffness is not increased remarkably, but the lateral load capacity is increased by truss action of the precast panels. The columns strengthened by the cast in place side-wall technique reached almost the same strength as that of identical monolithic construction while the precast side-wall technique resulted in less strength but more ductility. Stiffnesses and strengths of the frames after strengthening with precast concrete panels were analyzed on the basis of an idealized load transfer mechanism.

Subsequently thirteen one storey, one bay, one-third scale reinforced concrete frames with poor transverse reinforcement in the columns were tested[Higashi et al 1980]. The frames were retrofitted using various infilling techniques which involved precast concrete panels, steel bracing, steel frames and steel trusses. The performance of the frames strengthened using infilling techniques was satisfactory in terms of lateral load strength and

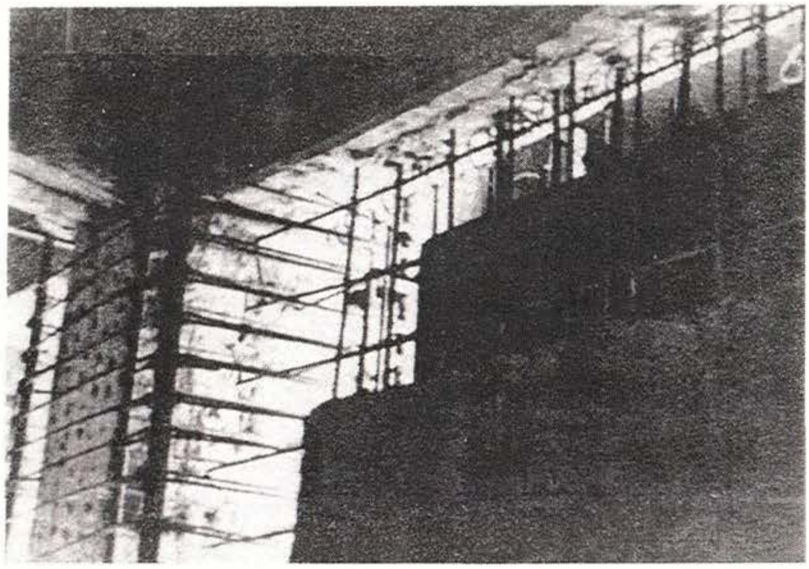

Fig.1.1 Infilling Wall Technique in Mexico City[Jara et al 1989]

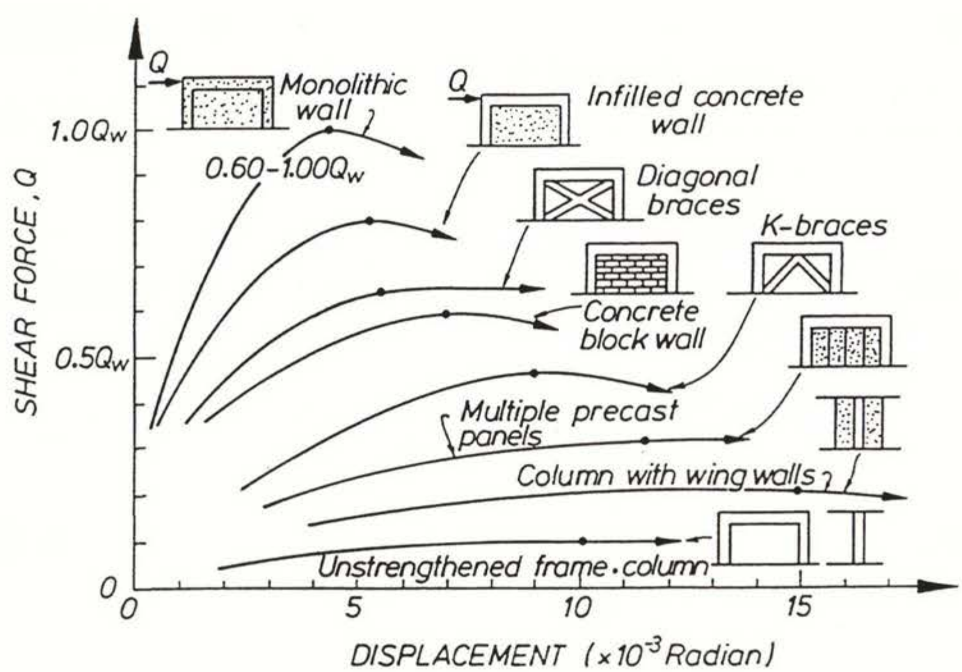

Fig.1.2 Typical Lateral Load versus Displacement Relationships for Different Infilling Techniques[Sugano 1981]

stiffness. Analytical models were proposed to determine the skeleton curves of the test specimens strengthened using the infilling techniques.

Further tests were carried out on one storey, one bay, one-third scale reinforced concrete frames strengthened using infilling wall techniques[Hayashi et al 1980]. The joining methods, mechanical shear connectors between the infilling wall and the existing frame, were varied. The test results showed a remarkable increase in the lateral load resistance of the frames strengthened by infilling walls inside the existing frame. It was also found that the joining methods affected the behaviour of the strengthened frames during the tests.

To investigate the seismic behaviour of reinforced concrete frames strengthened using various types of infilling techniques, ten one storey, one bay, one-third scale specimens were tested[Sugano and Fujimura 1980]. Typical lateral load versus displacement curves for the frames retrofitted using different infilling techniques are qualitatively shown in Fig.1.2. Those curves include the available test data reported by other researchers. As shown in this figure, the infilling techniques significantly increase the lateral load strengths and stiffnesses of frames. In general, a large increase in the strength is associated with a reduction in the ductility capacity of the original frame. It should be noted that each frame strengthened using a different infilling technique showed its own characteristic behaviour. Therefore, it is necessary to evaluate the effect of the infilling techniques on the seismic performance of the existing buildings in terms of the lateral load strength, displacement ductility and energy absorption capacity. In this study, reviewing available test data, a design guideline was proposed by Sugano and Fujimura with emphasis on improving the lateral load strength of the existing building. It was also mentioned in the guideline that to achieve more than 60% of the strength of a monolithic wall, it is necessary to provide connectors all around the existing frame in compliance with some special recommendations when using an infilling wall technique.

With reference to the above investigations, strengthening methods using mainly the infilling wall technique have been refined so as to be more effective for application to existing reinforced concrete buildings that were evaluated to be short of earthquake resistance. However, looking into practical applications of such methods, several problems became apparent. Most available data were obtained from the results of tests on one storey, one bay specimens. The confining effect of the frame surrounding a wall and the effect of window openings in postcast infilling walls had yet to be investigated. Furthermore, there were several detailing and construction problems, such as anchoring methods of wall reinforcement and the placement of postcast concrete. To investigate these problems, some tests were conducted as mentioned below.

Higashi et al carried out tests on specimens representing three storey, one bay frames[Higashi et al 1984]. The test results were compared with those of one storey, one bay frames[Higashi et al 1980]. It was found that infilling with cast-in-place wall techniques increased the lateral load strength of the original three storey frames significantly while infilling with precast concrete panels, steel frame and steel brace increased both the lateral load strength and the ductility capacity of the original frames. The behaviour observed for the three storey infilled frames was flexure dominant, in contrast to the shear dominant response obtained from the one storey infilled frames.

Aoyama et al 1984 tested twelve one-third scale, one storey, one bay specimens in order to investigate the confining effect of the frame surrounding a wall, the effect of window openings in the infilling walls, and the method of postcast construction. The test results indicated that the lateral load strengths of both postcast and monolithic walls increased with increase in the size and the quantities of reinforcement in the adjacent columns. It was also found that the lateral load strength of the postcast wall with openings could be evaluated in a manner similar to that for monolithic shear walls. The use of high strength chemical anchors in conjunction with expansive concrete was recommended for splicing the reinforcement at the top face of the postcast wall.

1.2.4 Steel Bracing Techniques

The use of steel bracing to strengthen and stiffen existing reinforced concrete frames is relatively new concept. Several applications using steel bracing systems, such as shown in Fig.1.3, can be found elsewhere[Kawamata and Ohnuma 1980, Mitchell et al 1988 and Badoux and Jirsa 1990]. Excellent performance during the devastating 1985 Mexico City earthquake of the reinforced concrete buildings retrofitted using steel bracing techniques, shown in Figs.1.3(b) and (c), was reported[Foutch et al 1989].

When only perimeter frames are braced, as in the case of applications mentioned above, most of the construction work can be performed on the exterior of the building to speed erection and to minimize disruption of the occupants. The comparatively small increase in mass associated with steel bracing technique may result in a reduction of the foundation cost when compared with that using the infilling wall technique. However, when using a bracing scheme, the original function and aesthetics of the building may not be maintained(see Fig.1.3). This is also the case when using infilling techniques. The methods to secure the anchorage of tension braces are not clear if tension braces are used. If compression braces are used, a large section of the brace is required to prevent buckling. However, little care is required for the anchorage.

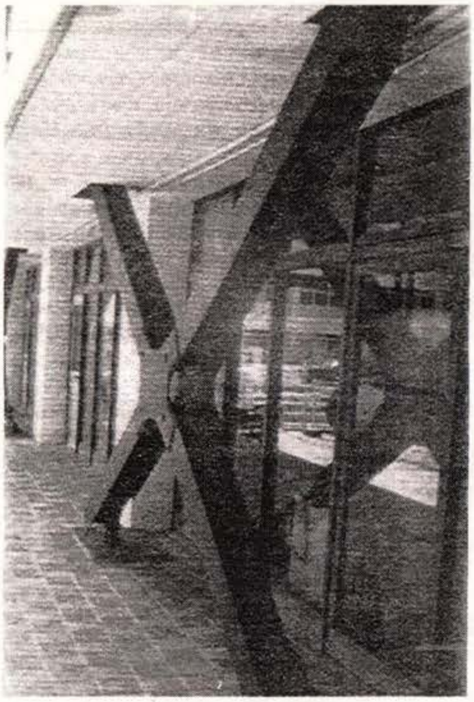

(a) School Building in Japan Following the 1978 Miyagiken-Oki Earthquake [Badoux and Jirsa 1990]

(b) Successful Use of Bracing for 12 storey Office Building in Mexico City [Mitchell et al 1988]

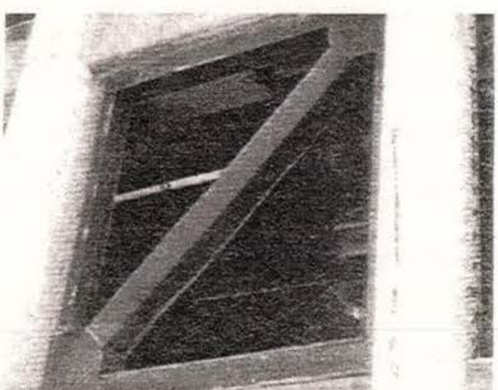

(c) Hospital Building in Mexico City [Badoux and Jirsa 1990]

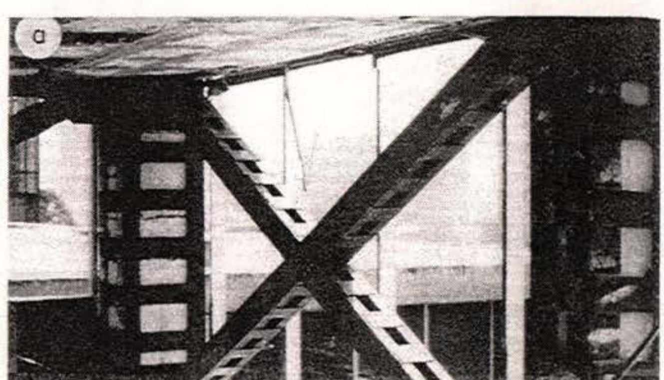

(d) 11 Storey Office Building Following the 1985 Mexico Earthquake [Mitchell et al 1988]

Fig.1.3 Applications of Steel Bracing Techniques

Although experimental and analytical research on the seismic behaviour of steel bracing systems added to existing frames has been conducted in Japan as well as in the U.S., the available test data on the response of steel braced frames is as yet limited.

An experimental study was undertaken to investigate the behaviour of the cross steel bracing system[Kawamata and Ohnuma 1980]. Based on the test results, braces were detailed to provide maximum energy dissipation in the inelastic range under lateral loading. These steel braces were added to the exterior frame in the long direction of a school building which had suffered heavy damage to several short columns during the 1978 Miyagiken-Oki earthquake(see Fig.1.3(a)). The bracing members were connected to existing exterior beams at every floor by prestressing steel rods through the steel members. Columns and beams of the frames serve as vertical and horizontal truss elements.

Bush et al 1986 conducted experimental research on a reinforced concrete frame with deep spandrel beams and short columns, which were considered typical of many buildings built in California in the 1950's and 1960's. The original test specimen was two storey, two bay, two-third scale and was retrofitted with a steel bracing scheme. The bracing scheme significantly improved the strength and stiffness of the original non-ductile frame. The ultimate load was reached when the welding at brace connections failed as a result of repeated loading. High local deformations were generated at the connections when the braces alternately buckled in compression and yielded in tension.

An analytical study was performed to obtain a better understanding of the behaviour of braced frames under cyclic loading, particularly a frame with weak short columns[Badoux and Jirsa 1990]. The results suggested that the bracing system should be designed for elastic response, but detailed for ductile behaviour in the case the design loads are exceeded. Inelastic buckling of the braces is the main problem in achieving ductile response. The brace slenderness ratio should therefore be kept low to limit inelastic buckling.

Bracing a weak column-strong beam frame may not be sufficient to guarantee the satisfactory behaviour of the retrofitted frame under severe earthquakes. The bracing system can compensate for inadequate frame strength and stiffness, but it cannot change the failure mode of the original frame. When failures of the weak columns cause a large decrease in axial load capacity, the vertical load carrying capacity of the braced frame will be impaired. To avoid this, the failure mode of the frame must be shifted to that of a strong column-weak beam system. This can be achieved by reducing the flexural capacities of the beams(beam alteration) or by increasing the strengths and ductility capacities of the columns(column alteration). The former is achieved by coring the compression zone or cutting flexural reinforcement of the beam near the column face, and the latter can be obtained using concrete jacketing or steel jacketing of columns. Beam alteration, which is more simple technique, was studied experimentally[Kawamata and Ohnuma 1980] and analytically[Badoux and Jirsa 1990] It was found that the beam alteration significantly improved the mode of failure : inelastic behaviour was transferred from the columns to the beams, thus providing protection against column damage and increasing the energy dissipation capacity of the frame.

The results of tests on a two storey, one bay, two-third scale reinforced concrete frame strengthened using a ductile steel bracing system have been reported[Goel and Lee 1990]. The steel bracing system consisted of inverted V-pattern braces, and horizontal and vertical members(collectors). The bracing system was added to a reinforced concrete frame designed to Mexican practice prior to the 1985 Mexico earthquake. The retrofitted frame behaved in a very ductile manner during the test. It was found that the vertical and horizontal members of the steel bracing system served a dual purpose, i.e., as truss members and as moment resisting members in combination with the original reinforced concrete frame members.

A new technique was recently proposed for strengthening low-rise reinforced concrete structures which are typical of school buildings in Mexico city. The strengthening technique consisted of the addition of high strength steel rods or prestressing cables which were post-tensioned to form a bracing system. One end of the diagonal bracing was anchored to the bottom end of the column at ground floor and the other end was anchored to top end of the column at the top floor of the structure. The inelastic dynamic analyses of a three storey school building frame were conducted to evaluate the effect of this bracing technique on the seismic behaviour of the frame[Miranda and Bertero 1990]. The results indicated that this technique with relatively small amount of materials produced a significant increase in stiffness and strength of the existing structure. It was also found that the level of prestress in the cable significantly modified the stiffness of the structure and that the prestress in the cable significantly enhanced moment resisting capacity of some columns due to an increase in axial load on the columns.

The seismic behaviour of two buildings retrofitted using a post-tensioned bracing system was also evaluated by performing inelastic dynamic analyses[Pincheira and Jirsa 1992]. The buildings represent typical low- and medium-rise non-ductile reinforced concrete frames built in the 1960's in the United States. The high level of prestress, (75% of the yield strength of the cable), was selected to allow the braces to yield in tension at relatively small drifts, resulting in energy dissipation at early stages of a severe earthquake. It was found that the post-tensioned bracing system can be used for the low-rise buildings on firm and soft soil sites. For the medium-rise buildings, the frame using the bracing system did not perform well on soft soil of Mexico city while satisfactory performance of the braced frame was achieved on firm soils. This is because the period of the braced medium-rise building on soft soil coincided with that corresponding to peak response of the Mexico earthquake.

1.2.5 Steel Jacketing Techniques

Generally, the columns with small shear span to depth ratio and/or widely spaced transverse reinforcement tend to fail in a shear dominated mode under severe earthquakes. Such non-ductile behaviour of the columns of the reinforced concrete building frames and of the bridge columns was demonstrated by the 1968 Tokachi-Oki earthquake and Californian earthquakes(the 1971 San Fernando, the 1987 Whitter Narrow, the 1989 Loma Prieta and the 1994 Nothridge). Steel or concrete jacketing techniques have been used to increase the shear strengths and ductility capacities of non-ductile columns following those earthquakes. In this section, steel jacketing techniques are reviewed.

Steel jacketing techniques involve steel encasement, steel straps and angles, and welded wire fabric, as shown in Fig.1.4. Voids between the steel encasement and the surface of the existing column are commonly filled with non-shrinkage cement grout or resin grout. A narrow gap at the ends of the column is provided to avoid an undesired increase in the flexural strength at those sections(see Fig.1.4). Special measures must be provided against fire and corrosion of the steel elements.

To investigate the effectiveness of the steel jacketing technique with steel straps shown in Fig.1.4(b), Arakawa 1980 tested 24 reinforced concrete columns. The shear span to depth ratio was 2.5 and the main variables of the test program were the spacing, width and thickness of the straps. The test results showed that the non-ductile behaviour of the original column could be changed to ductile response of the columns retrofitted with steel jacketing. In the case of the same width straps, a closer spacing was found to be effective to prevent the growth and expansion of shear cracks.

Four one-half scale reinforced concrete columns strengthened using mortar and welded wire fabric illustrated in Fig.1.4(c), were tested[Hayashi 1980]. The shear span to depth ratio ranged from 2.0 for the unstrengthened specimens to about 1.4 for the strengthened specimens. It was found that an effective increase in shear strength and displacement ductility capacity could be achieved by strengthening the original column using wire fabric wrapping.

Tests were carried out on five reinforced concrete columns : one column was designed to fail in shear during severe earthquake loading and the other columns were strengthened using steel encasement, as shown in Fig.1.4(a)[Fuse et al 1992]. The thickness of the steel encasement and the mortar thickness infill between the steel encasement and the original column surface were varied. The results indicated that the steel encasement technique could enhance the shear strength and ductility capacity of the original column.

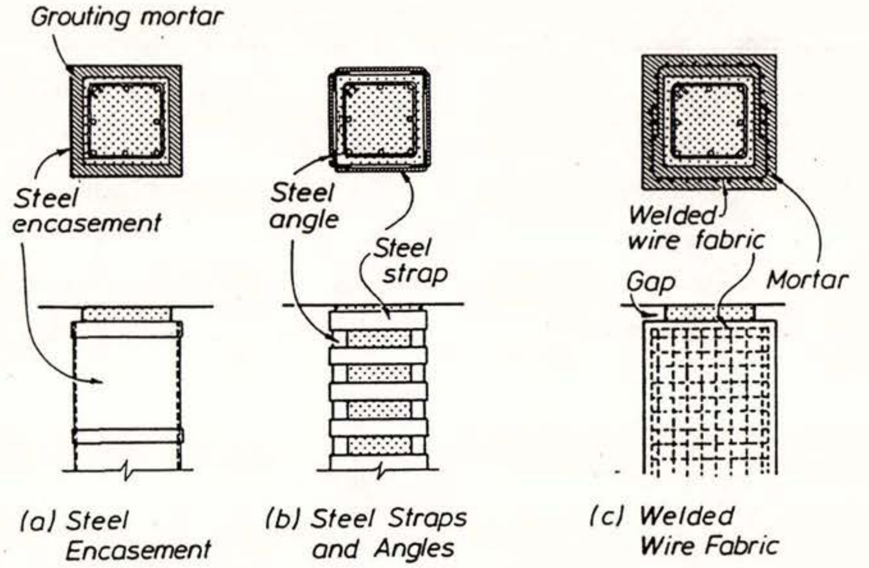

Fig.1.4 Steel Jacketing Techniques for Columns[Sugano and Endo 1983]

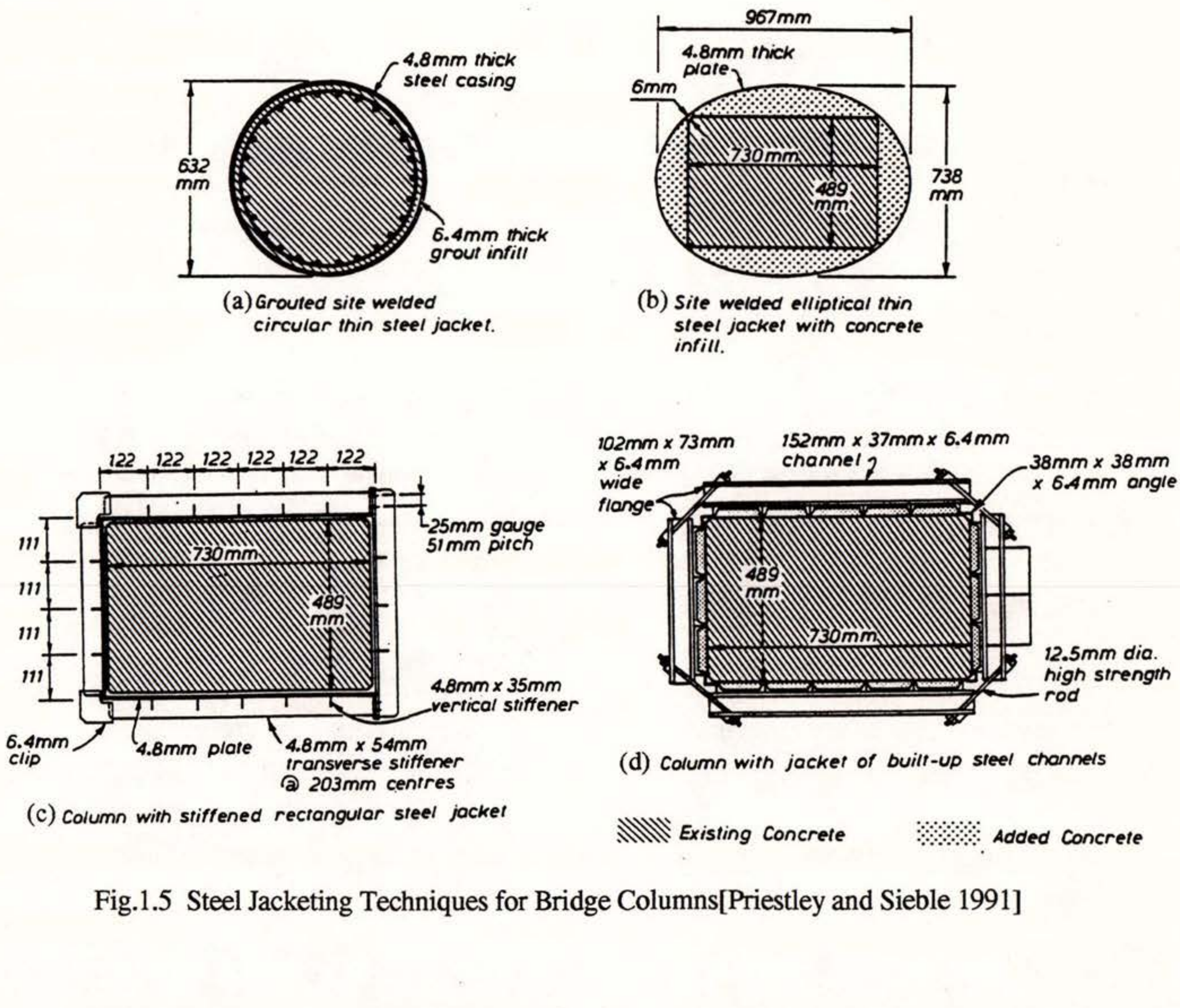

Fig.1.5 Steel Jacketing Techniques for Bridge Columns[Priestley and Sieble 1991]

Collapse or severe damage of many bridge structures in California caused by the 1971 San Fernando, the 1987 Whittier Narrow, the 1989 Loma Prieta and the 1994 Nothridge earthquakes emphasized the need to develop efficient retrofit measures to correct the deficiencies of bridge columns designed before the 1970's in the U.S. An extensive research program has been recently conducted in California to investigate various retrofit techniques to increase shear strengths and ductility capacities of the bridge columns using several different kinds of steel jacketing. Results from the test program indicated that cylindrical steel jacketing, as shown in Fig.1.5(a), provides an effective means of ensuring the ductile response with good energy dissipation of the circular reinforced concrete column. The circular jacket is constructed slightly oversize from two semi-circular halves welded up vertical seams in site. The gap between the steel jacket and the column is subsequently pressure filled with a cement-based grout which contains a small quantity of water reducing expansive additive. Similar ductile performance was also observed for the rectangular column encased with elliptical shape steel jacketing, with concrete placing between the jacket and the column, as illustrated in Fig.1.5(b). A rectangular thin steel jacket would not be so effective , due to the sides bowing out when dilation of the concrete occurs during a major earthquake, resulting in confinement applied mainly in the column corners. Rectangular jacket techniques, such as shown in Figs.1.5(c) and (d), found to be not so effective[Priestley and Seible 1991].

The column retrofit using steel jackets can be designed so as not to increase the flexural strength but to provide only additional transverse steel for concrete confinement, restraint against buckling of existing longitudinal bars, shear resistance and restraint against bond failure of lap splices of longitudinal reinforcement. In such case, the steel jacket is not continued beyond the ends of the column. The jacket is terminated about 25mm from the face of the beams or foundations.

The use of new material, such as carbon and glass fibre, to enhance the seismic performance of existing columns has been suggested and the effectiveness as a retrofit method has been verified by seismic loading test[Katsumata et al 1988, Priestley et al 1991 and Yamamoto 1992].

1.2.6 Concrete Jacketing Techniques

Concrete jacketing was the most commonly used repair and strengthening technique for reinforced concrete buildings after the 1985 Mexico earthquake[Jirsa 1987 and Jara et al 1989]. The jacket consists of added concrete, and longitudinal and lateral reinforcement around the existing column. A covering with concrete is efficient for fire protection. Several different kinds of concrete jacketing have been proposed in the UNIDO Manual 1983, one of which is shown in Fig.1.6 for increasing the concrete confinement, restraint against buckling of longitudinal bars, shear strength and strength of lap splices of existing columns.

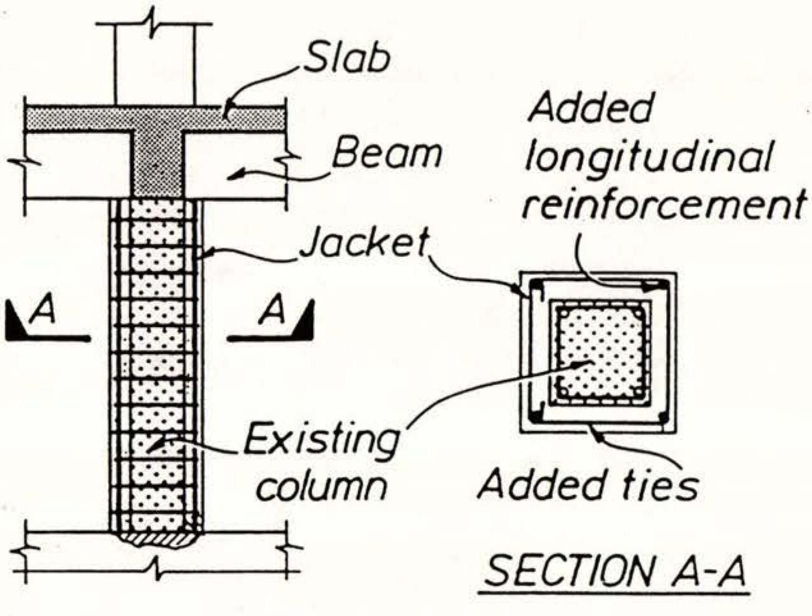

Fig.1.6 Concrete Jacketing Techniques to Enhance the Shear and Ductility Capacities of Columns[UNIDO 1983]

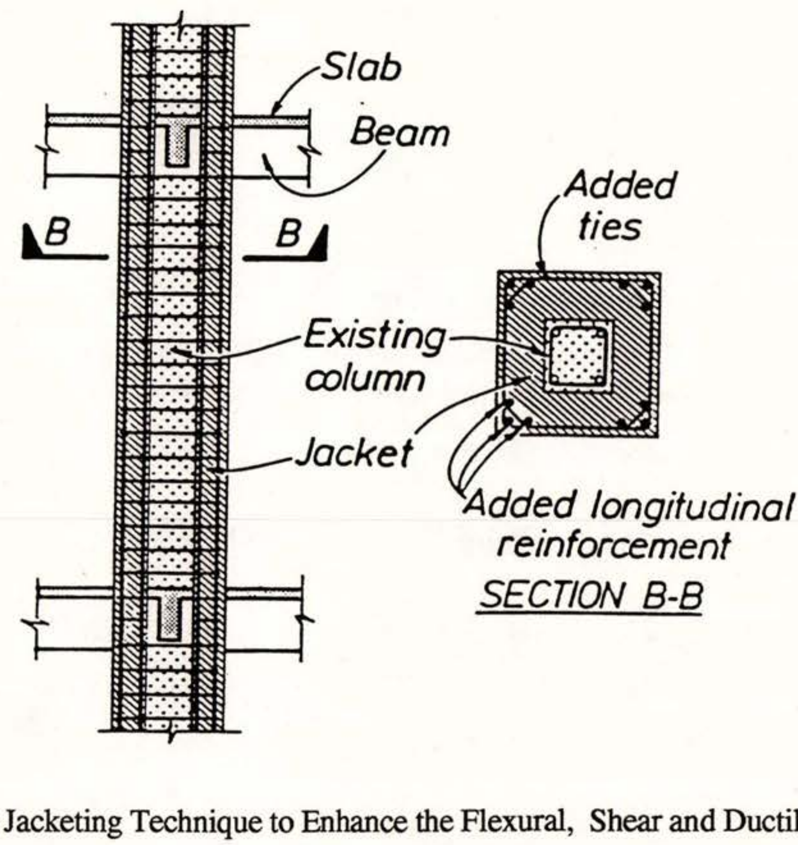

Fig.1.7 Concrete Jacketing Technique to Enhance the Flexural, Shear and Ductility Capacities of Columns[UNIDO 1983]

The effectiveness of concrete jacketing technique, as shown in Fig.1.6, was investigated on four two-thirds scale reinforced concrete short columns which were designed to typical practice in seismic regions of the U.S. in the 1950's and early 1960's[Bett et al 1988]. The unstrengthened column failed in shear during testing while the specimens strengthened using concrete jacketing showed either a flexural or a combined shear-flexural failure. It was found that the columns strengthened in shear by concrete jacketing were much stiffer and stronger as well as more ductile under lateral load than the original unstrengthened column.

Another type of concrete jacketing technique aimed at increasing the column flexural, as well as the shear strength and ductility is also given in the UNIDO Manual 1983. This is achieved by passing the new longitudinal reinforcement through holes drilled in the slab, and placing new lateral reinforcement and concrete around the existing column, as is illustrated in Fig.1.7. Four reinforced concrete columns have been tested to investigate the effectiveness of this type of repair and strengthening technique[Rodriguez and Park 1994]. The original columns in seven-eighth scale were designed and constructed to represent the column of a frame designed in the late 1950's in New Zealand. The main variables were the distribution of the new longitudinal reinforcement and the shape of the new transverse reinforcement in the retrofitted columns. The test results showed a significant increase in strength, stiffness and ductility compared with the unstrengthened column. It was also shown that two different details of the new longitudinal and transverse reinforcement had no significant influence on the overall seismic response of the jacketed columns. More details can be found elsewhere[Rodriguez and Park 1994].

Gulkan 1977 reported the results obtained from two three-fourth scale beam-interior column joints retrofitted using concrete jacketing technique. In this test, only the damaged columns were repaired with new longitudinal and lateral reinforcement. New lateral reinforcement was not placed in the joint core. It was concluded that the joint core might become the critical region.

The concrete jacketing techniques have been found to be effective for improving the seismic performance of non-ductile reinforced concrete columns. However, the jacketing of the columns and/or beams of an existing building frame does not necessarily ensure the satisfactory behaviour of the whole frame during severe earthquakes. Unless the beam-column joints are also retrofitted to improve the seismic behaviour, the weak link of the retrofitted frame may be shifted to the unstrengthened joints[Chai et al 1991]. The beam-column joints in moment resisting frames are normally subjected to large shear forces when the adjoining members develop their maximum flexural strengths. The large number of joint failures in the 1985 Mexico earthquake, as shown in Fig.1.8, strongly emphasized the need to address this problem[Rosenblueth and Meli 1986 and Mitchell et al 1988]. Very few

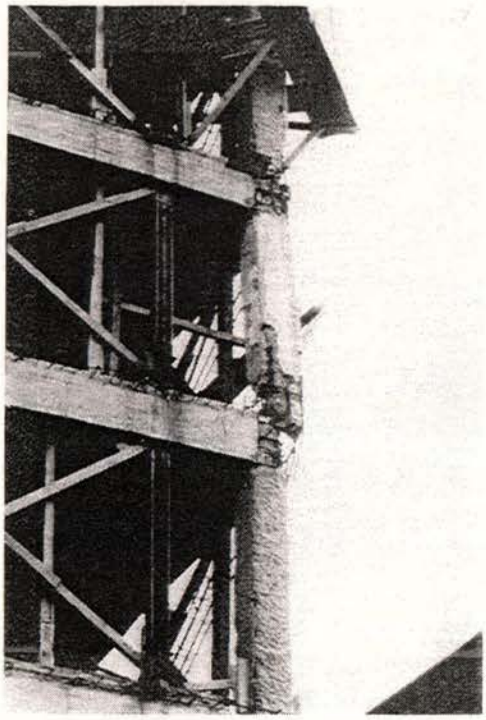

Fig.1.8 Joint Shear Failure During the 1985 Mexico Earthquake

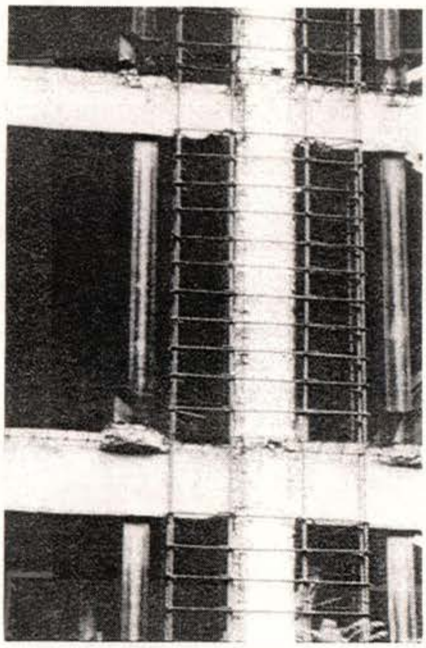

Fig.1.9 Enlarged Column Using Concrete Jacketing

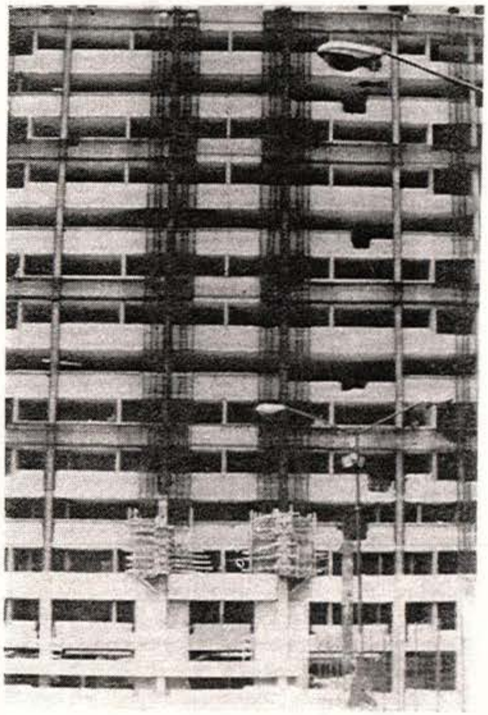

(a) Placement of New Beam and Column Reinforcement

(b) Building After Casting New Concrete

Fig.1.10 Building Frame Retrofitted Using Concrete Jacketing in Mexico City[Mitchell 1988] attempts have been made to assess experimentally the seismic behaviour of jacketed frame connections.

Alcocer et al reported the results tested on four full-scale beam-interior column connections with slab subjected to a bidirectional cyclic loading history[Alcocer and Jirsa 1990]. The original specimens were designed according to American and Mexican design practice of the 1950's. They lacked ductile detailing and had a strong beam-weak column characteristics. Furthermore, no shear reinforcement was placed in the joint core. The specimens were retrofitted by jacketing either only the columns or both the columns and beams. A structural steel cage was constructed by welding around the joint to confine the core concrete. The test results showed that concrete jacketing could change the behaviour of the frame from a strong beam-weak column system to that of a strong column-weak beam system. Although the steel cage maintained the integrity of the joint core concrete, the hysteresis curves of the retrofitted specimens exhibited severe stiffness degradation and pinching , indicating possible shear failure of the joint. It was also found that jacketing columns and beams required intensive labour and artful detailing.

An experiment was carried out on beam-exterior column joints with weak columns and very small amount of joint shear reinforcement[Paultre and Mitchell 1990]. The method of strengthening involved additional reinforced concrete around the existing exterior column to increase both the column and joint strengths. New lateral reinforcement were placed immediately above and below the joint region. The results of the test programme demonstrated that a significant improvement in strength, ductility and energy dissipation capacity of the unstrengthened exterior joints was achieved using concrete jacketing.

Hence, concrete jacketing of the columns and/or beams is very suitable technique for enhancing the lateral load strength and ductility of reinforced concrete moment resisting frames under seismic loading. One of the advantages of using concrete jacketing is the reduced cost in foundation strengthening required as compared with that when infilling wall or bracing techniques are used for strengthening. Little care is required for fire protection when compared with steel jacketing technique. In addition, the original function and aesthetics of the building may be maintained because no major changes in the original geometry of the existing building are necessary with this technique. As mentioned before, concrete jacketing techniques have been used as a retrofit measure for reinforced concrete building frames following the 1985 Mexico earthquake, as shown for example in Figs.1.9 and 1.10. However, the design and construction of the jacketing in most cases has been based on engineering judgement because of the lack of information about seismic assessment and retrofit procedures available to designers.

1.3 THE AIM OF THE RESEARCH PROJECT

In this research project, the seismic performance of details typical early reinforced concrete buildings constructed prior to 1970 in New Zealand is investigated. Design codes of that period did not specify capacity design nor ductile detailing procedures which ensure modes of inelastic deformation and ductility of the structure in the event of a major earthquake. The reinforcing details of such old buildings are adequate for gravity and wind loads but not for earthquake loading.

Some of the typical detailing problems found for old building frames are as follows:

(1) Columns with inadequate flexural strength to prevent column sidesway mechanisms(soft stories)

(2) Large diameter longitudinal beam bars passing through interior columns with small depth

(3) Poor anchorage of longitudinal beam reinforcement in exterior columns

(4) Small quantities of transverse reinforcement for shear, confinement of compressed concrete and restraint against premature buckling of longitudinal compression reinforcement in beams and columns

(5) Small quantities of shear reinforcement in beam-column joint cores

The effects of the poor reinforcing details mentioned above on the seismic behaviour of old building frames are examined in this study. The findings are for use by designers to assess the likely performance of old buildings for future earthquakes.

In addition, concrete jacketing techniques for retrofitting beam-column joint regions are also investigated in this research. The retrofit methods developed may be used for extending the life of existing reinforced concrete structures and the repair of damage arising from major earthquakes.

1.4 ORGANIZATION

In this thesis, first the seismic performance of a typical reinforced concrete building which was designed in the late 1950's in New Zealand is assessed. The results of the seismic assessment are presented in Chapter 2. This chapter also includes a review of the existing seismic assessment methods and a basic concept for redesign schemes of seismically inadequate buildings.

Then, experimental work carried out on full-scale replicas of the beam-column joint regions of the perimeter frame of the building mentioned above are described. Chapter 3 describes details of the test specimens, the retrofit techniques used in this study, and the loading programme. Three beam-interior column joint subassemblages with reinforcement details typical of reinforced concrete buildings designed in the late 1950's were constructed. One of the beam-column joint regions was tested as-built to investigate its seismic behaviour. The results are given in Chapter 4. The damaged beam-column joint replica and the other two undamaged beam-column joint replicas were retrofitted using jacketing with new reinforced concrete and tested. The seismic performance of the retrofitted specimens are compared in Chapter 5. Chapter 6 examines the behaviour of the beam-interior column joints without shear reinforcement subjected to simulated severe seismic loading, with emphasis on the effect of the bond condition along the longitudinal beam bars in the interior column. In addition, two beam-exterior column joint subassemblages were constructed. One of the exterior joints had the hooks of longitudinal beam bars not bent into the joint core of exterior column, which was common practice in some early frames. The other exterior joint had the hooks of the beam bars bent into the joint core. The test specimens were tested under simulated seismic loading and their behaviour is compared in Chapter 7.

In Chapter 8, the shear mechanisms of the beam-interior column joints with little or no shear reinforcement in the joint core are discussed. Based on the available test data, one approach to assess the seismic behaviour of such joints is proposed. A similar approach is also proposed for beams with a small amount of shear reinforcement.

Chapter 9 contains the conclusions of this research project and some recommendations for future research.

CHAPTER 2

AN EVALUATION OF A REINFORCED CONCRETE BUILDING DESIGNED IN THE LATE 1950'S IN NEW ZEALAND

2.1 INTRODUCTION

In recent years more attention has been focused on evaluating the seismic performance of existing buildings designed to early codes which may be now considered to provide inadequate protection against future earthquakes. Several seismic assessment methods have been proposed. Methodologies developed in Japan and the United States are briefly outlined below.

A reinforced concrete building frame designed in the late 1950's in New Zealand was chosen and its seismic behaviour was evaluated. Preliminary assessment was first attempted using the details of the building. Then non-linear inelastic analysis was carried out to obtain the probable strength, ductility and drift demands of the structure. The results of the seismic assessment of the building is presented below. Redesign schemes of seismically inadequate structures are also described.

2.2 REVIEW OF SEISMIC ASSESSMENT METHODS OF EXISTING REINFORCED CONCRETE STRUCTURES

2.2.1 General

In the seismic assessment of an existing structure, the details of the structure are usually given and therefore the available strength and deformation capacity in terms of ductility or storey drift angle can be estimated for the structure. Different from the ordinary design procedures and analysis, the maximum intensity of external disturbances such as lateral earthquake forces, under which the existing structure can survive with its lateral load carrying capacity and deformation capacity, is found in seismic evaluation[Aoyama 1980].

The deficiencies of reinforced concrete structures designed prior to about 1970 are mainly a consequence of the lack of structural ductility[Park 1992]. However, if the estimated lateral load strength of the existing structure exceeds the strength demand obtained from current code design spectra for elastic response, the safety of the structure can be assured to some extent, for example, in terms of annual probability of exceedance of a given level of peak ground acceleration.

2.2.2 Seismic Assessment Methods in Japan

In Japan, the 1968 Tokachi-Oki Earthquake heavily damaged a large number of low-rise buildings. The seismic safety of existing buildings became of particular concern after this event and the need for the evaluation of existing buildings was recognized. Several methods were developed for the evaluation of existing buildings[Miki et al 1973, Shiga 1977 and Umemura 1980].

In 1977, the "Standard for Seismic Capacity Evaluation of Existing Reinforced Concrete Buildings"[JABDP 1977] was compiled in Japan as the first complete document for the seismic assessment of existing reinforced concrete buildings and revised in 1990. This document is referred to as the "Standard" in this section. The method has been described in some detail in New Zealand[Aoyama 1980]. The evaluation method was developed mainly for low-rise reinforced concrete buildings in Japan, which contain shear walls and/or short columns likely fail in either shear or flexure. The "Standard" defines procedures for screening. The safety level of the existing buildings is assessed by the seismic index I_s for the total earthquake resisting capacity of a storey in each principal direction. The seismic index I_s is defined by the product of four indices as follows:

$$I_s = E_o\, G\, S_d\, T \tag{2.1}$$

where E_o = basic seismic index
G = geological index
S_d = structural design index
T = time index

The seismic index I_s indicates the ultimate strength of the building with regard to lateral loading or equivalent strength when the ductile behaviour is expected. Some factors which determine the right-hand terms of the Eq.2.1 are estimated in a relatively theoretical manner while the others are quantified on the basis of mainly engineering judgement. In the procedure, the safety of the existing building is judged based on the experience of earthquake damage. It is suggested that the value of the seismic index I_s of 0.6 to 0.7 be the border between damaged and undamaged buildings experiencing 250 to 300 gal level of ground motion[Sugano and Endo 1983, Okada et al 1983].

The basic seismic index E_o in Eq.2.1 in its simplest form is defined as follows:

$$E_o = \phi\, C\, F \tag{2.2}$$

where ϕ = storey index

C = strength index
F = ductility index

In Eq.2.2, it is assumed that the basic seismic capacity of a storey can be evaluated from the product of the strength index and ductility index, modified by a storey index. The ductility index is a function of the ductility factor and its evaluation is based on the inelastic response spectra using degrading trilinear hysteresis model. However, the ductility factor is not evaluated in a rational manner, especially for a frame with beam hinge mechanisms. This is because the primary emphasis of the "Standard" is placed on the vertical members such as the columns and walls, the failures of which have often been observed in Japan. It should be also mentioned that the "Standard" lacks the procedures to evaluate the seismic performance of beam-column joints. In Japan, the significance of the performance of beam-column joints was not appreciated at that time.

2.2.3 Seismic Assessment Methods in the United States

Two documents[ATC 1987 and 1989] have been prepared to provide minimum requirements for the evaluation of existing buildings in the United States. An existing building is evaluated to determine the potential life-safety hazards, that could endanger human lives during an expected future earthquake. The methodology was developed to identify the potential weak-links in an existing building, which could present a life-safety hazard. A check-list approach which compares the details of the existing structures with current code requirements is used in these documents and is written in the form of "True" or "False" which identify conditions that are acceptable or unacceptable. When the statements are false, more detailed investigation is required. Main aims of this investigation are the avoidance of brittle failure of members and joints, and to ensure that a beam hinging mechanism will form in the event of a severe earthquake.

It is recognised in these documents that the seismic performance of an existing building depends on not only the strength but also the drift control provided by the elements in the lateral force resisting system. Based on the flexural deformation of a representative column, including the effect of end rotation due to beam flexure, the drift is estimated and compared with the drift limitation. The strength of the existing building is assessed by the level of average shear stress of the members under specified lateral loads and hence the probable lateral load strength of the structure is not assessed for a critical failure mechanism.

The procedure includes the calculation of the capacity and demand ratios for lateral load carrying capacity of the building and for shear capacity of the member, which is the ATC-6-2 type approach[ATC 1983]. The capacities are calculated using appropriate building code provisions for the structural material although such provisions could only provide conservative values. Note that in both documents the required lateral load strengths of existing buildings are lower than those specified for new buildings. The recommended ratios are prepared and compared with the calculated values. Procedure to evaluate the non-structural elements is also covered in these documents.

It should be mentioned that the above method to assess the potential life-safety level of the existing building largely relies on the engineering judgement.

2.2.4 Seismic Assessment Method Using Capacity Design

2.2.4.1 The Approach

By applying the capacity design principles to existing reinforced concrete frame buildings, a realistic assessment procedure has been suggested by Priestley and Calvi 1991 which gets away from the check-list type approach and considers the overall performance of the structure. The suggested procedure is based on determining the lateral load strength and ductility of the critical post-elastic mechanism of deformation of the structure. This approach utilises recent experimental information relating to the interactions between the shear strength of members or joints and flexural ductility, the performance of lap-splices and anchorages and footing problems. Once the available lateral load strength and ductility of the structure has been established, reference to the current code response spectra for earthquake loading then enables the designer to assess the risk in terms of the annual probability of exceedance of the design earthquake.

2.2.4.2 Probable Strength of Members

In the assessment of an existing structure, realistic values for the material strengths should be used to obtain the best estimate of probable strength of the members. It follows that the use of nominal or specified material strengths, and of strength reduction factors, is inappropriate[Priestley and Calvi 1991].

Many existing reinforced concrete structures in New Zealand were constructed using reinforcing steel with a specified strength of about 240MPa. Park 1992 reports that it has been found by site sampling and testing that in structures built in New Zealand during the 1930 to 1970 period the reinforcement is likely to possess a characteristic yield strength 15 to 20% greater than the specified value. Hence, in the absence of other information, an actual yield strength of about 280MPa could be assumed in the assessment of structures of that age. Whenever possible, samples of steel from the structure should be tested to obtain a better estimation of the actual yield strength of the reinforcement.

Also, the actual compressive strength of old concrete is likely to considerably exceed the nominal value as a result of conservative mix design and age. Recent tests on the concrete of 30 year old bridges in California consistently showed compressive strengths approximately twice the nominal strength[Priestley and Calvi 1991]. Conservatively a value of 1.5 time the nominal compressive strength could be used in assessment. Wherever possible, cores should be taken from the structure to more accurately assess typical strengths. The quality of the concrete should also be inspected since if compaction was poor, a lower concrete strength may need to be assumed.

The estimated probable or the measured actual material strengths, and a strength reduction factor ϕ of unity, could be used to calculate the probable flexural and shear strengths of members and joints.

Park 1992 also reports that columns, if they were designed using elastic theory(working stress design), may often be found to have a high flexural strength when checked using current strength theory. Elastic theory design for column sections was very conservative (for example, a straight line interaction was commonly used between pure bending and pure concentric loading), resulting in eccentrically loaded columns with an actual flexural strength which is higher than expected. However, in spite of this, columns which were not designed for actions obtained using the capacity design process may not have sufficient flexural strength to avoid a column sidesway mechanism(soft storey).

2.2.4.3 Typical Examples of Poorly Detailed Reinforcement

Anchorage of Longitudinal Bars

Longitudinal reinforcement in existing structures may, according to current seismic design standards, not have adequate anchorage to develop and maintain the yield strength during the cyclic loading caused by a severe earthquake[Park 1992]. This deficiency is particularly found in early structures which used plain round bars, rather than deformed bars. Plain round bars require twice the development length of deformed bars[Erläuterungen et al 1961, SANZ 1982(a)].

Also, the configuration of hooks for longitudinal bars used in some early frames may not result in the best anchorage conditions[Nishimura and Minami 1986]. Fig.2.1(a) shows beam bars not bent into the joint core of exterior columns. This details does not provide the best configuration to enable the tensile bar force at the bend in the bar to be transferred into the diagonal compression strut which crosses the joint core. Current codes require the hooks to be bent into the joint core so that the bearing stresses at the inside of the bend are at the end of the diagonal compression strut.

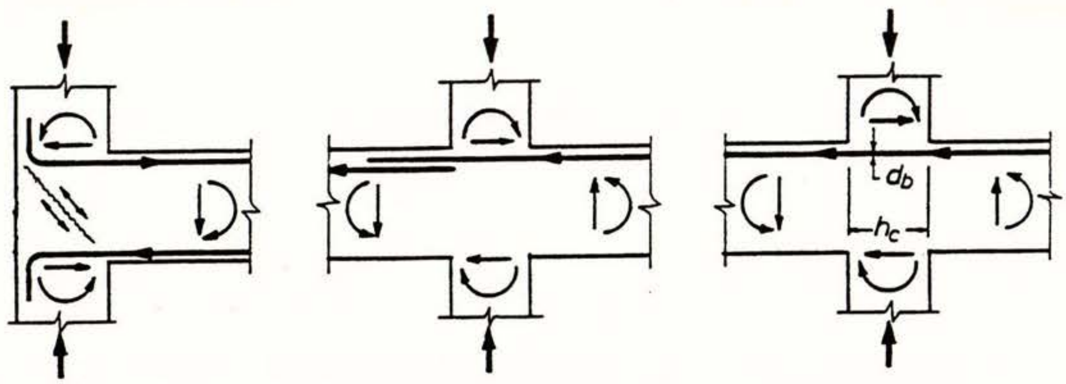

(a) Beam bar anchorages not bent into the joint core (b) Beam bar lap splice in plastic hinge region (c) Small h_c/d_b ratio for beam bars

Fig.2.1 Examples of Poor Detailing of Longitudinal Reinforcement[Park 1992]

Also, some early frames had longitudinal bars with lap splices in the potential plastic hinge regions of beams(see Fig.2.1(b)). This means that yielding may concentrate over small lengths of bar outside the lap and/or slip of bars may occur at the lap.

It will often also be found that beam bars of large diameter passing through relatively small columns will result in high bond stresses and bar slip. This occurs as a consequence of seismic loading which causes the bar to be in compression on one side of the column and in tension on the other side, which in the limit may require twice the yield force of the bar to be transferred to the joint core by bond. Current codes require the h_c/d_b ratio(see Fig.2.1(c)) to be large enough for the bond stress to be sufficiently low to prevent significant bar slip. If slip does occur, the bar will be in tension through the joint and the "compression" reinforcement in the beam on one side of the column may actually be in tension. Hence that steel will not act as compression reinforcement, with a resulting loss in beam ductility. Bond failure in beam-column joints will reduce the stiffness of the building, but it has been postulated that it may improve the shear strength of the joint core, since the beam compressive forces will be introduced into the joint by concrete compression rather than by bond along compression reinforcement. Hence the shear carried by the diagonal compression strut will be increased, reducing the diagonal tension stress introduced into the joint core by bond forces, resulting in an increase in the shear strength of the joint. Thus some slip of beam steel through the joint may actually increase the shear strength of the joint, although resulting in less ductile behaviour of the beam. This postulation has not been proved.

When considering the flexural strengths of beams subjected to seismic and gravity loading it is important to consider sections of the beam other than where the bending moment is maximum. In many frames designed in the 1950's and 1960's the curtailment of longitudinal reinforcement was governed more by gravity load moments than by the moment diagram corresponding to flexural strength. Hence unexpected locations of plastic hinges can occur where reinforcement is inappropriately terminated, especially taking into account the tension shift of bar forces due to diagonal tension cracking. For example, it may be found that negative moment plastic hinges in beams occur away from the column faces, due to too early curtailment of longitudinal top reinforcement.

Transverse Reinforcement for Shear Strength and Confinement

Transverse reinforcement is required in members to provide the confinement of compressed concrete, restraint against lateral buckling of longitudinal compression reinforcement and shear resistance[Park and Paulay 1975]. Inadequate quantities of transverse reinforcement will result in shear failure and a reduction in the flexural ductility of members.

Also, transverse reinforcement needs to be adequately anchored to be effective[Tanaka and Park 1987]. Transverse reinforcement will not be effective if lap spliced in the cover concrete without welding, or if the bend around longitudinal bars has inadequate bend angle or insufficient extension of free end into the core concrete. End hooks should preferably be bent at least 135°. 90° end hooks are definitely inadequate for perimeter hoops, since spalling of cover concrete will result in loss of anchorage. 90° end hooks could be tolerated when used for interior legs of hoops or ties which pass through the core concrete and are bent around intermediate column bars[Tanaka and Park 1987].

Shear Strength of Beam-Column Joints

The greatest uncertainty when assessing the seismic performance of reinforced concrete frames is the likely behaviour of beam-column joints. Most framed structures designed before about 1970 in New Zealand did not include shear reinforcement in the joint core. Very limited testing has been conducted on joints containing less shear reinforcement than required by current codes. Shear failure of joints is due to extensive diagonal tension cracking. One approach to the assessment of the shear strength of beam-column joints without shear reinforcement is to assume that the shear strength is reached at the stage of initial diagonal tension cracking of the joint core[Priestley and Calvi 1991]. If the diagonal tension strength of concrete is conservatively assesses to be $0.3\sqrt{f'_c}$ MPa, Mohr's circle for stress indicates that the horizontal shear stress required to induce this diagonal(principal) tension stress is:

$$v_c = 0.3\sqrt{f'_c}\sqrt{1+\frac{P_u}{0.3A_g\sqrt{f'_c}}} \text{ (MPa)} \tag{2.3}$$

where P_u=axial compressive column load(N) and A_g=gross area of column(mm^2).

To determine the level of seismic force which would be expected to cause diagonal tension cracking, the estimated horizontal shear stress at diagonal tension cracking given by Eq.2.3 can be compared with the horizontal shear stress v_{jh} imposed by the member actions on the joint where

$$v_{jh} = \frac{V_{jh}}{b_j h_c} \tag{2.4}$$

where V_{jh}=horizontal joint shear force, b_j=width of joint and h_c=column depth. It is suggested[Priestley and Calvi 1991] that the calculation of V_{jh} need not include the horizontal shear force carried by the diagonal compressive strut(C_B in Fig.2.2). That is, it could be assumed that:

$$V_{jh} = T_{Br} - V_{cu} \tag{2.5}$$

It is evident that joint core shear failure could be assumed to occur when $v_{jh} \geq v_c$.

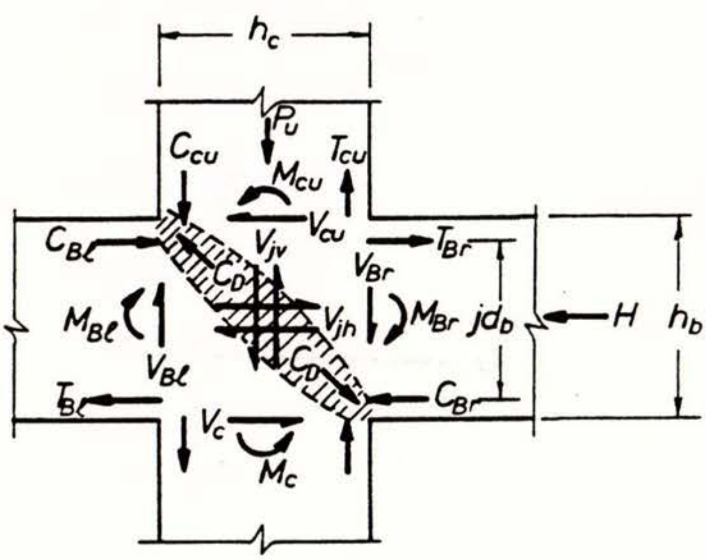

Fig.2.2 Forces in a Beam-Column Joint Caused by Member Actions
[Prirestley and Calvi 1991]

2.2.4.4 Assessment Procedure Suggested by Priestley and Calvi 1991

The assessment procedure should seek to identify the location, mode and probability of occurrence of post-elastic actions and deformations due to the design earthquake, and the critical collapse mechanism. The strength and ductility of the critical mechanism needs to be assessed.

Often for a building frame the critical mechanism is not simply a beam sidesway mechanism(see Fig.2.3(a)) or a column sidesway mechanism(see Fig.2.3(b)), but is a mixed mechanism involving flexural plastic hinges at some locations combined with shear failures of members and/or joints at other locations(for example, see Fig.2.3(c)). The consequences of particular failures need to be assessed relative to each other. For example, column shear failure is very serious, since it is associated with loss of gravity load capacity and could result in total collapse of the structure. Joint shear failure is less likely to result in catastrophic collapse. It must also be recognised that the shear strength of beams and columns in plastic hinge regions is dependent on the level of flexural ductility. Hence a mechanism which initiates with flexural plastic hinges may degenerate into plastic hinges with shear failure as the ductility demand increases[Priestley and Calvi 1991].

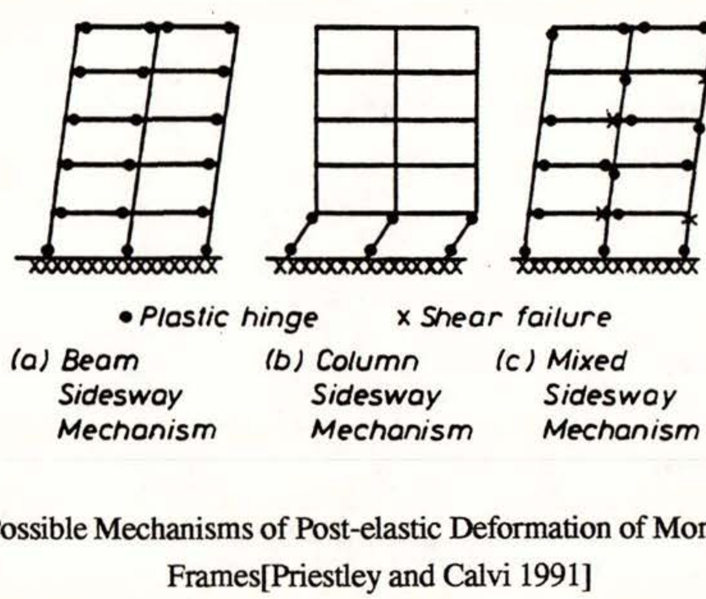

Fig.2.3 Possible Mechanisms of Post-elastic Deformation of Moment Resisting Frames[Priestley and Calvi 1991]

To investigate whether a column sidesway mechanism(soft storey) can be expected, a sway potential index S_p can be defined by comparing the probable flexural strengths of beams and columns at all joints at the level immediately above and below the suspect line of columns. For a line of j columns between levels n and n+1 of a frame[Priestley and Calvi 1991]:

$$S_p = \frac{\sum_{i=1}^{j} (\Sigma M_{Bn,j}) + \sum_{i=1}^{j} (\Sigma M_{Bn+1,j})}{\sum_{i=1}^{j} (\Sigma M_{Cn,j}) + \sum_{i=1}^{j} (\Sigma M_{Cn+1,j})} \qquad (2.6)$$

where $\sum M_{Bn,i}$ =sum of beam probable flexural strengths(left and right) at the centroid of joint i, level n and $\sum M_{Cn,i}$ =sum of column probable flexural strengths(upper and lower) at the centroid of joint i, level n.

When $S_p>1$, a column sidesway mechanism is expected. However, to include the effects of higher modes of vibration, it is suggested[Priestley and Calvi 1991] that a column sidesway mechanism be assumed if $S_p>0.85$.

The consequences of the development of various types of sidesway mechanisms and modes of post-elastic behaviour are discussed below:

Beam Sidesway Mechanism

When plastic hinge regions in beams are well detailed(for example, if the spacing s of transverse reinforcement satisfies $s \leq d/2$ or $s \leq 6d_b$, where d=effective depth of beam and d_b=diameter of longitudinal bars), an available displacement ductility factor of $\mu=6$ for the frame may be assumed. When the detailing is poor(for example, if $s \geq d/2$ or $s \geq 16d_b$), an available μ of 2 for the frame may be assumed, this being about the μ value when spalling of cover concrete commences. Intermediate values for the displacement ductility factor, in the range $2 \leq \mu \leq 6$, may be estimated according to the existing detailing of the members.

Similarly, the detailing of the potential plastic hinge regions at the column bases needs to be assessed(the spacing and quantity of transverse reinforcement, and the length and position of the confined region in the column, are all important) in order to estimate the available μ values. The assessment of the available curvature ductility factor of columns may require moment-curvature analysis using a stress-strain relationship for the confined concrete[Mander et al 1988]. The available μ can be estimated from the available curvature ductility factor[Park and Paulay 1975].

The above available ductilities apply only if the shear strength of the beams, columns and joints is adequate. Shear strength at plastic hinges degrades as the ductility demands increases, due to reduced shear carried by the concrete shear resisting mechanisms, V_c, particularly aggregate interlock. It is recommended[Priestley and Calvi 1991] that for beams the probable shear strength when $\mu \leq 2$ can be taken as:

$$V_p = v_c b_w d + \frac{A_v f_y d}{s} \tag{2.7}$$

where v_c=shear carried by the concrete mechanisms, b_w=width of beam web, d=effective depth of beam, A_v=area of vertical shear reinforcement at spacing s and f_y=probable yield strength of shear reinforcement.

When $\mu \geq 4$, degradation occurs and the probable shear strength can be taken as:

$$V_{pd} = A_v f_y d/s \tag{2.8}$$

Obviously the probable shear strength cannot be greater than the shear strength V_{fp} corresponding to the probable flexural strength. It is suggested[Priestley and Calvi 1991] that the available μ be found by interpolation as shown in Fig.2.4.

Also, the available μ value of the frame may be limited by the lack of shear strength of the beam-column joints.

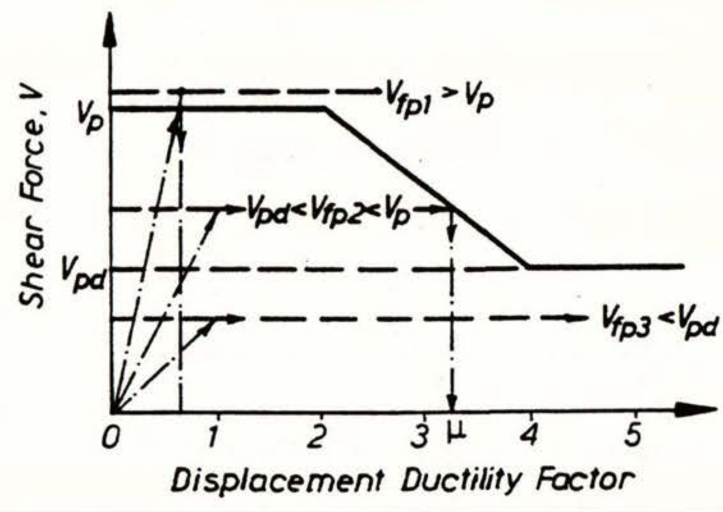

Fig.2.4 Proposed Relationship Between Shear Strength and Displacement Ductility Factor[Priestley and Calvi 1991]

Column Sidesway Mechanism

Column sidesway mechanisms in tall building can require very high plastic hinge rotations of the critical column regions[Park and Paulay 1975]. If the transverse reinforcing details are poor, an available μ of 1.5 may be conservatively assumed. Tests have indicated that the onset of concrete crushing in the plastic hinge regions of columns occurs in the range $2<\mu<3$. A moment-curvature analysis of the critical column sections can be conducted to determine the available curvature ductility factor, from which the available μ can be estimated taking into account the amount of confining steel and the number of storeys[Park and Paulay 1975].

Mixed Sidesway Mechanism

Combinations of beam and column plastic hinges and shear failures make up a variety of possible mixed sidesway mechanisms. As an example[Priestley and Calvi 1991], Fig.2.5 shows a line of beam-column joints when beam plastic hinges with available μ of 6 form except for one beam end where a flexure/shear failure is predicted with an available μ of 3. A conservative approach would be to assume the lower bound of $\mu=3$ for the whole mechanism. However, if it can be assessed that gravity loads can be carried at higher ductilities, it would be reasonable to ignore span 34 entirely and to assess the strength on the basis of spans 12 and 56 alone. Assuming that the equivalent elastic response strength $S_a(e)$ is proportional to the available μ multiplied by the sum of the flexural strengths, then if $\mu=3$ for all 6 plastic hinges

$S_a(e)$ is proportional to $3\times6\times M_f=18M_f$

and if $\mu=6$ for only 4 plastic hinges

$S_a(e)$ is proportional to $6\times4\times M_f=24M_f$

where M_f is the flexural strength of each beam plastic hinge. That is, this assumption which is equivalent to removing beam 34 from the mechanism results in a 33% increase in mechanism capacity.

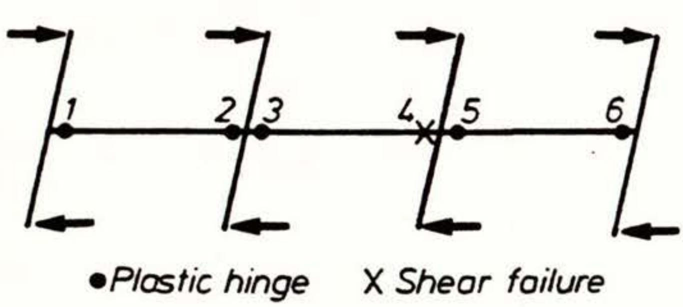

Fig.2.5 Mixed Sidesway Mechanism for a Storey[Priestley and Calvi 1991]

2.2.5 Summary of Needs for Improved Assessment Methods

In summary, the seismic assessment procedures mentioned above endeavour to find the probable lateral load strength and/or ductility of the existing building. Once the strength and ductility of the building are determined, reference to loading spectra(for example, SANZ 1992] will indicate whether the building for its period of vibration is able to withstand the design earthquake. The best estimate of the strength and ductility of the building can be obtained only when realistic strengths and deformation capacities of existing members and joints, and the critical collapse mechanism can be identified under seismic loading. It is also required to assess the stiffness of the existing building. Typically early building frames have inadequately low stiffnesses due to inadequate dimensions and reinforcing details of the members and joints. Further research on the available strengths, ductility capacities and stiffnesses of the members and subassemblages with dimensions and reinforcing details typical of early building frames is required to improve the seismic assessment methods mentioned above.

2.3 SEISMIC ASSESSMENT OF AN EXISTING REINFORCED CONCRETE BUILDING FRAME

2.3.1 Introduction

A seismic assessment of an existing reinforced concrete building frame, which was designed and built in the late 1950's, was made. A preliminary assessment was first attempted using details of the building. A non-linear 'static' analysis was carried out to estimate the lateral load strength of the structure, and the shear and ductility demands of the members and beam-column joints. A non-linear 'dynamic' analysis was also conducted to investigate the drift demands of the structure, and the shear and ductility demands of the members and joints under the given earthquakes.

2.3.2. Description of the Selected Structure

2.3.2.1 Configuration

The selected structure is that of a seven storey building with 5 spans in the x-direction and 3 spans in the y-direction as shown in Fig.2.6. The building was designed and constructed in Christchurch, New Zealand in the late 1950's. The foundation consists of large foundation beams and reinforced concrete piles. The structural walls enclosing a service core(see Fig.2.6(b)) are eccentrically located and hence may result in twisting about the vertical axis of the building when horizontal seismic load is applied. In this study, only the A and B-Frames in Fig.2.6(b) are assessed in the x-direction, neglecting the effect of the adjacent

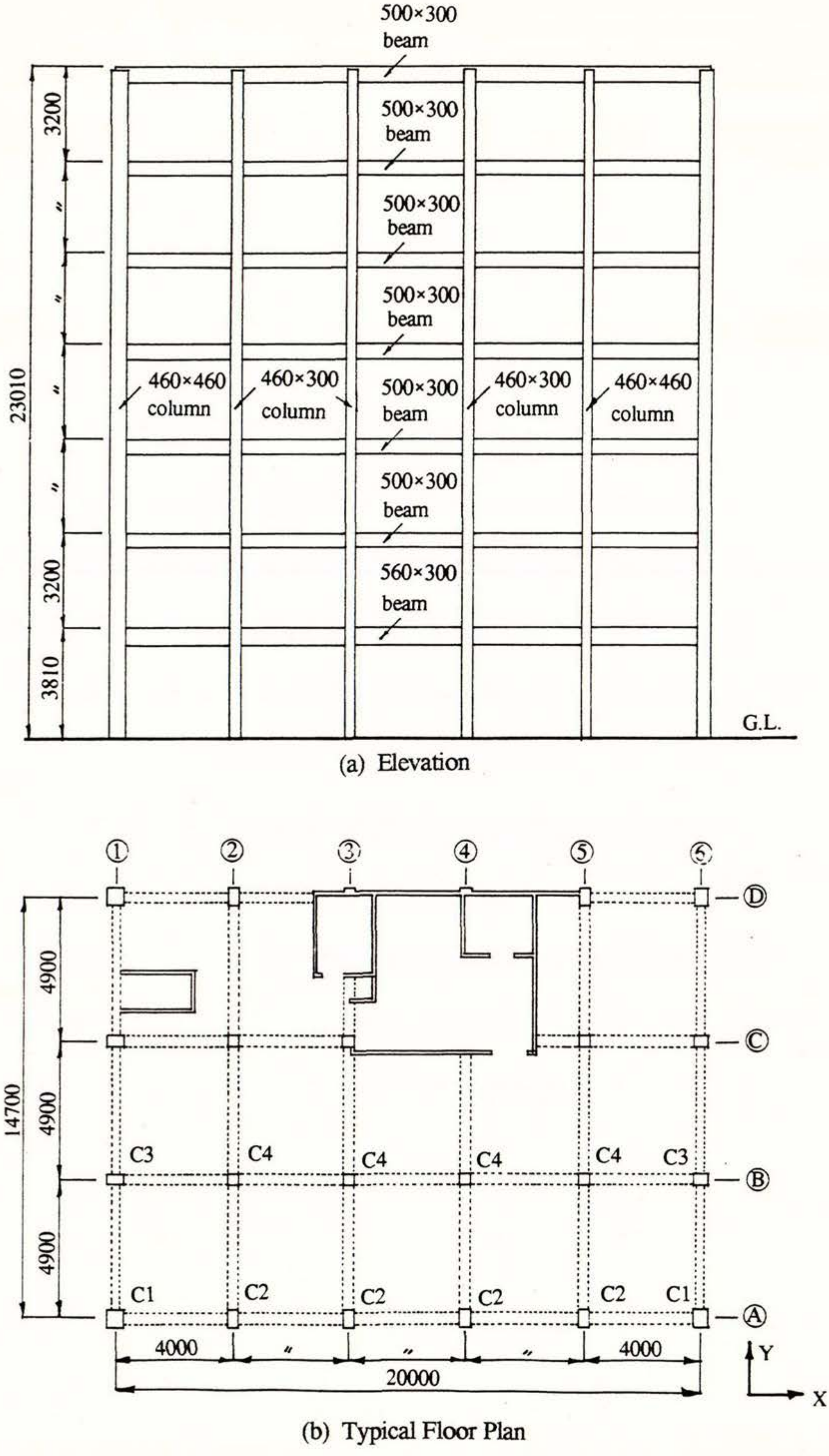

Fig.2.6 Elevation and Typical Floor Plan of Building

structural walls. Discontinuities in stiffness and strength exist between the 5th storey and the adjacent storey above or below, caused by the absence of the interior columns in the 5th storey of the B-Frame, as shown in Fig.2.7. This can lead to large ductility demands in the seismic resisting elements of that storey.

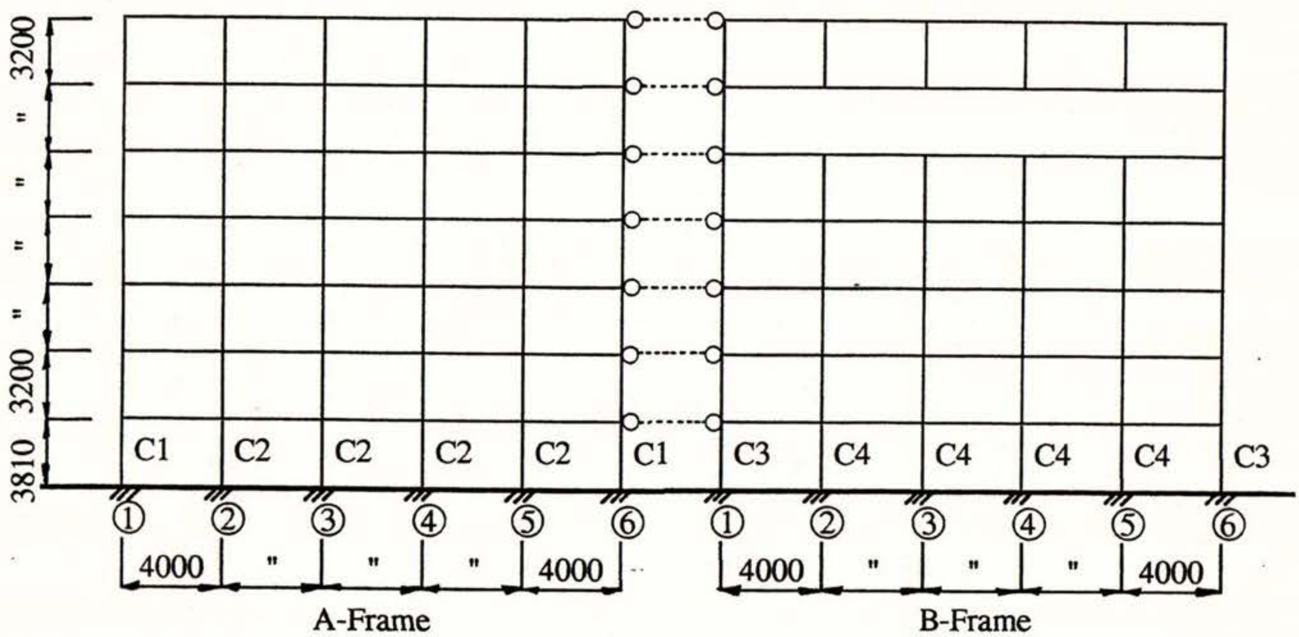

Fig.2.7 Selected Frames of the Building and Assumed Pin-Ended Rigid Links Connecting A and B-Frame in the Non-Linear Analysis

2.3.2.2 Reinforcing Details

In many building structures designed to early codes prior to about 1970, the reinforcing details are adequate for gravity and wind loads but not for earthquake loads. Earthquake design codes of that period did not specify capacity design nor detailing procedures which ensure strength and ductility of the structure in the event of a major earthquake.

The NZSS 95 New Zealand Standard Model Building By-Law published in 1955 superceded the 1939 edition. In this 1955 By-Law, the horizontal loading on a public building was recommended to be either that given by a uniform seismic coefficient of 0.1 up to the height of the building(0.08 was recommended for private buildings), or that given by a seismic coefficient which varied linearly from zero at the base to 0.12 at the top of the building(same for private buildings). The second option of a horizontal load distribution in the shape of an inverted triangle recognised approximately the deflected shape of the building in its first mode of dynamic response. Working stress design was recommended.

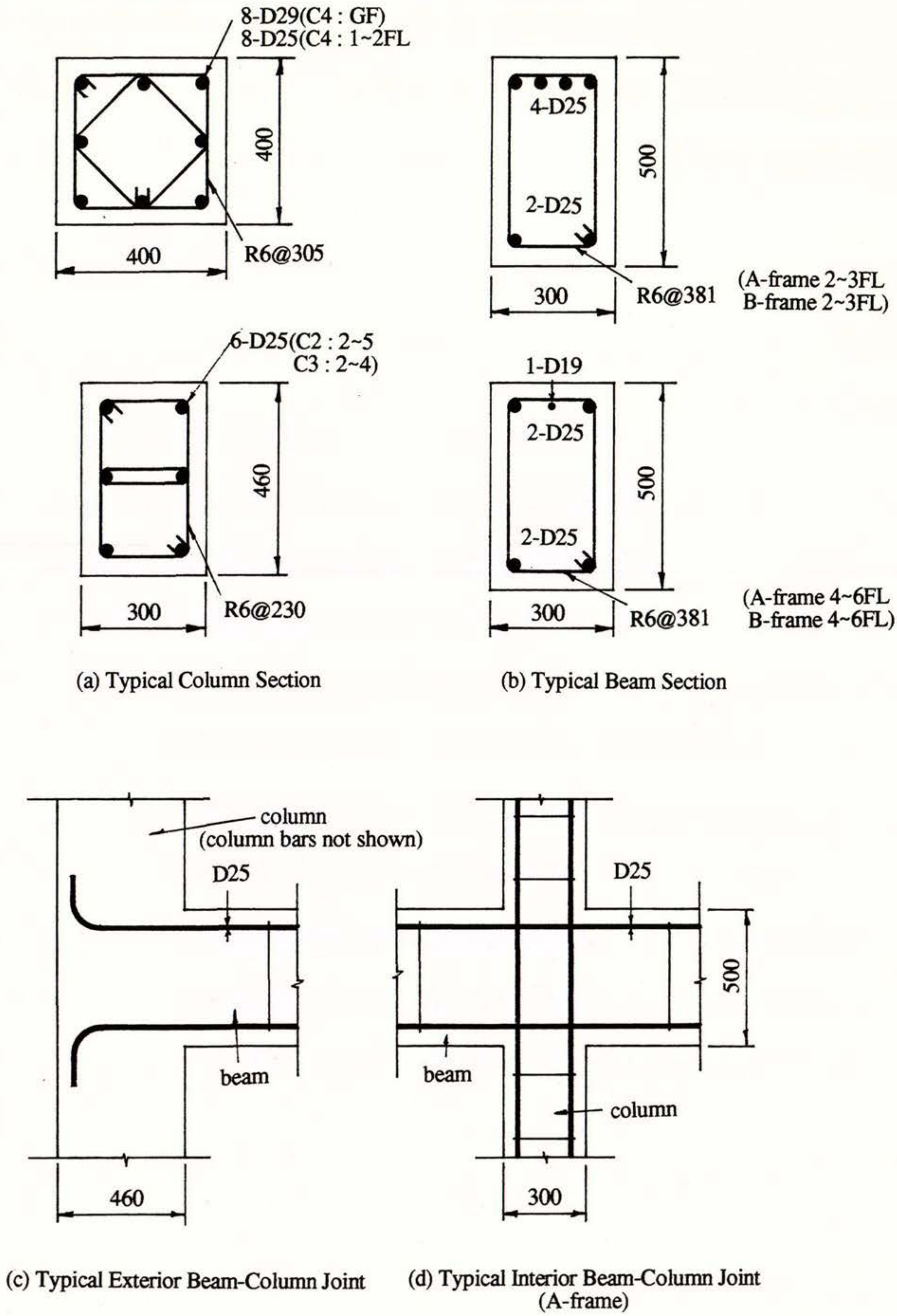

(a) Typical Column Section

(b) Typical Beam Section

(c) Typical Exterior Beam-Column Joint

(d) Typical Interior Beam-Column Joint
(A-frame)

Fig.2.8 Typical Dimensions and Reinforcement Details of Building Frame

Fig.2.8 shows the typical reinforcement details in the columns, beams and beam-column joint regions of the building. The spacings of transverse reinforcement are generally much greater than one-fifth of the least lateral dimension and six longitudinal bar diameters for the columns, and six longitudinal bar diameters for the beams which are specified as the maximum spacing in the current New Zealand Code NZS 3101[SANZ 1982(a)](see Figs.2.8(a) and (b)). This implies that the compressed core concrete is not confined effectively and that premature buckling of compression steel may occur, resulting in poor ductility capacity of the members. Since the transverse reinforcing bars have a small diameter in addition to a wide spacing mentioned above, brittle shear failure of the members are also expected during severe seismic loading.

A more critical aspect with respect to shear strength can be found in the beam-column joints. The joints of framed structures designed to early codes did not include any shear reinforcement, as illustrated in Fig.2.8(d). Hence joint shear failure may be expected during severe earthquake excitations. It is also found that longitudinal beam bars of large diameter pass through relatively small depth columns. The ratio of column depth to beam bar diameter is only 12 for the joint shown in Fig.2.8(d), while the current New Zealand code[SANZ 1982(a)] requires the ratio of 25 for Grade 300 reinforcing bars. Hence premature bond deterioration of beam bars passing through the joint can be predicted. Fig.2.8(c) shows that beam bars are not bent into the joint core of the exterior columns. This configuration of hooks for longitudinal beam bars at exterior joints may not provide the best anchorage conditions.

2.3.3 Evaluation of Member Strengths

2.3.3.1 Material Strengths

When assessing an existing building, realistic values for the material strengths should be used to obtain a good estimate of the probable strengths of the members. For assessment purpose, the following probable material strengths of the existing structure were used.

(1) The probable concrete compressive strength was estimated to be 30MPa, assuming 50% increase in strength from the originally specified compressive strength of 20MPa, taking into account conservative mix design and age. The probable concrete compressive strength is defined as f'_c in this chapter.

(2) The probable yield strength of the reinforcement was assumed to be 316MPa, assuming that the actual steel yield strength to be greater than the specified value by 15%.

In this chapter, the flexural and shear strengths calculated using both the probable material strengths defined above and a strength reduction factor of unity are termed the probable flexural and shear strengths, respectively.

Since the type of reinforcing bars could not be identified from the drawings of this building, it is assumed that deformed bars were used for the longitudinal reinforcement while plain round bars were used for the transverse reinforcement.

2.3.3.2 Flexural Strengths of Members

The flexural strengths of the members were calculated using an equivalent rectangular stress block for the compressed concrete of the current New Zealand code[SANZ 1982(a)] and assuming that plane sections before bending remain plane after bending. The contribution of the floor slab to the enhancement of the beam negative moment flexural strengths was considered by including the slab reinforcement over a width of 500mm each side of the beam. In this study, the area of slab bars which contribute to the negative moment flexural strength of a L-beam section was assumed to be 350mm^2 for the A-frame. For the B-frame, it was doubled, (that is, assumed to be 700mm^2) because the beams have flanges on both sides. In order to estimate the column flexural strength, column axial loads were obtained from the tributary floor areas and an assumed average floor loading of 8kPa, without a more accurate load evaluation. The above average floor loading was used consistently in this evaluation.

The strength ratios $\sum M_c/\sum M_b$ were assessed, where $\sum M_c$ is the total column moment at the beam centrelines and $\sum M_b$ is the total beam moment at the column centrelines, based on the probable flexural strengths of the columns and beams which were assumed to develop at the beam face or the column face. This strength ratio can be used to predict the probable failure mechanism of the frame. Fig.2.9 illustrates the strength ratio envelopes so determined. For interior joints, the strength ratios except for the top storey ranged from 0.92 to 1.36 for the A-Frame and 0.21 to 1.62 for the B-frame, respectively. It should be noted that for the B-frame the absence of the interior columns at the 5th storey results in the small ratios at the 5th and 6th floor. In general, it can be said that the column flexural strengths are not always large enough to ensure the development of a beam sidesway mechanism which is considered to be the preferred mechanism for tall building frames.

Note that in reality for this building, the presence of some walls would help to ensure that a beam sidesway mechanism develops.

2.3.3.3 Shear Strengths of Members

The shear strengths of the members were assessed using current design code[SANZ 1982(a)]. The shear design provisions of NZS 3101:1982 define two levels of the shear carried by concrete, v_c. One of them, referred to as the nominal shear strength in non-ductile regions, ${}_{nd}v_c$ is given by following equations from the code for the regions of members outside the plastic hinge regions:

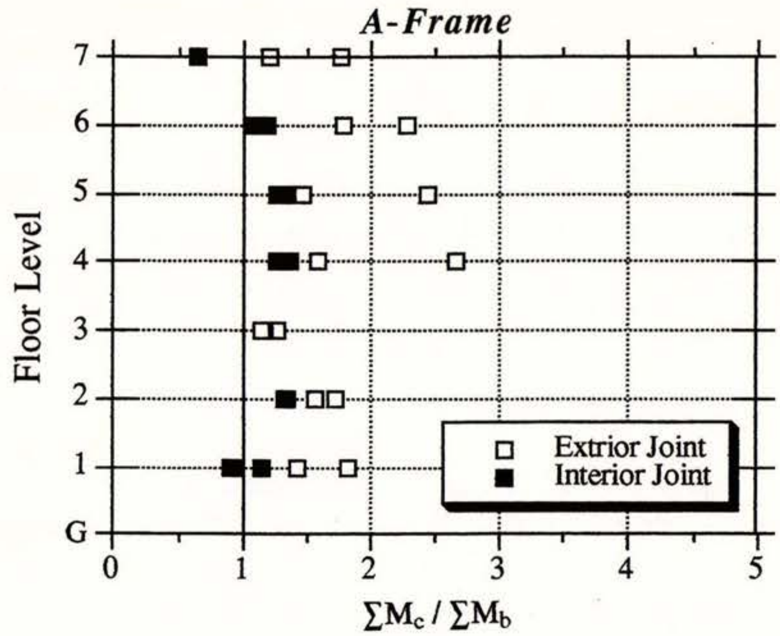

(a) A-Frame

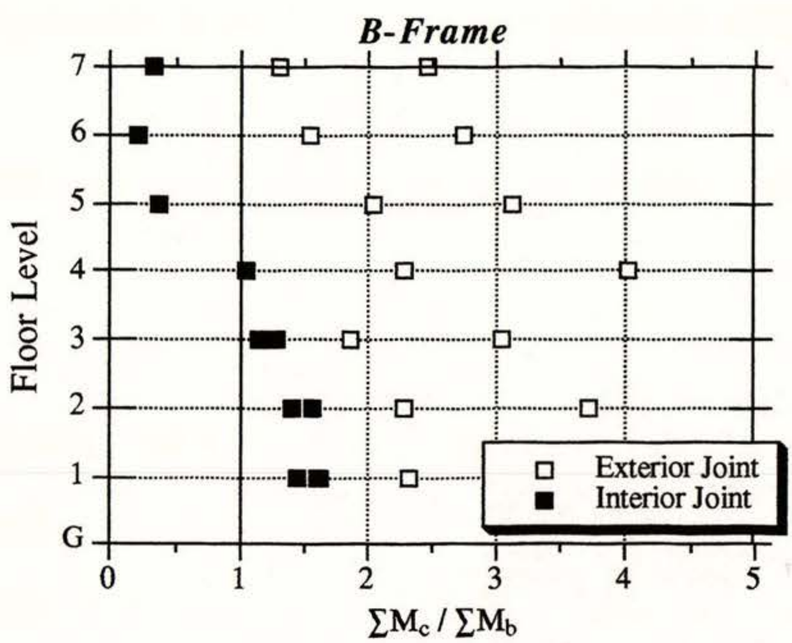

(b) B-Frame

Fig.2.9 The Ratio of Total Probable Flexural Strength of Columns to that of Beams

$$\text{Basic shear strength } v_b = (0.07+10\rho_w)\sqrt{f'_c} \tag{2.9}$$

$$\text{For beam} \quad {}_{nd}v_c = v_b \tag{2.10}$$

$$\text{For column} \quad {}_{nd}v_c = [1+\frac{3P_u}{A_g f'_c}]v_b \tag{2.11}$$

where $\rho_w = A_s/bd$, A_s=area of tension reinforcement, b=member width, d=distance from extreme compression fibre of concrete to centroid of tension reinforcement, f'_c=concrete compressive strength, P_u=axial load on column and A_g is gross area of column cross section.

Hence the nominal shear strength in regions where ductility is not expected is:

$$v_{nd} = {}_{nd}v_c + v_s \tag{2.12}$$

where v_s is the nominal shear stress carried by stirrups or hoops.

Cyclic reversed flexure in plastic hinge regions causes a degradation of the shear carried by the concrete shear resisting mechanisms of aggregate interlock and across the compression zone. Therefore the concrete contribution to shear is significantly reduced for beams in which large ductilities are expected(see Fig.2.4). According to SANZ 1982(a), the other level of shear carried by concrete v_c in potential plastic hinge regions, referred to as the nominal shear strength in ductile regions, ${}_{d}v_c$ is

$$\text{For Beam} \quad {}_{d}v_c = 0 \tag{2.13}$$

$$\text{For column} \quad {}_{d}v_c = 4v_b\sqrt{\frac{P_e}{A_g f'_c} - 0.1} \tag{2.14}$$

where P_e is the column load in compression due to the design gravity and seismic loading. The equation for a column implies that v_c shall be taken as zero if the axial force P_e produces an average compressive stress on the column less than $0.1f'_c$.

The non-ductile shear strength v_{nd} was used for the preliminary calculation of the shear strength in this study. For a conservative estimate, the specified yield strength of hoops or stirrups, 275MPa, was used to obtain the shear carried by hoops or stirrups, although the actual steel yield strength will likely be greater than the specified value.

Assuming the development of the probable flexural strength at the beam or column faces, the shear force V_f corresponding to the flexural strength(see Fig.2.10) was obtained for each member and compared with the probable non-ductile shear strength $V_p(=v_{nd}bd)$, where b is the member width and d is the effective depth of member. The contribution of gravity

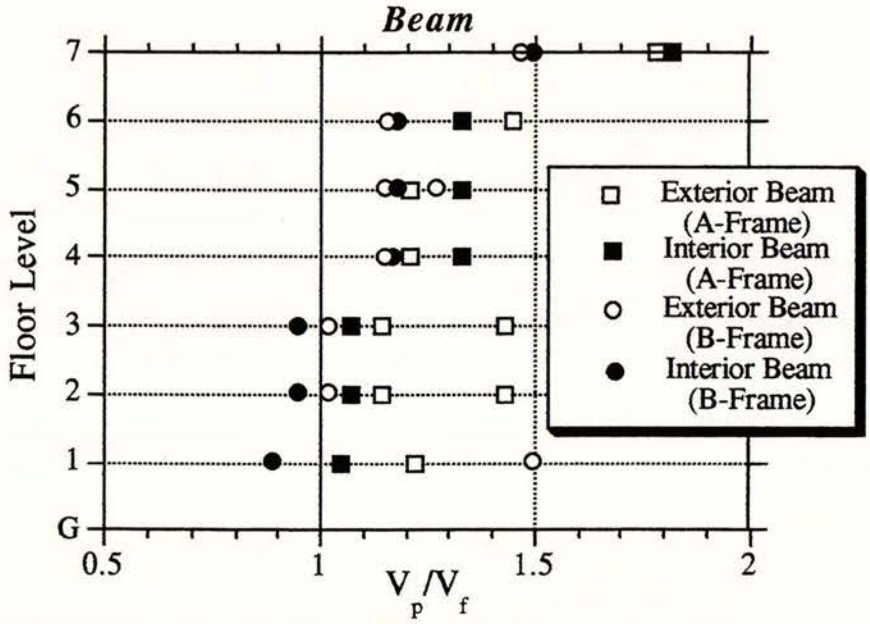

(a) Beams

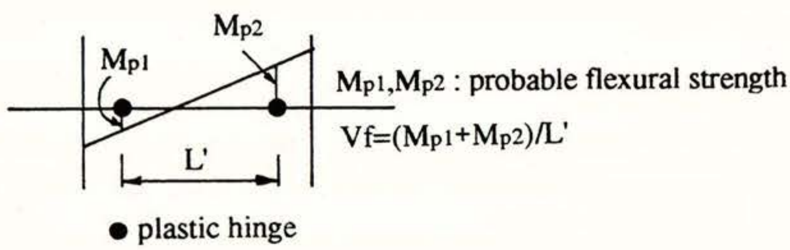

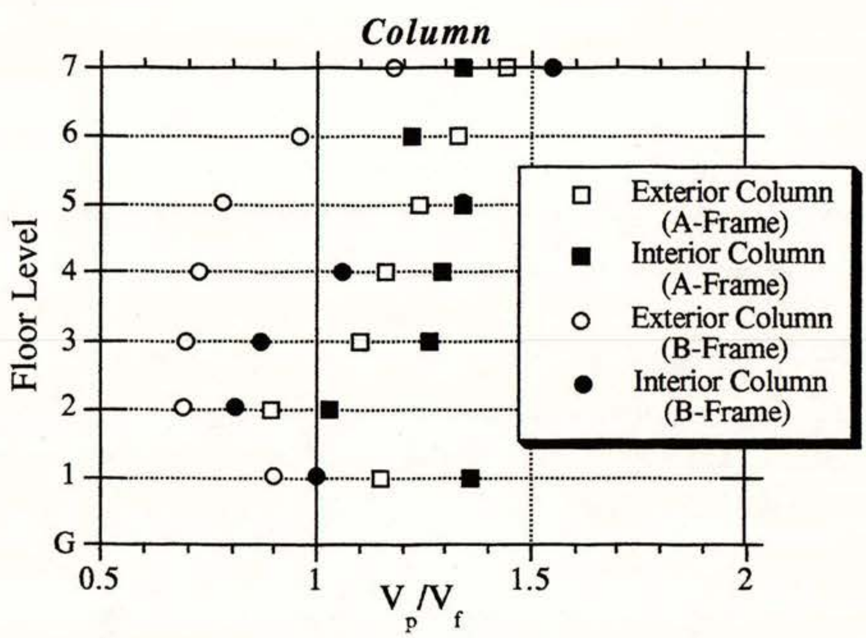

(b) Columns

Fig.2.10 The Ratio of Probable Shear Strength to the Shear Force Corresponding to the Probable Flexural Strength loading to the shear force V_f of beams was not considered. The strength ratios(V_p/V_f) are plotted in Fig.2.10. Shear failure is likely to occur when this ratio is less than one. As shown in this figure, shear failure can be expected: for example, in the exterior column at the 2nd floor level and some beams. In a severe earthquake where $_{nd}v_c$ would tend toward $_{d}v_c$, the strength ratio V_p/V_f would be less than in Fig.2.10. Hence it is identified that the amount of shear reinforcement is insufficient to prevent shear failure when the building is subjected to severe earthquake loading.

It is noted that column axial loads due to seismic loading have not been considered in the above assessment.

2.3.3.4 Anchorage of Longitudinal Reinforcement

To keep bond stresses to an acceptable level, the diameters of longitudinal bars d_b passing through an interior beam-column joint core are limited by NZS 3101:1982 as follows:

$$\frac{h_c}{d_b} \geq \frac{f_y}{12} \tag{2.15}$$

where f_y = specified yield strength of longitudinal bar
d_b = diameter of longitudinal bars
h_c = column overall depth

For interior column(C2, C4 in Fig.2.6) of the building, the ratio of the column depth to the beam bar diameter was

$$\frac{f_y}{23} \leq \frac{h_c}{d_b} \leq \frac{f_y}{17} \tag{2.16}$$

Hence slip of beam bars due to high bond stress could be expected during severe seismic loading.

To investigate the possibility of bond degradation, an index called the "beam bar bond index"[Kitayama et al 1987], was used. The average bond stress u_b over the column depth for simultaneous yielding of the beam reinforcement in tension and compression at the opposite faces of the joint is expressed as follows:

$$u_b h_c \pi d_b = f_y \frac{\pi}{4} d_b^2 \times 2$$

$$\therefore u_b = \frac{1}{2} f_y \left(\frac{d_b}{h_c}\right) \tag{2.17}$$

Beam Bar Bond Index

$$BI = u_b/\sqrt{f'_c}$$
$$= (f_y d_b / 2h_c)/\sqrt{f'_c}$$

where u_b=average bond stress
h_c=column depth
d_b=beam bar diameter
f_y=probable yield strength of the reinforcement
f'_c=probable compressive strength of concrete

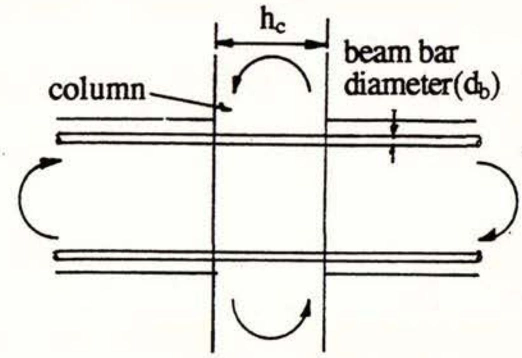

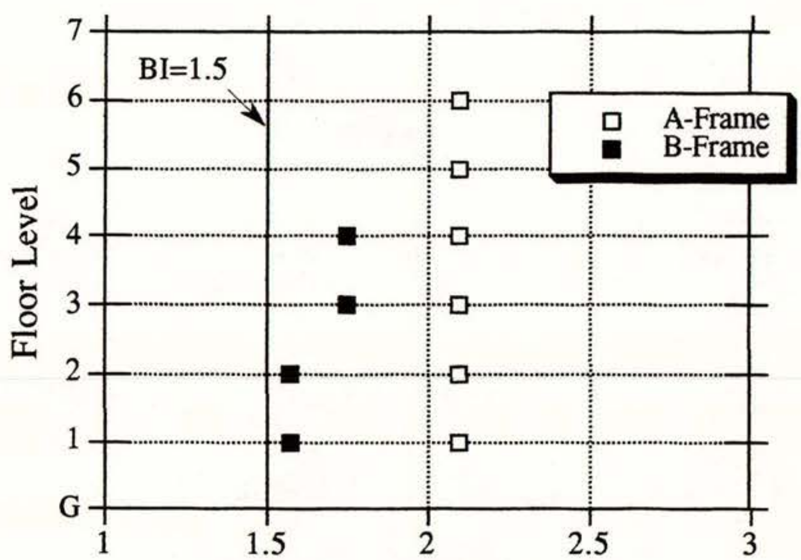

Fig.2.11 Beam Bar Bond Index Envelopes

If the bond strength is assumed to vary with the square root of the concrete compressive strength f'_c, the degree of bond degradation expected during seismic excitation may be expressed by a bond index, BI(see Fig.2.11), defined as

$$BI=u_b/\sqrt{f'_c} \tag{2.18}$$

The bond deterioration occurs more severely for a higher index value. The bond indices so obtained are plotted in Fig.2.11 and distributed the following range.

$$1.6<BI<2.1$$
$$\text{where } f'_c=30\text{MPa}$$

If the critical value of the bond index is assumed to be 1.5[Kitayama et al 1987], the bond indices obtained for the beam-interior column joint of the frames show values 7%~40% higher than critical. Hence premature bond deterioration can be expected for the beam bars passing through the interior joint during severe earthquakes.

As a result of the above preliminary assessment with regard to earthquake resistance, of a reinforced concrete moment resisting frame designed in the late 1950's, it is found that the columns have inadequate flexural strength due to insufficient longitudinal reinforcement and inadequate shear strength due to insufficient shear reinforcement, that the beams have inadequate shear strength due to insufficient shear reinforcement and that the beam-column joints have inadequate shear strength due to lack of shear reinforcement and inadequate development length for the beam bars.

2.3.4 Non-Linear Dynamic Analysis

2.3.4.1 Introduction

In order to provide information on the probable structural strength and the likely order of inelastic deformations of a reinforced concrete moment resisting frame designed in the late 1950's during earthquake shaking, a nonlinear dynamic analysis was carried out using the two-dimensional time-history non-linear frame analysis programme "RUAUMOKO".

2.3.4.2 Assumptions about the Structure

In non-linear response analyses, some simplifications are normally made to avoid a complicated and costly solution. However, such simplifications must not be unrealistic. The following assumptions were made.

(1) A beam or a column is a massless line element consisting of (a) infinitely rigid portions at ends in the beam-column joint, (b) a linear elastic portion in the middle, and (c) two rigid-plastic springs placed at the ends of the elastic portion. All inelastic deformations occur in these springs, and are expressed using the one-component model[Giberson 1969].

(2) The structure is a plane frame(see Fig.2.7) which displaces horizontally in its plane and rotates about an axis perpendicular to the plane of the structure.

(3) At each storey level, the horizontal displacements of all the joints are the same. Because of this assumption, axial deformations of the beams are not considered.

(4) At each storey level, A and B-Frame are linked together by rigid pin-ended links, so that the horizontal displacements of the two frames are the same(see Fig.2.7). This assumption is equivalent to assuming rigid diaphragm action of the floor and no torsional response of the building.

(5) Deformations are considered to be sufficiently small to allow the original geometry of the structure to be unchanged throughout the analysis.

(6) Beam-column joints are infinitely rigid.

(7) Masses are lumped at each floor level.

(8) The foundation of the structure is considered to be infinitely rigid. Columns at the ground floor are rigidly connected to this foundation.

(9) Gravity effects due to deflections, usually referred to "P-delta effects", are not taken into account.

(10) Base motions occur in the plane of the structure in the horizontal direction.

2.3.4.3 Member Stiffnesses, Strengths and Hysteresis Rules

A reasonably accurate assessment of member stiffness and strength is required for the analyses. The modulus of elasticity was calculated from the following equation[SANZ 1982(a)].

$$E_c=4700\sqrt{f'_c} \qquad (2.19)$$

where f'_c is probable compressive strength of concrete(=30MPa)

The following equivalent moments of inertia I_e are assumed based on the recommendation[Paulay and Priestley 1992].

$$\text{For beams} \quad : I_e=0.35I_g \tag{2.20}$$

$$\text{For columns} : I_e=0.60I_g \tag{2.21}$$

where I_g is moment of inertia of the gross concrete section

Probable flexural strengths obtained in Section 2.3.3.2 were used for the beams. The strengths of the columns were determined from the simplified moment-axial load interaction diagram shown in Fig.2.12. No strength degradation was assumed.

A bi-linear hysteresis model was used to express the moment-curvature hysteresis loops of the columns, as shown in Fig.2.13. For beams, the Q-Hyst model, as illustrated in Fig.2.14(a) was initially considered. This model can be considered as a modified bi-linear hysteresis model and adequately expresses the softening of beams during the unloading and load reversal stages. These two models are described in detail elsewhere[Saiidi and Sozen 1979]. However, the Q-Hyst model does not cover the case when pinching occurs due to slip of reinforcement. That is, the model cannot express the softening that can occur due to insufficient anchorage length of beam bars in the joint of the frames. Therefore another model which considers the pinching effect was also used for the hysteresis loops of the beams. The pinching model chosen for the beams is shown in Fig.2.14(b). Factors controlling the unloading and reloading stiffnesses were selected to make the hysteresis loop as thin as possible. Also, a post-yield stiffness of zero was used. This is because poor energy dissipation capacity could be expected for each member of the structure when subjected to severe earthquake motions.

The damping was represented using the Rayleigh damping model. The lumped nodal weights were determined by assuming the average weight of floor to be 8kPa as described in Section 2.3.3.2. Modal analysis was conducted to determine the fundamental period of vibration of the frames and it was found to be 1.32 seconds.

The El Centro 1940 NS earthquake record was selected since the NZS 4203:1984 design spectra[SANZ 1984] was based on Californian accelerograms scaled to El Centro magnitude. The Bucharest 1977 earthquake record containing significant long period ground motions was also chosen for this study. The structure was subjected to the first ten seconds of the selected earthquake records with a scale factor of unity.

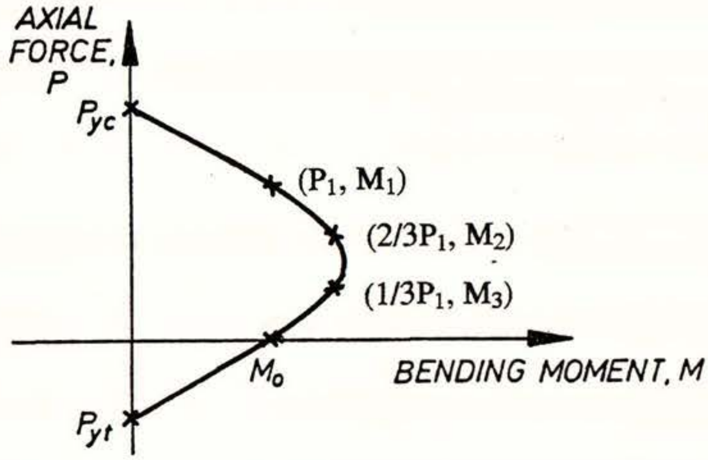

Fig.2.12 Simplified Moment - Axial Load Interaction Diagram

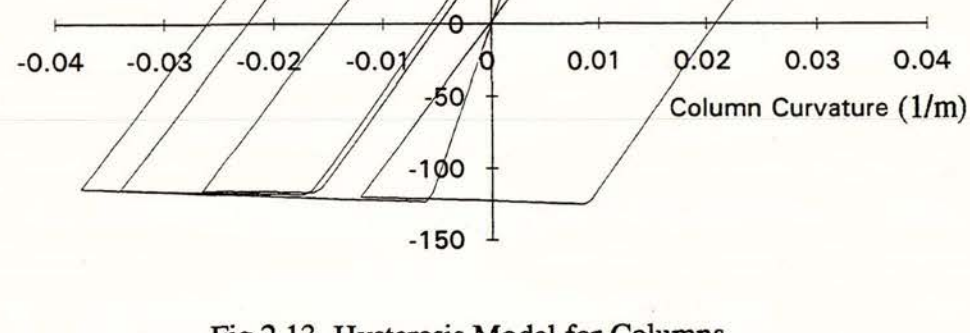

Fig.2.13 Hysteresis Model for Columns

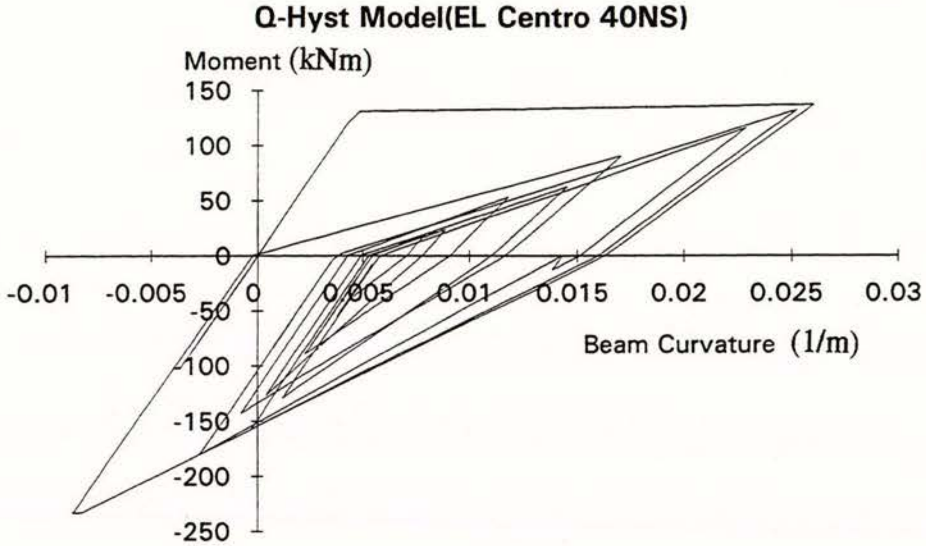

(a) Q-Hyst Hystersis Model

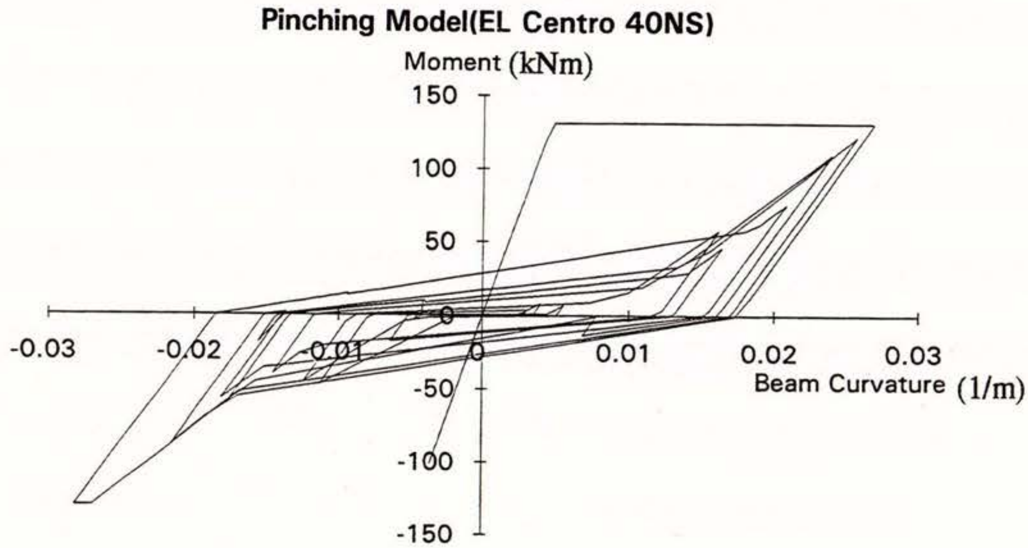

(b) Pinching Hystersis Model

Fig.2.14 Hysteresis Models for Beams

2.3.5 Results of Static Analysis

2.3.5.1 Method

First, the inelastic response analysis of the building subjected to statically applied monotonic lateral loading was carried out with the gravity load present. The lateral load applied at level i of the structure was obtained from

$$F_i = \frac{W_i h_i}{\Sigma W_i h_i} V \tag{2.22}$$

where W_i and h_i is the seismic weight and height at level i of the structure, respectively, and V is the total horizontal seismic force at the base of the structure.

Fig.2.15 shows the relationship between top roof horizontal displacement and the base shear force. The analysis was terminated when the top roof displacement reached approximately 1% of the total height of the building. The maximum values of the design parameters, for example, storey shear force and curvature ductility factor, were defined at this stage in this study.

2.3.5.2 Base Shear Force

Maximum storey shear force envelope (at 1% drift angle of the frame total height) is illustrated in Fig.2.16. Also shown are the design shear forces according to the NZS 4203:1984 and NZS 4203:1992[SANZ 1984 and 1992]. The design shear forces were determined from the following factors.

Using NZS 4203:1984

(1) Classification of the Building
  Category 4 (from Table 4 in the Code)

(2) Risk Factor
  R=1.0 (from Category 4)

(3) Structural Type Factor
  S=5 Elastically responding reinforced concrete structure

(4) Structural Material Factor
  M=0.8 Reinforced non-prestressed concrete

(5) The site subsoil category is assumed as
  Intermediate soil site

(6) Zone Factor
  Seismic Zone B is assumed

(7) Basic Seismic Coefficient

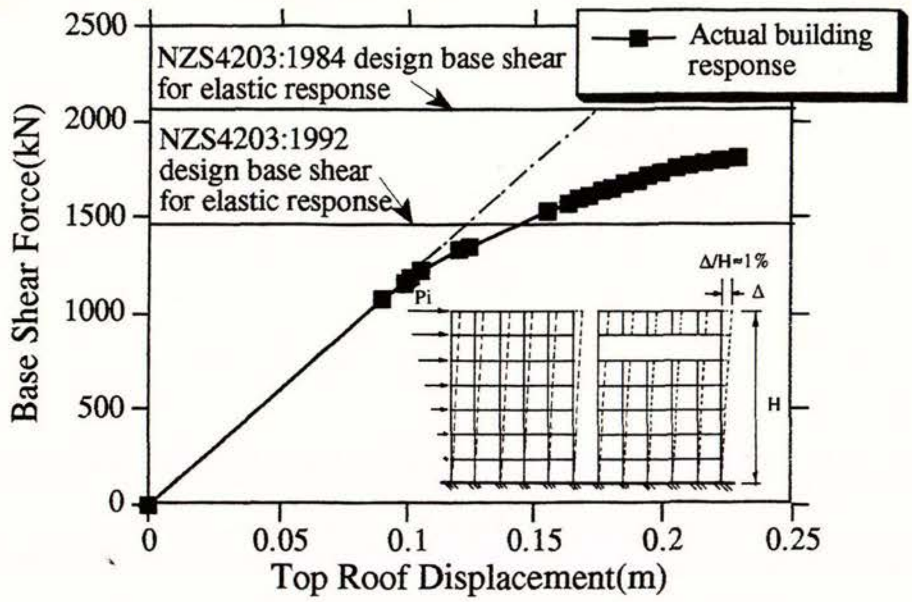

Fig.2.15 Base Shear Force versus Top Roof Displacement Relationship

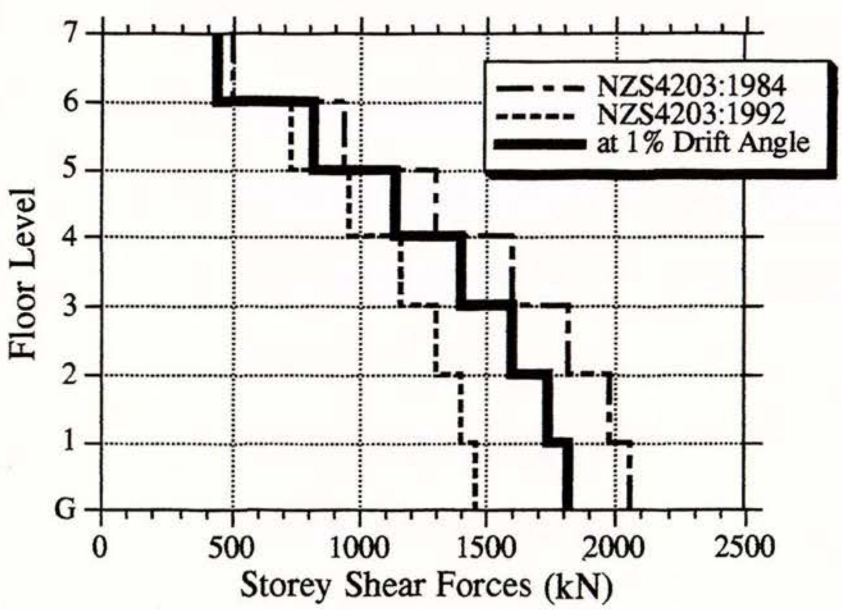

Fig.2.16 Maximum Storey Shear Force Envelopes

Period T=1.32 second, Intermediate soil site
C=0.0625 (from Fig.3 in the Code)

A total horizontal seismic force $V=C_d W_t$=2058kN
where C_d=CRSM=0.25 and W_t=8232kN

Using NZS 4203:1992

(1) Classification of the Building
Category 4 (from Table 2.3.1 in the Code)

(2) Risk Factor
R=1.0 (from Category 4)

(3) Structural Ductility Factor
μ=1.25 Elastically responding reinforced concrete structure

(4) Structural Performance Factor
S_p=0.67

(5) The site subsoil category is assumed as
Intermediate soil site

(6) Zone Factor
Z=0.8 (Fig.4.6.2 in the Code)

(7) Limit State Factor
L_u=1.0 (Ultimate)

(8) Basic Seismic Hazard Acceleration Coefficient
Period T=1.32 second, Intermediate soil site
$C_h(T1,\mu)$=0.33 (from Fig.4.6.1 or Table 4.6.1 in the Code)

(9) Lateral Force Coefficients for the Equivalent Static Method
$C=C_h(T1,\mu)\ S_p\ R\ Z\ L_u$=0.18

A total horizontal seismic force $V=C\ W_t$=1456kN

According to the static analysis, the base shear force at 1% drift angle of the total height was 1811kN which corresponds to 0.22g in terms of the base shear force coefficient. Hence the available storey shear strengths obtained from the static analysis, assuming inelastic behaviour up to 1% drift of the total height, were less than the design storey shear forces assuming elastic response from NZS 4203:1984 and larger than those from NZS 4203:1992(see Fig.2.16). However, because the actual building has some ductility(see Fig.2.15), it will survive the earthquake assumed in the both editions of NZS 4203, if the twist of the building due to the eccentric structural walls is neglected.

2.3.5.3 Maximum and Minimum Axial Loads on Columns

The axial force envelopes for the exterior and interior columns obtained at 1% drift angle of its total height are shown in Fig.2.17. In this figure, the axial force level $P_u/(A_g f'_c)$, which included gravity loads, are plotted with positive sign for compression, where P_u is the axial load on column, A_g is the gross area of column cross section and f'_c is the probable compressive strength of concrete. As illustrated in this figure, the maximum axial load level of 0.30 was observed for the exterior column of the B-Frame and the minimum axial load level of -0.07 was obtained for the exterior column of the A-Frame. For interior columns, the maximum and minimum axial load levels were 0.24 and 0.13, respectively.

In order to obtain the probable flexural and shear strengths of the columns, an approximation of the level of axial load under seismic loading should be made. The earthquake induced axial loads were investigated to provide some information related to this approximation. The earthquake induced axial load input may be estimated assuming the beams develop their probable flexural strengths at the ultimate stage of loading. The summation of such shear forces above the level under consideration would give an upper-bound estimate of the earthquake induced axial column force. The probable earthquake induced axial force P_{EP} can be expressed by the following equation.

$$P_{EP}=R_v \sum V_E \tag{2.23}$$

where $\sum V_E$ is the sum of the beam shear forces at the development of the probable beam flexural strengths above the level considered and R_v is the axial load reduction factor.

Values of R_v found for exterior columns are plotted in Fig.2.18 using the earthquake induced axial force P_{EP} obtained from static analysis. The recommended values in NZS 3101:1982[SANZ 1982(a)] are also shown in this figure. The recommended values recognize that with an increasing the number of storeys above the level to be considered, the number of beams which develop their probable flexural strength is likely to be reduced. As shown in this figure, however, the axial load reduction factors in some cases decreased with decrease in the number of stories above the level, indicating the different trend from the recommended values. The value of R_v depends on the number of the plastic hinges developed in the beams above the level. At roof level, where typically two beams and one column are joined, plastic hinges are hardly developed in the beams, resulting in a decrease of the axial load reduction factor. This trend is more obvious for the B-Frame due to the absence of the interior column at the 5th storey. The distribution of the beam hinging up to the height of the structure will also affect the axial load reduction factor.

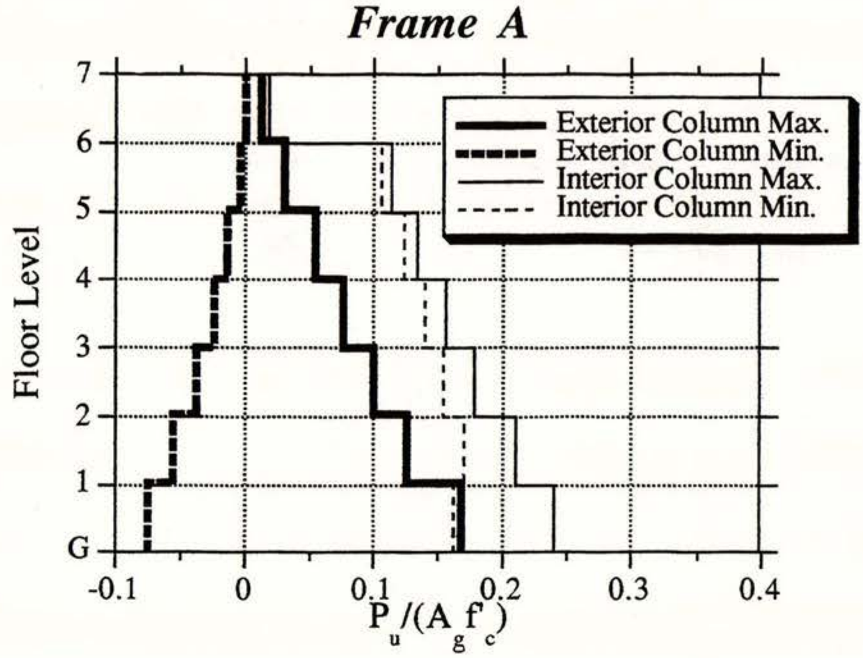

(a) A-Frame

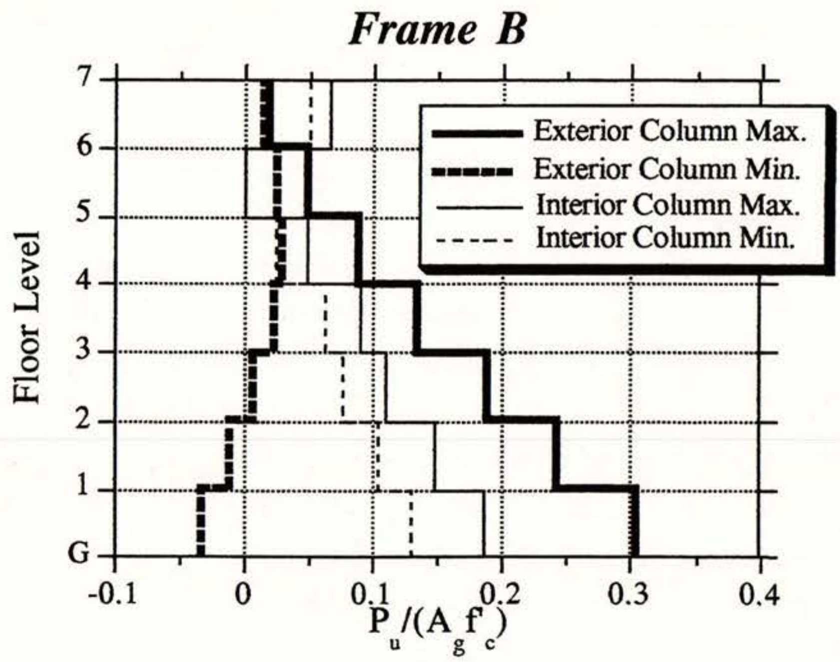

(b) B-Frame

Fig.2.17 Maximum and Minimum Axial Force Envelopes

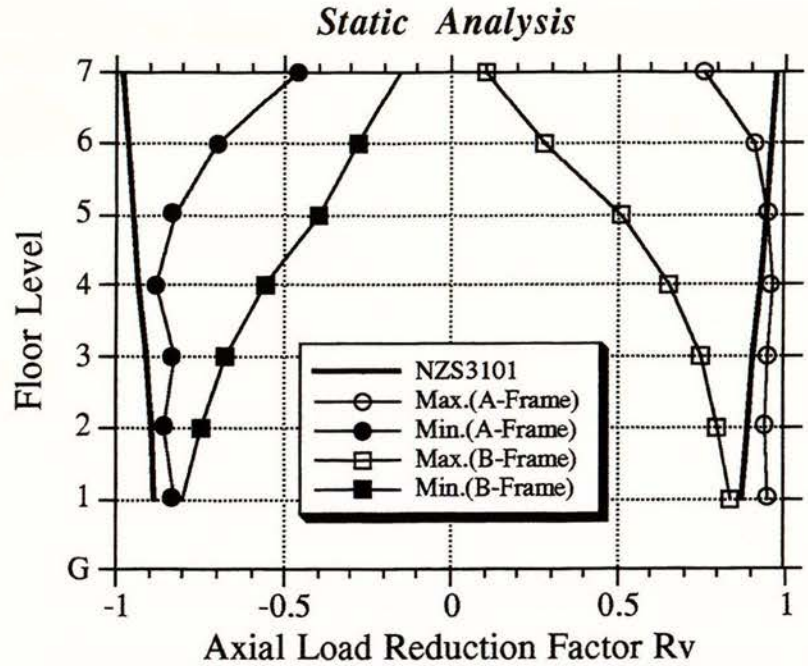

Fig.2.18 Axial Load Reduction Factor

2.3.5.4 Maximum Storey Drift Angle

The maximum horizontal displacement and interstorey drift angle at each level are plotted in Fig.2.19. The horizontal displacement envelope was reasonably proportional to its height and no detrimental effects due to the absence of the interior columns at the 5th floor of the B-Frame can be found. The maximum interstorey drift angle was approximately 1.20%, occurring at the 3rd through 5th floor.

2.3.5.5 Maximum Curvature Ductility

The maximum curvature ductility factor envelopes for the beams at each floor level are plotted in Fig.2.20. In the analysis, the equivalent plastic hinge length was assumed to be 50% of the member depth. A maximum curvature ductility factor demand of around 10 was observed for the beams of the frames when the drift angle of 1% of the total height was reached. In order to obtain the available curvature ductility factor of the beams, moment curvature analysis was carried out. Fig.2.21 shows the relationship between moment and curvature of a typical beam section in the lower storey. Despite the apparent poor detailing for ductility in the plastic hinge region shown in Fig.2.8, relatively large available curvature ductility factor can be reached assuming buckling of compression reinforcement and shear failure do not occur. If a maximum concrete compressive strain ε_{cu} of 0.4% is assumed, a curvature ductility factor of more than 10 can be expected for the typical beam section.

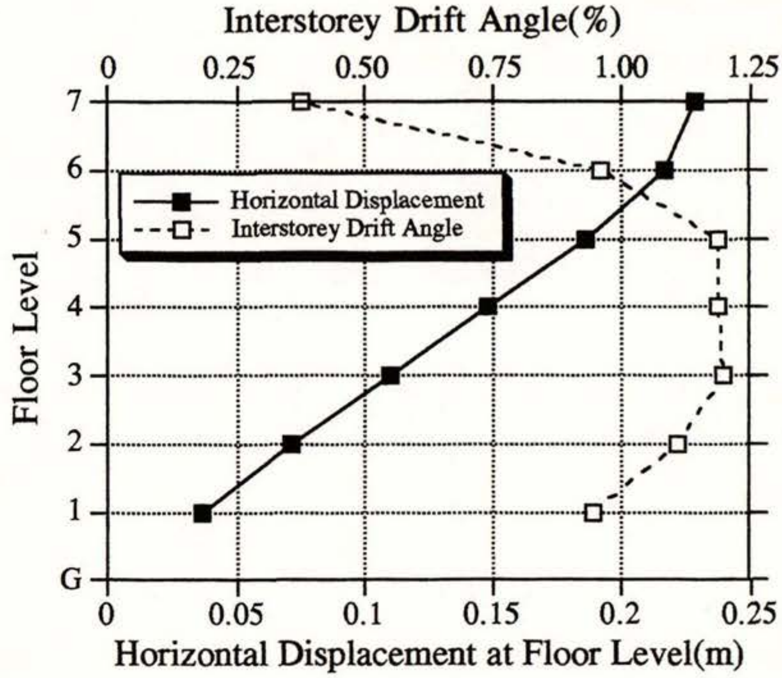

Fig.2.19 Maximum Horizontal Displacement and Interstorey Drift Angle Envelopes

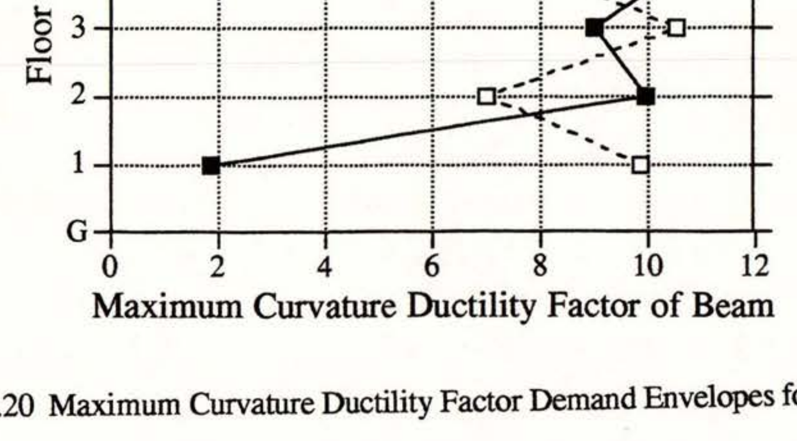

Fig.2.20 Maximum Curvature Ductility Factor Demand Envelopes for Beams

Hence theoretically the beams of the frames can survive during severe earthquake loading if compression steel buckling and shear failure can be avoided.

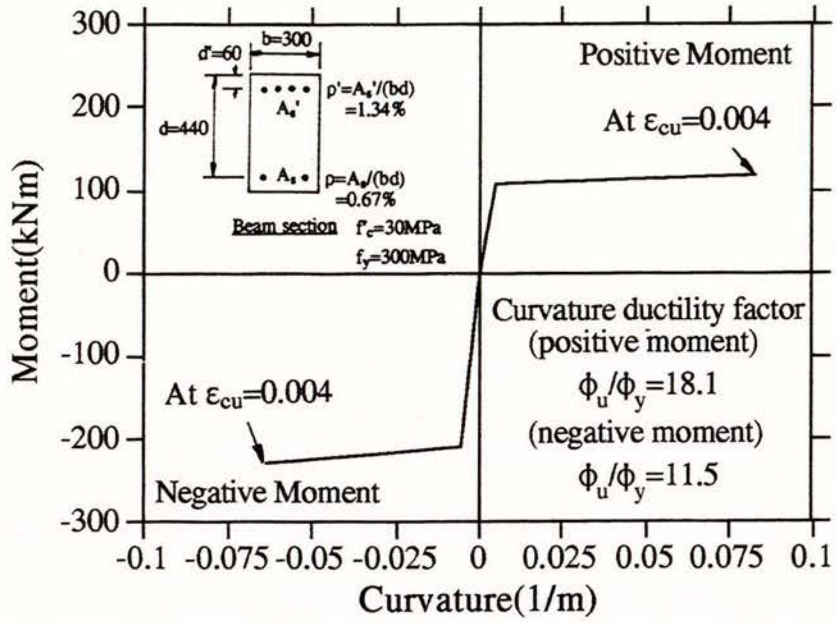

Fig.2.21 Moment versus Curvature Relationship of Typical Beam Section

2.3.5.6 Probable Mechanism

Fig.2.22 illustrates the ratio of the probable shear strength V_p to maximum shear input V_d for the beams and columns. The probable shear strength of the columns were calculated from the axial loads at 1% drift angle of the top roof displacement. As shown in this figure, the beams in the lower storey of the B-Frame and the exterior columns in the lower storey of the A-Frame can be expected to fail in shear. Note that the beam shear did not include the gravity loading.

At 1% drift angle of the roof displacement, the mechanism of the structure is shown in Fig.2.23. The critical mechanism of the building was not either a beam sidesway mechanism or a column sidesway mechanism, but a mixed mechanism involving flexural plastic hinges combined with shear failures of the beams and columns. Fig.2.23 indicates that the beam plastic hinge behaviour controls the inelastic response of the frame. Although flexural plastic hinges of the columns were observed at the top storey of the B-Frame and the exterior column at the 3rd storey of the A-Frame, a soft storey mechanism in which plastic hinges form at top and bottom of all the columns at one storey in the frame was not developed. Therefore, the curvature ductility demands of the column plastic hinges can be expected to be relatively low. When considering the low axial load level at the top storey and the inevitable axial loads in

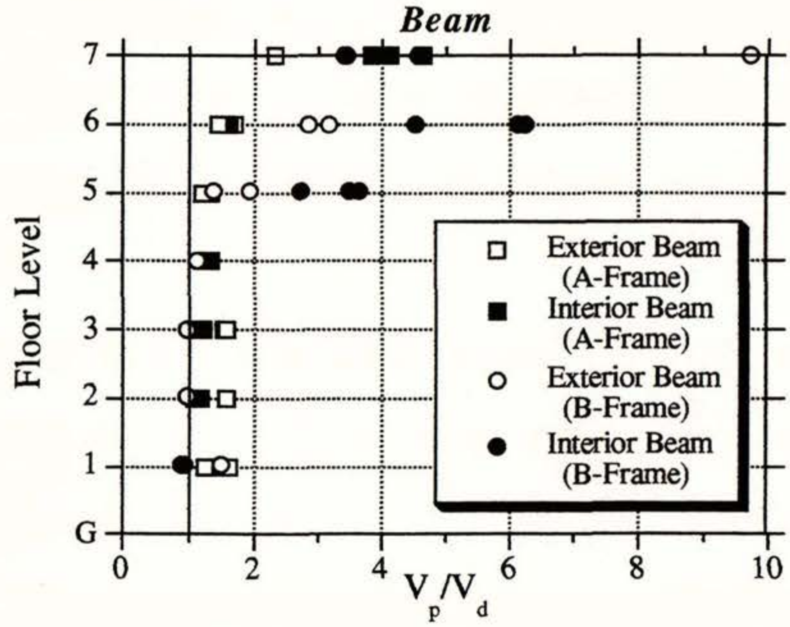

(a) Beams

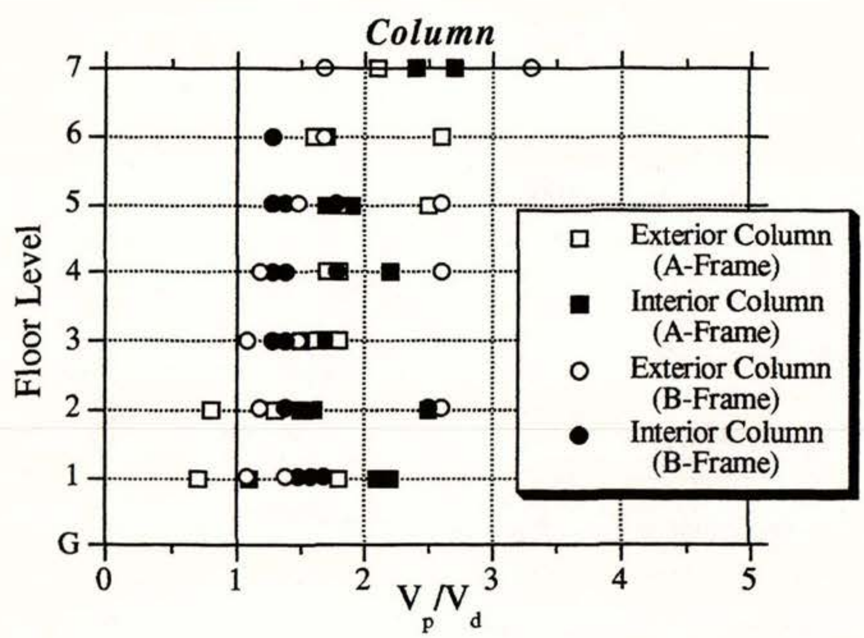

(b) Columns

Fig.2.22 The Ratio of Probable Shear Strength to Maximum Shear Input tension induced in the exterior column under seismic loading, the column plastic hinges shown in Fig.2.23 can be accepted.

Beam shear failure is less likely to result in catastrophic collapse of the structure. On the other hand, column shear failure is more serious since it is associated with loss of gravity load carrying capacity and could result in total collapse. As shown in Fig.2.23, shear failure of the exterior column in a tall building is likely to occur when subjected to severe seismic

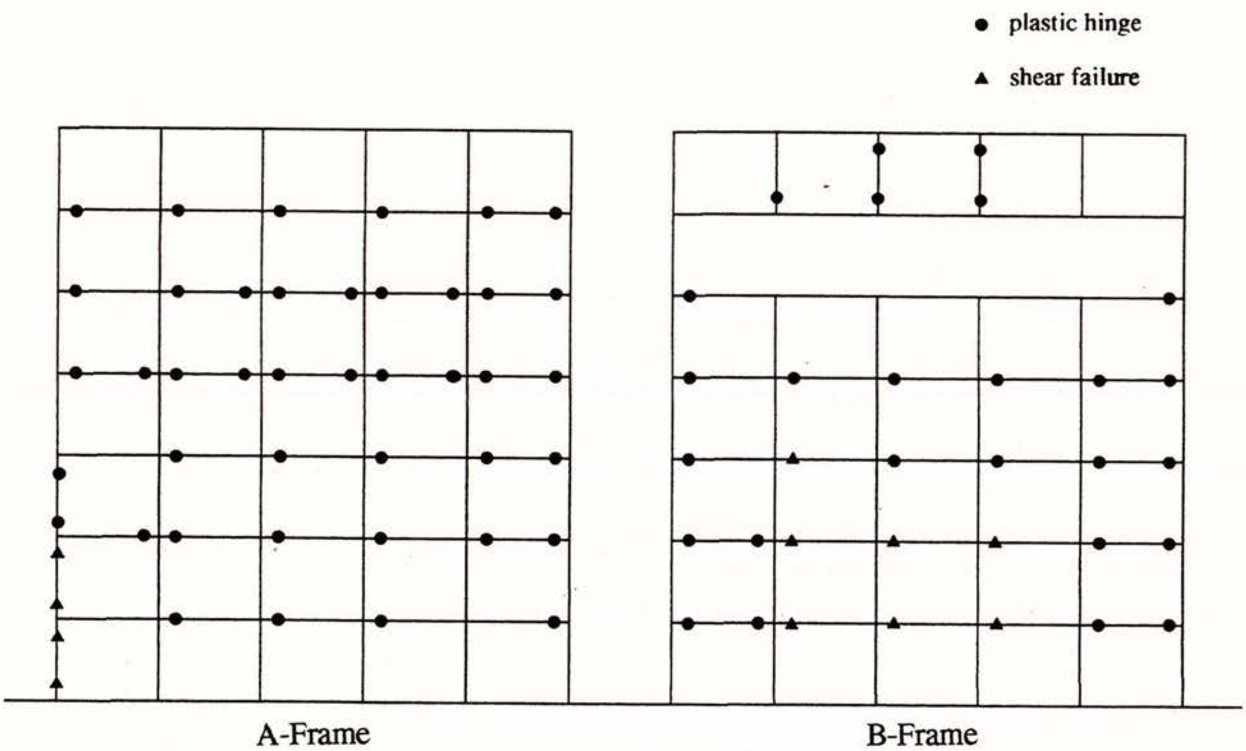

Fig.2.23 Mechanism at 1% Drift Angle of Roof Displacement

excitations because of the earthquake induced axial tension load input(see Fig.2.17). However, if the column shear failure under axial tension loading is not sudden, shear failure of the exterior column may be acceptable. Further investigation of this aspect is required.

2.3.5.7 Joint Shear Input

The joints of the structure have been assumed to be infinitely rigid. In this section, the seismic performance of the joints was investigated to determine whether the joint behaviour will affect the probable strength and mechanism of the structure during severe earthquake attack.

The maximum nominal joint shear stresses were calculated from the shear forces obtained from the beam face moments and column shear forces acting on the joint as illustrated in Fig.2.24 divided by the effective joint area shown in Fig.2.25[SANZ 1982(a)]. Fig.2.26 plots the maximum joint shear stresses expressed as a function of $\sqrt{f'_c}$. Maximum joint shear stresses in the lower storey ranged from $1.2\sqrt{f'_c}$ to $1.5\sqrt{f'_c}$ for interior joints and $0.6\sqrt{f'_c}$ to $1.0\sqrt{f'_c}$ for exterior joints of the frames, indicating severe joint shear input.

One approach to assess the joint shear strength without shear reinforcement is to assume that the shear strength is reached at the stage of initial diagonal tension cracking of the joint core. Joint shear failure could be assumed to occur when the principal tensile stress, f_{ct} indicated by Mohr's circle for stress is larger than the diagonal tension strength of concrete, f_t.

$$f_{ct} = -\frac{P_u}{2A_g} + \sqrt{\left(\frac{P_u}{2A_g}\right)^2 + (v_{jh})^2} \qquad (2.24)$$

where P_u is axial load on column, A_g is gross area of column cross section and v_{jh} is nominal horizontal joint shear stress. Also, f_{ct} is positive in tension and P_u is positive in compression. The diagonal tension strength of concrete was assessed to be $0.3\sqrt{f'_c}$[Priestley and Calvi 1991].

Fig.2.27 shows the maximum principal tensile stresses in the joints. Maximum principal tensile stresses in the lower storey ranged up to $1.1\sqrt{f'_c}$ for interior joints and $0.6\sqrt{f'_c}$ for exterior joints. These values are much larger than the above assumed diagonal tension strength of concrete, that is $0.3\sqrt{f'_c}$. The joints of the structure can be expected to suffer severe diagonal tension cracking and the strength of the structure is likely to be governed by the joint shear failure under severe earthquake loading.

2.3.6 Results of Dynamic Analysis

2.3.6.1 General

Following static analysis, dynamic analysis was conducted to investigate the inelastic response of the building subjected to the El Centro 1940NS and the Bucharest 1977 earthquake records.

2.3.6.2 Maximum Storey Shear Forces

Maximum storey shear force envelopes are shown in Fig.2.28. For the El Centro earthquake record, the observed maximum storey shear forces were smaller than those obtained from static analysis and the maximum base shear forces were also smaller (approximately 60%) of those obtained from static analysis. The base shear force coefficient was 0.14 for Q-Hyst model and 0.13 for Pinching model, respectively, used for the beams. On the contrary, the maximum base shear forces for the Bucharest earthquake motion were

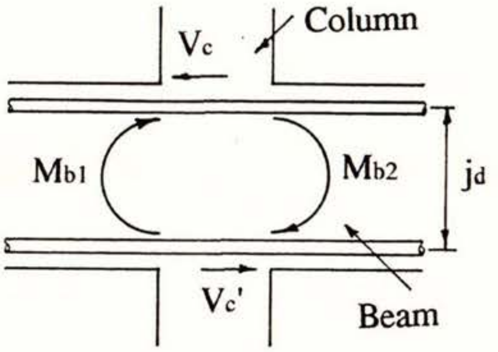

Horizontal joint shear force

$$V_{jh}=(M_{b1}+M_{b2})/j_d-V_c$$

where M_{b1}, M_{b2}=beam face moments

j_d=internal lever arm between resultant forces

V_c=column shear force

Fig.2.24 Beam Face Moment and Column Shear Forces Acting on the Joint

Effective joint area=b_jh_c

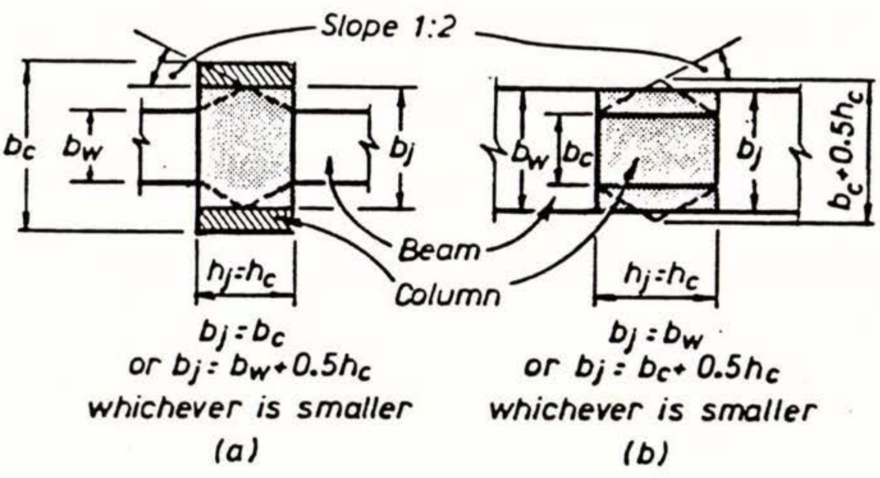

Fig.2.25 Assumption of Effective Joint Area[SANZ 1982(a)]

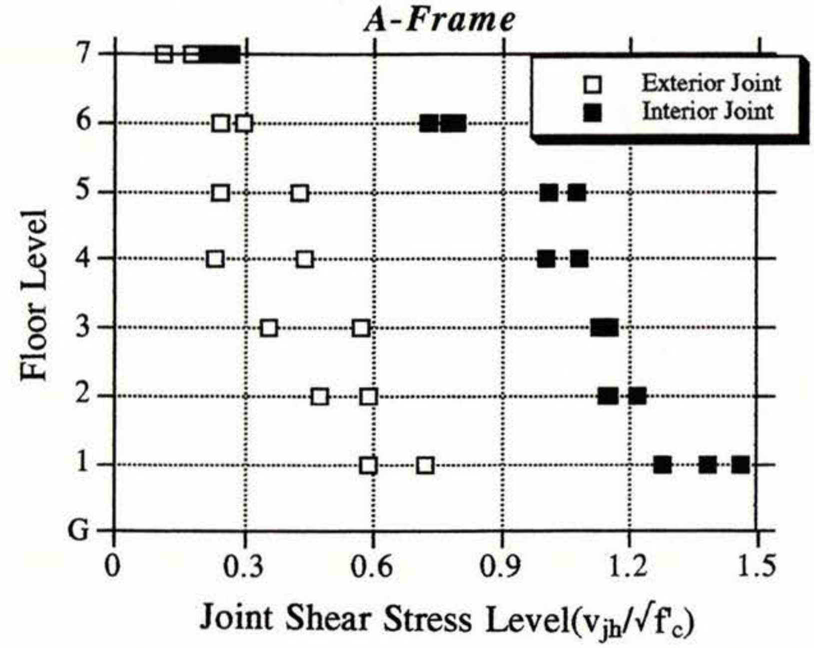

(a) A-Frame

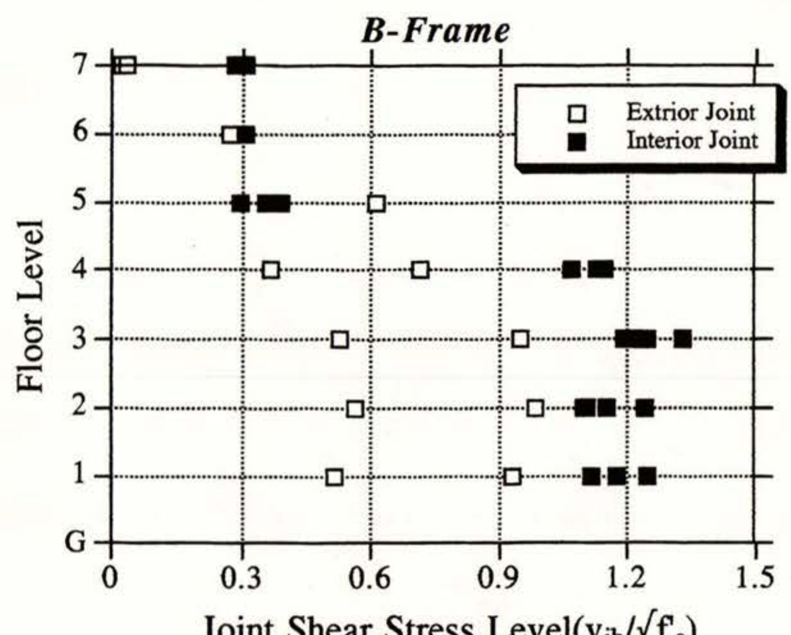

(b) B-Frame

Fig.2.26 Maximum Joint Shear Stress Input

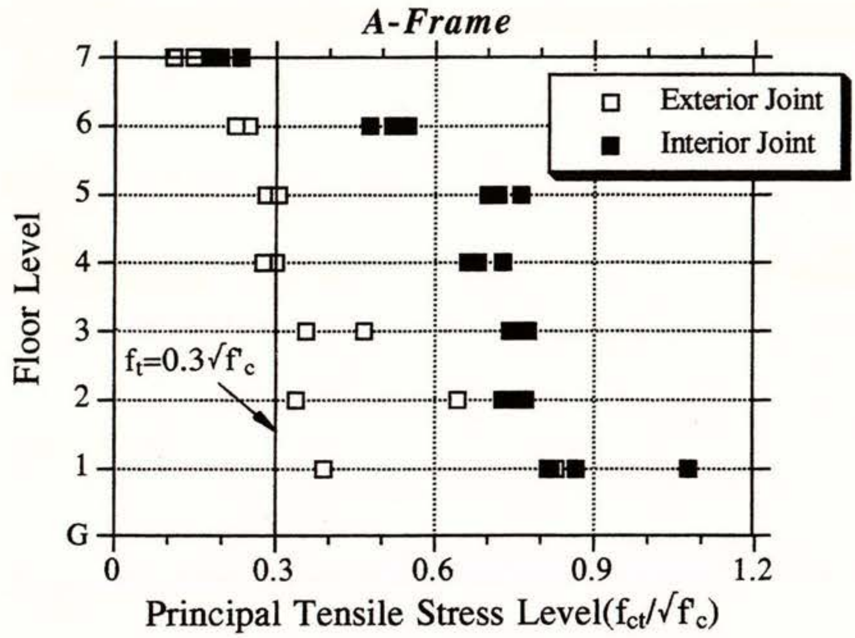

(a) A-Frame

f'_{ct}=principal tensile stress

f'_c=probable compressive strength of concrete

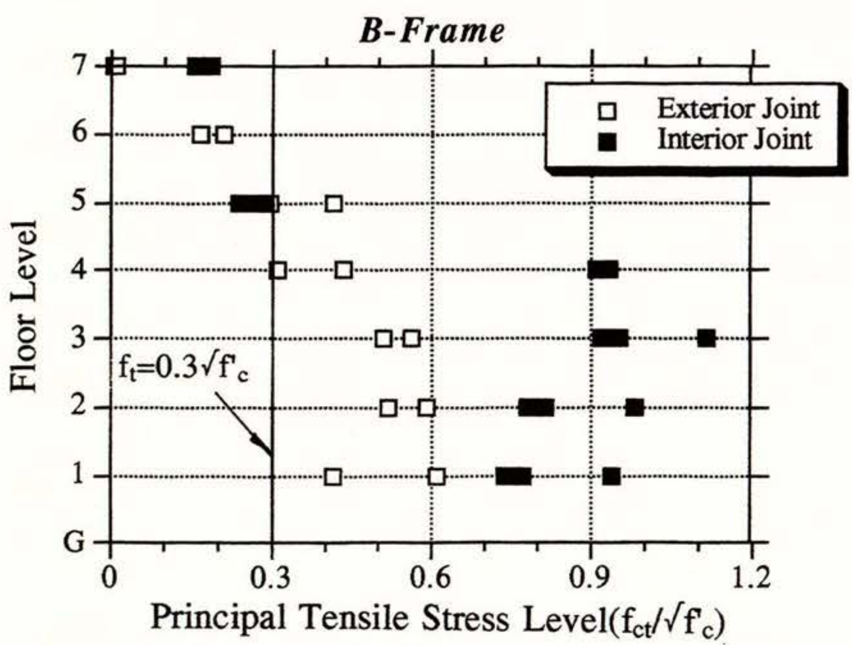

(b) B-Frame

Fig.2.27 Maximum Principal Tensile Stress in the Joints

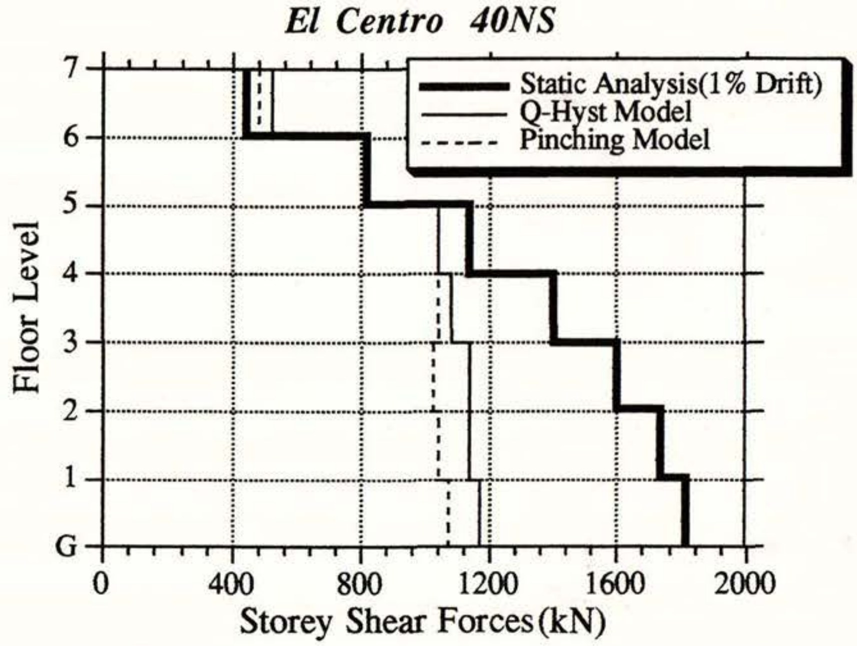

(a) El Centro 1940 NS Earthquake

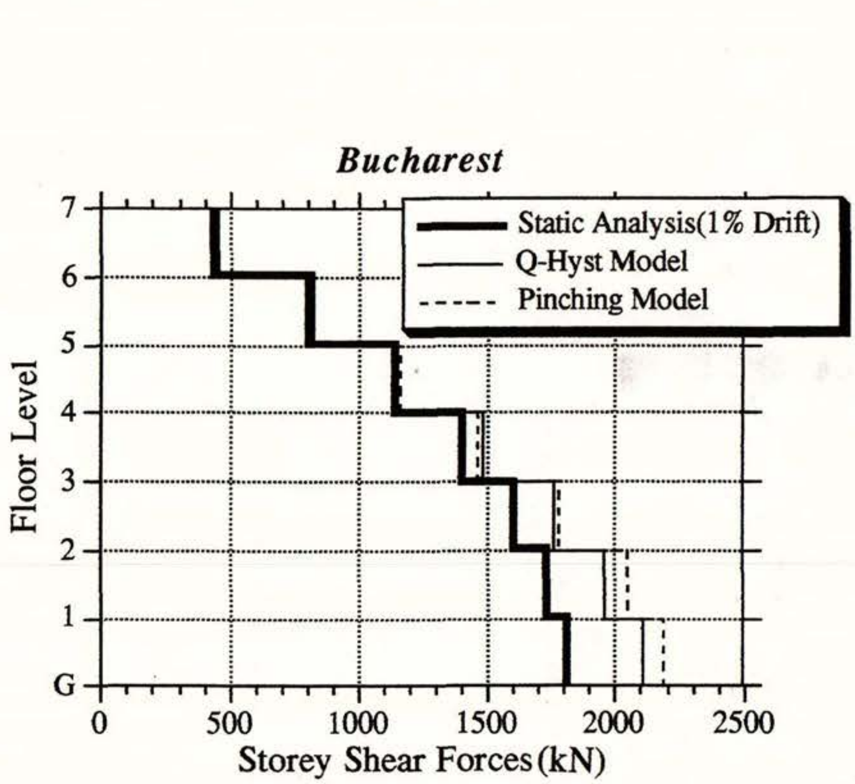

(b) Bucharest 1977 Earthquake

Fig.2.28 Maximum Storey Shear Force Envelopes about 20% larger than that observed from static analysis and the base shear coefficient was 0.26 for Q-Hyst model and 0.27 for Pinching model, respectively. The difference between the results of the Q-Hyst model and Pinching model could not be found for maximum storey shear input.

2.3.6.3 Maximum and Minimum Axial Loads on Columns

Maximum and minimum axial load level envelopes are plotted in Figs.2.29 and 2.30. In these figures, the axial load level, which included the gravity loading, is positive when in compression and negative in tension. For the El Centro record, the maximum axial load levels for the exterior columns at the 1st storey of approximately 0.13 and 0.27 were observed for the A-Frame and the B-Frame, respectively. The minimum axial load levels were -0.05 for the exterior column of the A-Frame and 0.01 for the B-Frame. Under the Bucharest record, the maximum axial load levels of 0.17 and 0.31 were observed for the A-Frame and the B-Frame, respectively. The minimum axial load levels were -0.09 for the A-Frame and -0.04 for the B-Frame. The variations of the earthquake induced axial loads on the exterior columns were larger for the Bucharest record. For interior columns, the maximum and minimum axial load levels ranged from 0.26 from 0.13 for both records. Differences in the results between Q-Hyst model and Pinching model could not be found for the maximum and minimum axial loads on the columns.

Axial load reduction factors R_v for exterior columns are plotted in Figs.2.31 and 2.32. The recommended values in SANZ 1982(a) are also shown in these figure. Similar trends as observed for static analysis are found. That is, the axial load reduction factors decreased with a decrease in the number of stories above the level. Although the Bucharest record gave the larger values of Rv for the lower storeys, little difference was observed for the higher storeys when compared with those obtained during the El Centro ground motion. The hysteresis models used in this study did not affect the axial load reduction factors. For the El Centro earthquake record, the recommended values gave only the maximum values for the structure. Some modifications are required to obtain better estimates of the axial load level on the exterior columns during severe earthquake loading.

2.3.6.4 Maximum Storey Drift Angle

Maximum storey drift angle envelopes are plotted in Fig.2.33. For the El Centro earthquake, the effect of discontinuities in stiffness and strength at the 5th storey of the B-Frame where no interior columns exist, could be found. Maximum storey drift angle of 0.7% initiated at the 5th storey. However, the observed maximum drift angle was at an acceptable level. On the other hand, the maximum storey drift angle obtained for the Bucharest record was significantly larger. The maximum storey drift angles observed at the

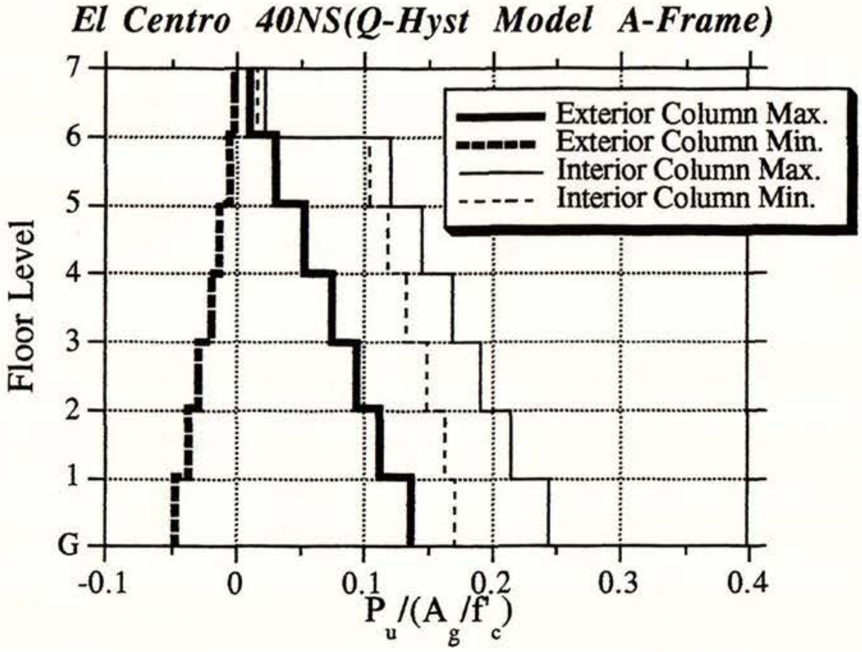

A-Frame

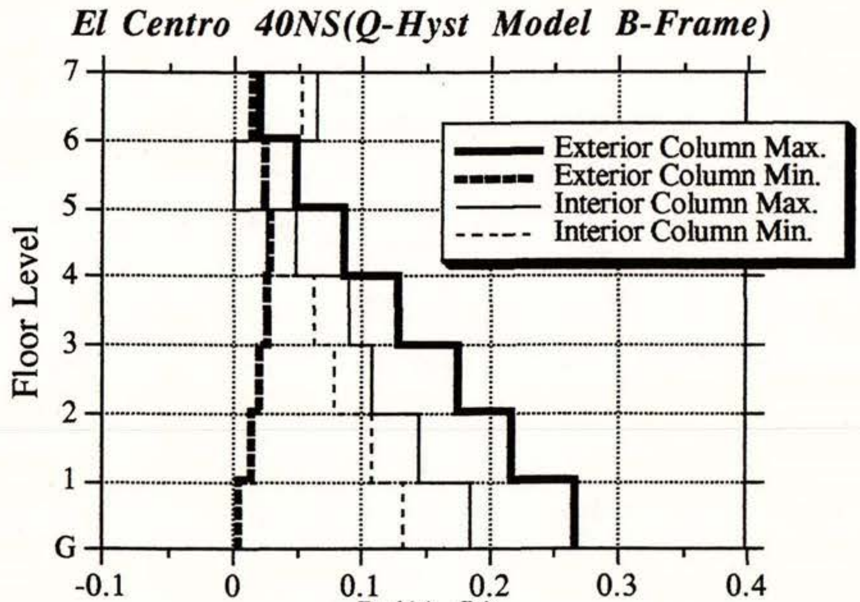

B-Frame

Fig.2.29(a) Maximum and Minimum Axial Load Level Envelopes
(El Centro 1940 NS Q-Hyst Model)

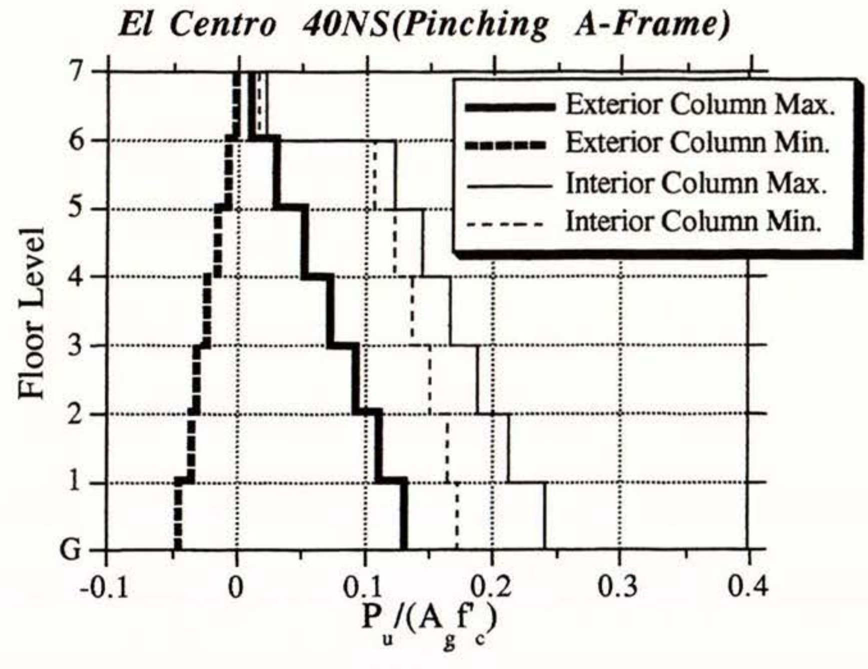

A-Frame

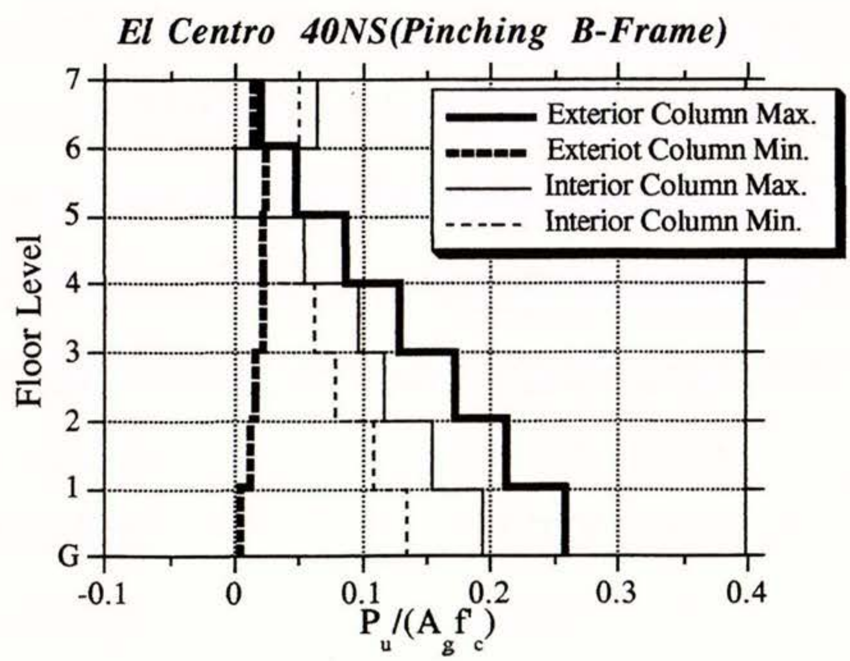

B-Frame

Fig.2.29(b) Maximum and Minimum Axial Load Level Envelopes
(El Centro 1940 NS Pinching Model)

Bucharest(Q-Hyst A-Frame)

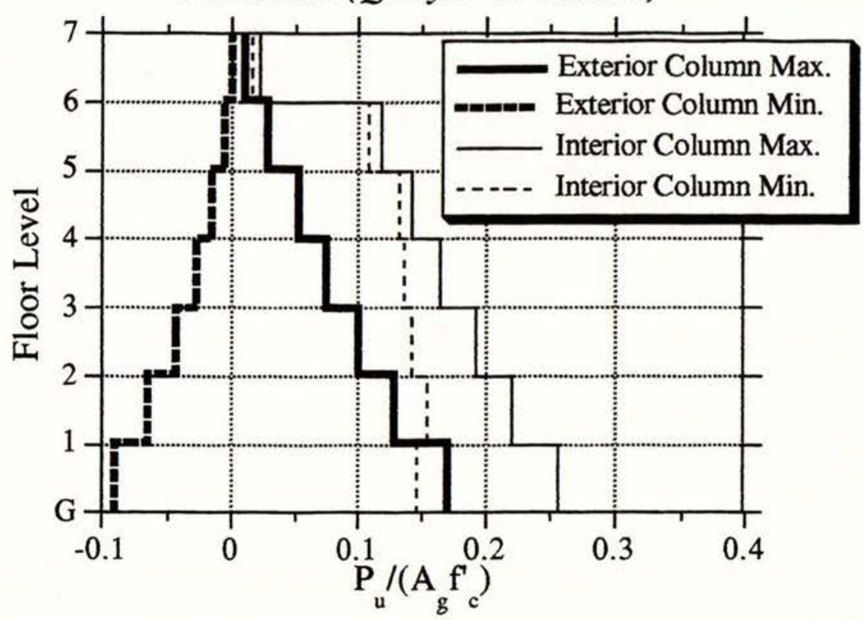

A-Frame

Bucharest(Q-Hyst B-Frame)

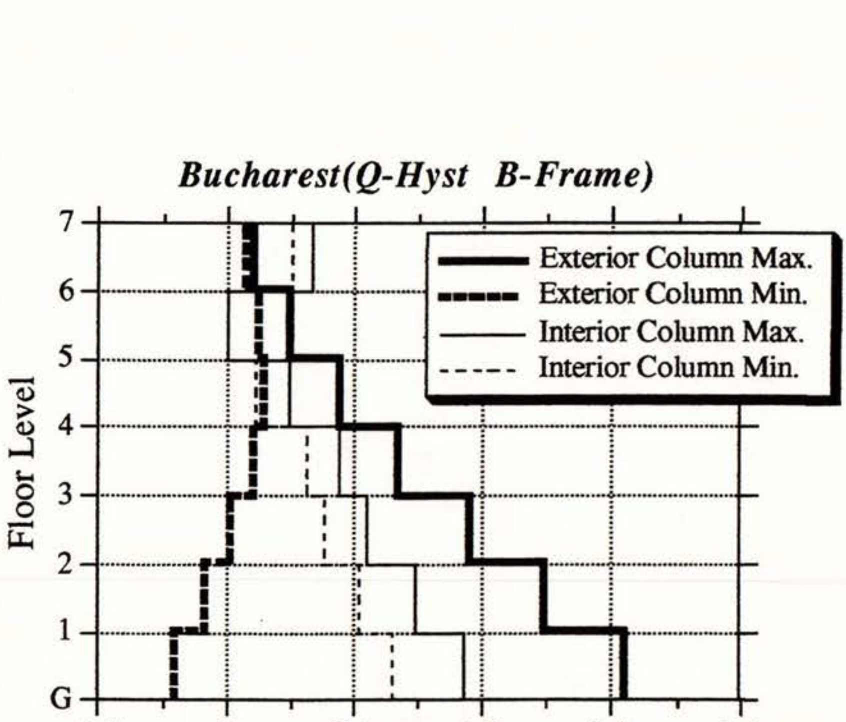

B-Frame

Fig.2.30(a) Maximum and Minimum Axial Load Level Envelopes
(Bucharest 1977 Q-Hyst Model)

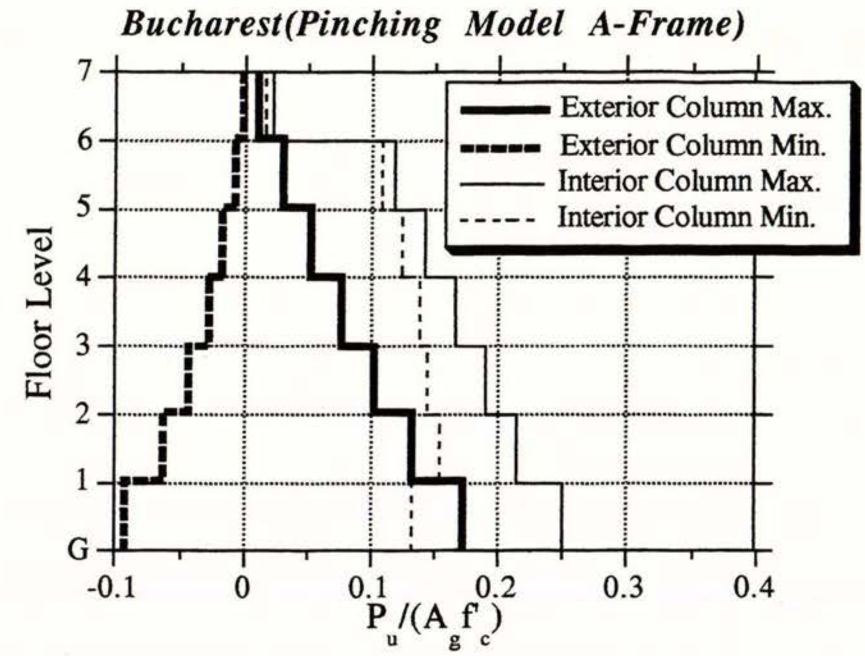

A-Frame

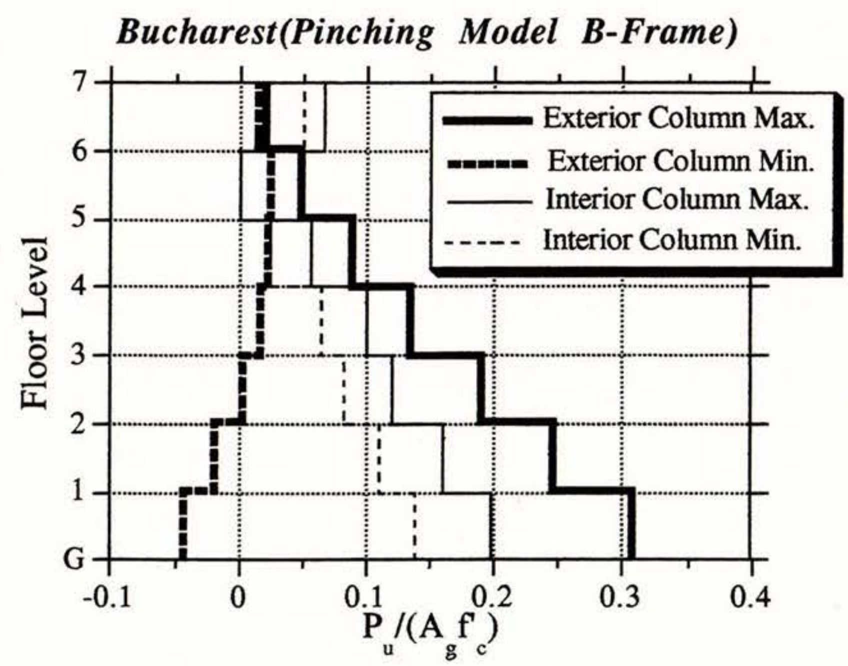

B-Frame

Fig.2.30(b) Maximum and Minimum Axial Load Level Envelopes
(Bucharest 1977 Pinching Model)

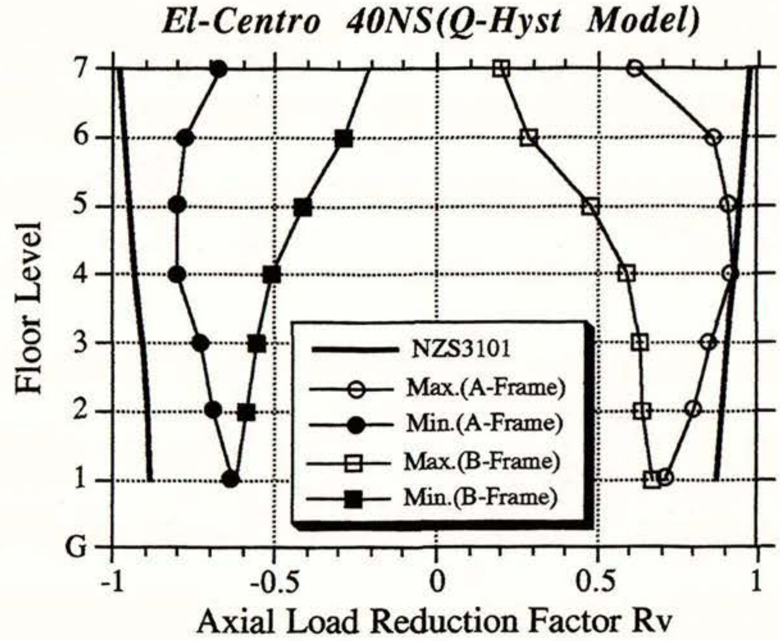

(a) Using Q-Hyst Model

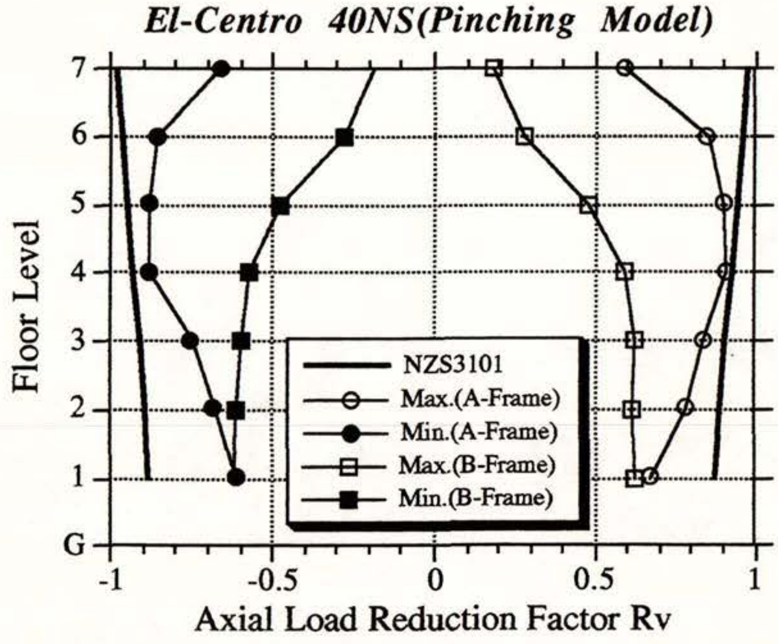

(b) Using Pinching Model

Fig.2.31 Axial Load Reduction Factor(El Centro 40NS)

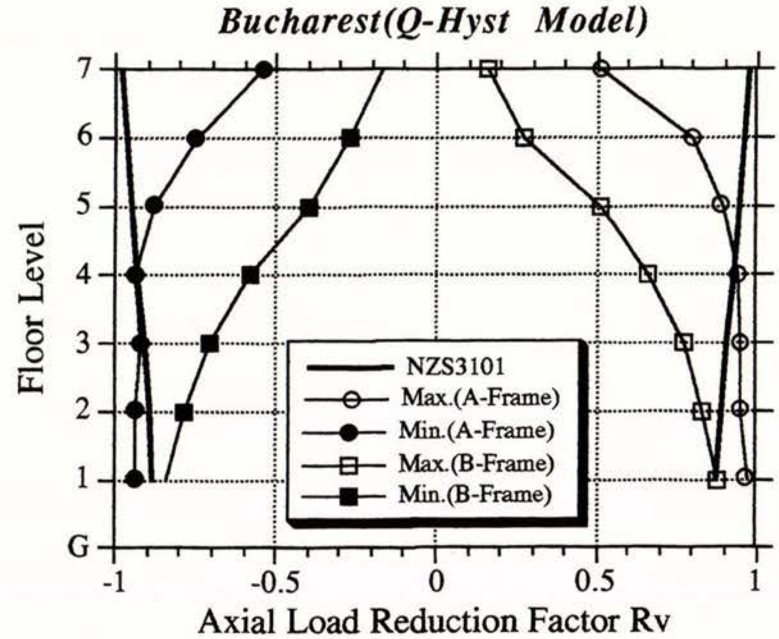

(a) Using Q-Hyst Model

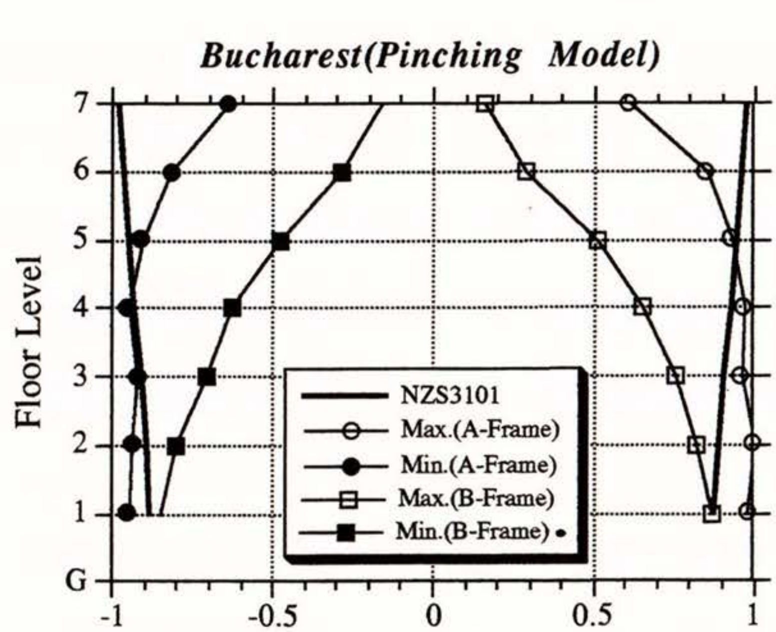

(b) Using Pinching Model

Fig.2.32 Axial Load Reduction Factor(Bucharest)

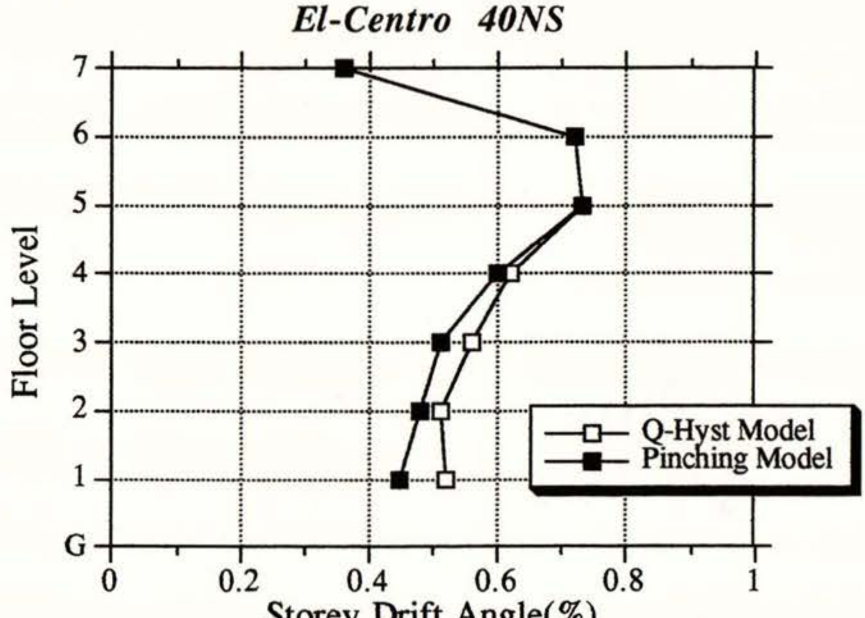

(a) El Centro 1940 NS Earthquake

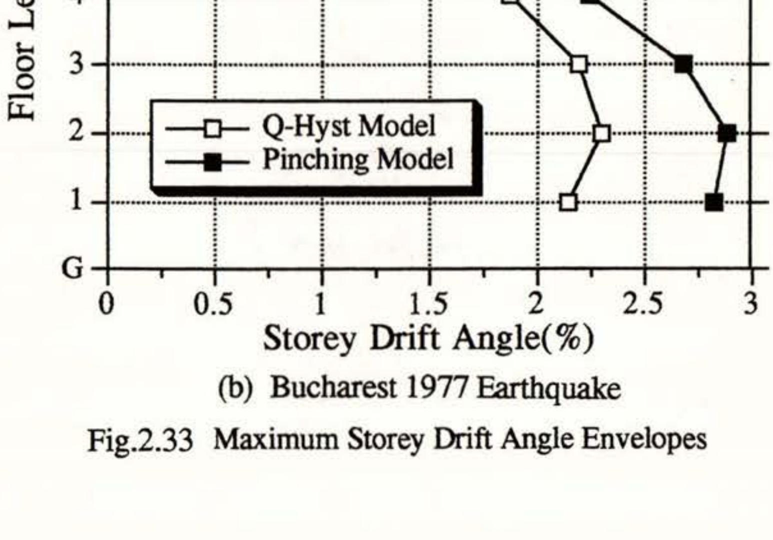

(b) Bucharest 1977 Earthquake

Fig.2.33 Maximum Storey Drift Angle Envelopes

2nd storey were 2.3% when using Q-Hyst model and 2.9% when using Pinching model, respectively. Those large drifts could cause the frame instability due to P-delta effects.

2.3.6.5 Maximum Curvature Ductility of Beams

Fig.2.34 shows the maximum curvature ductility factor demand envelopes for the beams. The maximum curvature ductility factor demands were up to 6 for the El Centro earthquake and 30 for the Bucharest earthquake, respectively. It is likely that the beams could not survive when the frames are subjected to earthquake motions containing long period ground motions as in the Bucharest record. The curvature ductility demands obtained using Pinching model show larger values than those obtained using Q-Hyst model. However, the difference is not so significant.

2.3.6.6 Probable Mechanism

The ratio of the probable shear strength V_p assuming limited ductility demand to the maximum shear input V_d , not taking into account the gravity loads, for the beams were calculated to investigate whether shear failure was likely. The results are plotted in Figs.2.35 and 2.36. The ratios for the El Centro record were larger than unity, indicating that the beams can be expected to fail not in shear but in flexure. It may be concluded that the beams of the structure can survive under the El Centro earthquake when considering the available curvature ductility obtained from section analysis mentioned in Section 2.3.5.5. However, it should be noted that the shear strength in plastic hinge regions degrades as the ductility demand increases due to the reduced shear carried by concrete. For the Bucharest record, the beams in the lower storey of the B-Frame can be predicted to fail in shear, as was also predicted by the results of static analysis.

The principal difficulty in assessing the possibility of column shear failures relates to the variable axial loads during earthquake loading which affect the shear strength of the member. One method to predict the possibility of shear failure is to compare the maximum shear input V_d, not taking into account the gravity loads, with the minimum probable shear strength V_p' of the column. The minimum shear strength can be calculated from the minimum axial load on the column during seismic excitations, since the shear strength had been assumed to decrease with a decrease in axial compression force linearly according to Eqs.2.9, 2.11 and 2.14 in Section 2.3.3.3.

Figs.2.37 and 2.38 show the ratio of the minimum probable shear strength assuming limited ductility demand to the maximum shear input for the columns. As shown in these figures, only the exterior column at the 1st storey of the A-Frame could be expected to fail in shear during the El Centro earthquake record. For the Bucharest record, the possibility of

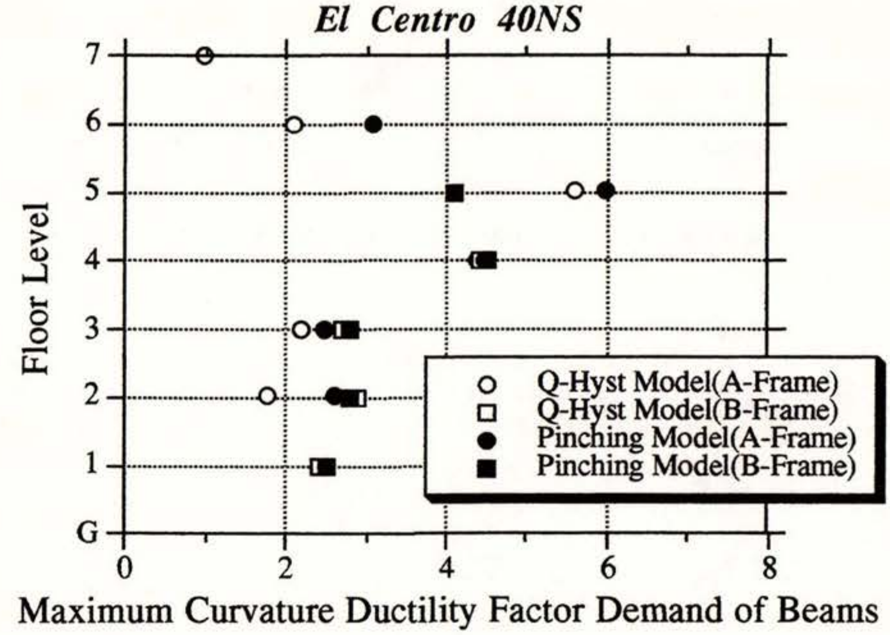

(a) El Centro 1940 NS Earthquake

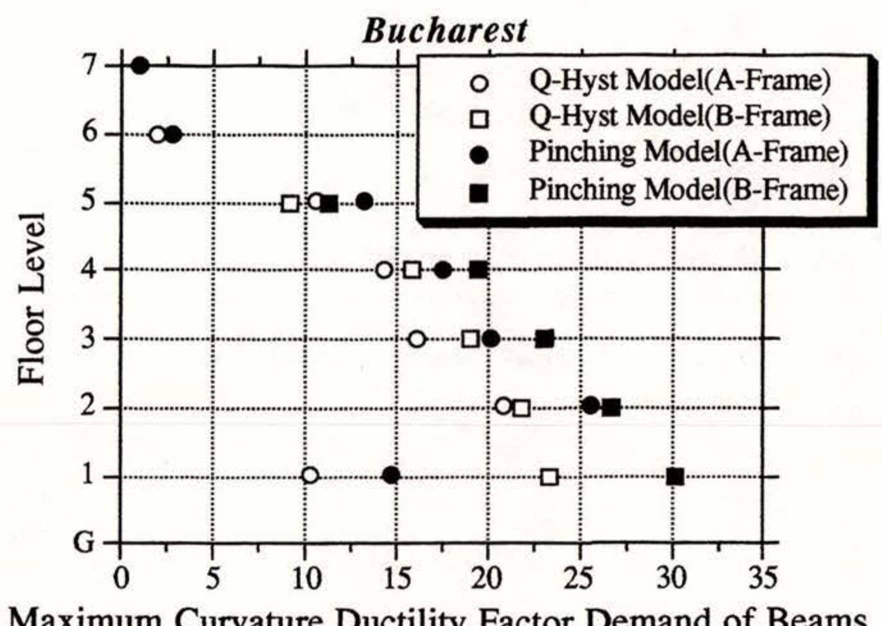

(b) Bucharest 1977 Earthquake

Fig.2.34 Maximum Curvature Ductility Envelopes for Beams

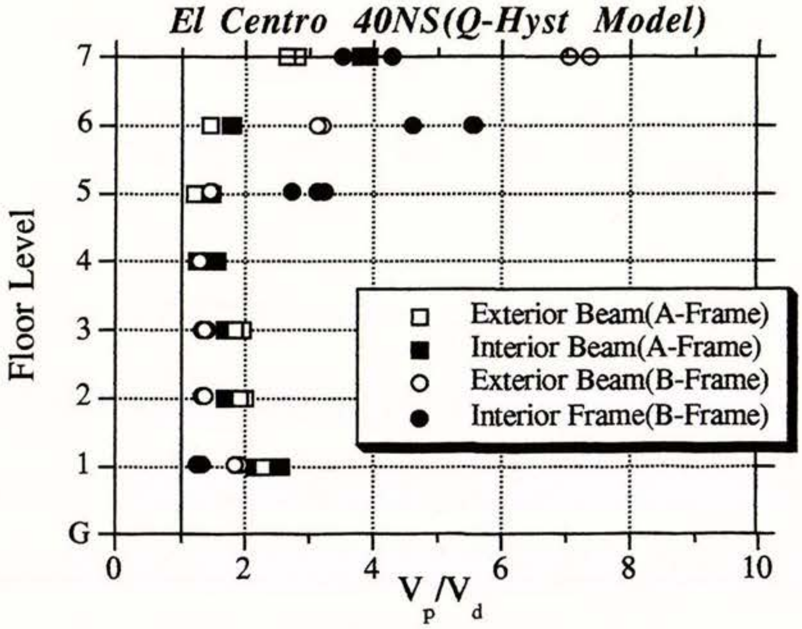

(a) Using Q-Hyst Model

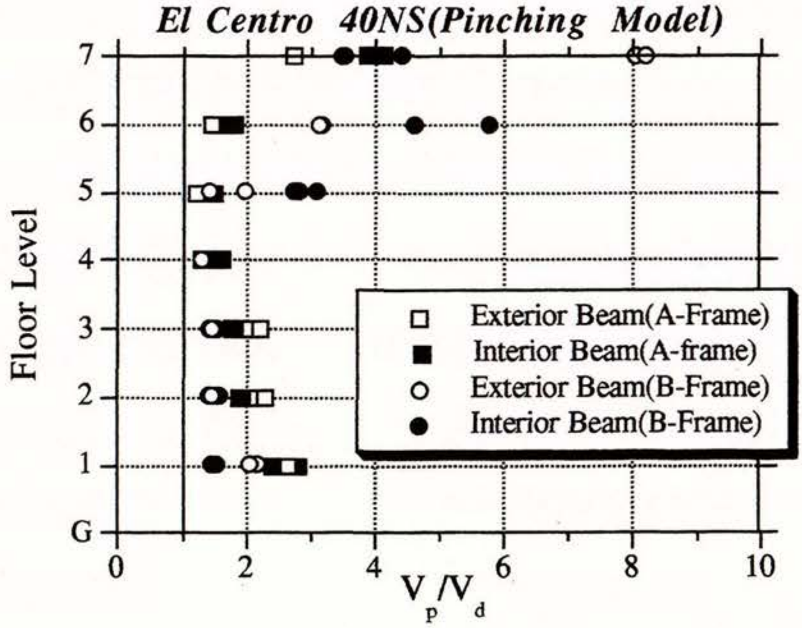

(b) Using Pinching Model

Fig.2.35 The Ratio of Probable Shear Strength to Maximum Shear Input for Beams (El Centro 40NS)

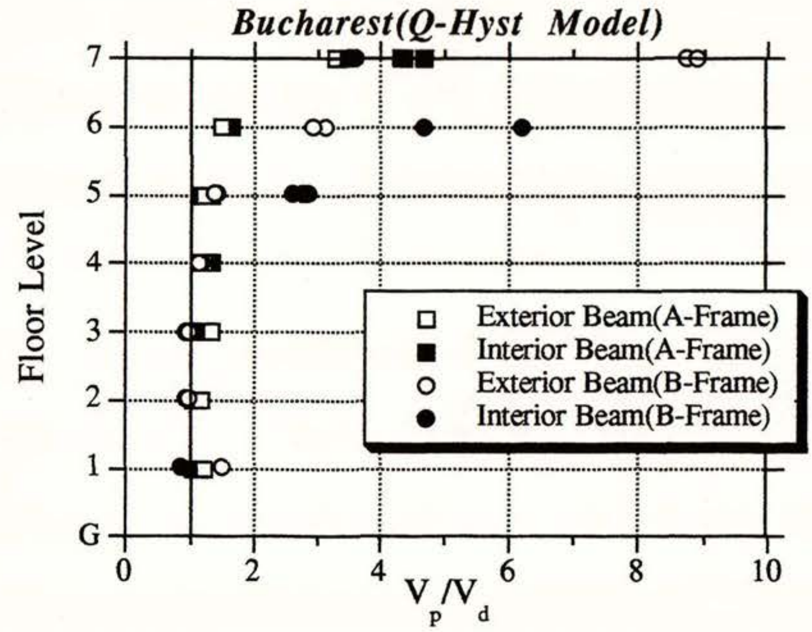

(a) Using Q-Hyst Model

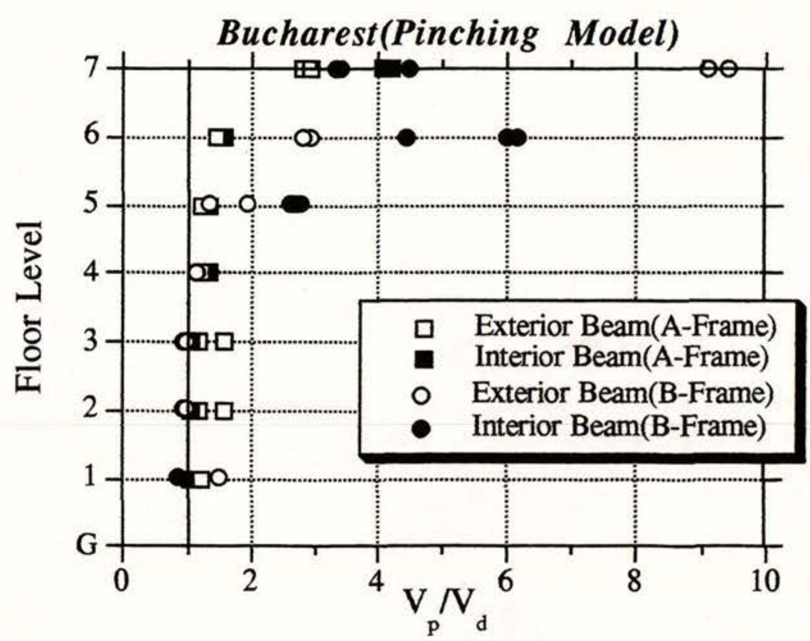

(b) Using Pinching Model

Fig.2.36 The Ratio of Probable Shear Strength to Maximum Shear Input for Beams (Bucharest)

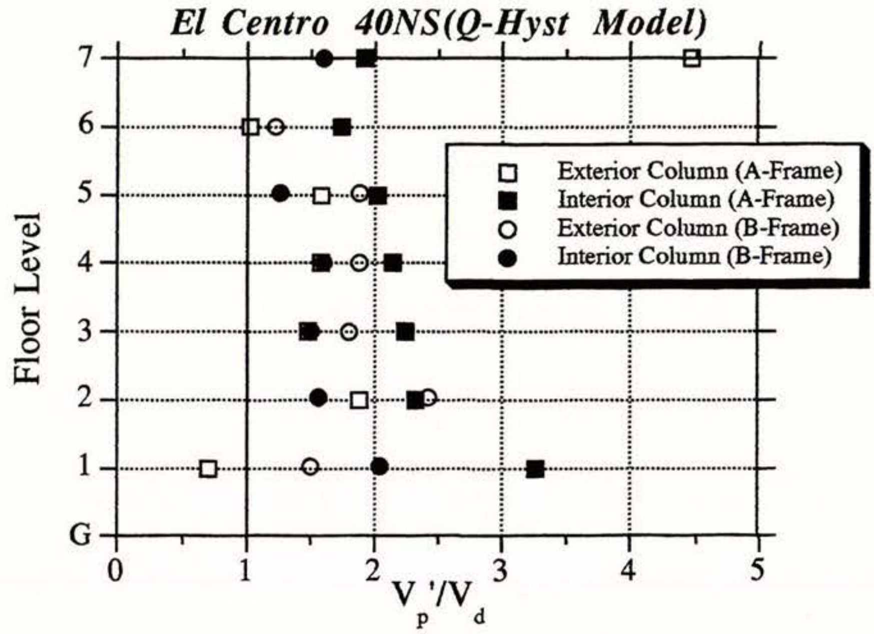

(a) Using Q-Hyst Model

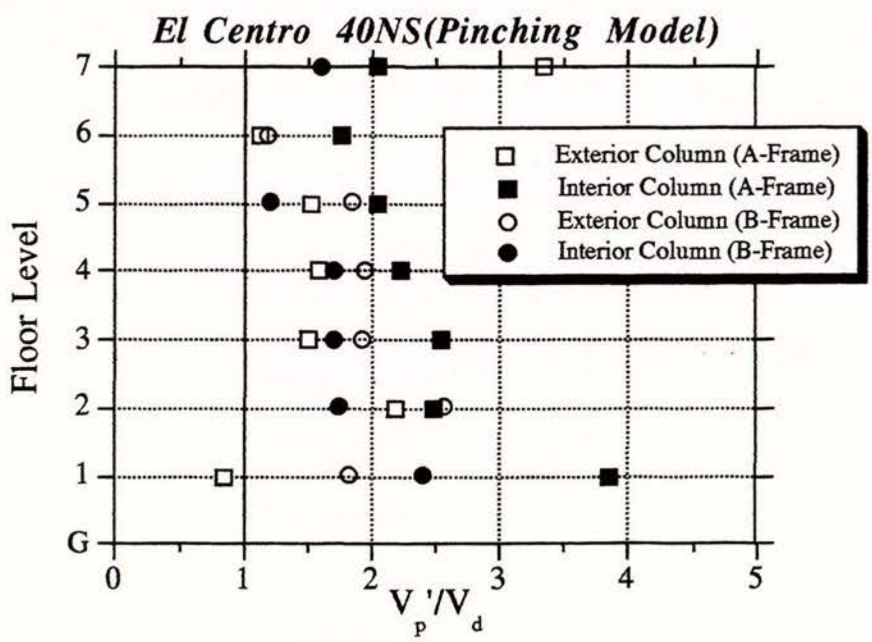

(b) Using Pinching Model

Fig.2.37 The Ratio of Probable Shear Strength to Maximum Shear Input for Columns (El Centro 40NS)

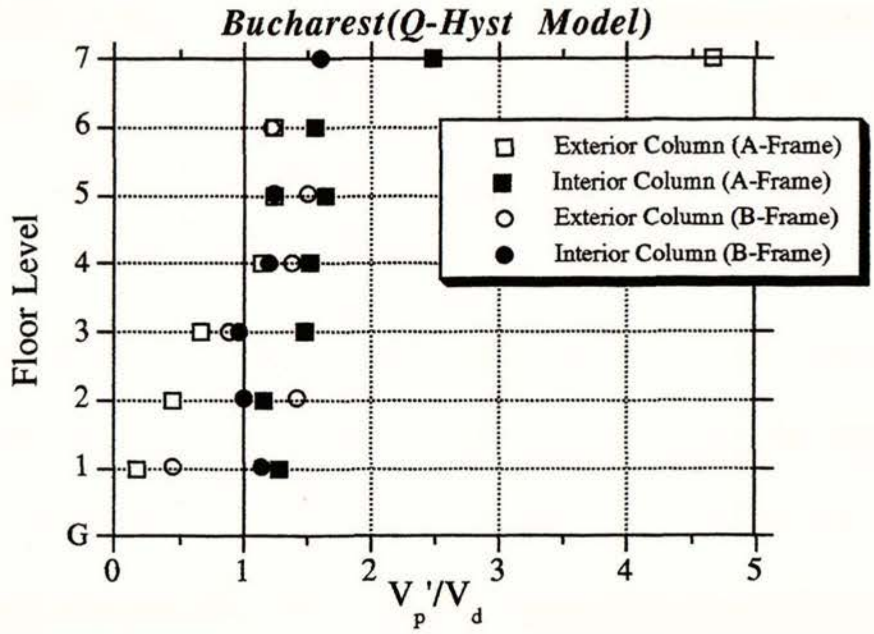

(a) Using Q-Hyst Model

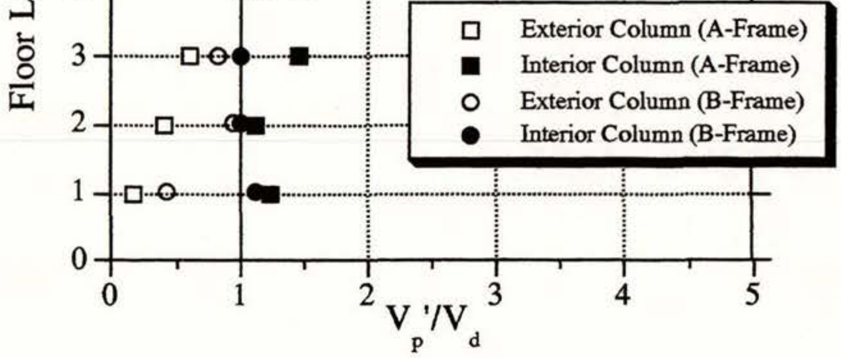

(b) Using Pinching Model

Fig.2.38 The Ratio of Probable Shear Strength to Maximum Shear Input for Columns (Bucharest)

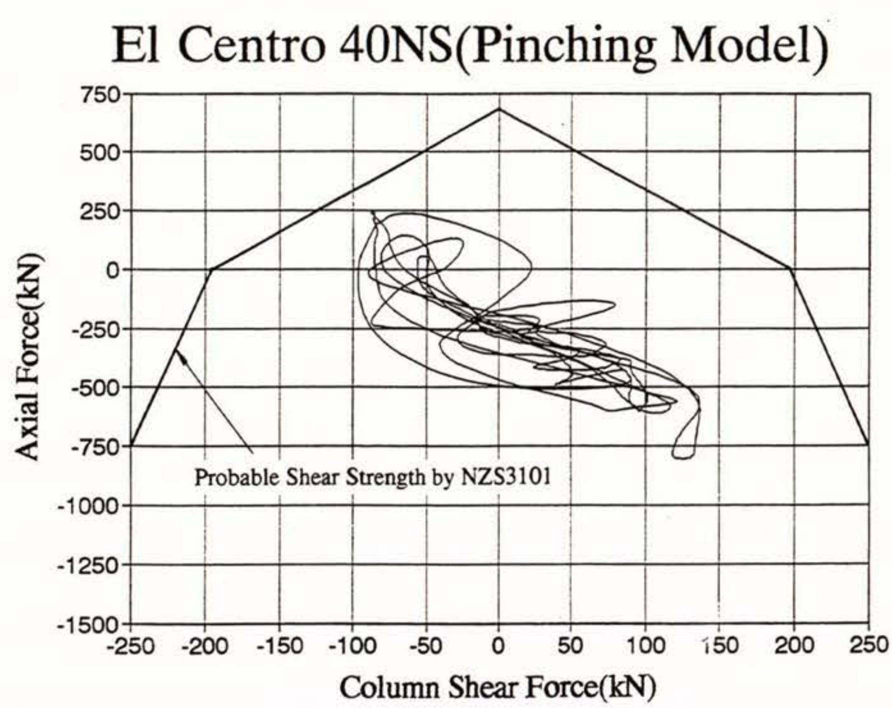

(a) El Centro 1940 NS Earthquake

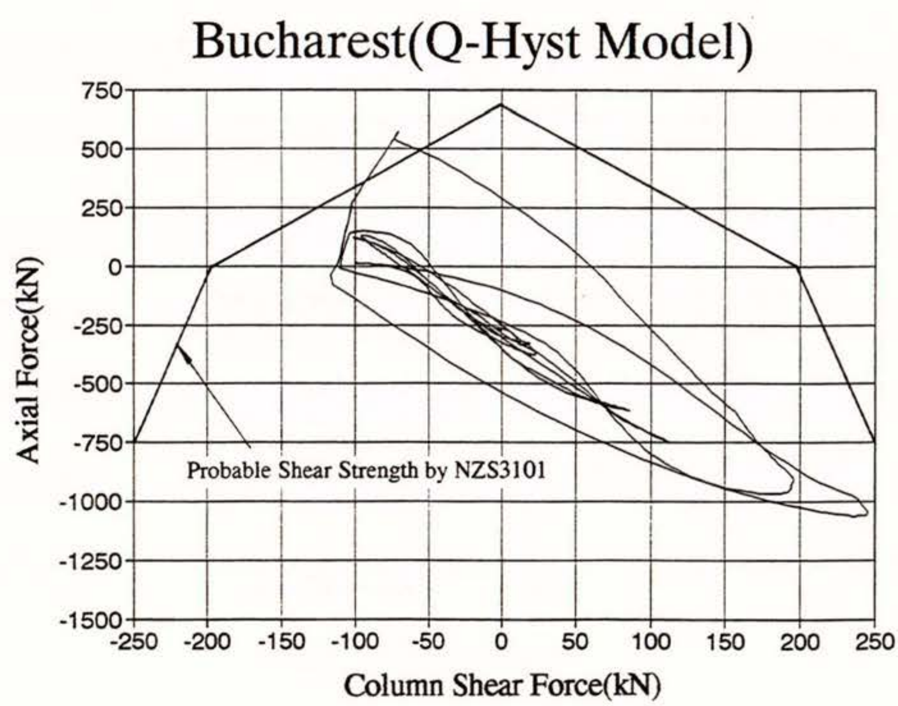

(b) Bucharest 1977 Earthquake

Fig.2.39 Axial Force versus Shear Force Relationship for the Exterior Columns

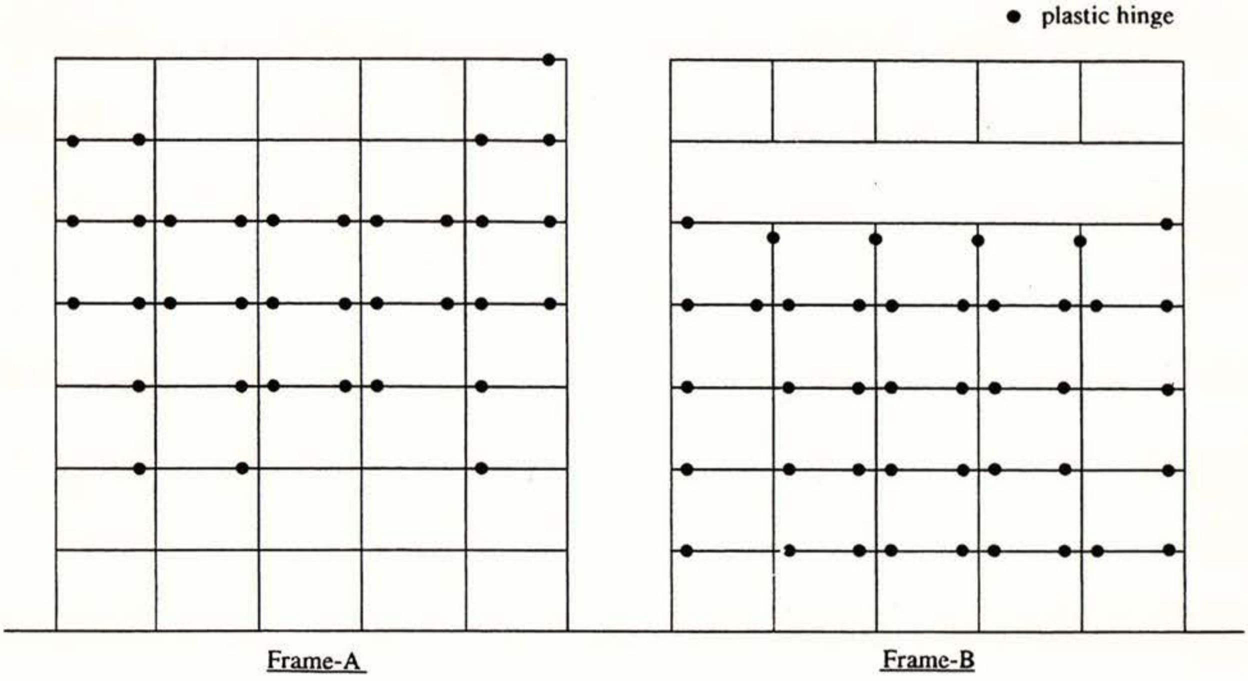

(a) Q-Hyst Model

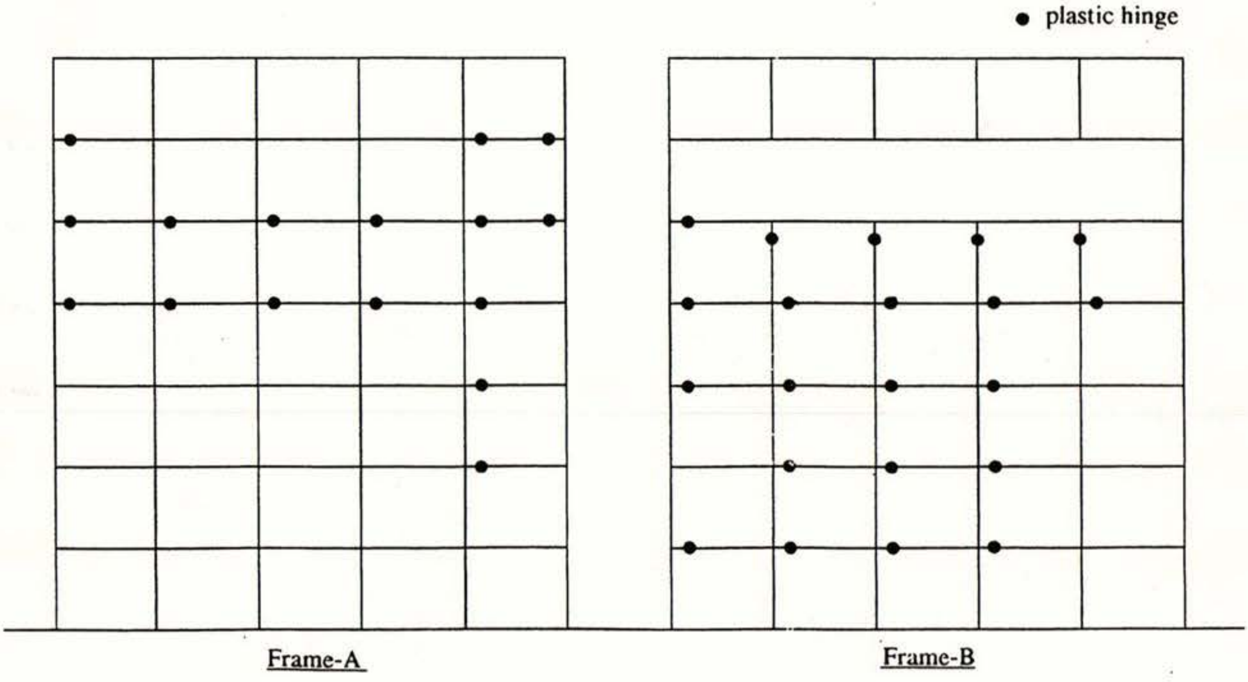

(b) Pinching Model

Fig.2.40 Mechanism(El Centro 1940 NS Earthquake)

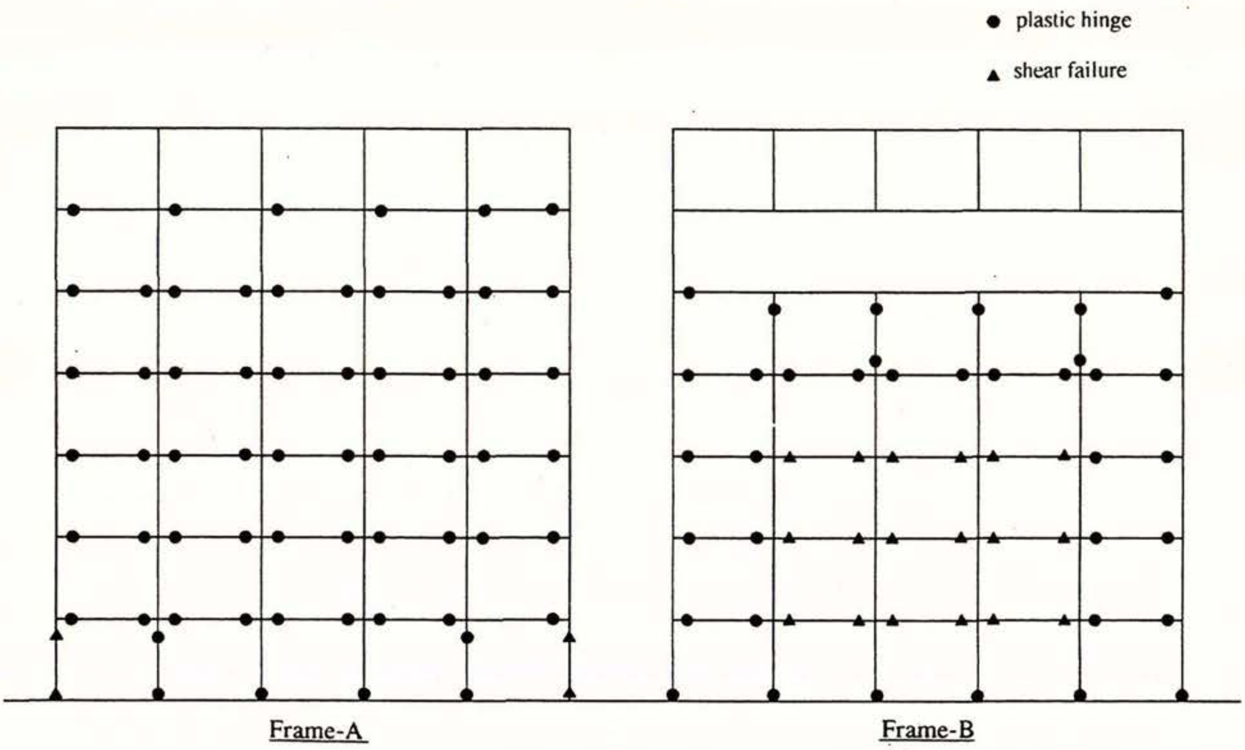

(a) Q-Hyst Model

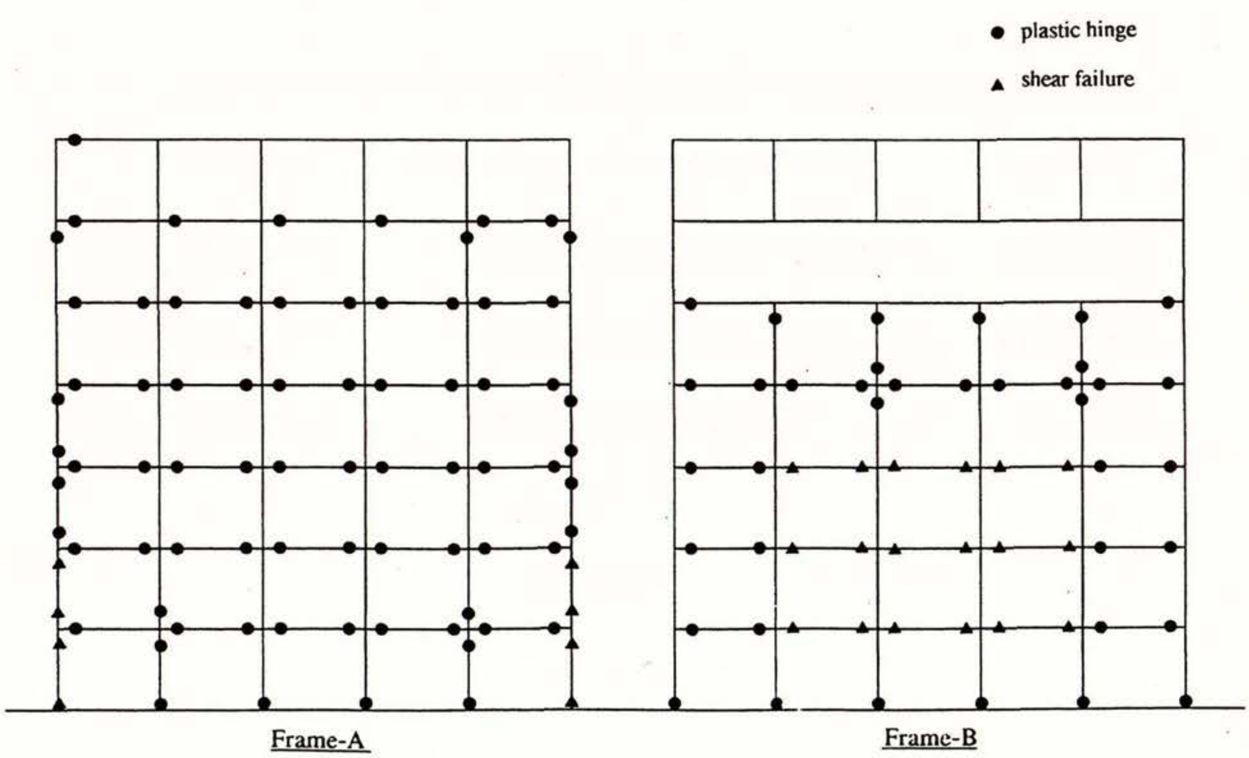

(b) Pinching Model

Fig.2.41 Mechanism(Bucharest 1977 Earthquake)

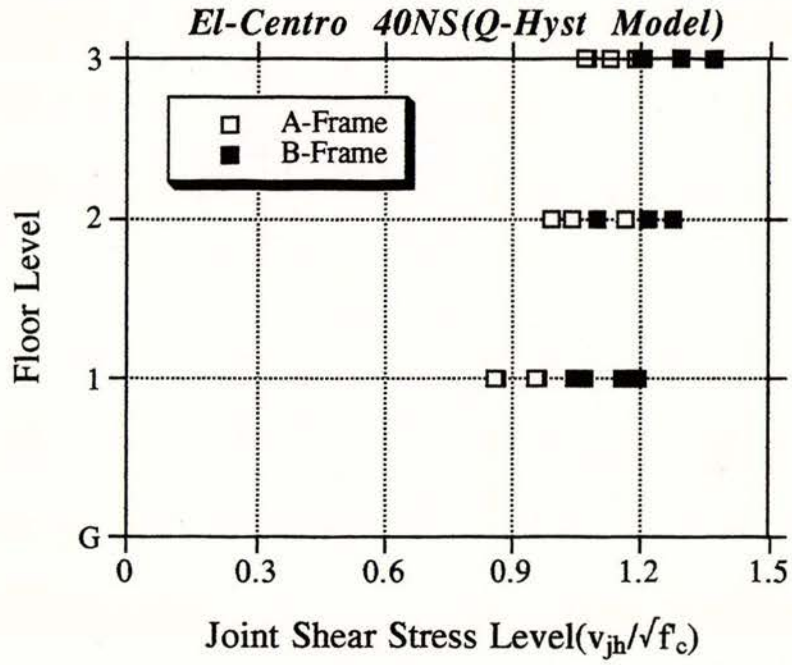

(a) Using Q-Hyst Model

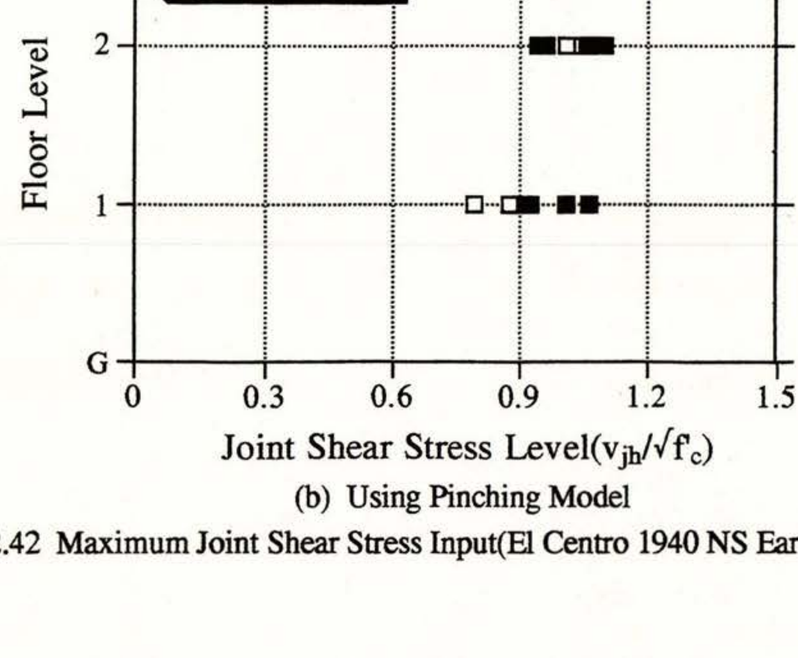

(b) Using Pinching Model

Fig.2.42 Maximum Joint Shear Stress Input(El Centro 1940 NS Earthquake) shear failure could be predicted for both the exterior and interior columns at the 1st through 3rd storeys. However, it should be noted that those columns could fail in shear only when the maximum shear input and the minimum probable shear strength (that is minimum axial force) develop at the same time. To solve this problem, the shear input in the columns were compared with the probable shear strength at each time step of the analysis, tracing the axial force and shear force curves for the column. Fig.2.39 shows the relationship between the axial force and shear input of the column. Also plotted are the probable shear strength obtained from the equations in Section 2.3.3.3. This figure indicates that the exterior columns would not fail in shear during the El Centro record. During the Bucharest record only the exterior columns could fail in shear under the axial tension force input on the columns.

Figs.2.40 and 2.41 illustrate the probable mechanism of the structure. Under the El Centro earthquake motion, only beam plastic hinges were developed for the A-Frame while for the B-Frame column plastic hinges were also observed at the floor level below the 5th storey where no interior columns exist. Use of the Pinching model resulted in a smaller number of plastic hinges forming. During the Bucharest record, plastic hinges in the beams and columns in conjunction with shear failure of beams and columns in the lower storey occurred. The structure is unlikely to survive during the Bucharest earthquake record.

2.3.6.7 Joint Shear Input

Maximum joint shear stresses were calculated using the approximations stated in Section 2.3.5.7 and illustrated in Fig.2.42. Only the nominal joint shear stresses of interior joints in the lower storey subjected to the El Centro record are plotted in this figure. The calculated maximum nominal joint shear stresses in the lower storey ranged from $0.9\sqrt{f'_c}$ to $1.4\sqrt{f'_c}$ for the Q-Hyst model and $0.8\sqrt{f'_c}$ to $1.2\sqrt{f'_c}$ for the Pinching model, respectively. The relatively large nominal joint shear stress level indicates the possibility of joint shear failure. As for the results from static analysis, joint shear failure can be identified to be the most critical for the building being investigated.

2.4 REDESIGN SCHEMES FOR EXISTING STRUCTURES

2.4.1 Introduction

A building may be retrofitted if the expected or observed seismic performance of the building during a future earthquake is assessed to be inadequate. The selection of the redesign schemes depends on

(1) Structural characteristics
(2) Available retrofit techniques

(3) Construction feasibility
(4) Requirements by owner or user

Economical and architectural considerations also play an important role in the selection.

2.4.2 Strength Requirements

The criteria for seismic redesign schemes are aimed at providing life safety of occupants in the event of a severe earthquake, at the "ultimate limit state". Generally, the emphasis of the redesign scheme for the ultimate limit state is placed on the strength and ductility of the structure against lateral loading .

Three basic alternative redesign schemes can be considered in terms of strength and ductility as follows:

(1) The strength is increased without an increase in ductility
(2) The strength is increased with an increase in ductility
(3) The strength is decreased with an increase in ductility

Those redesign schemes are qualitatively shown on the strength and ductility relationship in Fig.2.43. Current design procedures indicate that the required strength of the structure for a given earthquake can be related to the ductility capacity of the structure. The relationship between the strength and ductility is illustrated in Fig.2.44, indicating that the required strength of the structure at the ultimate limit state decreases with increase in ductility. Large ductility capacity means improved energy absorbing characteristic of the structure, but the damage during a severe earthquake may be significant. The strength of the redesigned structure must be larger than the minimum requirement for the ultimate limit state as shown in Fig.2.44, depending on the ductility capacity of the structure.

The required strength in terms of base shear capacity of a structure also depends on the natural period of the structure as shown in Fig.2.45, which is a function of the stiffness and mass of the structure. Therefore, the dynamic characteristics of the original and redesigned structures should be carefully examined. As shown in Fig.2.45, the required strength can be decreased for a more flexible structure while that must be increased for a more stiff structure, indicating that a reduction of the stiffness results in a decrease in the strength demand. Figs.2.44 and 2.45 can be used to identify adequate or inadequate seismic performance for the ultimate limit state with regard to the required strength of the structure.

In addition to surviving the major earthquake without collapse, the structure must resist smaller earthquakes with no damage to non-structural and structural elements. That is, the

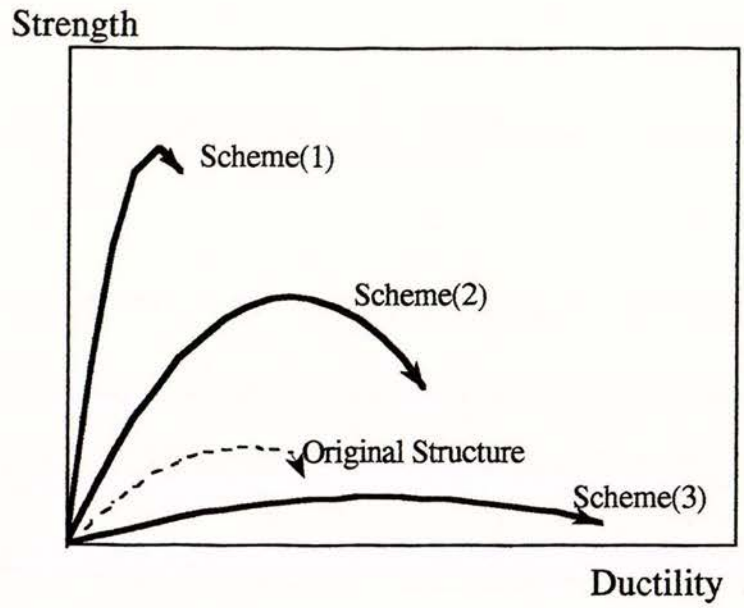

Fig.2.43 Strength versus Ductility Relation for Redesigned Structures

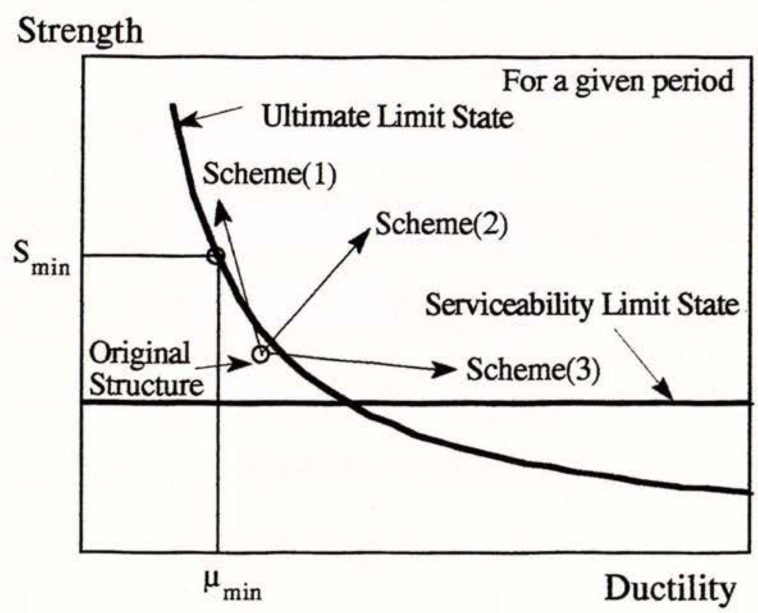

Fig.2.44 Redesign Scheme in the Strength and Ductility Plane

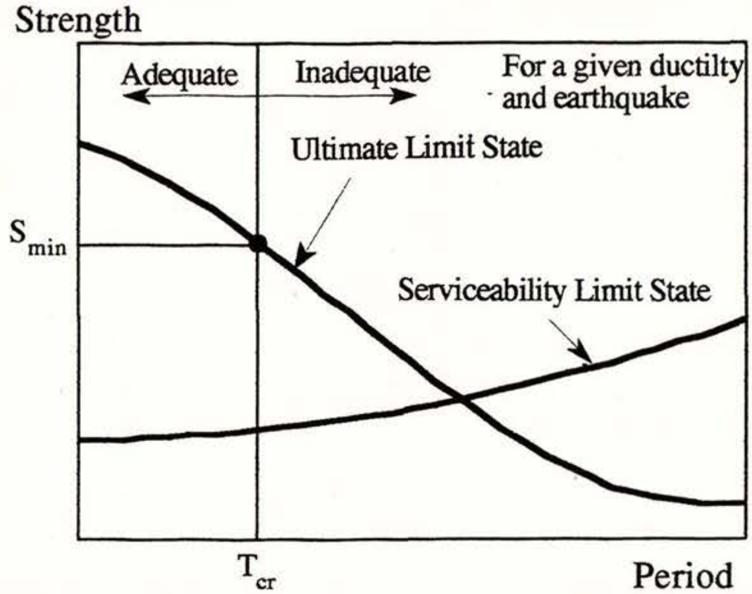

Fig.2.45 Redesign Scheme in the Strength and Period Plane

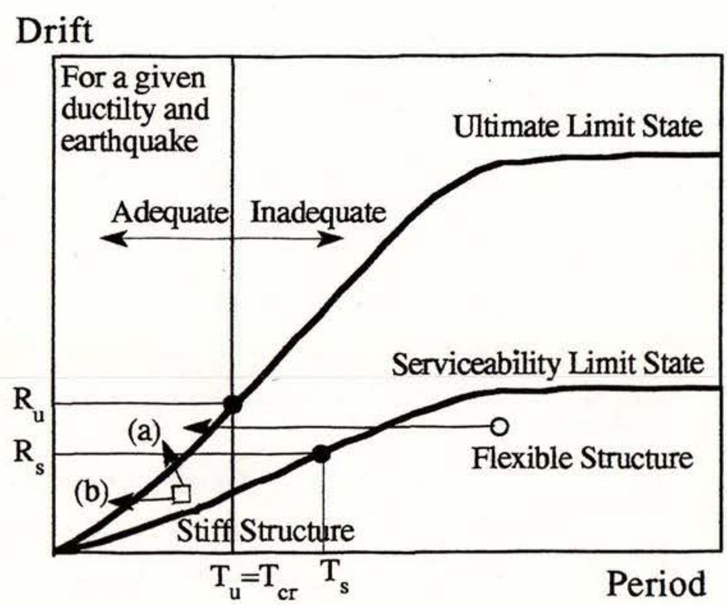

Fig.2.46 Redesign Scheme in the Drift and Period Plane

serviceability state requirements must be satisfied. When these requirements are met, the loss of operation of the facilities following the earthquake can be minimized. For the serviceability limit state, the lateral drift limit can be a criterion to protect the building against damage to non-structural elements. It should be noted that the deformation of the non-structural elements depend on the connection details of the elements. Another option may be to isolate the non-structural elements so that no large deformation will occur in those elements during large deformations of the structure. The required strength for the serviceability limit state of the former case is shown in Figs.2.44 and 2.45. In these figures, the strength requirement is assumed to be independent of the ductility but dependent on the period of the structure. The strength of the redesigned structure must be larger than that required at the serviceability limit state. As shown in Figs.2.44 and 2.45, the serviceability limit state requirement may be critical for flexible structures with long periods.

2.4.3 Drift Requirements

It is often found that early reinforced concrete building frames have a low stiffness due to inadequate dimensions and reinforcement details of the members and joints. Even when the available lateral load strength and ductility of the structure are larger than the demands, the drift of early building frames may be large during severe seismic loading. Excessively large drift is unacceptable. Unless the drift is limited to an acceptable level, the stability of the structure may be jeopardized due to P-delta effects[Carr and Moss 1980] and pounding against adjacent structures. To reduce the drift of a structure to an acceptable level, design strategies based on controlling the drift have already been proposed[Moehle 1992 and Pincheira 1993].

Fig.2.46 shows the relationship between the drift, in terms of interstorey drift, and the period of the structure for a given earthquake. Such relations can be estimated from inelastic displacement response spectra. The drift demand depends on the period of the structure and the requirements of the serviceability and ultimate limit states. For the short period structure, the ductility also affects the drift demand and the drift normally increases as the period of the structure increases. The drift demand for the long period structure is independent of the period, which is commonly referred to as the "equal displacement rule". The available drift of a structure must be larger than the drift demand estimated from inelastic response spectra. Even when the available drift of the structure with a given period is larger than the drift demand, the drift must be limited to an acceptable level for the serviceability and ultimate limit state requirements. Although the quantitative values for the drift limit are not well known for both the serviceability and ultimate limit states, the drift limit for the ultimate limit state R_u would be larger than that for the serviceability limit state R_s, as shown in Fig.2.46.

When the drift demand of the structure with a given period estimated from inelastic displacement response spectra is larger than the drift limits R_s and R_u, the structure must have its period made smaller than T_s and T_u(see Fig.2.46) to be adequate for the drift requirements. This is illustrated in Fig.2.46 for the case when the drift limit for the ultimate limit state of the structure becomes critical, and which the period for the serviceability limit state requirement T_s is larger than that for ultimate limit state requirement T_u ($T_s>T_u$). In such a case, the period of the structure must be made smaller than the critical period for the ultimate limit state requirement($T_{cr}=T_u$). Hence, one line can be produced for the structure with a given ductility and earthquake, which delineates adequate and inadequate relationships between the drift and period in terms of the drift limit, as illustrated in Fig.2.46. A similar line can also be drawn on the strength versus period relationship, as shown in Fig.2.45. The combination of the required period and strength can be used to identify adequate and inadequate seismic performance of the structure. The minimum requirement of strength S_{min} for the structure with a given ductility capacity can be found from Fig.2.45. The minimum requirement of strength S_{min} so obtained may be plotted on the relationship between the strength and ductility in Fig.2.44 with the critical period T_{cr}, and this will determine the ductility required for the structure μ_{min}.

The procedures mentioned above are illustrated using two structures with different fundamental periods. The original structure with a long period is plotted by an open circle on the drift versus period relationship in Fig.2.46. Since the period of this structure is larger than the critical period T_{cr} for the drift limit requirement R_u, the original structure must be stiffened to decrease the period at least down to T_{cr} to meet the drift limit requirement. Furthermore, the available drift of the retrofitted structure must be larger than the drift demand obtained from inelastic response spectra. The structure may be retrofitted by using infilling wall or steel bracing techniques. Those techniques can increase the stiffness as well as strength of the existing structure but would result in less ductile structure. The required strength and ductility can be estimated from the strength versus period relationship or the strength versus ductility relationship as described before.

The original structure with a short period is shown by an open square in Fig.2.46. Although the period of the structure is smaller than the critical period T_{cr}, the structure must be strengthened since the available drift of the original structure is smaller than the drift demand for the ultimate limit state obtained from inelastic response spectra as shown in Fig.2.46. In such a case, the original structure may be retrofitted to increase the available drift of the structure (scheme (2) in Fig.2.43) or to decrease the period of the structure (scheme (1) in Fig.2.43). For scheme(2), a jacketing technique may be used to increase the available drift of the original structure. In many cases, the retrofit is provided to only perimeter frames to minimize disruption of the occupants and functions of the building. While the members retrofitted using jacketing can have substantial strengths and ductilities, studies have shown that unless the retrofit scheme makes the existing structure stiff enough to significantly reduce the lateral drift, unacceptable damage to the existing unstrengthened elements can be expected[Pincheira 1993].

In summary, it has been shown that controlling the lateral drift is a very important of redesigning existing structures which are assessed to be inadequate for future earthquakes. Structures with inadequately low stiffness must be stiffened to limit the drift to an acceptable level under seismic loading. The required strength and ductility for the structure can be found from the required period to satisfy the drift demands, including the serviceability and ultimate limit state requirements. Only redesign schemes which consider strength, drift and ductility will result in seismically inadequate structures performing satisfactorily in future earthquakes.

2.5 CONCLUSIONS

The following conclusions can be drawn as a result of the seismic assessment of a reinforced concrete building frame designed in the late 1950's in New Zealand and other considerations:

(1) The available lateral load strength of the early frame, provided by the flexural strengths of the members, approached the design seismic forces assuming elastic response of New Zealand loading standards.

(2) The critical failure mechanism of the frame was a mixed mechanism including flexural plastic hinges combined with shear failures of the beams and columns. The results of the analyses indicated that the beam plastic hinge behaviour would control the inelastic seismic response of the frame.

(3) Moment-curvature analysis indicated that an available curvature ductility factor of at least 10 was achieved at the potential plastic hinge region of the typical beam section providing compression bar buckling and shear failure were prevented. This available curvature ductility factor was greater than the ductility demand obtained when the frame was subjected to the El Centro 40NS earthquake record.

(4) The column flexural strengths were not large enough to ensure the development of a beam hinge mechanism of the structure. However, the results of the analysis showed that a soft storey column mechanism was not developed in the event of a major earthquake although some column yielding was observed. When considering the low axial compression and tension loads acting on the columns where yielding was observed, column yielding can be accepted, but only if a column sidesway mechanism does not occur in that storey. That is, a small axial load means increased column flexural ductility but this ductility would not be sufficient to

meet the high curvature ductility demand of a column sidesway mechanism in multi-storey frame.

(5) Shear failures of the exterior columns in the lower storeys of the building frame were found to occur during severe seismic excitations. This is mainly due to the earthquake induced axial tension load acting on the columns. However, if column shear failure under axial tension loading is not sudden, shear failure of the exterior columns may not result in catastrophic collapse of the structure.

(6) A more critical aspect with respect to shear was found in the beam-column joints. Relatively large joint shear input during severe earthquakes indicated that the joints of the structure could suffer severe diagonal tension cracking and that the strength of the structure is likely to be governed by joint shear failure.

The seismic assessment methods proposed in Japan and the United States have been reviewed. Further investigations of the available strengths, stiffnesses and ductility capacities of the members and subassemblages with reinforcing details typical of the older buildings are required to refine the seismic assessment procedures.

It is shown that redesign schemes which consider the strength, drift and ductility will result in seismically inadequate structures performing satisfactorily during future earthquakes.

CHAPTER 3

EXPERIMENTAL PROGRAMME

3.1 INTRODUCTION

In Chapter 2, a reinforced concrete moment resisting frame designed in the late 1950's has been assessed. With regard to seismic resistance, it is found that when compared with the current New Zealand code requirements for ductile frames[SANZ 1982(a)], detailing of the longitudinal reinforcement in the columns is inadequate to ensure strong column-weak beam behaviour and that the transverse reinforcement details in the columns and beams are inadequate for shear resistance and for preventing premature buckling of compressed bars. Typically, no or little shear reinforcement is present in the joint core. This may result in the joint shear failure during severe seismic loading. Those deficiencies are common for the reinforced concrete buildings designed to the older codes in New Zealand[Park 1992] and in the United States[Pessiki et al 1990].

There is a need for more experimental investigations to provide further information regarding the seismic behaviour of the structures designed to the earlier codes. Also, the effectiveness of retrofit techniques needs to be clarified since most of the techniques have been based mainly on engineering judgement. Hence experimental studies were carried out with emphasis on examining the seismic behaviour of beam-column joint regions of frames with such deficiencies and those retrofitted by jacketing with new reinforced concrete.

3.2 TEST SPECIMENS

3.2.1 The Test Specimens

Tables 3.1 and 3.2 summarize the test specimens and Figs.3.1 to 3.8 show the dimensions and reinforcement details of all specimens. The dimensions of the test specimens were full-scale.

Three specimens identical to Specimen O1 were constructed. Specimen O1 was tested and then retrofitted by concrete jacketing to become Specimen R1. The other two specimens identical to Specimen O1 were retrofitted by concrete jacketing without previous testing to become Specimens R2 and R3. Specimens O4, O5, O6 and O7 were all different and were tested without concrete jacketing. Specimen O1(and hence Specimens R1, R2 and R3 before retrofitting) and Specimen O7 were identical full-scale replicas of parts of the 1950's frame which was assessed.

Table 3.1 Summary of Test Specimens

		As-Built Specimen O1	Specimen O4	Specimen O5	Specimen O6	As-Built Specimen O7
Beam	Size	300×500				
	Top Bars	4-D24 (ρ'=1.37%)	4-D24 (ρ'=1.37%)	2-D32 (ρ'=1.22%)	3-D24 (ρ'=1.03%)	
	Bottom Bars	2-D24 (ρ=0.68%)	4-D24 (ρ=1.37%)	2-D32 (ρ=1.22%)	2-D24 (ρ=0.68%)	
	Stirrups	2-R6@308				
Column	Size	300×460	600×460		460×460	
	Main Bars	6-D24 (ρ_t=1.96%)	6-D28 (ρ_t=1.34%)		4-D24 (ρ_t=0.85%)	
	Hoops	4-R6@230			2-R6@305	

Note : (1) $\rho=A_s/bd$, $\rho'=A'_s/bd$, $\rho_t=A_{st}/A_g$, where A_s=area of longitudinal tension reinforcement of beam, A'_s=area of longitudinal compression reinforcement of beam, A_{st}=total area of longitudinal reinforcement of column, b=width of beam d=distance from extreme compression fibre of concrete to centroid of tension reinforcement of beam, and A_g =gross area of column

(2) No shear reinforcement was placed in the joint core.

Table 3.2 Summary of Retrofitted Test Specimens

		Retrofitted Specimen R1	Retrofitted Specimen R2	Retrofitted Specimen R3
Beam	Size	500×600		300×500
	Top Bars	2-D12(ρ'=0.70%)		None
	Bottom Bars	2-D12(ρ=0.50%)		None
	Stirrups	2-D10@70		None
Column	Size	700×660		
	Main Bars	4-HD24 (ρ_t=0.98%)		4-D24 (ρ_t=0.98%)
	Hoops	2-D12@110		
Joint	Hoops	6-HR16	None	

Note : Only new reinforcement in the concrete jackets are shown.

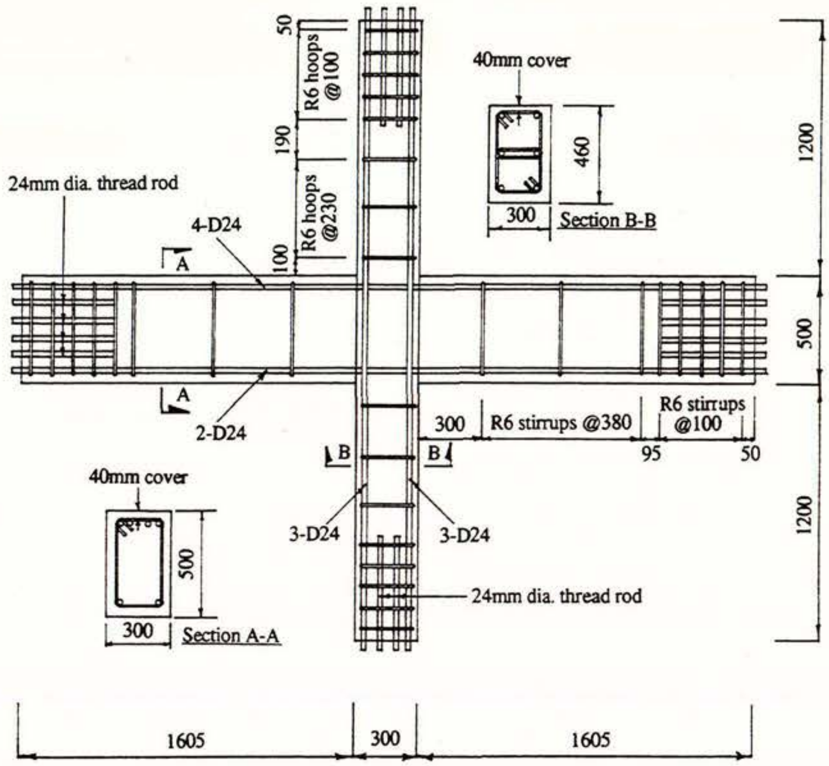

Fig.3.1 Dimensions and Reinforcement Details of the As-Built Specimen O1

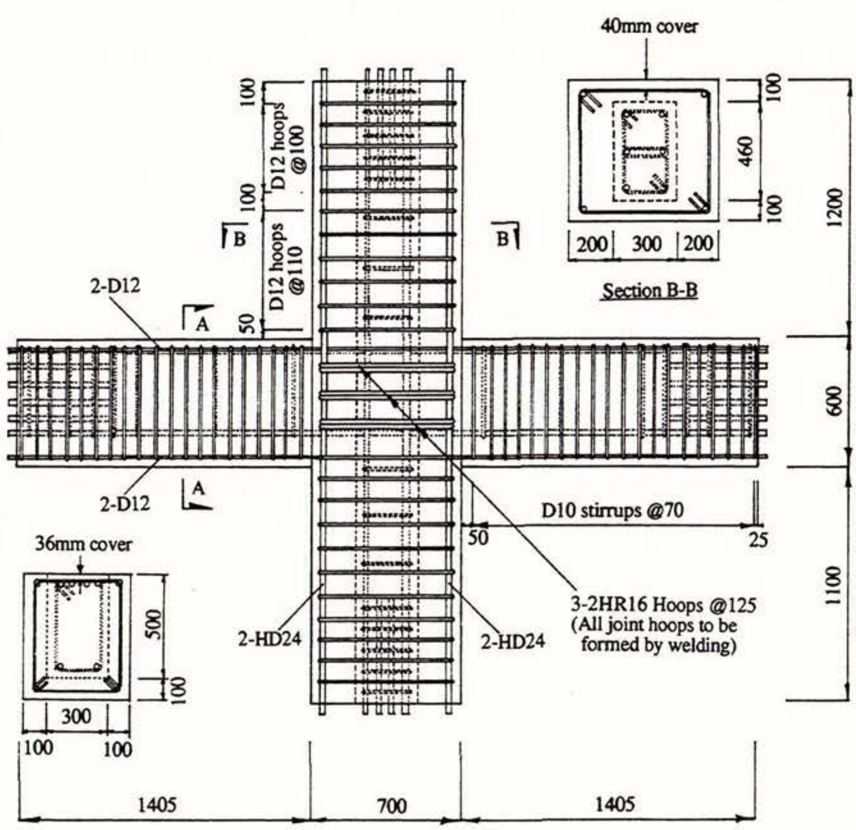

Fig.3.2 Dimensions and Reinforcement Details of the Retrofitted Specimen R1

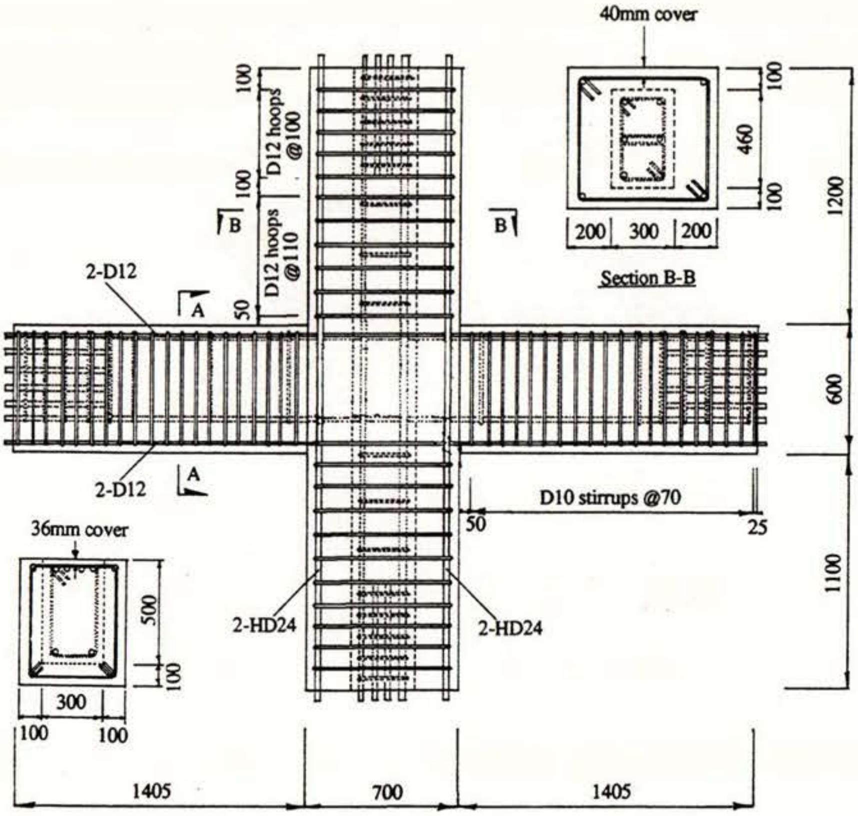

Fig.3.3 Dimensions and Reinforcement Details of the Retrofitted Specimen R2

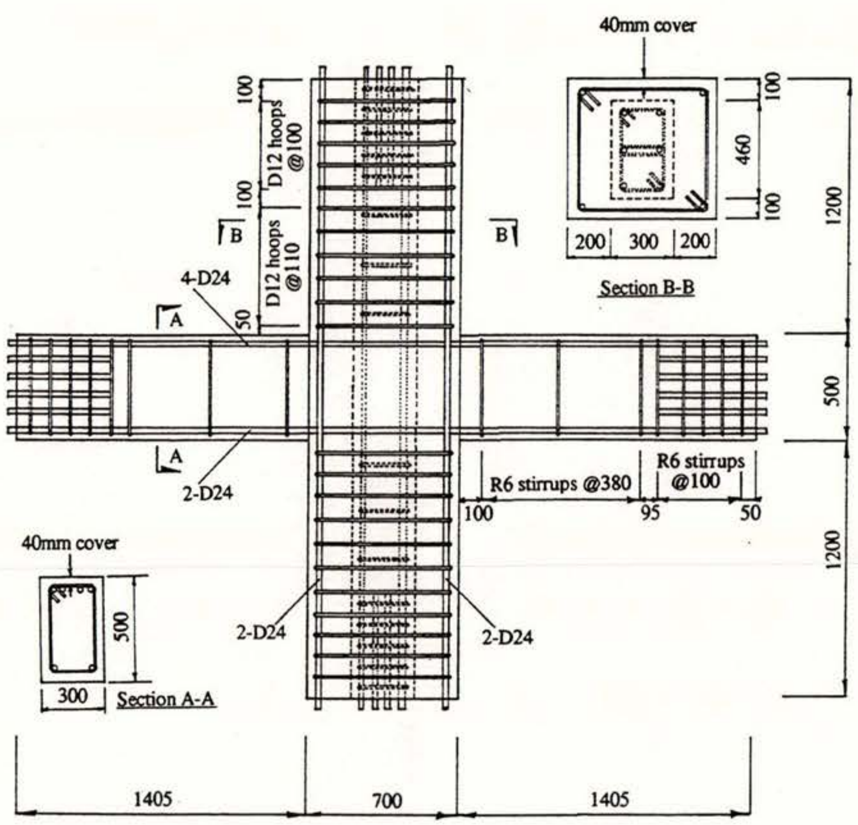

Fig.3.4 Dimensions and Reinforcement Details of the Retrofitted Specimen R3

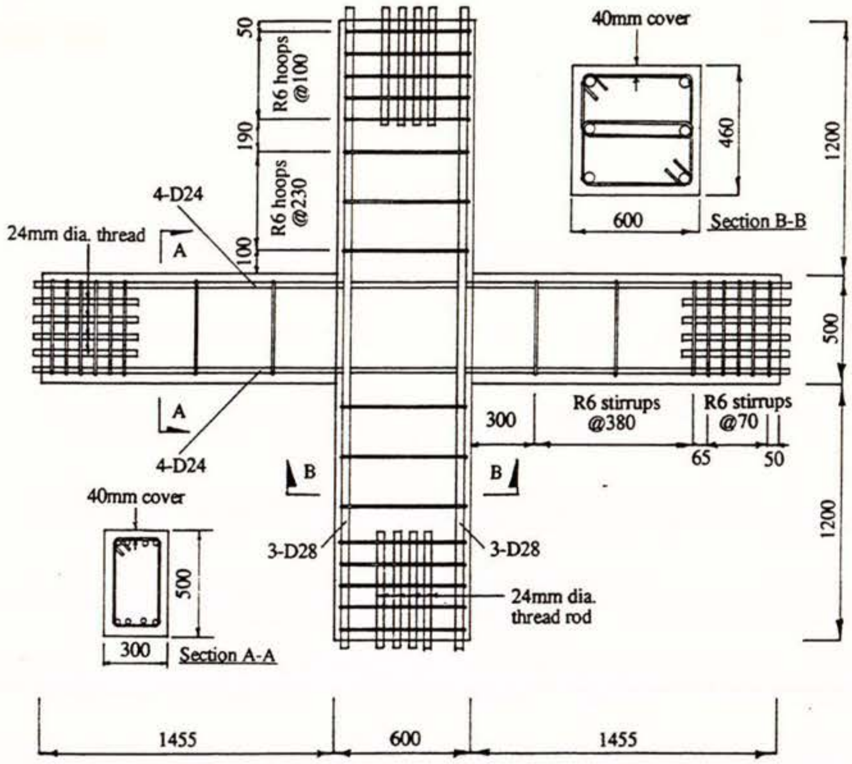

Fig.3.5 Dimensions and Reinforcement Details of Specimen O4

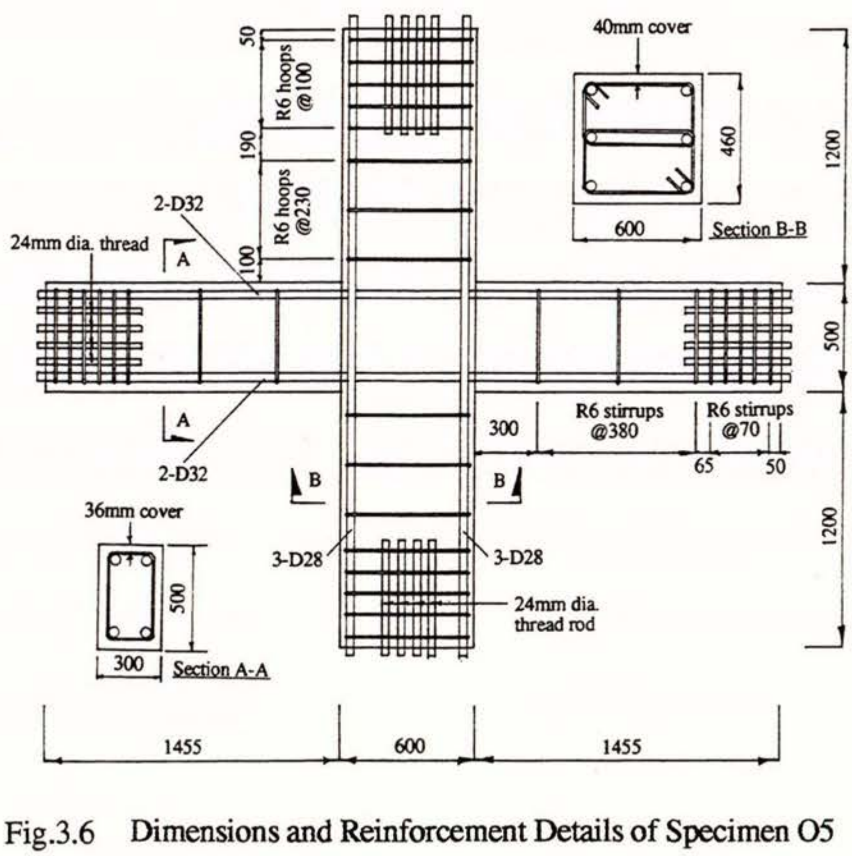

Fig.3.6 Dimensions and Reinforcement Details of Specimen O5

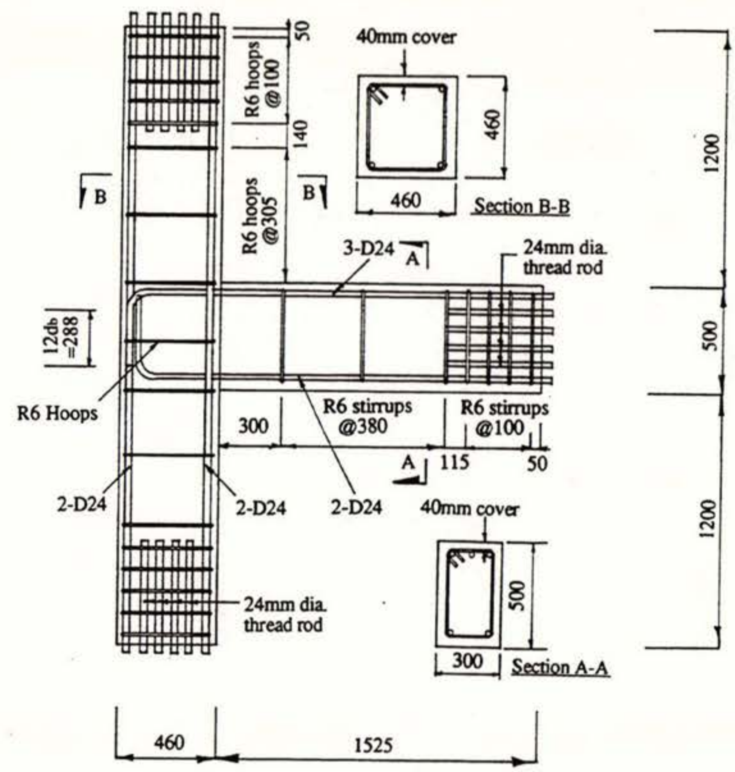

Fig.3.7 Dimensions and Reinforcement Details of Specimen O6

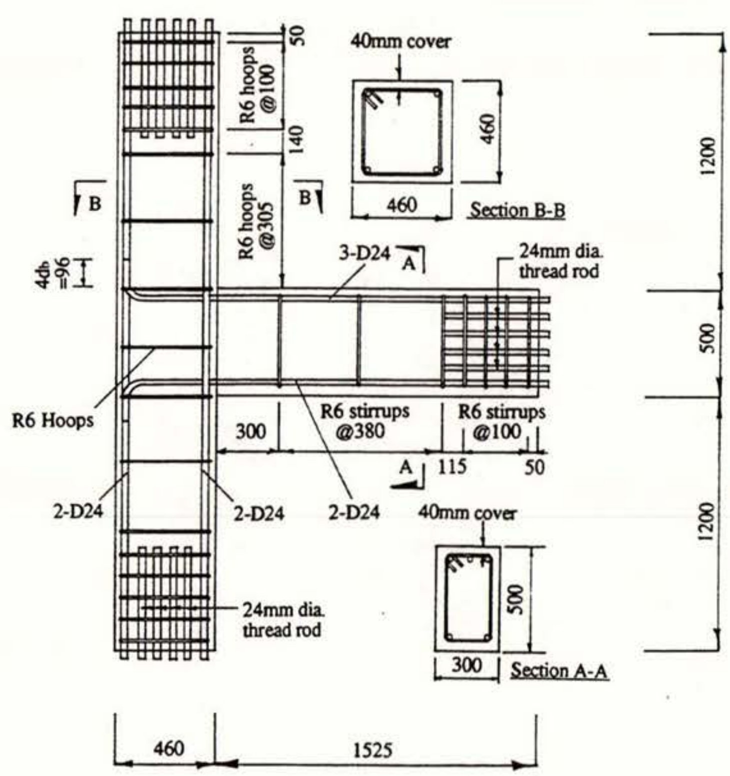

Fig.3.8 Dimensions and Reinforcement Details of Specimen O7

3.2.2 As-Built Specimen O1

Specimen O1 was a full-scale replica, referred to as the as-built specimen, of a critical beam-interior column joint region of the perimeter frame of the 1950's building being investigated. The dimensions and reinforcement details of Specimen O1 are shown in Fig.3.1. The beams had cross section of 500mm deep and 300mm wide and the columns had cross section of 300mm deep and 460mm wide. The longitudinal reinforcement of the columns and beams was of 24mm diameter deformed bars of Grade 300 steel. The transverse reinforcement was of 6mm diameter plain round bars of Grade 300 steel at 380mm spacing for the beams and 230mm spacing for the columns. No shear reinforcement was placed in the joint core.

The concrete of the as-built specimen was normal weight with a designed concrete compressive strength of 30MPa.

It is found from the reinforcing details of the as-built specimen with regard to earthquake resistance that according to NZS 3101[SANZ 1982(a)] the columns have inadequate longitudinal reinforcement to preclude their hinging when the axial load is zero, that the beams, columns and beam-column joint have inadequate transverse reinforcement for shear strength and restraining the compression reinforcement against premature buckling, and that the longitudinal beam bars have too large a diameter to pass through the column with small depth(see Table 3.3).

3.2.3 Retrofitted Specimens R1, R2 and R3

After testing Specimen O1 under simulated seismic loading, the damaged specimen was retrofitted by jacketing the beams, columns and joint with new reinforced concrete in an attempt to achieve a favourable beam hinge mechanism under severe earthquake loading. The dimensions and reinforcement details of the retrofitted Specimen, referred to as Specimen R1, are shown in Fig.3.2. The total column size was made 700mm deep and 660mm wide by a four-sided concrete jacket containing new longitudinal bars at the four corners of the jacket and new transverse reinforcement. The beams were made 600mm deep and 500mm wide by a four-sided jacket, in which new longitudinal bars and transverse reinforcement were placed. The new longitudinal reinforcement in the column jackets were deformed bars of Grade 430 steel while those in the beam jackets were deformed bars of Grade 300 steel. The transverse reinforcement in both the column and beam jackets were deformed bars of Grade 300 steel. Plain round bars of Grade 430 steel were used for the new horizontal joint shear reinforcement as illustrated in Fig.3.2. The reinforcement in the beams, columns and joint met the requirements of the current New Zealand code for ductile frames[SANZ 1982(a)](see Table

Table 3.3 Comparison of Details of As-Built Beam-Interior Column Specimen O1(and R1, R2 and R3 before Retrofitting) with Requirements of NZS 3101:1982[SANZ 1982(a)]

Actual for Specimens				Required by NZS 3101:1982				
Flexural strength based on measured material strengths Column M_c=120kNm Beam (+)M_b=132kNm (-)M_b=246kNm $\sum M_c/M_b$=0.69				$\sum M_c/M_b \geq 1.81$				
Transverse reinforcement				For shear	For restraint against bar buckling			For confinement
	Area (mm^2/mm)	Longitudinal Spacing(mm)	Transverse spacing(mm)	Area (mm^2/mm)	Area (mm^2/mm)	Longitudinal Spacing(mm)	Transverse spacing(mm)	Area (mm^2/mm)
Column	0.49	230	170	0.54*	0.85(4-legs)	60	200	2.15
Beam	0.15	380	180	0.35*	1.13(2-legs)	110	200	
Shear reinforcement in beam-column joint Area(mm^2) Horizontal 0 Vertical 0				Area(mm^2) Horizontal 771 Vertical 3213				
Diameter of beam bar / column depth=24/300=1/12.5 Diameter of column bar / beam depth=24/500=1/20.8				Diameter of beam bar / column depth≤1/20 Diameter of column bar / beam depth≤1/20				

* At flexural strength of column and based on v_c outside plastic hinge zones.

Comparison based on actual(measured) strengths of concrete and steel

Table 3.4 Comparison of Details of Retrofitted Beam-Interior Column Specimen R1 with Requirements of NZS 3101:1982[SANZ 1982(a)]

Actual for Specimens				Required by NZS 3101:1982				
Flexural strength based on measured material strengths Column M_c=592kNm Beam (+)M_b=180kNm (-)M_b=387kNm $\sum M_c/M_b$=2.10				$\sum M_c/M_b \geq 1.81$				
Transverse reinforcement				For shear	For restraint against bar buckling			For confinement
	Area (mm2/mm)	Longitudinal Spacing(mm)	Transverse spacing(mm)	Area (mm2/mm)	Area (mm2/mm)	Longitudinal Spacing(mm)	Transverse spacing(mm)	Area (mm2/mm)
Column	2.06	110	540	1.31	0.57(2-legs)	132	200	1.86
Beam	2.24	70	380	1.43	1.27(2-legs)	72	200	
Shear reinforcement in beam-column joint Area(mm2) Horizontal 2413(Grade 430) Vertical 2714				Area(mm2) Horizontal 3473 Vertical 1190				
Diameter of beam bar / column depth=24/700=1/29.1 Diameter of column bar / beam depth=24/600=1/25				Diameter of beam bar / column depth≤1/25 Diameter of column bar / beam depth≤1/15				

Comparison based on actual(measured) strengths of concrete and steel

Table 3.5 Comparison of Details of Retrofitted Beam-Interior Column Specimen R2 with Requirements of NZS 3101:1982[SANZ 1982(a)]

Actual for Specimens				Required by NZS 3101:1982				
Flexural strength based on measured material strengths								
Column	M_c=598kNm							
Beam	$(+)M_b$=182kNm							
	$(-)M_b$=389kNm							
	$\sum M_c/M_b$=2.11			$\sum M_c/M_b \geq 1.81$				
Transverse reinforcement				For shear	For restraint against bar buckling			For confinement
	Area (mm^2/mm)	Longitudinal Spacing(mm)	Transverse spacing(mm)	Area (mm^2/mm)	Area (mm^2/mm)	Longitudinal Spacing(mm)	Transverse spacing(mm)	Area (mm^2/mm)
Column	2.06	110	540	1.31	0.57(2-legs)	132	200	1.86
Beam	2.24	70	380	1.42	1.27(2-legs)	72	200	
Shear reinforcement in beam-column joint								
	Area(mm^2)				Area(mm^2)			
Horizontal	0			Horizontal	3473			
Vertical	2714			Vertical	1190			
Diameter of beam bar / column depth=24/700=1/29.2				Diameter of beam bar / column depth≤1/25				
Diameter of column bar / beam depth=24/600=1/25				Diameter of column bar / beam depth≤1/15				

Comparison based on actual(measured) strengths of concrete and steel

Table 3.6 Comparison of Details of Retrofitted Beam-Interior Column Specimen R3 with Requirements of NZS 3101:1982[SANZ 1982(a)]

Actual for Specimens				Required by NZS 3101:1982				
Flexural strength based on measured material strengths								
Column	M_c=450kNm							
Beam	(+)M_b=127kNm							
	(-)M_b=235kNm							
	$\sum M_c/M_b$=2.41			$\sum M_c/M_b \geq 1.81$				
Transverse reinforcement				For shear	For restraint against bar buckling			For confinement
	Area (mm^2/mm)	Longitudinal Spacing(mm)	Transverse spacing(mm)	Area (mm^2/mm)	Area (mm^2/mm)	Longitudinal Spacing(mm)	Transverse spacing(mm)	Area (mm^2/mm)
Column	2.06	110	540	0.77	0.57(2-legs)	132	200	1.86
Beam	0.15	380	180	0.35*	1.13(2-legs)	110	200	
Shear reinforcement in beam-column joint								
	Area(mm^2)				Area(mm^2)			
Horizontal	0			Horizontal	2997			
Vertical	2714			Vertical	856			
Diameter of beam bar / column depth=24/700=1/29.2				Diameter of beam bar / column depth≤1/25				
Diameter of column bar / beam depth=24/500=1/20.8				Diameter of column bar / beam depth≤1/15				

* At flexural strength of beam and based on v_c outside plastic hinge zones.

Comparison based on actual(measured) strengths of concrete and steel

3.4), except that in both the columns and beams the horizontal spacing of the tied longitudinal bars exceeded the code permitted maximum spacing of 200mm. This specimen was denoted as Specimen R1 and tested to investigate the effect of the concrete jacketing on the seismic behaviour of the as-built specimen.

Another as-built specimen, similar to Specimen O1 but not previously damaged, was originally planned to be retrofitted in the same manner to permit a comparison of the effect of the previous damage. After testing Specimen R1, however, it became obvious that no joint distress was likely to occur if tested as planned. Therefore, new joint hoops were not placed in the joint core to create critical conditions for the joint core as shown in Fig.3.3 . This specimen was referred to as Specimen R2. Comparison of the details of Specimen R2 with the code requirements is shown in Table 3.5. The seismic behaviour obtained from Specimen R2 was compared with that from Specimen R1.

The other as-built specimen, similar to Specimen O1 but not damaged, was retrofitted by jacketing the columns alone. This specimen was referred to as Specimen R3. The columns were jacketed in a fashion similar to Specimen R2 except that the longitudinal reinforcement in the column jacket was deformed bars of Grade 300 steel as shown in Fig.3.4. No new joint hoops were placed in the joint core (similar to Specimen R2). Comparison of the details of Specimen R3 with the code requirements is shown in Table 3.6. This method of concrete jacketing was investigated since it could significantly mitigate the labour required for jacketing both the columns and beams. This aspect will be described later in this chapter. It was expected that the beams would fail in shear under severe seismic loading since the beams, not retrofitted, had a small amount of shear reinforcement .

A designed concrete compressive strength of new concrete for the retrofitted specimens was 40MPa.

3.2.4 Specimens O4 and O5

In order to investigate the effect of the bond conditions along the beam bars passing through the joint on the shear strength of the joint without shear reinforcement, Specimens O4 and O5 were constructed. These two specimens were not replicas of the investigated 1950's frame but represented details common in other early frames. Fig.3.5 shows the dimensions and reinforcement details of Specimen O4 which was designed to have good bond conditions along the beam bars in the joint. The longitudinal beam reinforcement was of 24mm diameter deformed bars of Grade 300 steel. The ratio of beam bar diameter to column depth was $d_b/h_c=24/600=1/25$, which satisfied the requirements of NZS 3101[SANZ 1982(a)] for ductile frames. The longitudinal column bars were designed to preclude column hinging. The transverse reinforcement was of 6mm diameter plain round bars of Grade 300 steel spaced at

380mm for the beams and 230mm for the columns. As shown in Fig.3.5, no joint shear reinforcement was placed.

The dimensions and reinforcement details of Specimen O5 were the same as Specimen O4 except that the longitudinal reinforcement of the beams were 32mm diameter bars as shown in Fig.3.6. The ratio of beam bar diameter to column depth was $d_b/h_c=32/600=1/18.75$. Therefore, more severe bond conditions along the beam bars in the joint was expected for Specimen O5 when compared with Specimen O4.

Concrete with a designed concrete compressive strength of 30MPa was used for Specimens O4 and O5. Comparison of the details of Specimen O4 and O5 with the requirements of the code are shown in Table 3.7.

The two specimens were tested under simulated severe seismic loading and their behaviour was compared.

3.2.5 Specimens O6 and O7

One full-scale beam-exterior column joint with beam bar anchorage typical of the 1950's reinforced concrete building being investigated was constructed. This specimen was referred to as Specimen O7. The dimensions and reinforcement details of Specimen O7 are shown in Fig.3.8. As shown in this figure, the longitudinal beam bars were not bent into the joint core and the straight extension beyond the bend was four times the bar diameter. In order to investigate the effect of the configuration of the hooks at the ends of the beam bars, Specimen O6 was also constructed as shown in Fig.3.7. The beam bars were bent into the joint core and the extension was twelve times bar diameter which satisfied the current code requirements[SANZ 1982(a)]. Only one 6mm diameter hoop was placed in the joint core of both specimens. Only a small amount of transverse reinforcement was provided in the beams and columns as shown in Figs.3.7 and 3.8.

Concrete with a designed concrete compressive strength of 30MPa was used for Specimens O6 and O7. Comparison of the details of Specimens O6 and O7 with the requirements of the code are shown in Table 3.8.

The two specimens were tested under simulated seismic loading and their behaviour was compared.

Table 3.7 Comparison of Details of Beam-Interior Column Specimens O4 and O5 with Requirements of NZS 3101:1982[SANZ 1982(a)]

Actual for Specimens				Required by NZS 3101:1982				
Flexural strength based on measured material strengths								
	Specimen O4	Specimen O5						
Column	M_c=323kNm	M_c=307kNm						
Beam	M_b=239kNm	M_b=202kNm						
	$\sum M_c/M_b$=1.35	$\sum M_c/M_b$=1.52		$\sum M_c/M_b \geq 1.81$				
Transverse reinforcement				For shear	For restraint against bar buckling			For confinement
	Area (mm2/mm)	Longitudinal Spacing(mm)	Transverse spacing(mm)	Area (mm2/mm)	Area (mm2/mm)	Longitudinal Spacing(mm)	Transverse spacing(mm)	Area (mm2/mm)
Column	0.49	230	170	0.54*	1.15(4-legs)	92	200	1.56
Beam	0.15	380	180	0.35*	1.13(2-legs)	110	200	
Shear reinforcement in beam-column joint					Specimen O4		Specimen O5	
	Area(mm2)				Area(mm2)		Area(mm2)	
Horizontal	0			Horizontal	4020		3567	
Vertical	0			Vertical	1340		1189	
Diameter of beam bar / column depth for				Diameter of beam bar / column depth≤1/25				
	Specimen O4=24/600=1/25							
	Specimen O5=32/600=1/18.75							
Diameter of column bar / beam depth=28/500=1/17.9				Diameter of column bar / beam depth≤1/15				

* At flexural strength of beam and based on v_c outside plastic hinge zones.

Comparison based on actual(measured) strengths of concrete and steel

Table 3.8 Comparison of Details of Beam-Exterior Column Specimens O6 and O7 with Requirements of NZS 3101:1982[SANZ 1982(a)]

Actual for Specimens			Required by NZS 3101:1982
Flexural strength based on measured material strengths			
	Specimen O6	Specimen O7	
Column	M_c=115kNm	M_c=114kNm	
Beam	(+)M_b=121kNm	(+)M_b=119kNm	
	(-)M_b=174kNm	(-)M_b=173kNm	
	$\sum M_c/(+)M_b$=1.38	$\sum M_c/(+)M_b$=1.37	$\sum M_c/M_b \geq 1.81$

Transverse reinforcement				For shear	For restraint against bar buckling			For confinement
	Area (mm2/mm)	Longitudinal Spacing(mm)	Transverse spacing(mm)	Area (mm2/mm)	Area (mm2/mm)	Longitudinal Spacing(mm)	Transverse spacing(mm)	Area (mm2/mm)
Column	0.19	305	340	0.54*	0.57(2-legs)	92	200	1.34
Beam	0.15	380	180	0.35*	0.85(2-legs)	110	200	

Shear reinforcement in beam-column joint			
	Area(mm2)		Area(mm2)
Horizontal	56.5	Horizontal	1513
Vertical	0	Vertical	657

Actual for Specimens	Required by NZS 3101:1982
Specimen O6 : Beam bars bent into the joint core and tweleve times bar dimeter of straight extension beyond the bend. Specimen O7 : Beam bars not bent into the joint core and four times bar dimeter of straight extension beyond the bend.	Beam bars bent into the joint core and tweleve times bar dimeter of straight extension beyond the bend.

* At flexural strength of beam and based on v_c outside plastic hinge zones.

Comparison based on actual(measured) strengths of concrete and steel

3.3 SPECIMEN FABRICATION

3.3.1 Formwork

The formwork for all specimens were made from plywood(see Figs.3.9(a) and (f)). In order to minimize any bowing outwards of the plywood moulds during the casting of concrete, the moulds were stiffened with timber blocks, steel angles and steel plates. The moulds were coated with lacquer to avoid water absorption by the plywood during the concreting of the specimens. For each casting of concrete, the moulds were repainted. All edges were sealed with parcel tape to prevent any leaking of the water of the fresh concrete. Before the concreting of each test specimen, the moulds were oiled to make it easy to remove them when required.

3.3.2 Reinforcing Cages

All of the longitudinal reinforcement was cut to length and threaded at both ends by a local firm. Stirrups and hoops were also cut and bent by a local firm except that the new joint hoops for Specimen R1 were cut and bent in the laboratory.

Before constructing the steel cages for each test specimen, wire strain gauges were attached on reinforcing bars in the critical regions to measure the local strains. For all specimens except Specimens O1, R1 and R2, 10mm diameter steel rods were also welded to the main beam bars so as to protrude laterally through the cover concrete to measure bar deformations. This will be described later in this chapter.

After the stirrups and hoops of the test specimens were tied to the longitudinal bars, the reinforcing cages were placed in the formwork, including some additional 10mm diameter steel rods required to hold some parts of the instrumentation during the test. Both ends of the longitudinal bars with threads passed through the holes of the moulds drilled at the position of the longitudinal reinforcement by about 50mm (as seen in Figs.3.1 to 3.8) and were tightened to the moulds by nuts to lock their positions. This procedure made it possible to keep the reinforcement in the correct position during the casting of concrete.

3.3.3 Casting of Concrete

The concrete was provided by a commercial ready-mix plant. The specified 28 day compressive strength was 30MPa and the specified slump was 100mm for the as-built Specimen O1, Specimens R2 and R3 before retrofitting, and Specimens O4 to O7. On the other hand, for new concrete used in retrofitted Specimens R1 to R3, 40MPa concrete was specified which was 10MPa greater than the compressive strength of the concrete specified for

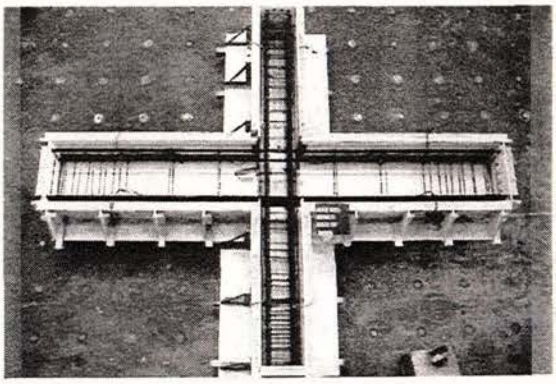

(a) As-Built Specimen O1 before Casting

(b) Casting Concrete for As-Built Specimen O1

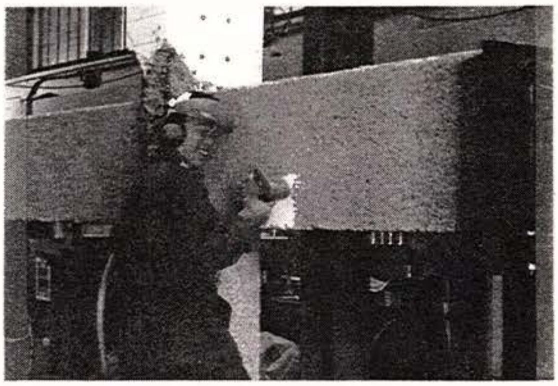

(c) Surface Preparation after Testing Specimen O1

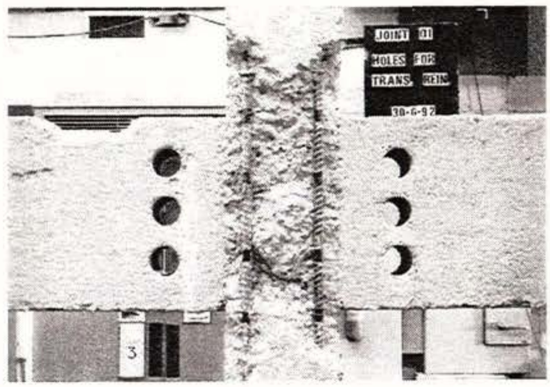

(d) After Finishing the Surface Preparation before Jacketing Specimen O1

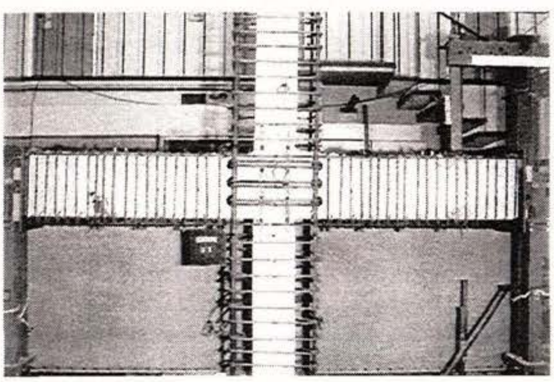

(e) New Reinforcement of Specimen R1

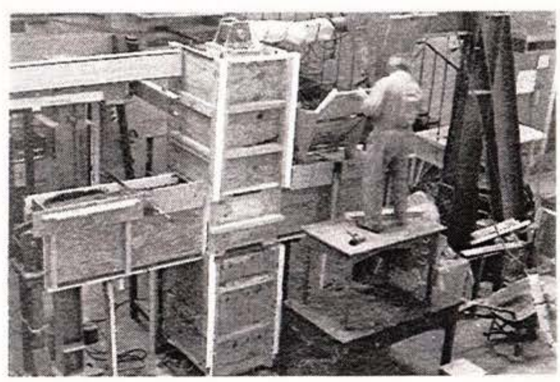

(f) Casting New Concrete of Specimen R1

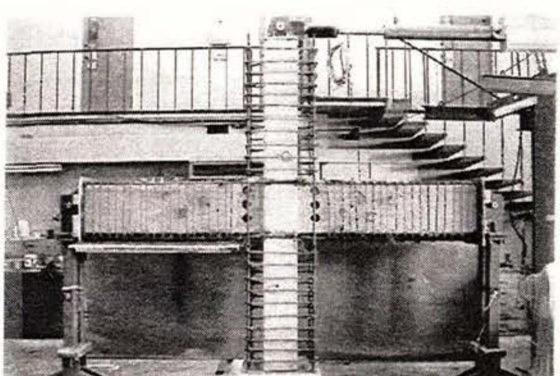

(g) New Reinforcement of Specimen R2

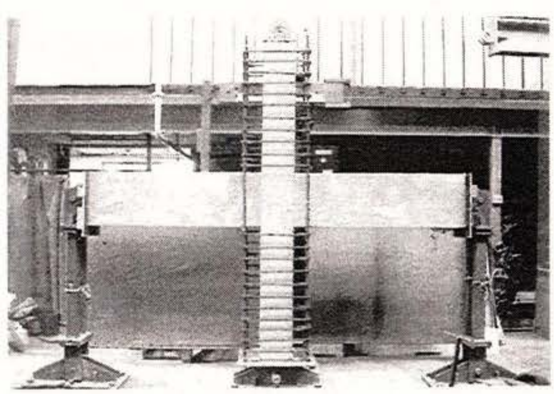

(h) New Reinforcement of Specimen R3

Fig.3.9 Construction of the Retrofitted Specimens the as-built specimens. A slump of 180mm was specified for the new concrete. The specified maximum aggregate size was 20mm for all test specimens except for the new concrete of Specimens R1 to R3, where the specified maximum aggregate size was 13mm because of the congestion of the new reinforcement, especially in the holes drilled through the beams where new joint hoops were present in Specimen R1.

For the as-built Specimen O1, Specimens R2 and R3 before retrofitting, and Specimen O4 to O7 the casting of concrete was conducted with the specimens in the horizontal position(see Fig.3.9(b)). On the other hand, the new concrete for the jackets of Specimens R1, R2 and R3 were cast in vertical position as shown in Fig.3.9(f). The concrete was placed by a hopper and portable electric vibrators were used to compact the concrete.

Casting of the concrete for all specimens was carried out in one stage. The time required to complete concreting was about three hours for the new concrete of the retrofitted specimens and about thirty minutes for the other specimens, respectively.

After casting the concrete, all specimens were cured with damp fabric and with plastic sheets for seven days. Then the plywood moulds were removed and the test specimens were placed in the laboratory before testing. Details of the concrete cylinders are given in Section 3.4.2.

3.3.4 Jacketing of the Columns and Beams with New Reinforced Concrete

After testing the as-built Specimen O1, the test specimen was loaded back to the zero residual horizontal displacement position measured at the top of the column and then retrofitting process started for Specimen R1.

The existing concrete of the as-built specimen and the new concrete were intended to act monolithically. To improve shear transfer across the interface of the new and existing concrete[Bass et al 1989], the surface of the as-built specimen was lightly roughened to a peak amplitude of approximately 1mm by a scrabbler as shown in Fig.3.9(c). In the case of Specimen O1, the loose concrete of the joint region damaged during the previous test was completely removed by an electric jackhammer. The cover concrete of the top face of the beams were also chipped off where new transverse reinforcement was placed. The roughened or chipped off surfaces were cleaned with a vacuum cleaner to remove small particles and dust. The time required for the surface preparation was approximately one to two days. This process was the most labour intensive part of the retrofit procedure. Specimen R1 after finishing the surface preparation but before jacketing can be seen in Fig.3.9(d).

In order to place the new joint hoops in the retrofitted specimen R1, holes were made through the beams between top and bottom main beam bars of Specimen O1 with a core boring machine(see Fig.3.9(d)). The holes had a diameter of 75mm, which was considered to be large enough to facilitate the casting of new concrete in the holes around the new hoops.

Fig.3.10 shows the details of the beam and column section of the retrofitted Specimens R1 and R2. The new longitudinal beam reinforcement was first placed in the correct positions and then the beam transverse reinforcement was placed. The new beam stirrups were made from two portions. A U-shaped portion was placed over the top and around the sides of the as-built concrete, and a straight portion was placed along the bottom. All ends were anchored by 135° hooks but some hooks were formed after placing the stirrups to make the placing easier(see Fig.3.10(a)). The new column hoops were made from two L-shaped portions with 135° end hooks that overlapped in diagonally opposite corners(see Fig.3.10(b)). The L-shaped ties were stacked at the base of the bottom column, alternating the diagonal of overlapping corners at each layer. Then the new longitudinal column bars were placed and the hoops were lifted to the correct positions and tied. For Specimen R1, horizontal joint shear reinforcement were also placed. This process will be described in detail in the following section. The new beam and column steel cages of Specimen R1 are shown in Fig.3.9(e).

The jacketing of the retrofitted Specimen R2 was carried out in a similar fashion. The placement of the new joint hoops was not made as seen in Fig.3.9(g). Nevertheless, intensive labour was still required for the surface preparation, as for Specimen R1.

For the retrofitted Specimen R3, the columns alone were retrofitted. As shown in Fig.3.9(h), no new hoops were placed in the joint core. This retrofit procedure significantly reduced the intensive labour required for jacketing of both the columns and beams.

As mentioned before, casting of the new concrete was carried out in one stage. For Specimens R1 and R2, extreme care was needed to ensure that new concrete reached the underside of the beams and that in the case of Specimen R1 the new concrete was adequately placed in the holes where new joint hoops were placed.

3.3.5 Placement of New Joint Hoops

Fig.3.11 illustrates the method used to place the new hoops in the joint core. The procedure was labour intensive but in practice the jacketing of the beams and columns with new reinforced concrete may only need to be conducted for the perimeter frames of the existing building(see Fig.3.11(a)). Jacketing only the perimeter frame would minimize the disruption of the occupants and the function of the building. Plain round bars of Grade 430 steel were

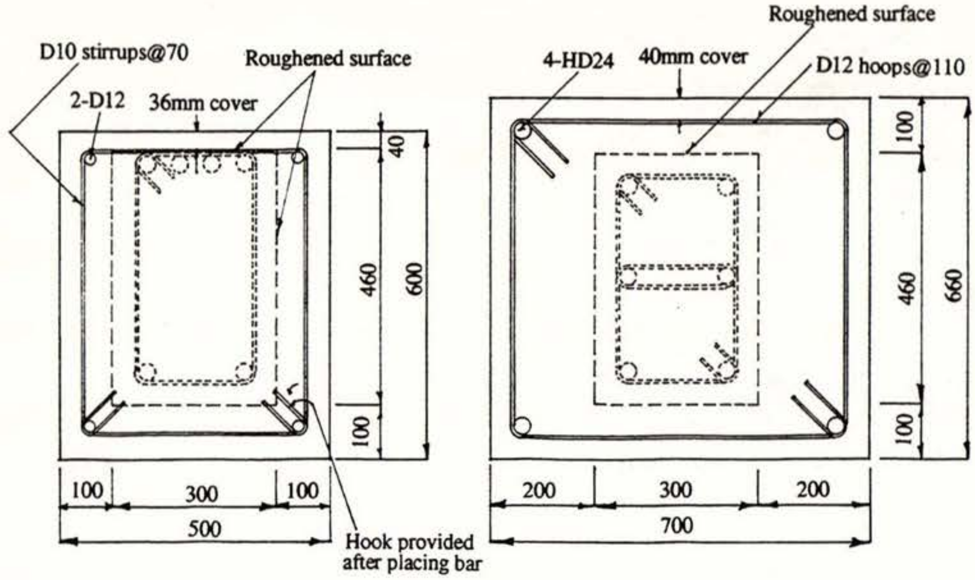

(a)Beam Section

(b)Column Section

Fig.3.10 Details of Beam and Column Sections of Retrofitted Specimen R1 and R2

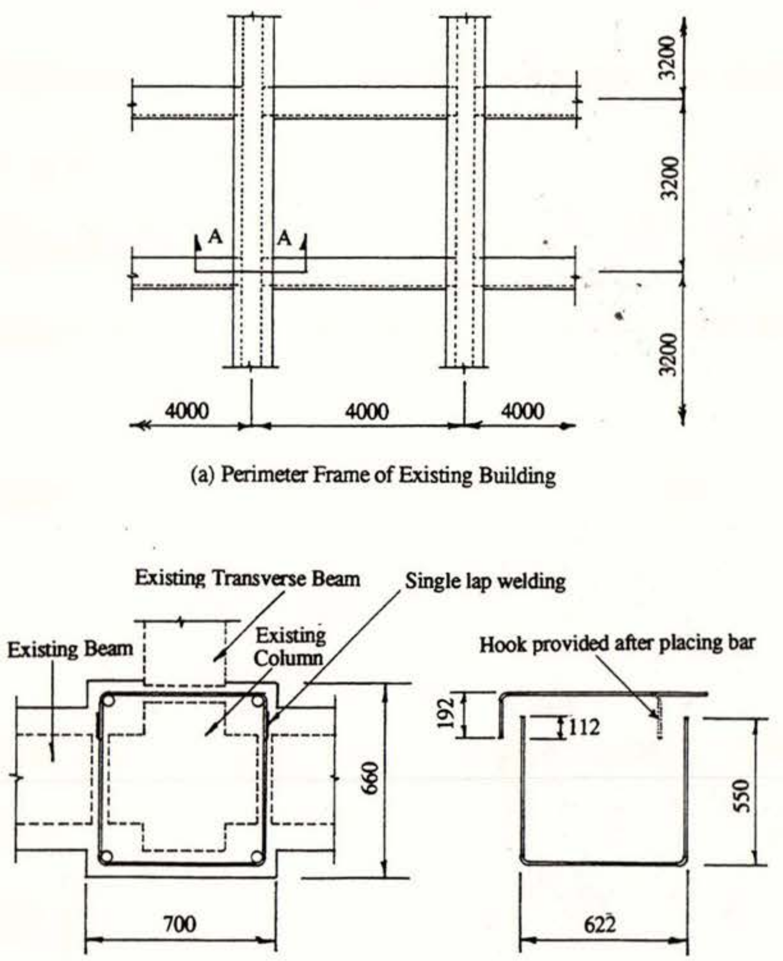

(a) Perimeter Frame of Existing Building

(b)A-A Section

(c)Shear Reinforcement for Joint (HR16)

Fig.3.11 Methods to Place New Joint Hoops used for the new joint hoops. As shown in Fig.3.11(c), new joint hoops were made from two U-shaped ties. When a transverse beam connects to the joint as shown in Fig.3.11(b), the 90 degree hook of one end of the tie which passes through the transverse beam must be provide at the construction site after placing the tie through the hole of the transverse beam(see Fig.3.11(c)). After placing the ties through holes drilled in the beams, both ties were connected by lap welding to form closed hoops as shown in Fig.3.11(b). According to SANZ 1982(b), a minimum throat thickness of $0.4d_b$ is required for the single lap welding of Grade 275 steel reinforcing bars with a minimum lap length of $9d_b$, where d_b is the bar diameter. However, when considering conditions of a construction site, the length for the lap welding is limited due to the existence of the transverse beams. Therefore, the throat thickness of $0.7d_b$ with a lap welding length of $7d_b$ was chosen in this study. Fig.3.12 shows the joint hoops after welding in the laboratory. Specimen R1 is a plane frame and no floor slab is present. It is clear that the existence of both the slabs and transverse beams of the existing building will make this welding much more difficult.

Before welding the new joint hoops of Specimen R1, tensile tests of bars welded using the procedure described above were carried out to investigate their performance. Test results and test specimens after fracture are shown in Table 3.9 and Fig.3.13, respectively. The yield strengths as well as ultimate strengths of the welded bars were somewhat larger than those of the bar itself due to the effect of heat by welding(compare with values in Table.3.10). As shown in Fig.3.13, no fracture in the welded regions were observed for three test coupons. It was concluded that the chosen welding method would not affect the joint behaviour during the test.

3.3.6 Retrofitting of the Beams of Specimens O4 and O5

During the test of Specimens O4 and O5, shear failure initiated in the beams of the test specimens. At this stage, the test was temporarily terminated. The beams were retrofitted to obtain further information about the seismic behaviour of the joint and retested. The retrofit method used for the damaged beams involved placing vertically clamped external stirrups to increase the shear resistance. As shown in Fig.3.14, the clamping action was achieved by steel rods with threads at both ends which were tightened by nuts on to channels placed across the top and bottom faces of the beams. The specified yield strength of the 20mm steel rods was 700MPa. The steel rods were placed at 300mm spacing, which was 0.6 of the overall depth of the beams, so that the maximum beam shear force associated with a beam hinge mechanism could be resisted by the steel rods as part of a truss mechanism.

Fig.3.15 shows Specimen O4 after retrofitting the beams. During the test, this retrofit technique performed quite well. The diagonal tension cracks in the beams were well

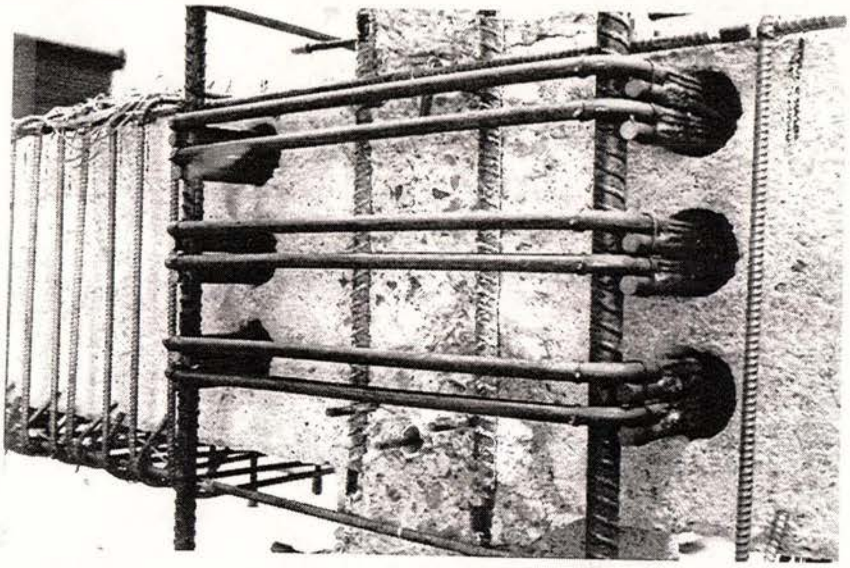

Fig.3.12 Joint Hoops after Welding of Specimen R1

Table 3.9 Test Results of Welded Bars

Grade of Steel	430			
Bar Size	HR16			
	No.1	No.2	No.3	Average
Yield Strength, f_y(MPa)	450	458	*	454
Ultimate Strength, f_u(MPa)	612	614	612	613

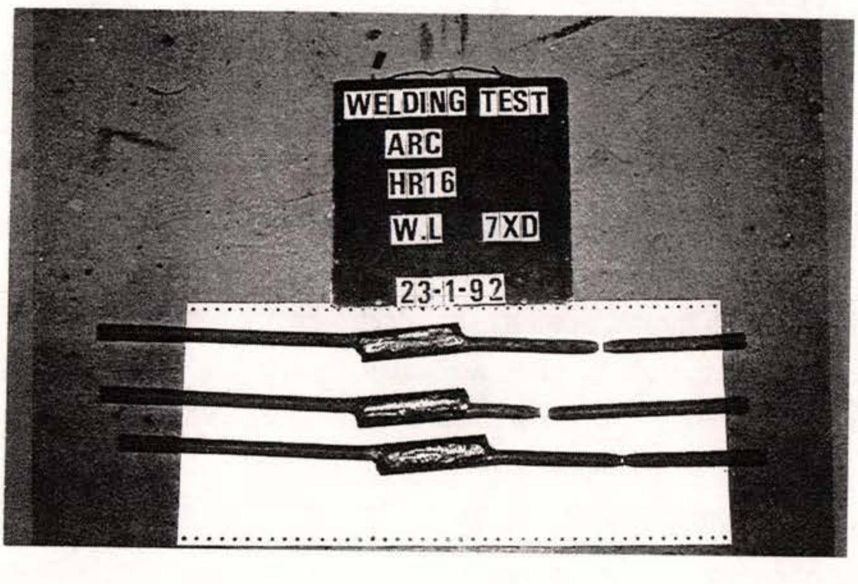

Fig.3.13 Welded Bars after Fracture

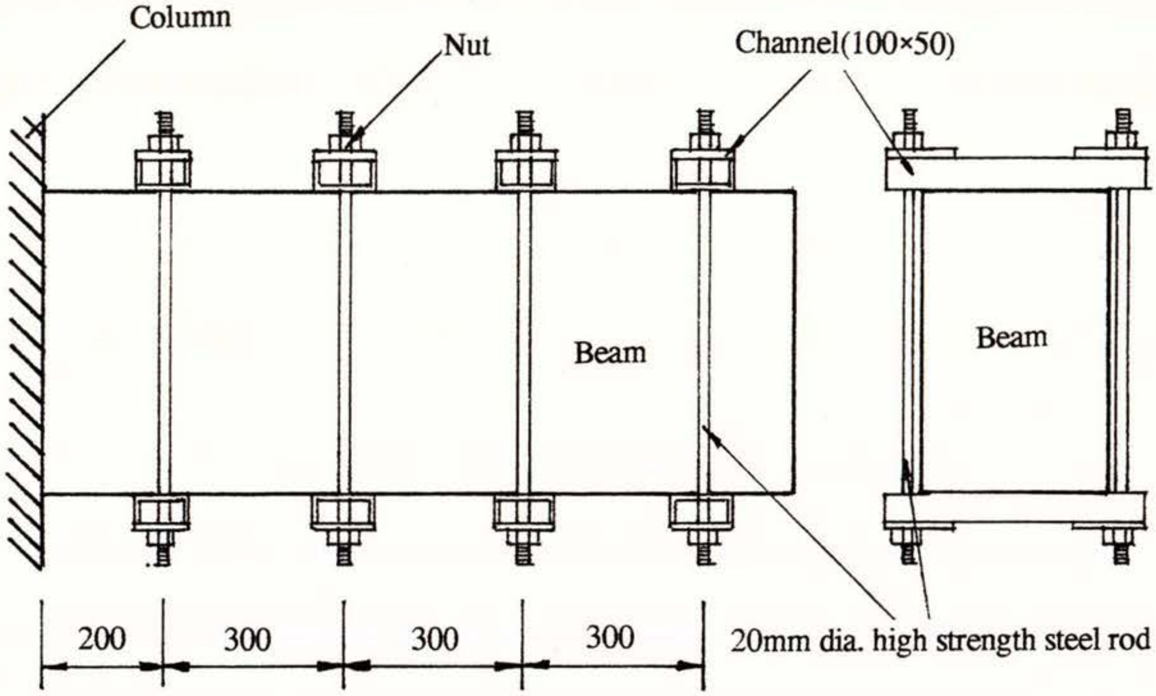

Fig.3.14 Retrofit Method for the Damaged Beam of Specimens O4 and O5

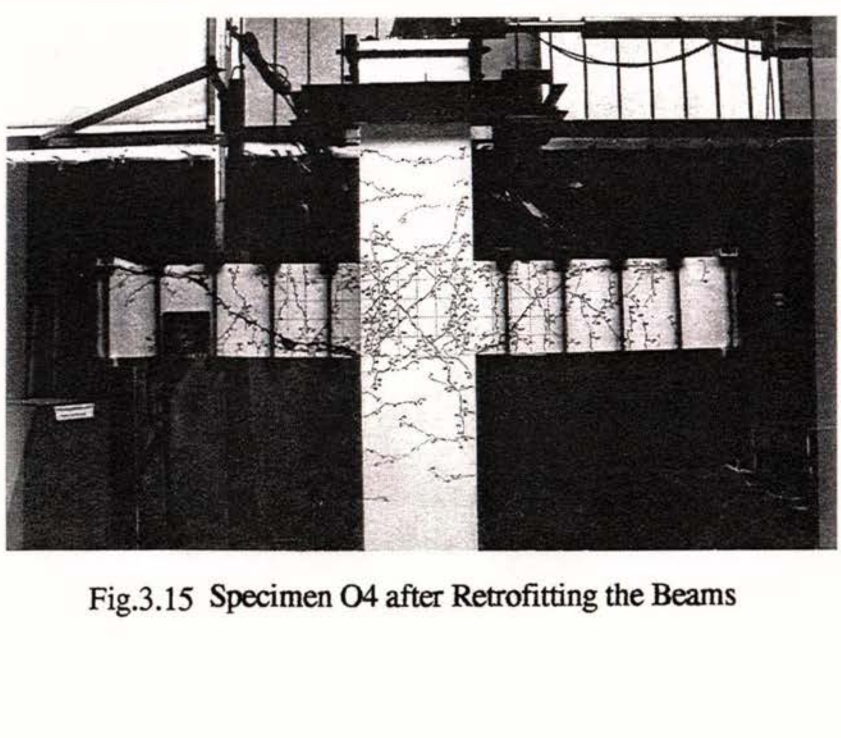

Fig.3.15 Specimen O4 after Retrofitting the Beams

confined due to the external clamping actions and the specimens were able to achieve their flexural capacity.

It can be concluded that this retrofit technique using external clamping actions can be used to increase the shear resistance of the beams damaged under cyclic loading.

3.4 MATERIAL PROPERTIES

3.4.1 Reinforcing Steel

The longitudinal reinforcement used for all test specimens were deformed bars of Grade 300 except that the new longitudinal column bars in Specimens R1 and R2 were deformed bars of Grade 430. The transverse reinforcement in the as-built specimens and Specimens O4 to O7 were plain round bars of Grade 300 while the new transverse reinforcement in the retrofitted Specimens R1 to R3 were deformed bars of Grade 300. The new joint hoops in the retrofitted Specimen R1 was plain round bar of Grade 430.

Tables 3.10 and 3.11 list the measured tensile properties of the reinforcing bars used in the test specimens. The average values obtained from three coupons are tabulated. The measured properties were obtained from monotonic loading tests by an Avery Universal Testing Machine. Typical stress-strain curves for the reinforcing steel used are plotted in Figs.3.16 and 3.17. Also shown is the clear rib spacing of the deformed bars used for the longitudinal bars. The strain was measured using a Batty Gauge Extensiometer with a gauge length of 51mm. The measured yield strengths were larger than the specified values by 1% to 33% for the Grade 300 steel bar and by 1% to 7% for the Grade 430 steel bar, respectively. As can be seen in Figs.3.16 and 3.17, earlier strain hardening was observed for the Grade 430 steel and the Grade 300 plain round bar of 6mm diameter.

3.4.2 Concrete Cylinders and Modulus of Rupture Beams

Twelve 100mm diameter × 200mm test cylinders were prepared for each test specimen. Three test cylinders were cured in a fog room at 20°C constant and approximately 100% relative humidity and tested at twenty eight days to obtain the standard 28 day compressive strength of the concrete. The other test cylinders were cured under the same conditions as the test specimens mentioned in Section 3.3.3. Three of those test cylinders were tested to determine the compressive strength of the concrete just before testing the specimens. Immediately after testing, two sets of three test cylinders were then used to obtain the compressive strength and split cylinder tensile strength, respectively. To obtain the modulus of rupture, three 120 × 120 × 480mm concrete beams were also prepared and tested under two-point loading after testing. All tests were carried out by an Avery Universal Testing

Table 3.10 Measured Reinforcing Steel Properties used for Specimens O1, R1 and R2

Grade of Steel	300				430	
Bar Size	R6	D10	D12	D24	HR16	HD24
Yield Strength, f_y(MPa)	339	330	302	325	436	462
Yield Strain, ε_y	0.00161	0.00182	0.00143	0.00175	0.00214	0.00231
Strain at commencing strain hardening, ε_{sh}	0.0946	0.304	0.368	0.195	0.189	0.146
Ultimate Strength, f_u(MPa)	463	451	422	481	599	613

Note : R6=plain round bar of 6mm diameter
D10=deformed bar of 10mm diameter
HR16=plain round high strength bar of 16mm diameter
HD24=deformed high strength bar of 24mm diameter
Each value was obtained from the average of three coupons

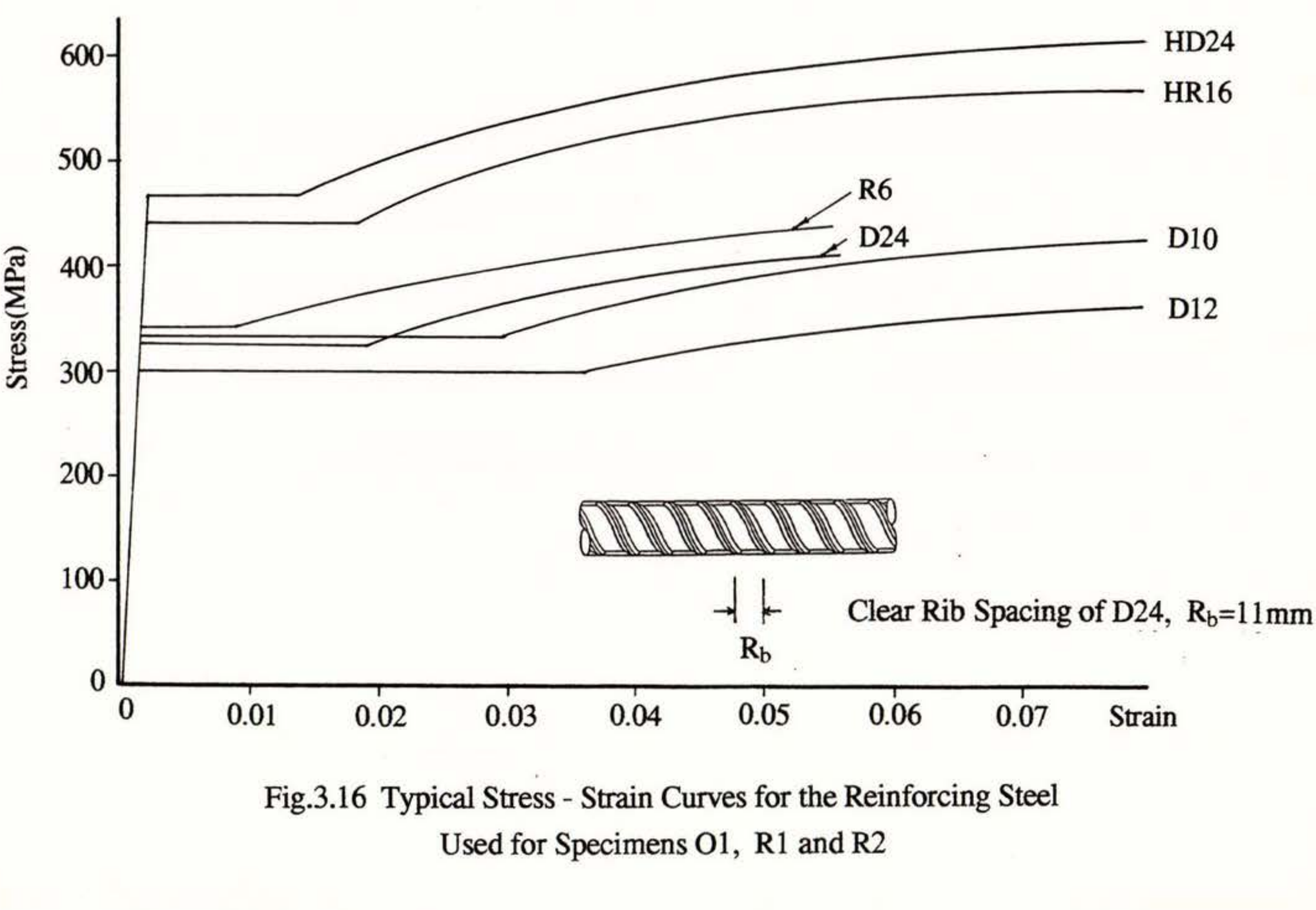

Fig.3.16 Typical Stress - Strain Curves for the Reinforcing Steel
Used for Specimens O1, R1 and R2

Table 3.11 Measured Reinforcing Steel Properties used for Specimens R3 and O4 to O7

Grade of Steel	300				
Bar Size	R6	D12	D24	D28	D32
Yield Strength, f_y(MPa)	398	358	308	321	306
Yield Strain, ε_y	0.00206	0.00167	0.00165	0.00170	0.00160
Strain at commencing strain hardening, ε_{sh}	0.0205	0.0077	0.0206	0.0236	0.0193
Ultimate Strength, f_u(MPa)	505	476	462	480	479

Note : R6=plain round bar of 6mm diameter

D12=deformed bar of 12mm diameter

Each value was obtained from the average of three coupons

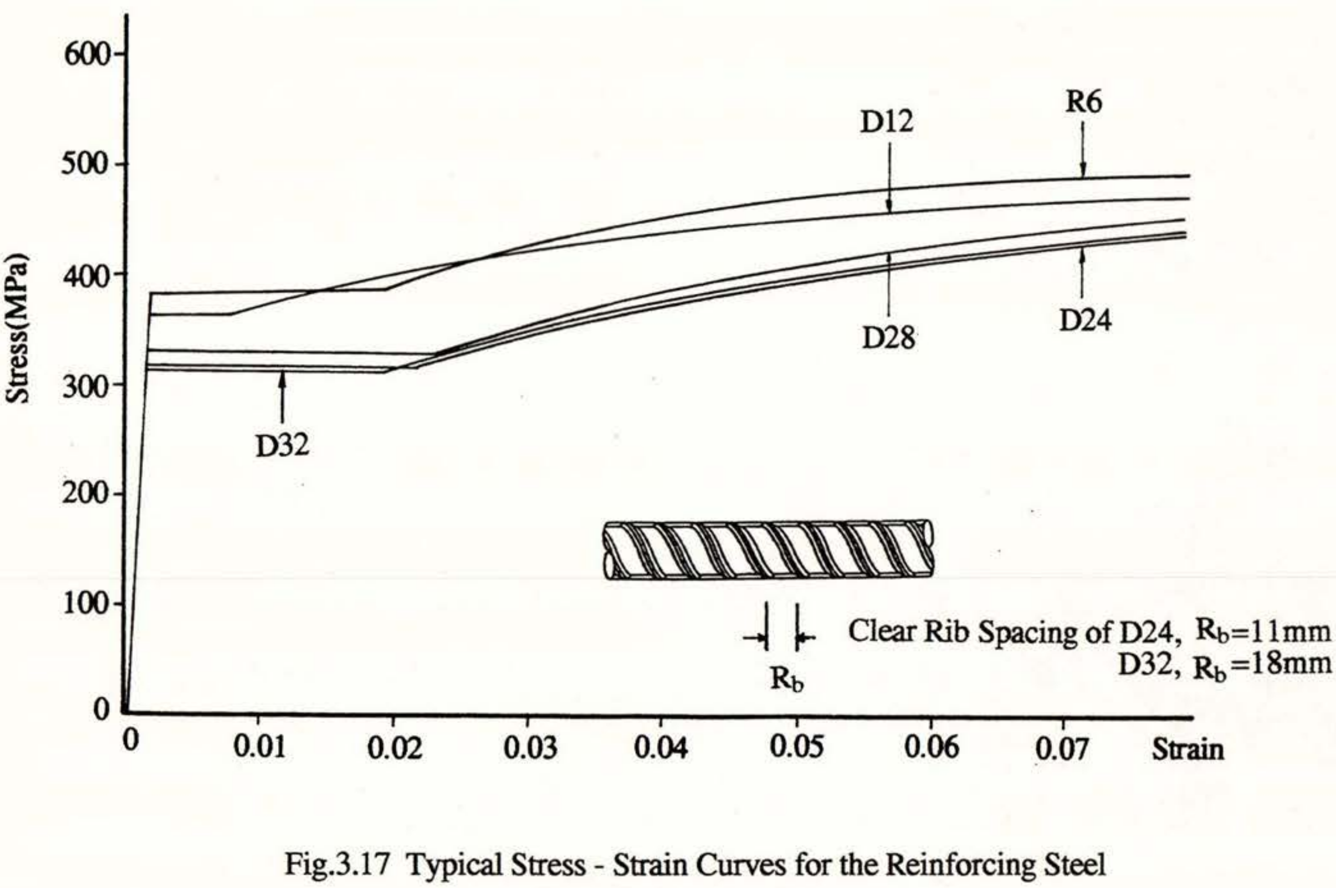

Fig.3.17 Typical Stress - Strain Curves for the Reinforcing Steel
Used for Specimens R3 and O4 to O7

Table 3.12 Measured Concrete Properties

		slump (mm)	At 28days f'c(MPa)	Just before testing f'c(MPa)	Immediately after testing f'c(MPa)	ft(MPa)	fr(MPa)
Specimen O1	original concrete	55	33.7	40.7 (107days)	44.8 (114days)	4.25 (114days)	4.30 (114days)
Specimen R1	original concrete	55	33.7	42.3 (175days)	42.7 (189days)	3.91 (189days)	
	jacketing concrete	150	40.1	54.4 (42days)	58.8 (56days)	3.80 (56days)	
Specimen R2	original concrete	125	35.4	43.4 (182days)	42.0 (186days)	4.11 (186days)	5.12 (186days)
	jacketing concrete	180	47.9	61.4 (38days)	59.9 (42days)	4.46 (42days)	3.34 (42days)
Specimen R3	original concrete	125	35.7	43.4 (182days)	46.7 (186days)	4.40 (186days)	5.03 (186days)
	jacketing concrete	130	32.8	42.0 (38days)	40.8 (42days)	4.09 (42days)	4.58 (42days)
Specimen O4	original concrete	56	40.8	52.9 (81days)	53.0 (100days)	4.45 (100days)	5.46 (100days)
Specimen O5	original concrete	75	26.9	32.8 (54days)	35.1 (63days)	3.68 (63days)	5.02 (63days)
Specimen O6	original concrete	110	30.8	34.3 (69days)	34.3 (74days)	3.78 (74days)	4.48 (74days)
Specimen O7	original concrete	75	27.4	31.0 (43days)	32.2 (48days)	3.22 (48days)	3.65 (48days)

Note : f'_c=compressive strength of 100mm dia. × 200mm concrete cylinder

f_t=split cylinder tensile strength

f_r=modulus of rapture of 120 × 120 × 480mm concrete prism under two-point loading

Each value was obtained from the average of three specimens

(43days)=age is 43 days

Table 3.13 Weighted Average Concrete Compressive Strengths Before Testing

	Beam f'_c*(MPa)	Column f'_c*(MPa)
Specimen R1	48.4	50.8
Specimen R2	52.4	56.0
Specimen R3	not retrofitted	42.4

Machine with monotonic loading applied. The average values obtained from the tests are shown in Table 3.12. In this study, the compressive strengths obtained just before testing were used to calculate the initial stiffnesses and strengths of the test specimens.

The measured compressive strengths were larger than the specified compressive strength of 30MPa by 3% to 76% and of 40MPa by 2% to 54%. In terms of $\sqrt{f'_c}$, the mean split cylinder tensile strength f_t was $0.61\sqrt{f'_c}$ while the mean modulus of rupture f_r was $0.74\sqrt{f'_c}$, where f'_c is the measured compressive strength of concrete.

The retrofitted specimens consisted of two different concretes. To estimate the concrete compressive strengths in those members, a weighted average concrete compressive strength $f'_c{}^*$ was defined in this study. The weighted average concrete compressive strength was given by

$$f'^*_c = \frac{A_1 f'_{c1} + A_2 f'_{c2}}{A_1 + A_2} \tag{3.1}$$

where A_1 =cross section area of original member

A_2 =cross section area of jacket around original member

f'_{c1}=measured compressive strength of original concrete

f'_{c2}=measured compressive strength of jacket concrete

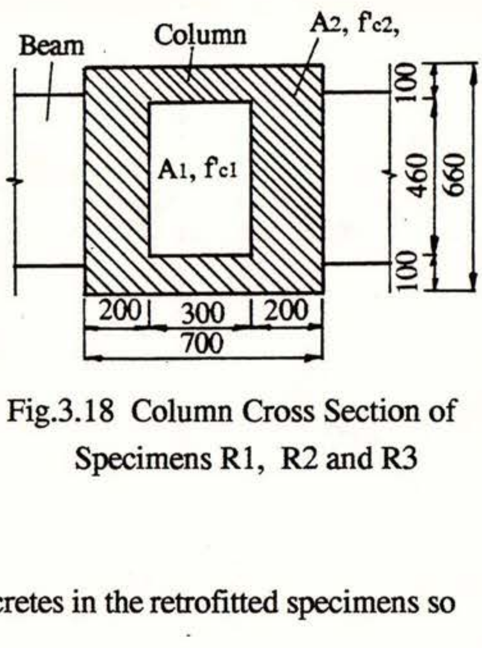

Fig.3.18 Column Cross Section of Specimens R1, R2 and R3

The weighted average compressive strengths of concretes in the retrofitted specimens so obtained are shown in Table 3.13.

3.5 LOADING SYSTEM

In order to simulate the seismic loading, two loading systems were designed for this experimental programme. They are shown in Figs.3.19 to 3.22.

The ends of the members of the subassemblages coincide with the mid-span and mid-storey height points of the building frame being investigated. The ends of the members were connected to steel plates by steel rods with threaded ends which were embedded in the specimens(see Figs.3.1 to 3.8). This connection allowed the applied forces to be distributed

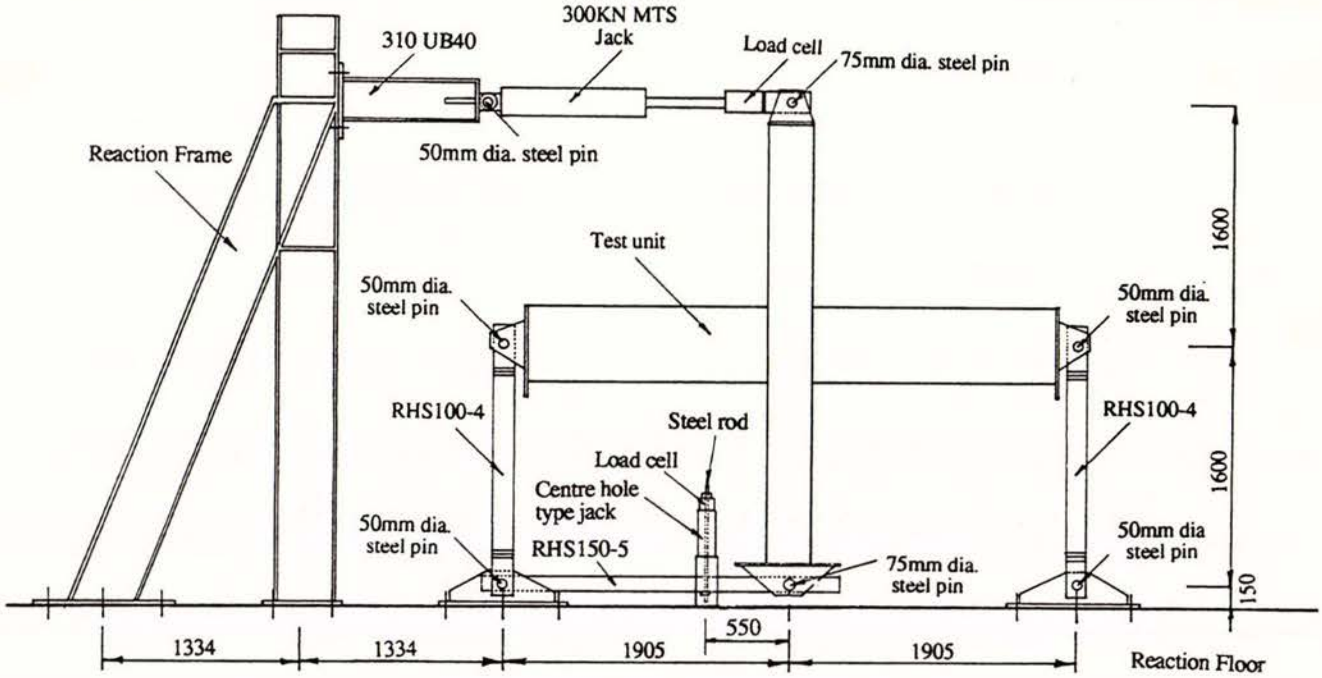

Fig.3.19 Loading Rig for Specimen O1

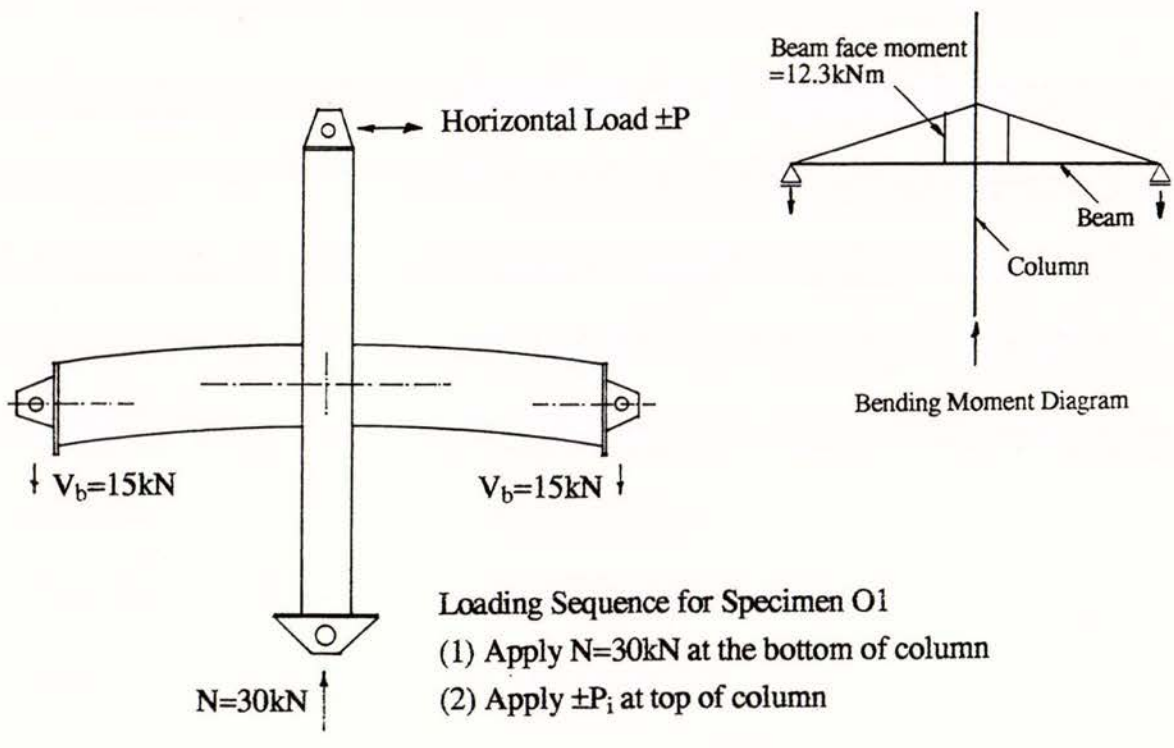

Loading Sequence for Specimen O1

(1) Apply N=30kN at the bottom of column

(2) Apply $\pm P_i$ at top of column

Fig.3.20 Simulated Gravity Loading for Specimen O1

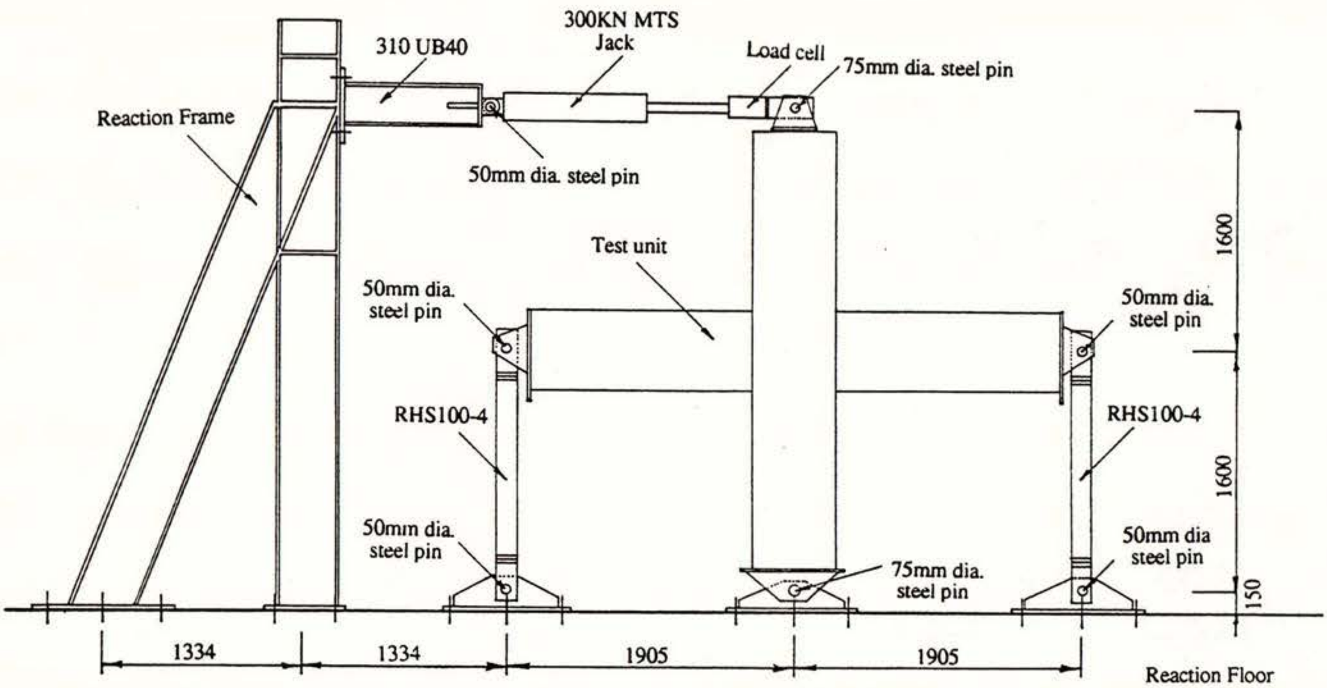

Fig.3.21 Loading Rig for Specimens R1 to R3 and O4 to O5

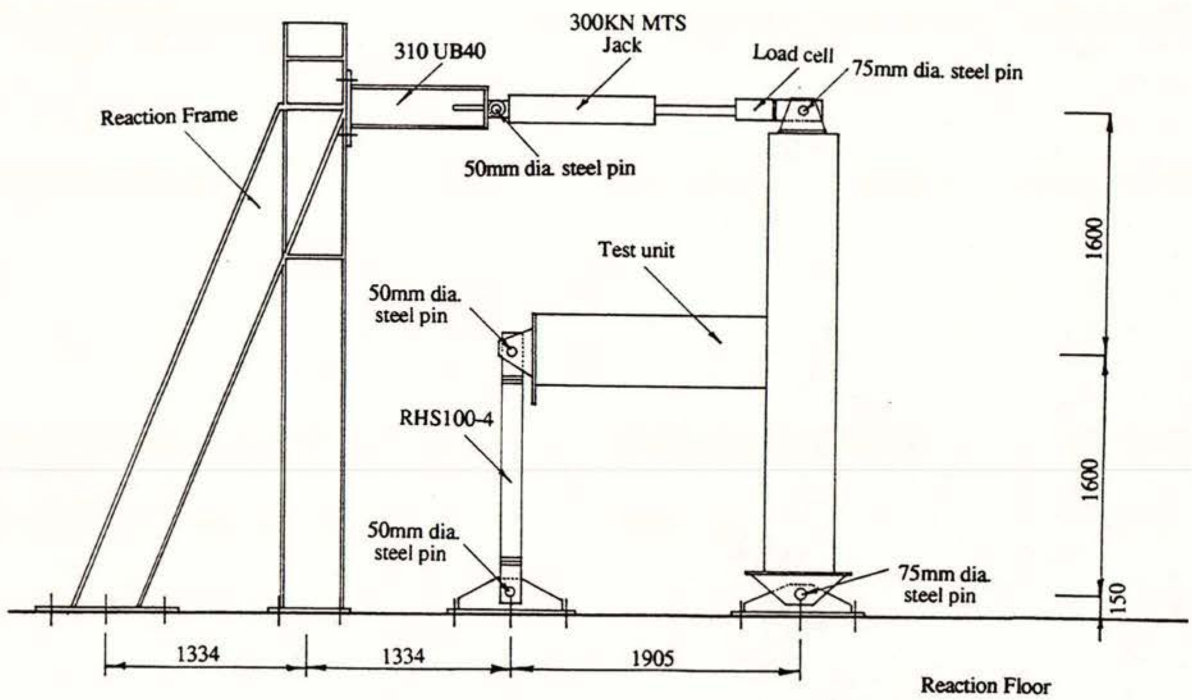

Fig.3.22 Loading Rig for Specimens O6 and O7

over the cross sections of the members. The steel end plates were connected by pins to the loading rig which allowed free rotation. Horizontal cyclic load P was applied to the ends of the columns of the test specimens using a double acting 300kN capacity hydraulic jack. The ends of the beams were held against vertical displacement. No axial loads were applied to the column, that being the most unfavourable condition for the joint core.

Fig.3.19 shows the loading system designed for the as-built Specimen O1. Specimen O1 was expected to develop plastic hinges in the columns. The end of the bottom column was held against horizontal displacement using a steel member, both ends of which were connected by steel pins, allowing free elongation of the bottom column. In order to simulate the negative moment in the beams at the column faces due to gravity load, the end of the bottom column of Specimen O1 was lifted up by a centre hole jack acting through a steel rod connected to the pinned steel member as shown in Figs.3.19 and 3.20.

Fig.3.21 shows the loading system for Specimens R1 to R3 and Specimens O4 to O5, while that for Specimens O6 and O7 is shown in Fig.3.22. Those specimens were expected to develop plastic hinges in the beams. As shown in Figs.3.21 and 3.22, the bottom columns were not allowed free elongation. This would induce some axial load in the bottom column.

3.6 TEST SEQUENCE

All test specimens were loaded under quasi-static simulated seismic loading except that the as-built Specimen O1 was loaded under both simulated seismic and gravity loading.

As mentioned in the previous section, the bottom column of Specimen O1 was lifted up to induce the beam negative moment at the column faces before the simulated seismic loading was applied to the specimen(see Fig.3.20). In this study, the beam negative moment at the column faces due to gravity load was selected to be 12.3kNm. This was obtained from the assumption that the average weight of floor in the building investigated was 8kPa. The beam negative moment due to gravity load was held constant during the test.

The quasi-static cyclic loading applied to all test specimens is shown in Fig.3.23. The first two cycles were load controlled and the remainder of the test was displacement controlled.

In all tests, two cycles of horizontal loading to $\pm 0.5P_i$ and $\pm 0.75P_i$ were initially applied, where P_i is the horizontal load at the top of the column associated with the theoretical flexural strength M_i being reached at the critical sections of the members, calculated using the conventional compressive stress block for the concrete with an extreme fibre concrete compressive strain of 0.003 and the measured concrete compressive cylinder strength and the

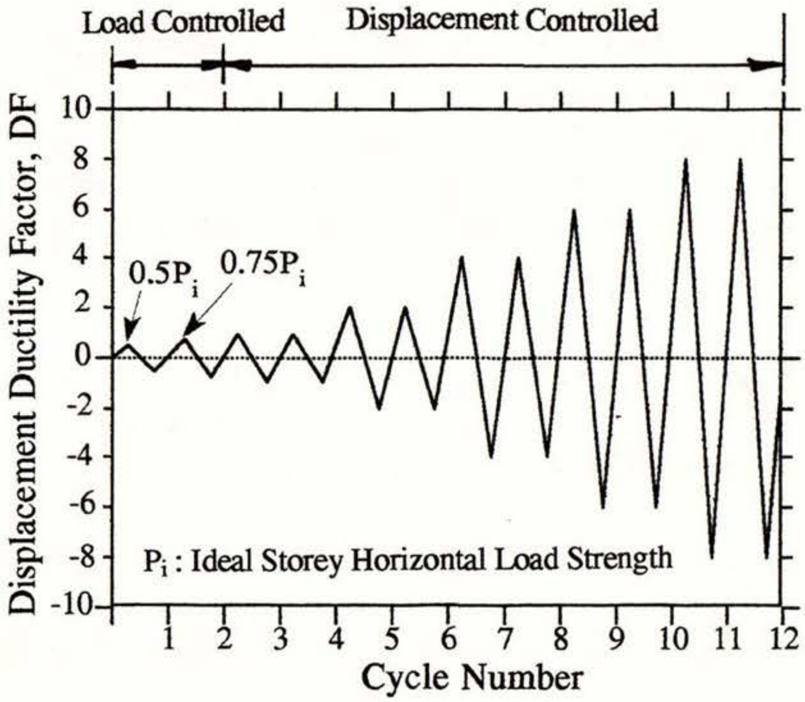

Fig.3.23 Cyclic Lateral Loading and Displacement History Applied to the Test Specimens

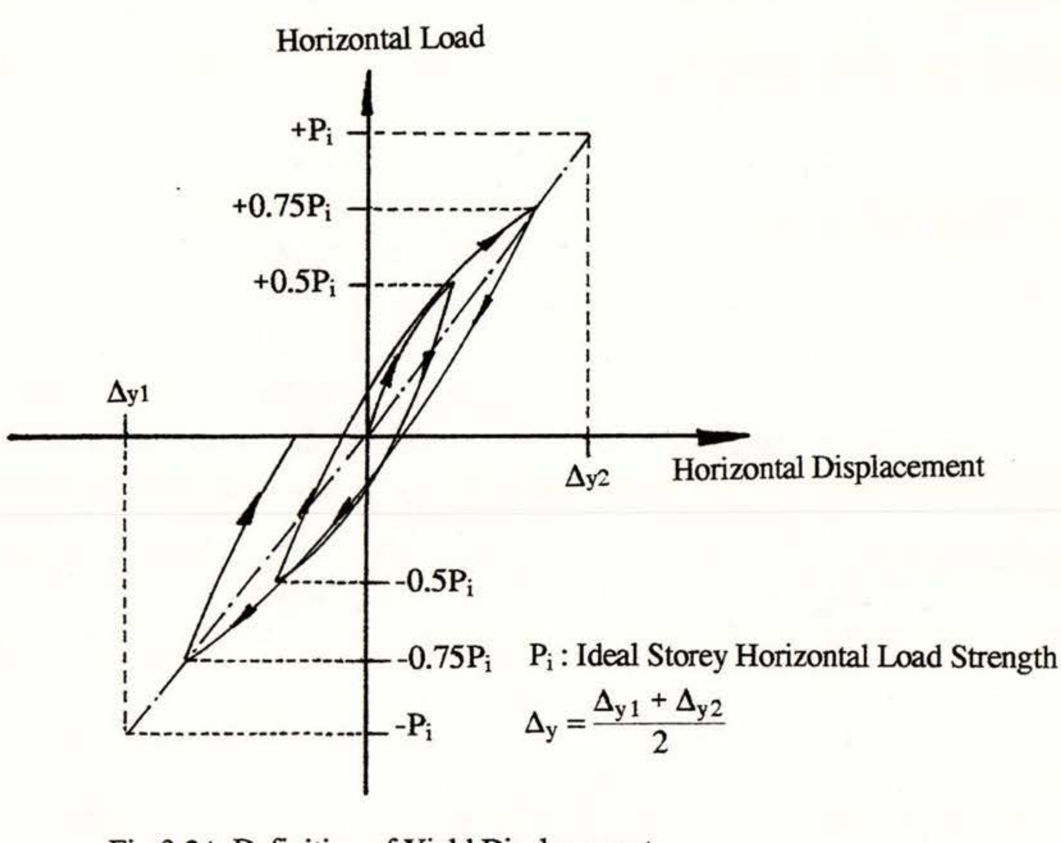

Fig.3.24 Definition of Yield Displacement

steel yield strengths. The yield displacements Δ_y for all test specimens were calculated using the stiffness at the interstorey horizontal displacement measured at $0.75P_i$, extrapolated linearly to P_i(see Fig.3.24). The applied cyclic loading in the inelastic range was displacement controlled. The test specimens were subjected to two cycles of loading to DF of ± 1, ± 2, ± 4, ± 6 and ± 8, where DF is the displacement ductility factor defined as Δ/Δ_y where Δ is the interstorey horizontal displacement of the test specimen. The initial stiffness of the test specimen K_e was then given by

$$K_e = \frac{P_i}{\Delta_y} \tag{3.2}$$

The procedures to obtain the interstorey horizontal displacement of the test specimen will be described later in this chapter.

In this study, the interstorey drift is also used as an index for the level of the displacement imposed on the test specimens. The interstorey drift can be obtained by dividing the interstorey horizontal displacement by the storey height. However, caution must be adopted in the use of this index because the imposed displacement needs to be related to the stiffness of the specimen and the displacement ductility factor[Park 1989].

3.7 INSTRUMENTATION

3.7.1 Measurement of Loads

A 300kN capacity load cell was used to measure the horizontal load, or storey shear force applied to the specimens(see Fig.3.19). Two full-bridge circuits were installed in the load cell. One circuit was connected to a X-Y recorder to monitor the applied horizontal load during the test. The other circuit was connected to a data logger unit.

In order to obtain the beam end forces, wire strain gauges forming a full bridge were attached on the steel columns connected at the end of the beams(see Fig.3.19).

The load cell and the instrumented steel columns were calibrated in compression by an Avery Universal Testing Machine. It was assumed that the tensile characteristics of the load cell and the instrumented steel columns would be the same as those obtained in compression.

The horizontal load was measured with a resolution of 0.52kN and within 1.0kN error while the measurements of the beam end forces were made with a resolution of 0.71kN and within 2.2kN error.

3.7.2 Measurement of Horizontal Displacement

Six linear potentiometers were used to estimate the interstorey horizontal displacement of the test specimens. Fig.3.25 shows the positions of those linear potentiometers on the test specimen. In order to estimate the horizontal displacement at the top column end pin, two linear potentiometers with 300mm travel were used. The horizontal displacement measured at the top face of the column(point 1 in Fig.3.25) was connected to the X-Y recorder so that a plot of the applied horizontal load versus the horizontal displacement could be obtained. This assisted in controlling the imposed horizontal loading in the displacement controlled cycles. Another two linear potentiometers with 100mm travel measured the horizontal displacement at the bottom column end pin. Those measurements made it possible to calculate the gross horizontal displacement at the top column end pin relative to the bottom column end pin of the test specimen. However, the horizontal displacement so obtained includes the horizontal displacement due to rigid body rotation of the specimen. Two vertical linear potentiometers with 50mm travel were used to estimate the horizontal displacement due to rigid body rotation except that for Specimens O6 and O7, one vertical linear potentiometer was used(see Fig.3.25).

The interstorey horizontal displacements of the test specimens were then estimated from the following equations:

$$\text{For interior joints : } \Delta=(\Delta_1+\frac{\Delta_1-\Delta_2}{500}150) - (\Delta_4 - \frac{\Delta_3-\Delta_4}{200}300) - (\Delta_5-\Delta_6)\frac{3200}{2910} \quad (3.3)$$

$$\text{For exterior joints : } \Delta=(\Delta_1+\frac{\Delta_1-\Delta_2}{500}150) - (\Delta_4 - \frac{\Delta_3-\Delta_4}{200}300) - \Delta_5\frac{3200}{1455} \quad (3.4)$$

where Δ is the interstorey horizontal displacement and Δ_1 to Δ_6 are the displacements measured at points 1 to 6, respectively(see Fig.3.25). The interstorey horizontal displacement so calculated is referred to as the horizontal displacement of the test specimen in this study.

3.7.3 Measurement of Average Curvatures and Shear Distortions

A large number of liner potentiometers with 30 or 50mm travel were used to obtain the average curvatures and shear distortions. The linear potentiometers were mounted on steel brackets screwed into the 10mm steel rods embedded in the concrete or welded on the main beam bars. Figs.3.26 to 3.29 illustrate the locations of the linear potentiometers on the test specimens.

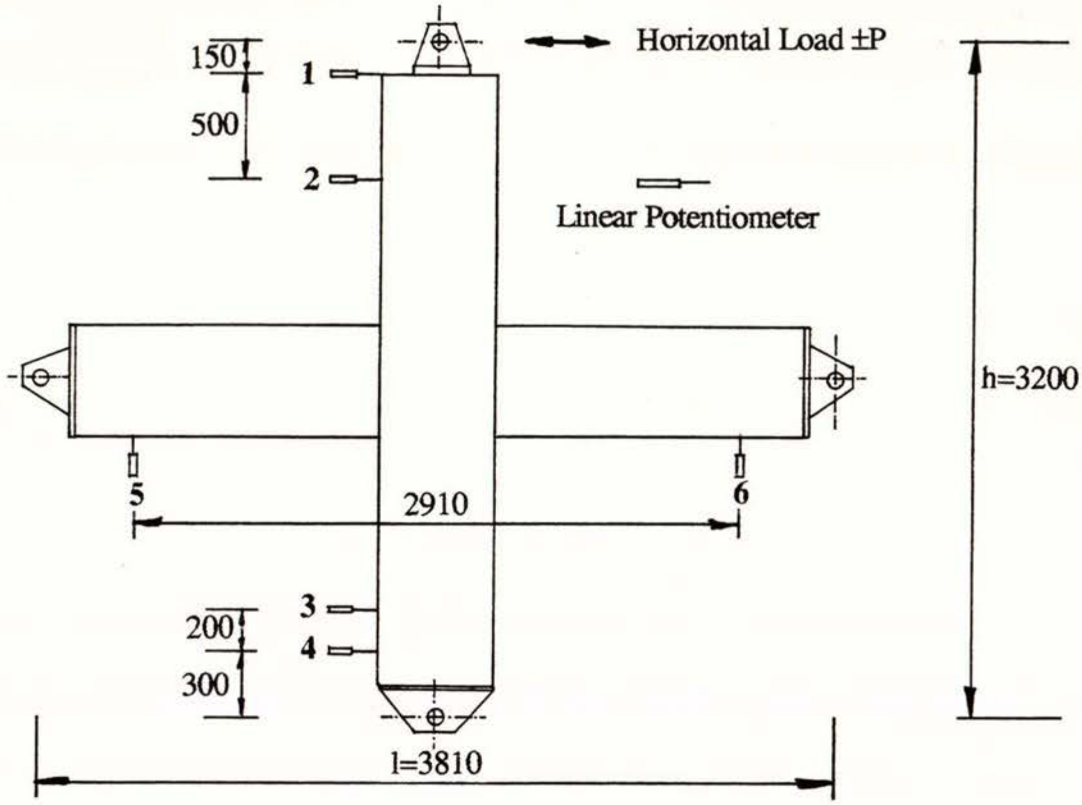

(a) Interior Joint

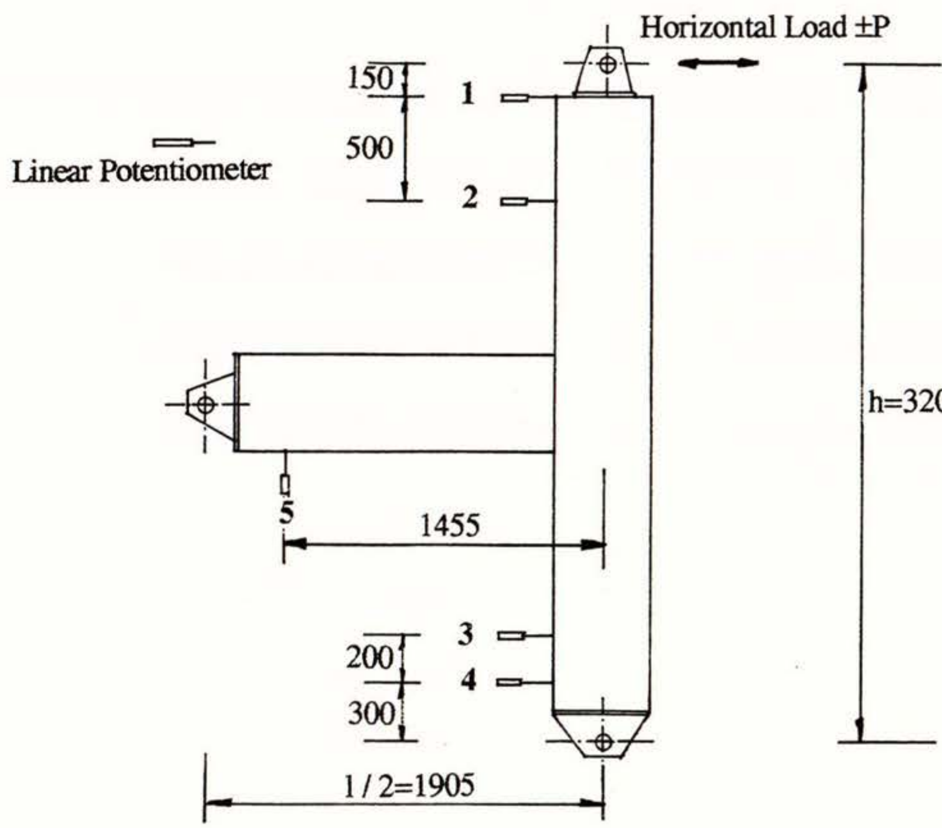

(b) Exterior Joint

Fig.3.25 Positions of Linear Potentiometers to Measure the Horizontal Displacement

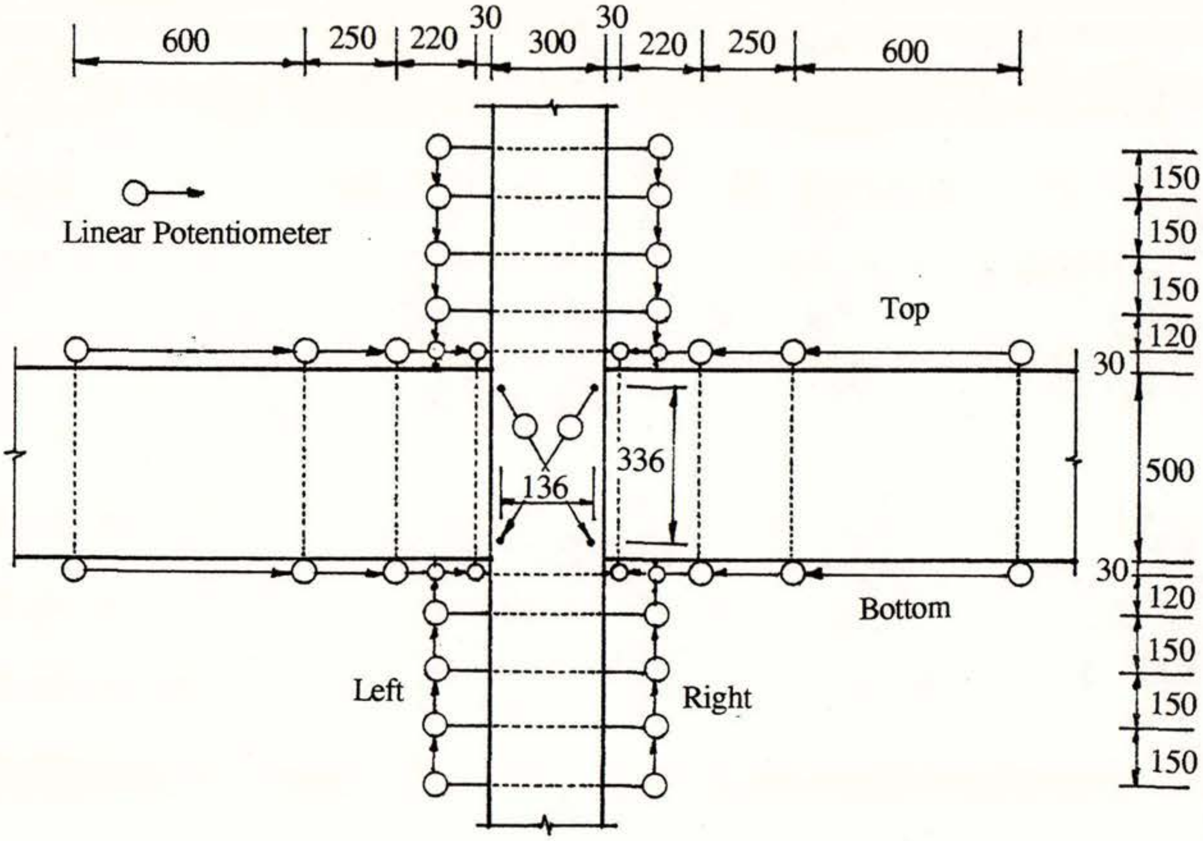

Fig.3.26 Locations of Linear Potentiometers for Specimen O1

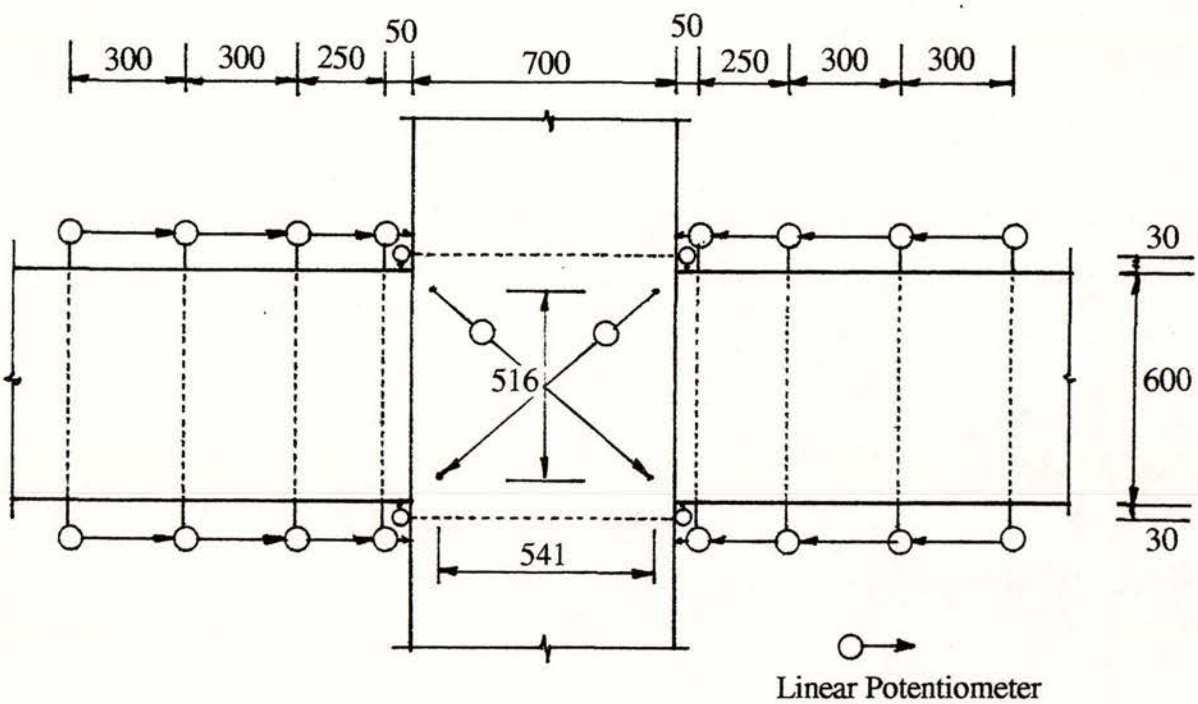

Fig.3.27 Locations of Linear Potentiometers for Specimens R1 and R2

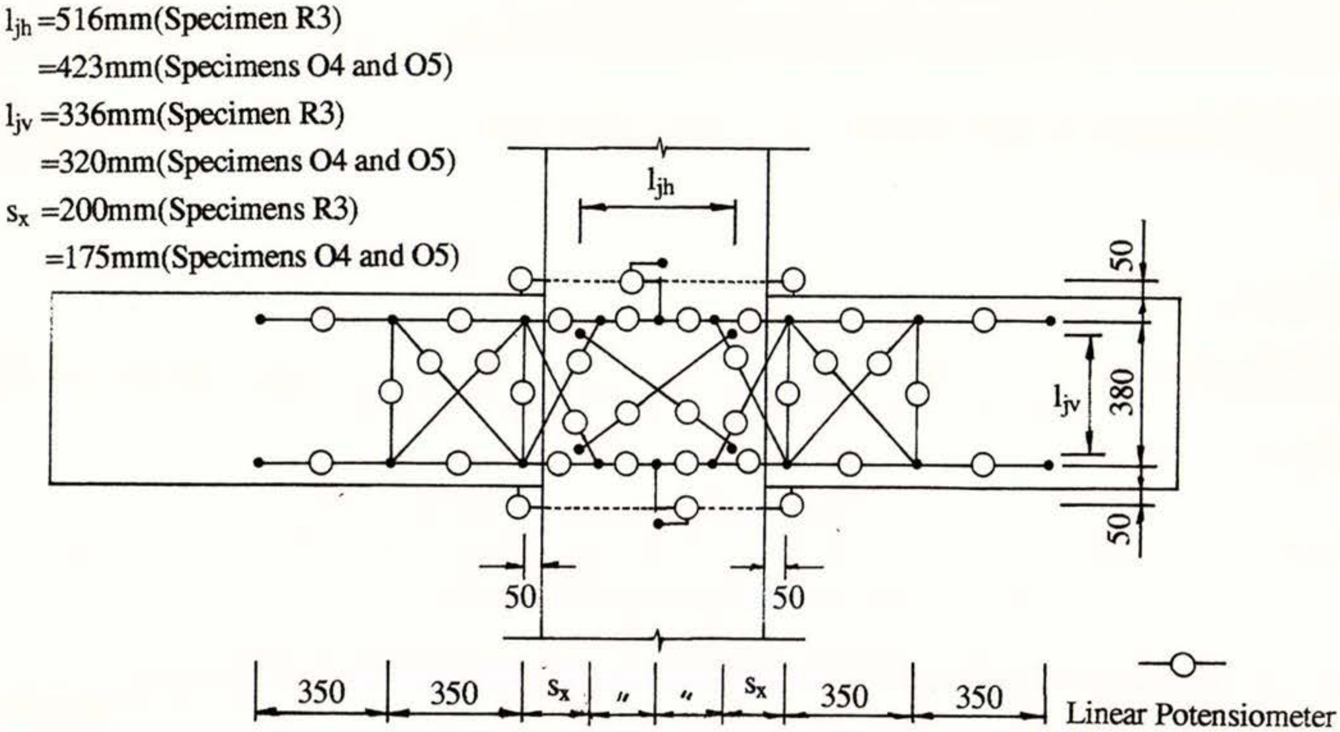

Fig.3.28 Locations of Linear Potentiometers for Specimens O4 and O5

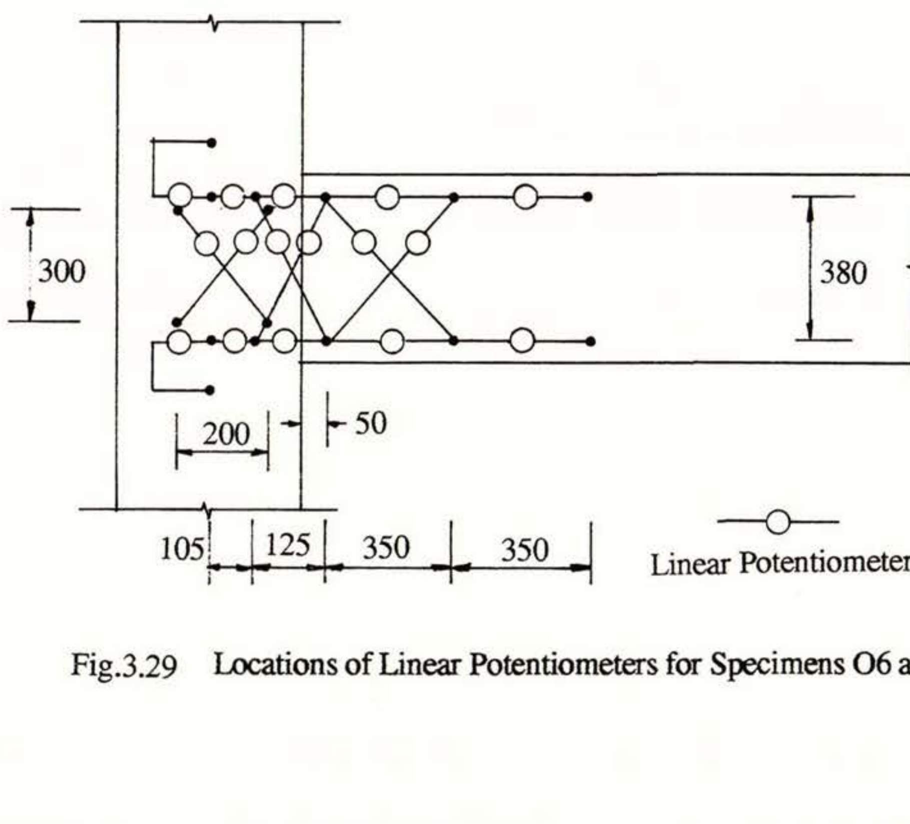

Fig.3.29 Locations of Linear Potentiometers for Specimens O6 and O7

The average curvatures of the beams were estimated for all specimens. As shown in Fig.3.30, a pair of linear potentiometers measured the average rotation over a region. From these measurements, the average curvature could be derived over the region as follows:

$$\phi_{b,i} = \theta_{b,i} / s_i \tag{3.5}$$

$$\theta_{b,i} = ({}_t\delta_i - {}_b\delta_i) / h_i \tag{3.6}$$

where $\phi_{b,i}$ is the average curvature over the region i in the beam, $\theta_{b,i}$ is the rotation measured over the region i in the beam, s_i is the gauge length of the region i in the beam, ${}_t\delta_i$ and ${}_b\delta_i$ are the top and bottom displacements measured over the region i in the beam, and h_i is the distance between top and bottom linear potentiometers in the region i(see Fig.3.30).

The average curvatures of the columns were also estimated for Specimen O1 in which column plastic hinge mechanisms were expected. Using the same method as above, the average column curvature is given by

$$\phi_{c,i} = \theta_{c,i} / s'_i \tag{3.7}$$

$$\theta_{c,i} = ({}_r\delta_i - {}_l\delta_i) / h'_i \tag{3.8}$$

where $\phi_{c,i}$ is the average curvature over the region i in the column, $\theta_{c,i}$ is the rotation measured over the region i in the column, s'_i is the gauge length of the region i in the column, ${}_r\delta_i$ and ${}_l\delta_i$ are the left and right displacements measured over the region i in the column(see Fig.3.26), and h'_i is the distance between left and right linear potentiometers in the region i.

The average shear distortions in the critical regions of the beams were estimated for Specimen R3 and Specimens O4 to O7 using the method shown in Fig.3.31. Assuming that the rotation due to flexure in the region is constant, the average shear distortion γ_s can be obtained from the change in the length of the two diagonals as follows:

$$\gamma_s = \frac{\delta_s - \delta'_s}{2l_s}\left(\tan\alpha_s + \frac{1}{\tan\alpha_s}\right) \tag{3.9}$$

where δ_s and δ'_s are the changes in the lengths of the diagonals, l_s is the initial length of the diagonal and α_s is the angle of the diagonal to the beam axis(see Fig.3.31).

3.7.4 Measurement of Beam Bar Slip

The slip of the longitudinal beam bars passing through the beam-column joint was estimated for Specimen R3 and Specimens O4 to O7. As shown in Fig.3.32, the slip was defined as the relative displacement measured between a steel rod embedded in the concrete of the column at the column centre line and a target steel rod welded to the longitudinal bar in the

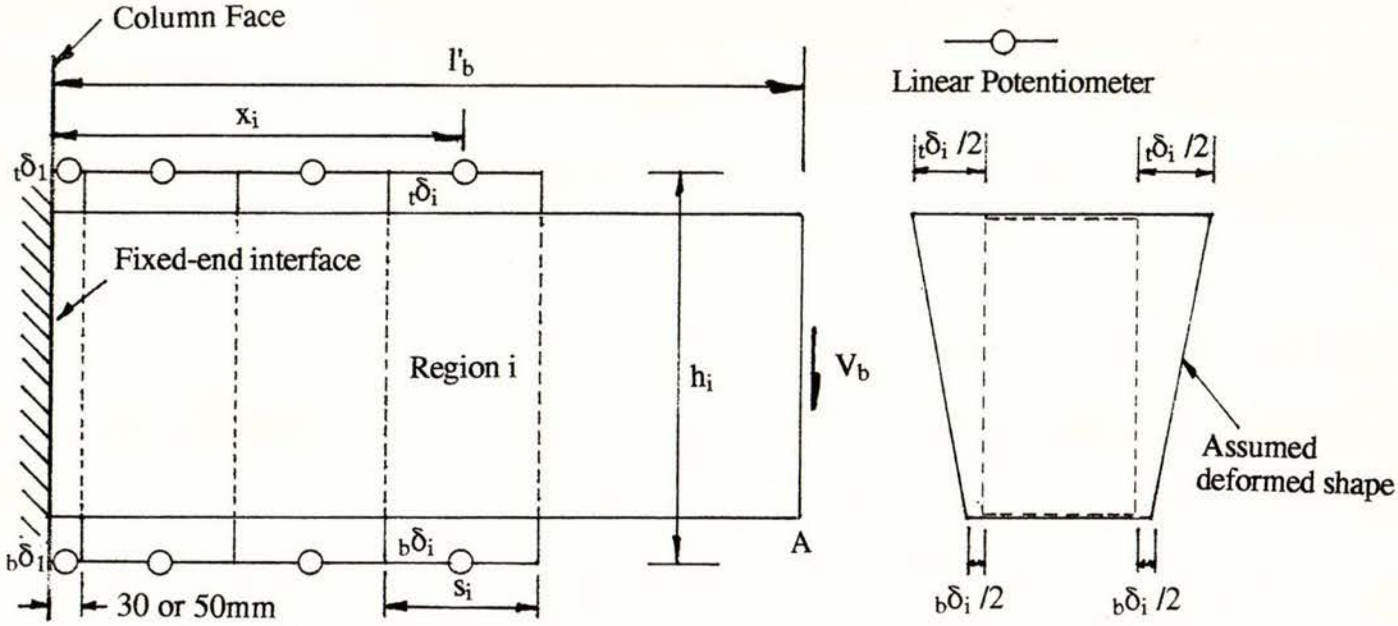

Curvature $:\phi_{b,i}=\theta_{b,i}\,/\,s_i$

Rotation $:\theta_{b,i}=({}_t\delta_i - {}_b\delta_i)\,/\,h_i$

Fixed-end rotation $:\theta_{b,fe}=({}_t\delta_1 - {}_b\delta_1)\,/\,h_1$

Deformation at A due to flexure : $\delta_{b,f}=\Sigma\dfrac{({}_t\delta_i - {}_b\delta_i)}{h_i}(l'_b - x_i)$

Deformation at A due to fixed-end rotation : $\delta_{b,fe}=\theta_{b,fe}l'_b$

Fig.3.30 Estimation of Fixed-End Rotation, Curvature and Flexural Deformation

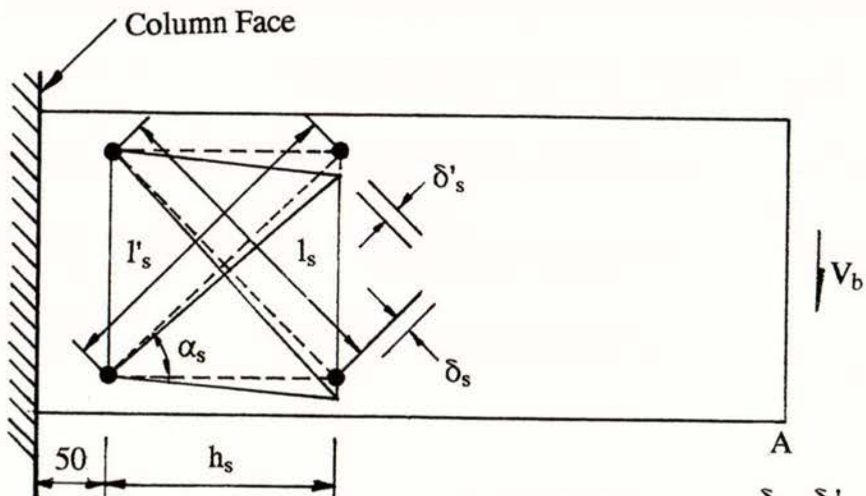

Shear distortion $:\gamma_s=\dfrac{\delta_s-\delta'_s}{2l_s}(\tan\alpha_s+\dfrac{1}{\tan\alpha_s})$

Shear deformation at A : $\delta_{b,s}=\gamma_s h_s$

Fig.3.31 Estimation of Beam Shear Distortion and Shear Deformation

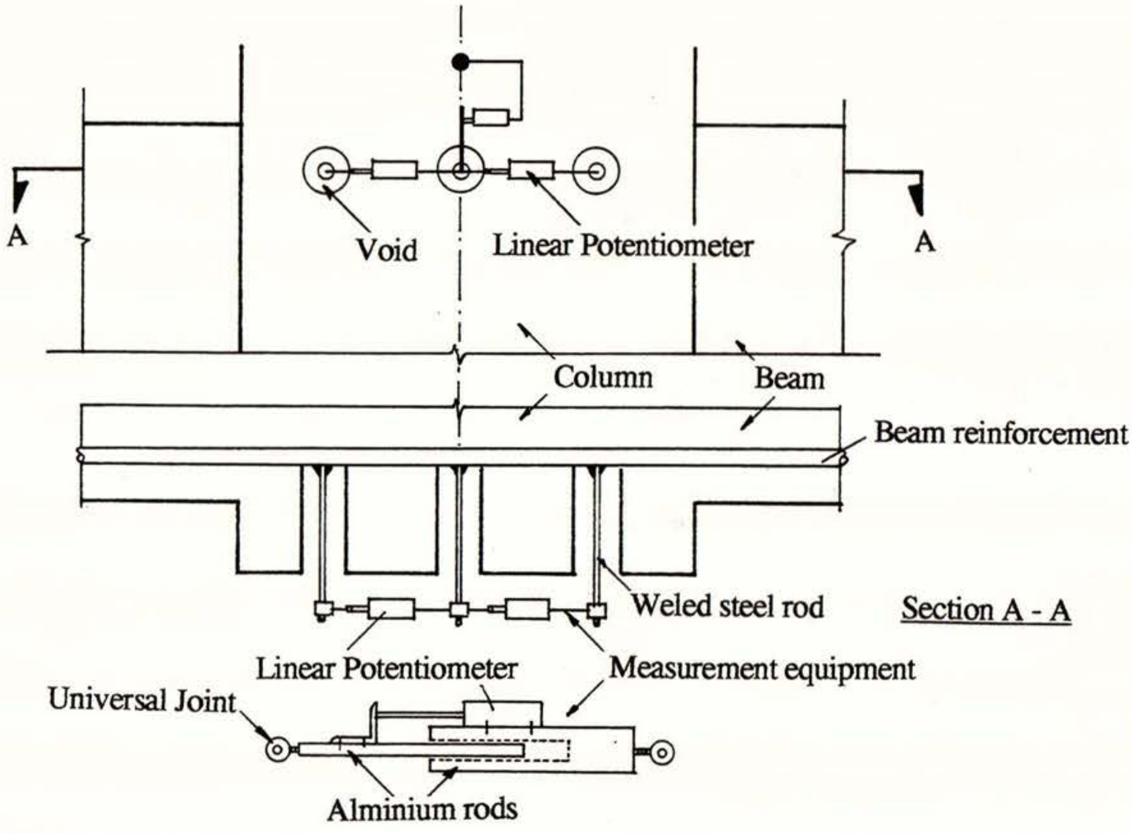

Fig.3.32 Estimation of Beam Bar Slip

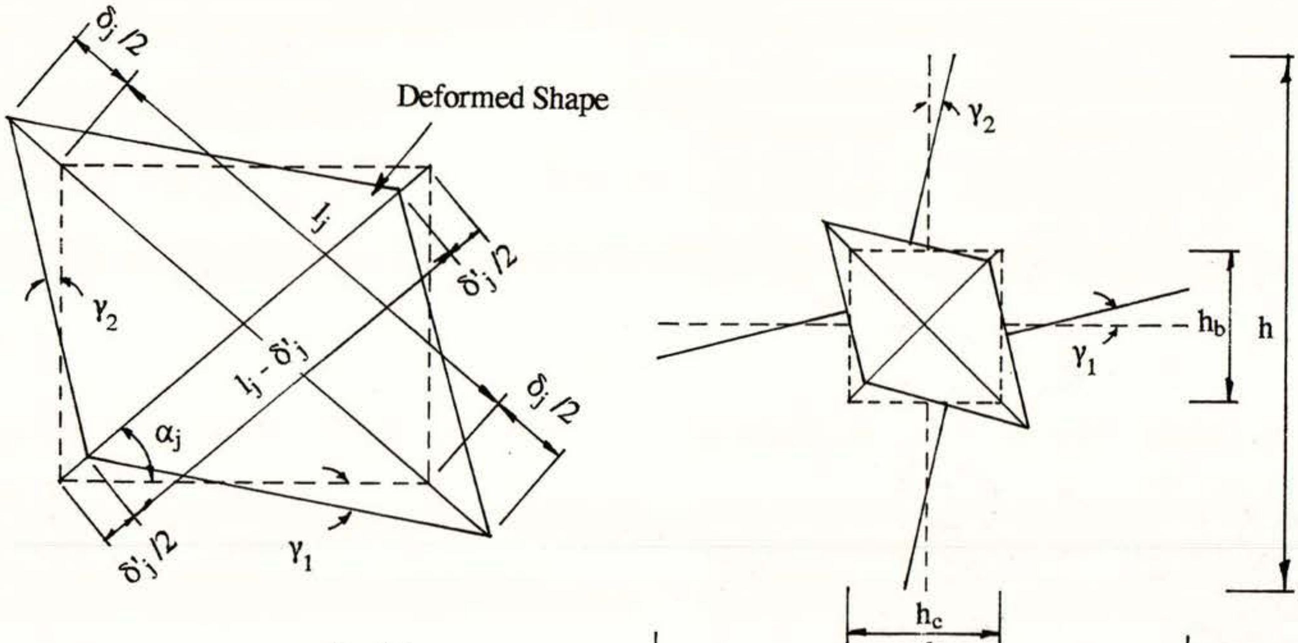

Joint shear distortion : $\gamma_j = \gamma_1 + \gamma_2 = \dfrac{\delta_j - \delta'_j}{2l_j}(\tan\alpha_j + \dfrac{1}{\tan\alpha_j})$

Joint expansion : $(\delta_j + \delta'_j)/2$

Horizontal displacement due to joint shear

: $\Delta_j = \gamma_j\,(h - h_b - \dfrac{h}{l}h_c)$

Fig.3.33 Measurement of Joint Shear Distortion and Expansion joint core. Three 30mm travel linear potentiometers were used to estimate the slip at three different locations for each beam bar in the joint core. For one reinforcing bar, one linear potentiometer measured the slip at the column centre line. The other two linear potentiometers measured the elongation of the bar between the target at the column centre line and the other two target as illustrated in Fig.3.32. By adding the slip at the column centre line to the elongations of the bar, the slip at the other two targets could be estimated.

This measurement is strictly valid only when the concrete in the region measured is infinitely rigid.

3.7.5 Measurement of Strains in Reinforcing Bars

The local strains in the reinforcing bars in the beams, columns and joint were measured using electric resistance wire strain gauges(Showa N11-FA-120-1 or Tokyo Sokki FLA-5-11). The strain gauges were attached on both sides of the longitudinal beam reinforcement at the column faces. In the case of Specimen O1, these gauges were placed at both the beam and column faces. The strain gauges for stirrups and hoops were also attached on both sides of the reinforcement. The average values of the two measurements were used to minimize the effect of bending of the reinforcing bars. The strain gauges at the other positions were attached on only one side of the reinforcing bars. The local strains were measured with a resolution of about 10 micro strain. Details of the position of the strain gauges on the reinforcing bars will be given with the test results in the following chapters.

Average strains along the longitudinal beam bars were measured using linear potentiometers with 30 or 50mm travel for Specimen R3 and Specimens O4 to O7. The linear potentiometers were connected to the aluminium rods specially designed for this study shown in Fig.3.32. Both ends of the rods have universal joints which allowed free rotation and were locked to the drilled steel rods that had been welded to the main beam bars.

Average strain ${}_{ave}\varepsilon_i$ was calculated from:

$$ {}_{ave}\varepsilon_i = \delta_i / s_i \tag{3.10} $$

where δ_i is the displacement measured over the region i by linear potentiometers and s_i is the gauge length of the region i. These average strains were measured up to about 4% in the inelastic loading cycles. These strains were obtained with a resolution of approximately 30 to 90 micro strain.

3.7.6 Measurement of Shear Distortions and Expansions of the Joints

The measurements of the linear potentiometers placed diagonally on the joint core enabled the average shear distortions and expansions to be estimated. When assuming the deformed shape of the joint core concrete due to shear distortion illustrated in Fig.3.33, the average joint shear distortion γ_j can be given by

$$\gamma_j = \gamma_1 + \gamma_2 = \frac{\delta_j - \delta'_j}{2l_j} (\tan\alpha_j + \frac{1}{\tan\alpha_j}) \tag{3.11}$$

where δ_j and δ'_j are the changes in the lengths of the diagonals, l_j is the initial length of the diagonal in the joint core and α_j is the angle of the diagonal to the horizontal.

Joint core expansion was also estimated from the diagonal measurements for all specimens. In this study, joint expansion is defined as the average value of the diagonal displacements, that is $(\delta_j+\delta'_j) / 2$. The joint expansions so obtained are proportional to the increase in the volume of the joint core concrete. Therefore, the joint expansion so obtained can be used as an index to gauge the failure of the joint core concrete.

3.7.7 Observation of Cracking

All cracks observed for each test specimen were marked on the white painted concrete surface. To record the development of the cracks, photographs were taken at the peak of each loading cycle and at other stages when desired. Crack widths were also measured by a crack magnifier with 0.02mm division at the peak of each loading cycle. When the measurements became out of range, a steel rule with 0.5mm division was used. Only the crack widths in the joint and critical regions of the test specimen were measured.

3.8 COMPONENTS OF HORIZONTAL DISPLACEMENT

3.8.1 General

The horizontal displacements of the test specimens defined in Section 3.7.2 are composed of various deformation contributions from the beams, columns and joint. The measurements mentioned in Section 3.7 enabled the estimation of the different sources of the horizontal displacement to be made. The procedures to estimate those sources of the horizontal displacement are described below.

3.8.2 Beam Deformations

3.8.2.1 Flexural Deformations

Flexural deformations of the beams $\delta_{b,f}$ were obtained from the rotation of each region in the beam measured from a pair of top and bottom linear potentiometers $\theta_{b,i}$ defined in Section 3.7.3. As shown in Fig.3.30, the flexural deformation of the beam can be derived as follows:

$$\delta_{b,f} = \sum \frac{({}_t\delta_i - {}_b\delta_i)}{h_i} (l'_b - x_i) \tag{3.12}$$

where ${}_t\delta_i$ and ${}_b\delta_i$ are the top and bottom displacements measured over the region i, h_i is the distance between top and bottom linear potentiometers in the region i, l'_b is the distance from the column face to the centre of the beam end pin and x_i is the distance from the column face to the centre of the region i.

The horizontal displacement at the column top due to the beam flexural displacement is

$$\Delta_{b,f} = \frac{h}{l} \delta_{b,f} \tag{3.13}$$

where $\Delta_{b,f}$ is the equivalent horizontal displacement due to beam flexural deformation, h is the storey height or vertical distance between the column end pins(=3200mm) and l is the beam span or horizontal distance between the beam end pins(=3910mm).

3.8.2.2 Shear Deformations

As mentioned earlier, the average shear distortions of the beams were estimated for Specimen R3 and Specimens O4 to O7. Those shear distortions were obtained in the critical regions of the beams.

From Fig.3.31, shear deformation $\delta_{b,s}$ of the beam can be given by

$$\delta_{b,s} = \gamma_s h_s \tag{3.14}$$

where γ_s is the average shear distortion defined in Section 3.7.3 and h_s is the horizontal distance of the region estimating the average shear distortion.

The horizontal displacement at the column top due to the beam shear deformation $\Delta_{b,s}$ can be expressed by

$$\Delta_{b,s} = \frac{h}{l}\,\delta_{b,s} \tag{3.15}$$

where h is the storey height or vertical distance between the column end pins(=3200mm) and l is the beam span or horizontal distance between the beam end pins(=3910mm).

The beam shear deformation so obtained includes the effect of flexural deformation since the rotation due to flexure cannot be represented by the assumed deformed shape shown in Fig.3.30[Hiraishi 1984]. This results in an overestimate of the shear deformation. However, the shear deformation was estimated at 50mm away from the column face shown in Fig.3.31 so that the effect of the fixed-end rotation could be eliminated which significantly affects the shear deformation.

3.8.2.3 Fixed-End Rotation

The beam fixed-end rotations were estimated for Specimen O1 and Specimens R1 to R2. The fixed-end rotation of the members adjacent to the joint is caused by the tensile strains or slip of the longitudinal bars anchored in the joint core. In this study, the fixed-end rotation of the beam is estimated by a pair of linear potentiometers located next to the column face, fixed-end interface. From Fig.3.30, the fixed-end rotation $\theta_{b,fe}$ can be derived by

$$\theta_{b,fe} = ({}_t\delta_1 - {}_b\delta_1) / h_1 \tag{3.16}$$

where ${}_t\delta_1$ and ${}_b\delta_1$ are the top and bottom displacement measured at the fixed-end interface and h_1 is the distance between the linear potentiometers at the fixed-end interface.

The deformation due to fixed-end rotation of the beam, $\delta_{b,fe}$ can be obtained as

$$\delta_{b,fe} = \theta_{b,fe}\, l'_b \tag{3.17}$$

where $\theta_{b,fe}$ is the beam fixed-end rotation defined above and l'_b is the distance from the column face to the centre of the beam end pin.

The horizontal displacement at the column top due to fixed-end rotation can be expressed by

$$\Delta_{b,fe} = \frac{h}{l}\,\delta_{b,fe} \tag{3.18}$$

where $\Delta_{b,fe}$ is the equivalent horizontal displacement due to beam fixed-end rotation, h is the storey height or vertical distance between the column end pins(=3200mm) and l is the beam span or horizontal distance between the beam end pins(=3910mm).

Although the linear potentiometers were placed as close as possible to the column face, the fixed-end rotation so obtained includes some rotation due to elongation of the longitudinal bars over that region.

3.8.3 Column Deformations

3.8.3.1 Flexural Deformations

Measurements to obtain the flexural deformations of the columns were made only for Specimen O1, in which plastic hinges were expected to form in the columns. The column flexural deformation component of the horizontal displacement $\Delta_{c,f}$ can be obtained by the same procedures mentioned in Section 3.8.2.1 as follows:

$$\Delta_{c,f} = \sum \frac{({}_l\delta_i - {}_r\delta_i)}{h'_i} (l'_c - y_i) \tag{3.19}$$

where ${}_l\delta_i$ and ${}_r\delta_i$ are the left and right displacements measured over the region i, h'_i is the distance between left and right linear potentiometers in the region i, l'_c is the distance from the beam face to the column end pin and y_i is the distance from the beam face to the centre of the region i.

3.8.3.2 Fixed-End Rotation

The column fixed-end rotations were obtained for all specimens except Specimens O6 and O7.

The component of horizontal displacement due to fixed-end rotation of the column, $\Delta_{c,fe}$ can be obtained using the same procedures used for the beam as

$$\Delta_{c,fe} = \theta_{c,fe}\, l'_c \tag{3.20}$$

$$\theta_{c,fe} = ({}_l\delta_1 - {}_r\delta_1) / h'_1 \tag{3.21}$$

where $\theta_{c,fe}$ is the column fixed-end rotation, l'_c is the distance from the beam face to the centre of the column end pin, ${}_l\delta_1$ and ${}_r\delta_1$ are the left and right displacement measured at the fixed-end interface and h'_1 is the distance between the linear potentiometers.

3.8.4 Joint Deformation due to Shear Distortion

The average shear distortion in the joint core has been defined in Section 3.7.6. The joint shear distortion contributes the horizontal displacement of the specimen. Fig.3.33 illustrates the deformed shape of the test specimen due to joint shear distortion when the beam and column ends are not supported. When considering the support conditions of the loading systems used in this study, the horizontal displacement due to joint shear distortion Δ_j can be derived as follows:

$$\Delta_j = \gamma_j \, (h - h_b - \frac{h}{l} h_c) \tag{3.22}$$

where γ_j is the joint shear distortion defined in Section 3.7.6, h is the storey height or vertical distance between the column end pins(=3200mm), l is the beam span or horizontal distance between the beam end pins(=3910mm), h_b is depth of beam and h_c is the overall depth of column.

3.9 ESTIMATION OF YIELD DISPLACEMENTS AND INITIAL STIFFNESSES OF THE TEST SPECIMENS

The theoretical yield displacements $\Delta_{y,theoretical}$ and initial stiffnesses $K_{theoretical}$ of all test specimens were calculated. The theoretical values will be compared with those obtained from the test results. The methods used to calculate the yield displacement Δ_y and initial stiffness K_e from the test results have already been described in Section 3.6. For each test specimen, it was assumed that the theoretical flexural strength M_i was reached simultaneously at the critical sections of the members when the ideal storey horizontal load strength P_i of the test specimen developed.

The elastic flexural and shear deformations of the beams and columns when the ideal storey horizontal load strength of the specimen was developed were estimated as follows:

$$\text{(for beam)} \qquad \delta_b = \delta_{b,f} + \delta_{b,s} = \frac{V_b \, l'^3_b}{3 \, E_c \, I_e} + \frac{V_b \, f \, l'_b}{0.2 \, E_c \, b \, h_b} \tag{3.23}$$

$$\text{(for column)} \qquad \delta_c = \delta_{c,f} + \delta_{c,s} = \frac{V_c \, l'^3_c}{3 \, E_c \, I_e} + \frac{V_c \, f \, l'_c}{0.2 \, E_c \, b_c \, h_c} \tag{3.24}$$

where δ_b and δ_c are the elastic deformations of the beam and column, $\delta_{b,f}$ and $\delta_{c,f}$ are the flexural deformations of the beam and column, $\delta_{b,s}$ and $\delta_{c,s}$ are the shear deformations of the beam and column, V_b and V_c are the beam and column shear forces at developing the ideal horizontal load strength of the specimen, l'_b is the distance from the column face to the centre of the beam end pin, l'_c is the distance from the beam face to the centre of the column end pin, f is the shape factor(=1.2), b is the width of beam, h_b is the depth of beam, b_c is the width of column, h_c is the depth of column, E_c is the modulus of elasticity of concrete(=$4700\sqrt{f'_c}$ or $4700\sqrt{f'_c*}$), f'_c is the measured concrete compressive strength, f'_c* is the weighted average compressive strength defined in Section 3.4.2 and I_e is the effective moment of inertia.

In estimating flexural deformation, approximate allowance was made for the effect of cracking of the concrete on the stiffnesses of the beams and columns. Several expressions are available to determine the effective moments of inertia of the members[Park and Paulay 1975, Paulay and Priestley 1992]. In this study, it was assumed that the effective moments of inertia I_e were

$$\text{For beam} \quad I_e = 0.5\, I_g \tag{3.25}$$

$$\text{For column} \quad I_e = 0.5\, I_g \tag{3.26}$$

where I_g is the moment of inertia based on uncracked gross concrete area. The assumed I_e value for the column is the same as for the beam since no axial load was on the column.

The shear deformation of the cracked member was approximated as twice the shear deformation of an uncracked member.

In terms of the horizontal displacement of the top of the column of the test specimen, the elastic deformation contributions of the beams and columns can be given by

$$\Delta_b = \frac{h}{l}\,\delta_b \tag{3.27}$$

$$\Delta_c = \delta_c \tag{3.28}$$

where Δ_b and Δ_c are the horizontal displacement due to the beam and column deformations defined above, h is the storey height and l is the beam span.

In addition to the flexural and shear deformations of the beams and columns mentioned above, the deformation due to joint shear distortion was assumed to contribute to the total horizontal displacement by 20%, as found by several researchers, for example Cheung 1991. That is

$$\Delta_j = 0.2\,\Delta_{y,\,\text{theoretical}} \tag{3.29}$$

where Δ_j is the horizontal displacement of the test specimen due to joint shear distortion.

The theoretical yield displacements $\Delta_{y,theoretical}$ and initial stiffnesses $K_{theoretical}$ of all test specimens are then derived by

$$\Delta_{y,theoretical} = \Delta_b + \Delta_c + \Delta_j \tag{3.30}$$

$$K_{theoretical} = \frac{P_i}{\Delta_{y,theoretical}} \tag{3.31}$$

The theoretical yield displacements and initial stiffnesses of all test specimens will be given with the test results in the following chapters.

3.10 JOINT AND BEAM SHEAR STRESSES

To estimate the relative severity of joint and beam shear forces, it is convenient to express these in terms of the nominal shear stresses. In this study, the nominal horizontal joint shear stress v_{jh} and beam shear stress v_b are defined as follows:

Nominal horizontal joint shear stress $$v_{jh} = \frac{V_{jh}}{b_j\, h_j} \tag{3.32}$$

Nominal beam shear stress $$v_b = \frac{V_b}{b\, d} \tag{3.33}$$

where V_{jh} is the horizontal joint shear force(see Fig.2.24 in Chapter 2) , V_b is the beam shear force, b_j is the the effective width of a joint defined in Fig.2.25 in Chapter 2, h_j is taken as the overall depth of the column(=h_c), b is the width of beam and d is the effective depth of beam.

The shear stresses so obtained are useful indices to assess the severity of the shear forces in the joint and beam although they have no physical meaning.

The estimation of average bond stress along longitudinal beam bars passing through beam-column joints should be based on the forces to be transferred at each face of the joint. It should be noted that these forces are not always tension at one face and compression at the other face. If the neutral axis depth in beam is small the bar may be in tension at both faces.

3.11 CONCLUSIONS

(1) This chapter described the construction and testing methods of the beam-column joint subassemblages. The methods to obtain the applied forces, displacements and strains were also described. The experimental studies were conducted to investigate the seismic

behaviour of beam-column joint regions with reinforcement details typical of concrete buildings designed in the late 1950's and effectiveness of retrofit techniques using concrete jacketing.

(2) It was identified that jacketing the beams, columns and joint with new reinforced concrete was very labour intensive. The placement of the new joint core hoops, passing through holes in the existing beams, was very difficult. However, jacketing the columns alone could significantly reduce the intensity of labour required for jacketing both the columns and beams.

(3) A retrofit technique using externally clamped stirrups was very effective way of increasing the shear resistance of the beams.

CHAPTER 4

EXPERIMENTAL RESULTS OF THE AS-BUILT SPECIMEN O1

4.1 INTRODUCTION

Three full-scale beam-interior column joint replicas, referred to as the as-built specimens, of critical regions of the reinforced concrete moment resisting frame investigated were constructed. As mentioned in Chapter 3, one typical feature of reinforcing details is that no shear reinforcement is present in the beam-column joint core, and that the amount of shear reinforcement in the beams and columns is very small. Other features are that longitudinal beam bars of large diameter pass through columns of relatively small depth, and that the columns are flexurally weaker than the beams. One of the as-built beam-interior column joint specimens, referred to as Specimen O1, was tested subjected to simulated seismic loading to establish experimentally its behaviour. This chapter reports the test results conducted on Specimen O1.

4.2 SPECIMEN O1

For Specimen O1, the ratio of the theoretical ideal flexural strength of the column, when the axial load was zero, to that of the beam was 0.69. Hence plastic hinges were expected to form in the columns during the test. The ratio of beam bar diameter to column depth was d_b/h_c=24/300=1/12.5, which did not satisfy the requirements of NZS 3101[SANZ 1982(a)] for ductile frames. The ratio of column bar diameter to beam depth was d_b/h_b=1/20.8 which does satisfy NZS 3101. The concrete of the specimen at the stage of testing had a compressive cylinder strength f'_c of 40.7MPa. The details of the specimen and the method of testing under simulated seismic loading are described in Chapter 3.

4.3 GENERAL BEHAVIOUR

The final crack pattern and the measured horizontal storey shear force versus horizontal displacement hysteresis loops are shown in Figs.4.1 and 4.2, respectively. Also shown are the theoretical ideal storey horizontal load strength P_i when the column plastic hinges were developed and the theoretical stiffness $K_{theoretical}$ based on the assumptions mentioned in Chapter 3. Fig.4.3 illustrates observed crack patterns at the peak of each loading cycle.

In the loading to $\pm 0.5P_i$, flexural cracks initiated in the columns and the beams. Bond splitting cracks along the main beam bars also formed in the joint(see Fig.4.3(a)). In the

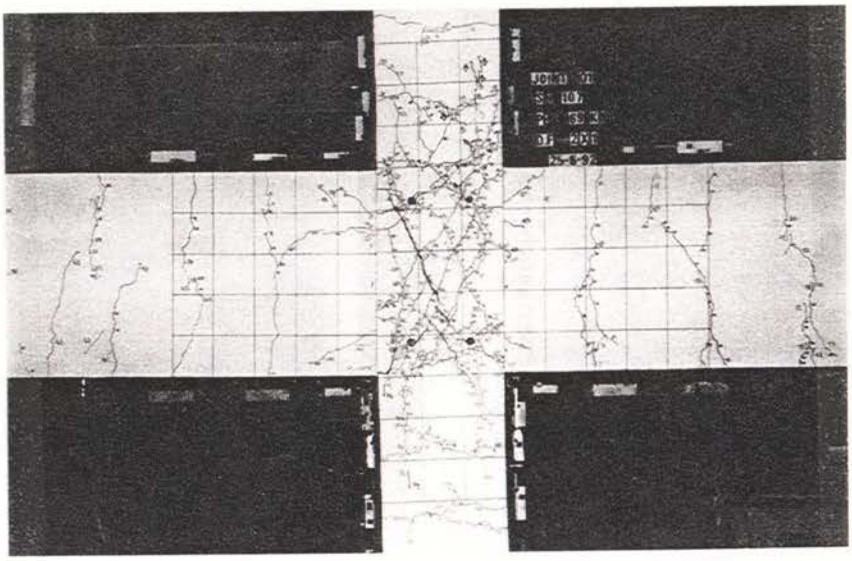

Fig.4.1 Observed Cracking of Specimen O1
at second cycle of DF=+2

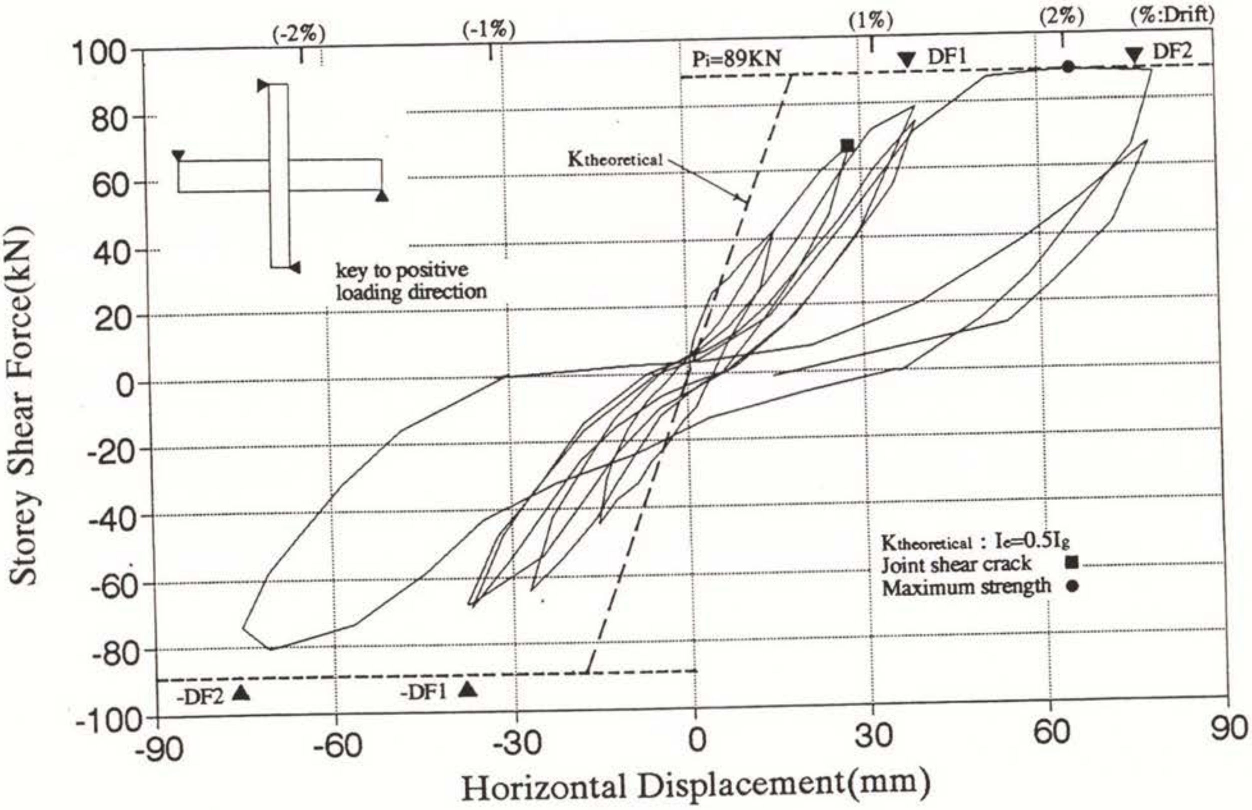

Fig.4.2 Storey Shear Force versus Horizontal Displacement Relationship
for Specimen O1

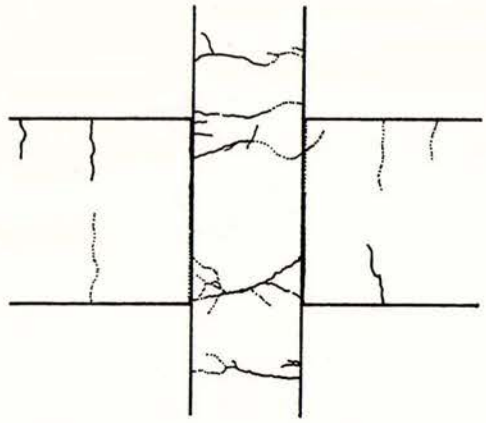

(a) at the peak of 0.5Pi
(R=0.48%)

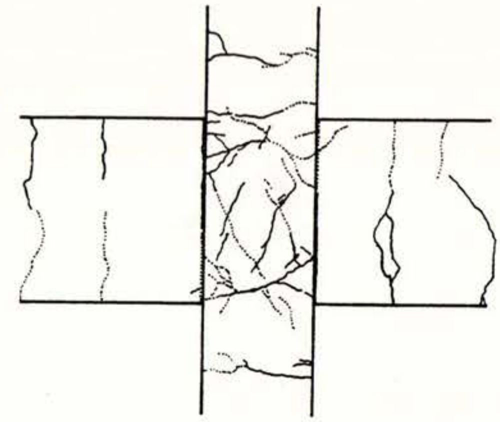

(b) at the peak of 0.75Pi
(R=0.88%)

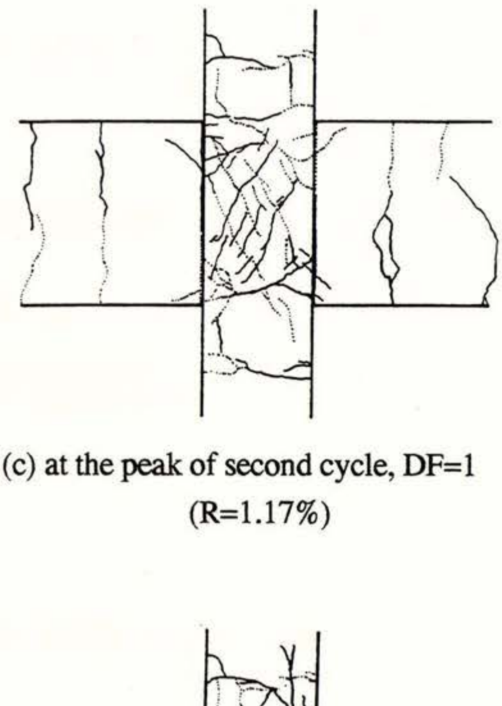

(c) at the peak of second cycle, DF=1
(R=1.17%)

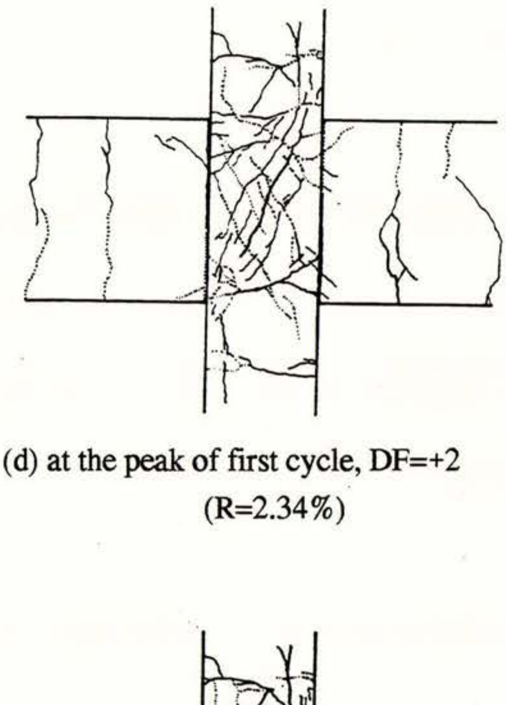

(d) at the peak of first cycle, DF=+2
(R=2.34%)

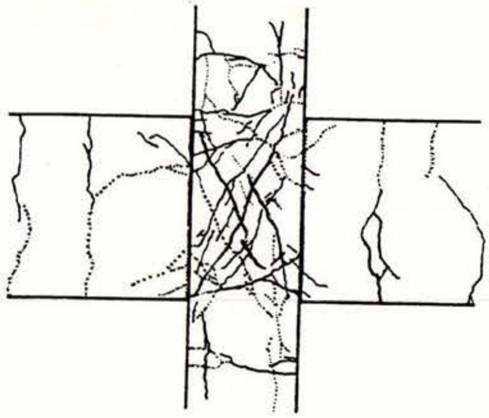

(e) at the peak of first cycle, DF=-2
(R=2.34%)

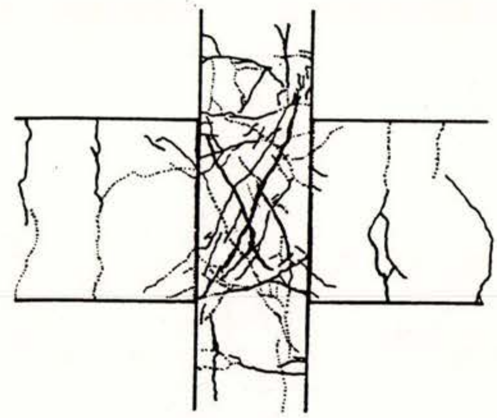

(f) at the peak of second cycle, DF=+2
(R=2.34%)

Fig.4.3 Observed Cracking of the Joint(Specimen O1)

loading to $\pm0.75P_i$, corner to corner diagonal tension cracks developed in the joint(see Fig.4.3(b)) and column flexural cracks at the beam face opened wide. Some pinching was observed in the hysteresis loops (see Fig.4.2). The yield displacement obtained from the measured load-displacement curves was extremely large, corresponding to a storey drift angle of 1.2%, due to joint cracking and bond splitting at that early stage.

In the loading to displacement ductility factor DF of 1, diagonal tension cracks in the joint extended and the number of those cracks increased. Also observed were bond splitting cracks along the main column bars in the flexural compression zones near the beam face(see Fig.4.3(c)). The flexural cracks in the beams did not open wide, unlike those in the columns, although those cracks ran through the whole depth of the beam at the column face. At this stage, more pinching of the hysteresis curves was observed due to the bond deterioration along the beam bars and the formation of diagonal tension cracks in the joint, and the column flexural cracks opened wide.

In the first cycle of loading to DF of 2, the strains in the column longitudinal bars obtained from wire strain gauges reached their yield strain and crushing of concrete was observed in the column flexural compression zone. In the joint, one dominant diagonal tension crack opened wide. Bond splitting cracks along the column bars extended and connected to the joint diagonal tension cracks(see Fig.4.3(d)). In the first positive cycle of loading to DF of 2, the maximum horizontal load strength of 89kN, which was equal to the ideal storey horizontal load strength of Specimen O1, was reached at the corresponding storey drift angle of about 2%. In the negative loading cycle, however, the measured maximum horizontal load strength of 81kN did not reach the ideal horizontal load strength due to shear failure of the joint core. The hysteresis loops were significantly pinched due to severe bond deterioration along the beam and column bars in the joint and joint diagonal tension cracking(see Fig.4.3(e)). The distress of the joint was evident with the formation of one dominant diagonal tension crack and the extension of some joint shear cracks into the beams(see Fig.4.3(f)).

In the second cycle of loading to DF of 2, only 75% of the theoretical ideal horizontal load strength was developed. An extensive enlargement of joint diagonal tension cracks caused the severe strength and stiffness degradation. The shape of hysteresis curves were dominated by the response of the most damaged element, shown in Fig.4.1, namely the joint.

After completion of the second positive cycle of loading to DF of 2, the test was terminated since a storey drift angle of more than 2% had been reached and the specimen was to be repaired and retrofitted.

4.4 INITIAL STIFFNESS

The theoretical initial stiffness $K_{theoretical}$ of Specimen O1, assuming the effective moment of inertia of the beams and columns to be $0.5I_g$ and that the deformation due to joint shear distortion contributed to the total horizontal displacement by 20%, where I_g is the moment of inertia based on the uncracked gross concrete area, was given by

$$K_{theoretical}=4.79\text{kN/mm}$$

The theoretical initial stiffness $K_{theoretical}$ is shown in Fig.4.2. The initial stiffness of Specimen O1 was estimated by using the secant of the horizontal storey shear force versus horizontal displacement relationship passing through the point at which 75% of the ideal horizontal load strength P_i was attained. The initial stiffnesses so obtained were 2.39kN/mm for the positive loading cycle and 2.37kN/mm for the negative loading cycle, respectively. The average value of the stiffnesses obtained for positive and negative loading cycle was 2.38kN/mm which was only 50% of the theoretical value. This is mainly due to the bond deterioration along the main beam bars in the joint core in the early stages of loading, as mentioned before.

The yield displacement of Specimen O1 was estimated from the stiffness at $0.75P_i$, extrapolated linearly to P_i. The yield displacement so obtained was 37.3mm which could be converted to 1.2% in terms of a storey drift angle. The as-built specimen was far more flexible than that required by the current requirement of NZS 4203[SANZ 1992]. This significant flexibility of the frame may result in the smaller response to a major earthquake but the damage to the frame would be significant.

4.5 BEAM BEHAVIOUR

4.5.1 Longitudinal Beam Bar Strains

The strains in the longitudinal beam bars obtained from wire strain gauges are plotted in Fig.4.4. Up to the loading to DF of 2, gradual increase in tensile strains along the beam bars are shown. The strains in the top beam bar were about a half of those in the bottom beam bar, as would be expected since the area of bottom steel in the beam was one half of that of the top steel. The beam bar strains measured did not reach the yield strain although the strains in the bottom beam bar at the column face almost reached the yield strain.

A typical feature of the strain profiles for the beam bars of the as-built specimen was that tensile strains were measured over the whole column depth during the test. Even in the loading to $\pm 0.5P_i$, tensile strains were measured at the part of the column face subjected to

Top Beam Bar(Positive Loading Cycle)

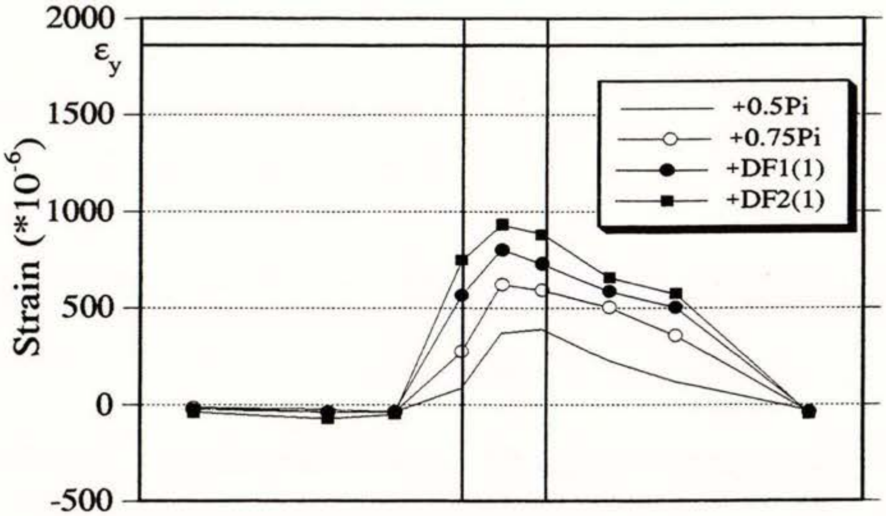

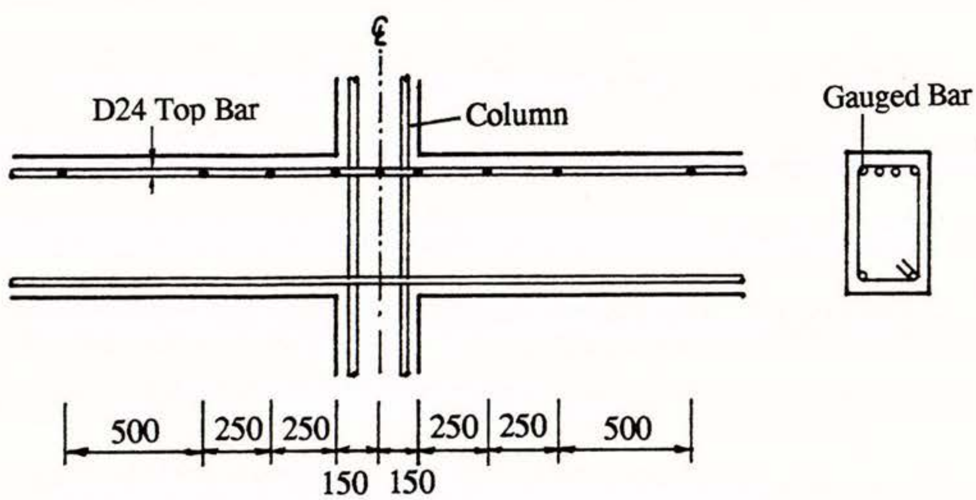

Top Beam Bar(Negative Loading Cycle)

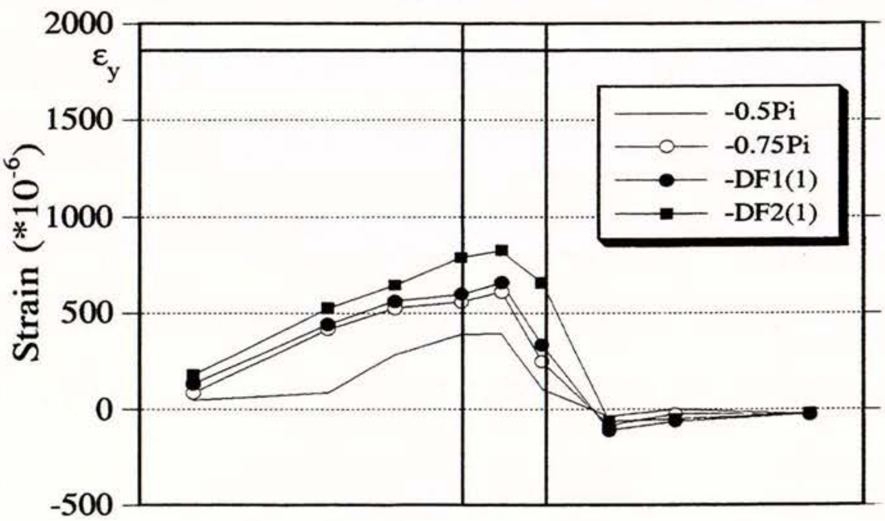

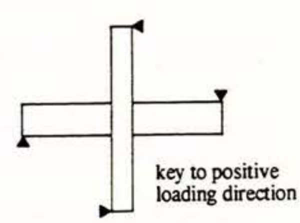

Fig.4.4(a) Strain Profiles of Top Beam Bar of Specimen O1

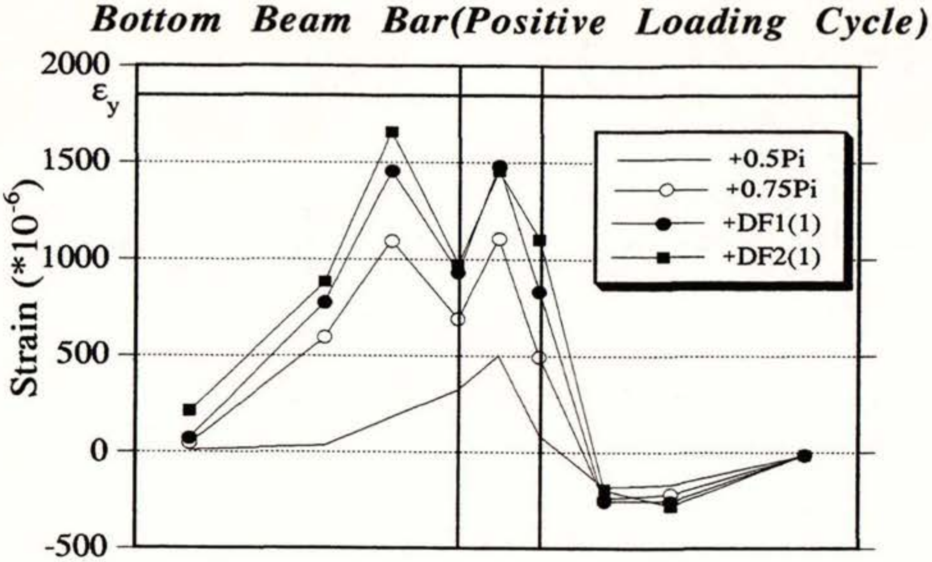

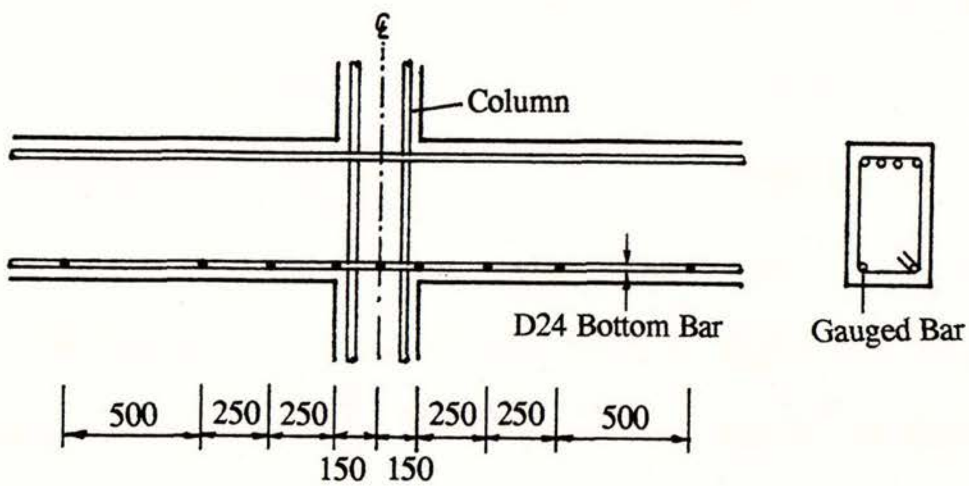

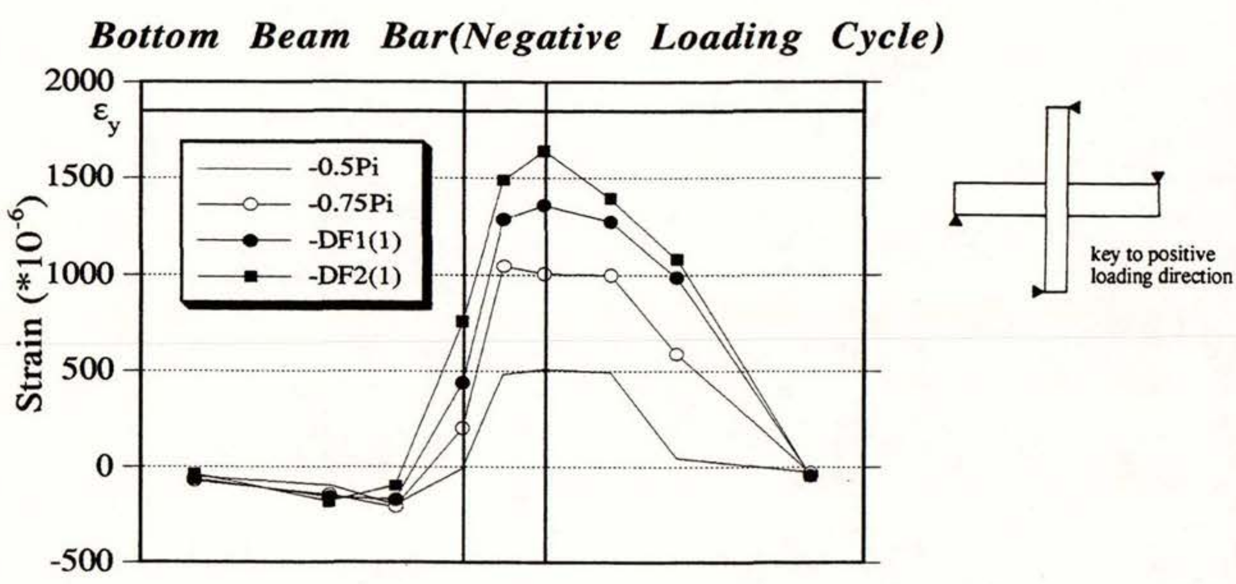

Fig.4.4(b) Strain Profiles of Bottom Beam Bar of Specimen O1

beam flexural compression force, indicating that the "compression" reinforcement in the beam on one side of the joint was actually in tension. This is because of the large ratio of beam bar diameter to column depth of the as-built specimen. As shown in Fig.4.4, anchorage was developed at a short distance into the flexural compression zone of the beam, as indicated by the change to compressive strain at the first strain gauge located 250mm in the opposite beam from the column face. It is evident that the beam bars of Specimen O1 were not well anchored in the joint core, causing an increase in flexibility of the as-built specimen.

Another typical feature of the strain distributions along the beam bars is that the tensile strains measured at the centre of the joint core were larger than those at the column face. This trend became more apparent, especially after the loading to $\pm 0.75P_i$, at which diagonal tension cracking occurred in the joint core. For the as-built specimen without joint shear reinforcement, the longitudinal beam bars in the joint core were significantly stressed in tension during the test.

4.5.2 Beam Curvature Distributions

Fig.4.5 illustrates the beam curvature distributions estimated from the potentiometer readings over a region of length $2.1h_b$, where h_b is the beam depth. The theoretical yield curvatures of 0.0056(1/m) for beam positive moment and 0.0062(1/m) for beam negative moment calculated from section analysis are also shown in this figure. A gradual increase in the beam curvatures was observed during the test. With beam positive moment, the curvatures estimated over the region nearest to the column face reached the theoretical yield curvature in the loading to DF of 1. However, rapid increase in the curvature over that region was not observed in the subsequent loading cycles . On the other hand, the curvatures with beam negative moment were below the theoretical yield curvature. Hence it can be concluded that the beams of Specimen O1 remained essentially in the elastic range up to the end of testing.

4.6 COLUMN BEHAVIOUR

4.6.1 Longitudinal Column Bar Strains

The strain profiles along the longitudinal column bars are shown in Fig.4.6. Those strains were measured from wire strain gauges. Strains along the column bars increased gradually up to the loading to DF of 1 as the test progressed. In the first positive cycle of loading to DF of 2, in which the ideal storey horizontal load strength of the specimen was attained, the strains measured at the beam face reached the yield strain and increased rapidly for both the top and bottom columns. At this stage, yield penetration into the joint core was also observed(see Fig.4.6). In the first negative cycle of loading to DF of 2, the strains

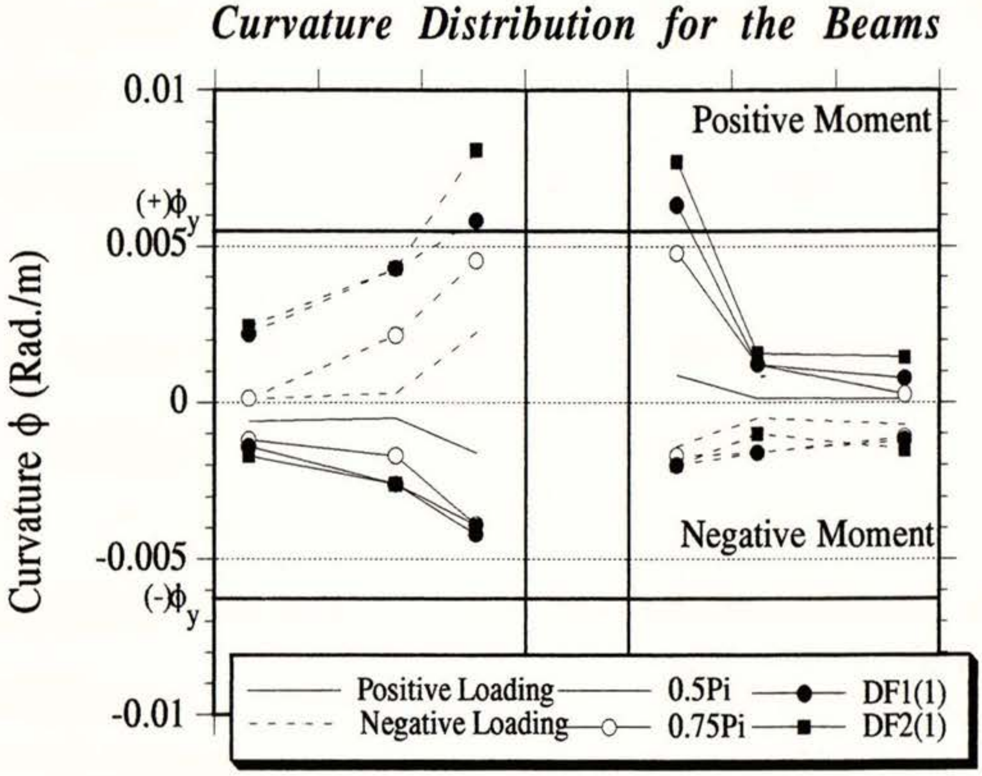

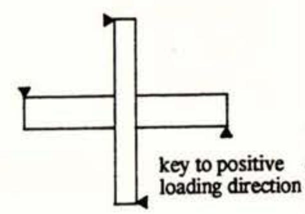

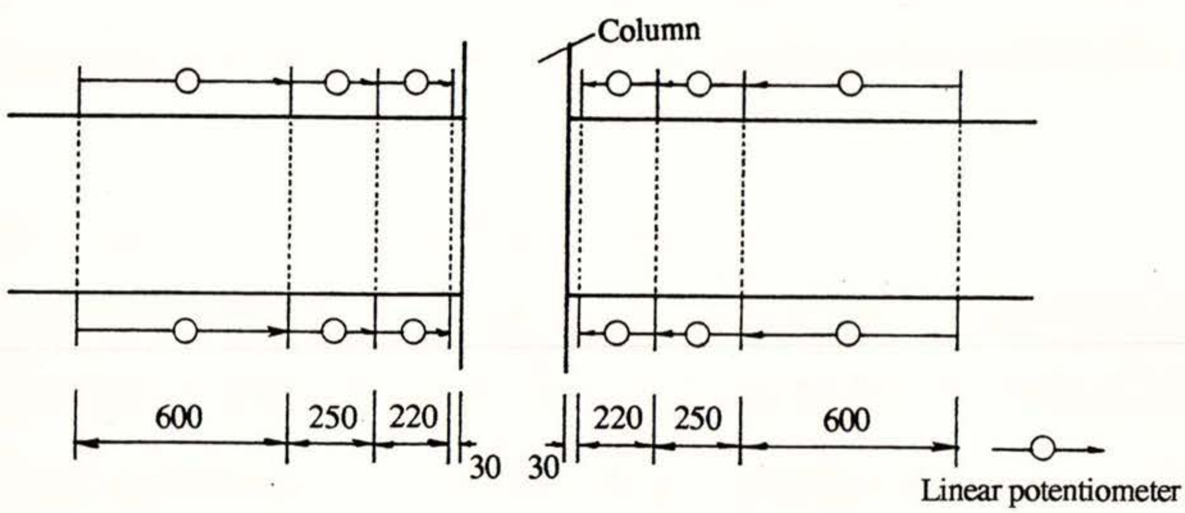

Fig.4.5 Curvature Distribution for the Beams of Specimen O1

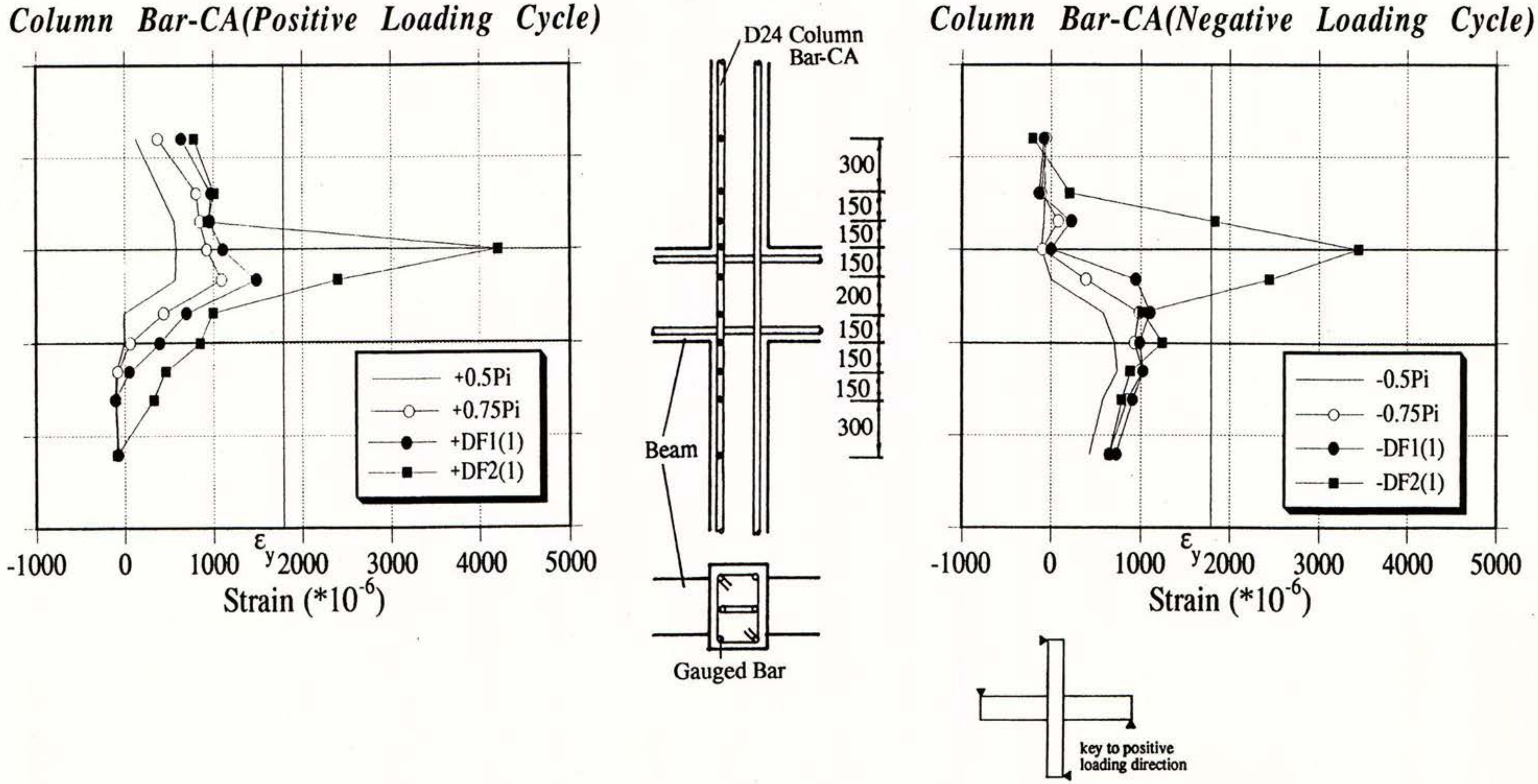

Fig.4.6(a) Strain Profiles of Column Bar of Specimen O1

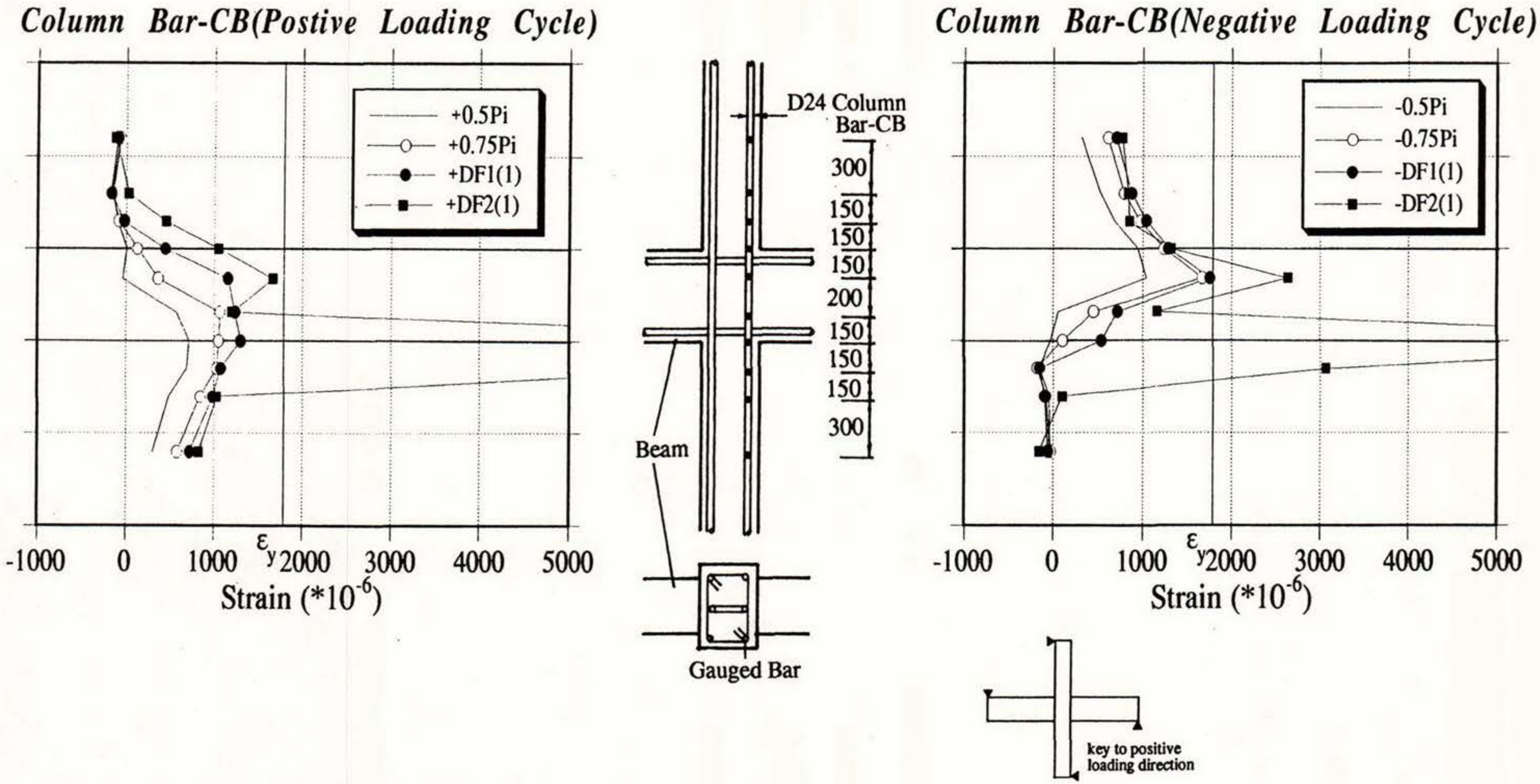

Fig.4.6(b) Strain Profiles of Column Bar of Specimen O1

measured at the beam face did not reach the yield strain although the strain measured at the position immediately inside the joint core yielded in tension. This is because the ideal storey horizontal load strength could not be reached in this loading cycle due to shear failure of the joint core.

In the loading to $\pm 0.75P_i$, in which diagonal tension cracks were observed in the joint, tensile strains along the column bars were measured through the joint. Subsequent loading cycles resulted in an increase in those tensile strains. As shown in Fig.4.6, the column bars of the test specimen were anchored at a distance of approximately 600mm from the beam face in the opposite column in the loading to DF of 2. Some measurements in the joint core were larger than those obtained at the beam face. This trend was also observed for the beam bars as mentioned before.

The column bars in the joint core of the as-built specimen were stressed in tension significantly during the test as observed for the beam bars.

4.6.2 Column Curvature Distributions

Fig.4.7 plots the column curvature distributions estimated over a region of length $1.9h_c$, where h_c is overall depth of the column. Yield curvatures shown in this figure were estimated using the curvatures obtained at $\pm 0.75P_i$ extrapolated linearly to P_i. The column curvature profiles showed similar trends to that observed from the strain profiles along the column bars. Up to the loading to DF of 1, column curvatures gradually increased as the storey shear force applied to the specimen increased. In the loading to DF of 1, the curvatures estimated over the region nearest to the beam face reached the yield curvature. In the first positive cycle of loading to DF of 2, the curvatures estimated over that region increased rapidly. In the first negative cycle of loading, however, yield curvature was not reached for the bottom column as shown in Fig.4.7, indicating that the as-built specimen could reach the ideal horizontal load strength only in one direction of loading due to shear failure of the joint core.

4.7 JOINT BEHAVIOUR

4.7.1 General Behaviour

In the loading to $\pm 0.5P_i$, bond splitting cracks formed along the main beam bars in the joint(see Fig.4.3(a)). Initial corner to corner diagonal tension cracks were initiated in the loading to $\pm 0.75P_i$(see Fig.4.3(b)). In the loading to DF of 1, the joint diagonal tension cracks extended and opened wide. A maximum nominal horizontal shear stress in the joint core of $0.61\sqrt{f'_c}$ was obtained in the first positive cycle of loading to DF of 2, where f'_c is the

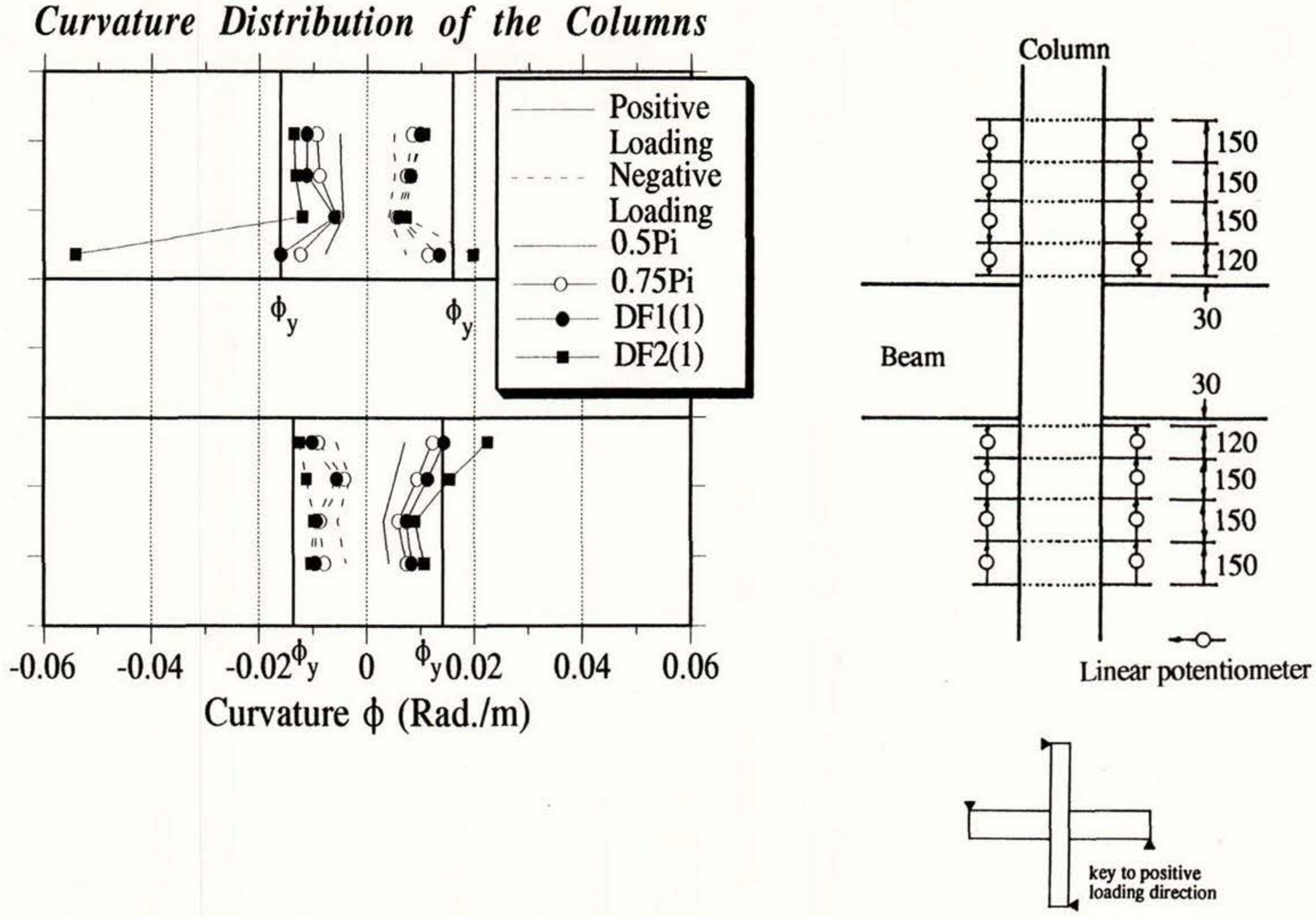

Fig.4.7 Curvature Distribution of the Columns of Specimen O1

measured compressive cylinder strength of concrete. Subsequent loading cycles resulted in severe strength and stiffness degradation due to joint diagonal tension cracking and bond deterioration along the beam bars in the joint core(see Figs.4.1 and 4.2).

4.7.2 Bond Stresses of the Longitudinal Beam and Column Bars in the Joint

The average bond stresses measured along the longitudinal beam and column bars in the joint, assumed to be uniformly distributed over the gauge length of 150mm or 200 mm, were calculated using the wire strain gauge readings. The average bond stresses so obtained are plotted in Fig.4.8 for beam bars and in Fig.4.9 for column bars. Only the bond stresses at the peaks of the selected loading cycles are plotted until the bars yielded.

In the loading to $\pm 0.5P_i$, bond splitting cracks along the beam bars were initiated at bond stresses of 0.2MPa to 0.7MPa for the top beam bar and 0.2MPa to 1.6MPa for the bottom beam bar. That range of bond stresses can be expressed by $0.03\sqrt{f'_c}$ to $0.3\sqrt{f'_c}$, where f'_c is the measured concrete compressive cylinder strength.

As shown in Fig.4.8, only small bond stresses were developed in the beam bars estimated over the region subjected to transverse column flexural tension force during the test. The bond stresses were generated mainly over the region subjected to transverse column flexural compression force. Maximum bond stresses obtained over that region were 2.9MPa($=0.45\sqrt{f'_c}$) for top beam bar and 6.8MPa($=1.1\sqrt{f'_c}$) for bottom beam bar, respectively. Those maximum bond stresses were attained in the loading to $\pm 0.75P_i$. In the subsequent loading cycles, however, the bond stresses began to decrease gradually as shown in Fig.4.8. Bond deterioration along the beam bars in the joint core of the as-built specimen was initiated in the loading to DF of 1.

In the loading to $\pm 0.5P_i$, bond stresses in the column were developed mainly over the central region in the joint. In the loading to $\pm 0.75P_i$, the bond stresses estimated over the region subjected to transverse beam flexural tension force began to decrease and only small bond stresses were developed over that region during the test. On the other hand, the bond stresses over the region subjected to transverse beam flexural compression force began to increase. This trend became more apparent in the loading to DF of 1. At this stage, however, the bond stresses obtained over the central region began to decrease as shown in Fig.4.9. The maximum bond stresses over the region subjected to beam flexural compression force were 7.6MPa($=1.2\sqrt{f'_c}$) developed in the loading to DF of 1.

The bond stress profiles along the beam bars in the joint of the as-built specimen without shear reinforcement demonstrated that the bond forces in terms of bond stress could be hardly generated over the region subjected to transverse column flexural tension force in the early

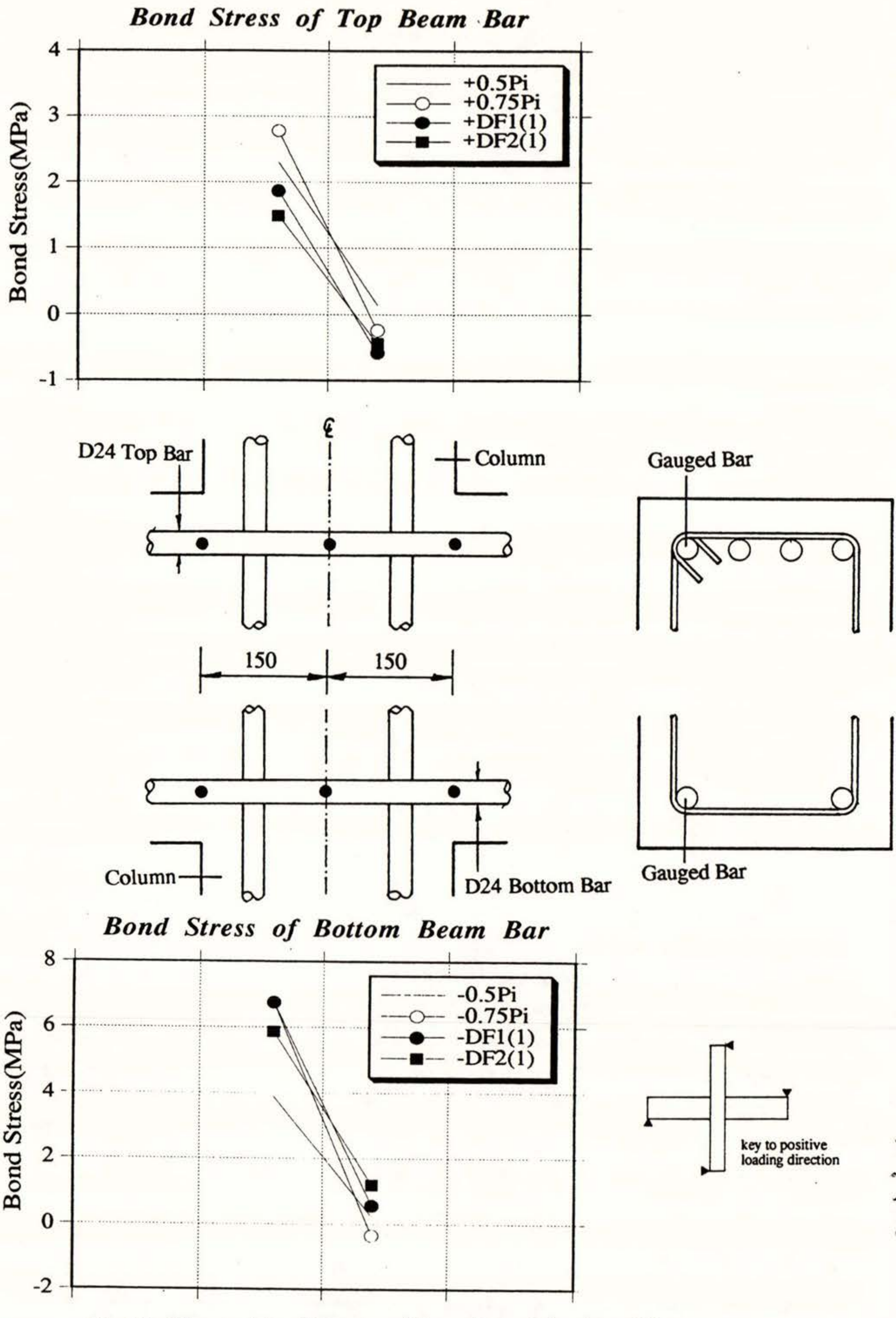

Fig.4.8 Measured Bond Stresses of Beam Bars of Specimen O1

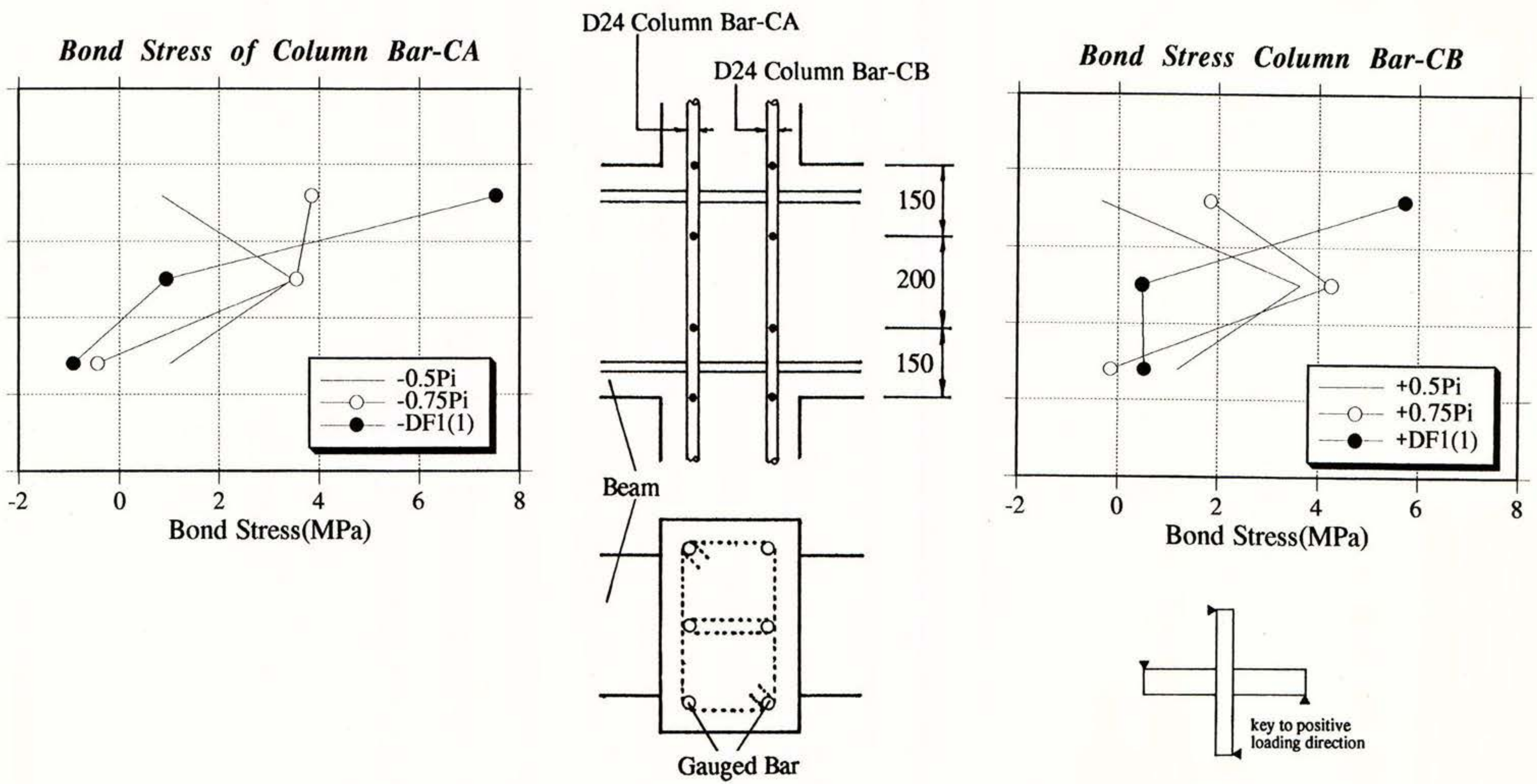

Fig.4.9 Measured Bond Stresses of Column Bars of Specimen O1

stages of loading, indicating premature bond deterioration. The bond stresses were reduced over the region of approximately six times bar diameters in length from the tension side of the column. The bond forces were developed mainly over the region subjected to transverse column flexural compression force during the test. This was also observed for the column bars in the joint.

4.7.3 Joint Shear Distortion and Expansion

The measured joint shear distortion and expansion are shown in Fig.4.10. The procedures for estimating the joint shear distortion and expansion were described in Section 3.7.6.

In the loading to $\pm 0.5P_i$, there was a small joint shear distortion and expansion. In the loading to $\pm 0.75P_i$, in which diagonal tension cracks were observed in the joint, the joint shear distortion increased rapidly. At this stage, the joint expansion also began to increase. In the loading to DF of 1, joint shear distortion increased to approximately 0.5%. Joint expansion became notable at the stage of this loading. This could be expected because of the relatively large tensile strains measured along both the beam and column bars in the joint core. Subsequent loading cycles resulted in the consistent increase of joint expansion as illustrated in Fig.4.10. The joint shear distortion also increased consistently and the maximum joint shear distortion of 0.76% was obtained in the second cycle of loading to DF of 2.

In summary it was observed that, for the as-built Specimen O1 without joint shear reinforcement, joint shear distortion and expansion increased rapidly after diagonal tension cracking occurred in the joint core, indicating joint shear failure.

4.8 DECOMPOSITION OF HORIZONTAL DISPLACEMENT

Fig.4.11 illustrates the components of the horizontal displacement measured for Specimen O1 at the peaks of the selected loading cycles, expressed as a percentage of the storey drift angle. The definition of each displacement was explained in Section 3.8.

The major source of the storey drift was the column displacement, indicating a "strong beam-weak column" response. The contribution to the total drift of column flexure and fixed-end rotation were 25% to 28% and 27% to 30%, respectively. Although some increase in the column displacement due to fixed-end rotation was observed, the contribution of the column displacement was fairly constant during the test. The beam displacement accounted for 12% to 14% due to flexure and 9% to 12% due to fixed-end rotation. The contribution of the beam displacement did not change significantly during testing.

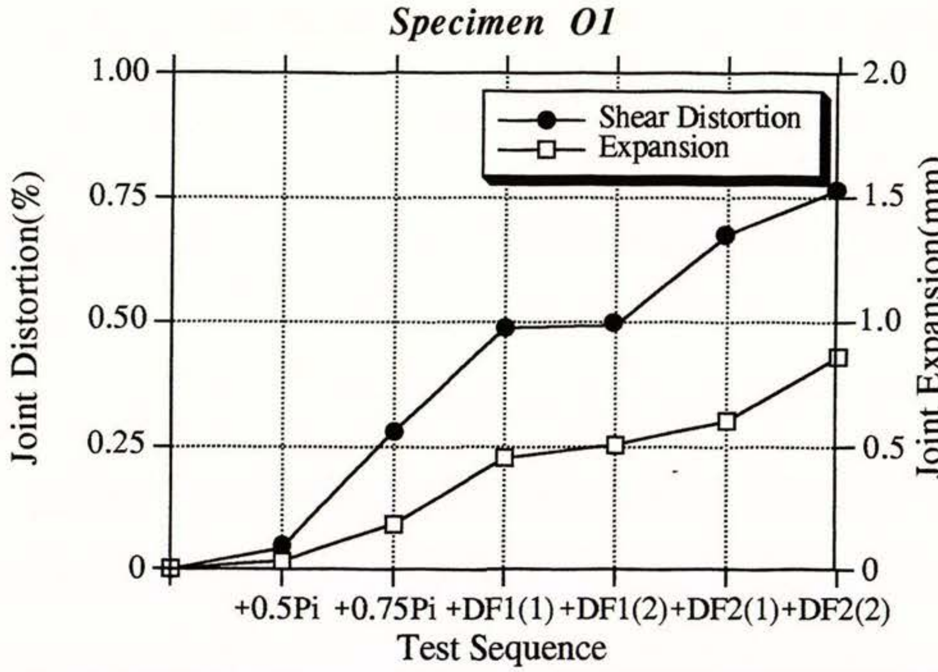

Fig.4.10 Joint Shear Distortion and Expansion of Specimen O1

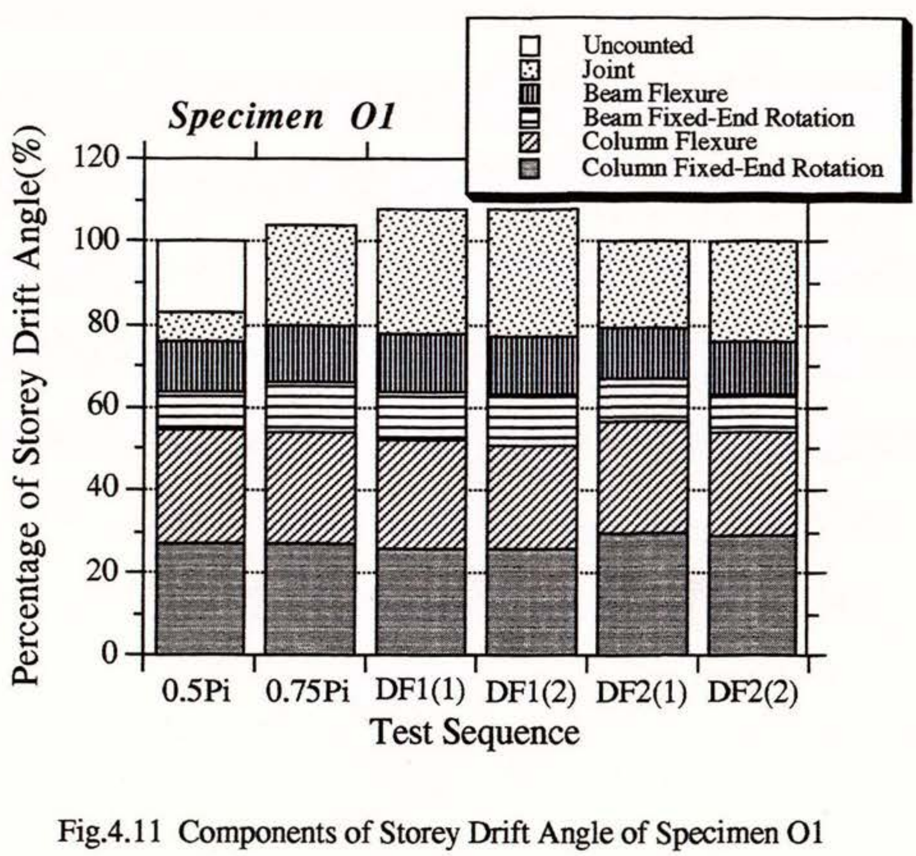

Fig.4.11 Components of Storey Drift Angle of Specimen O1

The contribution of the displacement due to joint shear distortion increased rapidly to 24% in the loading to ±0.75P_i. The joint contribution to the storey drift angle increased up to the loading to DF of 1. The maximum contribution of 31% was obtained in the second cycle of loading to DF of 1, indicating severe deterioration of the joint core. Although the contribution due to joint shear displacement decreased in the loading to DF of 2, the joint contribution to the storey drift angle was still significant.

Even in the elastic loading cycles, the displacement due to fixed-end rotation of the beams and columns contributed to the storey drift of the as-built specimen by approximately 30 to 40%. The large contribution due to fixed-end rotation could be expected because of the large diameter longitudinal beam bars passing through interior columns of small depth. Premature bond deterioration along the beam bars was initiated over the tension side of the column. The large tensile strains in the column bars in the joint also attributed to the horizontal displacement due to fixed-end rotation. The effect of the fixed-end rotation of the members adjacent to the joint without shear reinforcement should be taken into account when assessing the stiffness of the frame building.

4.9 CONCLUSIONS

Based on the results tested on the as-built Specimen O1, the following conclusions are reached.

(1) Specimen O1 was a beam-interior column joint subassemblage which is a critical region of the reinforced concrete moment resisting frame investigated. No joint shear reinforcement was present in the joint core and the diameter of longitudinal beam bars to column depth ratio was 1/12.5. The beams were flexurally stronger than the columns. The maximum nominal horizontal joint shear stress was $0.61\sqrt{f'_c}$ MPa. The test on Specimen O1 demonstrated that the performance of the beam-interior column joint region of the as-built frame would be poor in a major earthquake in terms of the stiffness, strength and ductility of the structure. This is mainly due to the lack of shear reinforcement and inadequate anchorage of longitudinal beam bars in the joint core.

(2) Specimen O1 could not reach the ideal horizontal load strength in one direction of loading due to shear failure of the joint core.

(3) The initial stiffness of Specimen O1 was significantly low when compared with the theoretical value calculated using the normal method. The main reasons are that large diameter longitudinal beam bars passed through the column of small depth and that premature bond deterioration was initiated in both the beam and column bars, and that the joint developed severe diagonal tension cracking.

(4) During the test, the bond forces along the beam and column bars were mainly generated over the region subjected to flexural compression forces applied transverse to the embedded bars.

(5) After diagonal tension cracking, large tensile strains prevailed along the beam and column bars in the joint core, resulting in significant joint expansion.

CHAPTER 5

EXPERIMENTAL RESULTS OF THE RETROFITTED SPECIMENS R1, R2 AND R3

5.1 INTRODUCTION

In Chapter 4, the seismic behaviour of the as-built beam-interior column joint with poor reinforcing details which are typical of many older buildings was investigated. It was found that the performance of the beam-interior column joint regions of the building frame would be poor in a severe earthquake. It is evident that the retrofit solution would be to jacket the frame with new reinforced concrete in order to enhance the strength and ductility of the building. This chapter examines the seismic behaviour of the three as-built beam-column joint replicas which were retrofitted by jacketing with new reinforced concrete.

One of the as-built beam-column joint replicas, referred to as Specimen O1, had already been tested(see Chapter 4). The damaged beam-column joint replica was then retrofitted by jacketing both the beams and columns with added reinforced concrete as described in Chapter 3, and became Specimen R1. Another as-built beam-column joint replica, not previously damaged, was retrofitted in the same manner except that new joint hoops were not placed in the joint core, and became Specimen R2. The two retrofitted specimens were then tested under simulated severe seismic loading to permit a comparison of the effect of the presence of the joint hoops and the previous damage.

As described in Chapter 3, jacketing the columns and beams is extremely labour intensive. In order to develop more economical retrofit methods, the remaining undamaged as-built beam-column joint replica was retrofitted by jacketing the columns alone and then tested subjected to simulated seismic loading. No horizontal shear reinforcement were placed in the joint core.

Chapter 3 describes in detail the retrofit procedures used and the method of testing under simulated seismic loading.

This chapter describes the results obtained from the three retrofitted beam-column joint regions and the effectiveness of the retrofit technique using jacketing with new reinforced concrete.

5.2 RETROFITTED SPECIMEN R1

5.2.1 The Specimen

Specimen R1 was the specimen retrofitted by jacketing the beams, columns and joint with new reinforced concrete. The compressive strengths of the existing and new concrete were 42.3MPa and 54.4MPa, respectively, at the time of testing. The ratio of the theoretical ideal flexural strength of the column to that of beam was 2.1 based on the measured material strengths, and hence plastic hinges were expected to form in the beams during the test. When the beam plastic hinges developed, the ideal storey horizontal load strength P_i was 217kN.

5.2.2 General Behaviour

Final crack pattern and the measured storey shear force versus horizontal displacement hysteresis curves are shown in Figs.5.1 and 5.2, respectively. Also shown are the theoretical ideal storey horizontal load strength P_i mentioned above and the theoretical initial stiffness $K_{theoretical}$ calculated by conventional frame analysis. Fig.5.3 shows crack patterns at the peak of each loading cycle.

In the loading to $\pm 0.5P_i$, flexural cracks initiated in the beams and columns. Flexural-shear cracks were also observed in the beams. The new bottom beam bars(2-D12) reached the yield strain at the column face. In the loading to $\pm 0.75P_i$, corner to corner diagonal tension cracks developed in the joint(see Fig.5.3(a)). Beam flexural cracks at the column face extended and opened wide. The new top beam bars(2-D12) started to yield at the column face at the stage of this loading.

In the loading to displacement ductility factor DF of 1, crushing of concrete in the beam flexural compression zones was observed. The width of beam flexural cracks at the column face and joint diagonal tension cracks were measured to be 1.5mm and 0.4mm, respectively. Existing top(4-D24) and bottom beam bars(2-D24) started to yield at the column face.

In the loading to DF of 2, concrete crushing in the beams became more apparent and beam flexural crack at the column face opened wide to a maximum crack width of 5mm at the top face and 7mm at the bottom face. In the first positive loading cycle, the maximum horizontal load strength of 231kN was reached at a storey drift angle of about 1%(see Fig.5.2). The maximum horizontal load strength obtained for the retrofitted Specimen R1 was 106% of the ideal storey horizontal load strength. Some pinching was observed in the hysteresis loops in the second cycle of this loading. Columns and joint showed only minor flexural and shear cracking(see Fig.5.3(c)).

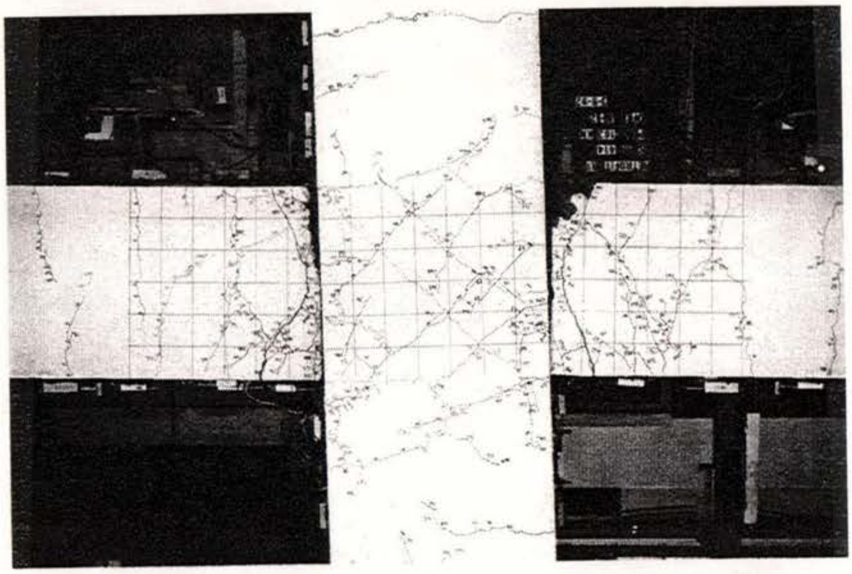

Fig5.1 Observed Cracking of Specimen R1
at second cycle of DF=-8

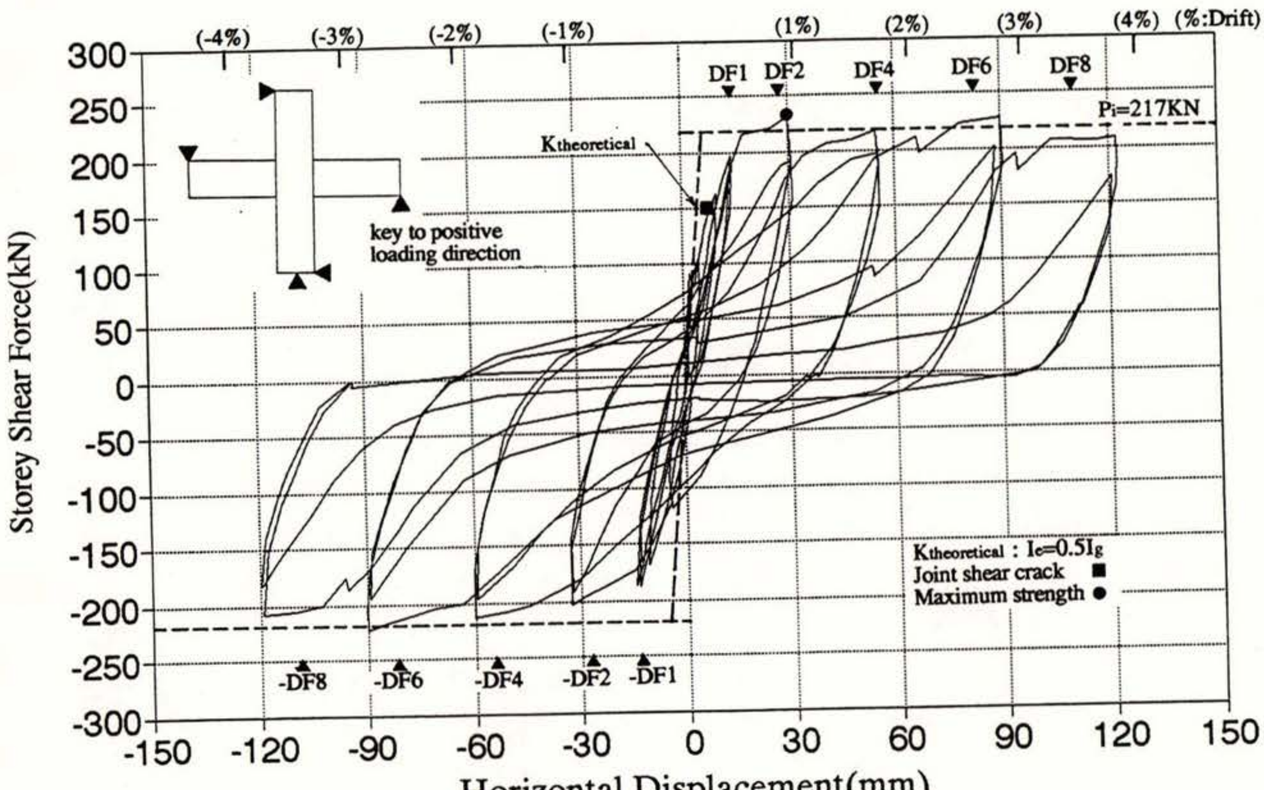

Fig.5.2 Storey Shear Force versus Horizontal Displacement Relationship
for Specimen R1

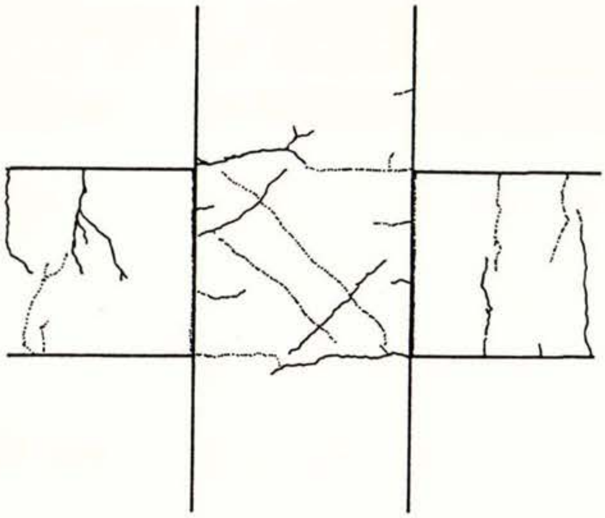

(a) at the peak of 0.75Pi
(R=0.30%)

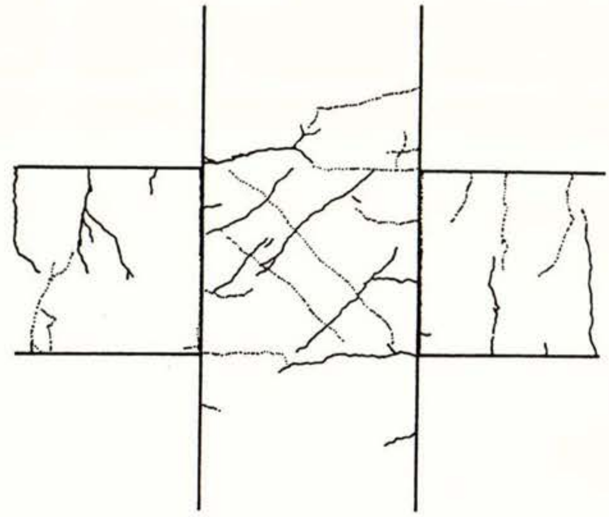

(b) at the peak of second cycle, DF=1
(R=0.41%)

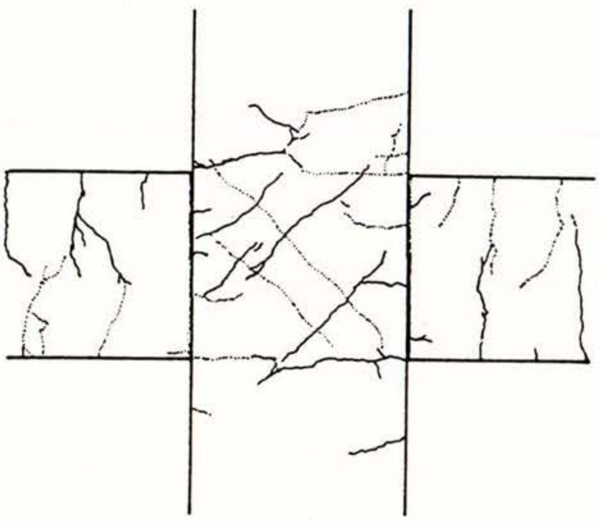

(c) at the peak of second cycle, DF=2
(R=0.82%)

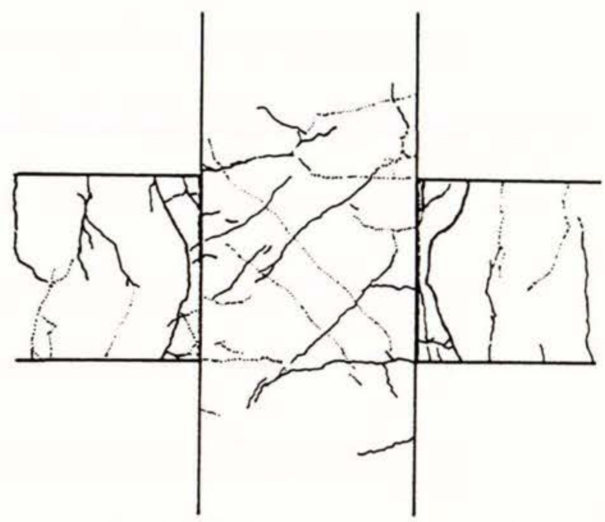

(d) at the peak of second cycle, DF=4
(R=1.62%)

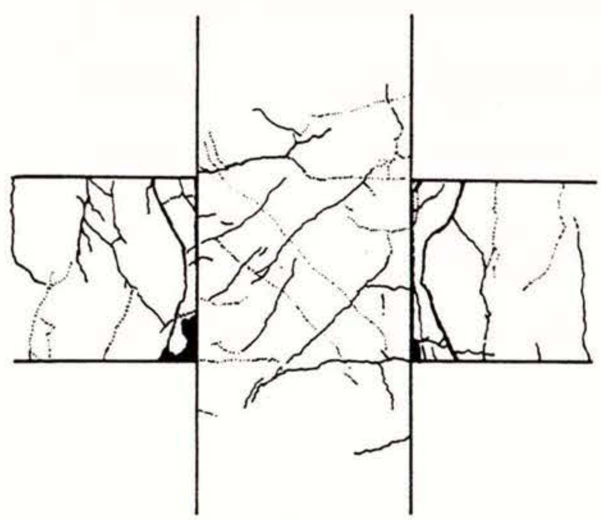

(e) at the peak of second cycle, DF=6
(R=2.44%)

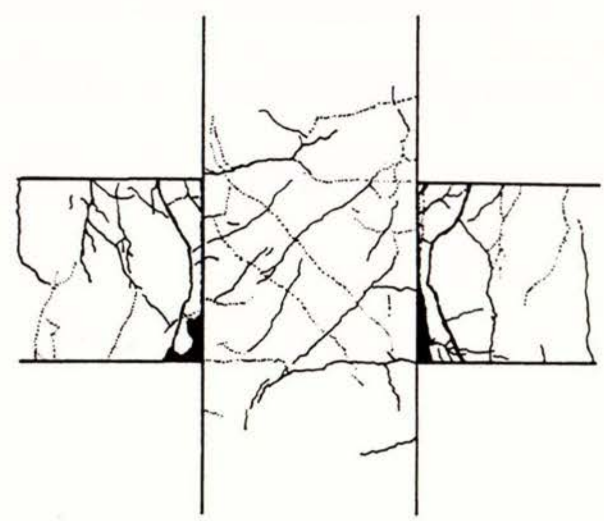

(f) at the peak of second cycle, DF=8
(R=3.25%)

Fig.5.3 Observed Cracking of the Joint(Specimen R1)

In the loading to DF of 4, the beam flexural cracks at the column face opened to a maximum crack width of approximately 10mm at the top beam face and 20mm at the bottom beam face. Diagonal tension cracks initiated in the beam plastic hinge regions(see Fig.5.3(d)). Cover concrete at the bottom beam face started to spall off and some sliding shear deformation of the beam occurred along the full depth flexural crack at the column face. The maximum width of the joint diagonal tension cracks was 0.5mm. Bond splitting cracks initiated along the column corner bars in the column flexural compression zone near the beam face. More pinching appeared in the hysteresis curves, mainly due to the open beam flexural cracks(see Fig.5.2). However the hysteresis loops indicated only a little reduction in strength.

In the loading to DF of 6, the cover concrete of the bottom beam face spalled off significantly(see Fig.5.3(e)). In the second loading cycle, buckling of the new bottom beam bars(2-D12) occurred at the column face and eventually those longitudinal bars fractured as a consequence of successive buckling and straightening. However, this fracture did not affect the overall response of the test specimen significantly, because of the relatively small amount of new longitudinal bars provided in the beams. Diagonal tension cracks in the beams widened to 4mm although the maximum flexural crack widths of beams at the column face were almost the same as those observed in the previous loading cycles. As shown in Fig.5.2, strength degradation was not so significant although considerable pinching was observed in the hysteresis loops.

In the loading to DF of 8, significant concrete crushing and spalling were observed at the beam soffit at the column face(see Fig.5.3(f)). On the other hand, the columns showed only minor flexural and bond splitting cracks. Until the end of testing, no indication of joint distress was found although the joint diagonal tension cracks extended and connected to the bond splitting cracks along the column corner bars in the flexural compression region near the beam face. The maximum width of the joint diagonal tension cracks was 0.5mm, indicating that the joint core was well confined during the test. In the second loading cycle, the hysteresis curves showed some strength degradation.

The retrofitted Specimen R1 demonstrated a desirable beam hinging failure mechanism as intended. Comparing the response of Specimen R1 with that of the as-built Specimen O1(Fig.4.2), it is evident that jacketing the columns, beams and joint with new reinforced concrete is a useful technique for enhancing the stiffness, strength and ductility of poorly detailed as-built beam-column joint regions.

The test results also showed that the new column bars in the column jacketing performed satisfactorily, in spite of the fact that these column bars were 580mm apart(NZS 3101[SANZ

1982(a)] requires the spacing of tied longitudinal column bars not to exceed 200mm). Similar results for this aspect have also been found in seismic load tests of reinforced concrete columns strengthened by jacketing conducted at the University of Canterbury[Rodriguez and Park 1994].

5.2.3 Initial Stiffness

The theoretical initial stiffness of Specimen R1 was estimated using the procedures outlined in Section 3.9. When calculating the stiffness of the test specimen, a weighted average concrete compressive strength was used since both the beam and column consisted of two different concretes having different compressive strengths. The method used to obtain the weighted average concrete compressive strength was described in Section 3.4.2.

The theoretical initial stiffness of Specimen R1 was calculated to be

$$K_{theoretical}=42.1\text{kN/mm}$$

The theoretical stiffness $K_{theoretical}$ is shown in Fig.5.2. The stiffness estimated at 75% of the theoretical ideal storey horizontal load strength of the test specimen was 17.4kN/mm for the positive loading cycle and 16.0kN/mm for the negative loading cycle. The average value of the stiffnesses obtained for the positive and negative loading cycle, 16.7kN/mm was only 40% of the theoretical stiffness. This is mainly attributed to the effect of the previous damage to the as-built specimen, especially bond deterioration along the beam bars in the joint core. However the measured stiffness of the retrofitted specimen was about seven times that of the as-built specimen. A significant increase in stiffness as a result of jacketing was obvious.

The yield displacement of the retrofitted specimen was 13.0mm which was 0.41% in terms of a storey drift angle. It is seen that the measured yield displacement of the retrofitted specimen was somewhat larger than that limited by the current code NZS 4203[SANZ 1992].

5.2.4 Available Displacement Ductility Factor

The available displacement ductility factor μ_a [Park 1989] was calculated from the cumulative displacement ductility factor obtained from the measured horizontal storey shear force versus horizontal displacement hysteresis loops of Specimen R1. The available displacement ductility factor is defined for four loading cycles as follows:

$$\mu_a = \Sigma\mu / 8 \tag{5.1}$$

where $\sum\mu$ is the cumulative displacement ductility factor, calculated for when the horizontal storey shear force is not less than 80% of the maximum applied shear force. Using this definition, $\mu_a=8$ for Specimen R1. The New Zealand concrete design code NZS 3101[SANZ 1982(a)] specified that structures with "adequate ductility" should reach horizontal displacement of at least 4 to 6 times the displacement at first yield during four loading cycles, without significant reduction in strength. Available displacement ductility factor obtained from the retrofitted Specimen R1 met the requirement for structures with "adequate ductility" in the code, indicating a considerable improvement in the displacement ductility capacity due to jacketing the poorly detailed as-built beam-column joints.

5.2.5 Beam Behaviour

5.2.5.1 Beam Shear

The maximum nominal beam shear stress $v_b=V_b/bd$ was estimated to be $0.14\sqrt{f'_c{}^*}$ during beam negative moment and $0.08\sqrt{f'_c{}^*}$ during beam positive moment, where V_b is the applied beam shear force obtained from the measured end reaction, b is the beam width, d is the effective depth of the beam and $f'_c{}^*$ is the weighted average concrete compressive strength defined in Section 3.4.2.

5.2.5.2 Longitudinal Beam bar Strains

The strains on the new and existing longitudinal beam bars measured from the wire strain gauges are plotted in Figs.5.4 and 5.5, respectively. The new bottom beam bars at the column face started to yield during the loading to $\pm 0.5P_i$, while the new top beam bars yielded in the loading to $\pm 0.75P_i$. In the loading to DF of 2, the measured strains in the beam bars at the column face increased to more than 1.5% and most of the wire strain gauges at the column face were damaged after those loading cycles. The small tensile strains measured at the centre of the column as illustrated in Fig.5.4 indicates that the new main beam bars were well anchored in the joint core up to the loading to DF of 2.

As shown in Fig.5.5, the existing top and bottom main beam bars at the column face started to yield in the loading to DF of 1. In the loading to DF of 2, the maximum tensile strains measured at the column face were 1.36% for the top beam bars and 1.46% for the bottom beam bars. Although the column depth of the retrofitted specimen was great enough to accommodate the development length of the beam bars, tensile strains were measured over the column depth even in the elastic loading cycle. In the positive cycle of loading to DF of 2, the strains along the existing bottom beam bar measured over the column depth approached the yield strain, indicating severe bond deterioration. This is because the bond condition along the existing beam bars in the joint had deteriorated during the previous test conducted on

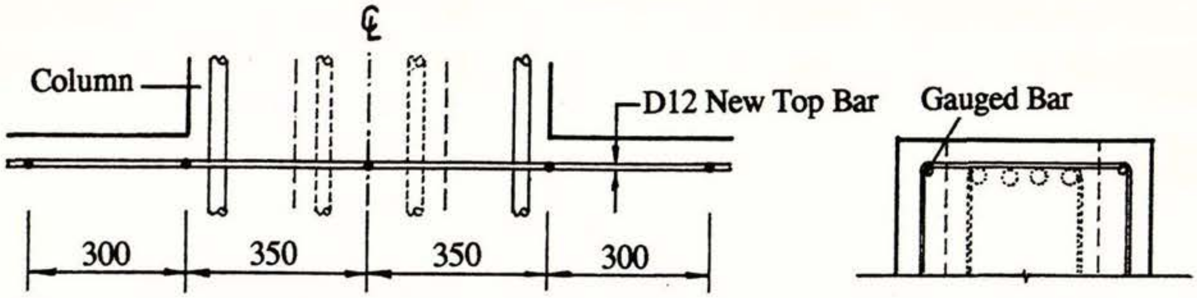

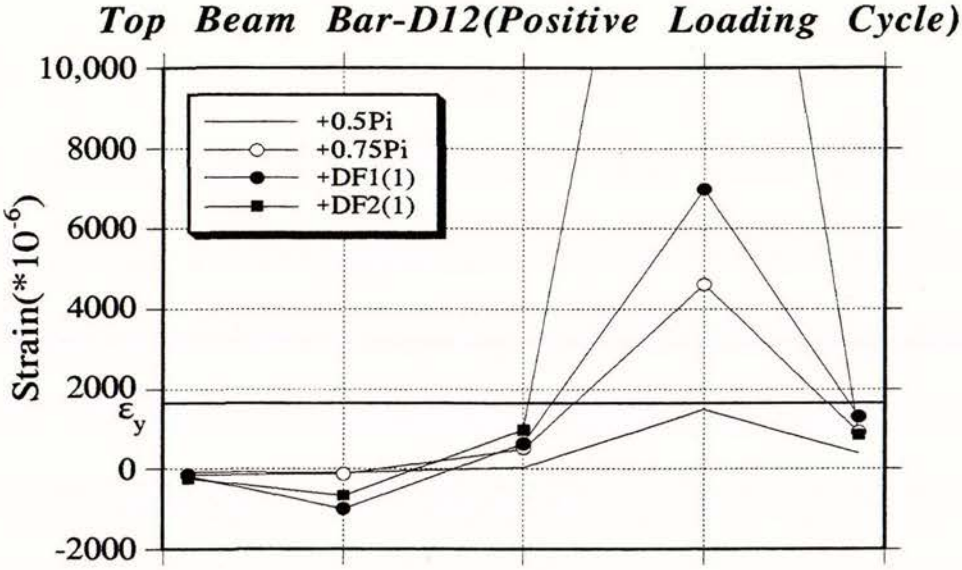

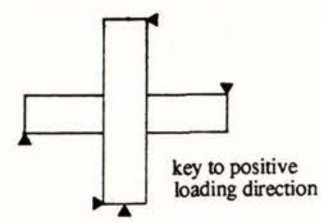

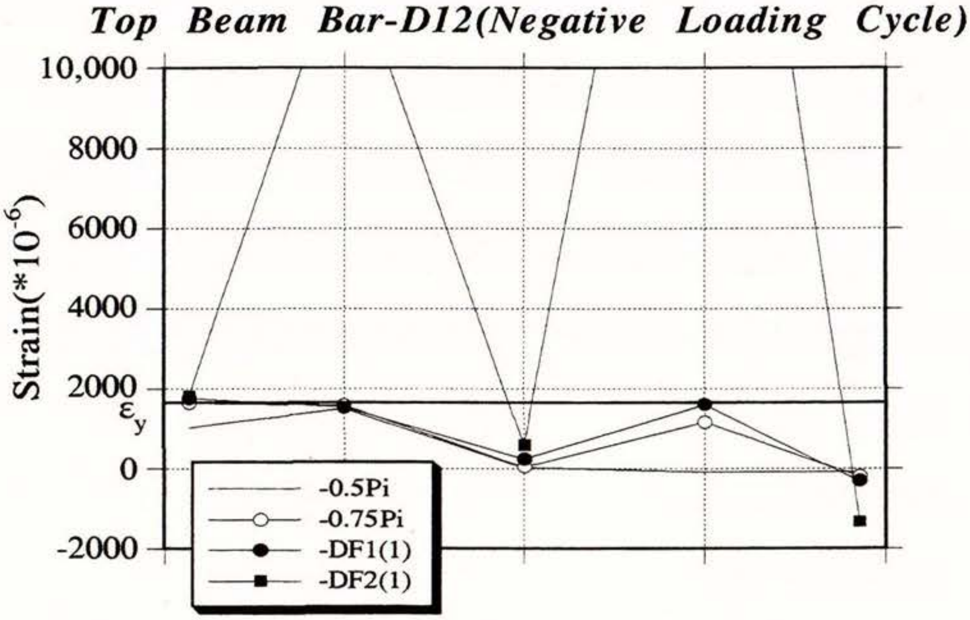

Fig.5.4(a) Strain Profiles of New Top Beam Bar(D12) of Specimen R1

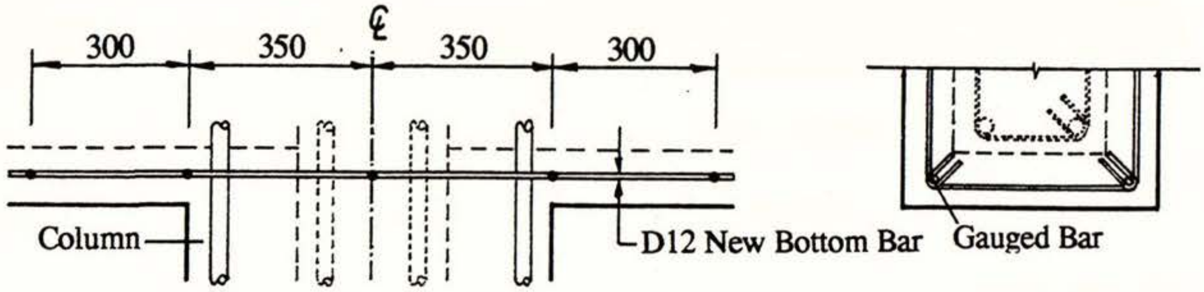

Bottom Beam bar-D12(Positive Loading Cycle)

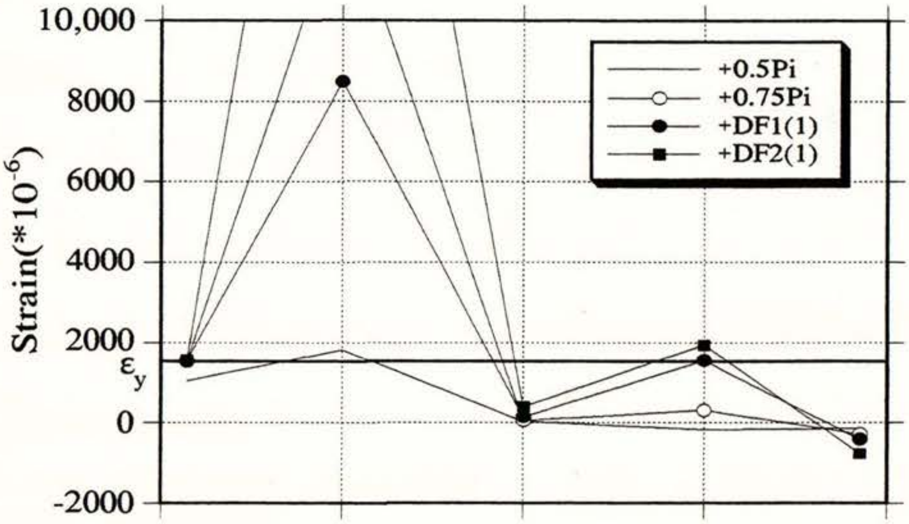

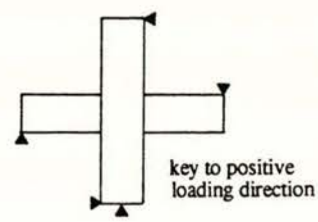

Bottom Beam Bar-D12(Negative Loading Cycle)

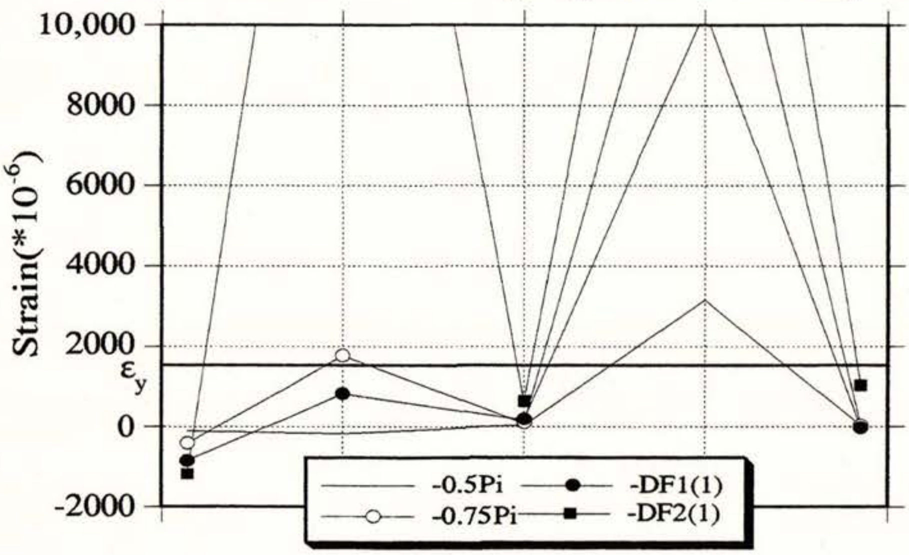

Fig.5.4(b) Strain Profiles of New Bottom Beam Bar(D12) of Specimen R1

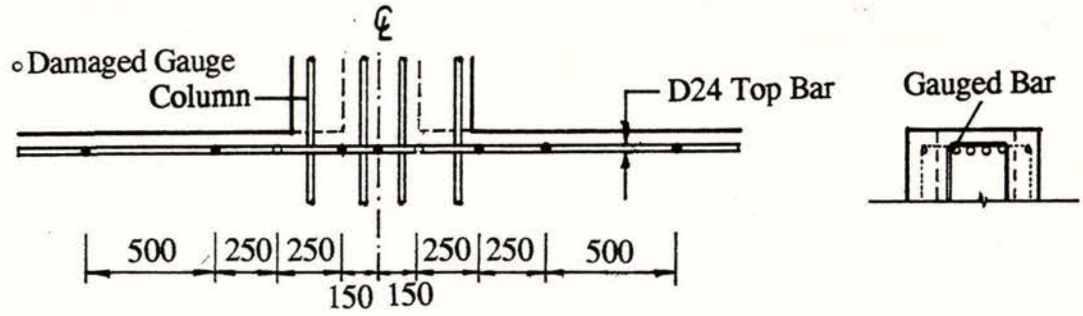

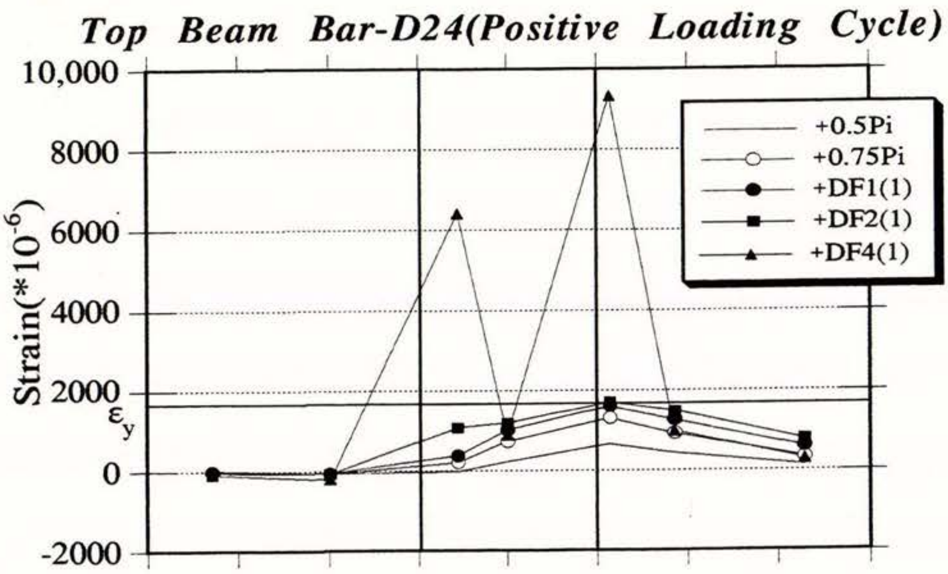

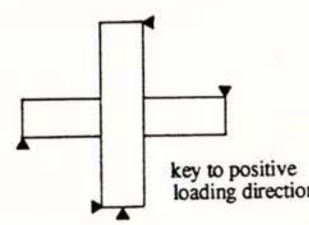

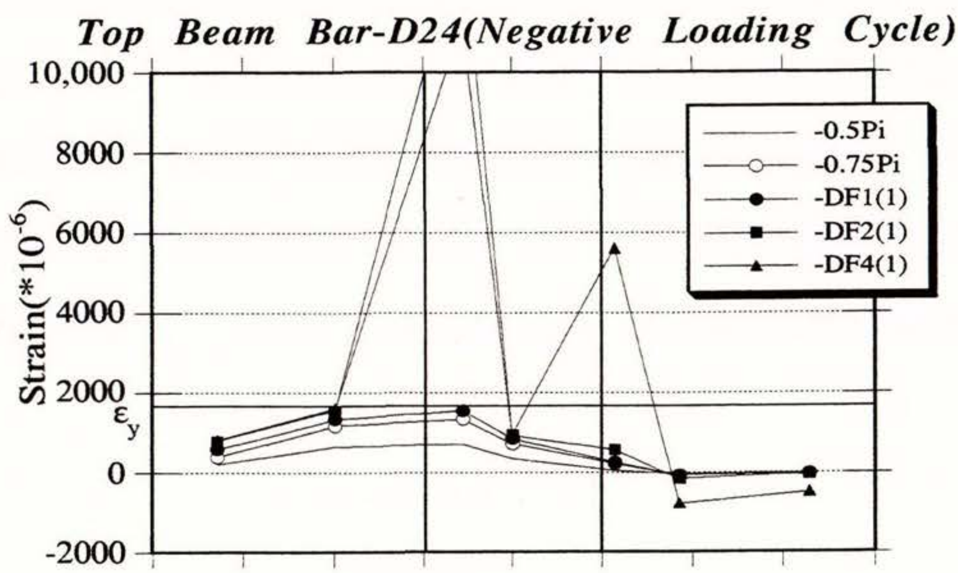

Fig.5.5(a) Strain Profiles of Existing Top Beam Bar(D24) of Specimen R1

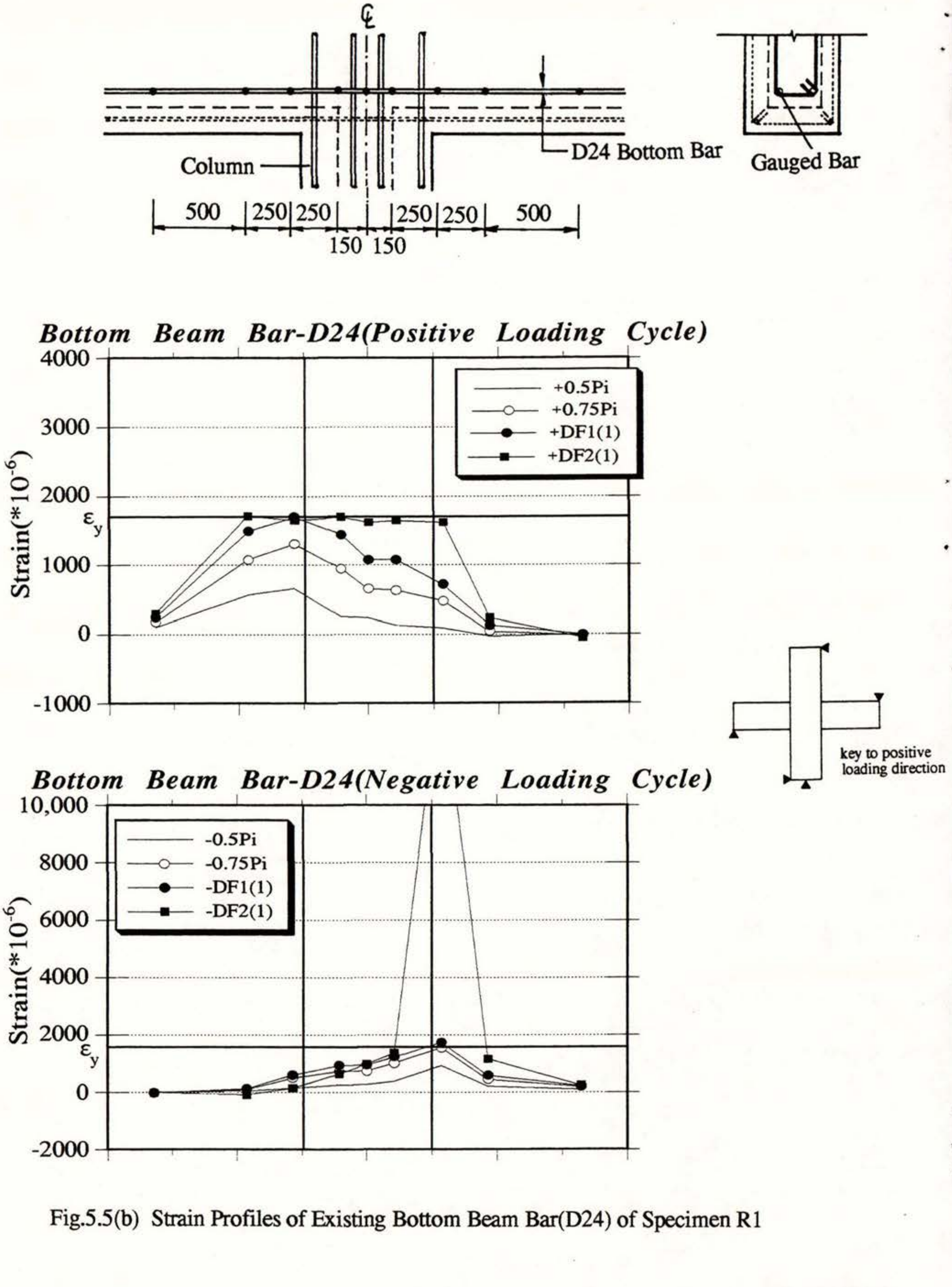

Fig.5.5(b) Strain Profiles of Existing Bottom Beam Bar(D24) of Specimen R1

Specimen O1. Chipping off the cover concrete of the beam top face to place the new transverse reinforcement as well as removing the loose concrete in the joint region aggravated the bond condition along the existing beam bars in the joint.

It can be concluded that bond deterioration along the existing beam bars in the joint of the as-built specimen cannot be improved by concrete jacketing. This resulted in the relatively flexible structure as discussed in Section 5.2.3.

5.2.5.3 Beam Curvature Ductility Factor

Fig.5.6 shows the measured curvature ductility factors of the beams. The curvatures were obtained from the second set of the linear potentiometers placed commencing at 50mm away from the column face. The gauge length for calculating the curvature was $0.42h_b$, where h_b is beam depth(=600mm). The yield curvature ϕ_y was calculated using the curvature ϕ_{75} measured at $\pm 0.75P_i$, extrapolated linearly to M_i, where M_i is the ideal flexural strength of the beam based on the measured material strengths. The yield curvature was then calculated by following equation.

$$\phi_y = \phi_{75} M_i / M_{75} \tag{5.2}$$

where M_{75} is the applied beam face moment at $0.75P_i$. The yield curvatures so obtained are shown in Fig.5.6. Theoretical yield curvature of the beam calculated by conventional section analysis is 0.0034(1/m) during beam positive moment and 0.0038(1/m) during beam negative moment.

The curvature ductility factors with beam positive moment and negative moment measured in the loading to DF of 2 were very comparable. With beam positive moment, however, the measured curvature ductility factor increased rapidly as the displacement ductility factor imposed on the specimen increased. The maximum curvature ductility factors measured during beam positive moment were 37 for the east beam and 16 for the west beam. With beam negative moment, the curvature ductility factors increased gradually after the loading to DF of 2. The maximum curvature ductility factor measured during beam negative moment was 6 for the east beam and 7 for the west beam. The beams retrofitted by jacketing with additional reinforced concrete demonstrated that significantly large curvature ductility factors could be obtained when detailed according to NZS 3101[SANZ 1982(a)].

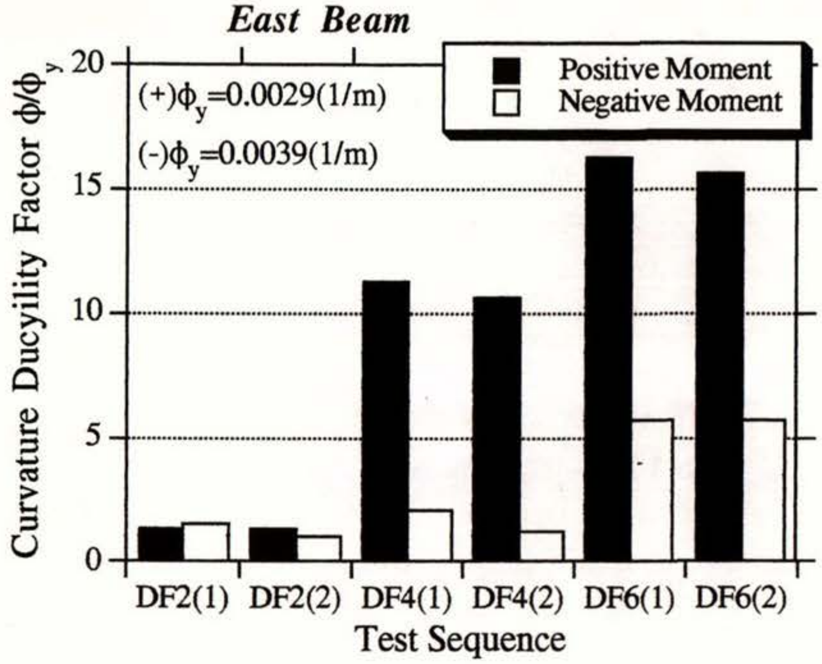

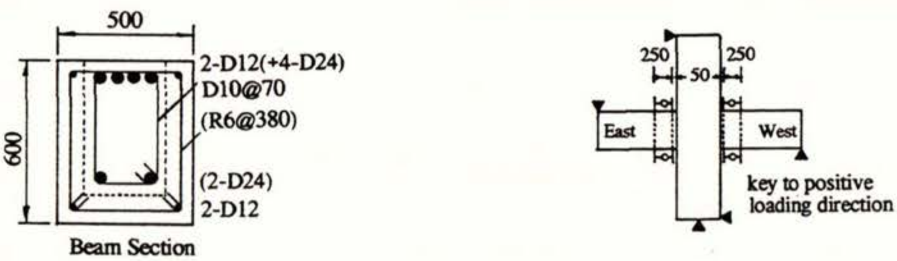

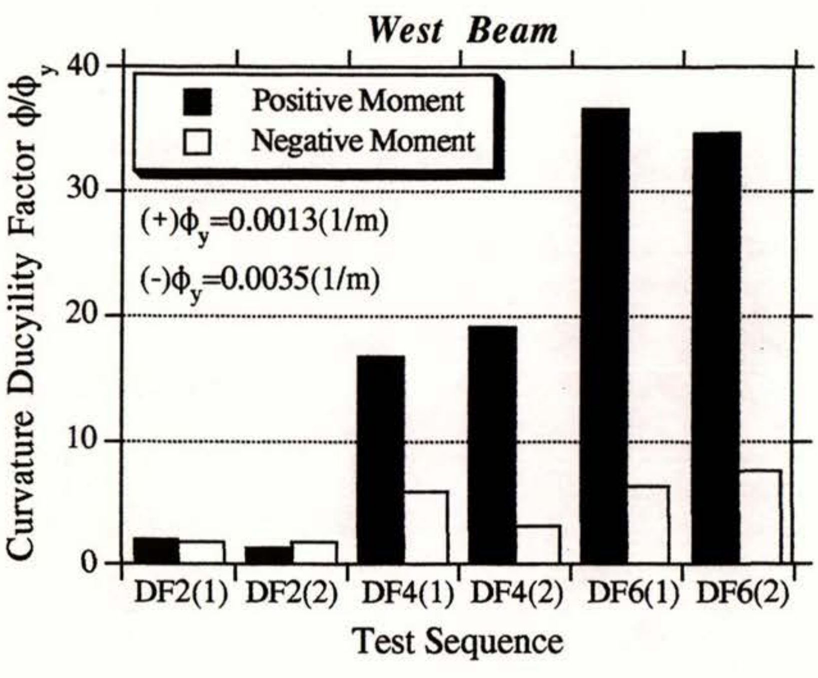

Fig.5.6 Curvature Ductility Factors of Beams of Specimen R1

5.2.5.4 Equivalent Plastic Hinge Lengths of the Beams

The equivalent plastic hinge length L_p of the beams retrofitted by concrete jacketing was calculated at the peak of each loading cycle. Based on the assumed curvature distribution illustrated in Fig.5.7, following equation was used to obtain L_p.

$$\delta_b=\delta_y+(\phi-\phi_y)\,L_p\,(l'_b-\frac{L_p}{2}) \tag{5.3}$$

where δ_b=beam end displacement due to flexure obtained from the linear potentiometer readings, not including the displacement due to fixed-end rotation, δ_y=beam yield displacement(=$\delta_{75}M_i/M_{75}$), δ_{75}=the calculated beam end displacement at $0.75P_i$, M_i=the theoretical ideal flexural strength of the beam, M_{75}=the applied beam face moment at $0.75P_i$, ϕ_y=beam yield curvature obtained from the average curvature measured at the second set of linear potentiometers placed at 50mm away from the column face(=$\phi_{75}M_i/M_{75}$), ϕ_{75}=the measured curvature at $0.75P_i$, l'_b=shear span of beam from column face(=1555mm), ϕ=curvature measured at the second set of linear potentiometers placed at 50mm away from the column face.

As shown in Fig.5.7, it was assumed that the distribution of elastic curvature was linear along the beam and that the distribution of plastic curvature was constant spread over L_p. The equivalent plastic hinge lengths for each beam so obtained were plotted as the ratio of the beam depth.

With beam positive moment, the obtained equivalent plastic hinge lengths were scattered widely in the loading to DF of 2. In the loading to DF of 4, however, the equivalent plastic hinge lengths became fairly constant and were approximately 0.40 to 0.45 of the beam depth for both beams. In the loading to DF of 6, the equivalent plastic hinge length with beam positive moment increased slightly to 0.49 of the beam depth. With beam negative moment, the range of the equivalent plastic hinge length was 0.27 to 0.40 times the beam depth up to the loading to DF of 6.

The equivalent plastic hinge length of the beams retrofitted by concrete jacketing of Specimen R1 was somewhat smaller than the 0.5 of the beam depth, which is generally accepted for design purposes but was very close to the value obtained from the following equation proposed by Priestley and Park 1987:

$$\begin{aligned} L_p &= 0.08l'_b+6d_b \\ &= 268\text{mm}(=0.45h_b) \end{aligned} \tag{5.4}$$

where d_b is the bar diameter(=24mm) and l'_b is shear span of beam.

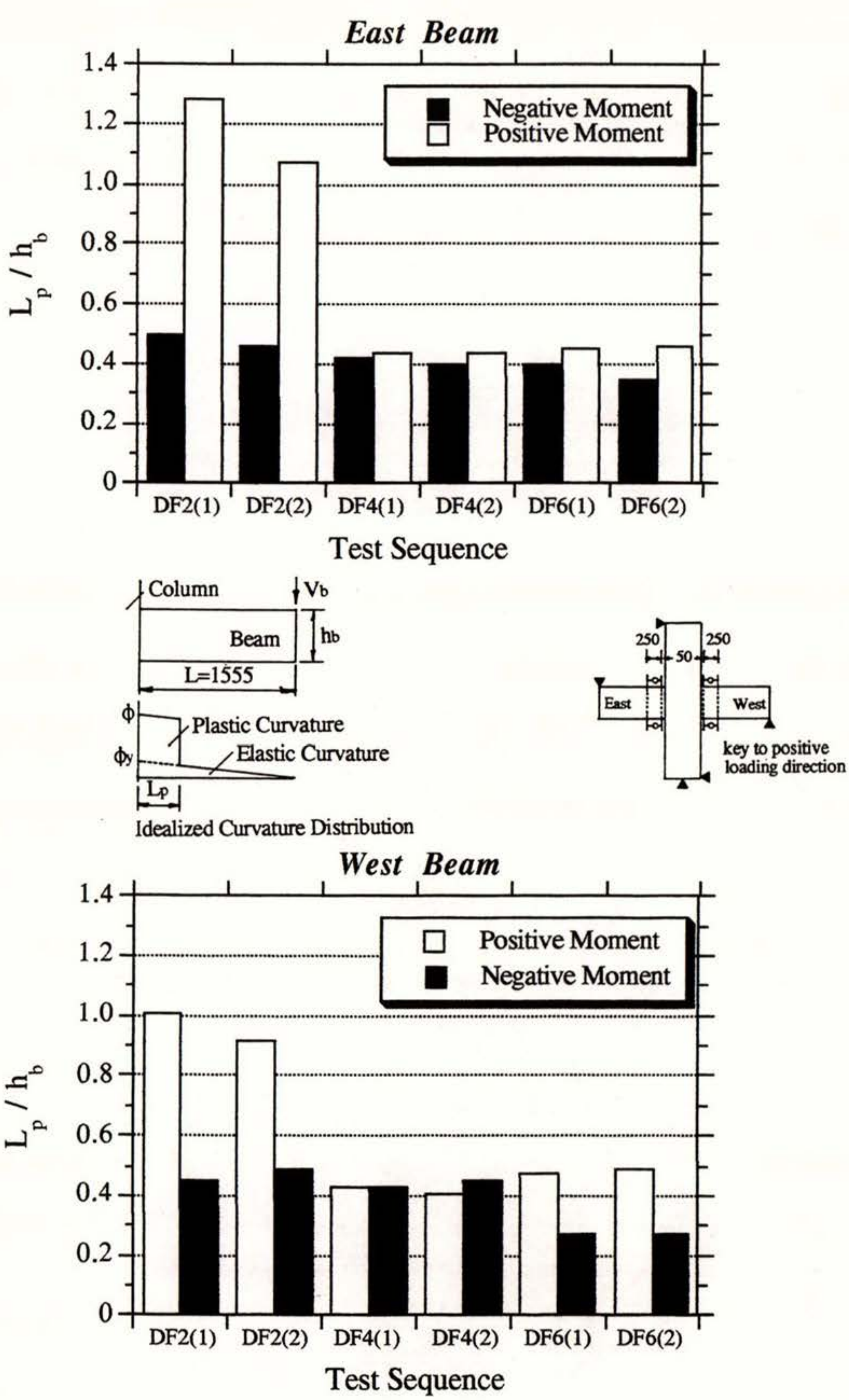

Fig.5.7 Equivalent Plastic Hinge Length of the Beams of Specimen R1

5.2.6 Column Behaviour

5.2.6.1 Column Cracking

During the test, only minor flexural cracks and bond splitting cracks along the column corner bars were observed(see Fig.5.1). The widths of those cracks remained very small until the end of testing.

5.2.6.2 Longitudinal Column Bar Strains

The strains along the new longitudinal column reinforcement are shown in Fig.5.8. Those strains were obtained from the wire strain gauges. Only strains at the beam face were measured.

The strains increased gradually as the test progressed. The beam depth of the test specimen was increased by jacketing the beam soffit alone so that column flexural tension force at beam top face was larger than that at beam bottom face. Therefore the strains measured at beam top face were somewhat larger than those measured at beam bottom face. In the loading to DF of 6, the strains measured at the beam top face subjected to column flexural tension force reached its yield strain. As shown in Fig.5.8, however, no significant tensile strains were measured during the test. On the other hand, the strains measured in flexural compression zone were in compression or small tension up to the loading to DF of 8. For Specimen R1 in which horizontal shear reinforcement were provided in the joint core, it is likely that the new column longitudinal bars were well anchored in the joint and that large column bond forces were transferred into the joint core.

It can be concluded that the columns of the retrofitted Specimen R1 remained essentially in the elastic range during the test.

5.2.7 Joint Behaviour

5.2.7.1 Joint Shear

The maximum nominal horizontal joint shear stress was $0.29\sqrt{f'_c{}^*}$, where $f'_c{}^*$ is the weighted average compressive strength of two concretes (existing and added) of the joint core. In the loading to $\pm 0.75P_i$, diagonal tension cracks initiated in the joint core. However, the crack widths remained very small until the end of testing.

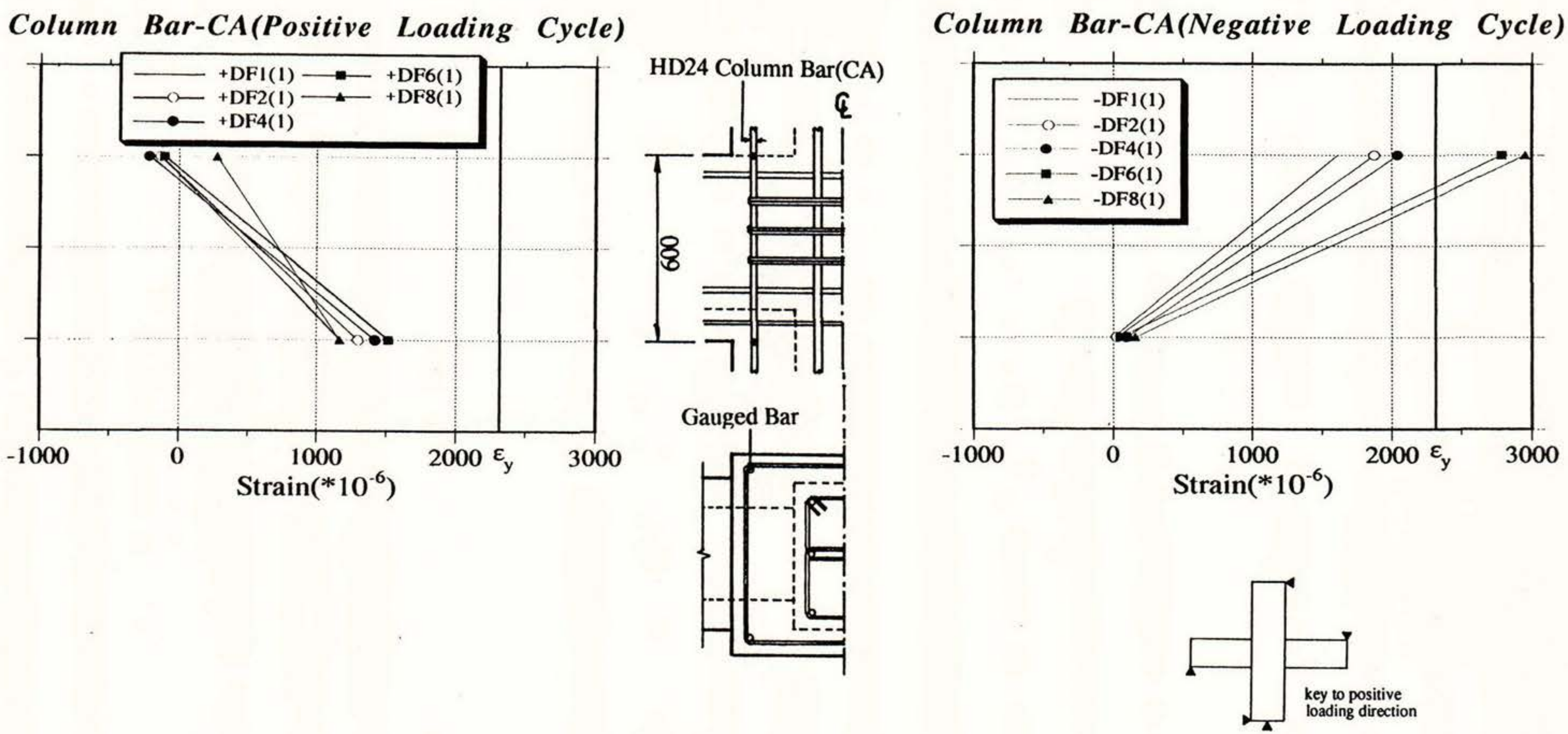

Fig.5.8(a) Strain Profiles of Column Bars of Specimen R1

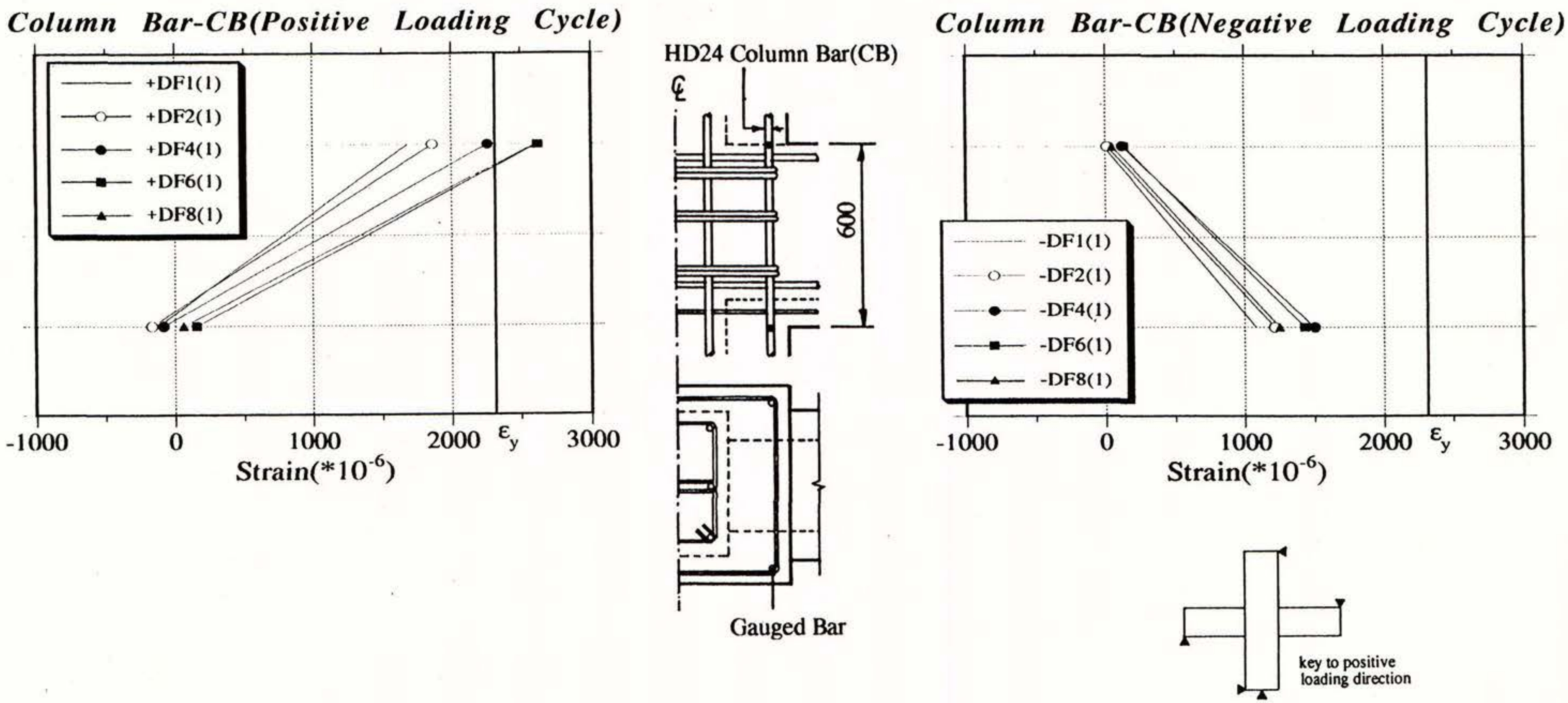

Fig.5.8(b) Strain Profiles of Column Bars of Specimen R1

5.2.7.2 Joint Hoop Strains

Three pairs of wire strain gauges attached on both sides of the reinforcement were used to measure the strains in the new joint hoops . Fig.5.9 illustrates the joint hoop strains measured at the peak of each loading cycle.

After diagonal tension cracks formed in the joint, the joint hoop strains increased gradually with the increase in displacement ductility factor imposed on the test specimen. During the test, the strains measured were below the yield strain as shown in Fig.5.9. The maximum tensile strains were 0.081% for the positive loading cycle and 0.093% for the negative loading cycle during the test. These values were only 38% to 43% of the yield strain of the horizontal joint shear reinforcement. It is evident that the new joint horizontal reinforcement were well detailed and that the joint core remained in the elastic range.

5.2.7.3 Joint Shear Distortion and Expansion

The joint diagonal movements were monitored to obtain the joint shear distortion and expansion during the test. Those are shown in Fig.5.10. As observed for the joint hoop strains, the joint shear distortion and expansion increased gradually as the test progressed. However, no rapid increases were observed during the test. The maximum joint shear distortion was 0.27% while the joint expansion was 1.21mm measured in the first cycle of loading to DF of 8. The small shear distortion and expansion measured in the joint are mainly due to the reduced nominal horizontal joint shear stress as a result of the enlargement of the column cross section area and the well detailed transverse reinforcement in the joint core.

In summary, the test conducted on Specimen R1 demonstrated that the previous damage to the joint of the as-built Specimen O1 had little effect on the response of Specimen R1.

5.2.8 Decomposition of Horizontal Displacement

In Fig.5.11, the components of the horizontal displacement of the specimen at the peaks of the selected loading cycles are shown.

The major source of storey drift was the beam displacement, indicating a "strong column-weak beam" behaviour. The beam fixed-end rotation accounted for about 30% of the total displacement up to the loading to DF of 4. In the subsequent loading cycles, its contribution increased to 52%. The contribution of the beam flexural displacement was approximately 30% to 40% of the imposed storey drift angle and did not change significantly during the test.

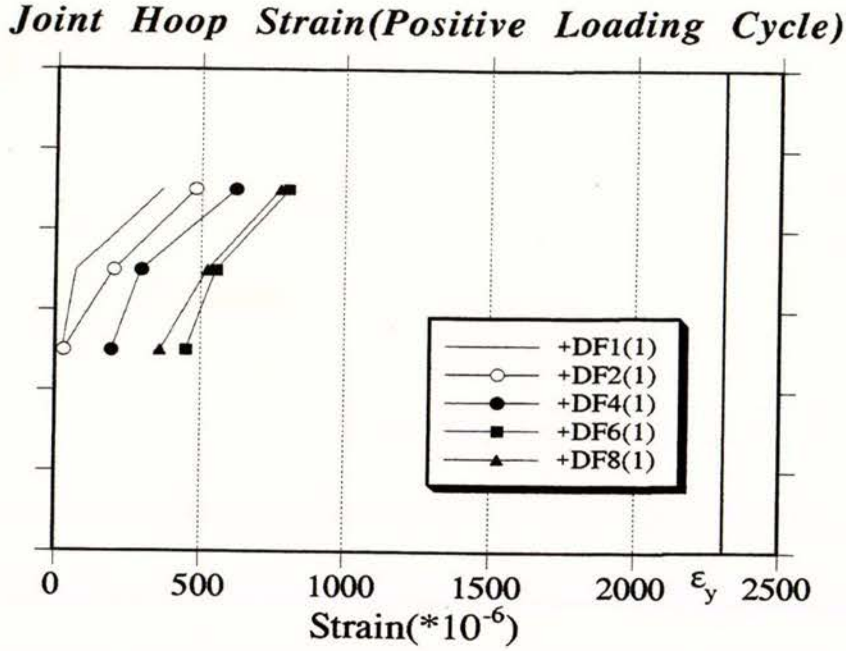

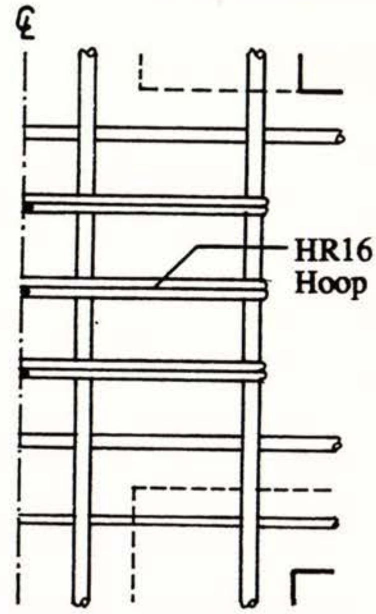

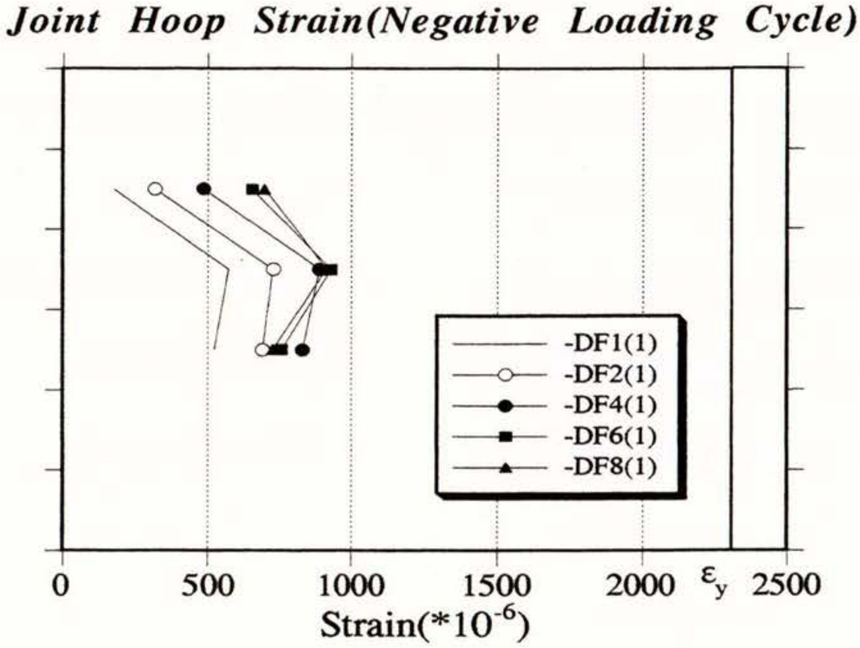

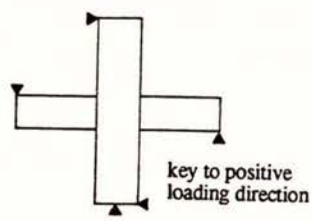

Fig.5.9 New Joint Hoop Strains of Specimen R1

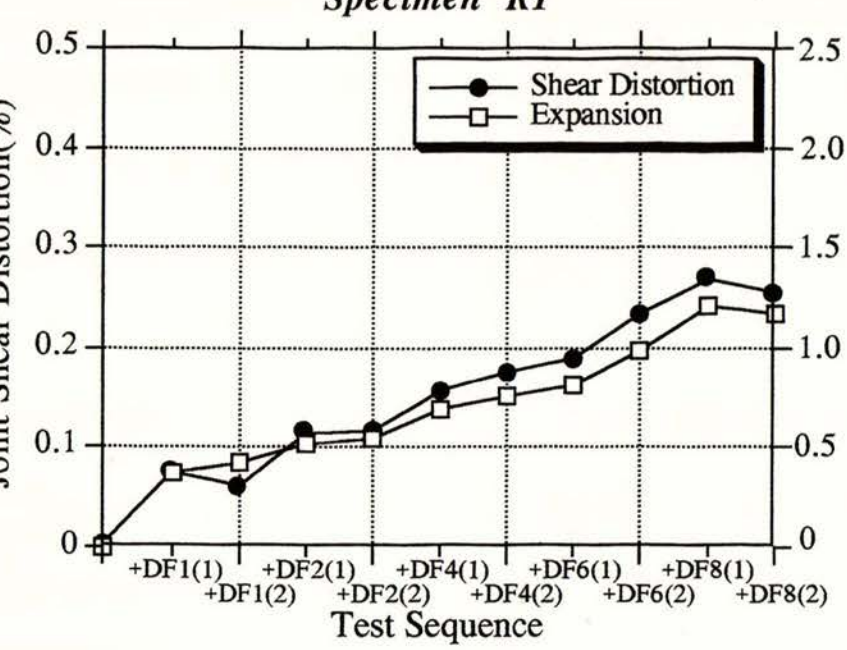

Fig.5.10 Joint Shear Distortion and Expansion of Specimen R1

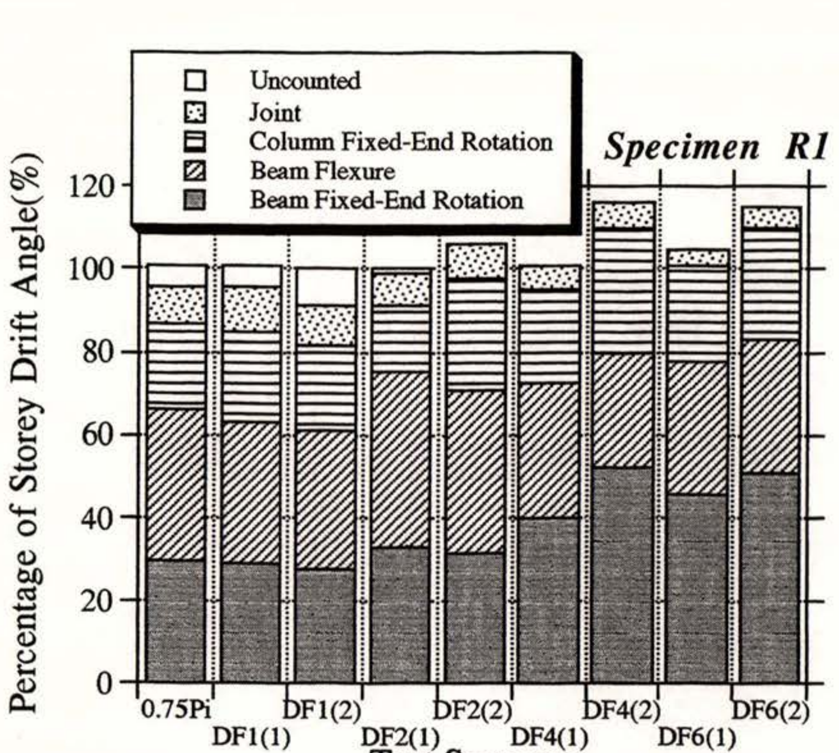

Fig.5.11 Components of Storey Drift Angle of Specimen R1

As shown in Fig.5.11, the fixed-end rotation of the columns contributed about 20% to 30% of the drift angle during testing. The contribution of the columns was relatively constant during the test. The contribution of the joint shear distortion accounted for up to 11% of the total displacement until the loading to DF of 1. However, its contribution became insignificant since the joint remained essentially elastic during the test, as mentioned before.

5.3 RETROFITTED SPECIMEN R2

5.3.1 The Specimen

Specimen R2 was the specimen retrofitted in the same manner as Specimen R1 except that new joint hoops were not placed in the joint core. The existing and new concrete had compressive cylinder strengths of 43.4MPa and 61.4MPa, respectively, at the time of testing. The ratio of the theoretical ideal flexural strength of the column to that of beam was 2.1 based on the measured material strengths. When the plastic hinges were formed in the beams, the calculated ideal storey horizontal load strength P_i was 218kN.

5.3.2 General Behaviour

The final crack pattern is shown in Fig.5.12 Fig.5.13 illustrates the measured storey shear force versus horizontal displacement hysteresis curves. The theoretical ideal storey horizontal load strength P_i and the theoretical stiffness $K_{theoretical}$ calculated by conventional frame analysis are also shown in this figure. Crack patterns at the peak of each loading cycle are shown in Fig.5.14.

In the loading to $\pm 0.5P_i$, flexural cracks were observed in the beams and columns. Flexural-shear cracks also developed in the beams. The new bottom beam bars yielded in tension at the column face. In the loading to $\pm 0.75P_i$, beam flexural cracks extended and the number of those cracks increased(see Fig.5.14(a)). The new top beam bars also yielded at the column face at the stage of this loading.

In the loading to displacement ductility factor DF of 1, the beam flexural cracks at the column face opened to a maximum crack width of 0.9mm at the beam bottom face and 0.3mm at the beam top face. The strains in the existing top and bottom beam bars reached the yield strain at the column face.

In the loading to DF of 2, crushing of concrete in the beam flexural compression zones occurred. The width of the beam flexural crack at the column face was up to 3mm for the top face and 4mm for the bottom face, respectively. The maximum horizontal load strength of

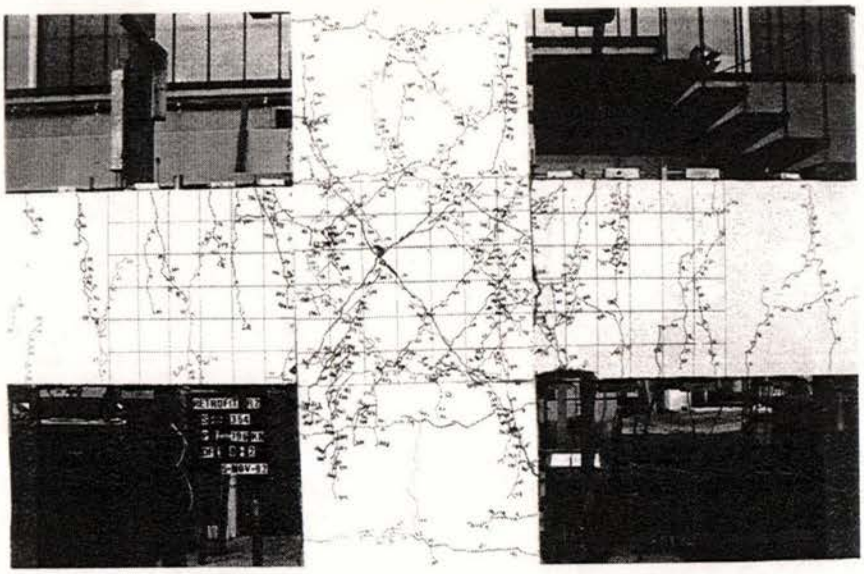

Fig.5.12 Observed Cracking of Specimen R2
at second cycle of DF=-8

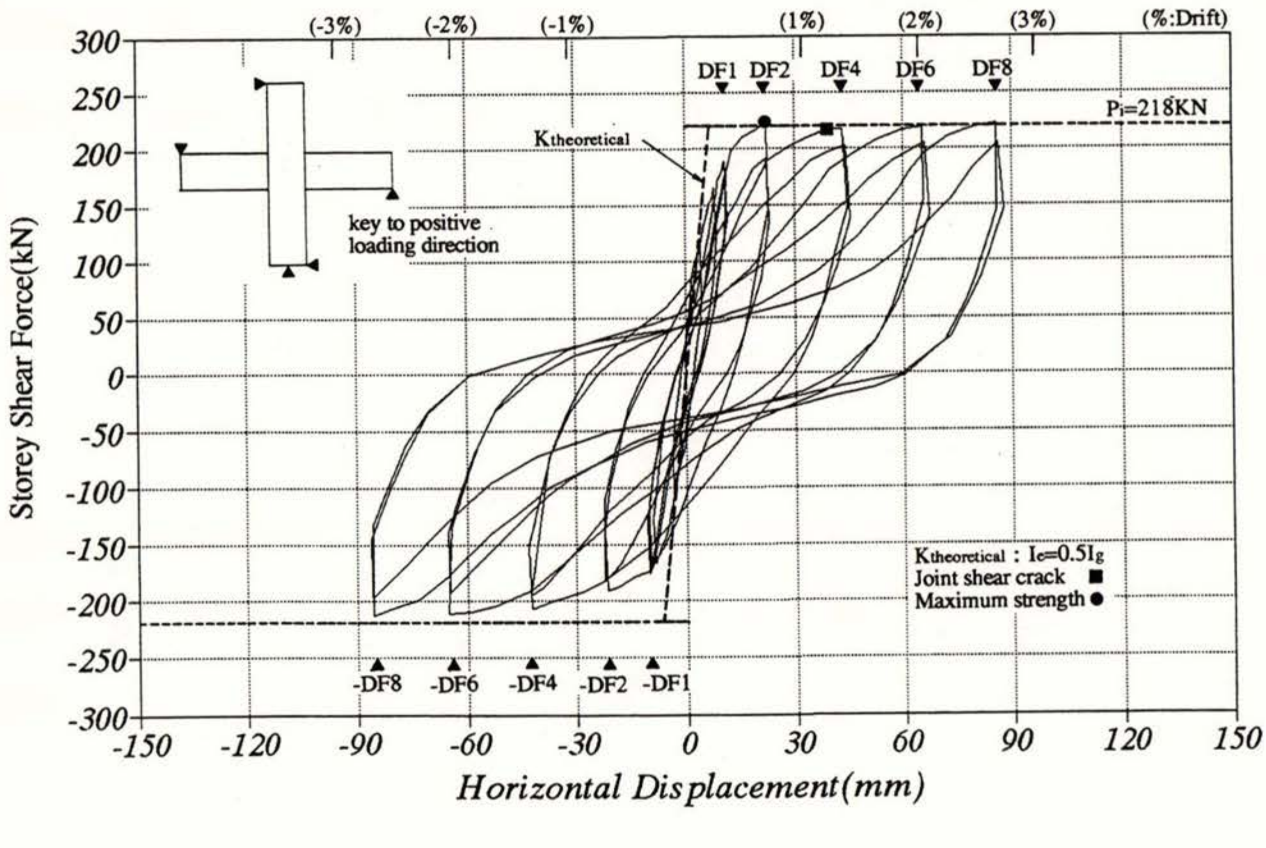

Fig.5.13 Storey Shear Force versus Horizontal Displacement Relationship
for Specimen R2

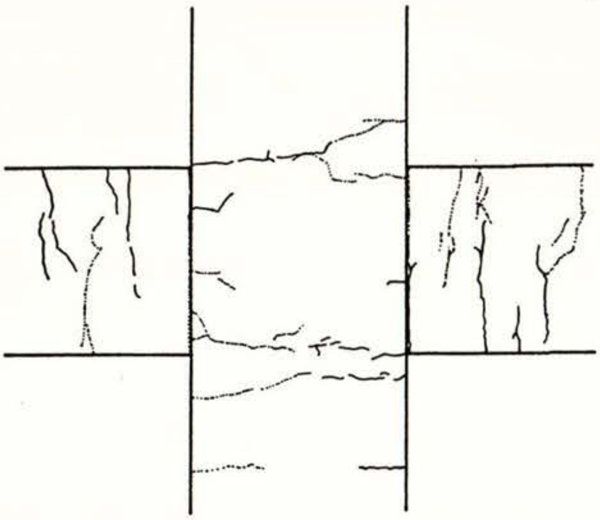

(a) at the peak of 0.75Pi
(R=0.25%)

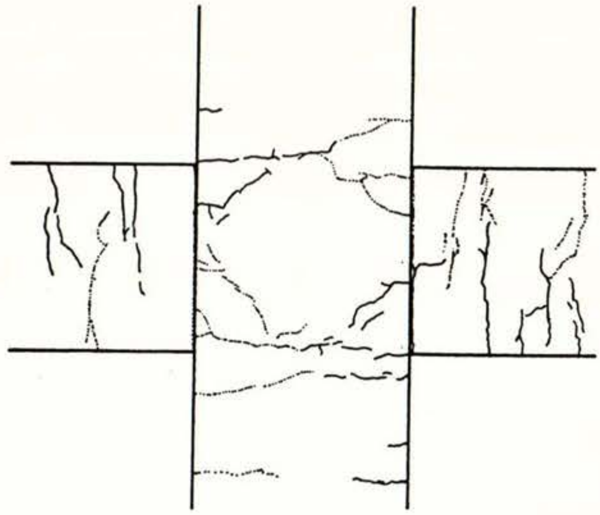

(b) at the peak of second cycle, DF=1
(R=0.34%)

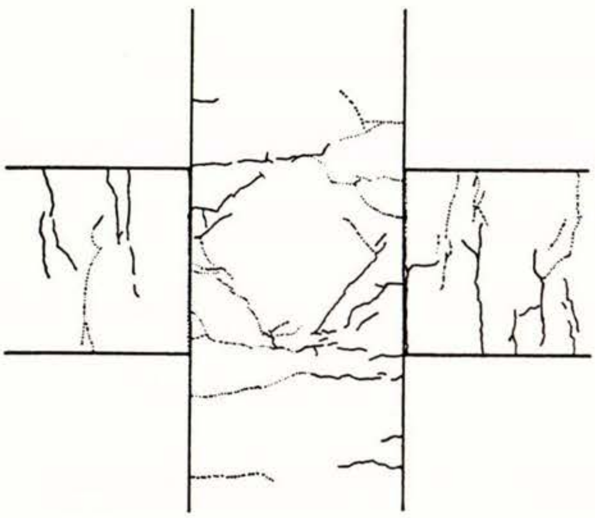

(c) at the peak of second cycle, DF=2
(R=0.67%)

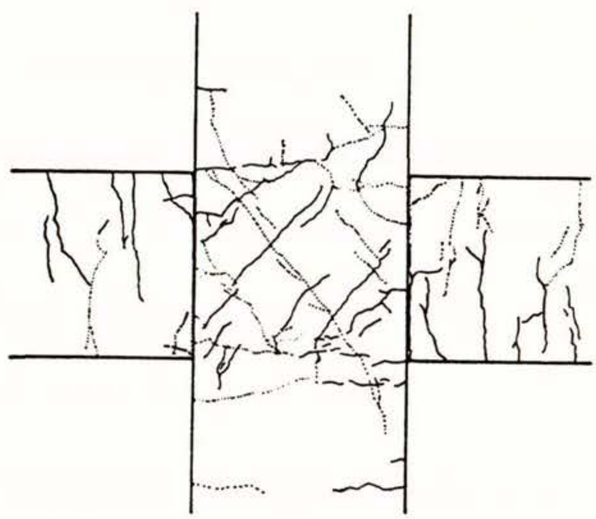

(d) at the peak of second cycle, DF=4
(R=1.34%)

(e) at the peak of second cycle, DF=6
(R=2.01%)

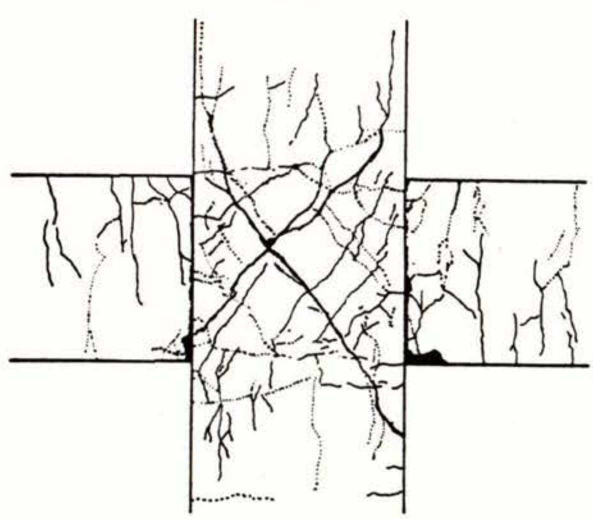

(f) at the peak of second cycle, DF=8
(R=2.68%)

Fig.5.14 Observed Cracking of the Joint(Specimen R2)

223kN was measured at a storey drift angle of about 0.7%. The measured maximum horizontal load strength was 103% of the ideal storey horizontal load strength of the specimen. The columns and joint showed only minor flexural and shear cracking(see Fig.5.14(c)).

In the first cycle of loading to DF of 4, corner to corner diagonal tension cracks developed in the joint core(see Fig.5.14(d)). Concrete crushing in the beam flexural compression zone became more apparent. The beam flexural cracks at the column face opened to a maximum crack width of about 7mm at the top beam face and 9mm at the bottom beam face, respectively. In the second cycle of this loading, corner to corner diagonal tension cracks opened to a maximum width of 1.8mm. Some pinching was observed in the storey shear force versus horizontal displacement hysteresis curves. However only a little reduction in strength was measured in the hysteresis loops(see Fig.5.13).

In the loading to DF of 6, the cover concrete at the beam soffit started to spall off. Bond splitting cracks along the column corner bars initiated near the beam face. Joint diagonal tension cracks extended and connected to those bond splitting cracks(see Fig.5.14(e)). The measured maximum width of the joint diagonal tension crack was 2.2mm. The beam flexural cracks at the column face widened significantly. As shown in Fig.5.13, the pinching became more apparent in the hysteresis curves, mainly due to the wide open beam flexural cracks.

In the loading to DF of 8, the cover concrete of the beam soffit in the plastic hinge regions spalled off(see Fig.5.14(f)). Flexural and flexural-shear cracks extended and opened wide in the beam plastic hinge regions. However, the observed damage in the beams was concentrated in a relatively small length from the column face. The joint diagonal tension cracks widened to a maximum crack width of 3.6mm Bond splitting cracks along the column corner bars extended. Although significant pinching was observed in the hysteresis loops as shown in Fig.5.13, only a 12% reduction in the storey horizontal load strength was measured in the second cycle of loading to DF of 8.

The response of the retrofitted Specimen R2 was very similar to that obtained from Specimen R1, that was ductile due to the beam hinge failure mechanism. This suggests that the previous damage to the as-built Specimen O1 had little effect on the response of the retrofitted specimen. Although diagonal tension cracks developed in the joint core during the test, the behaviour of the joint of Specimen R2 had no detrimental effect on the seismic performance of the retrofitted specimen, in spite of the fact that new horizontal shear reinforcement were not placed in the joint core.

5.3.3 Initial Stiffness

The theoretical initial stiffness of Specimen R2 was calculated by the same procedure as used for Specimens O1 and R1. The theoretical stiffness of Specimen R2 was

$$K_{theoretical}=43.8kN/mm$$

The theoretical stiffness $K_{theoretical}$ is shown in Fig.5.13. The stiffnesses estimated at 75% of the theoretical ideal storey horizontal load strength of the specimen were 21.1kN/mm for the positive loading cycle and 19.6kN/mm for the negative loading cycle. The average value of the stiffnesses obtained for the positive and negative loading cycle, 20.3kN/mm was 27% larger than that obtained from Specimen R1. However, the measured initial stiffness of Specimen R2 retrofitted by jacketing the columns, beams and joint was far below the theoretical value as observed for Specimen R1. The main reason for this low stiffness is likely to be caused by micro cracking and reduction of the effectiveness of the existing concrete associated with chipping off the cover concrete in the beams of the as-built specimen to place the new transverse reinforcement. Chipping off also had a detrimental effect of the bond condition along the beam bars in the joint. Therefore chipping off the existing concrete should be minimised if required. However the measured stiffness of Specimen R2 was nine times that of the as-built Specimen O1, indicating a significant increase in initial stiffness.

The yield displacement measured for the test specimen was 10.7mm which could be converted to 0.33% in terms of a storey drift angle. The yield displacement obtained from Specimen R2 approached the limiting value recommended by the current code[SANZ 1992].

5.3.4 Available Displacement Ductility Factor

The available displacement ductility factor μ_a of 10 was obtained for Specimen R2. This value was comparable to that calculated for Specimen R1. As mentioned before, the behaviour of the joint did not affect the overall response of Specimen R2 although the widths of the joint diagonal tension cracks were much larger than those observed for Specimen R1.

It can be concluded that even when no new horizontal shear reinforcement were placed in the joint core, the response required of structures with "adequate ductility" in the current code could be achieved by jacketing the poorly detailed as-built beam-column joints in this study.

5.3.5 Beam Behaviour

5.3.5.1 Beam Shear

The maximum nominal beam shear stress $v_b=V_b/bd$ measured was $0.12\sqrt{f'_c{}^*}$ during beam negative moment and $0.07\sqrt{f'_c{}^*}$ during beam positive moment, respectively, where V_b is applied beam shear force obtained from the measured end reaction, b is the beam width, d is the effective depth of the beam and $f'_c{}^*$ is the weighted average compressive strength of the two concretes of the beam.

5.3.5.2 Longitudinal Beam Bar Strains

The strain distributions obtained using the readings of wire strain gauges attached to the new and existing beam longitudinal bars are shown in Figs.5.15 and 5.16, respectively. The strains of the new bottom beam bars measured at the column face reached the yield strain during the loading to $\pm 0.5P_i$ as illustrated in Fig.5.15(b). On the other hand, the strains of the new top beam bars reached the yield strain in the loading to $\pm 0.75P_i$(see Fig.5.15(a)). In the loading to DF of 2, the measured bar strains at the column face increased to larger than 1.3% and yielding of top and bottom beam bars spread over 0.5 times the beam overall depth from column face in the beam. The measured strains at the centre of the column were less than the yield strain until the loading to DF of 2. The strain profiles measured along the new beam bars in Specimen R2 were very similar to those measured in Specimen R1.

As shown in Fig.5.16, the strains in the existing top and bottom beam bars at the column face reached the yield strain during the loading to $\pm 0.75P_i$ or DF of 1. In the loading to DF of 2, the maximum tensile strains measured at the column face were about 2.14% for the top beam bars and 2.33% for the bottom beam bars. Up to the loading to DF of 4, the strains at the centre of the joint were smaller than yield strain and no yield penetration into the joint core was measured. As was observed for Specimen R1, tensile strains in the beam bars were measured through the column depth even in the elastic loading cycles. The tensile strains measured in the joint core would cause beam fixed-end rotation, resulting in a more flexible structure. Although the tensile strains in the beam bars measured at the column face subjected to beam flexural compression force were somewhat smaller than those obtained from Specimen R1, the difference was not so significant.

5.3.5.3 Beam Curvature Ductility Factor

The curvature ductility factors of the beams were calculated using the same method as used for Specimen R1, described in Section 5.2.5.3. The gauge length for calculating the curvature ductility factor was 250mm($=0.42h_b$), where h_b is beam depth(=600mm). The

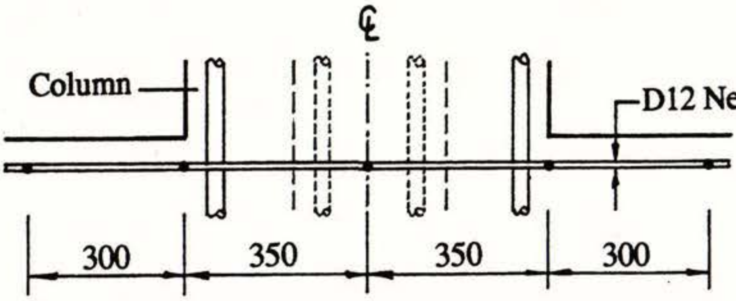

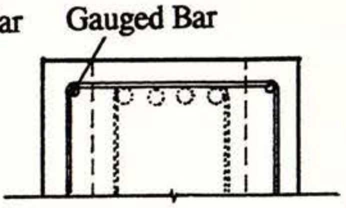

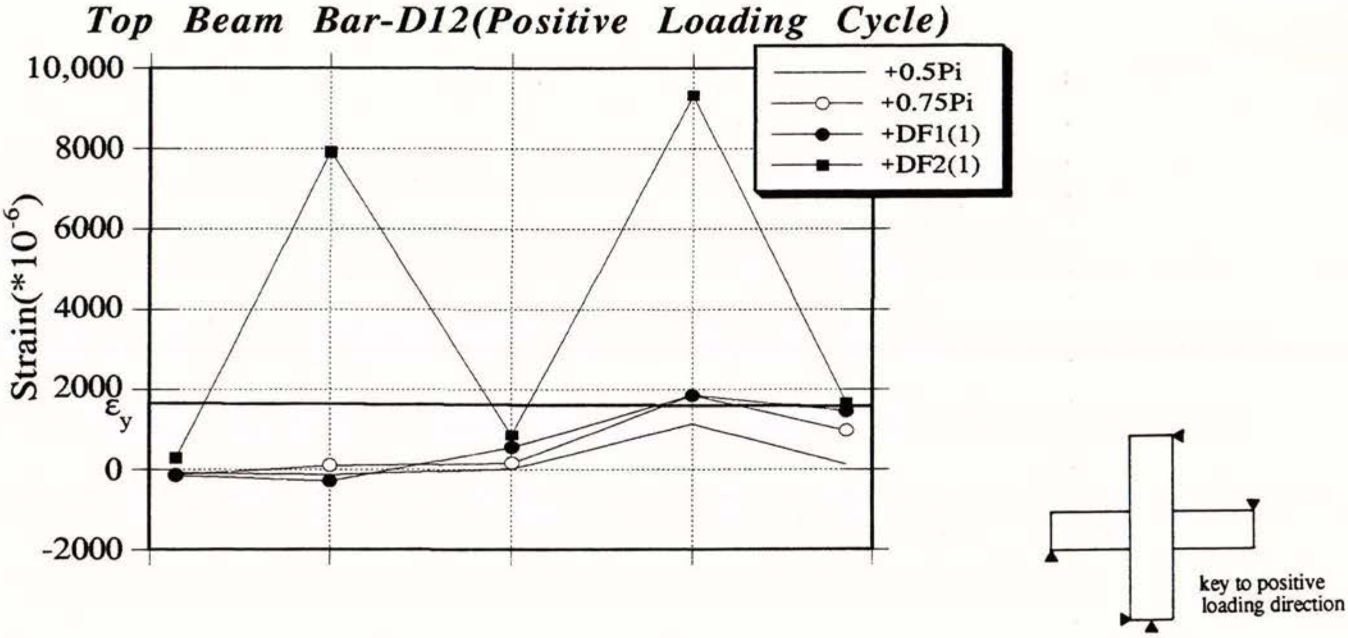

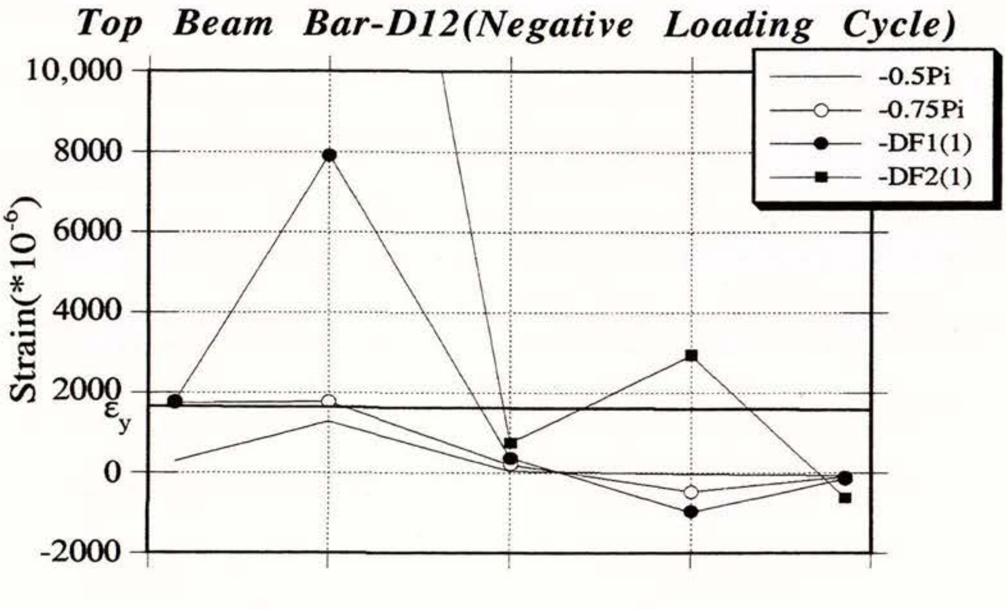

Fig.5.15(a) Strain Profiles of New Top Beam Bar(D12) of Specimen R2

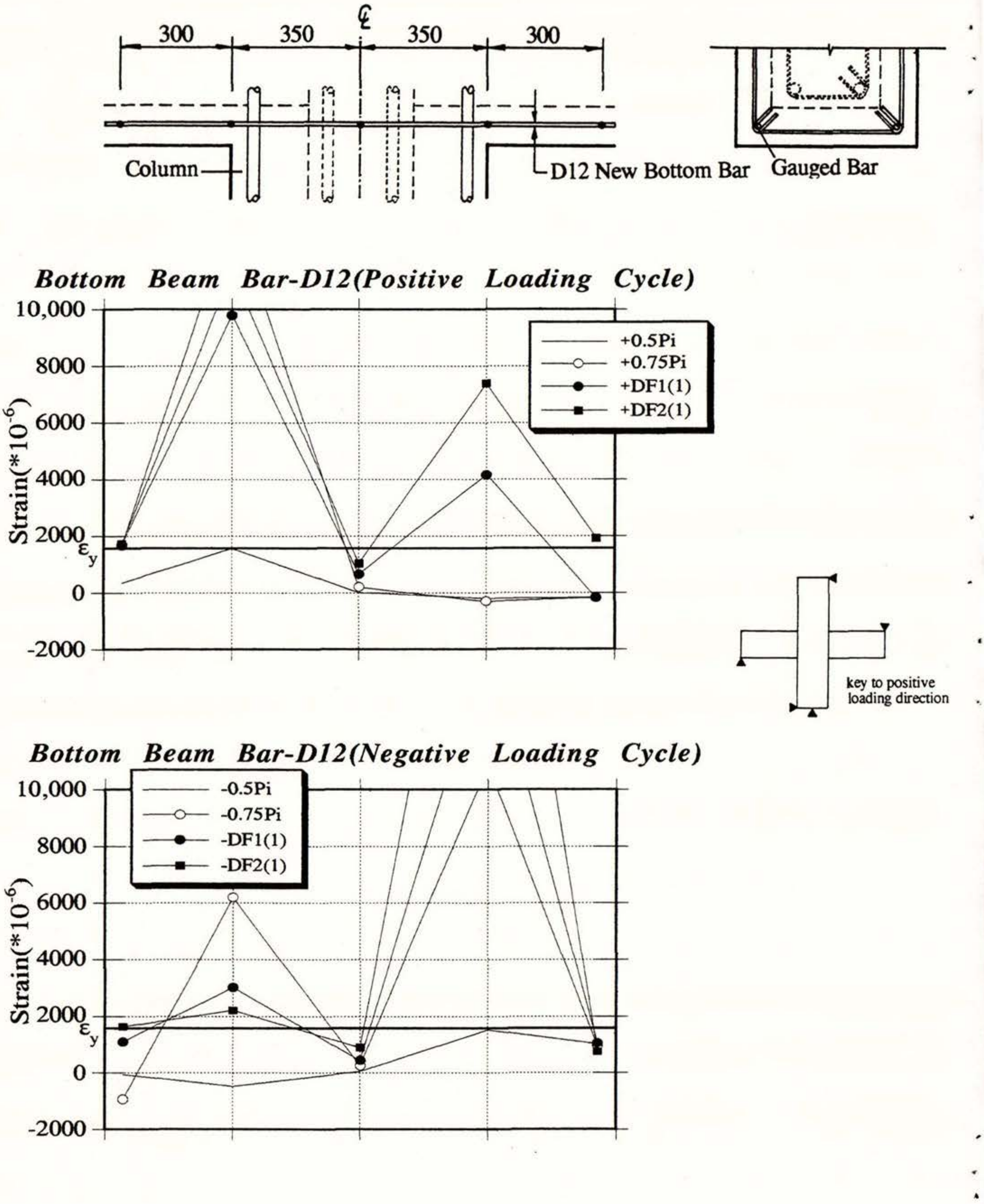

Fig.5.15(b) Strain Profiles of New Bottom Beam Bar(D12) of Specimen R2

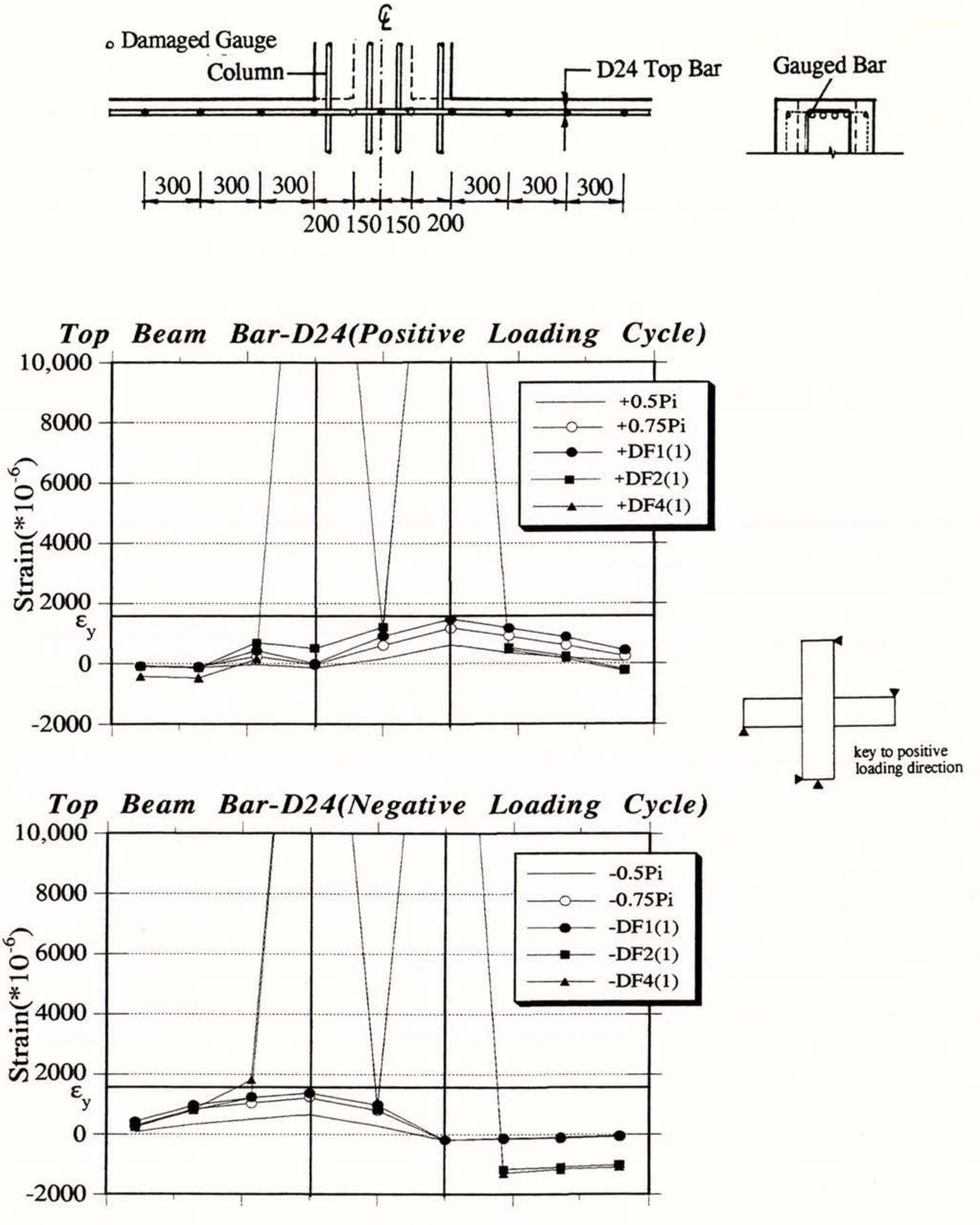

Fig.5.16(a) Strain Profiles of Existing Top Beam Bar(D24) of Specimen R2

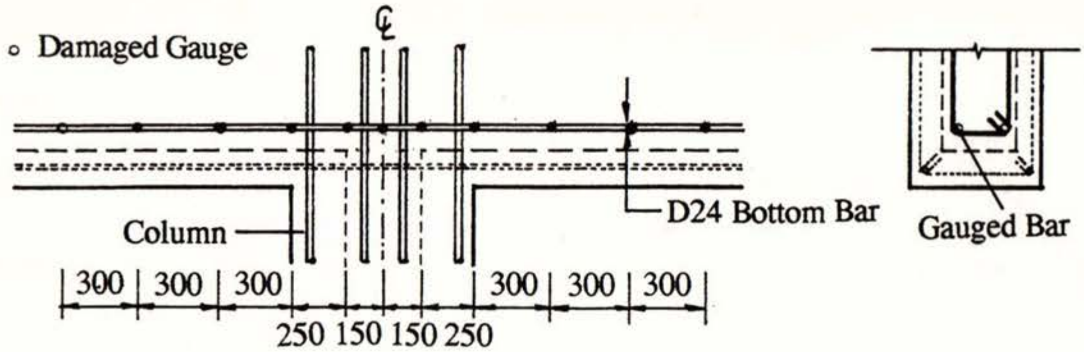

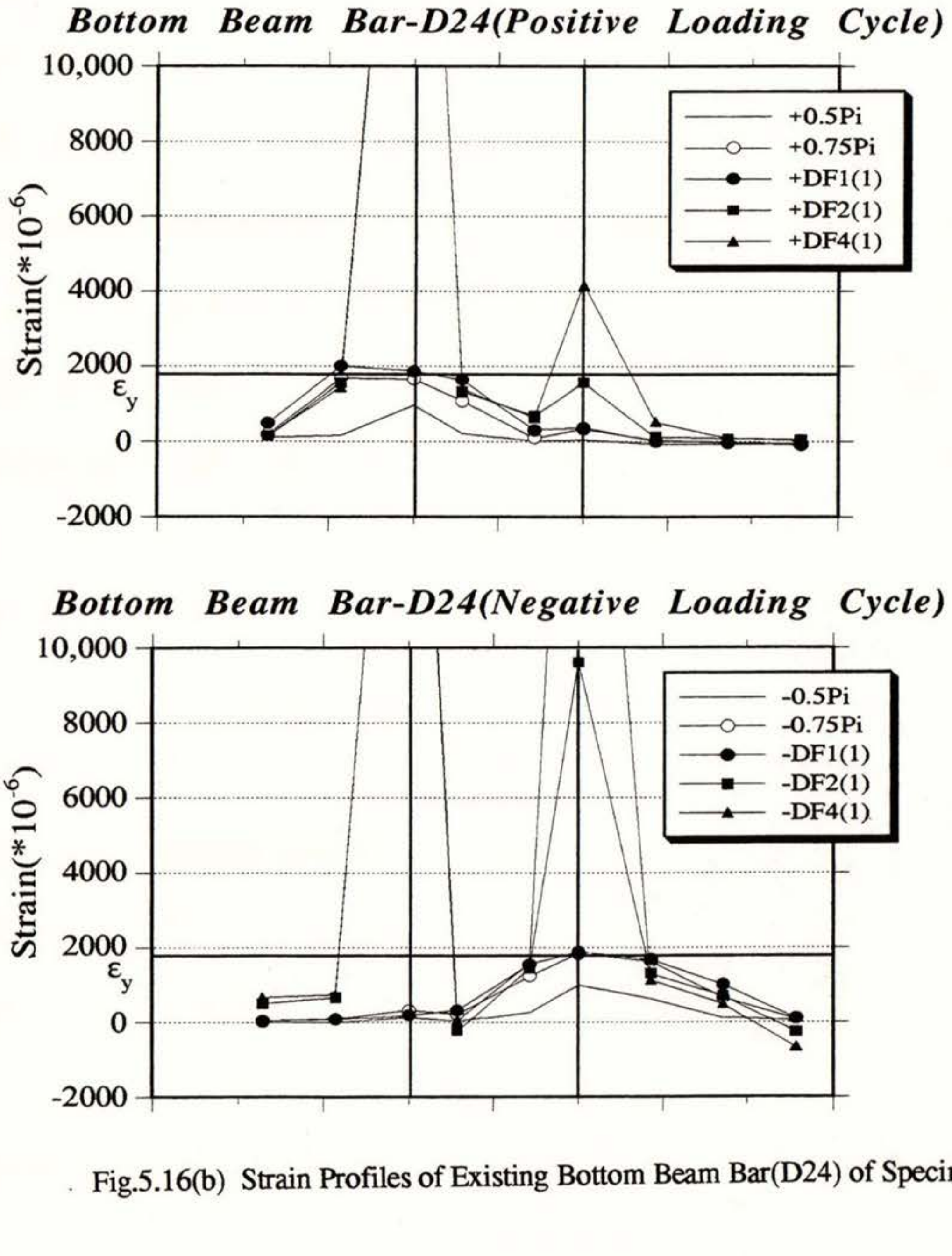

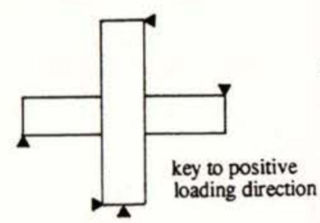

Fig.5.16(b) Strain Profiles of Existing Bottom Beam Bar(D24) of Specimen R2

curvature ductility factors so obtained were plotted in Fig.5.17. The yield curvatures estimated at $\pm 0.75P_i$ are also shown. Theoretical yield curvatures by conventional section analysis are 0.0033(1/m) during beam positive moment and 0.0037(1/m) during beam negative moment.

In the loading to DF of 2, the curvature ductility factors with beam positive moment were very similar to those with beam negative moment. In the loading to DF of 4, however, the curvature ductility factors with beam positive moment increased rapidly while those with beam negative moment increased gradually. Up to the loading to DF of 8, the maximum curvature ductility factor during beam positive moment was 18 for the west beam and 23 for the east beam. During beam negative moment, the maximum curvature ductility factor was 6 for the east beam and 4 for the west beam. It is evident that the beams retrofitted by jacketing with new reinforced concrete designed to the current code[SANZ 1982(a)] could reach large curvature ductility factors in this study.

5.3.5.4 Equivalent Plastic Hinge Lengths of the Beams

The equivalent plastic hinge length L_p for the retrofitted beams of Specimen R2 was estimated at the peak of each loading cycle. The procedures for estimating the equivalent plastic hinge length were described in Section 5.2.5.4 in detail. The equivalent plastic hinge lengths for each beam so obtained are shown in Fig.5.18 expressed as a proportion of the beam depth.

As was observed for Specimen R1, the values of the equivalent plastic hinge length exhibited a wide scatter in the loading to DF of 2. In the loading to DF of 4, however, the equivalent plastic hinge length became fairly constant for both beams. Until loading to DF of 8, the range of values of the equivalent plastic hinge lengths were 0.41 to 0.44 times the beam depth during beam positive moment and 0.39 to 0.47 times the beam depth during beam negative moment, respectively. The equivalent plastic hinge length estimated for Specimen R2 was very comparable to that estimated for Specimen R1.

5.3.6 Column Behaviour

5.3.6.1 Column Cracking

During the test, column flexural cracks and bond splitting cracks along the column corner bars were observed. The crack widths of flexural cracks remained very small while the bond splitting cracks extended and connected to the joint diagonal tension cracks.

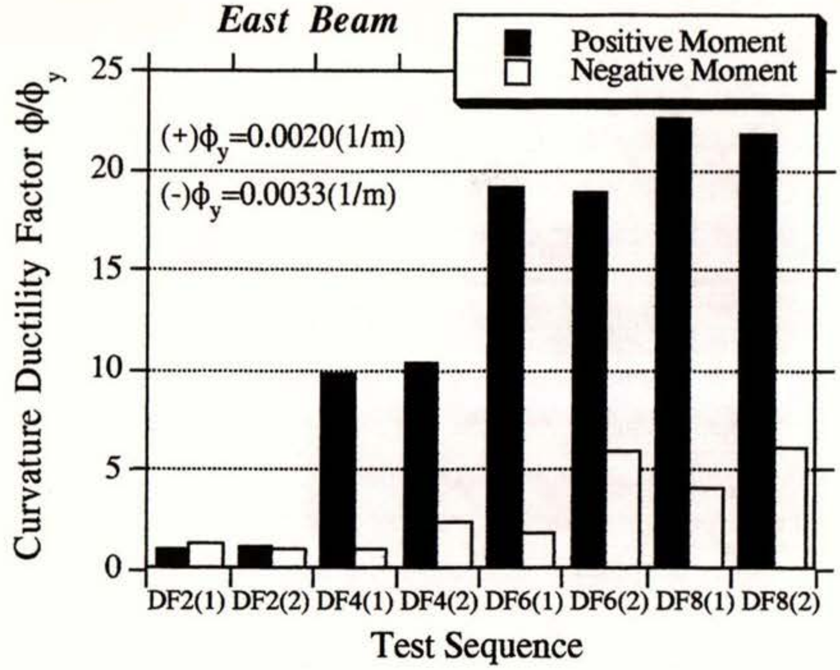

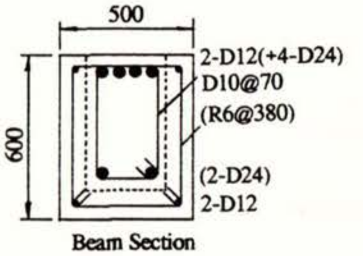

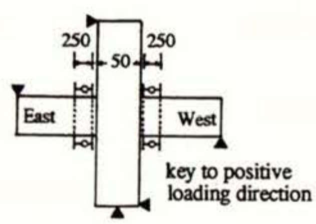

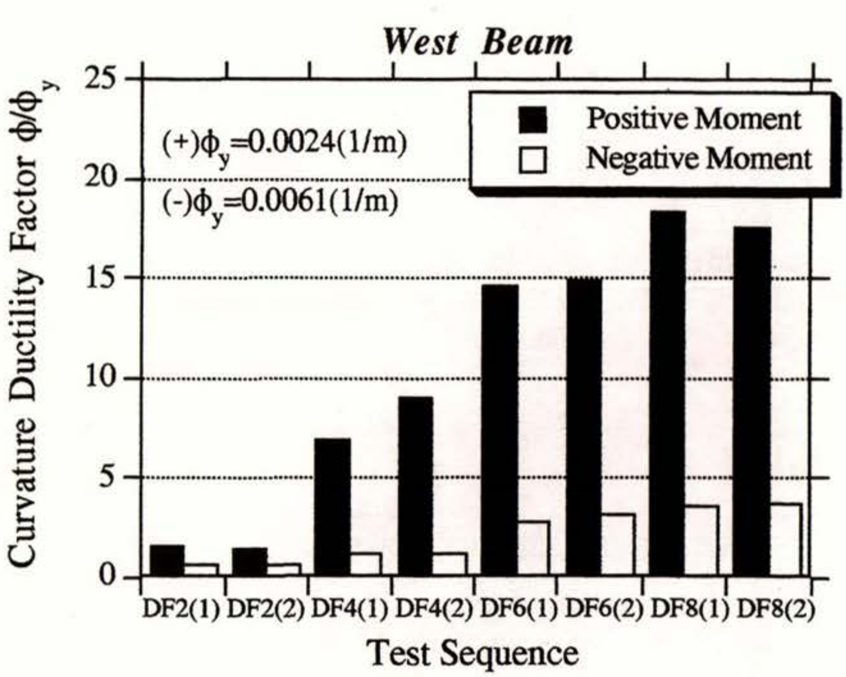

Fig.5.17 Curvature Ductility Factors of Beams of Specimen R2

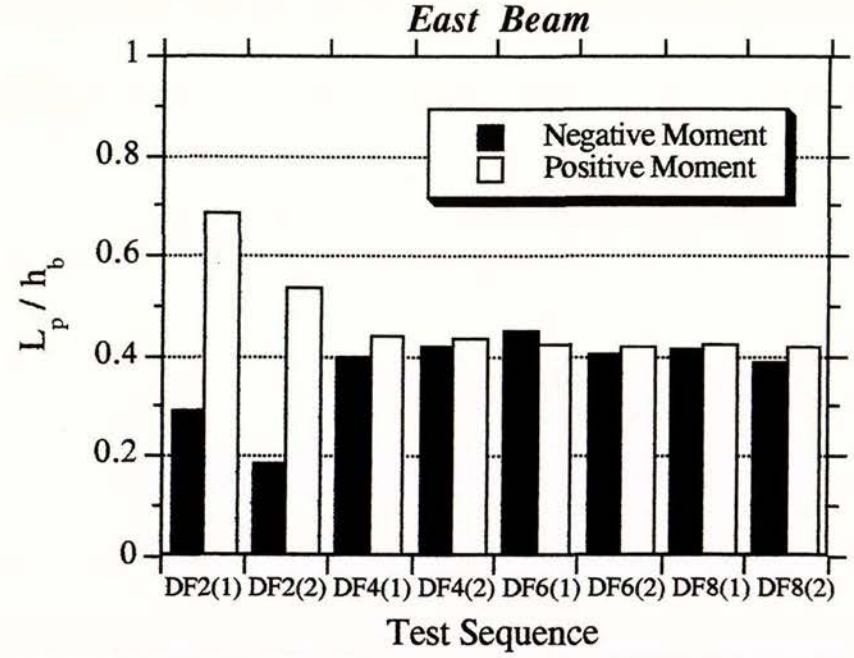

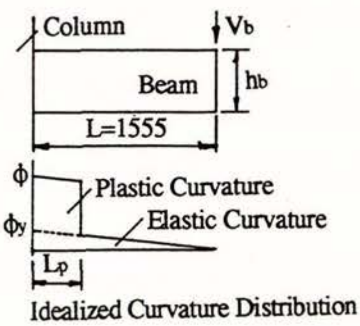

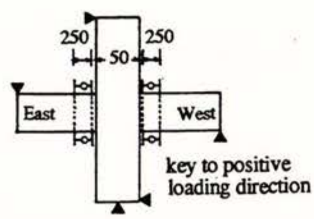

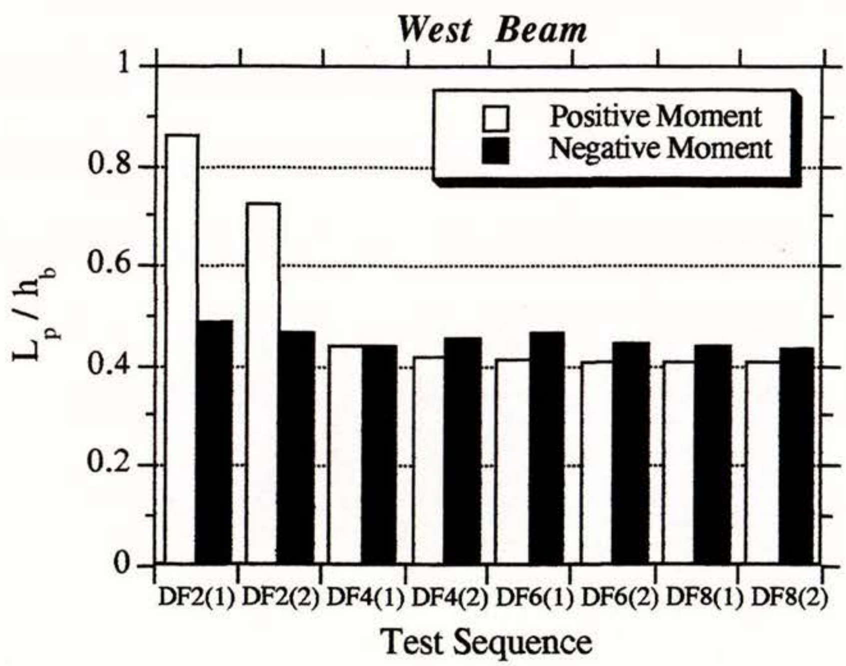

Fig.5.18 Equivalent Plastic Hinge Length of the Beams of Specimen R2

5.3.6.2 Longitudinal Column Bar Strains

The strains in the new longitudinal column bars at the beam face are shown in Fig.5.19. Those strains were measured using the wire strain gauges. Up to the loading to DF of 2, the strains increased gradually and the strains measured at the beam face when subjected to column flexural compression force showed small compressive strain. In the loading to DF of 4, however, in which corner to corner diagonal tension cracks developed in the joint core, those strains shifted to tensile strains. Subsequent loading cycles resulted in a rapid increase in tensile strains. The tensile strains prevailed along the column bars in the joint and the bond forces along the column corner bars to be transmitted into the joint core were significantly reduced. This would cause fixed-end rotation of the columns, resulting in a more flexible structure. As mentioned earlier, bond splitting cracks were observed along the column corner bars at this stage.

When comparing the strain profiles obtained from Specimen R1(compare Fig.5.8 with Fig.5.19), it is clearly shown that after diagonal tension cracking occur in the joint, the bond forces along the new column corner bars could be hardly generated in the joint without horizontal shear reinforcement.

5.3.7 Joint Behaviour

5.3.7.1 Joint Shear

The maximum nominal horizontal joint shear stress was $0.27\sqrt{f'_c{}^*}$, where $f'_c{}^*$ is the weighted average compressive strength of two concretes of the joint core. In the loading to DF of 4, corner to corner diagonal tension cracks developed in the joint core. Those cracks extended and opened as the displacement ductility factor imposed on the test specimen increased.

5.3.7.2 Strains of Column Intermediate Reinforcement

The longitudinal column bars of the as-built specimen became the column intermediate reinforcement of the retrofitted specimens R1 and R2. Strains measured along the column intermediate bars in the joint of Specimen R2 are plotted in Fig.5.20.

Up to the loading to DF of 2, the strain profiles of the column intermediate bar indicate the role of flexural reinforcement. In the loading to DF of 4, in which corner to corner diagonal tension cracks were observed in the joint, the strains measured in the joint core increased gradually. In the subsequent loading cycles, rapid increase in tensile strain was observed where joint diagonal tension cracks crossed. On the other hand, the strains

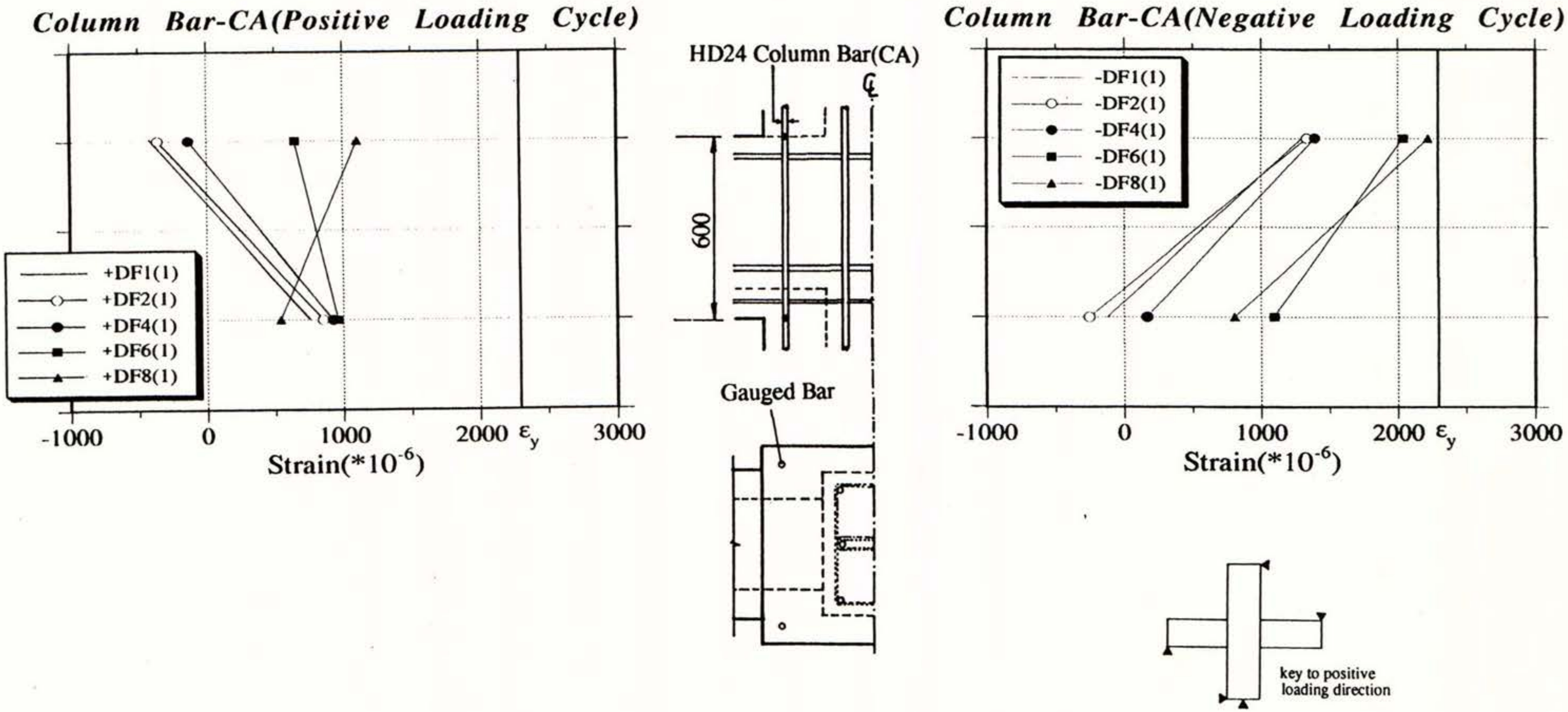

Fig.5.19(a) Strain Profiles of Column Bars of Specimen R2

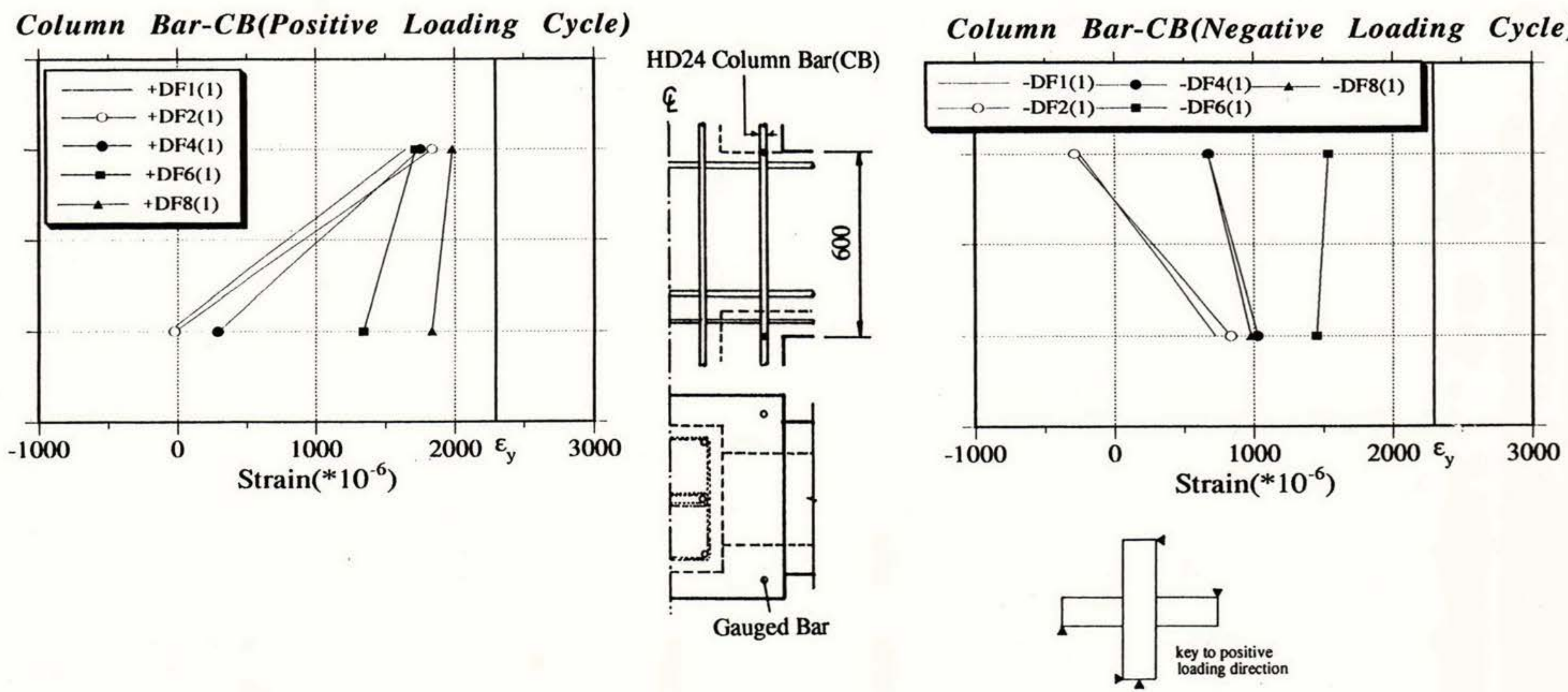

Fig.5.19(b) Strain Profiles of Column Bars of Specimen R2

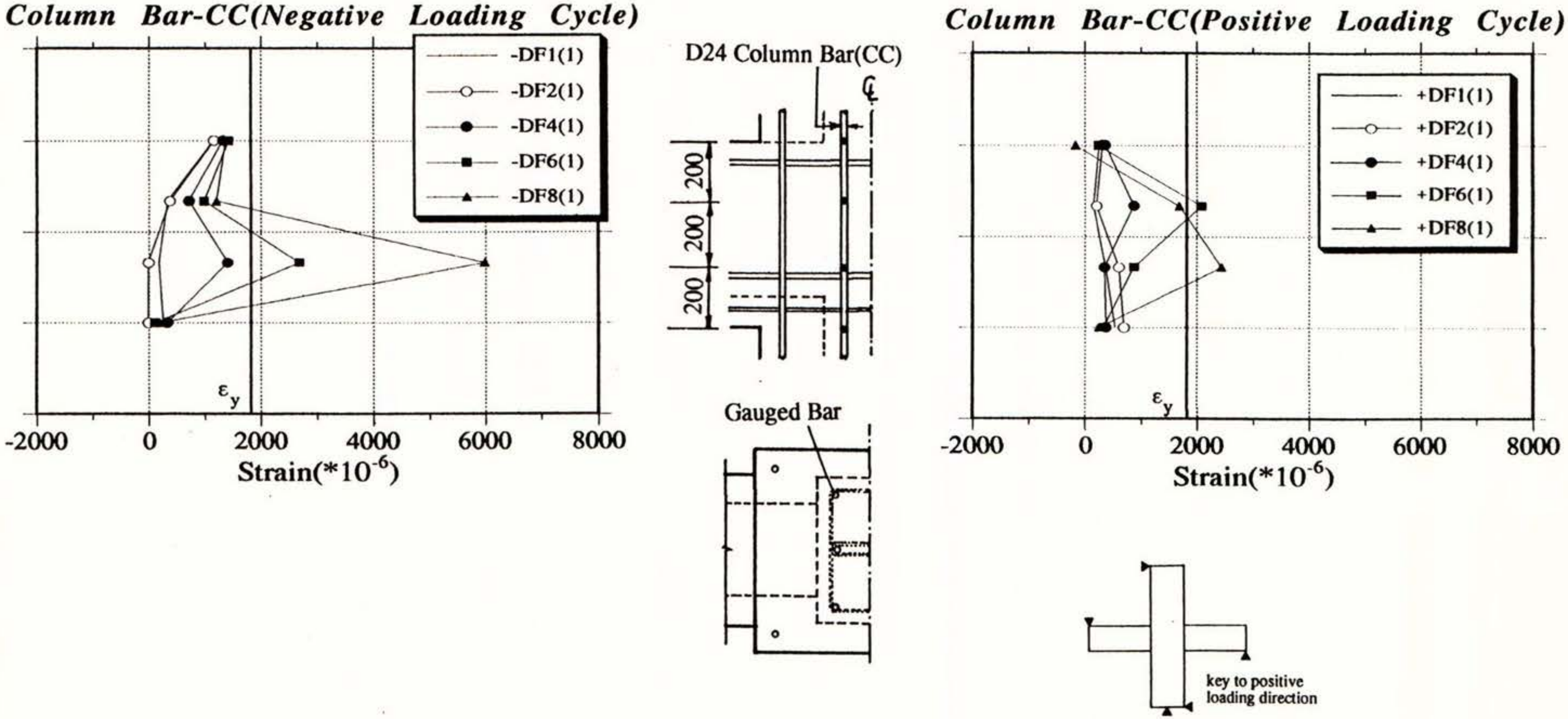

Fig.5.20(a) Intermediate Column Bar Strains of Specimen R2

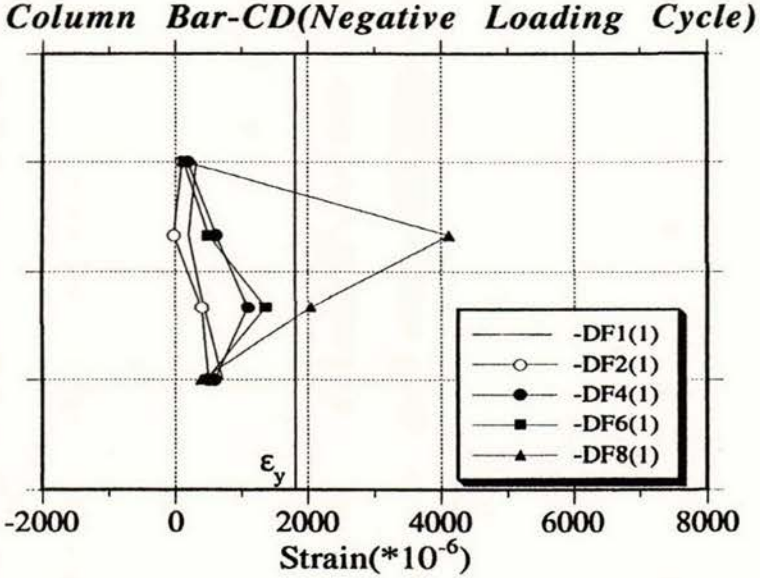

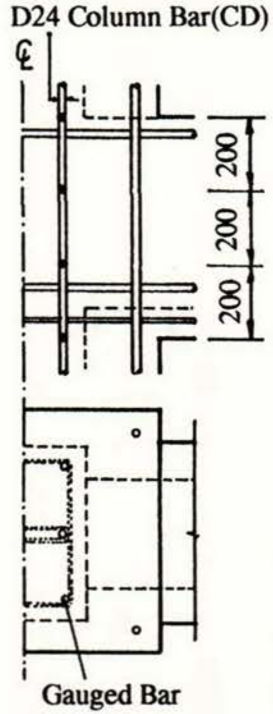

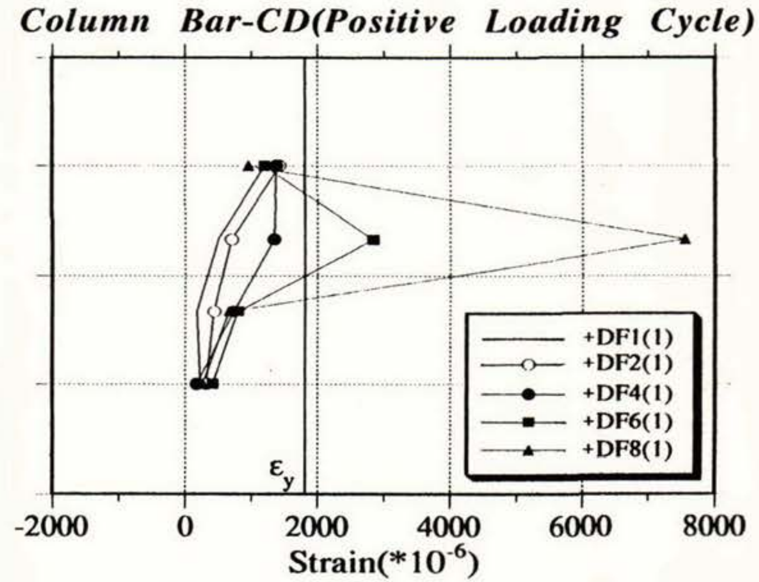

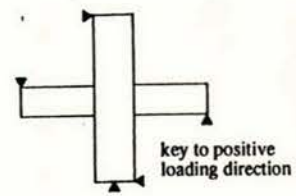

Fig.5.20(b) Intermediate Column Bar Strains of Specimen R2

measured at the beam face were fairly constant during the test. The measured strains in the joint core reached the yield strain in the loading to DF of 6 and the maximum strains measured were about 0.6 to 0.8%.

5.3.7.3 Joint Shear Distortion and Expansion

The joint shear distortion and expansion of Specimen R2 are shown in Fig.5.21. Up to the loading to DF of 2, joint shear distortion and expansion increased gradually. In the loading to DF of 4, in which corner to corner diagonal tension cracks developed, those measurements increased rapidly. The rate of increase was rather constant until the end of testing. The maximum joint shear distortion was 0.56%, measured in the second cycle of loading to DF of 8, which was twice that of Specimen R1. On the other hand, a maximum joint expansion of 3.2mm was obtained and this value was approximately three times of that measured for Specimen R1.

The joint shear distortion and expansion obtained from Specimen R2 were much larger than those from Specimen R1 due to the absence of the new joint hoops. However, the joint behaviour did not affect the overall response of this test specimen. This is mainly due to the reduction in the horizontal shear stress in the joint as a result of the enlargement of the column cross section area.

5.3.8 Decomposition of Horizontal Displacement

Fig.5.22 shows the components of the horizontal displacement at the peaks of the selected loading cycles.

The beam displacement due to flexure and fixed-end rotation contributed about 60% to 70% to a storey drift angle during the test. Of this, the beam fixed-end rotation accounted for approximately 35% to 45% while the beam flexure accounted for approximately 25% to 30%. The contribution due to beam fixed-end rotation increased slightly as the test progressed. On the other hand, the contribution due to beam flexure decreased as the test progressed. The trend of the beam contribution to the storey drift angle was very similar to that obtained from Specimen R1.

As shown in Fig.5.22, the fixed-end rotation of the columns contributed about 20% to 40% of a storey drift angle during the test. The contribution of the columns was fairly constant up to the loading to DF of 4. However, the contribution increased gradually in the subsequent loading cycles, as could be expected from the strain profiles of column corner bars shown in Fig.5.19. The contribution of column fixed-end rotation was somewhat larger than that of Specimen R1.

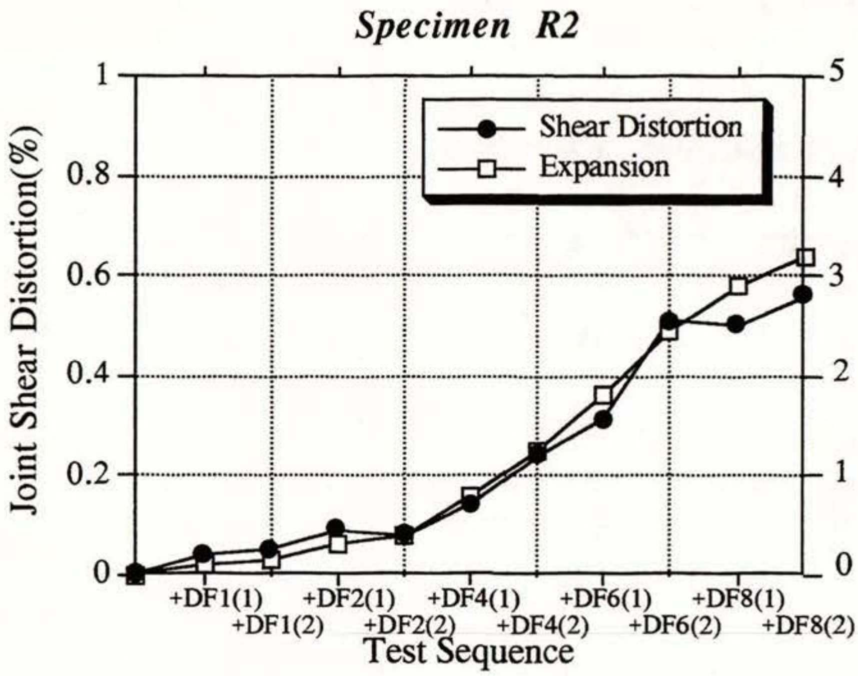

Fig.5.21 Joint Shear Distortion and Expansion of Specimen R2

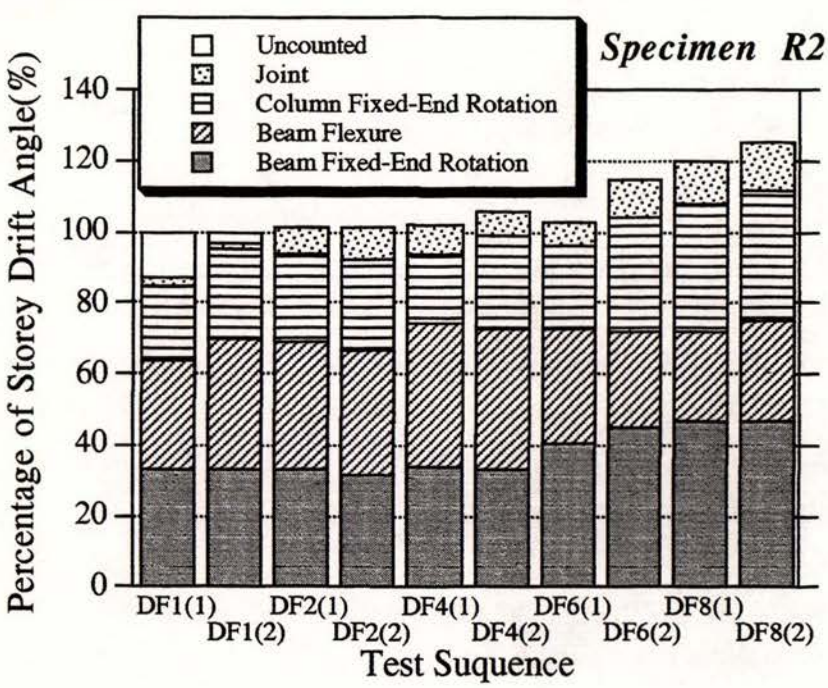

Fig.5.22 Components of Storey Drift Angle of Specimen R2

The contribution due to joint shear distortion increased gradually until the end of the test. The maximum contribution was 16% obtained in the second cycle of loading to DF of 8. Although the absence of the joint hoops caused larger contribution of the joint shear distortion to the storey drift angle when compared with that of Specimen R1, its contribution was not so significant during the test.

5.4 RETROFITTED SPECIMEN R3

5.4.1 The Specimen

Specimen R3 was the retrofitted specimen in which only the columns were jacketed with new reinforced concrete. The compressive cylinder strengths of the existing and new concrete were 43.4MPa and 42.0MPa, respectively, at the time of testing. The ratio of the theoretical ideal flexural strength of the column to that of the beam was 2.4 based on the measured material strengths. When the beam plastic hinge mechanisms developed, the calculated ideal storey horizontal load strength P_i was 139kN.

5.4.2 General Behaviour

The observed cracking after testing and the storey shear force versus horizontal displacement hysteresis curves are shown in Figs.5.23 and 5.24, respectively. The theoretical ideal storey horizontal load strength P_i and the theoretical stiffness $K_{theoretical}$ are also shown in Fig.5.24. Observed cracking at the peaks of the selected loading cycles are shown in Fig.5.25.

In the loading to $\pm 0.5P_i$, flexural and flexural-shear cracks initiated in the beams. Column flexural cracks were also observed. In the loading to $\pm 0.75P_i$, those cracks extended and the number of the cracks also increased(see Fig.5.25(a)).

In the loading to displacement ductility factor DF of 1, diagonal tension cracks initiated at approximately 45 degree to the beam axis in the west beam(see Fig.5.25(b)). At this stage, the longitudinal beam bars started to yield in tension at the column face.

In the loading to DF of 2, the flexural-shear cracks in the beams extended and tended to open wide. The maximum width of those cracks was measured to be 2.2mm for the beam bottom face and 0.5mm for the beam top face, respectively. In the first negative loading cycle, the diagonal tension cracks in the east beam also developed at approximately 45 degree to the beam axis. In the west beam, the diagonal tension cracks extended. In this case, however, the diagonal tension cracks began to shift direction to become more acute to the

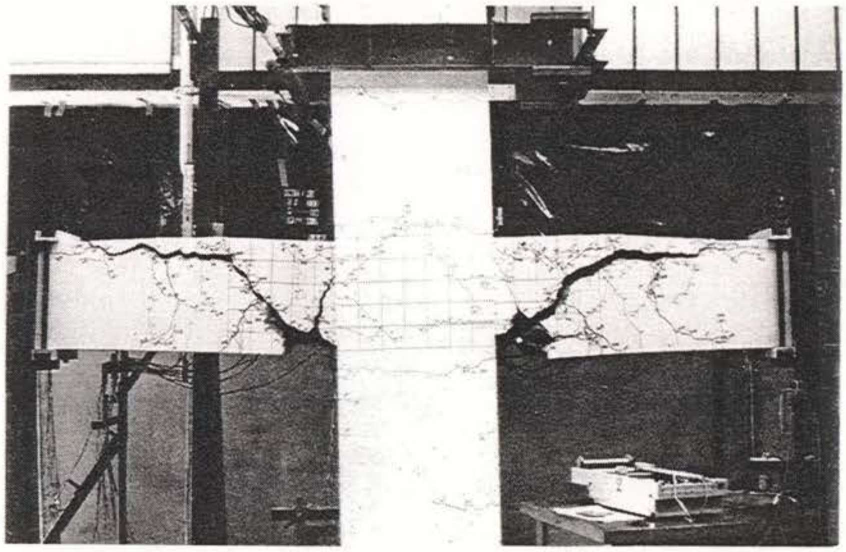

Fig.5.23 Observed Cracking of Specimen R3
at second cycle of DF=-8

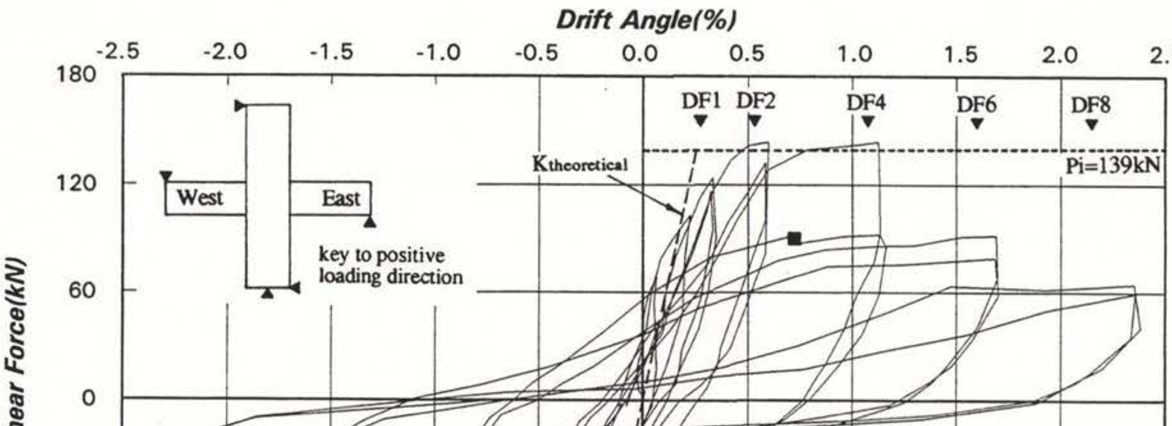

Fig.5.24 Storey Shear Force versus Horizontal Displacement Relationship
for Specimen R3

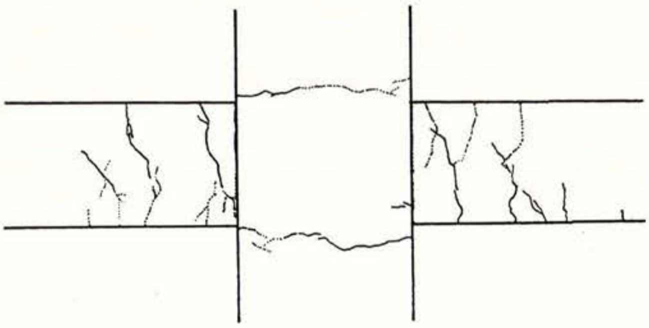

(a) at the peak of 0.75Pi
(R=0.20%)

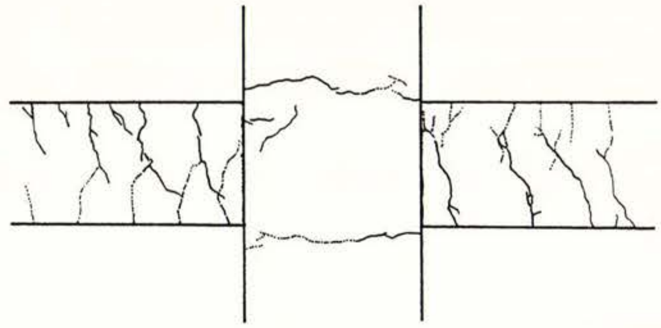

(b) at the peak of second cycle, DF=1
(R=0.27%)

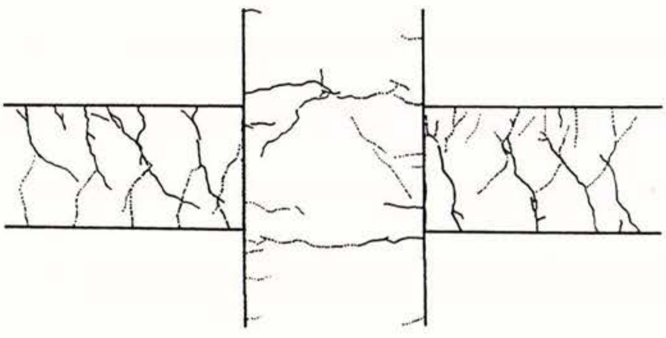

(c) at the peak of second cycle, DF=2
(R=0.54%)

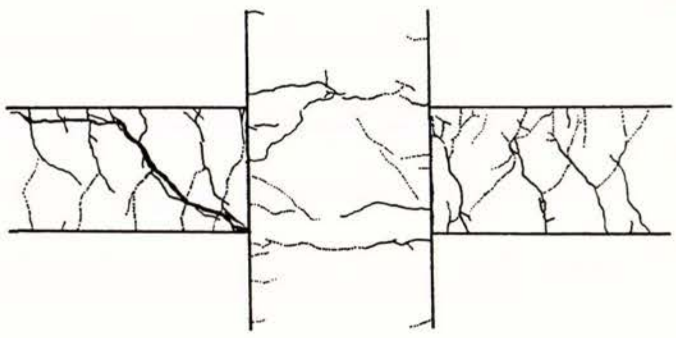

(d) at the peak of second cycle, DF=4
(R=1.08%)

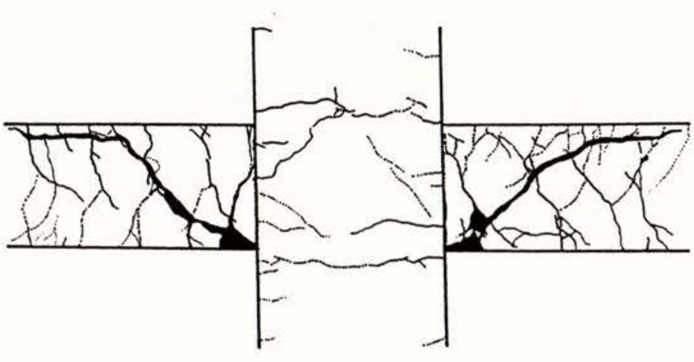

(e) at the peak of second cycle, DF=6
(R=1.61%)

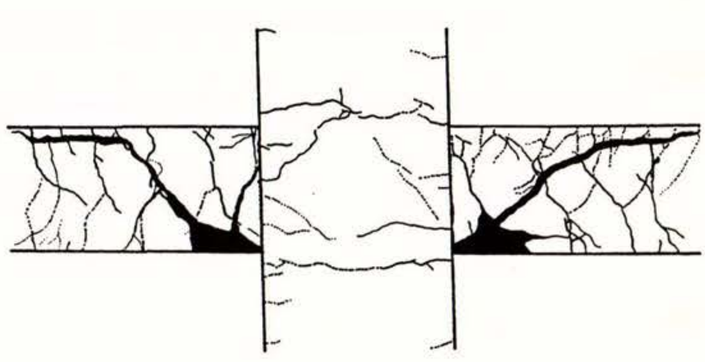

(f) at the peak of second cycle, DF=8
(R=2.15%)

Fig.5.25 Observed Cracking of the Joint(Specimen R3)

beam axis(see Fig.5.25(c)). The stirrup placed at 100mm from the column face in the west beam started to yield. Columns and joint showed only minor flexural and shear cracking. The theoretical ideal storey horizontal load strength of the specimen based on the measured material strengths was reached during the first cycle of loading to DF of 2. Only small strength degradation was observed in the second loading cycle(see Fig.5.24).

In the first cycle of loading to DF of 4, the maximum horizontal load strength of the specimen was reached at a storey drift angle of approximately 1.1%(see Fig.5.24). The measured maximum horizontal load strength was 144kN for the positive loading cycle and 145kN for the negative loading cycle. The maximum strength was 104% of the theoretical ideal storey horizontal load strength when the plastic hinges were formed in the beams. The flexural-shear cracks extended and opened wide to a maximum crack width of 2.8mm at the beam bottom face and of 1.2mm at the top beam face, respectively. The diagonal tension cracks also extended and opened wide. In the second positive loading cycle, one dominant diagonal tension crack with an inclination of approximately 35 to 45 degree to the beam axis extended toward the flexural compression zone of the beam at the column face in conjunction with the bond splitting cracks along the top beam bar in the west beam. The diagonal tension crack opened wide and resulted in a shear failure during beam negative moment(see Fig.5.25(d)). The maximum width of the diagonal tension crack was larger than 10mm. Beam shear failure initiated at a storey drift angle of approximately 0.74%. Severe strength degradation during the positive loading cycle was observed in the hysteresis loops shown in Fig.5.24. In the negative loading cycle, little strength degradation could be found although a diagonal tension crack similar to that observed in the west beam developed. During beam positive moment, the beam shear cracks extended and opened with an inclination of larger than 45 degree to the beam axis. Significant tensile strains of larger than 1.5% were measured by all of the wire strain gauges attached to the stirrups.

The east beam also failed in the same manner at a storey drift angle of approximately 0.56% during the first cycle of loading to DF of 6(see Fig.5.25(e)). Severe strength and stiffness degradation was obvious during the negative loading cycle as shown in Fig.5.24. In the subsequent loading cycles, the beam diagonal tension cracks opened more wide to a measured maximum crack width of approximately 25mm. The 6mm diameter stirrups with a spacing of 380mm fractured where crossing the wide diagonal tension cracks. Near the column face, the cover concrete of the beams at the bottom face spalled off significantly(see Figs.5.25(e) and (f)) and the 135 degree hooks of the stirrups were bent to 90 degrees. Although beam shear cracks at obtuse angle to the beam axis also opened wide with beam positive moment , no indication of shear failure could be found. In the second cycle of loading to DF of 8, only 45% of the measured maximum horizontal load strength developed as shown in Fig.5.24.

Until the end of the test, only minor flexural cracks could be observed in the columns. For the joint, no critical corner to corner diagonal tension cracks initiated(see Fig.5.25(f)). Hence it could be concluded that the shape of hysteresis curves was governed by the response of the most damaged elements, namely the beams(see Fig.5.23).

5.4.3 Initial Stiffness

The theoretical initial stiffness was calculated to be as follows:

$$K_{theoretical}=17.3kN/mm$$

The procedures for calculating the theoretical initial stiffness were described in Section 3.9. The theoretical stiffness $K_{theoretical}$ is shown in Fig.5.24. The stiffness estimated at 75% of the theoretical ideal storey horizontal load strength of the test specimen was 20.0kN/mm for the positive loading cycle and 12.5kN/mm for the negative loading cycle. The theoretical stiffness predicted the average value of the measured initial stiffness, 16.2kN/mm with good accuracy. On the other hand, the initial stiffnesses obtained from Specimens R1 and R2, in which the beams as well as the columns were retrofitted by jacketing, were very low when compared with the theoretical values. It can be concluded that the main reason for the low stiffness of Specimens R1 and R2 is micro cracking and reduction of the effectiveness of the existing concrete due to chipping off the cover concrete of the beams to place the new transverse reinforcement.

The measured yield displacement of the test specimen was 8.58mm which converted to 0.27% in terms of the storey drift angle. The measured storey drift angle at yielding met the current code requirements[SANZ 1992].

5.4.4 Available Displacement Ductility Factor

An available displacement ductility factor μ_a of 2.5 was obtained from the measured storey shear force and horizontal displacement hysteresis loops of Specimen R3. The method for calculating the available displacement ductility factor was explained in Section 5.2.4. According to the New Zealand code[SANZ 1992], the test specimen was categorized as "Limited Ductility". The results tested on this specimen which was retrofitted by jacketing the columns alone showed the beam shear failure after the plastic hinges were formed in the beams, resulted in a poor displacement ductility capacity.

5.4.5 Beam Behaviour

5.4.5.1 Longitudinal Beam Bar Strains

The strains along the longitudinal beam bars obtained from the readings of wire strain gauge are shown in Fig.5.26. Fig.5.27 illustrates the beam bar strains measured from the linear potentiometer attached to the steel rods welded to the beam bars. Up to the loading to DF of 1, both figures show the gradual increase in tensile strains along the beam bars and the attainment of the yield strain at the column face. In the loading to DF of 2, the tensile strains measured at the column face increased rapidly. After the second cycle of loading to DF of 4 in which diagonal tension cracks extended and opened wide in the beams, yielding of the beam bars spread in the beams from the column face, as shown in Figs.5.26(b) and 5.27(b).

In the central region of the joint, large tensile strains were not attained until the loading to DF of 6, indicating that the beam bars were well anchored in the joint during the test.

5.4.5.2 Slip of Beam Bars

The slip of the top and bottom beam D24 bars in the joint are shown in Fig.5.28. The clear distance between two ribs of the beam bar used was 11mm. The methods to estimate the bar slip were mentioned in Section 3.7.4.

The bar slip measured at each location increased as the test progressed. The maximum bar slip was only 0.61mm, indicating that no significant slippage initiated until the end of the test. This is because the enlarged column depth of Specimen R3 was great enough to accommodate the development length of the beam bars.

5.4.5.3 Beam Shear Stress and Shear Distortion

In this study, beam shear distortions were estimated using the second set of the linear potentiometers placed diagonally at 50mm away from the column faces as illustrated in Fig.5.29. The linear potentiometers were attached to the steel rods which were welded to top and bottom beam bars.

Fig.5.29 plots the relationship between shear stress level $v_b/\sqrt{f'_c}$ and shear distortion of the beams so obtained. Also plotted is the shear carried by stirrups using the average strains measured from the wire strain gauges attached on both sides of the stirrup, assuming a 45 degree truss mechanism.

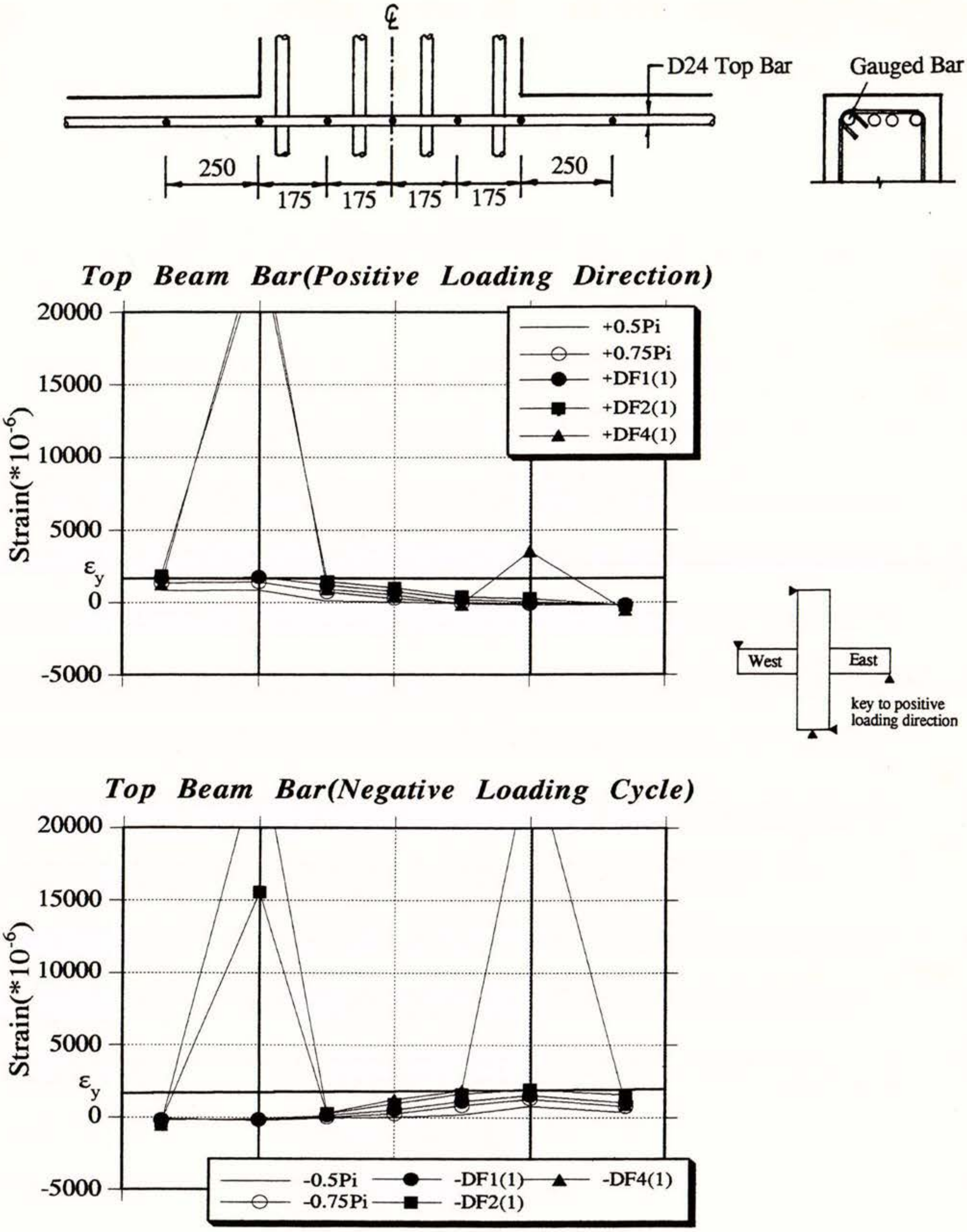

Fig.5.26(a) Strain Profiles of Top Beam Bar Measured by Wire Strain Gauges of Specimen R3

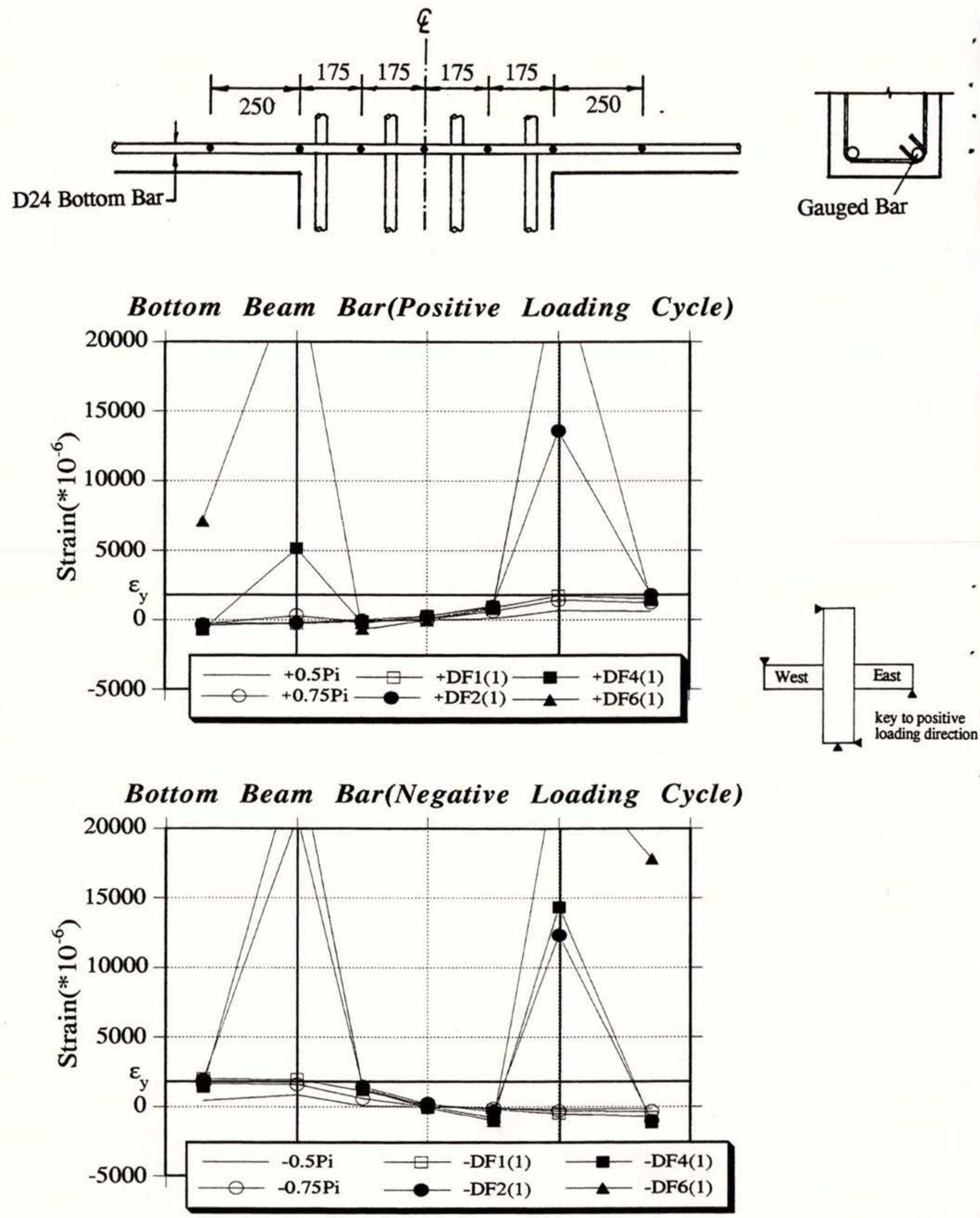

Fig.5.26(b) Strain Profiles of Bottom Beam Bar Measured by Wire Strain Gauges of Specimen R3

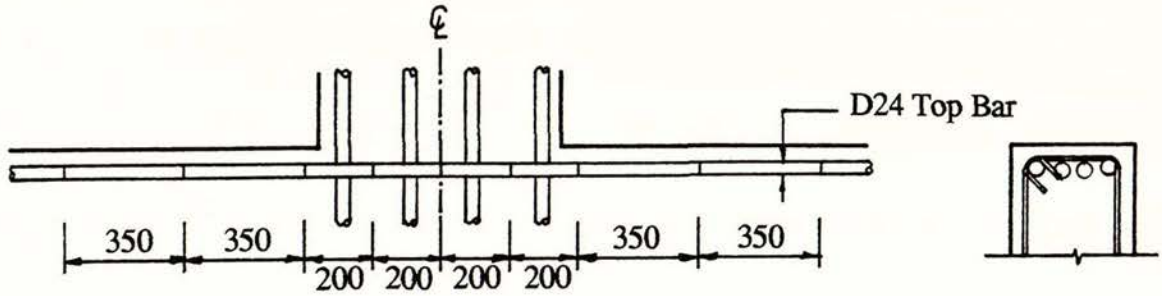

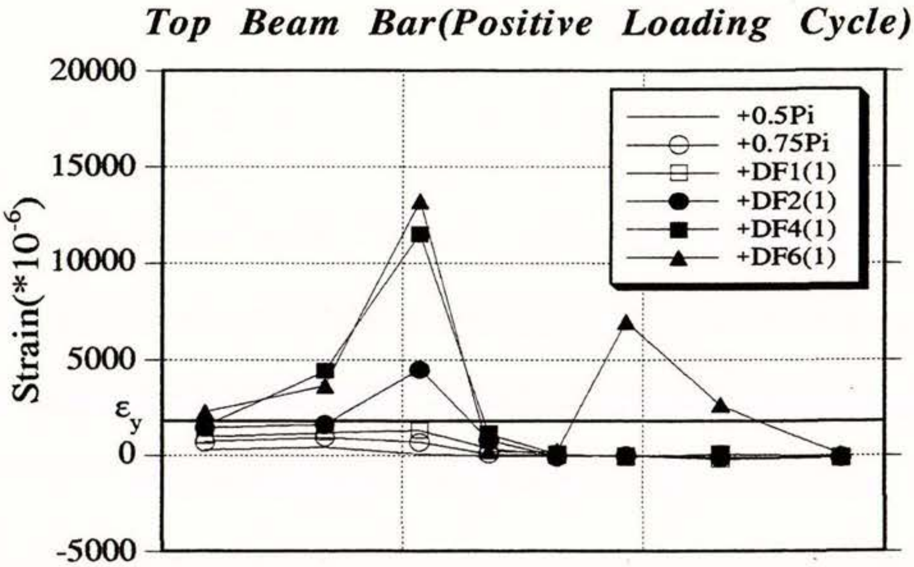

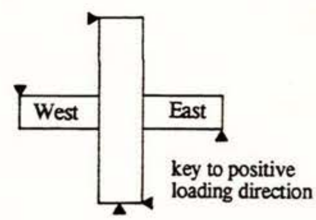

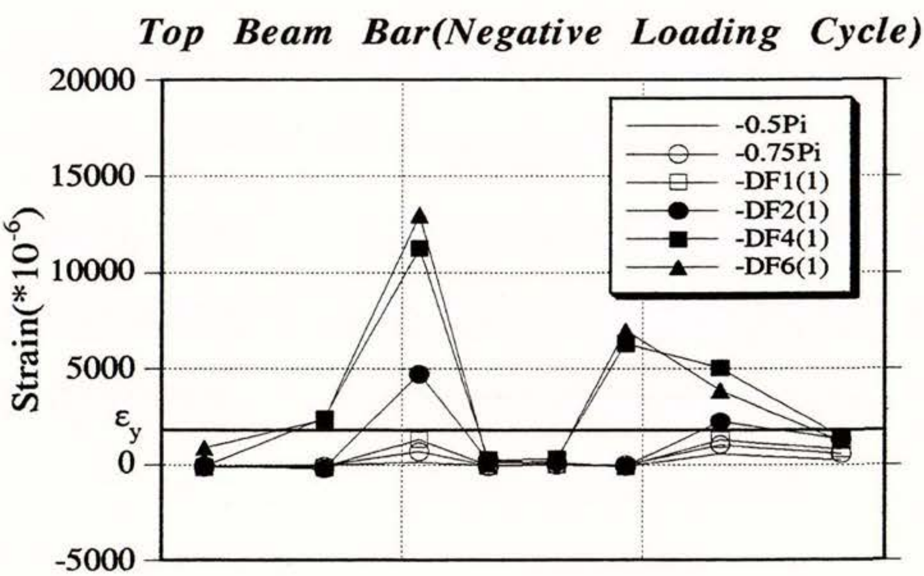

Fig.5.27(a) Strain Profiles of Top Beam Bar Measured by Linear Potensiometers of Specimen R3

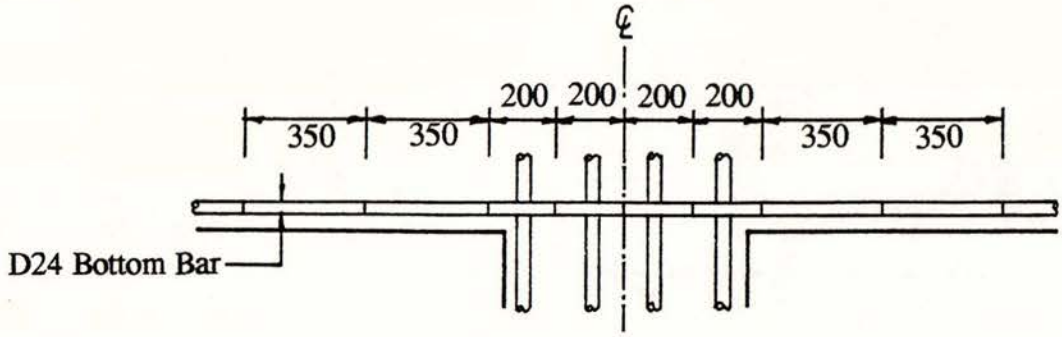

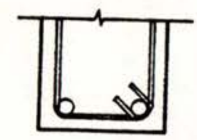

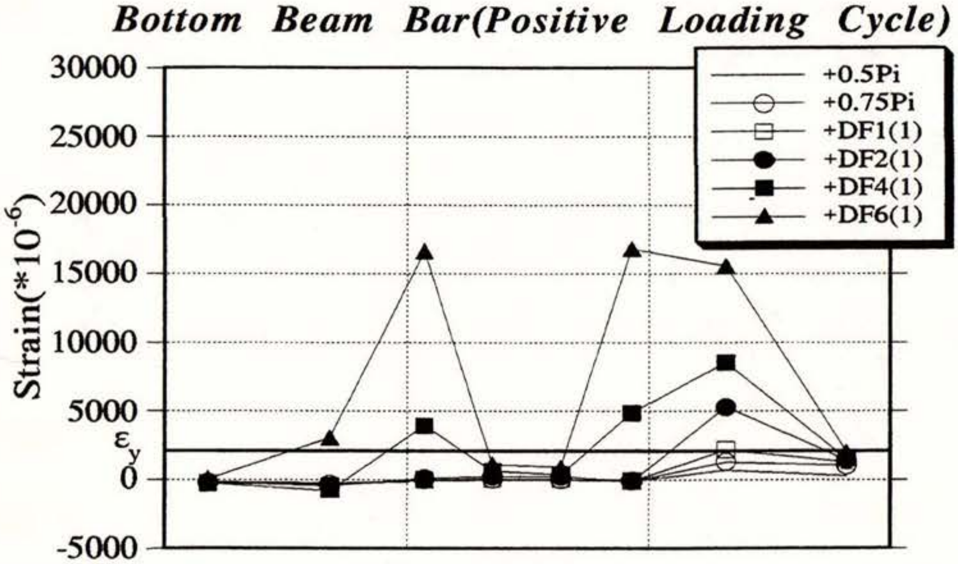

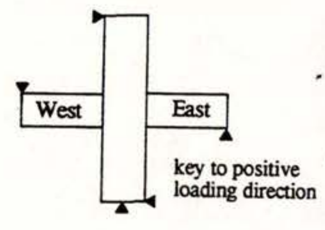

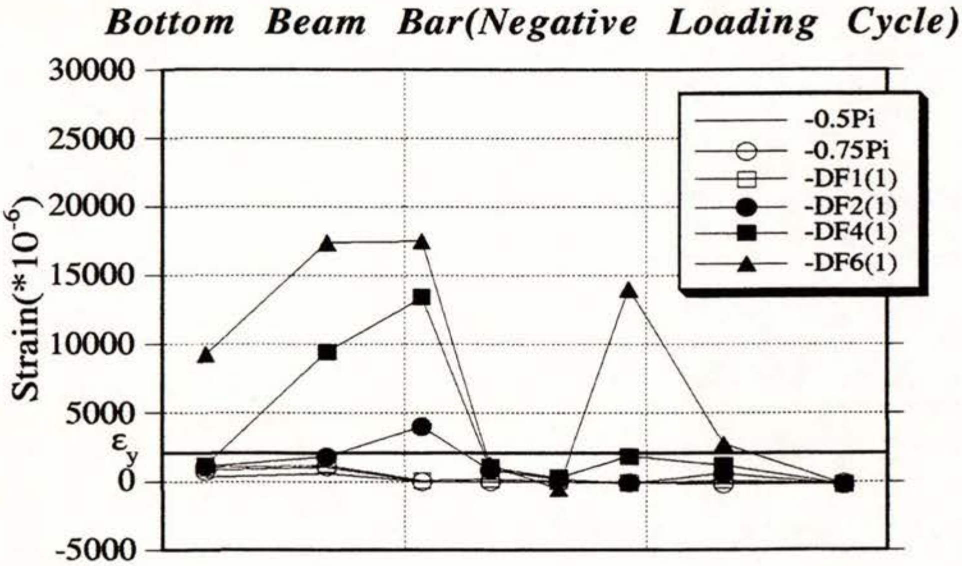

Fig.5.27(b) Strain Profiles of Bottom Beam Bar Measured by Linear Potensiometers of Specimen R3

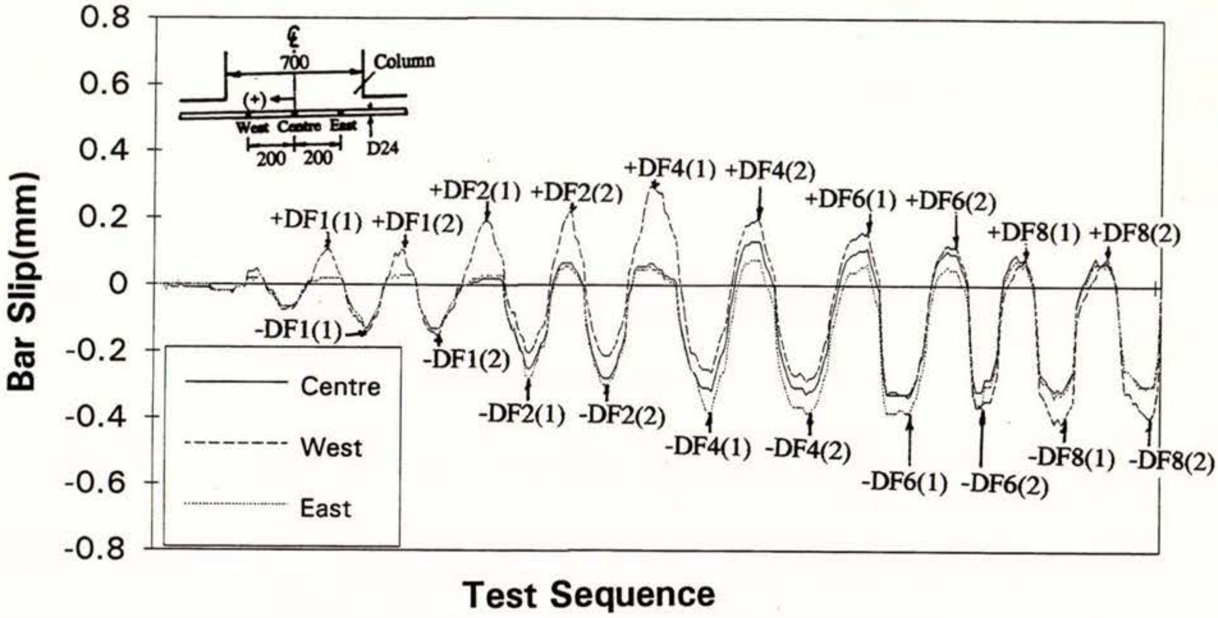

(a) Slip of Top Beam Bar

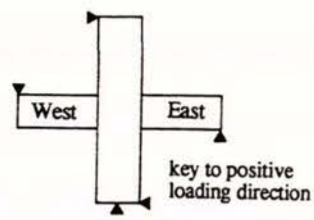

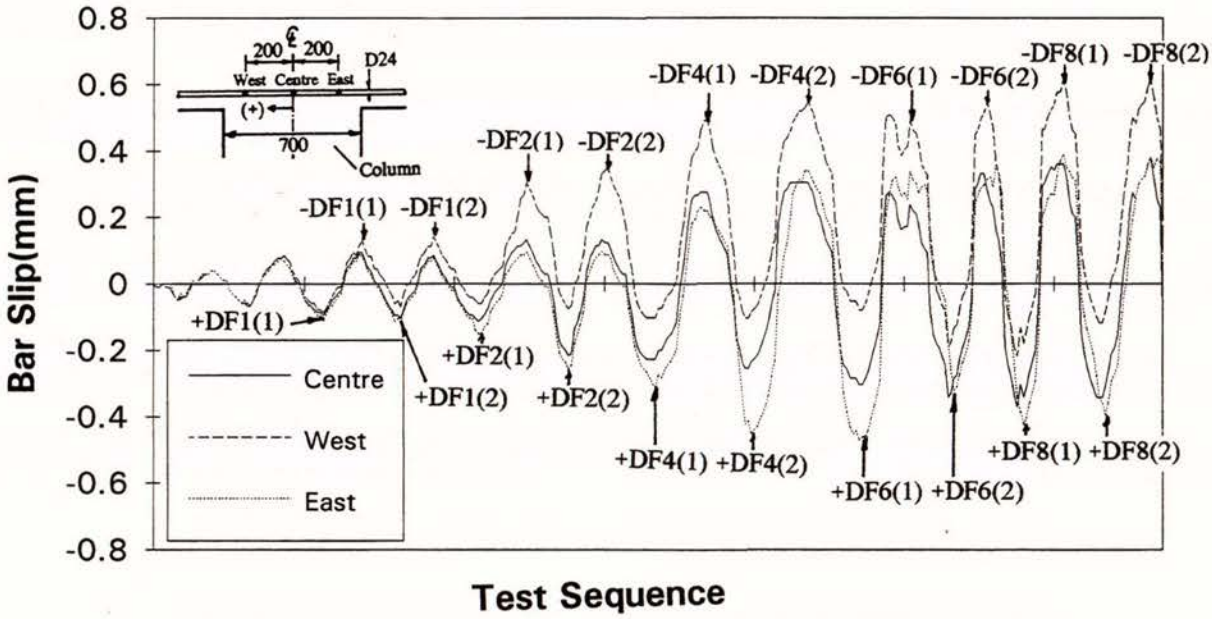

(b) Slip of Bottom Beam Bar

Fig.5.28 Measured Slip of Beam Bars of Specimen R3

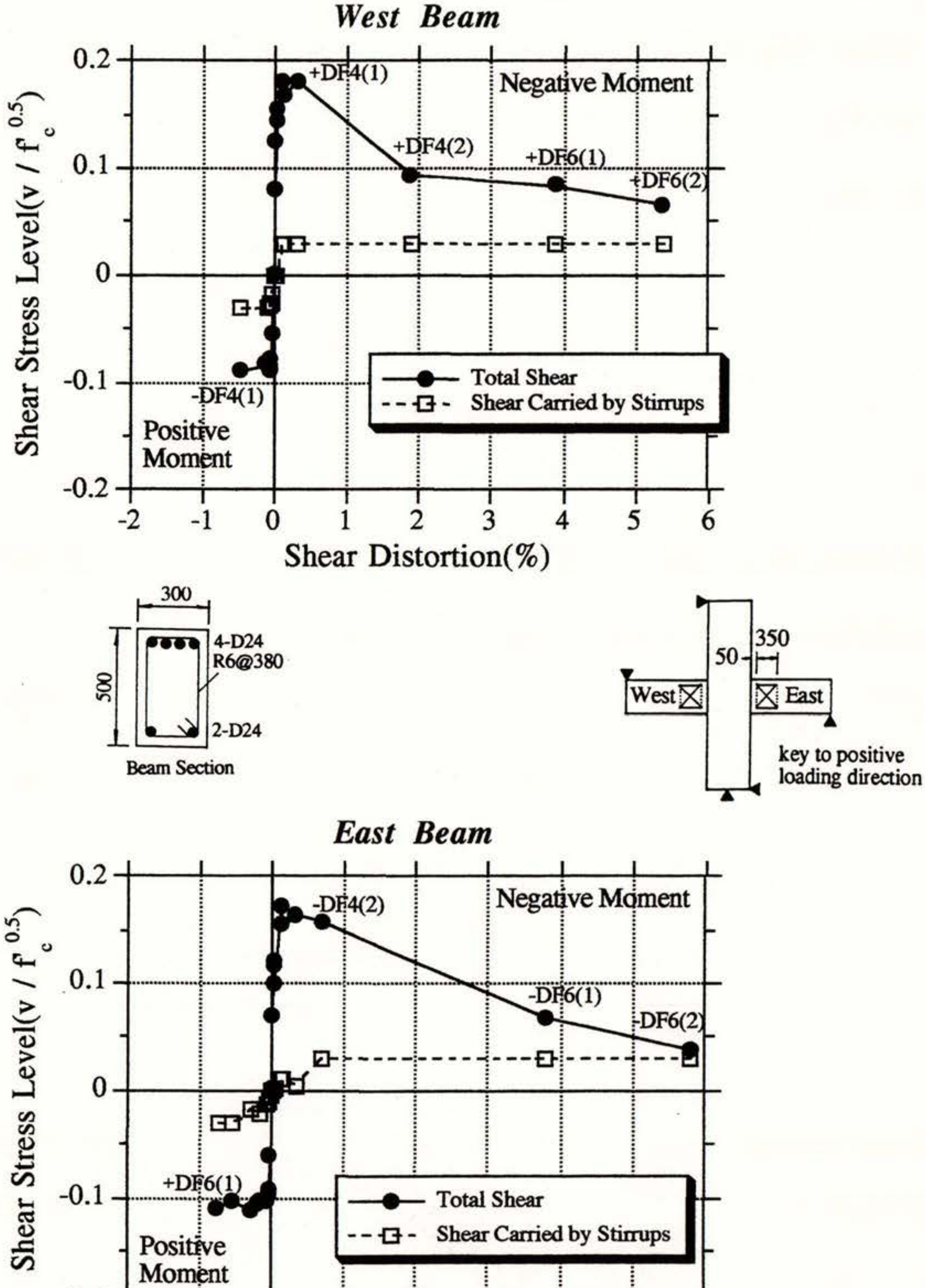

Fig.5.29 Relationship between Shear Stress Level and Shear Distortion of Beams of Specimen R3

With beam negative moment, the shear stress at onset of diagonal tension cracks was $0.13\sqrt{f'_c}$ for the east beam and $0.12\sqrt{f'_c}$ for the west beam. After the development of the diagonal tension cracks in the beam, the beam shear stress increased slightly and the maximum shear stress during beam negative moment was measured to be 1.19MPa($=0.18\sqrt{f'_c}$) for the west beam and 1.13MPa($=0.17\sqrt{f'_c}$) for the east beam, where f'_c is the measured concrete compressive cylinder strength. As shown in Fig.5.29, shear distortion increased rapidly to a value of approximately 0.6 to 0.7% with beam negative moment. At this stage, the stirrups yielded in tension. The shear carried by the stirrups was 0.20MPa which was only 16 to 17% of the maximum shear stress measured in the beams, assuming a 45 deg truss. The aggregate interlock mechanism became ineffective due to the diagonal tension cracks opening wide. Shear carried by dowel action was also reduced due to the bond splitting cracks along the top beam bars. After the breakdown of the aggregate interlock mechanism and dowel force, rapid strength reduction could be observed during the loading to DF of 4 for the west beam and DF of 6 for the east beam, as shown in Fig.5.29. The total shear stress carried approached the shear carried by stirrups during beam negative moment.

With beam positive moment, the maximum shear stress obtained was 0.62MPa($=0.09\sqrt{f'_c}$) for the west beam and 0.74MPa($=0.11\sqrt{f'_c}$) for the east beam. Until the loading to DF of 6, the shear distortion was less than 0.75% and no strength reduction was observed during beam positive moment as illustrated in Fig.5.29.

5.4.5.4 Beam Curvature Ductility Factor

Fig.5.30 shows the curvature ductility factors of the beams obtained at the peaks of the selected loading cycles. The curvatures were obtained from the second set of the linear potentiometers placed at 50mm away from the column faces. The gauge length for calculating the curvatures was 350mm. As discussed in Section 5.2.5.3, the yield curvature ϕ_y was calculated using the curvature ϕ_{75} measured at $\pm 0.75P_i$, linearly interpolated to M_i, where M_i is the ideal flexural strength based on the measured material strengths.

During beam positive moment, the measured curvature ductility factor increased gradually as the imposed displacement ductility factor increased. The maximum curvature ductility factors attained were 14 for the west beam and 17 for the east beam. Despite the poor ductile detailing of the transverse reinforcement in the beam plastic hinge regions, relatively large curvature ductility factors could be attained during beam positive moment.

During beam negative moment, the beam curvature ductility factors increased up to the first cycle of loading to DF of 4 for the the west beam and the second cycle of loading to DF of 4 for the east beam. After these loading cycles, the curvature ductility factors decreased as the test progressed. Noting the rapid increase in the shear distortion of the beams observed

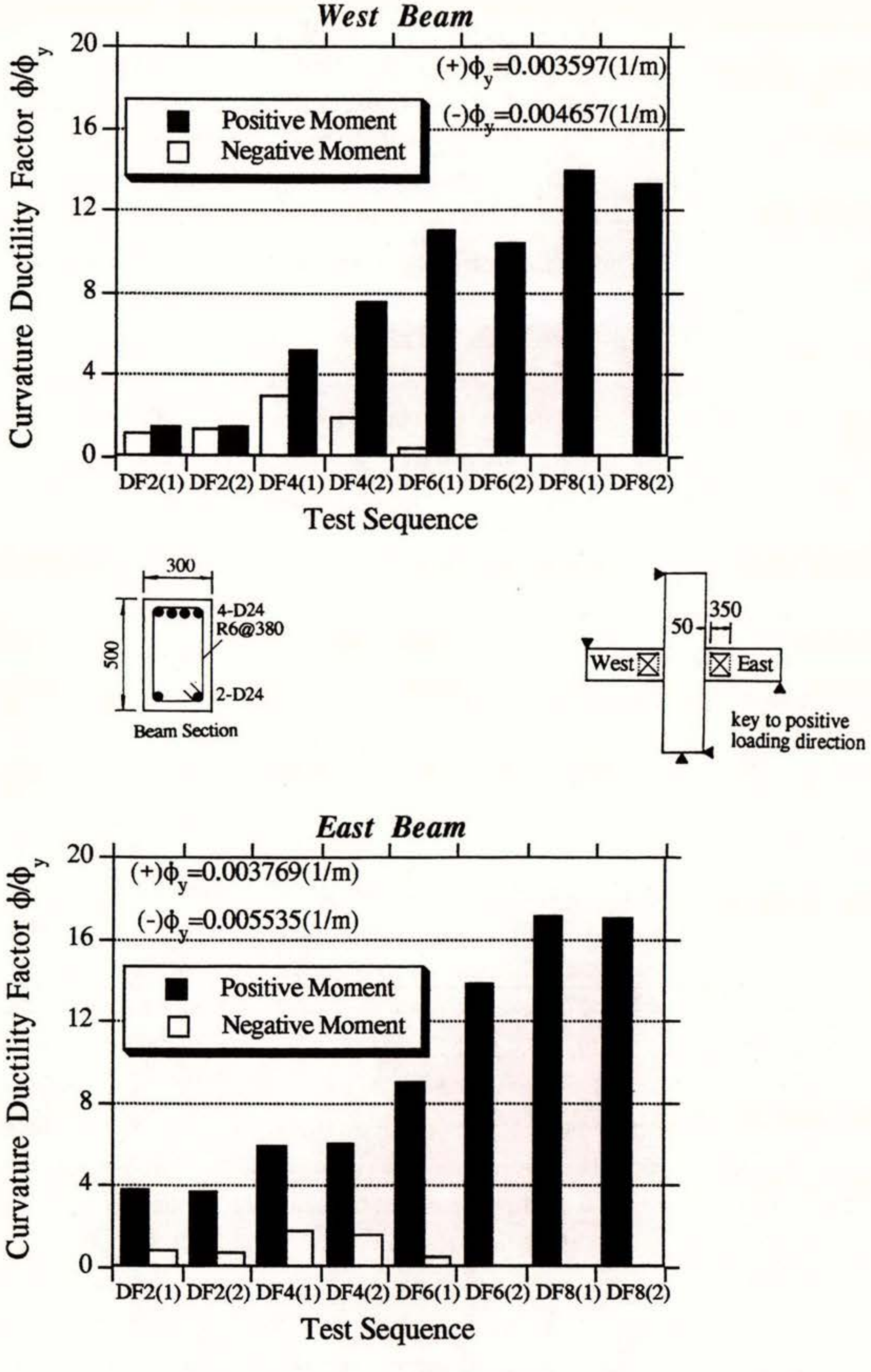

Fig.5.30 Curvature Ductility Factors of Beams of Specimen R3

during beam negative moment in those loading cycles(see Fig.5.29), it was identified that the shear deformations of the beams became dominant at this stage.

5.4.6 Column Behaviour

5.4.6.1 Column Cracking

During the test, only minor flexural cracks were observed in the columns(see Fig.5.25). The widths of those cracks remained very small during the test.

5.4.6.2 Longitudinal Column Bar Strains

Fig.5.31 shows the strains along the corner and intermediate bars in the column measured by wire strain gauges. As the displacement ductility factor imposed on the test specimen increased, the measured strains in the column corner and intermediate bars increased gradually. Up to the loading to DF of 6, the strain distribution of the corner column bar was almost linear and only small tensile strains were measured at the beam face subjected to the flexural compression force of the column. This implies that the large corner bar force was transferred by bond to the joint core concrete without bond deterioration. Although the strain measured at the beam face reached the yield strain in the loading to DF of 4, no significant tensile strains were measured at the other face.

The strain distribution in the intermediate column bars in Fig.5.31 indicates the role of column flexural resistance. The strains measured at the centre of the joint showed only small tensile strain up to the loading DF of 4 since no corner to corner diagonal tension cracks initiated in the joint core during the test.

It can be concluded that the columns remained essentially elastic during the test.

5.4.7 Joint Behaviour

When the beam plastic hinge mechanism was developed, the maximum nominal horizontal shear stress in the enlarged joint was $0.23\sqrt{f'_c{}^*}$, where $f'_c{}^*$ is the weighted average concrete compressive strength.

No critical corner to corner diagonal tension cracks were observed during testing(see Fig.5.25). Although several diagonal tension cracks initiated in the corners of the joint, the widths of those cracks remained very small until the end of the test. The joint behaviour was satisfactory due to the reduction in the horizontal shear stress in the joint core as a result of the enlargement of the joint.

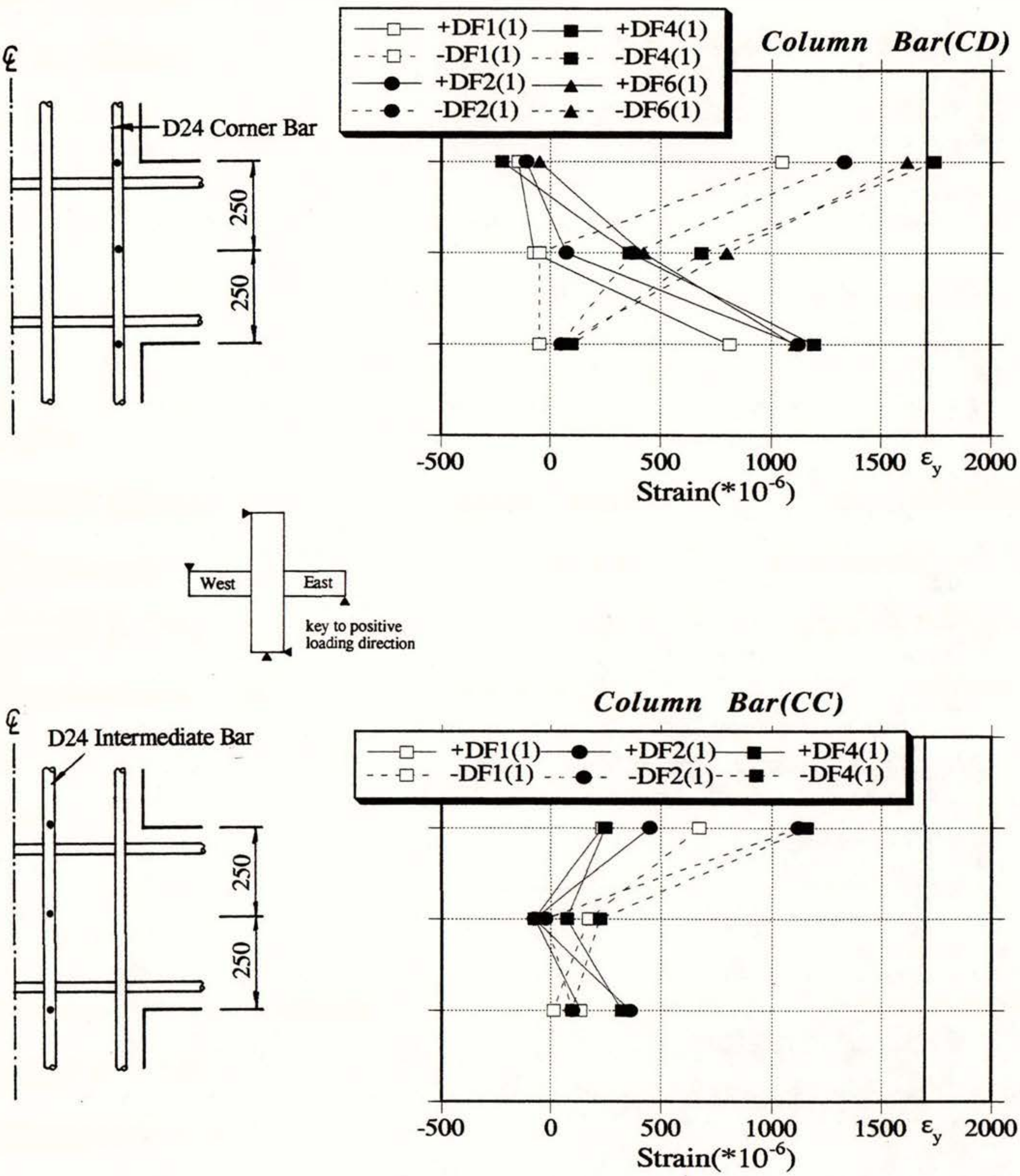

Fig.5.31 Strain Profiles of Column Bars of Specimen R3

5.4.7.1 Bond Stresses of Beam Bars

Fig.5.32 shows the average bond stress distributions along the beam bars in the joint at the peaks of the selected loading cycles. The bond stresses, assumed to be uniformly distributed over the gauge length of $7.3d_b$, were obtained from the wire strain gauge readings, where d_b is the beam bar diameter.

In the elastic loading cycles, the bond stresses were generated mainly over the region where the bars were in tension. Only small bond stresses were developed over the region where the bars were in compression. In the inelastic loading cycles, the bond stresses over the tension zone decreased and the maximum bond stresses were generated toward the centre of the joint. Bond stresses estimated over the region where the bars were in compression were still small. Until the loading to a displacement ductility factor DF of 2, the maximum bond stress was calculated to be $1.3\sqrt{f'_c}$ for bottom beam bar where f'_c is the measured compressive strength of the existing concrete.

It is likely that the bond stress profiles shown in Fig.5.32 represents a good bond condition along the beam bars in the joint since the enlarged column depth was great enough to keep the bond stress of longitudinal beam bars to be an acceptable level.

5.4.8 Decomposition of Horizontal Displacement

The components of the horizontal displacement at the peaks of the selected loading cycles are expressed as a percentage of the storey drift angle in Fig.5.33. The procedures for calculating those components were explained in Section 3.8.

Until the loading to DF of 1, the largest contribution was the beam flexural displacement which contributed 76 to 79% of a storey drift angle. The fixed-end rotation of the columns accounted for about 20% of a storey drift angle. However, this contribution became insignificant as the test progressed since the columns remained essentially elastic during the test.

In the loading to DF of 2, the contribution of the beam shear displacement increased gradually but its magnitude was always less than 5%. In the second cycle of loading to DF of 4, in which the beam shear failure occurred, the beam displacement by shear distortion increased rapidly and contributed 21% of the storey drift angle. A maximum contribution to the storey drift angle of 28% was calculated in the second cycle of loading to DF of 6. On the contrary, the contribution of the beam flexural displacement began to decrease.

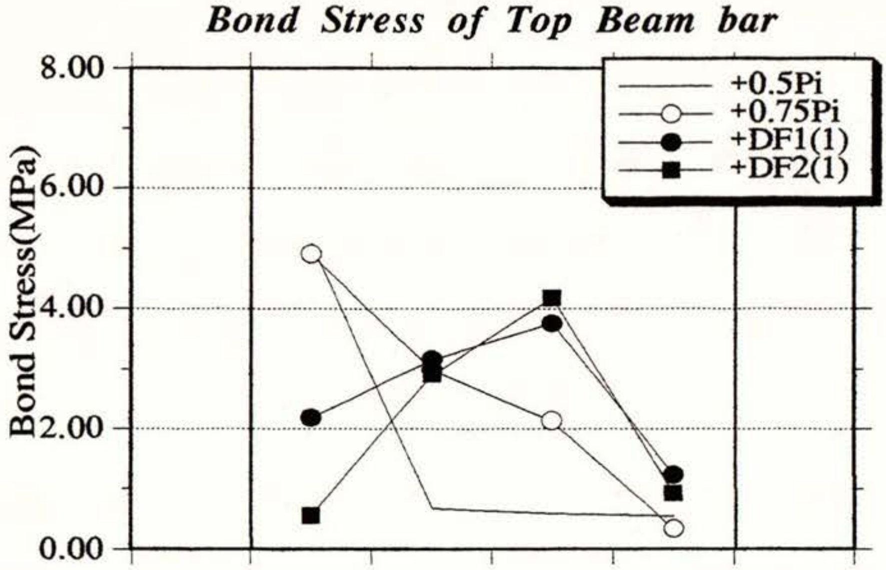

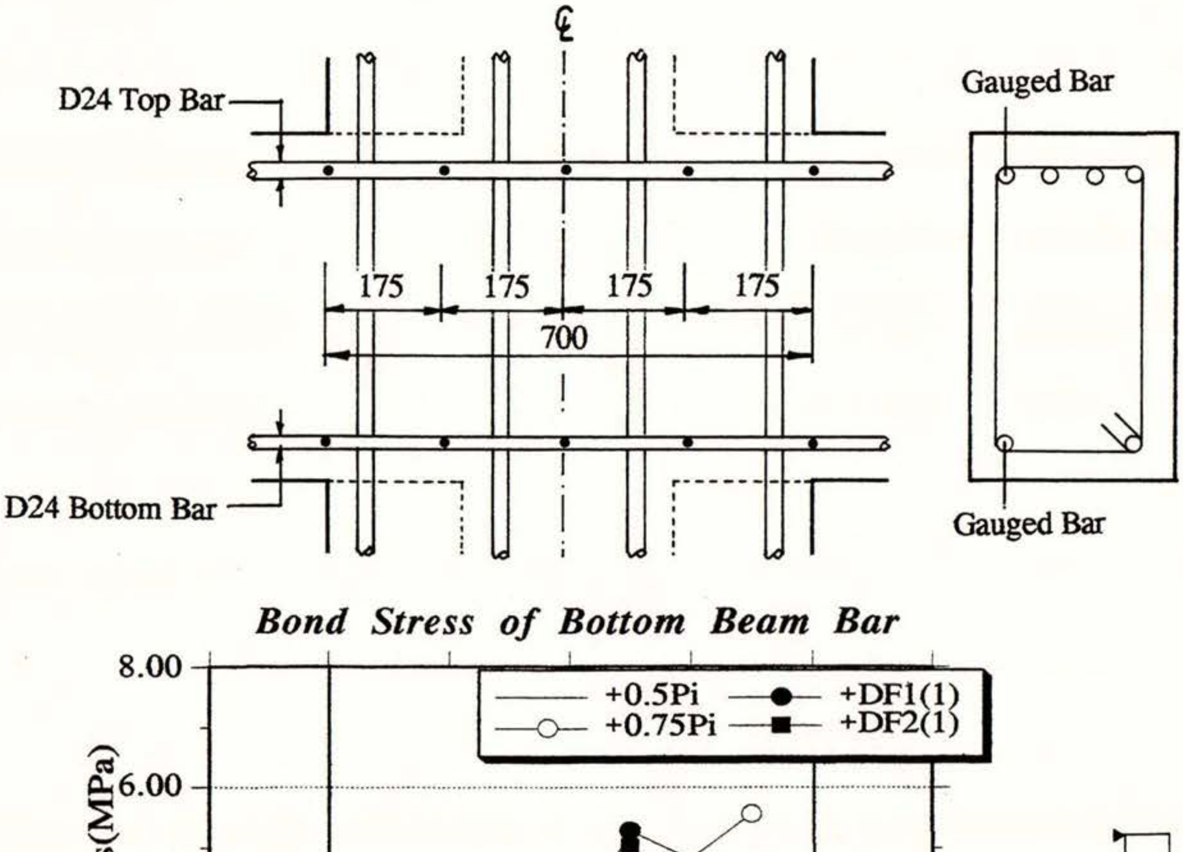

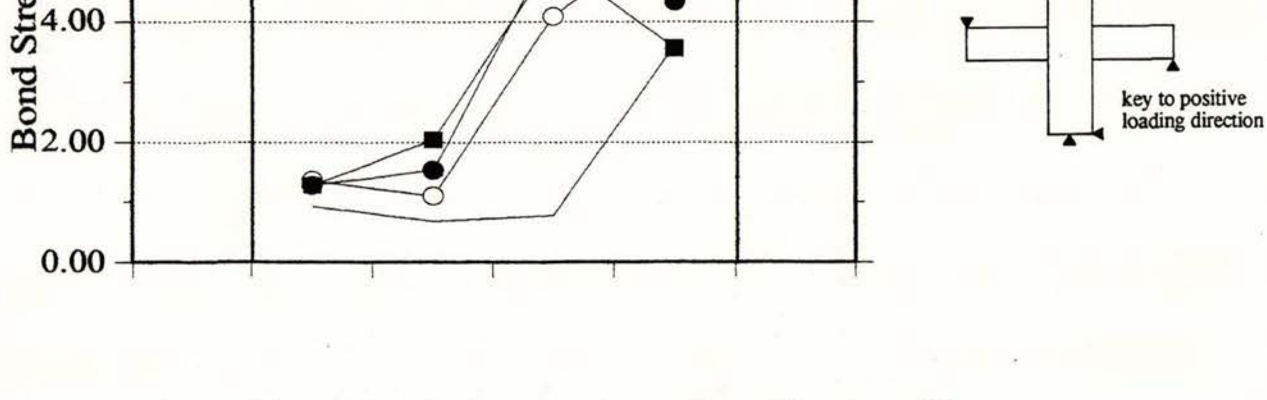

Fig.5.32 Bond Stress Distributions along Beam Bars of Specimen R3

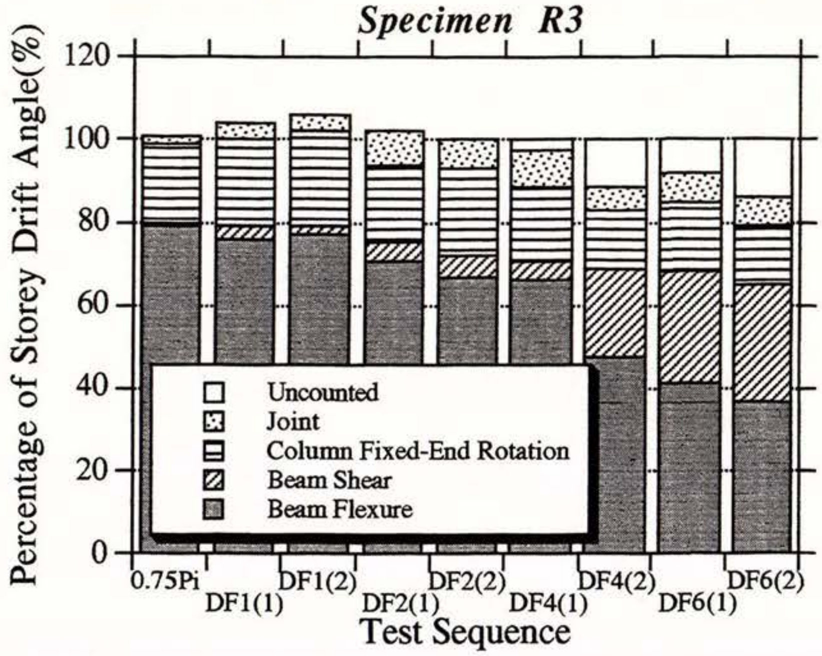

Fig.5.33 Components of Storey Drift Angle of Specimen R3

Table 5.1 Test Results

Specimen	f'_c (MPa)	Maximum Strength P_{max} (kN)	Initial Stiffness K_e (kN/mm)	Available Displacement Ductility Factor	Joint Cracking Stress $v_{j,cr}$ (MPa)	Maximum Joint Stress $v_{j,max}$ (MPa)
O1	40.7	89	2.38	NA	$0.41\sqrt{f'_c}$	$0.61\sqrt{f'_c}$
R1	50.8*	231	16.7	8	$0.27\sqrt{f'_c}$*	$0.29\sqrt{f'_c}$*
R2	56.0*	223	20.3	10	$0.27\sqrt{f'_c}$*	$0.27\sqrt{f'_c}$*
R3	42.4*	145	16.2	2.5	NA	$0.23\sqrt{f'_c}$*

f'_c : measured compressive cylinder strength of concrete

* : weighted average compressive strength of two concretes of the joint core

$v_{j,cr}$: nominal horizontal joint shear stress when joint diagonal tension cracks first formed

$v_{j,max}$: nominal horizontal joint shear stress when maximum storey horizontal load strength was reached

The maximum contribution of the joint shear displacement to the storey drift angle was only 9% in the loading to DF of 4 and its magnitude decreased as the imposed horizontal displacement increased, indicating that the joint remained in the elastic range.

5.5 EFFECTIVENESS OF THE RETROFIT TECHNIQUE USING CONCRETE JACKETING

Table 5.1 tabulates the test results obtained from Specimens R1, R2 and R3. The results obtained for the as-built Specimen O1 are also shown.

The retrofitted Specimens R1 and R2, in which both the beams and columns were retrofitted by jacketing with new reinforced concrete, had much higher maximum horizontal load strength, stiffness and available displacement ductility capacity than that of the as-built Specimen O1. The maximum nominal horizontal shear stress $v_{j,\,max}$ in the enlarged joint of Specimens R1 and R2 was $0.29\sqrt{f'_c{}^*}$ and $0.27\sqrt{f'_c{}^*}$, respectively, where $f'_c{}^*$ is the weighted average compressive strength of the joint core. The joint shear stress was evidently low enough not to result in the joint shear failure, since the joints of Specimens R1 and R2 behaved satisfactory, and almost similarly, with ductile plastic hinge behaviour in the beams in spite of the fact that Specimen R2 had no joint core hoops.

For the retrofitted Specimen R3, which was retrofitted by jacketing the columns alone, the maximum horizontal load strength and stiffness were significantly increased, compared with those of the as-built Specimen O1, as shown in Table 5.1. However, the available displacement ductility factor obtained from Specimen R3 was inferior to those from Specimens R1 and R2 since shear failure of the beams occurred. The maximum nominal horizontal shear stress $v_{j,\,max}$ in the enlarged joint of Specimen R3 was $0.23\sqrt{f'_c{}^*}$ and the joint behaviour was satisfactory, in spite of the absence of the joint core hoops.

When diagonal tension cracking occurred in the joint core, the nominal horizontal shear stress $v_{j,\,cr}$ in the enlarged joints of Specimen R1 and R2 was $0.27\sqrt{f'_c{}^*}$. For Specimen R3, corner to corner joint diagonal tension cracks were not observed until the end of the test. The joint shear stress at cracking $v_{j,\,cr}$ of the as-built Specimen O1 was $0.41\sqrt{f'_c}$, which was somewhat larger than those of the retrofitted specimens.

5.6 CONCLUSIONS

Three reinforced concrete beam-interior column joints representing the joint region of a frame constructed in New Zealand before the 1970's were retrofitted by jacketing with new reinforced concrete. One of the as-built interior joint specimen had been tested and damaged before retrofitting. Another as-built specimen, not previously damaged, was retrofitted in the same manner except that new joint hoops were not placed in the joint core The other non-damaged as-built specimen was retrofitted by jacketing the columns only.

Based on the test results obtained from the retrofitted Specimens R1, R2 and R3, the following conclusions can be reached:

(1) Results of the simulated seismic load tests showed that the jacketing of columns, beams and joints with new reinforced concrete was a useful technique for enhancing the stiffness, strength and ductility of poorly detailed as-built beam-column joint regions. The tests also showed that the effect of previous damage to the as-built specimen had no significant influence on the overall seismic response of the retrofitted specimen.

(2) It was found that, even when no joint core hoops are present in the existing beam-column joints, no new joint core hoops are required in the added jacket if the existing column is enlarged by jacketing so that the nominal horizontal shear stress in the joint core is reduced to less than $0.3\sqrt{f'_c}$MPa. This finding is for joints with no axial load on the columns. When axial compressive load is present on columns, a greater horizontal joint shear stress than $0.3\sqrt{f'_c}$ MPa would be tolerable.

(3) The overall response of Specimen R3, which was retrofitted by jacketing the columns alone, was governed by the beam shear failure which occurred after developing the theoretical ideal flexural strength of the beams. A limited ductility response, that is an available displacement ductility factor of 2.5, was attained for this specimen.

(4) Based on this test data, two limiting conditions were identified for the seismic behaviour of the beams with a small amount of shear reinforcement. At a maximum nominal shear stress level of less than $0.11\sqrt{f'_c}$ MPa, the beams did not fail in shear at least up to a curvature ductility factor of 14. However, when the maximum nominal shear stress level approached $0.18\sqrt{f'_c}$ MPa, beam shear failure commenced. At this stage, the hysteresis loops indicated rapid strength degradation, mainly due to the reduced shear carried by the concrete shear resisting mechanism, particularly aggregate interlock.

(5) The measured initial stiffnesses obtained from the retrofitted Specimens R1 and R2 were considerably lower than the theoretical values. One main reason is the damage to the existing concrete associated with surface preparation, especially chipping off the cover concrete of the beam to place the new transverse reinforcement. Therefore it is recommended that chipping off the concrete surrounding the longitudinal reinforcement should be avoided.

CHAPTER 6

EXPERIMENTAL RESULTS OF SPECIMENS O4 AND O5

6.1 INTRODUCTION

Two full-scale beam-interior column joint subassemblages, referred to as Specimens O4 and O5 were constructed and tested under simulated seismic loading. Typical features of the reinforcing details are that the test specimens had no shear reinforcement in the joint core and only a small amount of transverse reinforcement in the beams and columns, deficiencies which are common for in older building frames. Both specimens had the same dimensions and reinforcing details except for the longitudinal beam bar diameter. The beam bar diameter used was 24mm for Specimen O4 and 32mm for Specimen O5, respectively. The main aim of this test was to investigate the effect of the bond condition along the longitudinal beam reinforcement in the joint on the behaviour of the joint without shear reinforcement. This chapter presents the test results for Specimens O4 and O5.

6.2 SPECIMEN O4

6.2.1 Introduction

For Specimen O4, the ratio of the theoretical ideal flexural strength of the column to that of the beam was 1.35 based on the measured material strengths. When the beam plastic hinge mechanism was developed, the ideal storey horizontal load strength P_i was 177kN. The ratio of longitudinal beam bar diameter d_b to column depth h_c was d_b/h_c=24/600=1/25. Therefore, the column depth was great enough to accommodate the development length for beam bars according to NZS3101 for ductile frames[SANZ 1982(a)]. The concrete of Specimen O4 at the stage of testing had a compressive cylinder strength f'_c of 52.9MPa.

6.2.2 General Behaviour

The beams of the test specimen failed in shear during the loading to displacement ductility factor DF of 2 and 4. The test was temporarily terminated during the first negative cycle of loading to DF of 4. The beams were retrofitted to obtain further information about the seismic behaviour of the joint and retested. The retrofit methods used were described in detail in Section 3.3.6.

The observed cracking before retrofitting and the storey shear force versus horizontal displacement relationship are shown in Figs.6.1 and 6.2, respectively. The retrofit and the

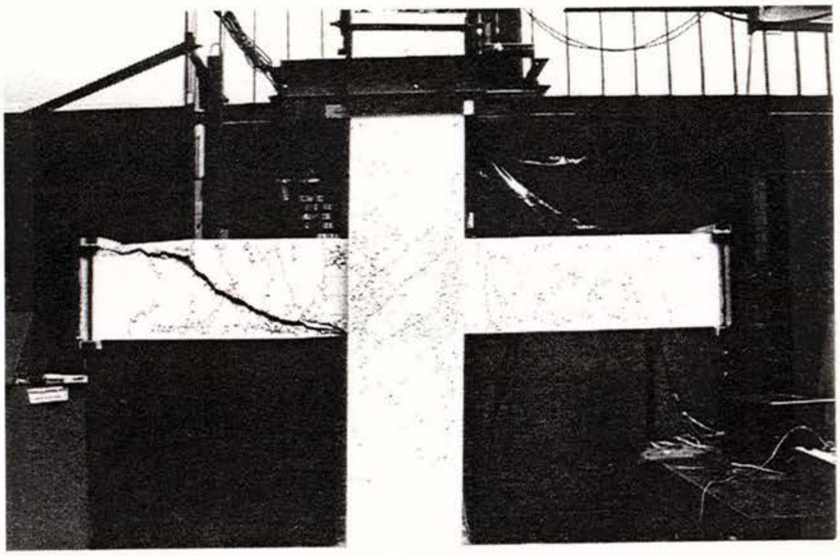

Fig.6.1 Observed Cracking of Specimen O4
at first cycle of DF=+4

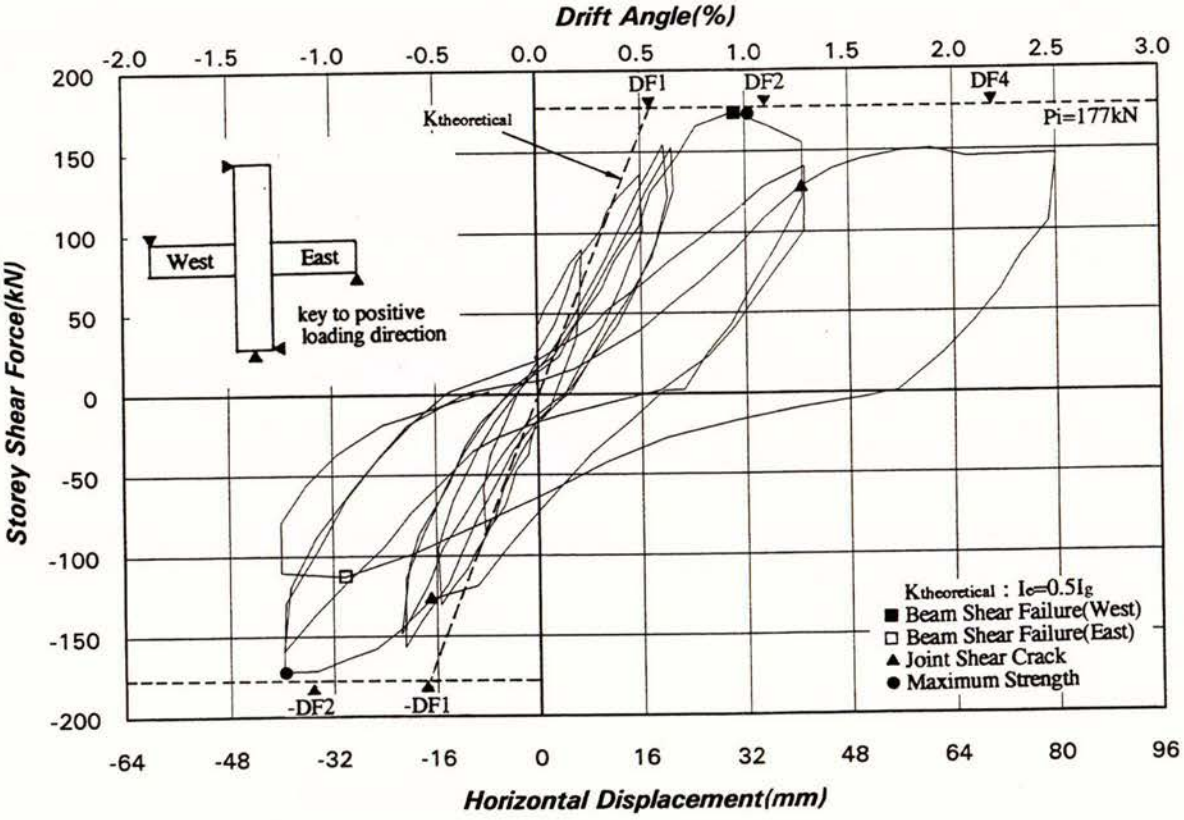

Fig.6.2 Storey Shear Force versus Horizontal Displacement Relationship
for Specimen O4

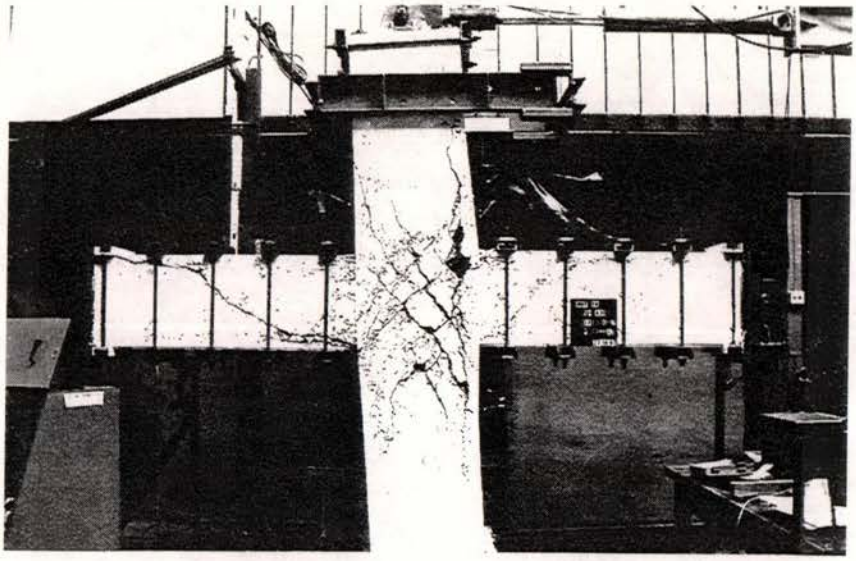

Fig.6.3 Observed Cracking of Specimen O4
at second cycle of DF=-8

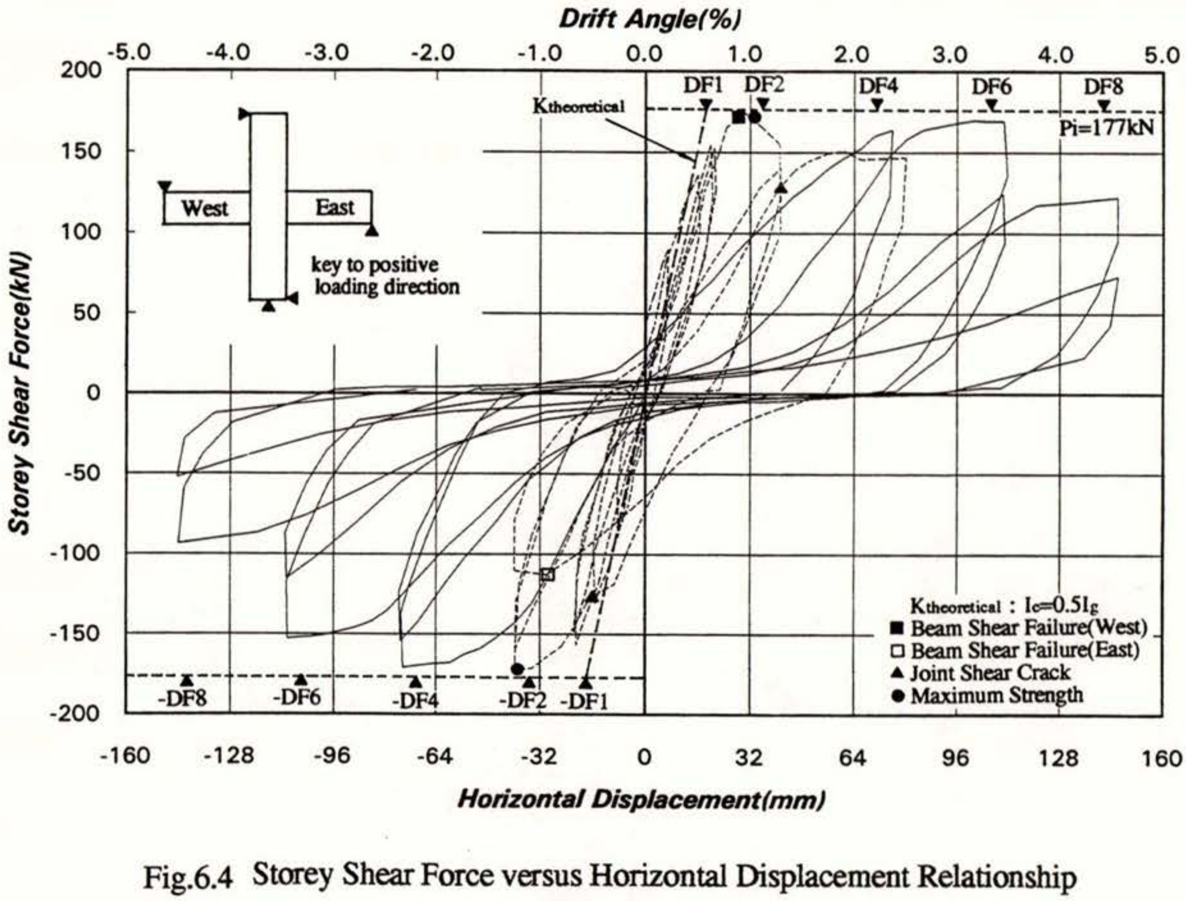

Fig.6.4 Storey Shear Force versus Horizontal Displacement Relationship
for Specimen O4

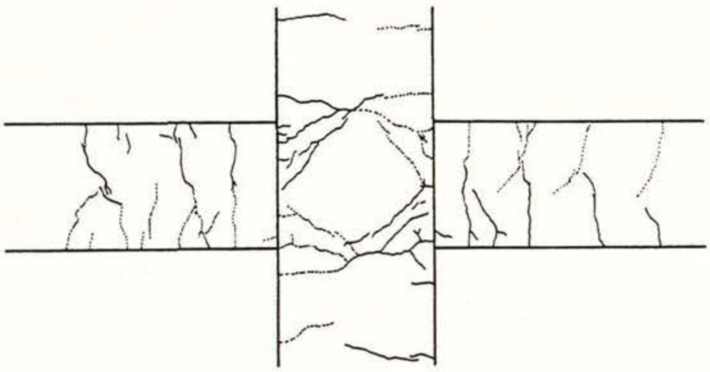

(a) at the peak of 0.75Pi
(R=0.41%)

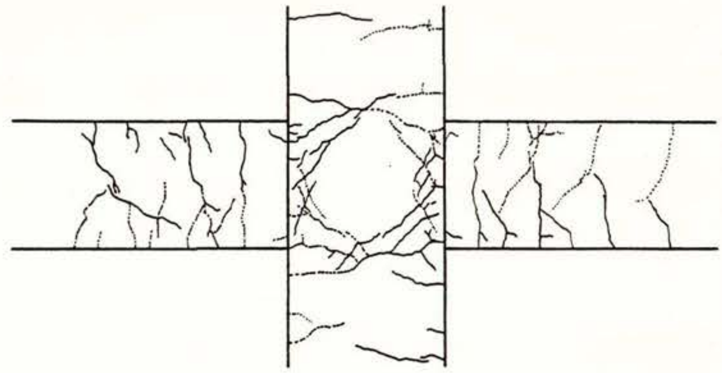

(b) at the peak of second cycle, DF=1
(R=0.55%)

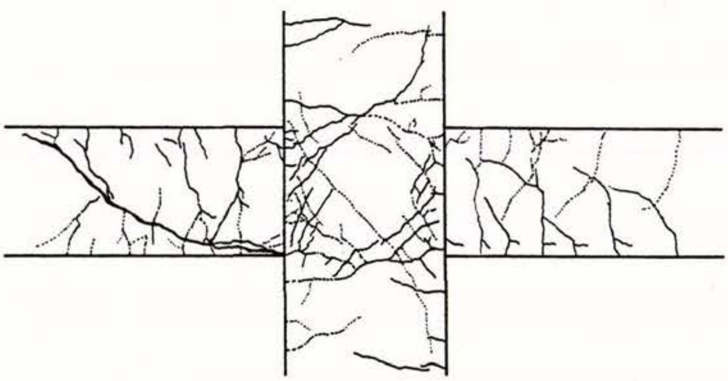

(c) at the peak of second cycle, DF=2
(R=1.10%)

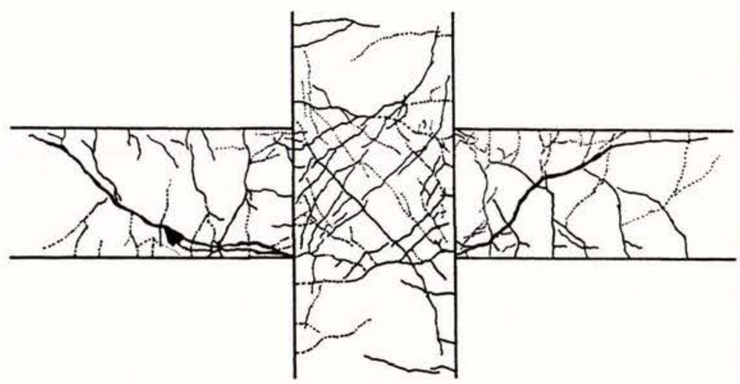

(d) at the peak of second cycle, DF=4
(R=2.20%)

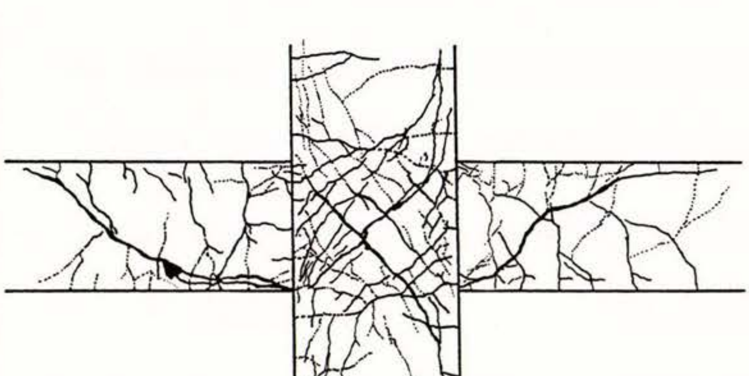

(e) at the peak of second cycle, DF=6
(R=3.30%)

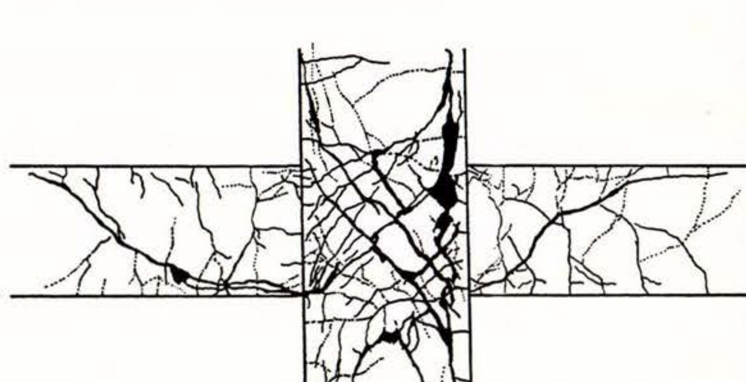

(f) at the peak of second cycle, DF=8
(R=4.40%)

Fig.6.5 Observed Cracking of the Joint(Specimen O4)

complete storey shear force versus horizontal displacement response is illustrated in Figs.6.3 and 6.4, respectively, in which the response before retrofit is expressed by dotted lines and that after retrofit is expressed by solid lines. Observed cracking after testing and that at the peak of the selected loading cycles are shown in Figs 6.3 and 6.5, respectively.

In the loading to $\pm 0.5P_i$, flexural and flexural-shear cracks initiated in the beams and column flexural cracks were also observed. In the loading to $\pm 0.75P_i$, those cracks extended and the number of the cracks also increased. Joint shear cracks initiated at the corners of the joint(see Fig.6.5(a)).

In the loading to displacement ductility factor DF of 1, bond splitting cracks were formed along the column bars in the joint(see Fig.6.5(b)). The diagonal tension cracks initiated near the flexural-shear cracks in the west beam. At this stage, the longitudinal beam bars started to yield in tension at the column face.

In the first positive cycle of loading to DF of 2, one dominant beam diagonal tension crack with an acute angle to the beam axis extended toward the flexural compression zone of the beam at the column face in conjunction with the bond splitting cracks along the top beam bar in the west beam. The diagonal tension crack opened wide and the west beam failed in shear at the storey drift angle of 0.95%(see Figs.6.2 and 6.5(c)). The maximum width of the beam diagonal tension crack was approximately 5mm. At this stage, the maximum horizontal load strength of the specimen was reached for the positive loading cycle. The measured maximum horizontal load strength was 175kN which was 99% of the ideal storey horizontal load strength when the beam plastic hinge mechanisms were developed. In the first negative cycle of loading to DF of 2, corner to corner diagonal tension cracks initiated at the storey drift angle of 0.53%. The maximum width of the joint diagonal tension crack was 1.8mm. At the peak of this loading cycle, the maximum horizontal load strength of 172kN was reached for the negative loading cycle(see Fig.6.2 or 6.4). In the second cycle of loading to DF of 2, the diagonal tension cracks extended and tended to open wide in the west beam. The splitting cracks along the column bars were also observed in the columns near the beam face and connected to the joint shear cracks(see Fig.6.5(c)).

In the first positive cycle of loading to DF of 4, the beam and joint diagonal tension cracks also extended and opened wide. However, strength degradation was not so significant(see Fig.6.2). During the first negative cycle of loading to DF of 4, the east beam also failed in shear in the same manner at the storey drift angle of approximately 0.94%(see Fig.6.2). At this stage, the test was terminated to retrofit the beams and retested. The horizontal load strength at the peak of the second cycle of loading to DF of 4 after retrofit was 94% of the maximum horizontal load strength obtained before retrofit during positive loading cycle and 99% of that during negative loading cycle, respectively. Joint diagonal tension cracks opened wide to the crack width of 4mm. Bond splitting cracks along the column bars also extended and opened wide(see Fig.6.5((d)). Although the hysteresis curves were significantly pinched, the strength degradation was not so significant at this loading stage.

In the loading to DF of 6, joint diagonal tension cracks opened wide significantly. Bond splitting cracks along the column bars also extended and opened wide in both the joint and the columns. In the second cycle of loading to DF of 6, severe strength degradation was observed in the hysteresis loops as illustrated in Fig.6.4. The maximum width of the joint shear crack was approximately 6.5mm. At this stage, shear cracks also initiated in the columns(see Fig.6.5(e)). For the beams, concrete crashing in the flexural compression zone was observed. The beam diagonal tension cracks did not extend nor did open wide due to the clamping action of the steel rods placed vertically on the beams.

In the loading to DF of 8, joint diagonal tension cracks opened wide to the crack width of approximately 10mm. Bond splitting cracks along the column bars also extended and opened wide significantly. The joint expansion could be seen by visual observation. In the second cycle of loading to DF of 8, cover concrete along the column bars in the joint spalled off and the joint was severely deteriorated(see Figs.6.3 and 6.5(f)). Column shear cracks also opened wide at this stage. Severe strength degradation and pinching were obvious in the hysteresis loops as shown in Fig.6.4.

After retrofitting, the beam diagonal tension cracks were well confined by the external clamping action of the steel rods attached to the beams, indicating that the aggregate interlock action along the beam diagonal tension cracks were fully mobilized until the end of the test. On the other hand, the joint diagonal tension cracks opened wide in conjunction with the bond splitting cracks along the column bars and the condition of the joint of the test specimen deteriorated. Hence it could be concluded that the shape of hysteresis curves were mainly governed by the response of the most damaged element, the joint(see Fig.6.3).

6.2.3 Initial Stiffness

The theoretical initial stiffness was calculated for Specimen O4 as follows:

$$K_{theoretical}=14.5\text{kN/mm}$$

The procedures for estimating the theoretical initial stiffness were described in detail in Section 3.9. The theoretical stiffness $K_{theoretical}$ is shown in Figs.6.2 and 6.4. The stiffness estimated at 75% of the theoretical ideal storey horizontal load strength of the test specimen was 10.4kN/mm for positive loading cycle and 9.7kN/mm for negative loading cycle, respectively. The average value of the stiffnesses estimated for the positive and negative loading cycle was 70 % of the theoretical stiffness.

The yield displacement of the test specimen estimated at $\pm 0.75P_i$ was 17.6mm. This value could be converted to 0.55% in terms of a storey drift angle. Specimen O4, which has no shear reinforcement in the joint core and good bond condition along the beam bars through the joint was significantly flexible according to the current code[SANZ 1992].

6.2.4 Available Displacement Ductility Factor

The available displacement ductility factor μ_a of 4.5 was obtained from the measured storey shear force and horizontal displacement relationship of Specimen O4. The method for calculating the available displacement ductility factor was explained in Section 5.2.4. Although severe strength degradation of the test specimen was observed mainly due to the joint shear failure after developing beam plastic hinge mechanisms, a moderate displacement ductility capacity could be obtained for Specimen O4 without joint shear reinforcement.

6.2.5 Beam Behaviour

6.2.5.1 Longitudinal Beam Bar Strains

Strains along the longitudinal beam bars are illustrated in Figs.6.6 and 6.7. Strain profiles obtained from the wire strain gauge readings are shown in Fig.6.6 while those measured from the linear potentiometers attached to the steel rods welded to the beam bars are shown in Fig.6.7. Up to the loading to DF of 1, both figures show the gradual increase in the tensile strains along the beam bars and the yield strain was reached at the column faces in the loading to DF of 1 or 2. In the loading to DF of 2, the tensile strains measured at the column face increased rapidly. For the west beam, the tensile strain measured at column face was not so large in the loading to DF of 2 since the west beam failed in shear during the first cycle of loading to DF of 2.

Typical feature of the strain profile along the beam bars is that tensile strains were measured over the column depth in the joint during the loading to DF of 1. This trend became more apparent in the loading to DF of 2, in which the corner to corner diagonal tension cracking was observed. The tension steel entering the joint found anchorage in the opposite beam at this stage. In the loading to DF of 2 and 4, yield penetration into the joint core was observed as shown in the Figs.6.6 and 6.7.

It was found from the results tested on Specimen O4 without shear reinforcement that even if the column depth was great enough to accommodate the development length for the

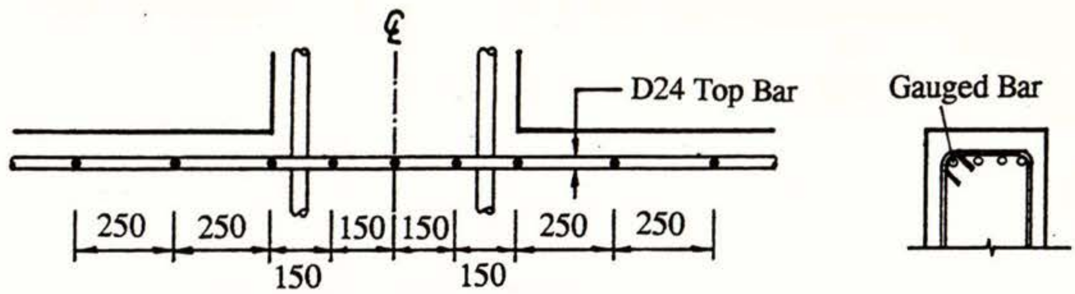

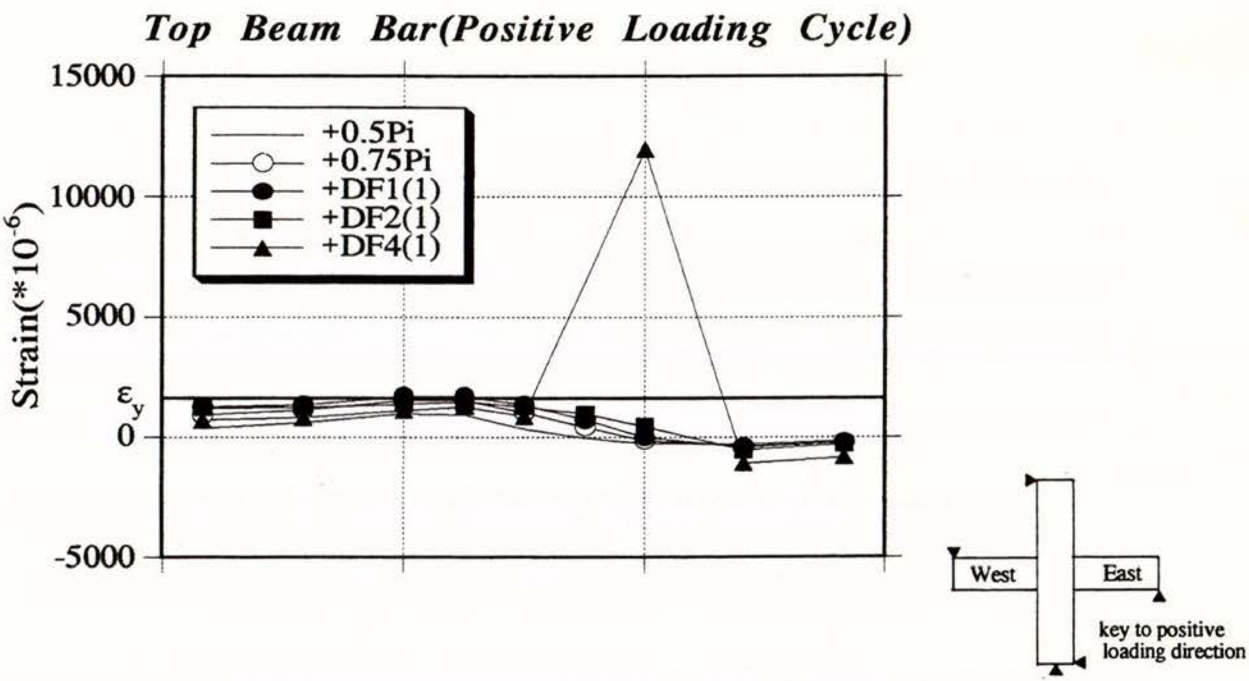

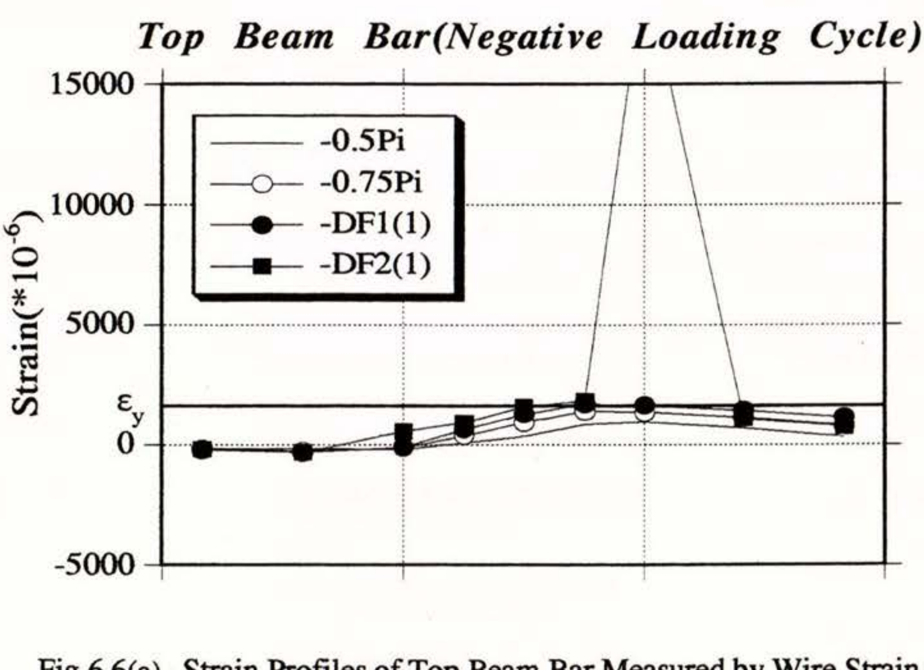

Fig.6.6(a) Strain Profiles of Top Beam Bar Measured by Wire Strain Gauges of Specimen O4

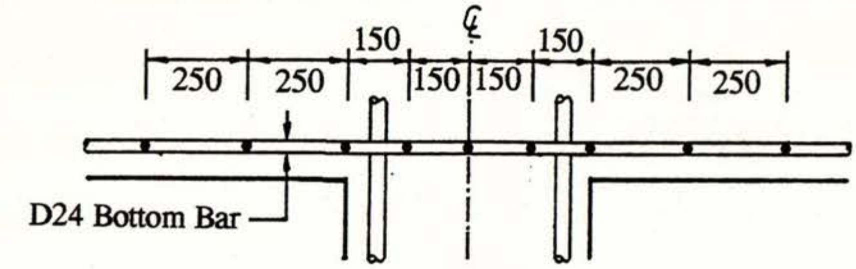

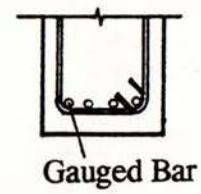

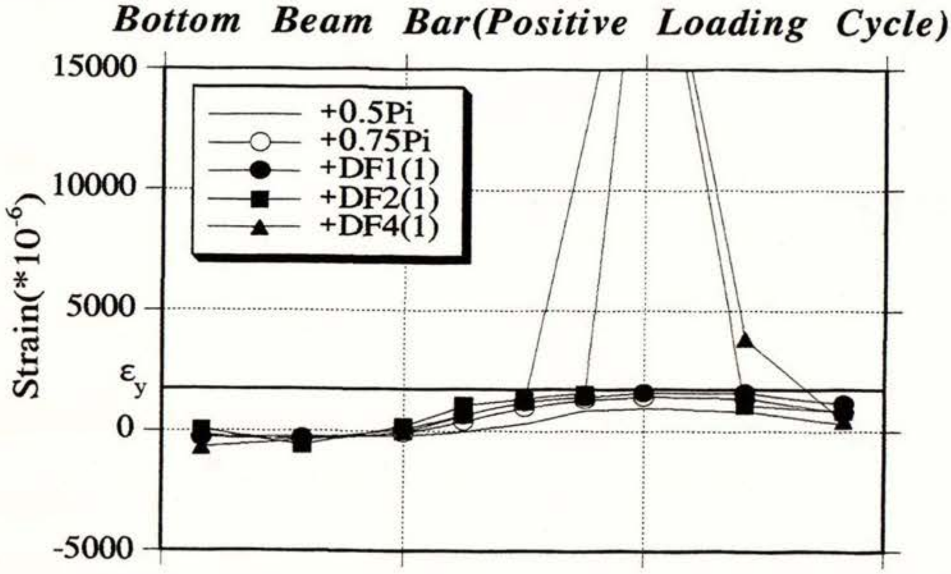

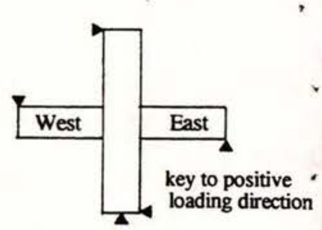

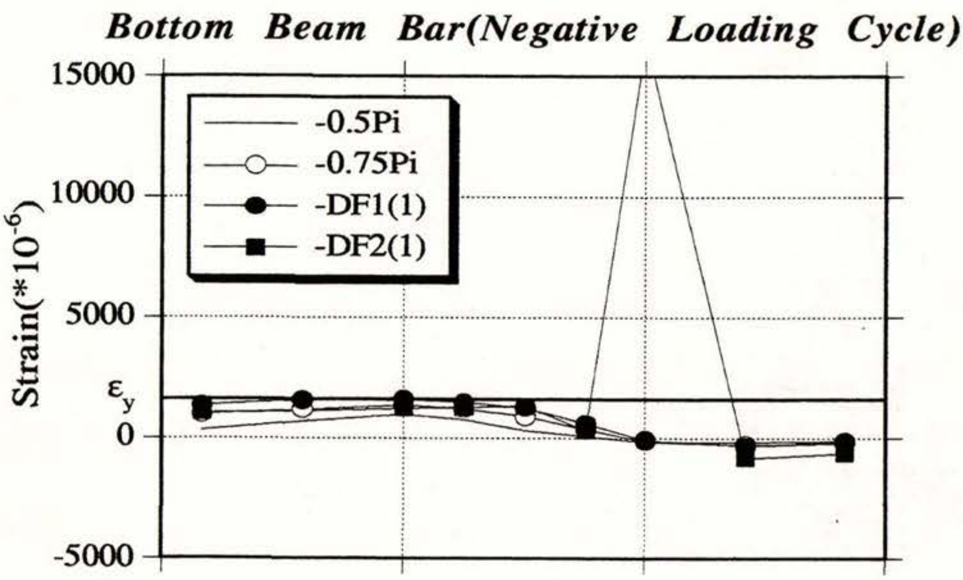

Fig.6.6(b) Strain Profiles of Bottom Beam Bar by Wire Strain Gauges of Specimen O4

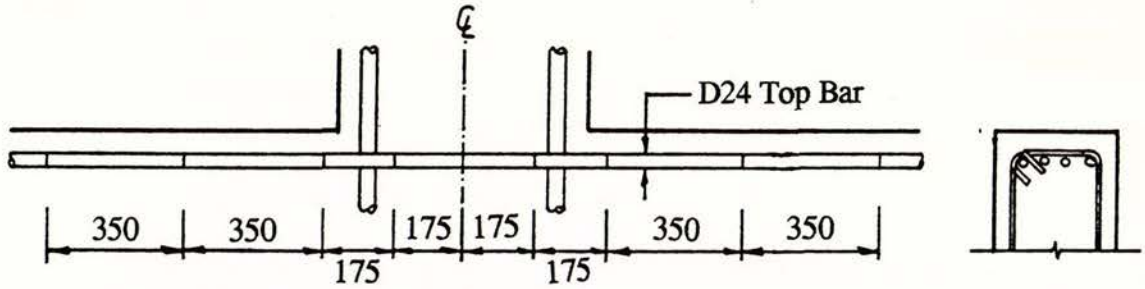

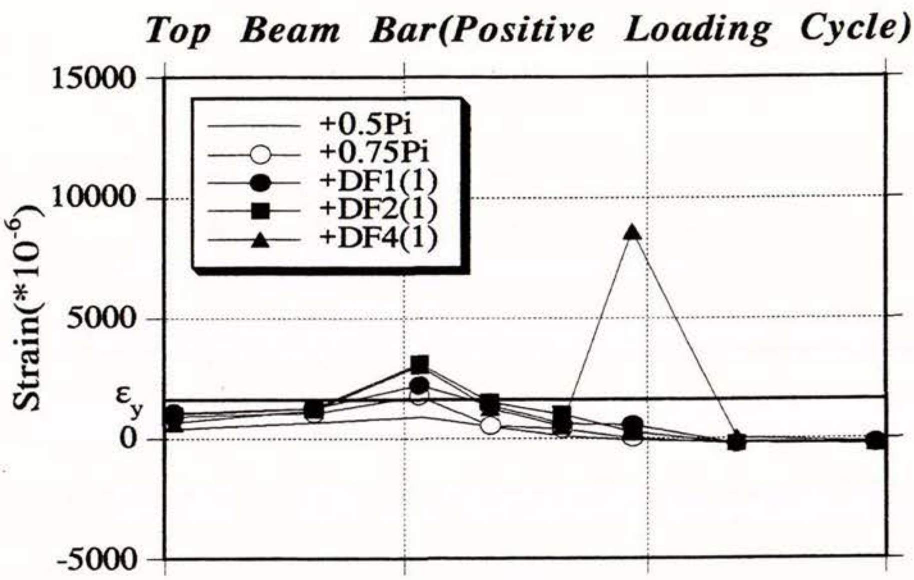

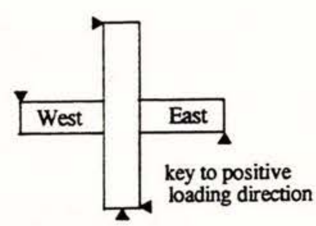

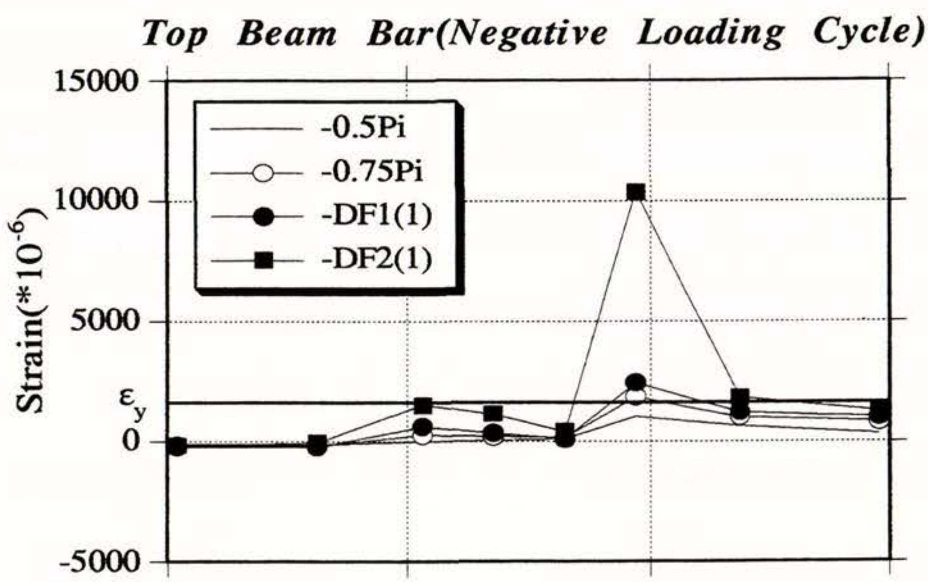

Fig.6.7(a) Strain Profiles of Top Beam Bar Measured by Linear Potensiometers of Specimen O4

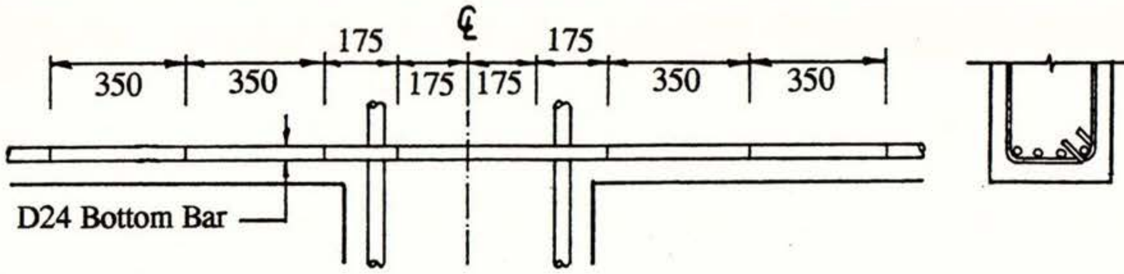

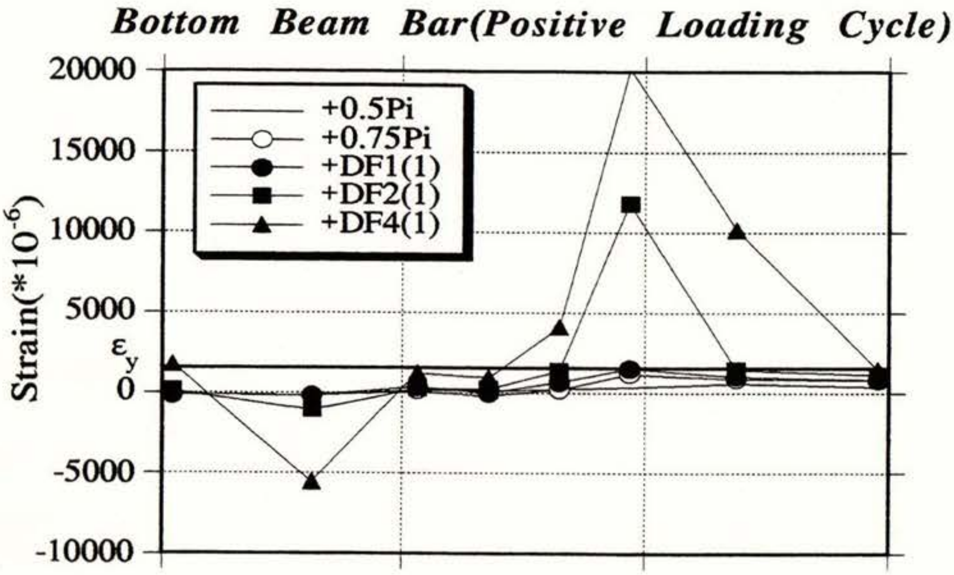

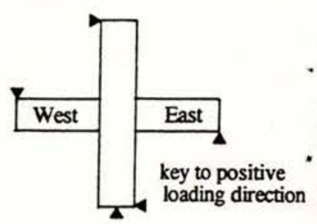

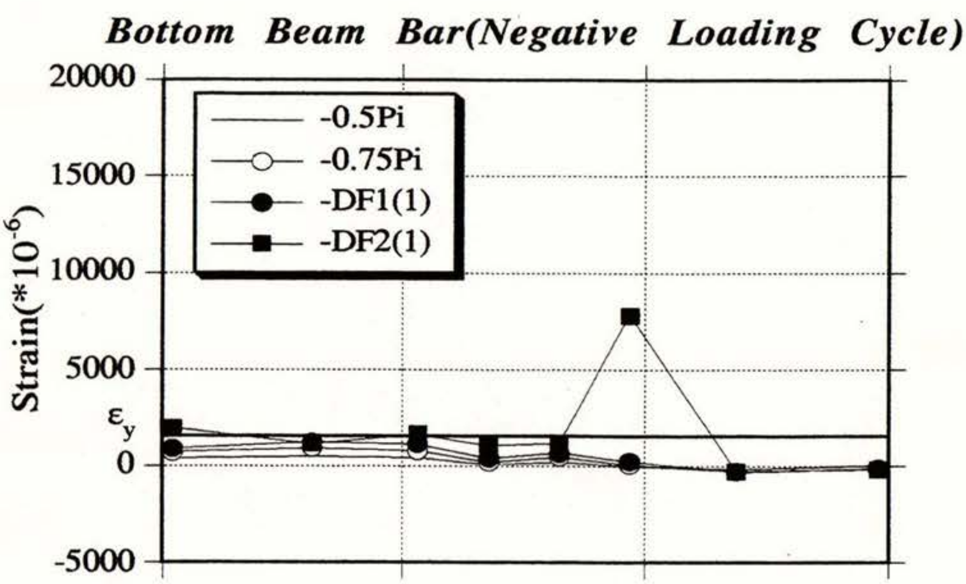

Fig.6.7(b) Strain Profiles of Bottom Beam Bar Measured by Linear Potensiometers of Specimen O4

beam bars required by current design code[SANZ 1982(a)], tensile strains in the beam bars were developed over the column depth at early loading stage, resulting in more flexible structure. The development of the diagonal tension cracks in the joint accelerated this trend.

6.2.5.2 Slip of Beam Bars

As mentioned earlier, the ratio of beam bar diameter d_b of column depth h_c for Specimen O4 was $d_b/h_c=24/600=1/25$, where h_c is the column overall depth and d_b is the longitudinal beam bar diameter. Therefore well anchorage condition for the beam bars could be expected through the joint.

The slip of the top and bottom beam bar in the joint are shown in Fig.6.8. The clear distance between two adjacent ribs of the beam bar was 11mm. The methods to obtain the bar slip were mentioned in detail in Section 3.7.4.

The bar slip measured at each location increased with the test progressed. Until the loading to DF of 6, the maximum bar slip was measured to 2.2mm for top beam bar and 1.9mm for bottom beam bar, respectively. No significant slippage of the beam bars in the joint was measured during the test.

6.2.5.3 Beam Shear Stress and Shear Distortion

Fig.6.9 plots the relationship between shear stress level $v_b/\sqrt{f'_c}$ and shear distortion of the beams, where $v_b=V_b/(b_w d)$, V_b is the applied beam shear force, b_w is the beam width and d is the effective depth of beam. Beam shear distortion was calculated using the second set of the linear potentiometers placed diagonally at 50mm away from the column faces as illustrated in Fig.6.9. Also plotted are the shear carried by stirrups using the average strains of the stirrups measured from the wire strain gauges attached on both sides of the stirrup, assuming 45 degree truss mechanism.

For the west beam, the beam diagonal tension crack was developed in the loading to DF of 1. In the loading to DF of 2, beam shear failure initiated at shear stress of $0.16\sqrt{f'_c}$ for the loading to negative moment, where f'_c is the measured concrete compressive strength. Shear distortion at failure was about 0.25%. Subsequent loading cycles resulted in a rapid increase in shear distortion of up to approximately 1%. The severe strength degradation for the west beam was caused by the diagonal tension cracks opened wide and bond splitting cracks along the top beam bar. At this stage, the stirrup in the west beam located at the closest to the column face yielded in tension and large strain was measured there. For the east beam, the maximum beam shear stress of $0.16\sqrt{f'_c}$ was obtained. In the first negative cycle of loading to DF of 4(shown in Fig.6.9 as DF2(3)), the shear distortion measured in the

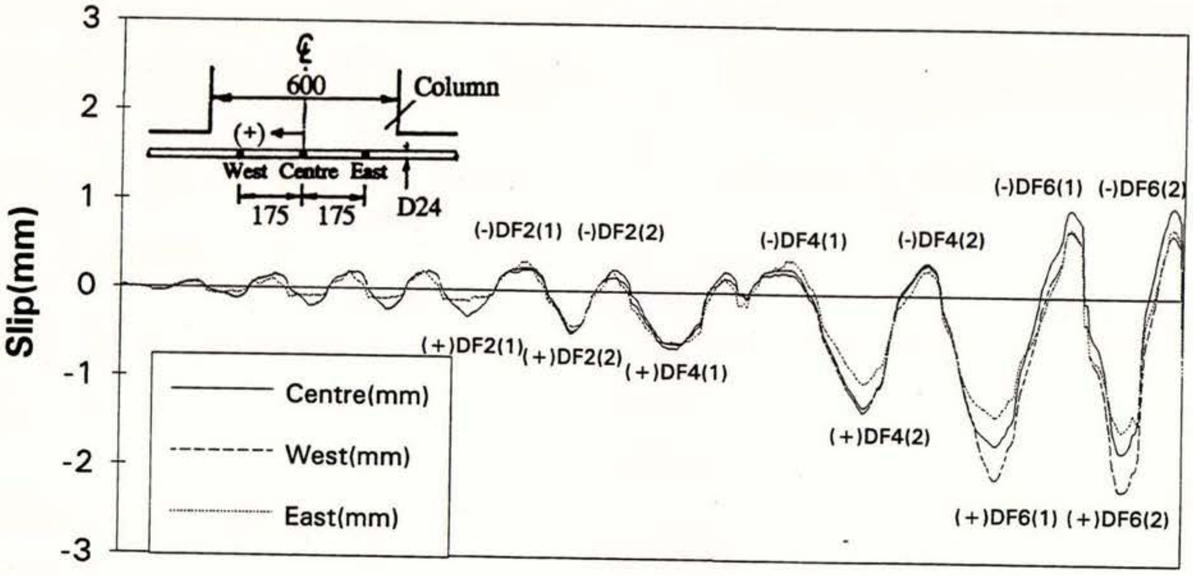

Test Sequence

(a) Slip of Top Beam Bar

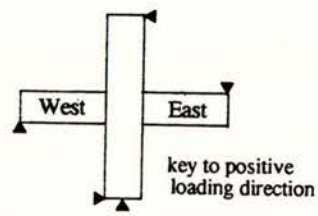

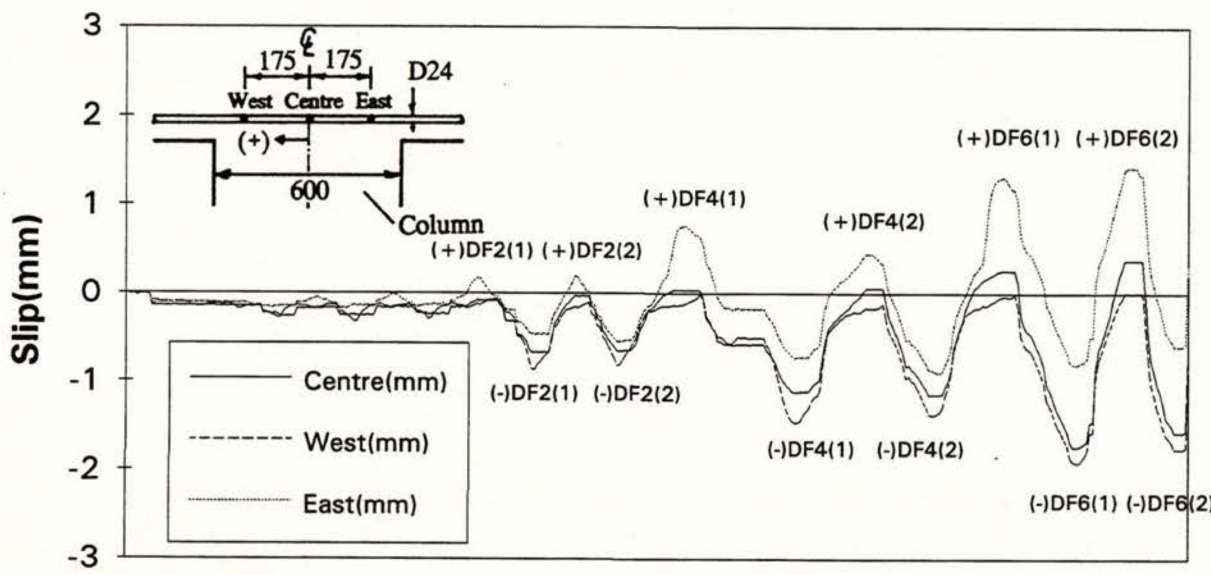

Test Suquence

(b) Slip of Bottom Beam Bar

Fig.6.8 Measured Slip of Beam Bars of Specimen O4

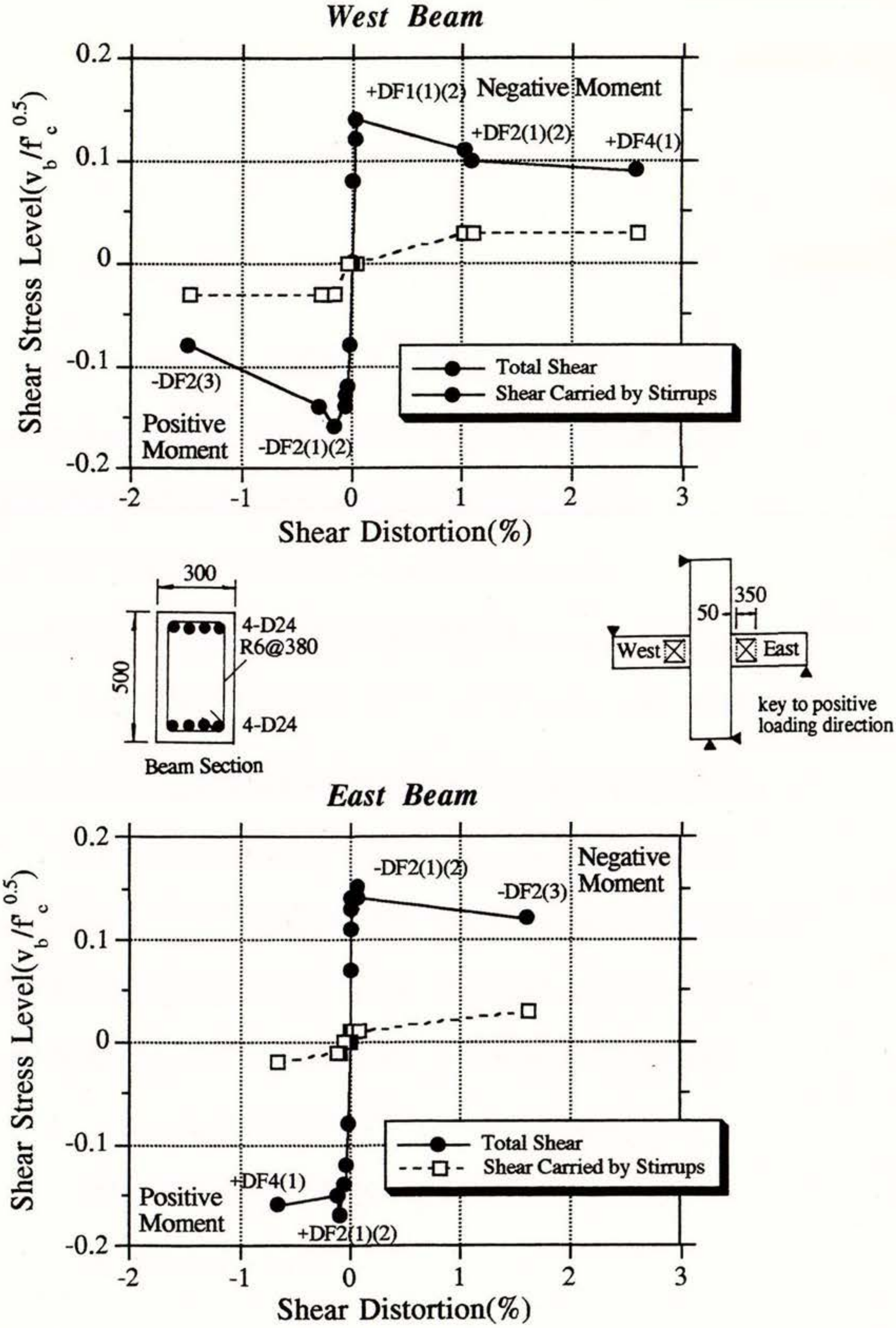

Fig.6.9 Relationship between Shear Stress Level and Shear Distortion of Beams of Specimen O4

east beam increased rapidly and the shear stress was reduced to $0.12\sqrt{f'_c}$ at shear distortion of 1.61% during negative moment. At this stage, the west beam also failed in shear with positive moment shown in Fig.6.9 and severe strength degradation was measured. The aggregate interlock mechanism became ineffective due to wide open diagonal tension cracks observed in both beams. Shear carried by dowel action was also reduced by the bond splitting cracks along the top beam bar.

6.2.6 Column Behaviour

6.2.6.1 Introduction

In the loading to DF of 1, bond splitting cracks along the column bars initiated in the joint. Those cracks extended and opened wide significantly as the test progressed. Shear cracks were observed in the columns in the loading to DF of 6 and opened wide in the loading to DF of 8.

6.2.6.2 Longitudinal Column Bar Strains

Fig.6.10 shows the strains along the longitudinal column bars in the joint. Those strains were obtained from the wire strain gauges. As the displacement ductility factor imposed on the test specimen increased, the measured strains of the column bars increased gradually. Until the loading to $\pm 0.75P_i$, the strains measured at the beam face showed small compressive strains when subjected to flexural compression force of the column while those showed tensile strains when subjected to flexural tension force of the column. In the loading to $\pm 0.75P_i$ in which joint shear cracks were developed at the corners of the joint, the tensile strain measured at the centre of the joint increased rapidly when compared with the other measurement. In the loading to DF of 1, this trend became more obvious and the tensile strains measured at the centre of the joint were equal to or larger than those measured at beam face when subjected to flexural tension force of the column. This implies that the column bond forces could not be developed in the flexural tension zones of the column in the joint. In the loading to DF of 2 in which a corner to corner diagonal tension crack was observed in the joint, the column bars at the centre of the joint yielded in tension as illustrated in Fig.6.10 (b). Yield strain was reached along the column bar through the joint in the first negative cycle of loading to DF of 2(see Fig.6.10 (a)).

The strain profiles of the column bars in the joint shown in Fig.6.10 indicated that the column bars in the joint core were stressed significantly larger than expected by the column flexural resistance alone, especially after the development of the joint diagonal tension cracks.

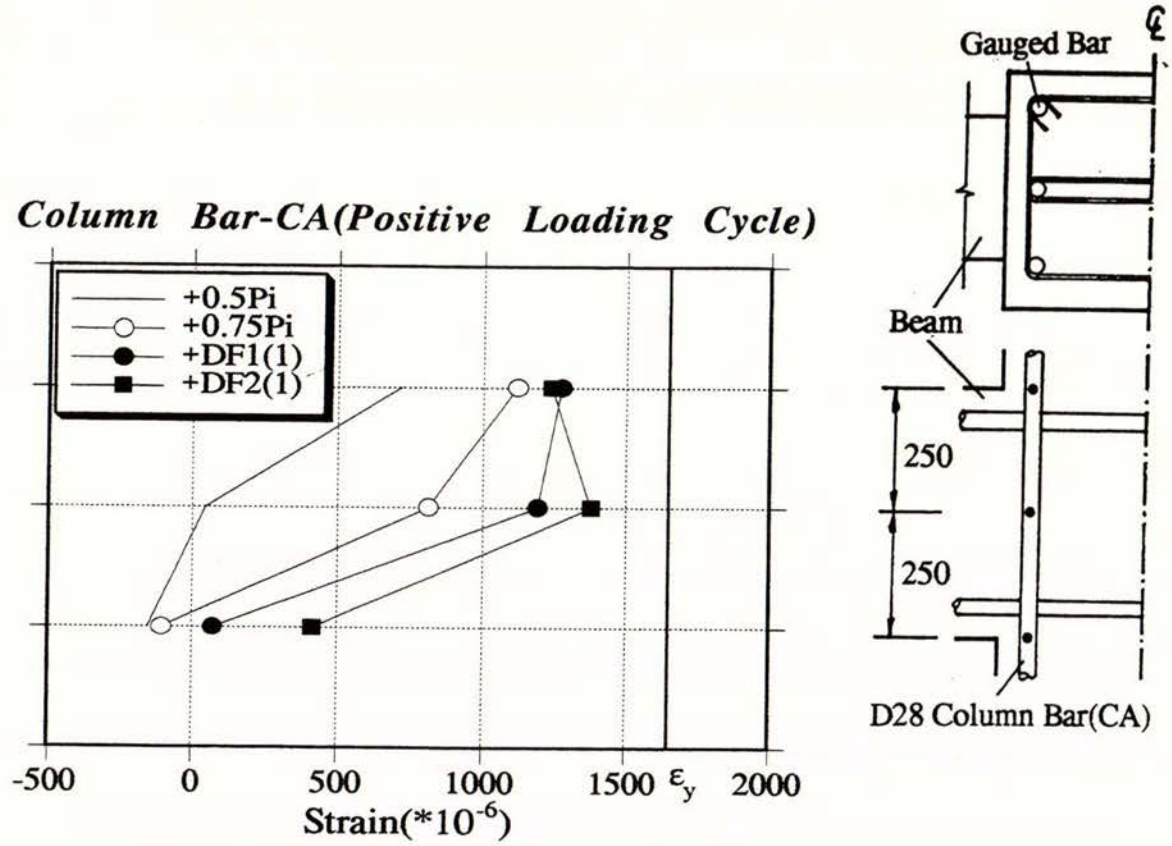

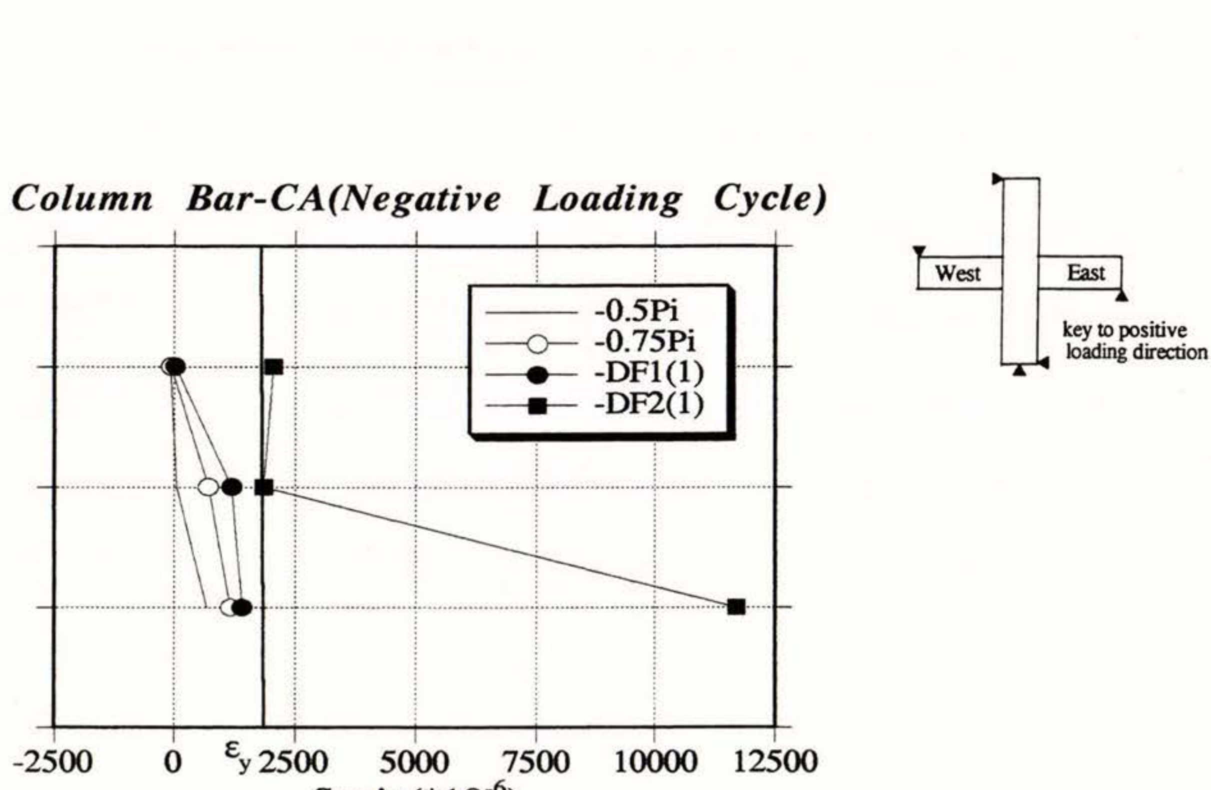

Fig.6.10(a) Strain Profiles of Column Bar of Specimen O4

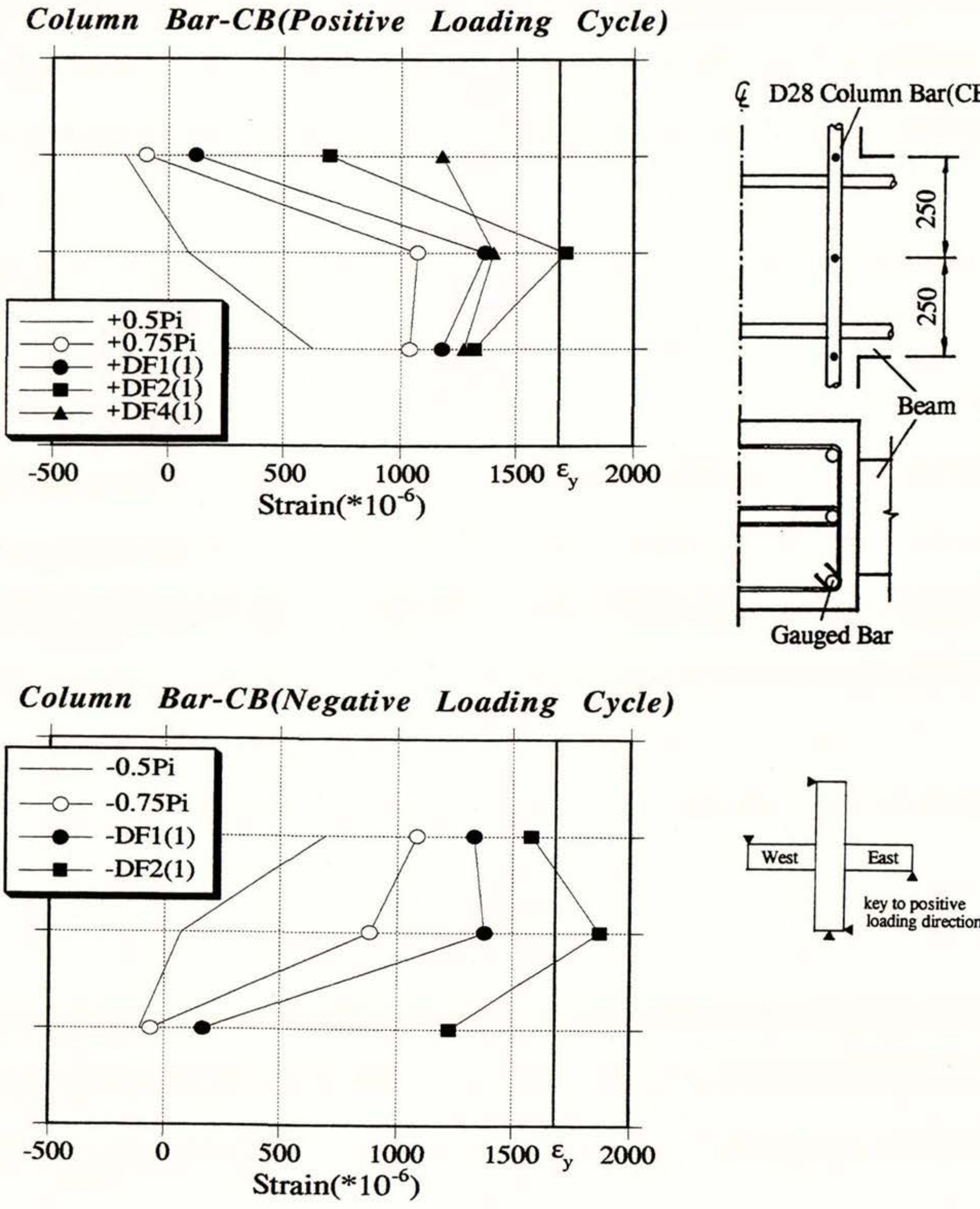

Fig.6.10(b) Strain Profiles of Column Bar of Specimen O4

6.2.7 Joint Behaviour

6.2.7.1 Introduction

Joint shear cracks initiated at the corners of the joint in the loading to $\pm 0.75P_i$. In the loading to DF of 1, bond splitting cracks were formed along the longitudinal column reinforcement in the joint(see Fig.6.5(b)). The maximum nominal horizontal joint shear stress was $0.47\sqrt{f'_c}$, where f'_c is the measured concrete compressive strength. Initial corner to corner diagonal tension crack was observed at storey drift angle of 0.53% in the loading to DF of 2(see Fig.6.2). The cracking shear stress was found to be $0.45\sqrt{f'_c}$. In the second cycle of loading to DF of 6, severe strength degradation was observed mainly due to the joint shear failure.

6.2.7.2 Bond Stresses of the Longitudinal Beam and Column Bars in the Joint

Average bond stresses along the longitudinal beam and column bars in the joint, assuming to be uniformly distributed over the gauge length of 150mm for the beam bars and 250mm for the column bars, were estimated using the wire strain gauge readings. Average bond stresses so obtained for the longitudinal beam and column bars in the joint are plotted in Figs.6.11 and 6.12, respectively. Only the bond stresses at the peak of the positive loading cycle are plotted until the loading to DF of 2 or 4.

In the loading to $\pm 0.5P_i$, the bond stresses in the beam bars estimated over the region located immediately inside the joint, where the column flexural tension force was imposed, began to decrease before the peak of the loading cycle was reached. Those bond stresses began to decrease at a bond stress of 1.5 to 2.7MPa. As shown in Fig.6.11, only small bond stresses were developed over that region. The maximum bond stress was generated mainly over the region located inside the joint from the beam flexural tension side in the loading to $\pm 0.5P_i$. After the loading to $\pm 0.75P_i$, in which joint shear cracks initiated at the corners of the joint, the bond stress profiles along the beam bars changed radically. The bond stresses estimated over the region, where the column flexural compression force was imposed, gradually increased as the test progressed. On the other hand, the bond stresses over the region subjected to the column flexural tension force diminished. As illustrated in Fig.6.11, the bond stresses distributed almost linearly in the inelastic loading cycle. The maximum bond stress over the region subjected to the column flexural compression force was 7.5MPa($=1.03\sqrt{f'_c}$) estimated in the first cycle of loading to DF of 2, where f'_c is the measured concrete compressive strength. At this stage, however, the bond stress began to decrease over the column depth.

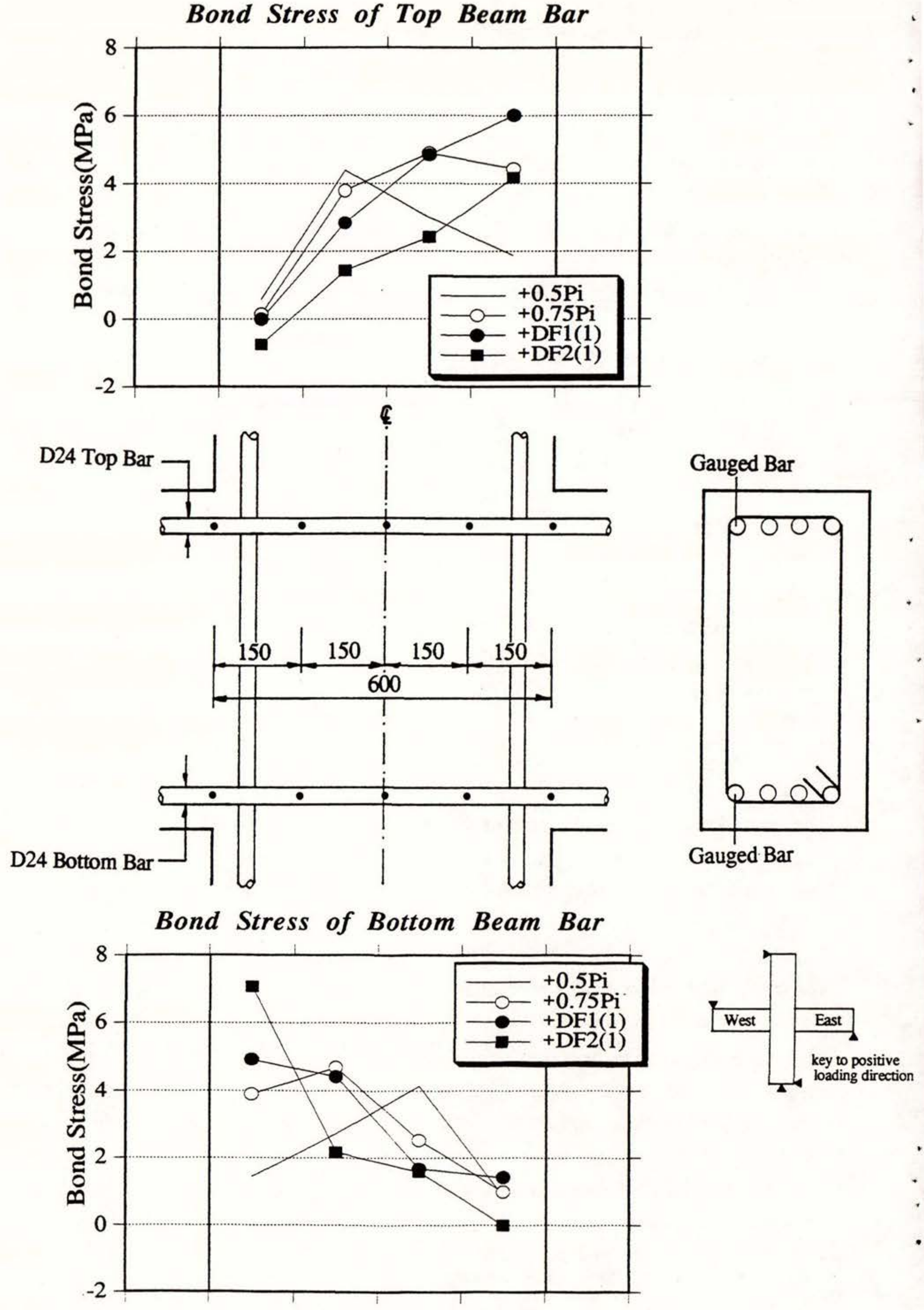

Fig.6.11 Measured Bond Stresses of Beam Bars of Specimen O4

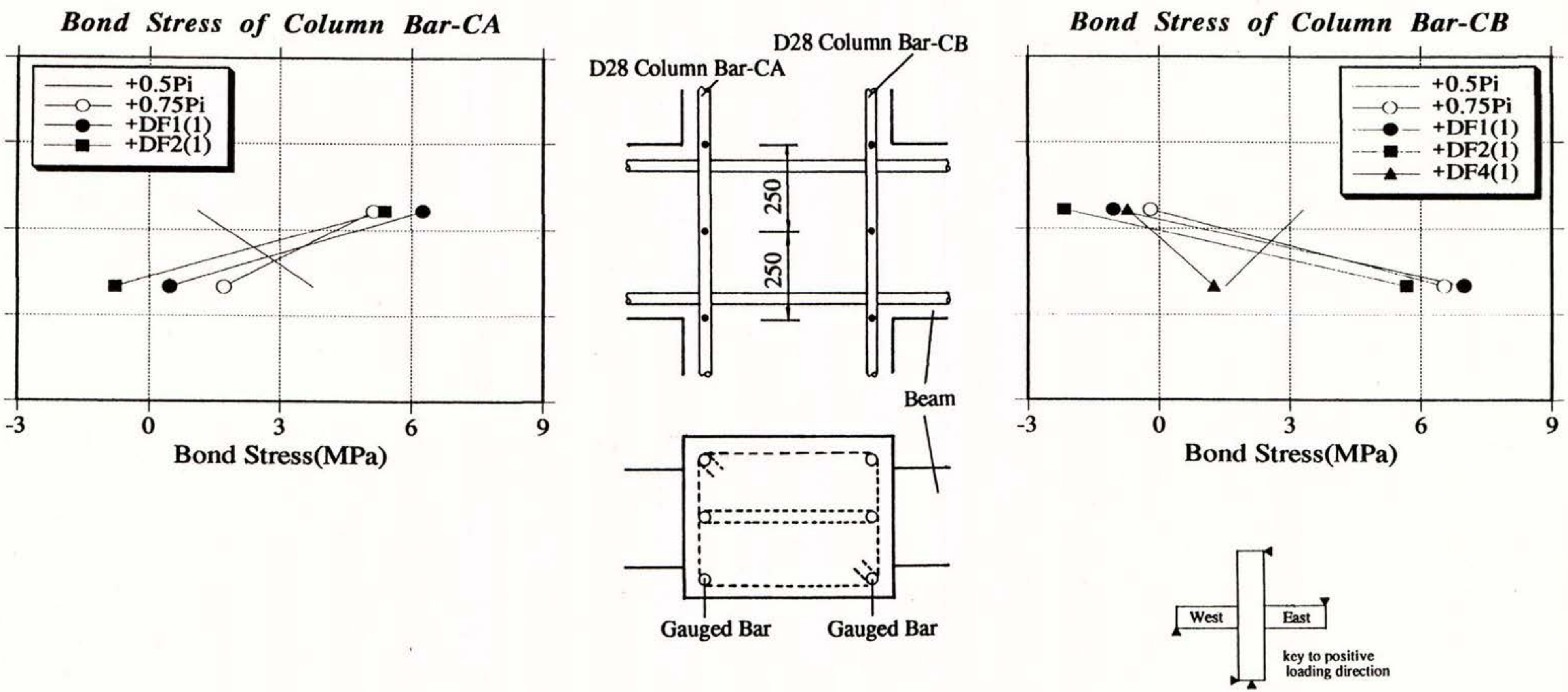

Fig.6.12 Measured Bond Stresses of Column Bars of Specimen O4

For the bond stress profiles along the longitudinal column bars, similar trends for the beam bars were observed as shown in Fig.6.12. In the loading to $\pm 0.5P_i$, the maximum average bond stress was developed over the region where the beam flexural tension force was imposed. After the loading to $\pm 0.75P_i$, however, the bond stresses estimated over the region subjected to the beam flexural tension force decreased while the bond stresses estimated over the region subjected to the beam flexural compression force increased rapidly. The maximum bond stress estimated for the column bars was 7.0MPa($=0.96\sqrt{f'_c}$) developed in the first cycle of loading to DF of 1 in which bond splitting cracks initiated(see Fig.6.1.5(b)). In the loading to DF of 2, the bond stresses began to decrease and significant bond deterioration could be found in the loading of DF of 4 as illustrated in Fig.6.12.

6.2.7.3 Joint Shear Distortion and Expansion

Fig.6.13 shows the joint shear distortion, together with the joint expansion The methods to obtain the joint shear distortion and joint expansion were defined in Section 3.7.6.

After the loading to $\pm 0.75P_i$, the joint shear distortion gradually increased. In the loading to DF of 2 in which a corner to corner diagonal tension crack initiated, the joint shear distortion increased rapidly. At this stage, the joint expansion also began to increase. In the second cycle of loading to DF of 4, the joint shear distortion was measured to be larger than 1%. Joint expansion became notable in this loading cycle as illustrated in Fig.6.13. This could be expected by the relatively large tensile strains along the beam and column bars measured overall depth of the column and beam in the joint. The maximum joint shear distortion of 1.5% was measured in the loading to DF of 6.

It is obvious that the joint shear distortion and expansion increased rapidly after the corner to corner diagonal tension cracks were developed in the joint. The absence of the joint shear reinforcement resulted in significant increase in joint shear distortion and expansion after the joint diagonal tension cracking.

6.2.8 Decomposition of Horizontal Displacement

The components of the horizontal displacement at the peak of the selected loading cycles are expressed as a percentages of the storey drift angle in Fig.6.14. The procedures for calculating those components were explained in Section 3.8.

Until the loading to DF of 1, the main contributions to the horizontal displacement were the beam flexural displacement and the fixed-end rotation of the columns. The beam flexural displacement contributed 32 to 48% of the imposed storey drift angle while the contribution of

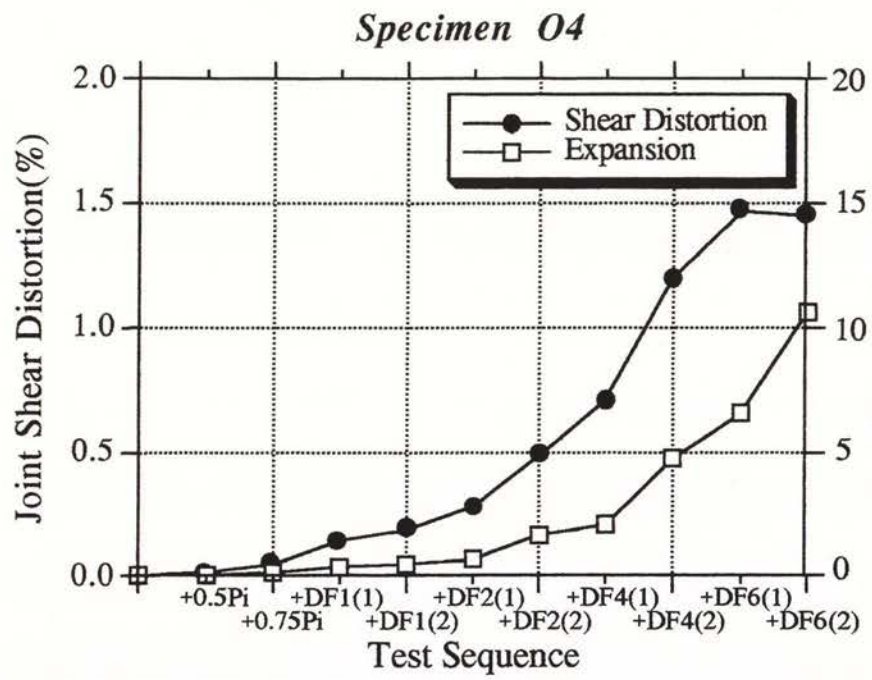

Fig.6.13 Joint Shear Distortion and Expansion of Specimen O4

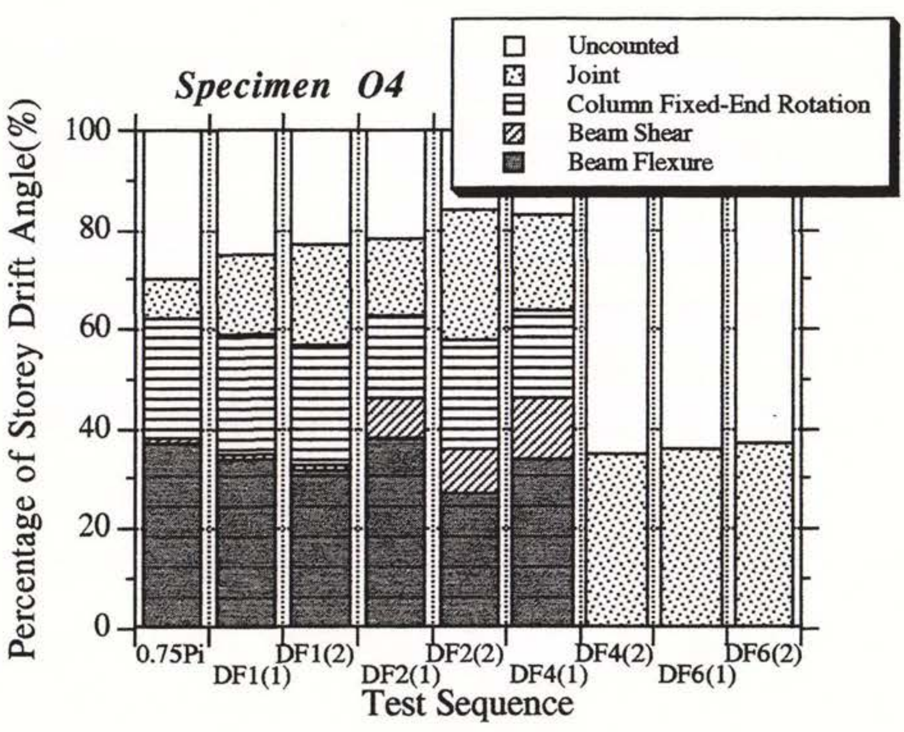

Fig.6.14 Components of Storey Drift Angle of Specimen O4

the fixed-end rotation of the columns was 24%. The contribution of the fixed-end rotation of the columns fairly constant until the loading to DF of 4.

In the loading to DF of 2, in which the west beam failed in shear, the contribution of the beam shear displacement increased gradually although its magnitude was less than 10%. In the first cycle of loading to DF of 4, the component by the beam shear displacement continued to increase up to 12% as could be expected by the shear failure observed in the east beam. On the contrary, the contribution of the beam flexural displacement became to decrease. No measurement for the beam flexure and shear, and column fixed-end rotation were made after the second cycle of loading to DF of 4.

The contribution of the joint shear distortion to the storey drift angle constantly increased as the imposed horizontal displacement increased as shown in Fig.6.14. Even in the elastic loading cycle, the joint shear accounted for 8% of the storey drift angle. Rapid increase of the joint shear contribution could be found in the second cycle of the loading to DF of 4. Maximum contribution of 37% was obtained in the loading to DF of 6, indicating severe joint deterioration.

6.3 SPECIMEN O5

6.3.1 Introduction

For Specimen O5, the ratio of the theoretical ideal flexural strength of the column to that of the beam was 1.52 based on the measured material strengths. When the theoretical flexural strength of the beam was reached at the column face, the ideal storey horizontal load strength P_i was 150kN. The ratio of longitudinal beam bar diameter d_b to column depth h_c was d_b/h_c=32/600=1/18.75, which did not satisfy the requirements by NZS3101 for ductile frames[SANZ 1982(a)]. The compressive strength of the concrete cylinder was 32.8MPa at the time of testing.

6.3.2 General Behaviour

After the first cycle of loading to DF of 4, the beams of the test specimen were retrofitted using the same method used for Specimen O4 since one dominant diagonal tension crack extended in the east beam.

The storey shear force versus horizontal displacement relationship is shown in Fig.6.16, in which the response of Specimen O5 before retrofit is expressed by dotted lines and that after retrofit is expressed by solid lines. Observed cracking after testing and those at the peak of the selected loading cycles are shown in Figs 6.15 and 6.17, respectively.

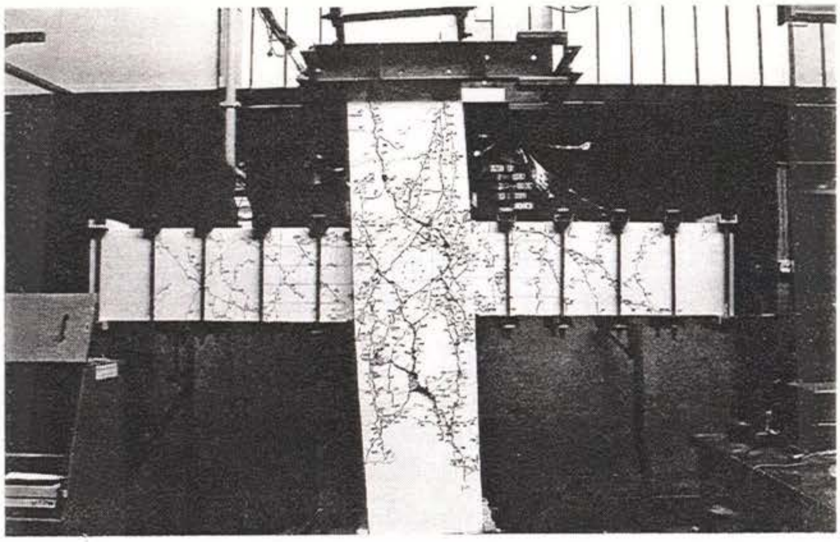

Fig.6.15 Observed Cracking of Specimen O5
at second cycle of DF=-8

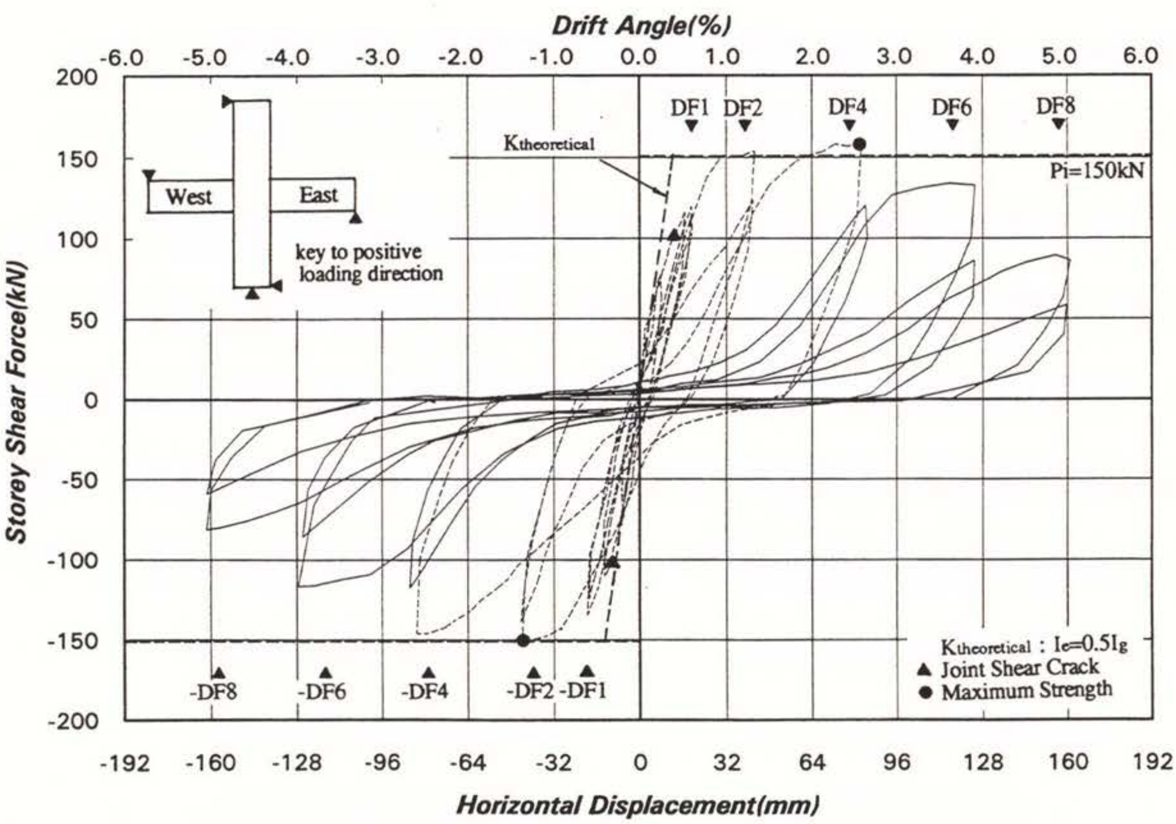

Fig.6.16 Storey Shear Force versus Horizontal Displacement Relationship
for Specimen O5

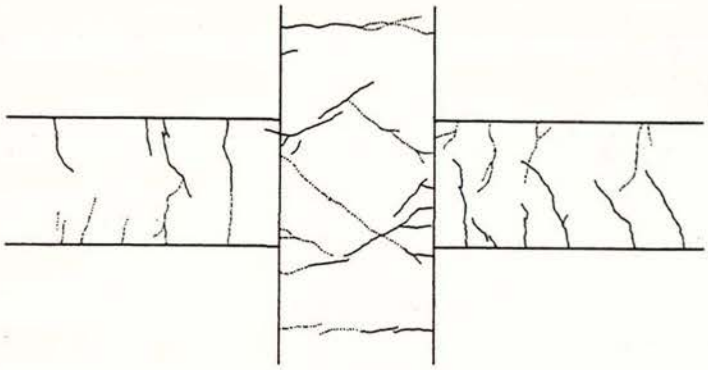

(a) at the peak of 0.75Pi
(R=0.41%)

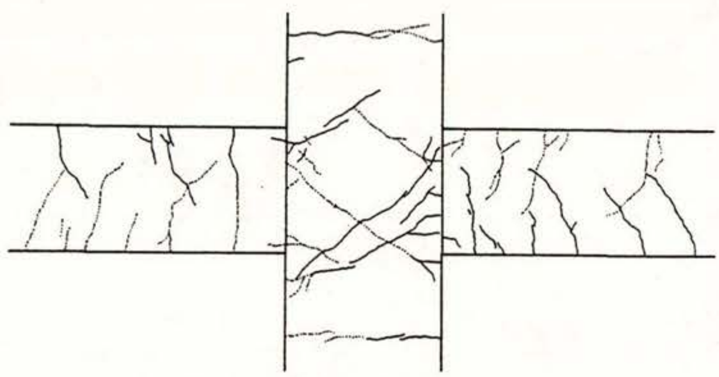

(b) at the peak of second cycle, DF=1
(R=0.62%)

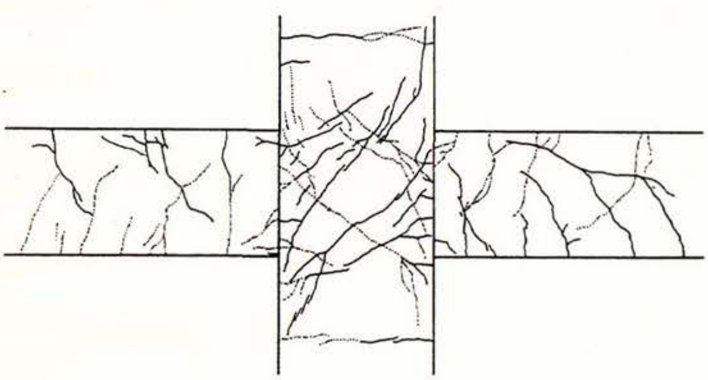

(c) at the peak of second cycle, DF=2
(R=1.23%)

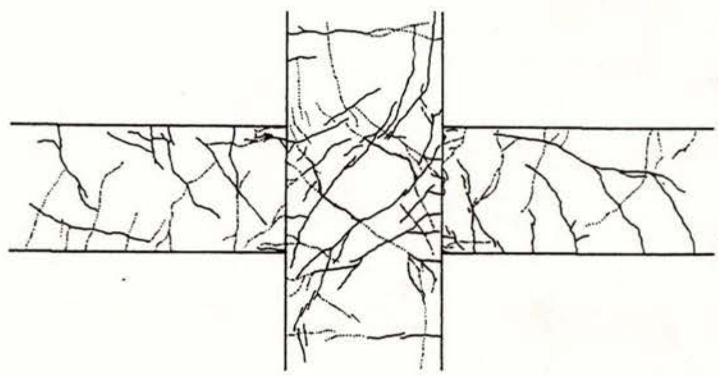

(d) at the peak of second cycle, DF=4
(R=2.46%)

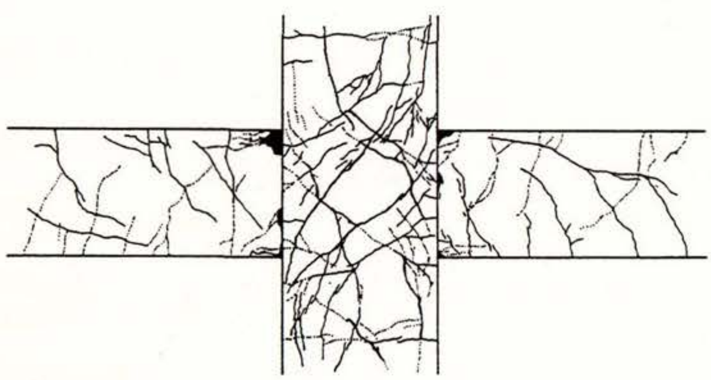

(e) at the peak of second cycle, DF=6
(R=3.69%)

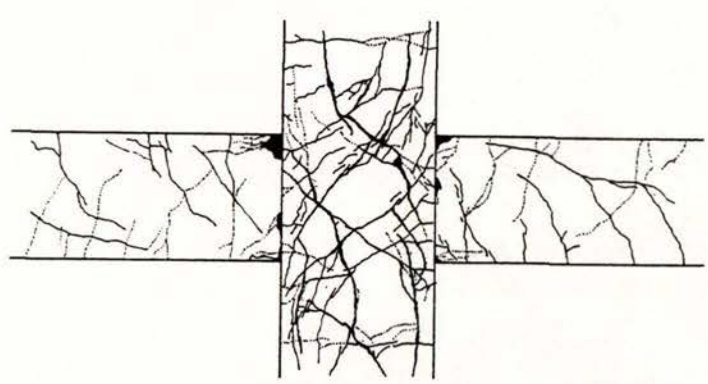

(f) at the peak of second cycle, DF=8
(R=4.92%)

Fig.6.17 Observed Cracking of the Joint(Specimen O5)

In the loading to $\pm 0.5P_i$, flexural and flexural-shear cracks initiated in the beams. Column flexural cracks were also observed at the beam face. In the subsequent loading cycle to $-0.75P_i$, a corner to corner diagonal tension crack was formed in the joint(see Fig.6.17(a)). Beam flexural and flexural-shear cracks, and column flexural cracks extended. The number of those cracks also increased.

In the loading to displacement ductility factor DF of 1, bond splitting cracks initiated along the column bars in the joint(see Fig.6.17(b)). In the first positive loading cycle, a joint diagonal tension crack was also observed. At this stage, the longitudinal beam bars started to yield in tension at the column face.

In the loading to DF of 2, a diagonal tension crack with an acute angle to the beam axis initiated in the east beam. Bond splitting cracks along the column bars in the joint became more apparent(see Fig.6.17(c)). Joint diagonal tension cracks opened wide and extended into the columns in the flexural compression zone near the beam face. The maximum width of the joint diagonal tension crack was measured to 1.6mm, which was somewhat smaller than that measured for Specimen O4. Beam flexural cracks at the column face opened wide to the crack width of approximately 4mm and crushing of cover concrete of the beams in the flexural compression region was observed near the column face. In the first cycle of loading to DF of 2, the ideal storey horizontal load strength was reached for both positive and negative cycle(see Fig.6.16). At the peak of this negative loading cycle, the maximum horizontal load strength of 150kN was developed. In the second cycle of loading to DF of 2, the reduction of the horizontal load strength was observed(see Fig.6.16).

In the first positive cycle of loading to DF of 4, the maximum horizontal load strength of 159kN was measured which was 106% of the ideal storey horizontal load strength(see Fig.6.16). In the first cycle of loading to DF of 4, the beam diagonal tension cracks extended in both beams. At this stage, the test was terminated to retrofit the beams and retested In the subsequent loading cycles, joint diagonal tension cracks extended and opened wide. The maximum width of the joint diagonal tension crack was approximately 4mm which was comparable to the crack width observed for Specimen O4. The bond splitting cracks along the column bars also extended and opened wide. Crushing of cover concrete in the beams at column face became more obvious and flexural cracks at the column face opened wide to the width of approximately 10mm. As shown in Fig.6.16, in the second cycle of loading to DF of 4, severe strength degradation was observed mainly due to the joint distress and the hysteresis curves were significantly pinched.

In the loading to DF of 6, joint diagonal tension cracks opened wide significantly. The maximum width of joint diagonal tension crack was measured to about 8mm for positive loading cycle and 6mm for negative loading cycle, respectively. Bond splitting cracks along the column bars extended and opened wide significantly both in the joint and in the columns near the beam face. Column shear cracks became more apparent in the second cycle of this loading stage. For the beams, concrete crushing in the flexural compression zone was more significant when compared with that of Specimen O4 and cover concrete started to spall off(see Fig.6.17(e)). As illustrated in Fig.6.16, strength degradation and pinching became more apparent in the hysteresis loops.

In the loading to DF of 8, joint diagonal tension cracks opened wide to approximately 10mm. Bond splitting cracks along the column bars also extended and opened significantly. The columns as well as the joint suffered severe shear cracks(see Fig.6.17(f)). In the second cycle of loading to DF of 8, cover concrete in the joint and the columns started to spall off. The joint and columns were severely deteriorated. Severe strength degradation and pinching were obvious in the hysteresis loops as shown in Fig.6.16.

6.3.3 Initial Stiffness

The theoretical initial stiffness was calculated for Specimen O5 as follows:

$$K_{theoretical}=12.0\text{kN/mm}$$

The calculated theoretical stiffness $K_{theoretical}$ is shown in Fig.6.16. The stiffness estimated at 75% of the theoretical ideal storey horizontal load strength of the test specimen was 6.9kN/mm for positive loading cycle and 8.3kN/mm for negative loading cycle, respectively. The average value of the stiffnesses obtained from the positive and negative loading cycle was 64% of the theoretical stiffness. As observed for Specimen O4, the initial stiffness estimated for the test specimen was considerably smaller than the theoretical value.

The yield displacement measured for the test specimen was 19.7mm which could be converted to 0.62% in terms of a storey drift angle. Specimen O5 which has no shear reinforcement in the joint core and bad bond condition along the beam bars through the joint was significantly flexible like Specimen O4 according to the current code requirements[SANZ 1992].

6.3.4 Available Displacement Ductility Factor

The available displacement ductility factor μ_a of 2.5 was obtained from the measured storey shear force and horizontal displacement relationship of Specimen O5, indicating a limited ductility response. When compared with the value of 4.5 obtained from Specimen O4, much less displacement ductility factor was observed for Specimen O5.

6.3.5 Beam Behaviour

6.3.5.1 Longitudinal Beam Bar Strains

Longitudinal beam bar strains are illustrated in Figs.6.18 and 6.19. Strain profiles obtained from the wire strain gauge readings are shown in Fig.6.18 while those measured from the linear potentiometers are shown in Fig.6.19. Up to the loading to DF of 1, tensile strains along the beam bars increased gradually and the yield strain was reached at the column face as shown in Fig.6.18. In the loading to DF of 2, the tensile strains measured in the beam plastic hinge regions increased rapidly. As illustrated in Fig.6.19, yield penetration along the beam bars was observed into the joint core in the loading to DF of 4. In the loading to DF of 6, significantly large tensile strains were measured over the column depth.

After the loading to DF of 1, the "compression" reinforcement in the beams at the column face were in tension as shown in Fig.6.18 and the tension steel entering the joint found anchorage in the opposite beam at this stage. This trend was also observed in the measured strain profiles of the longitudinal beam bars of Specimen O4 in which the column depth to beam bar diameter ratio meet the current code requirements[SANZ 1982(a)](see Fig.6.6).

The effect of the column depth to beam bar diameter ratio on the strain profiles of the longitudinal beam bars in the joint could not be found until the loading to DF of 2 in this study.

6.3.5.2 Slip of Beam Bars

The ratio of beam bar diameter to column depth for Specimen O5 was $d_b/h_c=32/600=1/18.75$, where d_b is beam bar diameter and h_c is column overall depth. Therefore poor anchorage condition for the beam bars in the joint could be expected.

The bar slip of the top and bottom beam bars in the joint of Specimen O5 are shown in Fig.6.20. The clear distance between two adjacent ribs of the beam bar was 18mm.

The bar slip measured at each location increased with the test progressed. In the loading to DF of 4 in which large tensile strains were measured along the beam bars in the joint, the beam bar slip increased rapidly. The measured maximum bar slip until the loading to DF of 6 was 11.7mm for top beam bar and 5.8mm for bottom beam bar, respectively. When compared with the beam bar slip measured for Specimen O4 shown in Fig.6.8, much larger bar slip was observed for Specimen O5 after the loading to DF of 2. The large slip of the beam bars through the joint resulted in severe crushing of concrete in the flexural

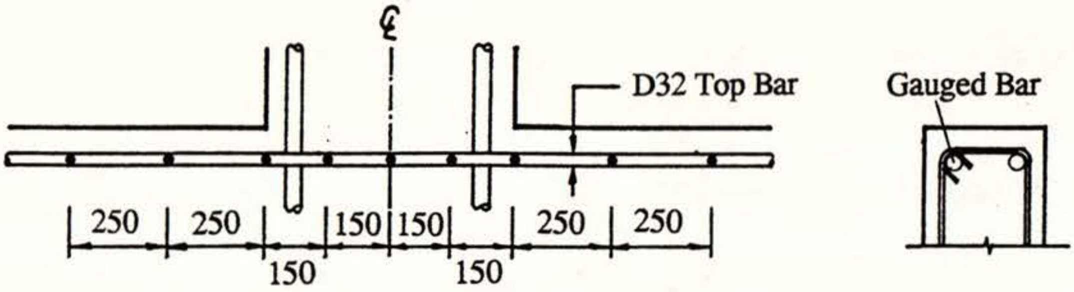

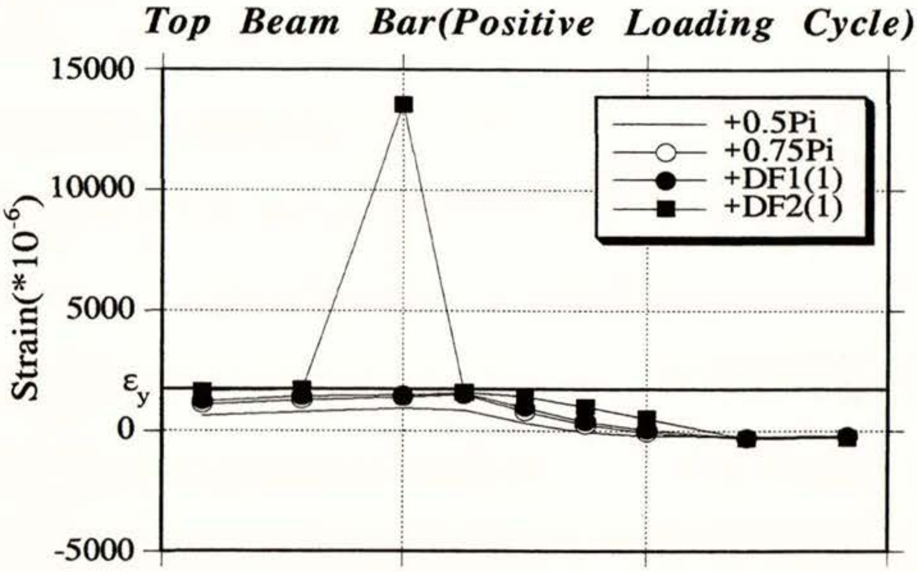

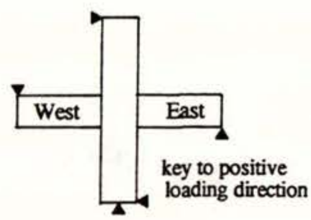

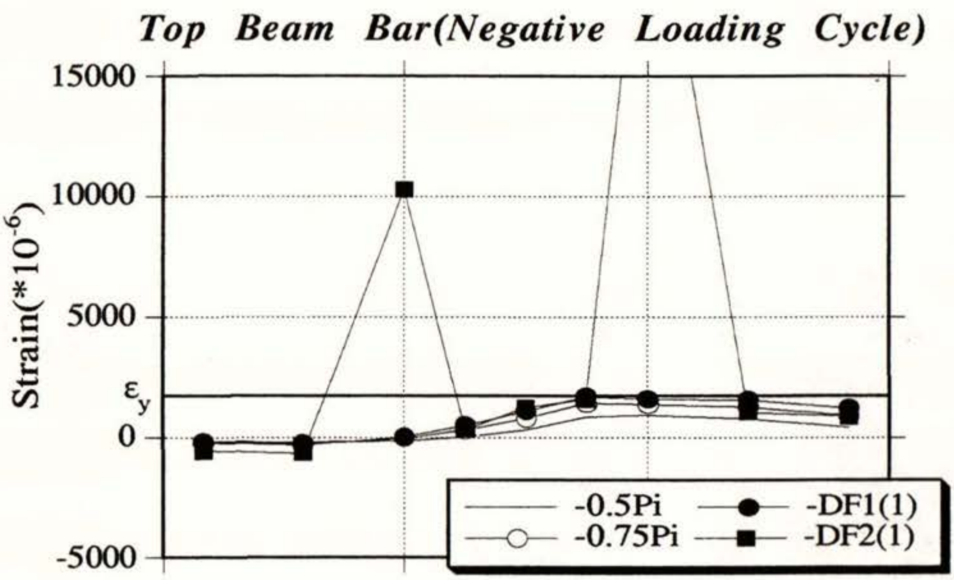

Fig.6.18(a) Strain Profiles of Top Beam Bar Measured by Wire Strain Gauges of Specimen O5

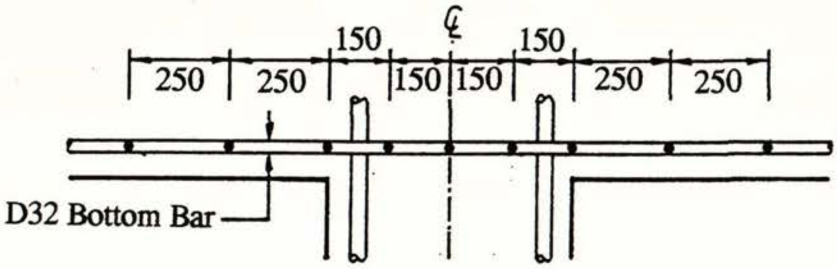

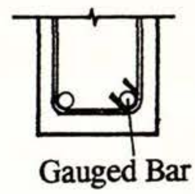

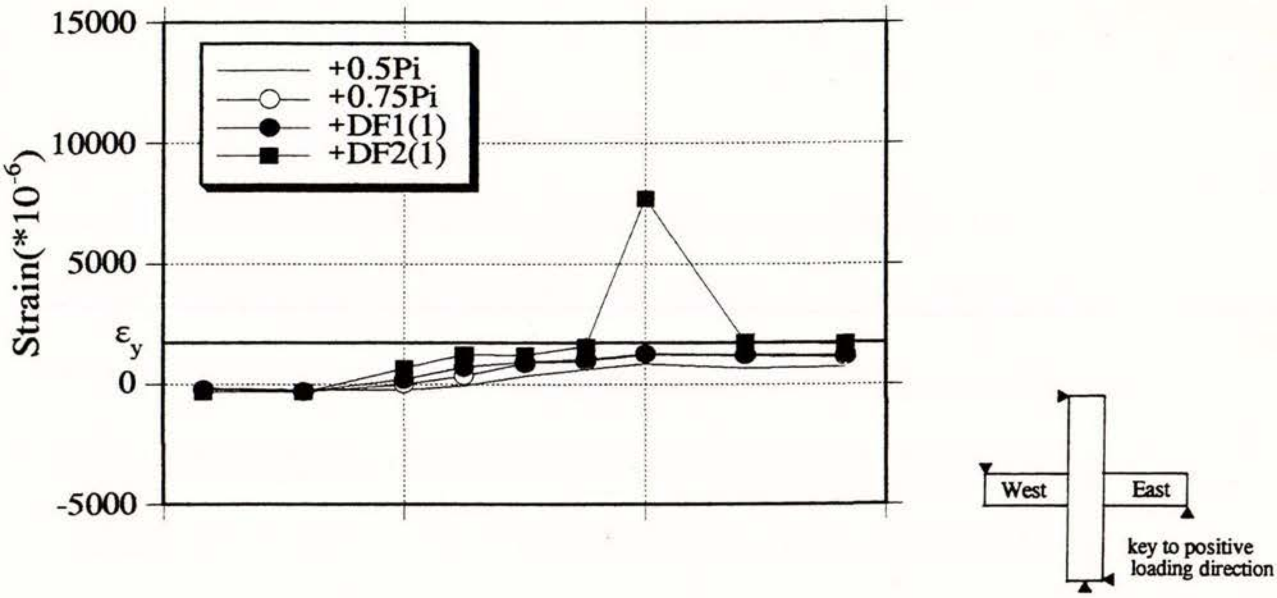

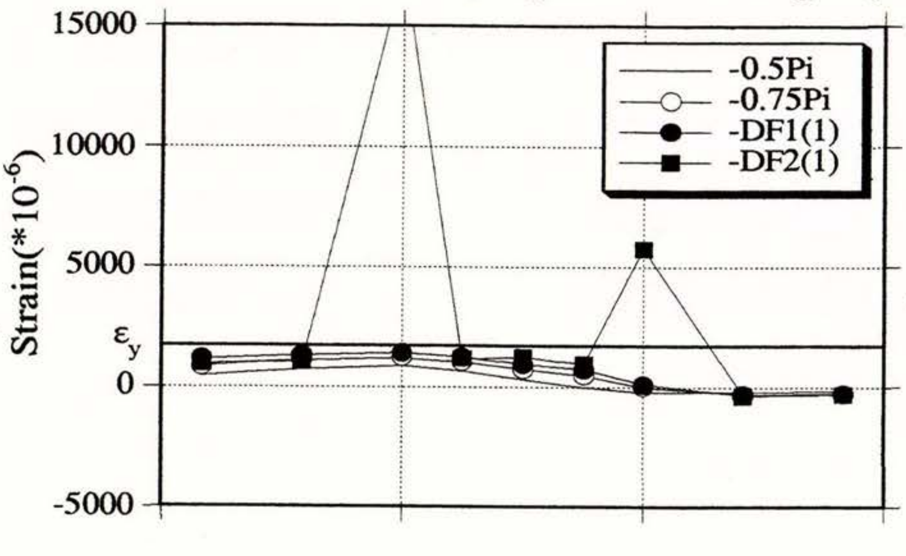

Fig.6.18(b) Strain Profiles of Bottom Beam Bar by Wire Strain Gauges of Specimen O5

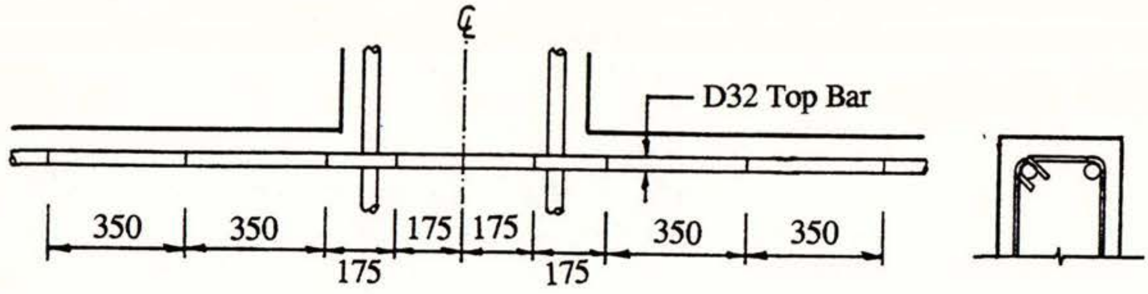

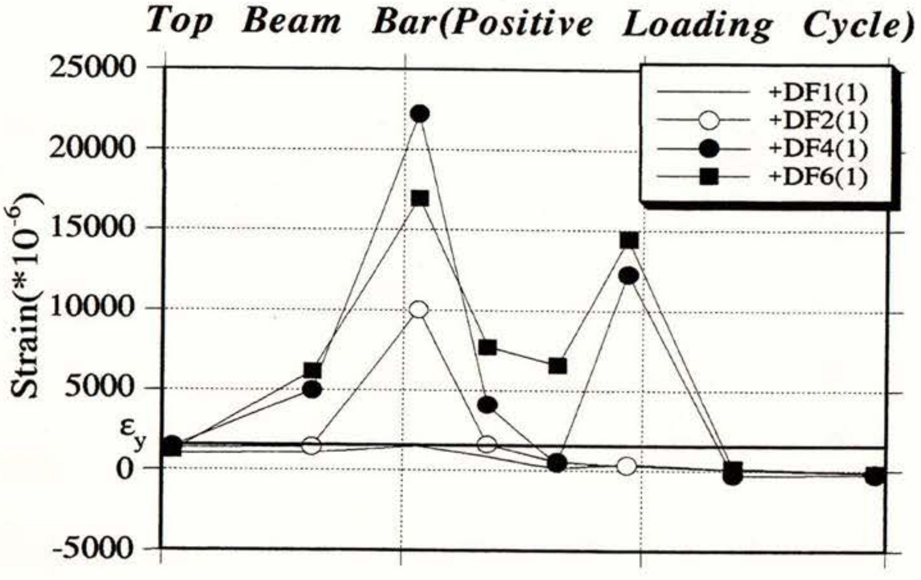

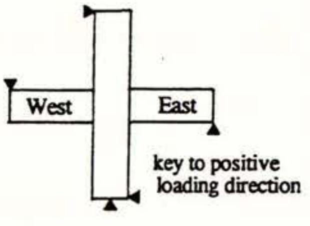

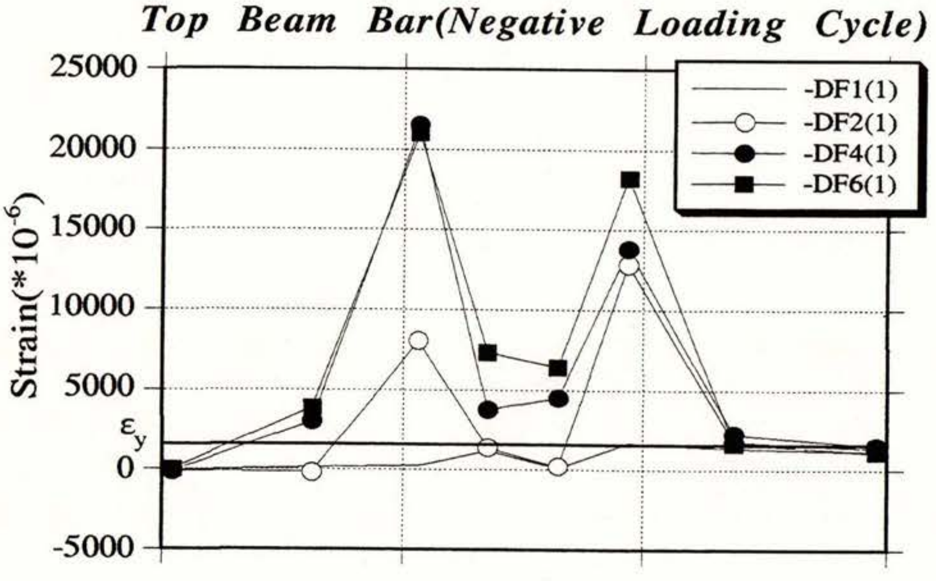

Fig.6.19(a) Strain Profiles of Top Beam Bar Measured by Linear Potensiometers of Specimen O5

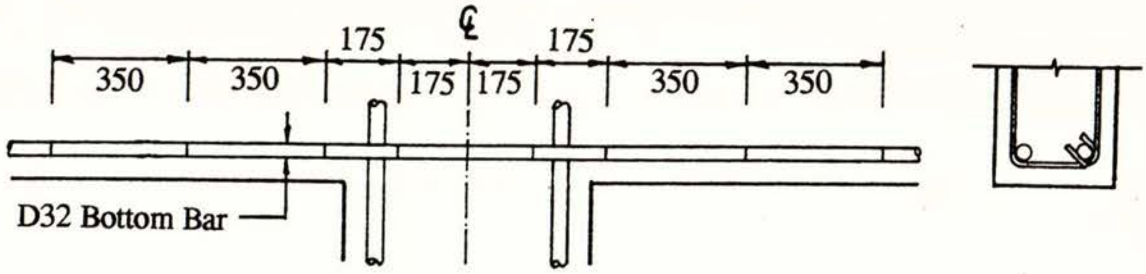

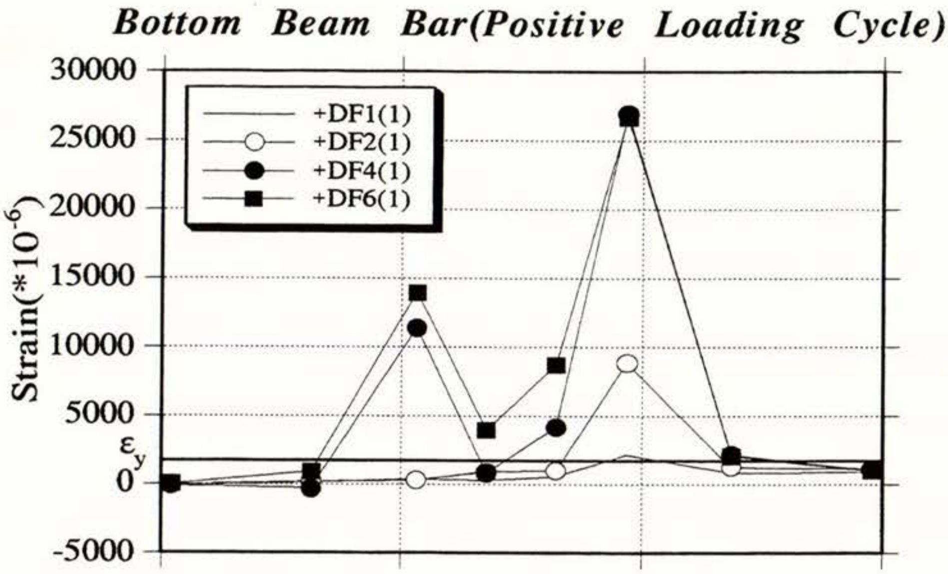

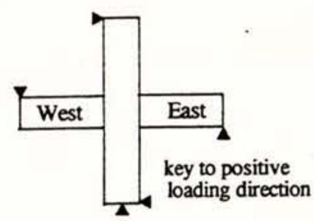

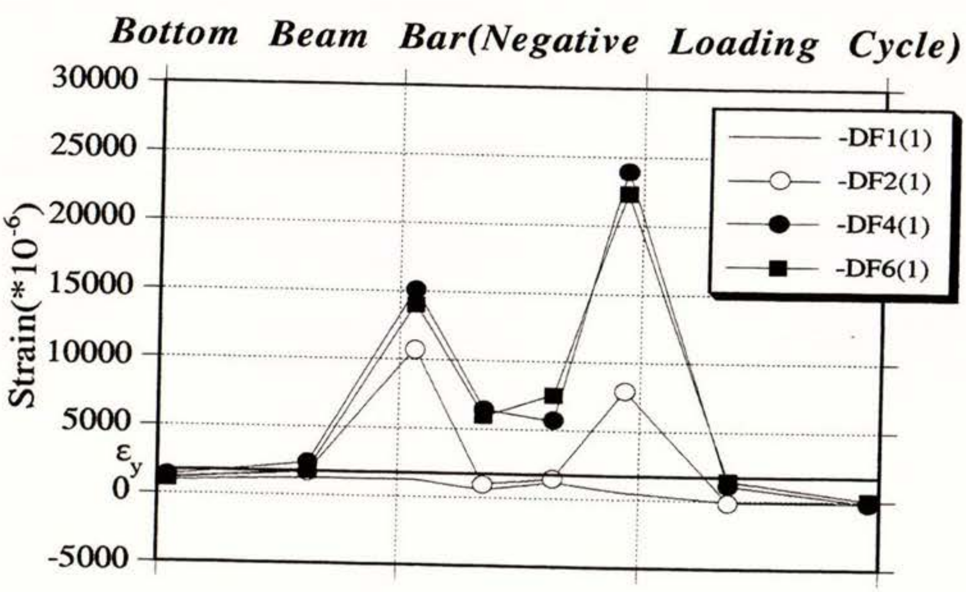

Fig.6.19(b) Strain Profiles of Bottom Beam Bar Measured by Linear Potensiometers of Specimen O5

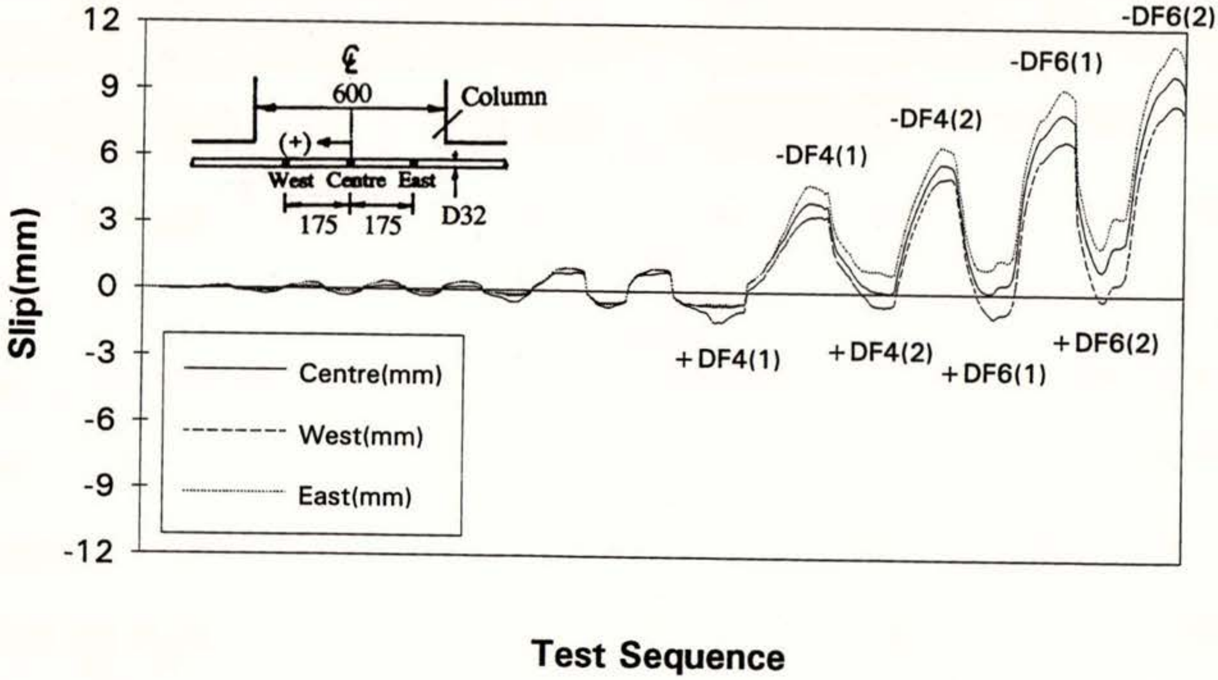

(a) Slip of Top Beam Bar

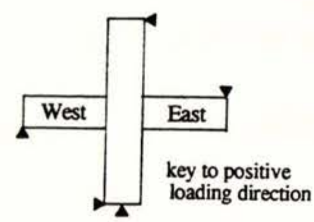

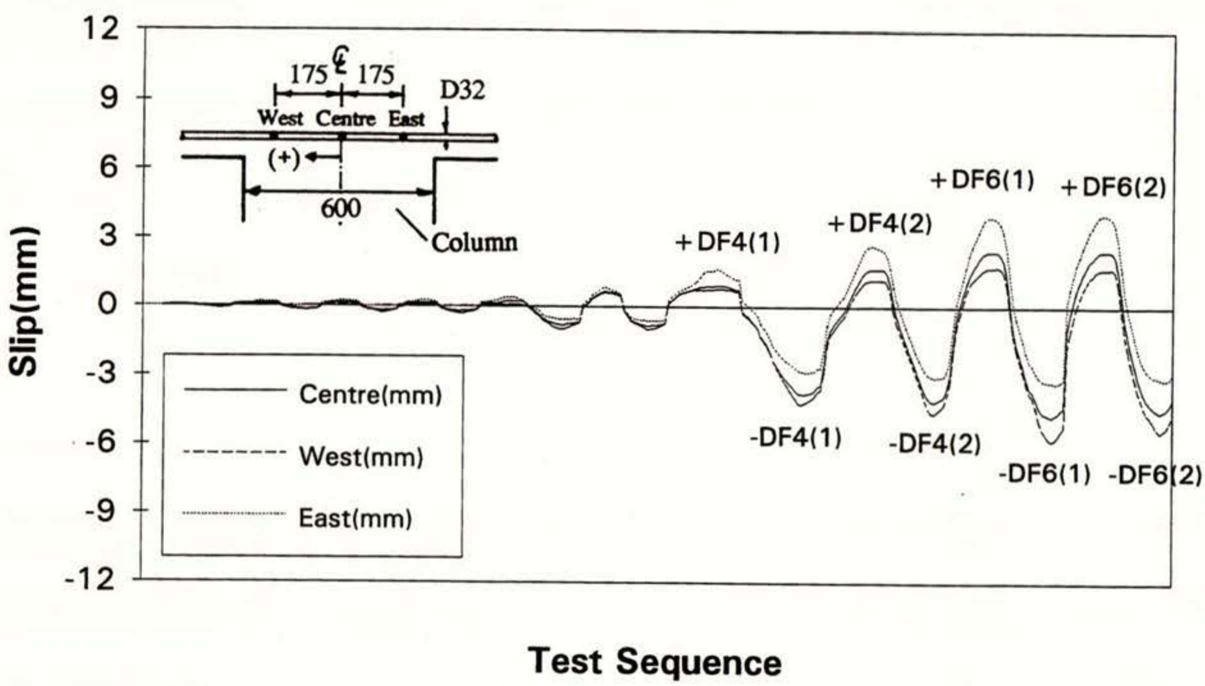

(b) Slip of Bottom Beam Bar

Fig.6.20 Measured Slip of Beam Bars of Specimen O5

compression zone of the adjacent beams. However, the effect on the overall response of Specimen O5 was not so significant.

6.3.6 Column Behaviour

6.3.6.1 Introduction

In the loading to DF of 1, bond splitting cracks along the column bars initiated in the joint. Those cracks extended and opened wide as the test progressed. Column shear cracks were developed in the column in the loading to DF of 6 and opened wide in the loading to DF of 8. Column shear cracks were more apparent for Specimen O5 when compared with those observed for Specimen O4.

6.3.6.2 Longitudinal Column Bar Strains

Fig.6.21 shows the strains along the longitudinal column bars in the joint. Those strains were obtained from the wire strain gauges. As the displacement ductility factor imposed on the test specimen increased, the measured strains of the column bars increased gradually. In the loading to $\pm 0.5P_i$, the strain distributions of the column bars in the joint were almost linear and the strains measured at the beam face showed small compressive strains when subjected to flexural compression force of the column. In the loading to $\pm 0.75P_i$ in which diagonal tension cracks were developed in the joint, tensile strains increased rapidly especially at the centre of the joint. In the loading to DF of 1, this trend became more apparent and the tensile strains measured at the centre of the joint were almost equal to that measured at beam face when subjected to flexural tension force of the column, indicating the reduction of bond stress along the column bar in the flexural tension zones. In the loading to DF of 2, the column bars at the centre of the joint reached the yield strain.

The strain profiles of the column bars in the joint measured for Specimen O5 were very similar to those obtained from Specimen O4(see Fig.6.10). It is likely that after joint diagonal tension cracking the strains of the column bars in the joint core with no shear reinforcement would be larger than expected by the column flexural resistance alone under severe earthquake loading.

6.3.7 Joint Behaviour

6.3.7.1 Introduction

An initial corner to corner diagonal tension crack was observed in the loading to $-0.75P_i$ for Specimen O5(see Fig.6.17(a)). The cracking shear stress was $0.42\sqrt{f'_c}$, where f'_c is the

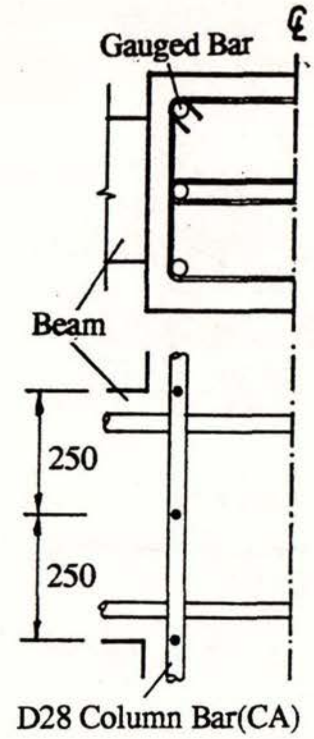

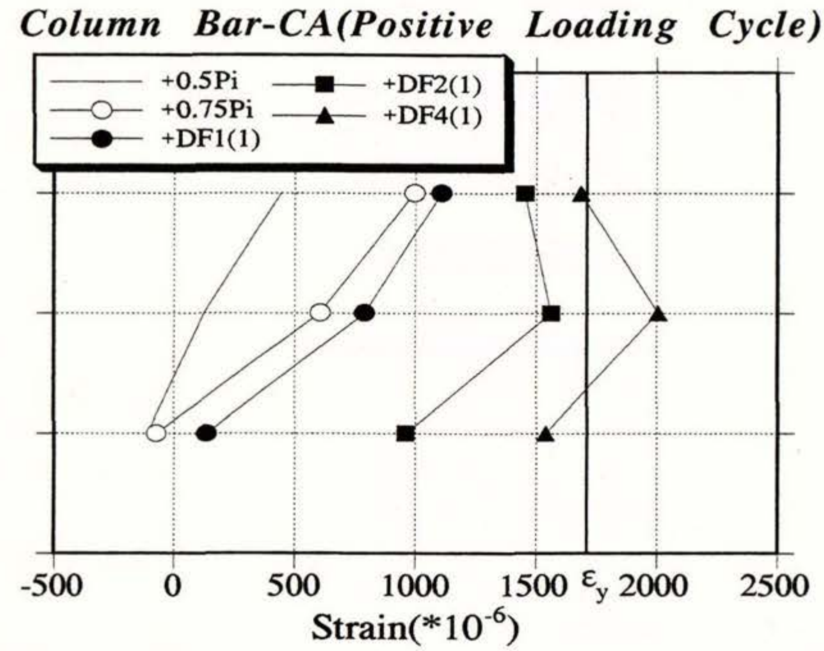

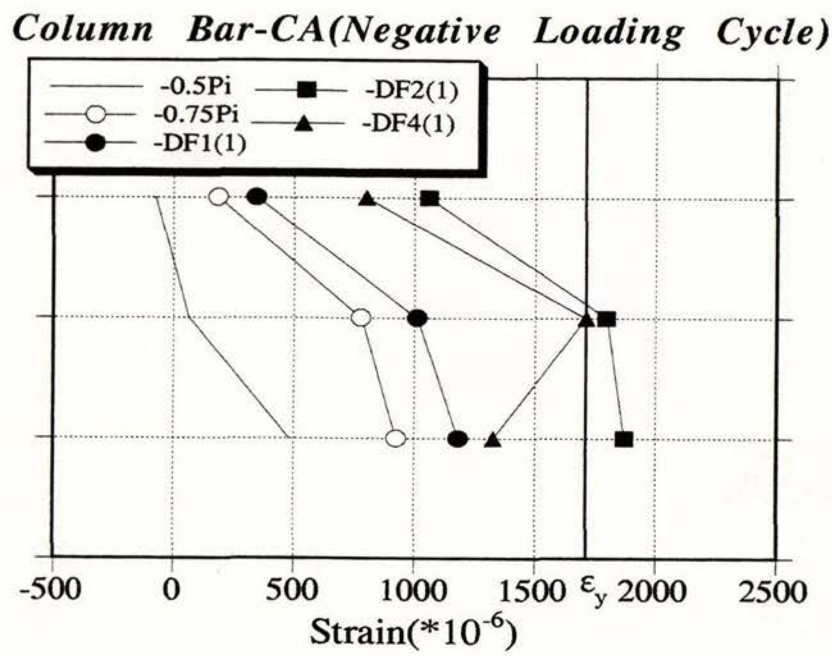

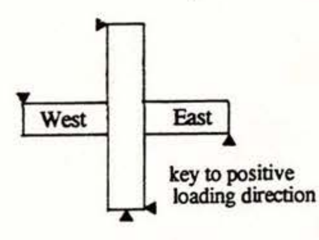

Fig.6.21(a) Strain Profiles of Column Bar of Specimen O5

Column Bar-CB(Positive Loading Cycle)

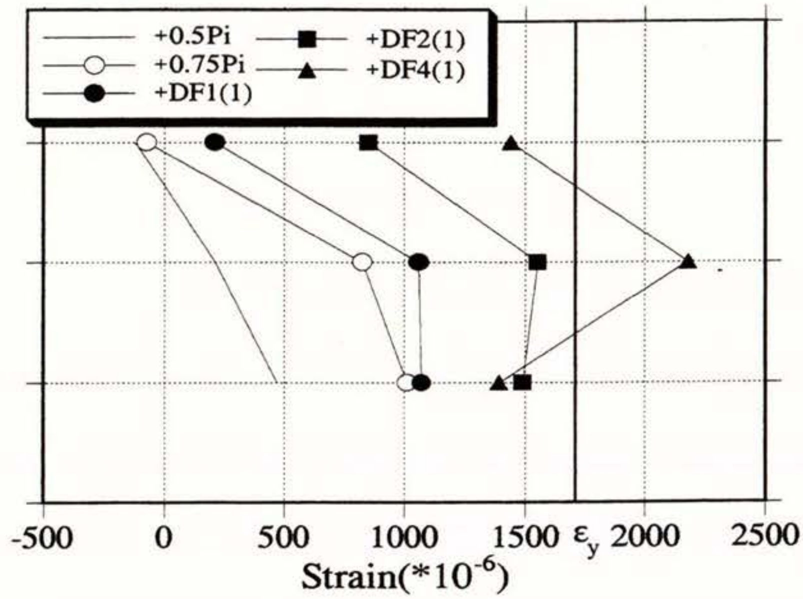

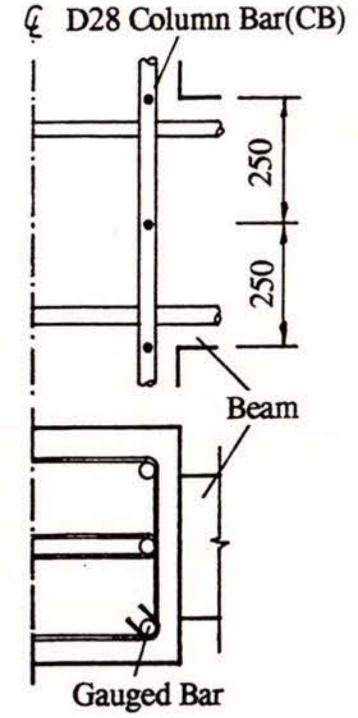

Column Bar-CB(Negative Loading Cycle)

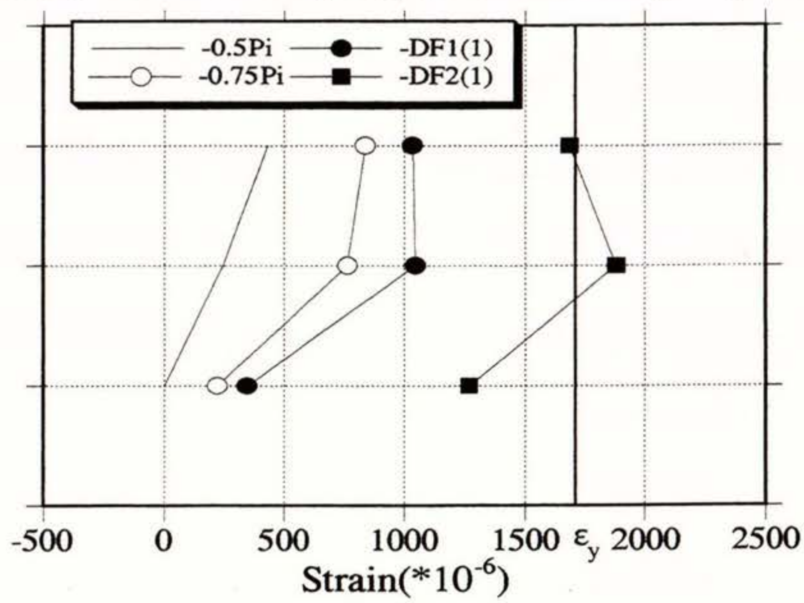

Fig.6.21(b) Strain Profiles of Column Bar of Specimen O5

measured concrete compressive strength. In the loading to DF of 1, bond splitting cracks initiated along the longitudinal column reinforcement in the joint(see Fig.6.17(b)). The maximum nominal horizontal joint shear stress was calculated to $0.61\sqrt{f'_c}$. The maximum joint shear stress was obtained in the loading to DF of 2 after the ideal storey horizontal load strength was reached. As the test progressed, joint diagonal tension cracks extended and opened wide, resulting in the strength reduction of the test specimen.

6.3.7.2 Bond Stresses of the Longitudinal Beam and Column Bars in the Joint

Average bond stresses along the longitudinal beam and column bars in the joint, assuming to be uniformly distributed over the gauge length of 150mm for the beam bars and 250mm for the column bars, were estimated using the wire strain gauge readings. Average bond stresses so obtained for the main beam and column bars in the joint are plotted in Figs.6.22 and 6.23, respectively. Only the bond stresses at the peak of the positive loading cycle are plotted.

In the elastic loading cycle, the maximum bond stresses along the beam bars were generated over the region located secondly or thirdly inside the joint from the beam flexural tension side. Subsequent loading cycles resulted in the decrease in the bond stresses over those regions. As shown in Fig.6.22, until the loading to DF of 2 only small bond stresses were developed over the region located immediately inside the joint, where the column flexural tension force was imposed. On the other hand, the bond stresses estimated over the region, where the column flexural compression force was imposed, gradually increased as the test progressed. As illustrated in Fig.6.22, the bond stresses distributed almost linearly at the peak of the loading of DF of 2 although some irregularities were observed for the bottom beam bar. The maximum bond stress over the region subjected to the column flexural compression force was 6.0MPa($=1.05\sqrt{f'_c}$) estimated in the first cycle of loading to DF of 2, where f'_c is the measured concrete compressive strength.

For the bond stress profiles along the longitudinal column bars in the joint, similar trends for the beam bars were observed as shown in Fig.6.23. In the loading to $\pm 0.5P_i$, the maximum average bond stress was developed over the region located immediately inside the joint, where the beam flexural tension force was imposed. After the loading to $\pm 0.75P_i$, however, the bond stresses estimated over the region subjected to the beam flexural tension force decreased while the bond stresses estimated over the region subjected to the beam flexural compression force increased rapidly. The maximum bond stress estimated for the column corner bars was 5.0MPa($=0.87\sqrt{f'_c}$) developed in the loading to $\pm 0.75P_i$. In the loading to DF of 1, the bond stresses began to decrease and significant bond deterioration could be found in the loading to DF of 4 as illustrated in Fig.6.23.

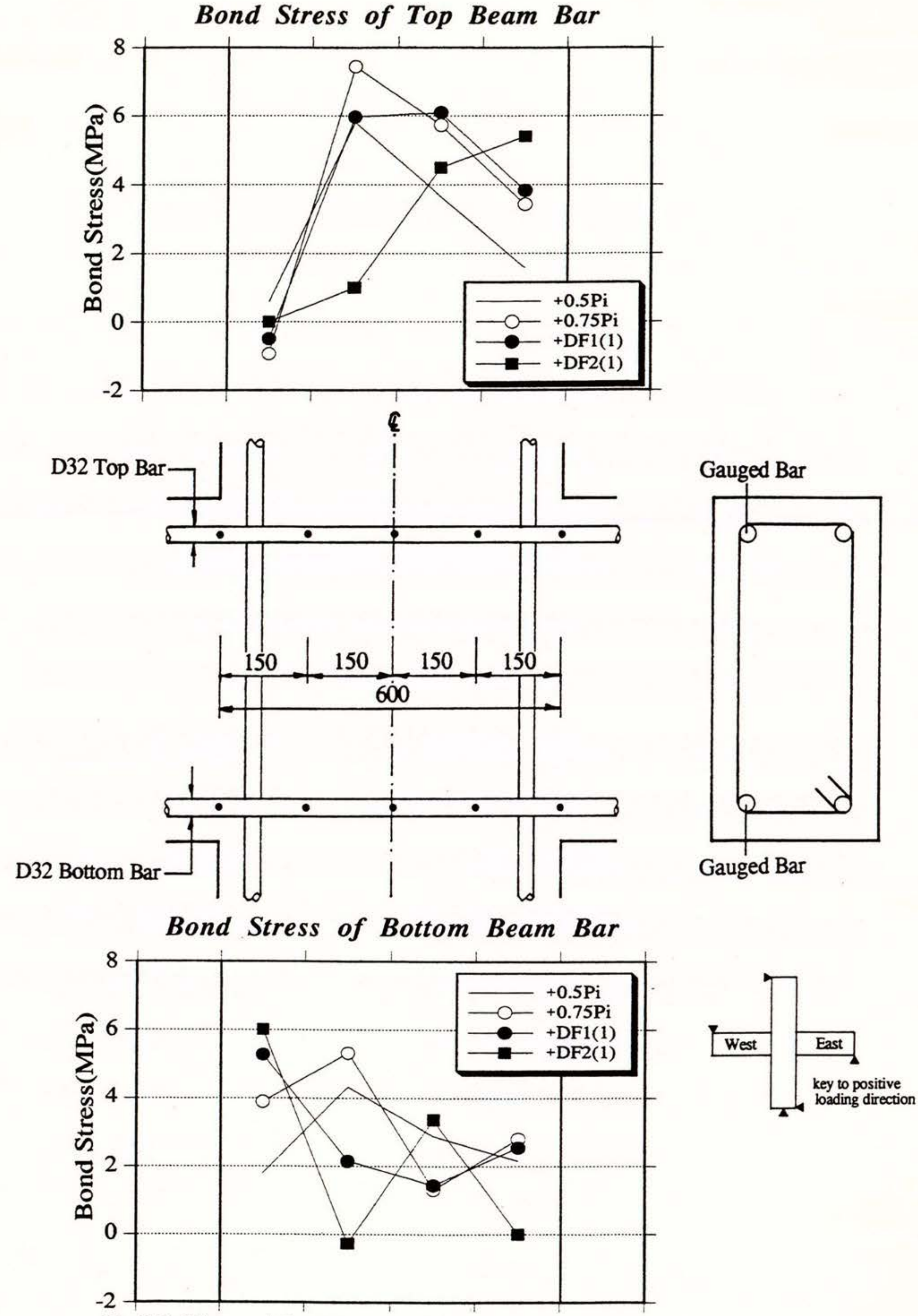

Fig.6.22 Measured Bond Stresses of Beam Bars of Specimen O5

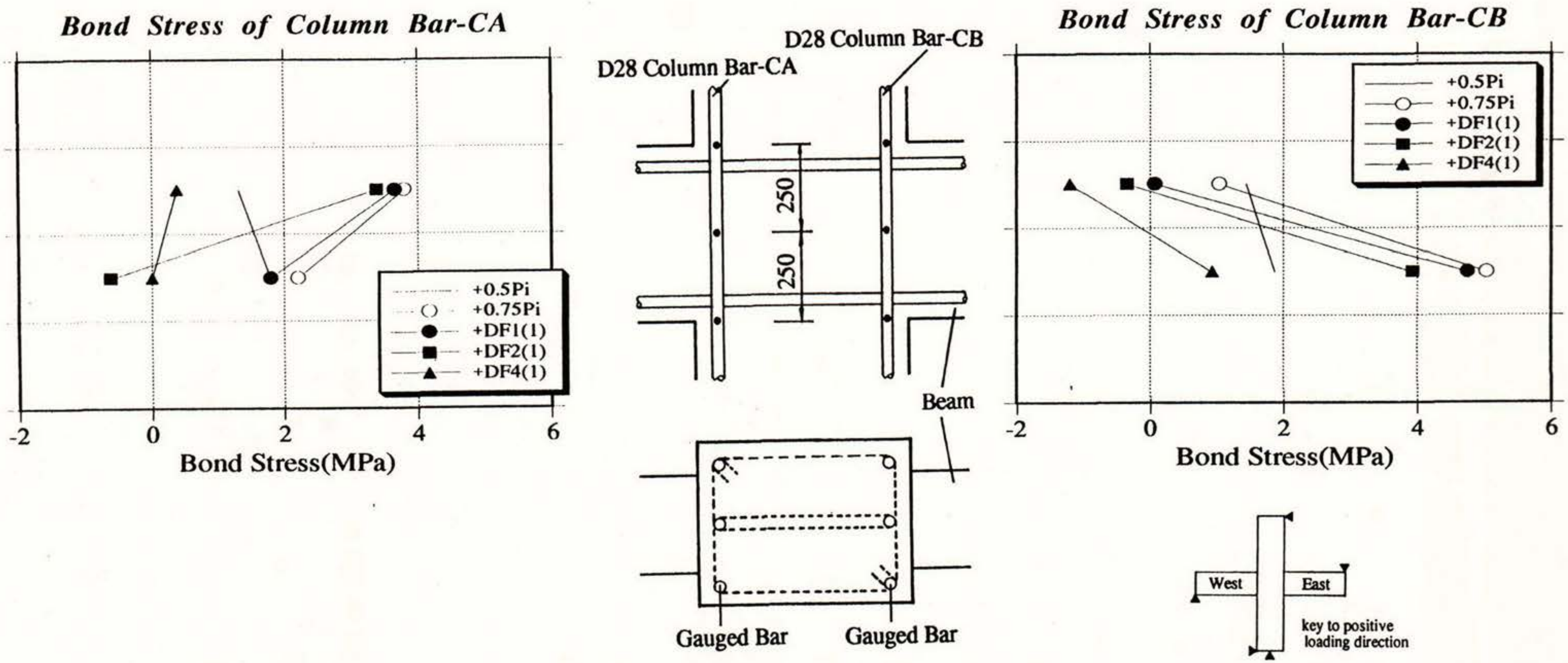

Fig.6.23 Measured Bond Stresses of Column Bars of Specimen O5

6.3.7.3 Joint Shear Distortion and Expansion

Fig.6.24 illustrates the joint shear distortion and expansion of Specimen O5.

After the loading to $\pm 0.75P_i$, in which corner to corner diagonal tension cracks initiated in the joint, the joint shear distortion gradually increased. In the loading to DF of 2, the joint shear distortion increased rapidly. At this stage, the joint expansion also began to increase. In the first cycle of loading to DF of 4, the joint shear distortion approached to 1%. Although some reduction in shear distortion was observed in the second cycle of loading to DF of 4, joint shear distortion increased up to 1.4% measured in the second cycle of loading to DF of 6. Joint expansion became notable in this loading cycle as illustrated in Fig.6.24.

When compared with the joint shear distortion and expansion measured for Specimen O4, the shear distortion and expansion measured for Specimen O5 were somewhat smaller than those for Specimen O4(compare Fig.6.24 with Fig.6.13). However the difference was not so significant. The effect of the difference in column depth to beam bar diameter ratio on the joint shear distortion and expansion could not be found in this study.

6.3.8 Decomposition of Horizontal Displacement

The components of the horizontal displacement at the peak of the selected loading cycle are expressed as a percentages of the storey drift angle in Fig.6.25. No measurements were made for beam flexural and shear displacement after the second cycle of loading to DF of 4.

Until the loading to DF of 4, the main contributions to the storey drift angle were the beam flexural displacement and the fixed-end rotation of the columns. The beam flexure displacement contributed 26 to 47% of the imposed storey drift angle while the contribution of the fixed-end rotation of the columns was 18 to 28%. The fixed-end rotation contribution increased up to 31% in the loading to DF of 6. The contribution of the beam displacement due to shear was less than 2% until the loading to DF of 4.

In the loading to $\pm 0.75P_i$, the joint shear distortion accounted for 16% of the storey drift angle. The contribution of the shear distortion of the joint fairly constant until the first cycle of loading to DF of 2. In the second cycle of loading to DF of 2, the component due to joint shear distortion increased rapidly and the maximum value of 31% was obtained. Although subsequent loading cycles resulted in the reduction of the contribution of the joint shear, its contribution was still important. The contribution in the second cycle of loading to DF of 6 was 24% of the storey drift angle.

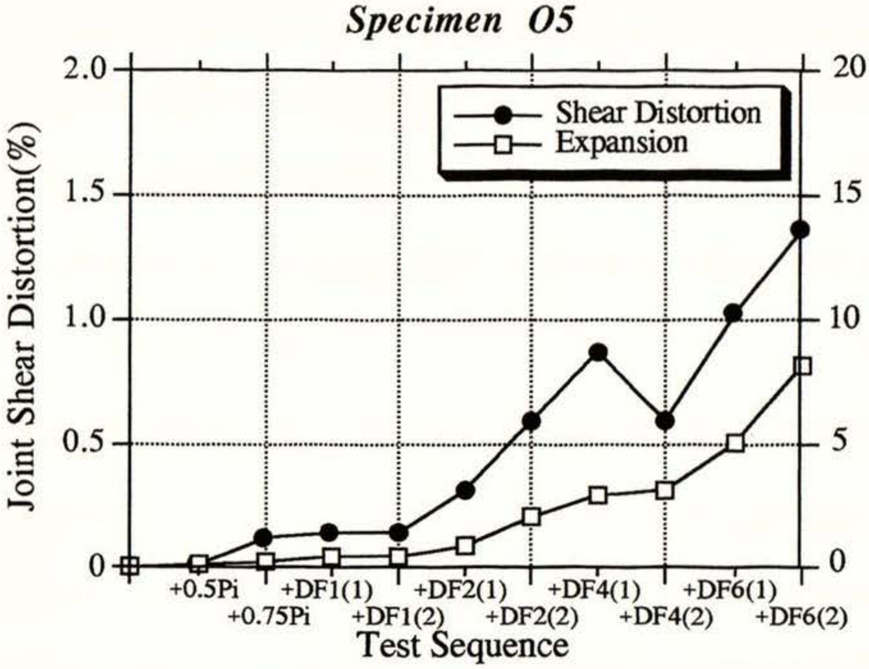

Fig.6.24 Joint Shear Distortion and Expansion of Specimen O5

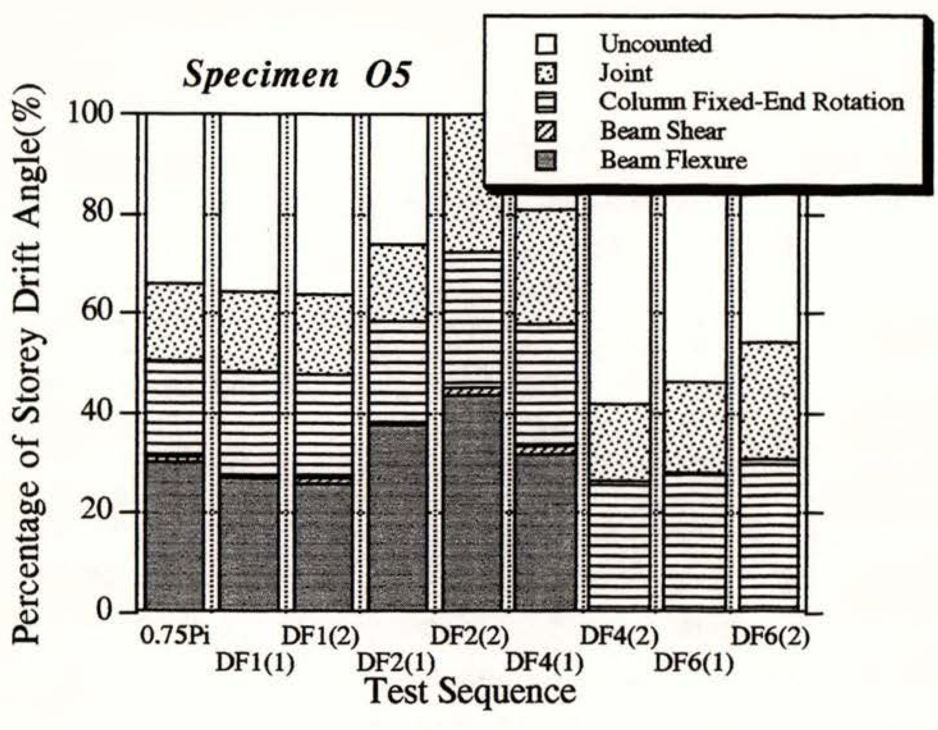

Fig.6.25 Components of Storey Drift Angle of Specimen O5

6.4 DISCUSSION OF THE TEST RESULTS

The comparison of the storey shear force and horizontal displacement relationship obtained from Specimen O4 with that from Specimen O5 indicates that the effect of the column depth to beam bar diameter ratio on the seismic behaviour of the joint without shear reinforcement was not significant. The somewhat inferior performance observed for Specimen O5 is mainly due to the lower concrete compressive strength when compared with that for Specimen O4.

The beam and column bar strains observed for Specimens O4 and O5 are again shown in Fig.6.26. As mentioned before, the strain profiles of the beam bars measured in the joint were almost similar despite the fact that the ratio of the column depth to beam bar diameter was different. Some difference may be found in the large tensile strains measured at flexural compression side of the bottom beam bar of Specimen O5. However, the effect of the column depth to beam bar diameter ratio on the beam bar strain profiles in the joint without shear reinforcement could not be found in this study. The strain profiles obtained along the column bars in the joint were also similar as illustrated in Fig.6.26.

The effect of the column depth to beam bar diameter ratio was observed in the loading to DF of 4, in which large beam bar slip initiated through the joint of Specimen O5 with large beam bar diameter. However, the slip of the beam bars through the joint did not affect the overall response of the test specimen significantly.

Based on the limited test data obtained from Specimens O1, O4 and O5, typical features of the strain profiles along the beam and column bars in the joint without shear reinforcement are as follows:

(1) Even in the early loading stages, only small bond stresses were generated in the flexural tension side where transverse tension forces are developed, irrespective of the column depth to beam bar diameter ratio. The bond stresses were mainly developed in the flexural compression side where transverse compression forces are present.

(2) The tensile strains measured along the longitudinal beam and column bars in the joint core were larger than those predicted by section analysis. This trend became more obvious after joint diagonal tension cracking.

(3) In the loading to DF of 1, the "compression" reinforcement in the beam on one side of the column was actually in tension. This observation could also be applicable to the strain profiles of the column bars.

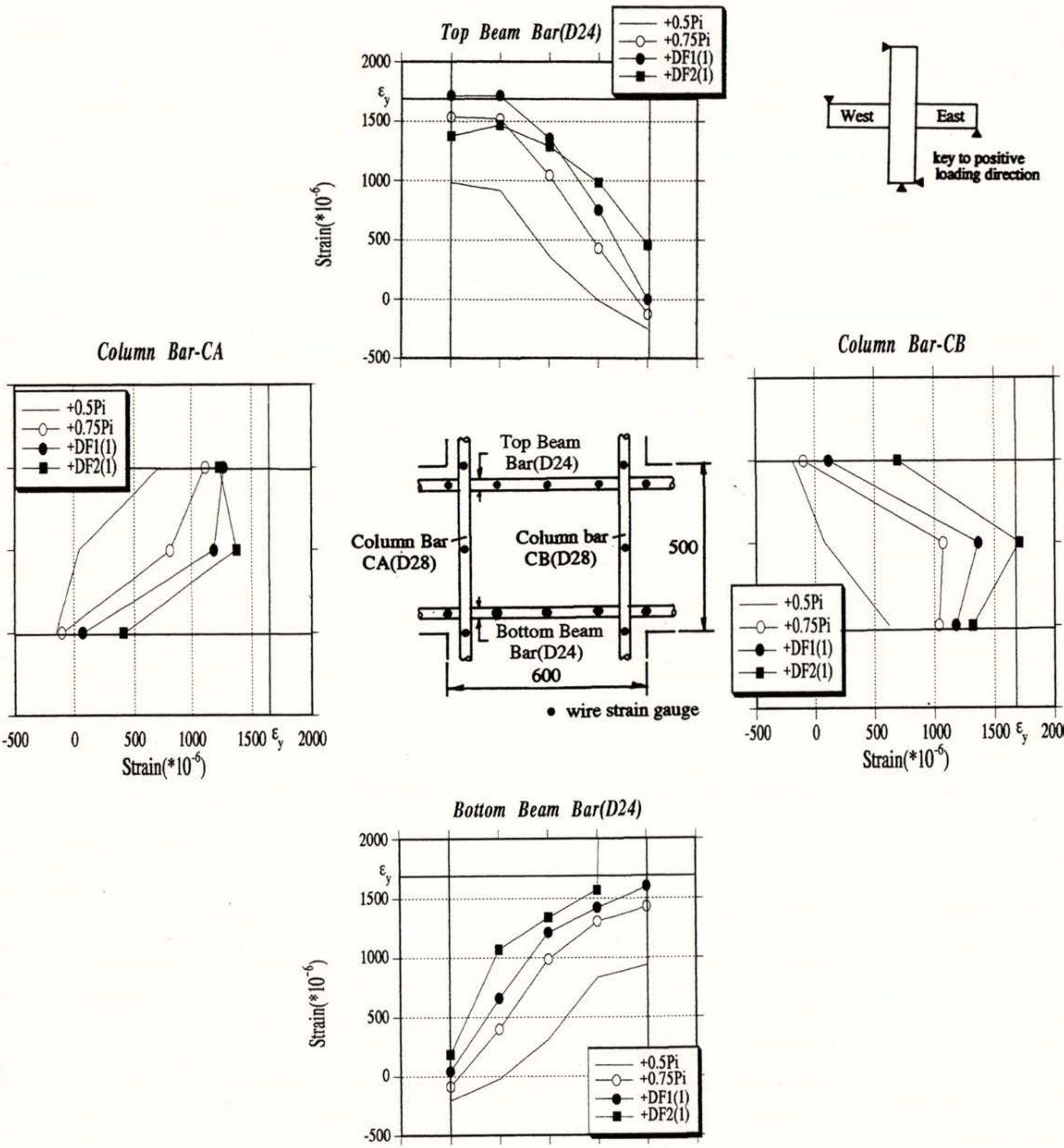

Fig.6.26(a) Strain Profiles of the Beam and Column Bars in the Joint of Specimen O4

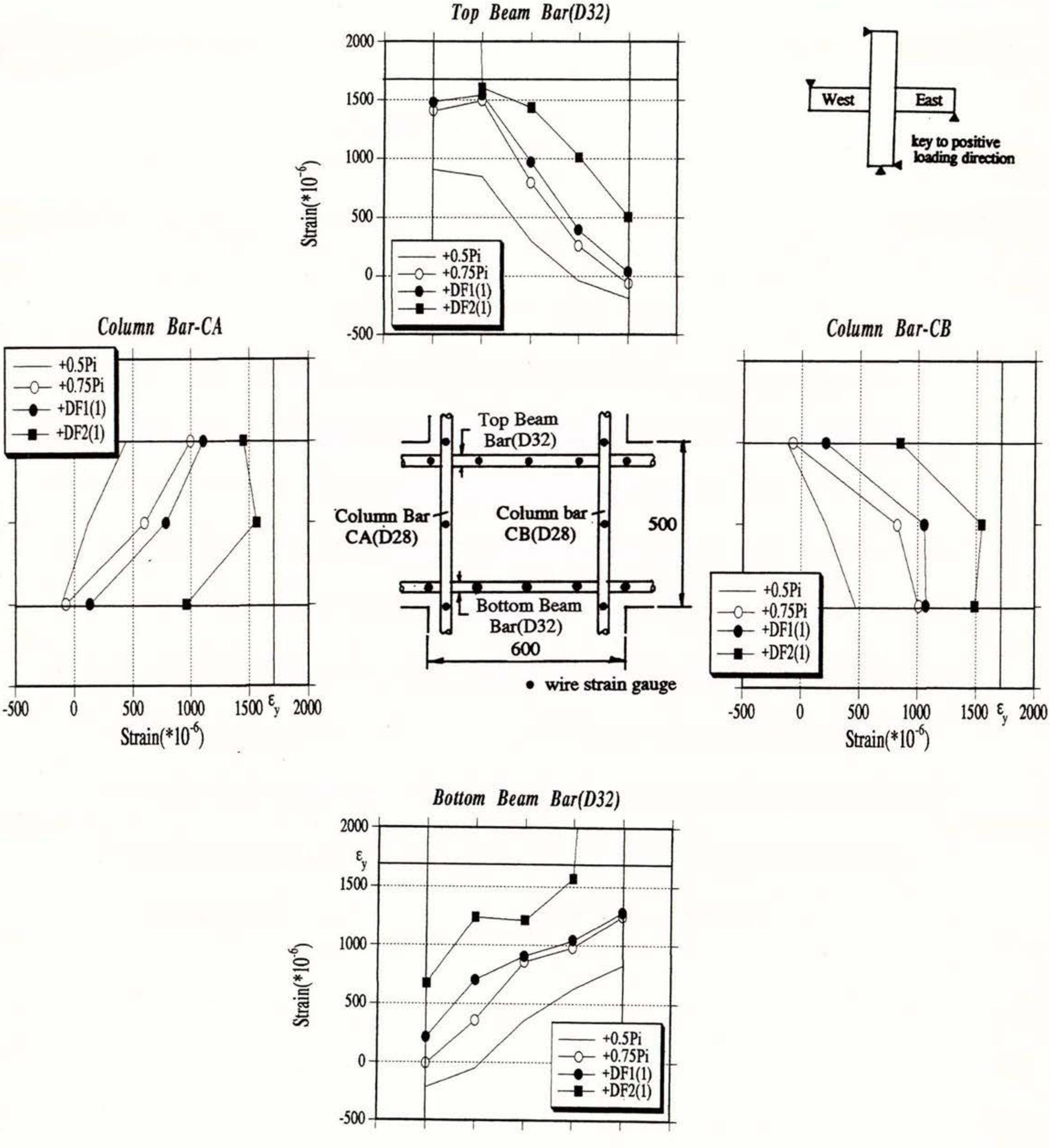

Fig.6.26(b) Strain Profiles of the Beam and Column Bars in the Joint of Specimen O5

It is believed that in the elastic loading cycles, bond splitting cracks initiated along the beam and column bars in the joint. In the joint without joint hoops and intermediate column bars which could significantly improve bond performance under seismic conditions, those cracks resulted in the decrease of the bond stress over the region subjected to transverse tension force, that is the column or beam flexural tension force, irrespective of the column depth to beam bar diameter ratio. Bond force in terms of the average bond stress in the joint without shear reinforcement could be generated mainly over the region subjected to transverse compression force which could exert clamping action across the bond splitting cracks. For the column corner bars situated outside the beam width, however, the clamping action due to the beam flexural compression force could be hardly mobilized. Therefore, the splitting cracks along the column corner bars in the joint without hoops could be easily developed and extended under the seismic loading, resulting in the reduction of bond resistance along the column corner bars(see Fig.6.3).

After diagonal tension cracking, the beam and column bars in the joint core were stressed in tension significantly, resulting in the deviation from the strain profiles obtained from section analysis. This mechanism will be discussed in Chapter 8.

For the joint without shear reinforcement, large tensile strains prevail along the beam and column bars in the joint under seismic loading, resulting in the considerable joint expansion. Fixed-end rotation of the members adjacent to the joint also become large, causing flexible structures. The beam and column bar strain profiles in such joints, which represent bond stress distributions, are quite different from those obtained from a well designed joint.

Based on the limited test data, the joint shear stress at diagonal tension cracking was found to be larger than $0.4\sqrt{f'_c}$ for the joint without shear reinforcement, where f'_c is the measured concrete compressive strength. This value was somewhat larger than the cracking shear stress of $0.3\sqrt{f'_c}$ which has been proposed by Priestley and Calvi 1991. When considering the bond stress distributions along the beam and column bars in the joint without shear reinforcement mentioned above, the shear carried by the diagonal compression strut will be increased, reducing the diagonal tension stress introduced into the joint core by bond force. Therefore, the cracking strength of the joint without shear reinforcement will be increased. Further investigation is necessary to obtain the shear strength at cracking for joints without shear reinforcement.

6.5 CONCLUSIONS

From the results tested on Specimens O4 and O5, the following conclusions are reached.

(1) Specimen O4, which had the beam bar diameter of 24mm and the maximum nominal horizontal joint shear stress of $0.47\sqrt{f'_c}$, showed a moderate ductility response during the test. Specimen O5 with the beam bar diameter of 32mm and the maximum nominal joint shear stress of $0.61\sqrt{f'_c}$ showed a limited ductility response. For joints without shear reinforcement, the effect of the column depth to beam bar diameter ratio on the seismic behaviour of the joint was not significant.

(2) In the elastic loading cycles, bond stresses along the beam and column bars in the joint without shear reinforcement were reduced in the flexural tension side, irrespective of the ratio of the column depth to beam bar diameter. On the contrary, bond stresses were generated mainly in the flexural compression side as the test progressed.

(3) After joint diagonal tension cracking, large tensile strains prevailed along the beam and column bars in the joint core without shear reinforcement, resulting in large joint expansion.

(4) The initial stiffnesses of the test specimens were found to be very low when compared with the theoretical values. This is mainly because the large tensile strains along the longitudinal beam and column bars prevailed in the joint, causing fixed-end rotation of the members adjacent to the joint.

(5) The nominal horizontal joint shear stresses at diagonal tension cracking for the joint without shear reinforcement were found to be larger than $0.4\sqrt{f'_c}$ in this study. This shear stress at cracking was somewhat larger than the value previously proposed for the joints with shear reinforcement, that is $0.3\sqrt{f'_c}$. This is due to the bond stress distribution along the main beam and column bars in the joint when joint reinforcement is not present.

CHAPTER 7

EXPERIMENTAL RESULTS OF SPECIMENS O6 AND O7

7.1 INTRODUCTION

One full-scale beam-exterior column joint subassemblage with beam bar end anchorages typical of the 1950's reinforced concrete building frames being investigated was constructed. The beam bars were not bent into the joint core and the end extension beyond the bend was four times bar diameter. This specimen was referred to as Specimen O7. In order to investigate the effect of such a configuration of the hooks at the ends of the beam bars, another specimen, referred to as Specimen O6, was also constructed, in which beam bars were bent into the joint core and the extension beyond the bend was twelve times bar diameter. Only one set of 6mm diameter hoops was placed in the joint core of both specimens. Small amounts of transverse reinforcement were provided in the beams and columns. The specimens were tested under simulated seismic loading and their behaviour was compared. This chapter describes the test results for Specimens O6 and O7.

7.2 SPECIMEN O6

7.2.1 Introduction

For Specimen O6 with beam bars bent into the joint core, the ratio of the theoretical ideal flexural strength of the column to that of the beam was 1.97 during beam positive moment and 1.37 during beam negative moment, respectively. When the beam plastic hinge mechanism was developed, the ideal storey horizontal load strength P_i was 43kN during beam positive moment and 62kN during beam negative moment, respectively. The concrete of the specimen at the stage of testing had a compressive cylinder strength f'_c of 34.3MPa.

7.2.2 General Behaviour

The final crack pattern and the storey shear force versus horizontal displacement relationship are shown in Figs.7.1 and 7.2, respectively. Observed cracking at the peak of the selected loading cycles are shown in Fig.7.3.

In the loading to $\pm 0.5P_i$, flexural cracks initiated in the beam and columns. In the subsequent loading cycle to $\pm 0.75P_i$, those cracks extended and the number of the cracks also increased. Flexural-shear cracks were also observed in the beam(see Fig.7.3(a)).

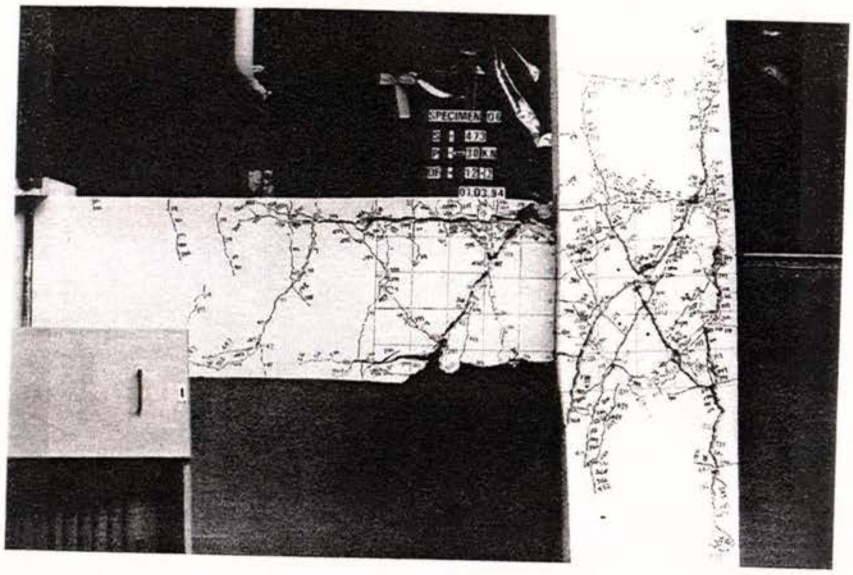

Fig.7.1 Observed Cracking of Specimen O6
at first cycle of DF=-12

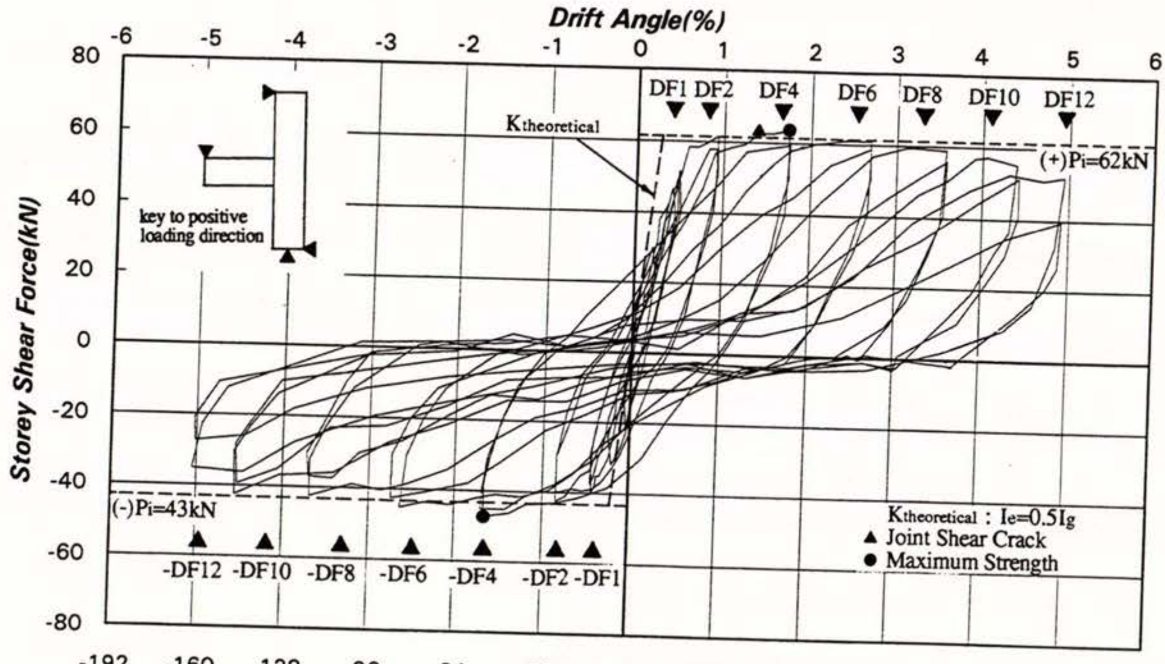

Fig.7.2 Storey Shear Force versus Horizontal Displacement Relationship
for Specimen O6

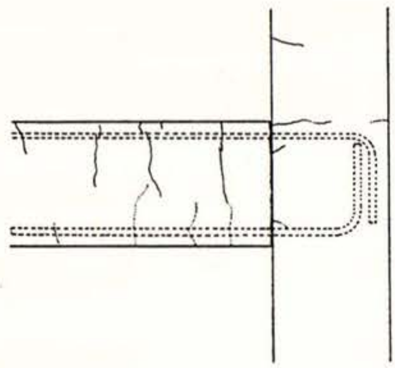

(a) at the peak of 0.75Pi
(R=0.31%)

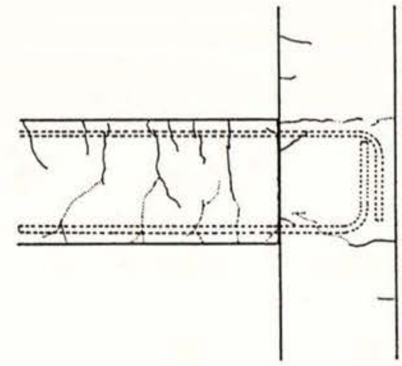

(b) at the peak of second cycle, DF=1
(R=0.41%)

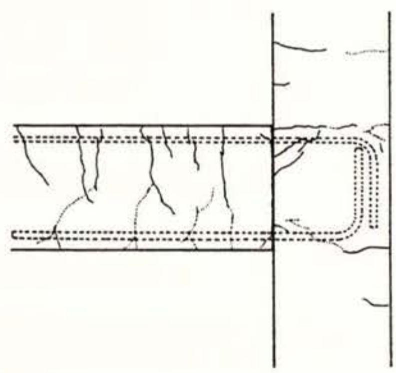

(c) at the peak of second cycle, DF=2
(R=0.83%)

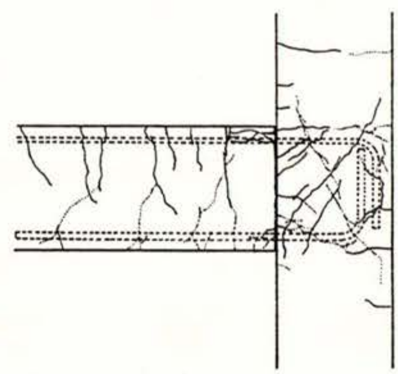

(d) at the peak of second cycle, DF=4
(R=1.66%)

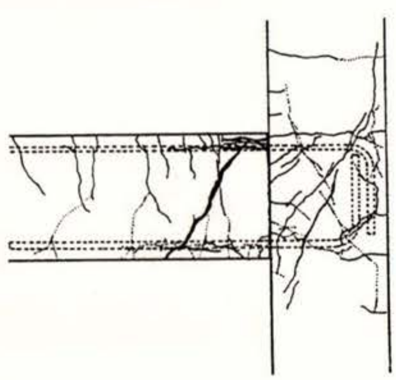

(e) at the peak of second cycle, DF=6
(R=2.49%)

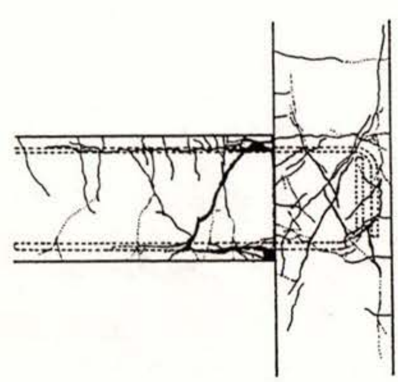

(f) at the peak of second cycle, DF=8
(R=3.33%)

Fig.7.3 Observed Cracking of the Joint(Specimen O6)

In the loading to displacement ductility factor DF of 1, flexural-shear cracks in the beam became more evident. Joint shear cracks initiated at the two corners adjacent to the beam(see Fig.7.3(b)). At this stage, bottom beam bars started to yield in tension at the column face.

In the loading to DF of 2, beam flexural and flexural-shear cracks extended and opened wide to a maximum crack width of 3.5mm. Top beam bars also yielded at the column face in this loading cycles. The ideal storey horizontal load strengths of the test specimen was reached during the positive and negative loading cycles(see Fig.7.2).

In the first cycle of loading to DF of 4, corner to corner diagonal tension cracks formed in the joint core. Also observed were bond splitting cracks along the outer column bars(see Fig.7.3(d)). Joint diagonal tension cracks extended and opened wide to a maximum crack width of 0.5mm. In the beam, cover concrete of the flexural compression zone in the plastic hinge region started to crush and bond splitting cracks initiated along the main beam bars near the column face. Beam flexural cracks at the column face opened wide to a maximum crack width of approximately 9mm. The maximum horizontal load strength was attained in the first cycle of loading to DF of 4 which was 47.2kN for the positive loading cycle and 63.6kN for the negative loading cycle, respectively. No significant strength degradation and pinching were observed in the hysteresis loops shown in Fig.7.2.

In the loading to DF of 6, joint diagonal tension cracks extended and connected to the splitting cracks along the column bars. The maximum width of the joint diagonal tension cracks and bond splitting cracks along the outer column bar was 11.4mm and 2.5mm, respectively. In the first negative cycle of loading to DF of 6, one dominant diagonal tension crack initiated in the beam with an angle of approximately 45 degree to the beam axis and opened wide to a maximum crack width of 11mm(see Fig.7.3(e)). Although some pinching was observed in the hysteresis curves, the reduction of the horizontal load strength was small.

In the loading to DF of 8, the damage of the joint due to diagonal tension cracks and bond splitting cracks along the column bars became more apparent. The maximum crack width was measured to 3mm for the joint diagonal tension cracks. In the beam, the diagonal tension crack during beam negative moment also initiated in this loading cycle(see Fig.7.3(f)). Bond splitting cracks along the beam bars extended and the cover concrete started to spall off. Hysteresis loops were significantly pinched mainly due to the cracks opened wide in the joint and beam. However, the horizontal load strength of the specimen was observed to be larger than 80% of the measured maximum horizontal load strength(see Fig.7.2).

In the loading to DF of 10, the beam diagonal tension cracks and splitting cracks along the main beam bars opened wide significantly. Most of the cover concrete in the beam flexural compression zone spalled off in the plastic hinge region. Sliding movement along the beam diagonal tension cracks were observed up to 18mm in vertical direction during beam positive moment. The maximum width of the beam diagonal tension cracks was 4mm during the positive loading cycle and 15mm during the negative loading cycle, respectively. Joint diagonal tension cracks also opened wide to a maximum crack width of about 4mm. The horizontal load strength of the specimen could still be maintained larger than 80% of the measured maximum horizontal load strength(see Fig.7.2).

In the loading to DF of 12, joint diagonal tension cracks opened wide to a maximum crack width of approximately 10mm. Bond splitting cracks along the outer column bars opened wide significantly. The hysteresis loops were significantly pinched and severe strength degradation was observed in the second cycle of this loading due to beam and joint shear failure(see Figs.7.1 and 7.2).

It is evident that for Specimen O6 in which beam bars were bent into the joint core, a ductile response could be achieved in spite of the fact that the joint and beam suffered severe diagonal tension cracking after the beam plastic hinge mechanism was developed.

7.2.3 Initial Stiffness

The theoretical initial stiffness was calculated for Specimen O6 as follows:

$$K_{theoretical}=9.0\text{kN/mm}$$

The procedures for calculating the theoretical initial stiffness were described in detail in Section 3.9. The calculated theoretical stiffness $K_{theoretical}$ is shown in Fig.7.2. The measured stiffness at 75% of the theoretical ideal storey horizontal load strength of the test specimen was 4.9kN/mm for the positive loading cycle and 3.5kN/mm for the negative loading cycle, respectively. The average value of the stiffnesses obtained for the positive and negative loading cycle was only 47% of the theoretical stiffness.

The yield displacement of the test specimen estimated from the stiffness at $0.75P_i$, extrapolated linearly to P_i was 13.3mm which could be converted to 0.42% in terms of the storey drift angle. The test specimen was rather flexible according to the current code requirements[SANZ 1992].

7.2.4 Available Displacement Ductility Factor

The available displacement ductility factor μ_a was calculated to be larger than 10 from the measured storey shear force and horizontal displacement relationship of Specimen O6. The method for calculating the available displacement ductility factor was explained in Section

5.2.4. Although the test specimen suffered beam and joint diagonal tension cracking during the test, large ductility capacity was attained for Specimen O6 with beam bars bent into the joint core.

7.2.5 Beam Behaviour

7.2.5.1 Longitudinal Beam Bar Strains

Strains measured along the longitudinal beam bars are shown in Figs.7.4 and 7.5. Fig.7.4 illustrates the strain profiles obtained from the wire strain gauge readings while Fig.7.5 indicates those measured from the linear potentiometers attached to the steel rods welded to the beam bars.

In the elastic loading cycles, the gradual increase in tensile strains along the beam bars was observed. In the loading to DF of 1, the bottom beam bars reached the yield strain at the column face and subsequent loading cycle resulted in significant large tensile strain of larger than 2.5%(see Fig.7.4(b)). In the loading to DF of 2, top beam bars also yielded in tension at the column face(see Fig.7.4(a)). The strains measured in the joint approached the yield strain at this loading stage.

After loading to DF of 4, in which joint diagonal tension cracks initiated, the strains measured in the joint core showed large tensile strains(see Fig.7.5), indicating yield penetration into the joint core. It could be expected that the bond forces diminished along the straight portion of the beam bars from the inner column face to the hook and the steel tensile forces were resisted around the bend of the hooks.

Yielding of the beam flexural reinforcement were also observed into the beam from the column face in the loading to DF of 4(see Fig.7.5) and large tensile strains were measured in the loading to DF of 6, in which diagonal tension cracks extended and opened wide in the beam. For the bottom beam bar, yielding spread over a length larger than 1.5d, where d is the beam effective depth.

7.2.5.2 Slip of Beam Bars

The slip of the top and bottom beam bars in the joint are shown in Fig.7.6. The clear distance between two adjacent ribs of the beam bar was 11mm. The extension of the hook was twelve times bar diameter. The methods to obtain the bar slip were described in Section 3.7.4.

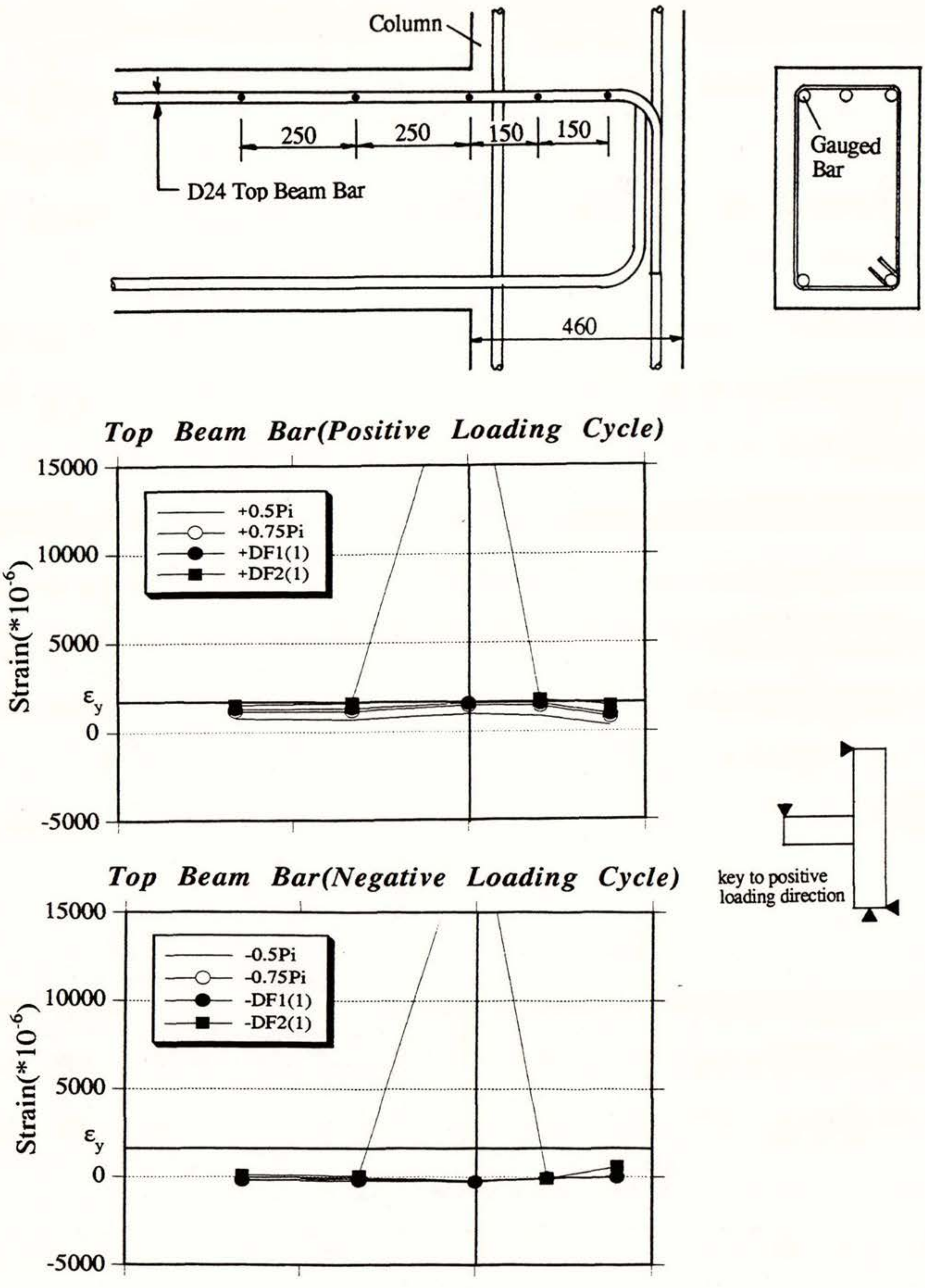

Fig.7.4(a) Strain Profiles of Top Beam Bar Measured by Wire Strain Gauges of Specimen O6

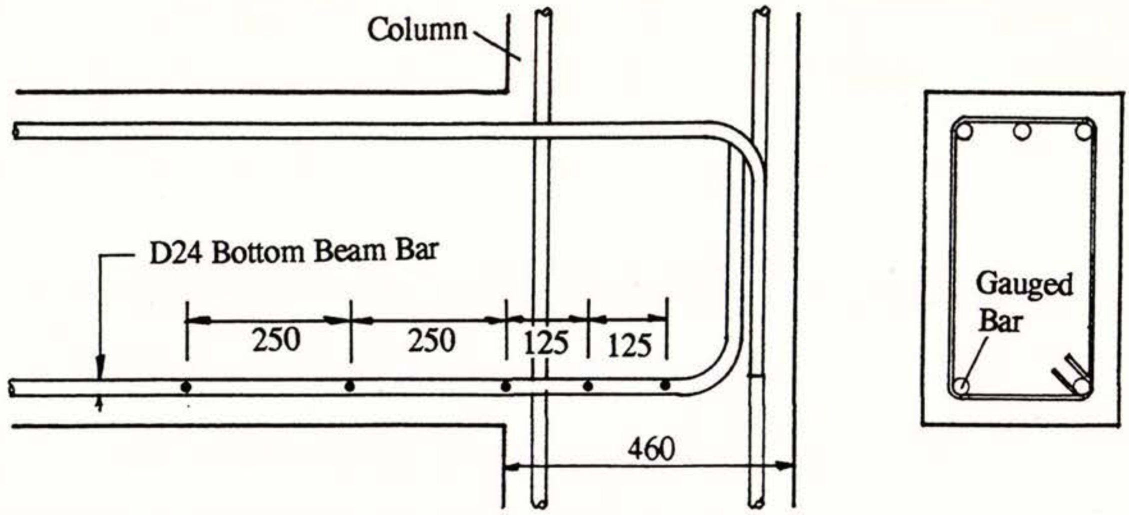

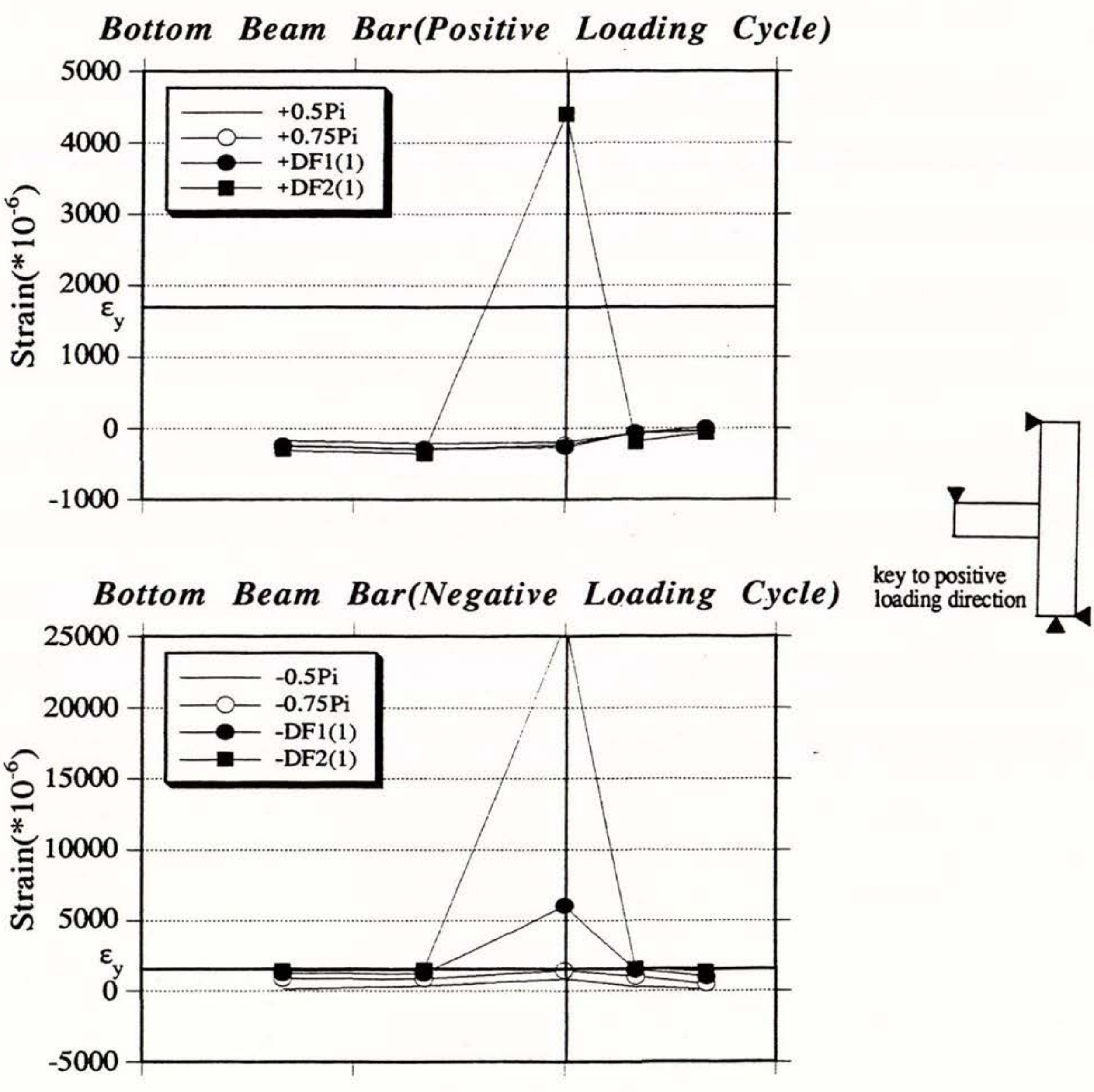

Fig.7.4(b) Strain Profiles of Bottom Beam Bar by Wire Strain Gauges of Specimen O6

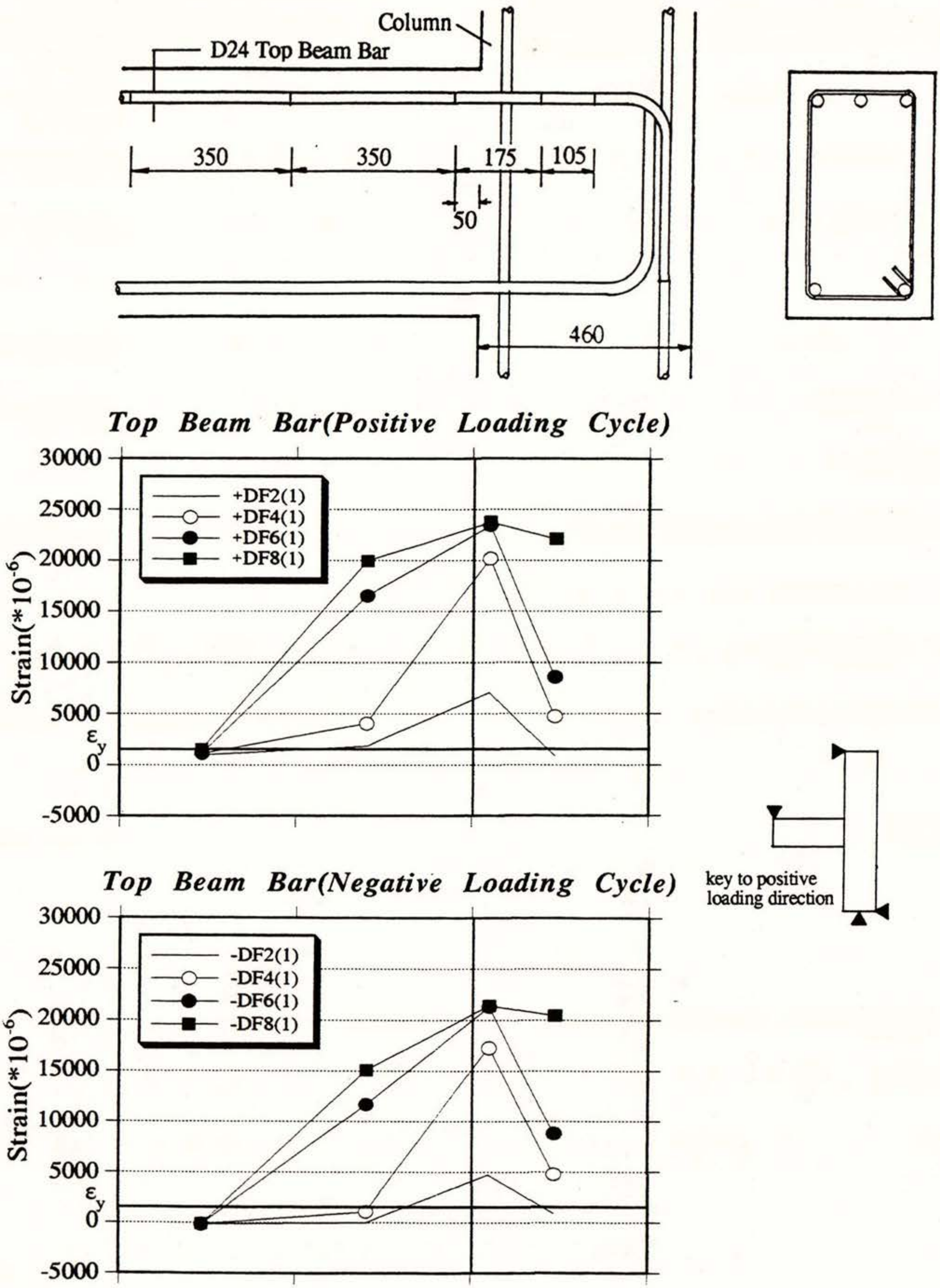

Fig.7.5(a) Strain Profiles of Bottom Beam Bar Measured by Linear Potensiometers of Specimen O6

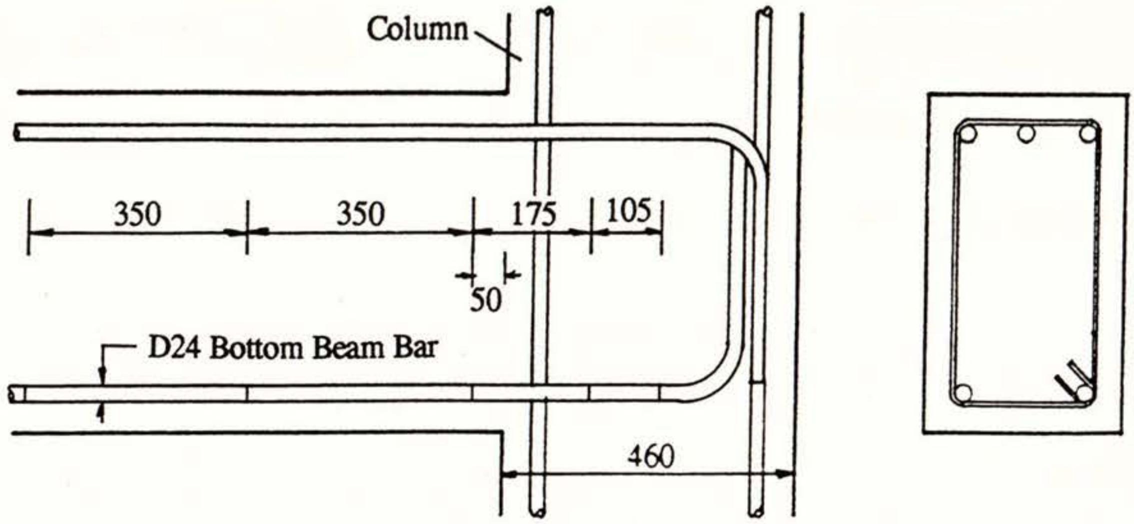

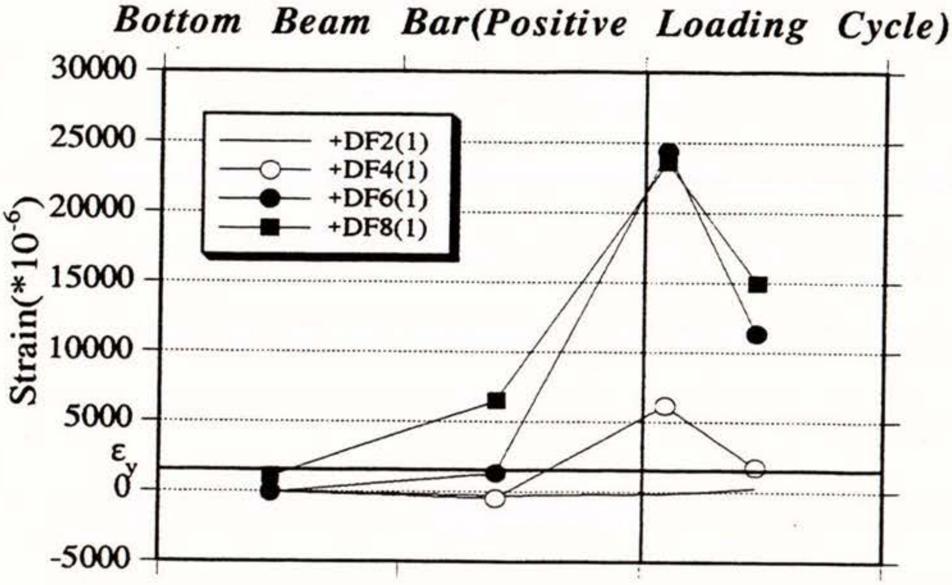

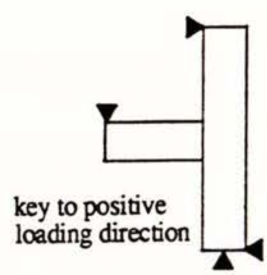

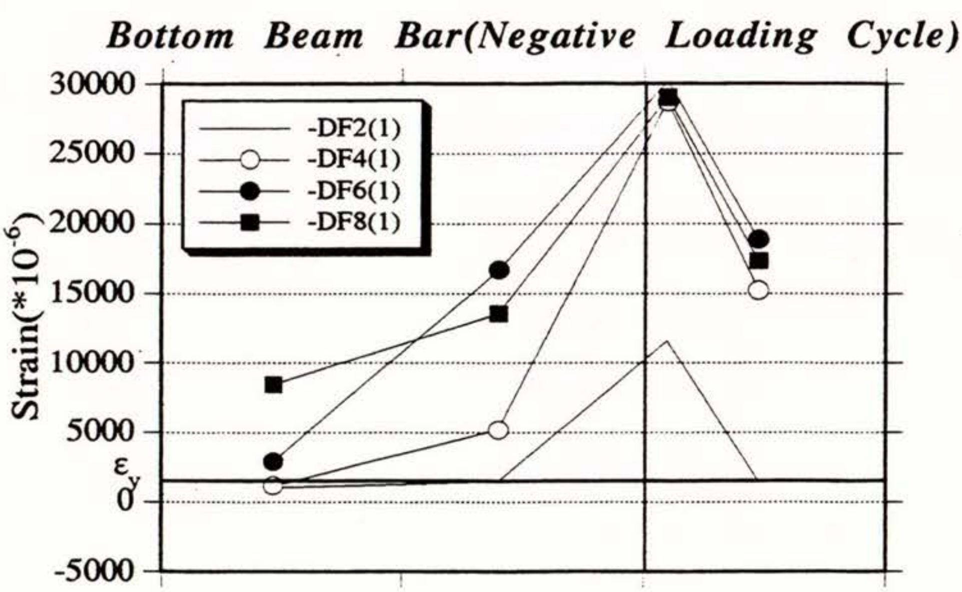

Fig.7.5(b) Strain Profiles of Top Beam Bar Measured by Linear Potensiometers of Specimen O6

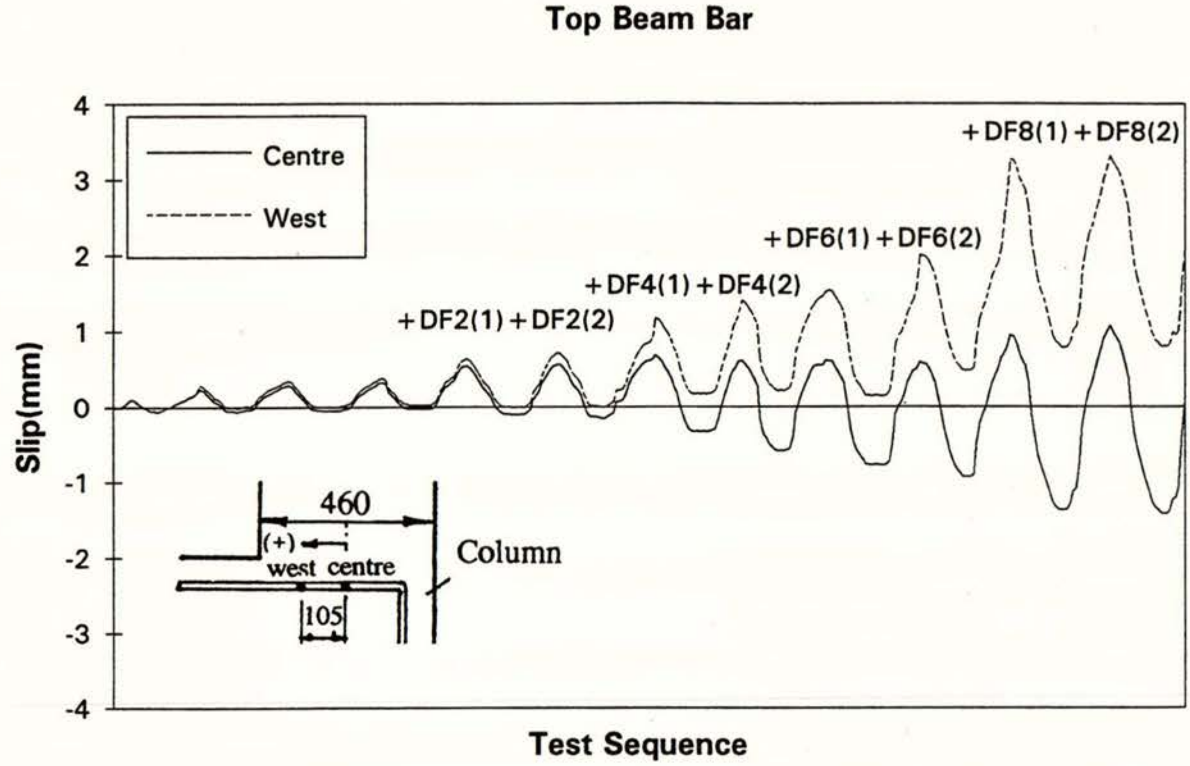

(a) Slip of Top Beam Bar

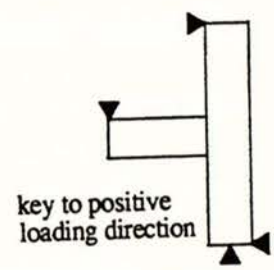

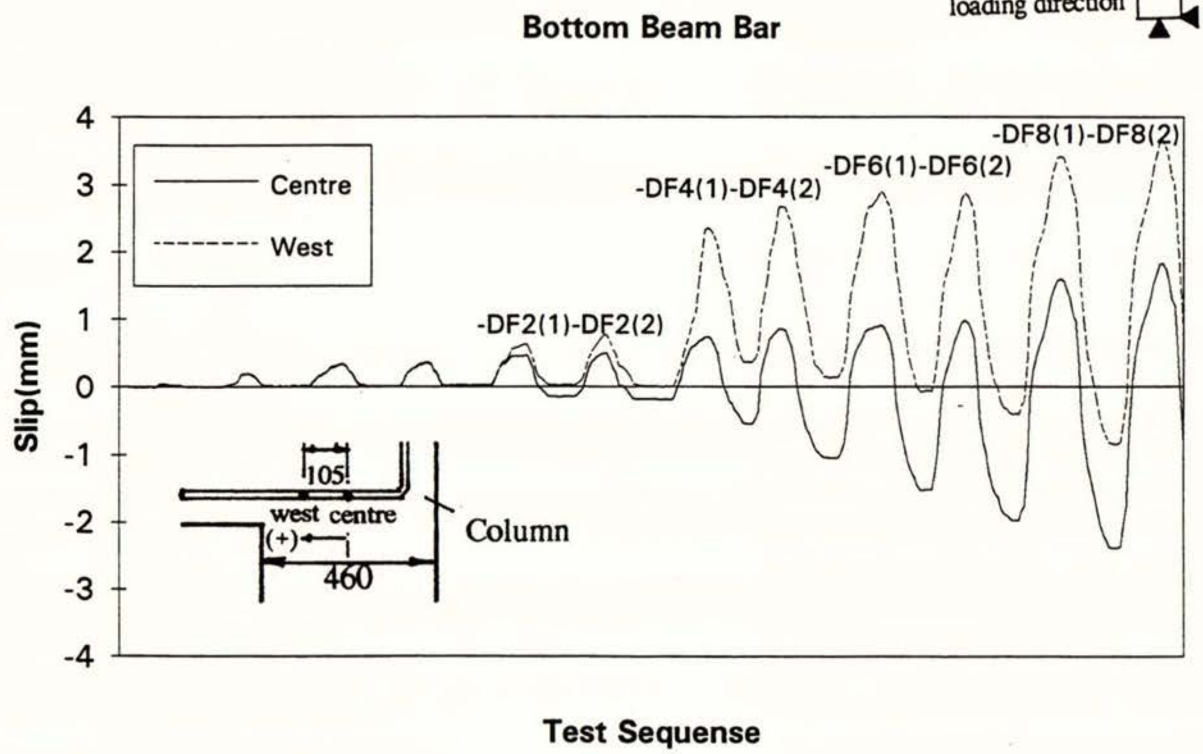

(b) Slip of Bottom Beam Bar

Fig.7.6 Measured Slip of Beam Bars of Specimen O6

The bar slip measured at each location increased with the test progressed. Until loading to DF of 8, the maximum bar slip was measured to 3.3 mm for top beam bar and 3.7mm for bottom beam bar, respectively. During the test, no significant slippage was measured for Specimen O6.

7.2.5.3 Beam Shear Stress and Shear Distortion

Fig.7.7 plots the relationship between shear stress $v_b/\sqrt{f'_c}$ and shear distortion of the beam, where $v_b = V_b/(bd)$, V_b is the applied beam shear force, b is the beam width and d is the effective depth of the beam and f'_c is the measured concrete compressive strength. Beam shear distortion was obtained from the second set of the linear potentiometers placed diagonally at 50mm away from the column face as illustrated in Fig.7.7. Also plotted is the shear carried by stirrups using the average strains of the stirrups measured from the wire strain gauges attached on both sides of the stirrup, assuming 45 degree truss mechanism.

During the test, the maximum nominal shear stress of the beam reached $0.14\sqrt{f'_c}$ with beam negative moment and $0.11\sqrt{f'_c}$ with beam positive moment.

For the negative loading cycles, which was during beam positive moment, diagonal tension cracks initiated in the loading to DF of 4 and those cracks extended and opened wide in the loading to DF of 6. At this stage, the stirrup in the beam plastic hinge region reached the yield strain and shear distortion increased rapidly up to larger than 2% as shown in Fig.7.7. Subsequent loading cycles resulted in a large increase in shear distortion. The aggregate interlock mechanism became ineffective due to the one dominant diagonal tension crack which opened wide. However, only a little reduction of the beam shear strength was observed up to the loading to DF of 8.

For the positive loading cycles, which was during beam negative moment, diagonal tension cracks were developed and extended in the loading to DF of 8. The shear distortion during this loading cycle was measured up to 1.4%(see Fig.7.7). The strength degradation was not so significant as was observed during beam positive moment.

7.2.5.4 Beam Curvature Ductility Factor

Until loading to DF of 8, the measured beam flexural strength during beam positive moment was 11% less than the theoretical ideal flexural strength based on the measured material strengths and was 3% less during beam negative moment. Fig.7.8 shows the curvature ductility factor of the beam estimated at the peak of the selected loading cycles. The curvature was obtained from the second set of the linear potentiometers placed at 50mm away from the column face, as shown in Fig.7.8. The gauge length for estimating the curvature

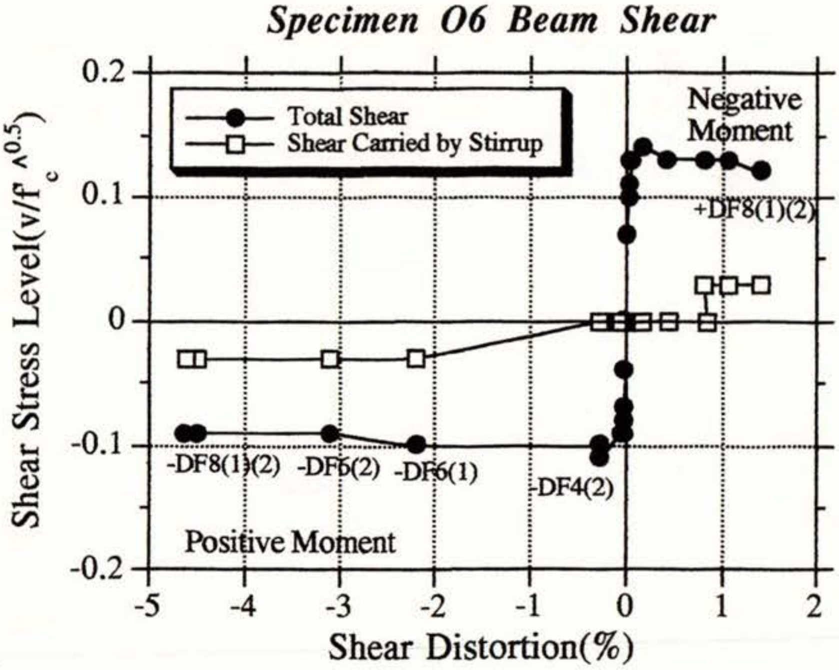

Fig.7.7 Relationship between Shear Stress Level and Shear Distortion of Beam of Specimen O6

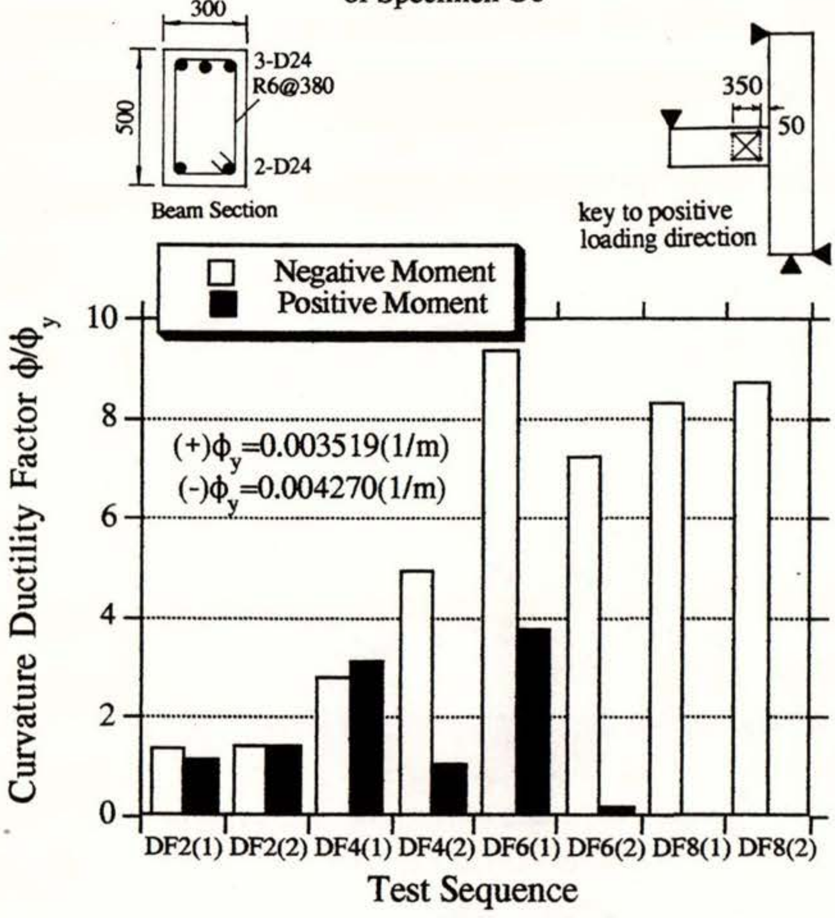

Fig.7.8 Curvature Ductility Factors of Beam of Specimen O6

was 350mm. The yield curvature ϕ_y was obtained by using the curvature at $0.75P_i$, extrapolated linearly P_i.

Up to the loading to DF of 4, the curvature ductility factor increased gradually as the test progressed. In the second cycle of loading to DF of 4, the measured curvature ductility factor began to decrease during beam positive moment. The reduction in the beam curvature ductility factor became more obvious in the loading to DF of 6. The rapid increase in beam shear distortion in this loading cycle shown in Fig.7.7 showed that shear deformations dominated for the deformation of the beam.

With beam negative moment, the measured curvature ductility factor increased up to the first cycle of loading to DF of 6 as illustrated in Fig.7.8. In the subsequent loading cycles, the curvature ductility factor did not increase. This was consistent to the increase in the shear distortion of the beam shown in Fig.7.7. The maximum curvature ductility factor was calculated to be about 9 for beam negative moment.

7.2.6 Column Behaviour

7.2.6.1 Introduction

In the loading to DF of 4, bond splitting cracks initiated along the column bars in the joint. Those cracks extended and opened wide significantly as the test progressed.

7.2.6.2 Longitudinal Column Bar Strains

Fig.7.9 shows the strains measured along the longitudinal column bars in the joint. Those strains were obtained from the wire strain gauges. As the displacement ductility factor imposed on the test specimen increased, the measured strains of the column bars increased gradually. Up to the loading to DF of 1, the strains measured in the column flexural compression zone were small compression or tension and fairly constant. In the loading to DF of 2, the strains measured throughout the joint began to increase. This trend became more obvious in the loading to DF of 4 in which the diagonal tension cracks formed in the joint. The tensile strains at the centre of the joint was notable. The strains at the centre of the joint and in the column flexural tension zone reached the yield strain in this loading cycle. Generally the inner column bar was more stressed in tension than the outer column bar as shown in Fig.7.9.

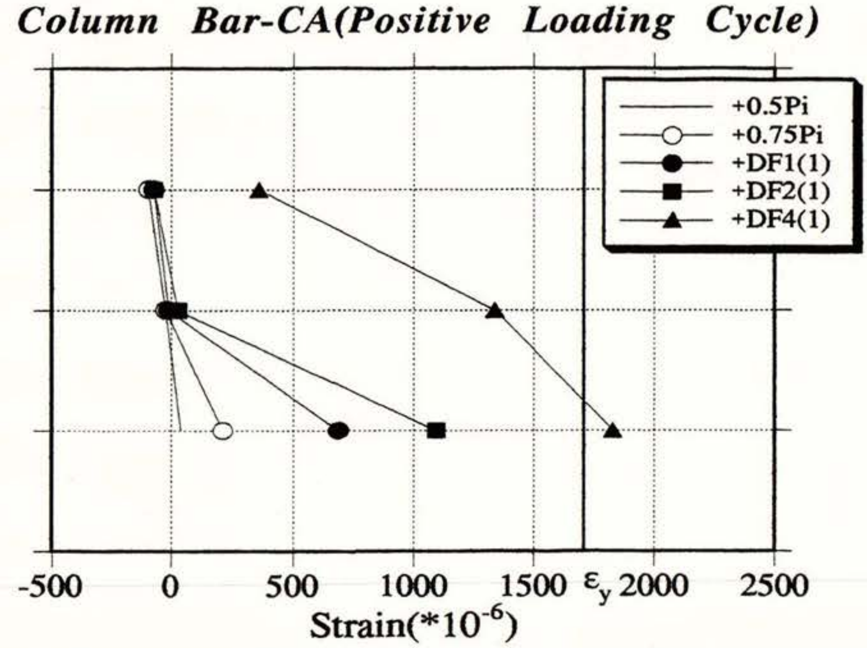

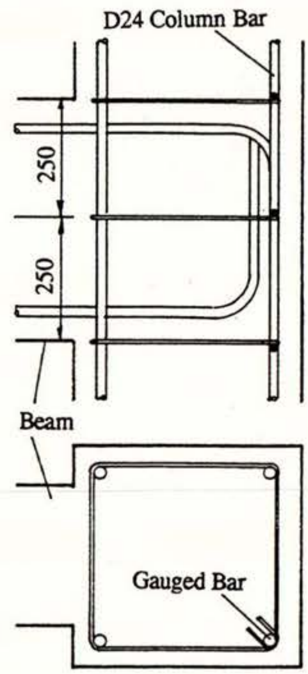

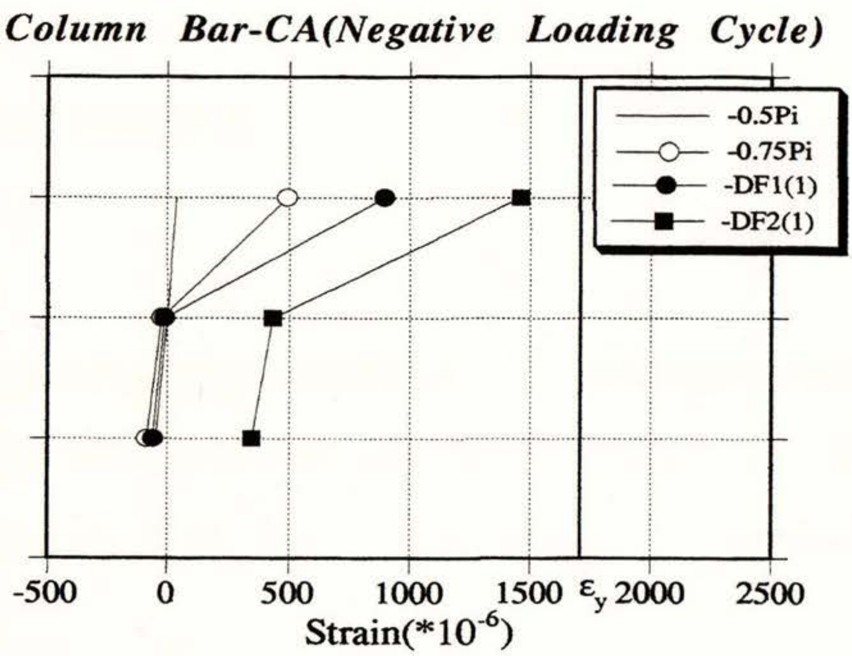

Fig.7.9(a) Strain Profiles of Column Bar of Specimen O6

Column Bar-CB(Positive Loading Cycle)

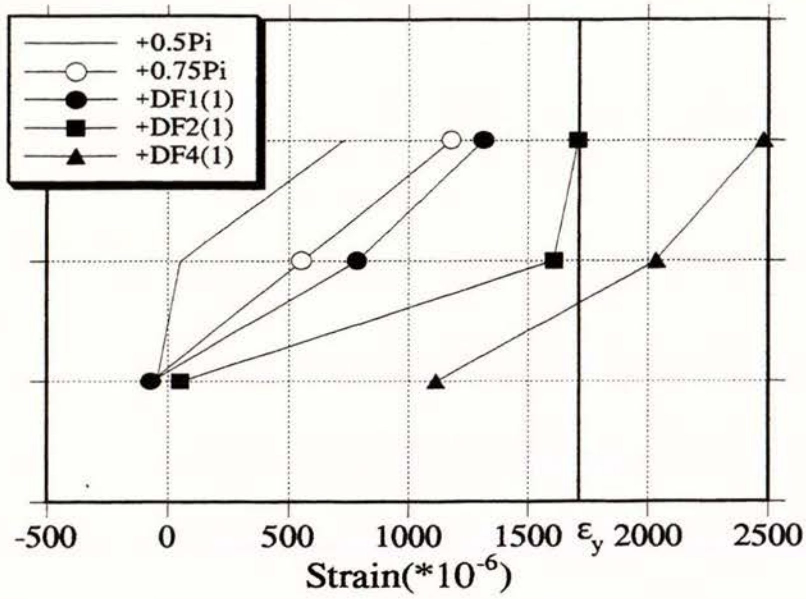

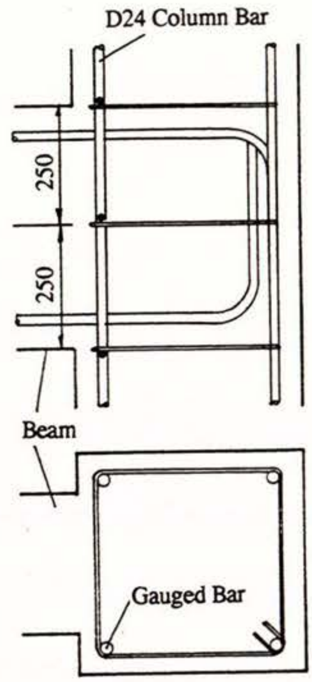

Column Bar-CB(Negative Loading Cycle)

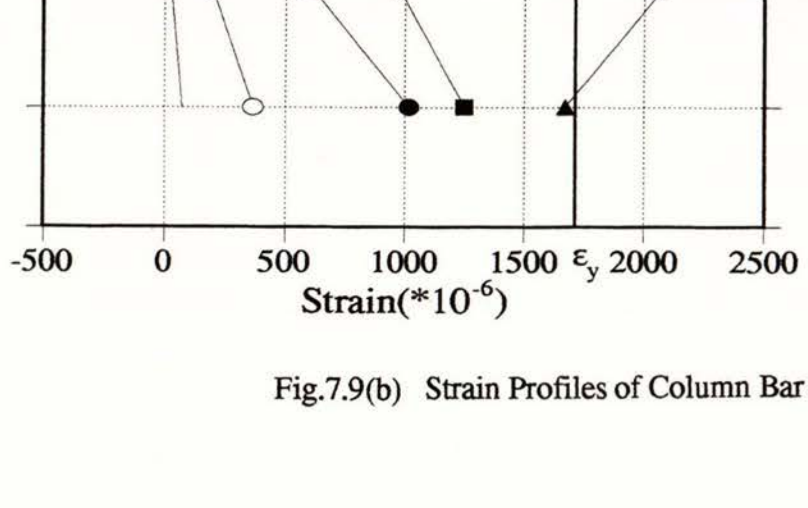

Fig.7.9(b) Strain Profiles of Column Bar of Specimen O6

7.2.7 Joint Behaviour

7.2.7.1 Introduction

Joint diagonal tension cracks initiated at the nominal horizontal joint shear stress of $0.31\sqrt{f'_c}$ in the loading to DF of 4, where f'_c is the measured concrete compressive strength. In the subsequent loading cycles, joint diagonal tension cracks extended and opened wide. The joint deteriorated as a result of diagonal tension cracking and bond splitting cracks along the column bars. The maximum nominal horizontal joint shear stress was calculated to be $0.32\sqrt{f'_c}$ for the positive loading cycle which gave the beam negative moment.

7.2.7.2 Joint Hoop Strains

The strains of three hoops, one located at the centre of the joint and the others at the beam face were measured using wire strain gauges. Fig.7.10 illustrates the hoop strains measured at the peak of the selected loading cycles.

After the diagonal tension cracks formed in the joint, the joint hoop strain increased gradually with an increase in the displacement ductility factor imposed on the test specimen. In the loading to DF of 4, the hoop placed at the centre of the joint started to yield and subsequent loading cycles caused a rapid increase in the tensile strain. As shown in Fig.7.10, the strains of the hoops placed at the beam face were far below the yield strain up to the loading to DF of 8, indicating small contribution of those hoops to the joint behaviour of the test specimen.

7.2.7.3 Joint Shear Distortion and Expansion

Fig.7.11 shows the joint shear distortion, together with the joint expansion. The methods to obtain the joint shear distortion and expansion were defined in Section 3.7.6.

After the loading to DF of 2, the joint shear distortion gradually increased. In the loading to DF of 4 in which corner to corner joint diagonal tension cracks initiated, the joint shear distortion increased rapidly. From the first cycle of loading to DF of 4, the joint shear distortion and expansion increased almost linearly up to the loading to DF of 8 for the positive loading cycle, that is during beam negative moment(see Fig.7.11). For the negative loading cycle, which is during beam positive moment, the joint shear distortion increased in the second cycle of loading to DF of 4. As mentioned in Section 7.2.5.4, the decrease in the beam curvature ductility observed in this loading cycle was partially attributed to the increase in the joint shear distortion. The maximum joint shear distortion was measured to be 1.5% during the positive loading cycle and 1.1% during the negative loading cycle. The maximum

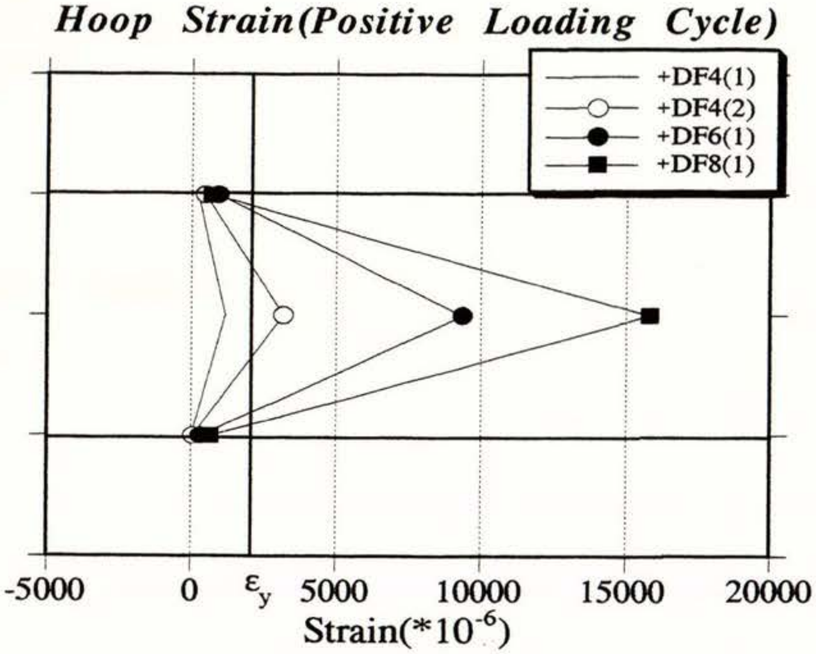

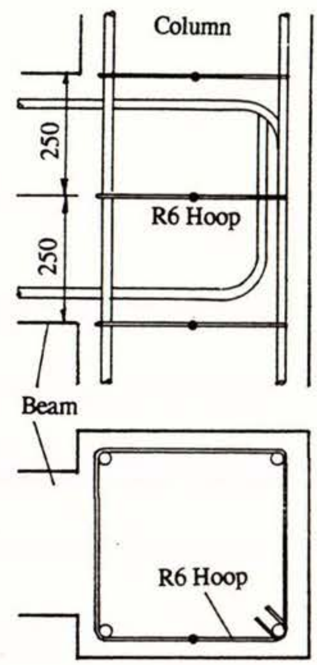

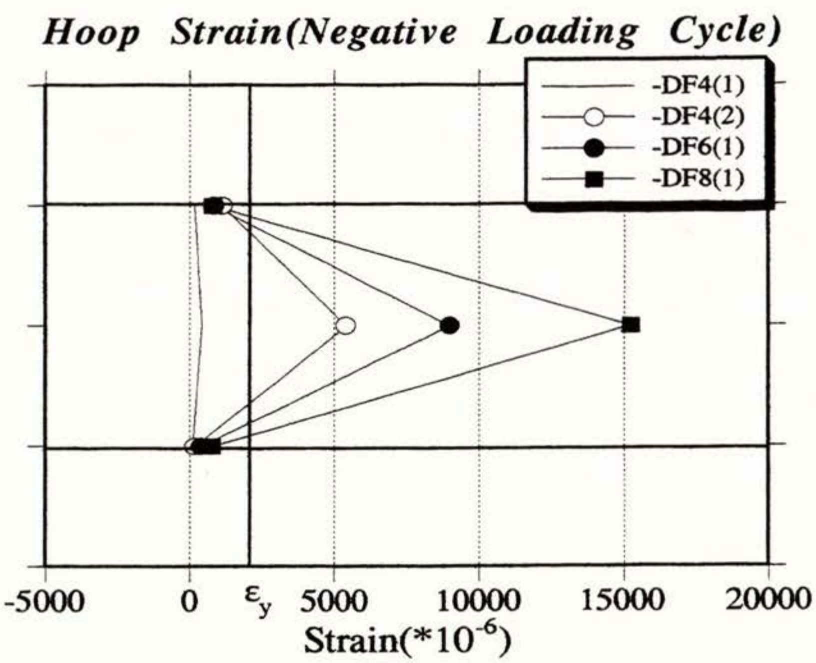

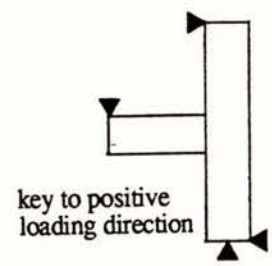

Fig.7.10 Hoop Strain Profiles of Specimen O6

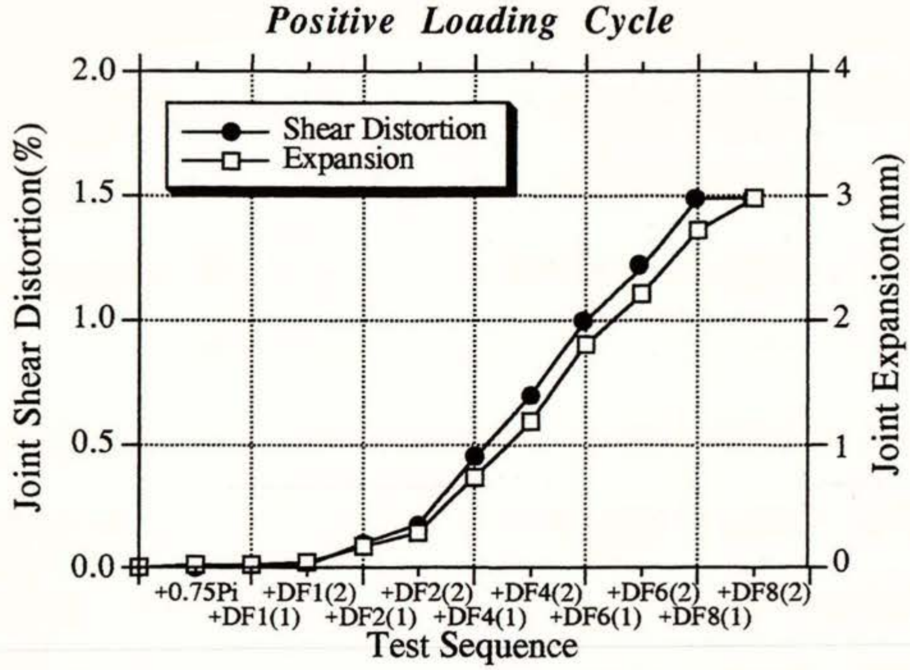

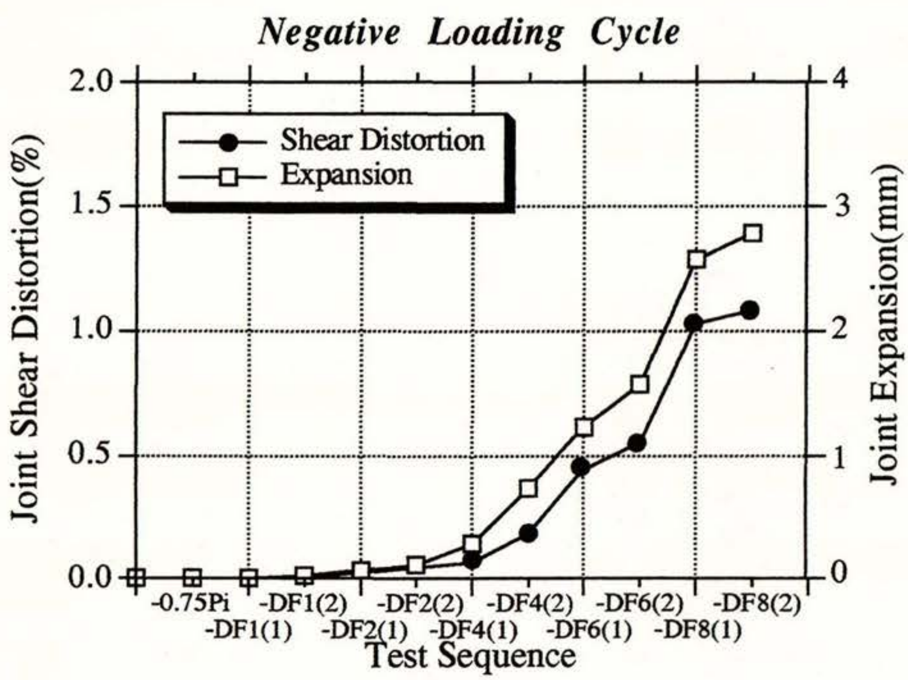

Fig.7.11 Joint Shear Distortion and Expansion of Specimen O6

joint expansion measured during both the positive and negative loading cycles were almost the same during the test.

7.2.8 Decomposition of Horizontal Displacement

The components of the horizontal displacement at the peak of the selected loading cycles are expressed as a percentage of the storey drift angle in Fig.7.12. The procedures for calculating those components were explained in Section 3.8.

Until loading to DF of 2, the main contribution was the beam flexural displacement. The beam flexural displacement contributed approximately 50 to 60% of the imposed storey drift angle in the loading to DF of 1. In the loading to DF of 2, in which plastic hinge was formed in the beam, the component of the beam flexural displacement increased to 75 to 90%. In the second cycle of loading to DF of 4, the contribution by beam flexure started to decrease as shown in Fig.7.12. Its contribution was only 20 to 30% in the loading to DF of 8. On the other hand, the component of the beam shear displacement began to increase in the loading to DF of 6 for the negative loading cycle, indicating that beam shear behaviour became dominant.

In the loading to DF of 2, the contribution of the joint shear distortion increased gradually, especially for the positive loading cycle, that was during beam negative moment. In the first cycle of loading to DF of 4, the joint shear contributed to the storey drift by 20% in the positive loading cycle. The contribution by joint shear continued to increase and its contribution was about 30% for the positive loading cycle and 20% for the negative loading cycle, respectively.

No measurements were made for the column displacement. Considering that the uncounted components were mainly due to column displacement, however, the contribution from column displacement started to increase in the second cycle of loading to DF of 4, in which the bond splitting cracks along the column bars were observed in the joint.

7.3 SPECIMEN O7

7.3.1 Introduction

Specimen O7 had the beam bars which were not bent into joint core. The ratio of the theoretical ideal flexural strength of the column to that of the beam was 2.00 during beam positive moment and 1.37 for beam negative moment, respectively. When the plastic hinge mechanism was formed in the beam, the ideal storey horizontal load strength P_i was 42kN

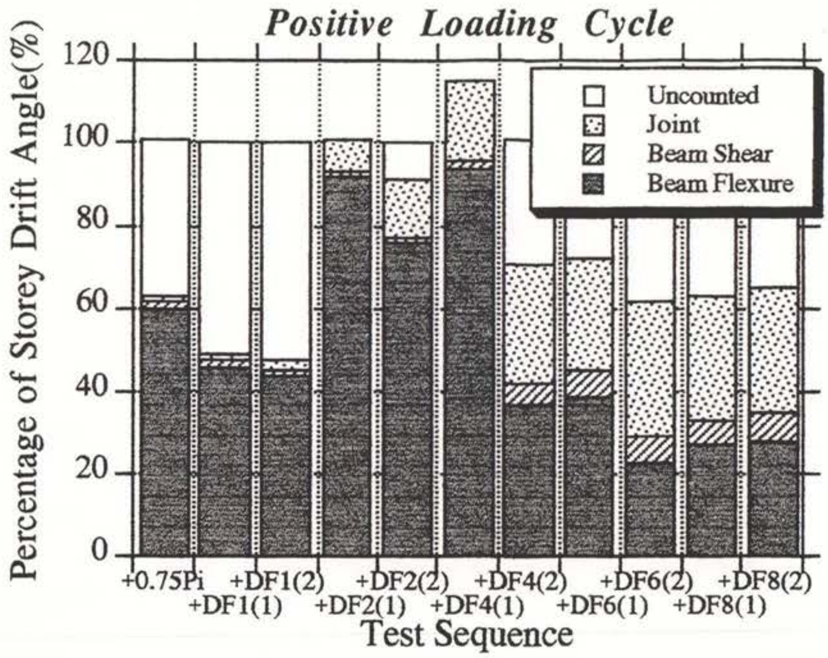

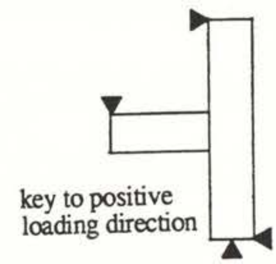

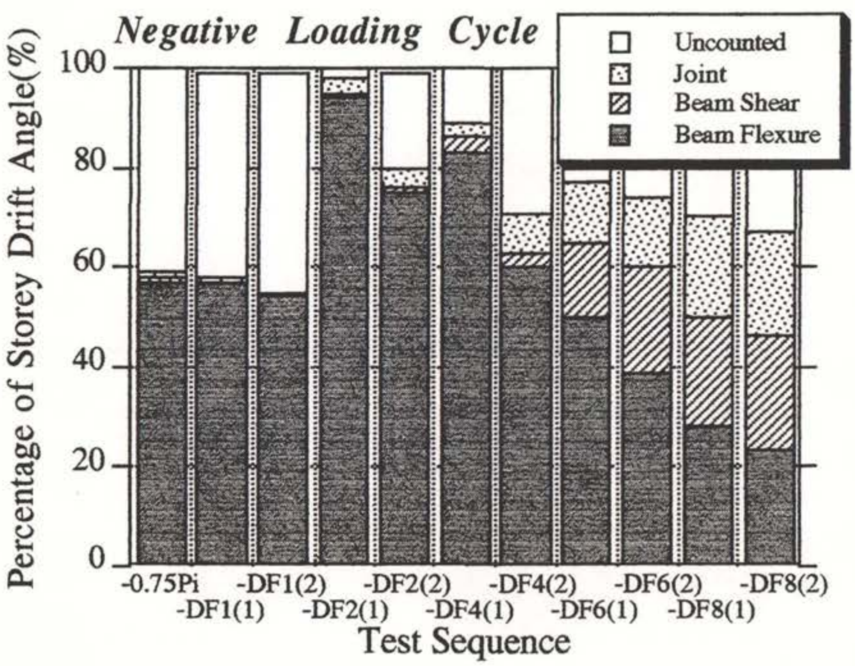

Fig.7.12 Component of Storey Drift Angle of Specimen O6

during beam positive moment and 61kN during beam negative moment. The compressive cylinder strength of the concrete was 31.0MPa at the time testing.

7.3.2 General Behaviour

Observed cracking after testing and the storey shear force versus horizontal displacement relationship are shown in Figs.7.13 and 7.14, respectively. Crack patterns observed at the peak of the selected loading cycles are shown in Fig.7.15.

In the loading to $\pm 0.5P_i$, flexural cracks initiated in the beam. Also observed were column flexural cracks at the column face.

In the loading to $\pm 0.75P_i$, beam and column flexural cracks extended and the number of those cracks also increased. Flexural-shear cracks formed in the beam. In the positive loading cycle, joint diagonal tension cracks initiated(see Fig.7.15(a)). The diagonal tension cracks were less inclined to the column axis when compared with those observed for Specimen O6(see Fig.7.13(d)). The maximum horizontal load strength of the test specimen for the positive loading cycle was 46kN in this loading cycle. The maximum horizontal load strength was only 75% of the theoretical ideal horizontal load strength of the specimen.

In the loading to displacement ductility factor DF of 1, the joint diagonal tension cracks opened wide and extended to the column flexural compression zone of the top column(see Fig.7.15(b)). The width of the diagonal tension cracks in the joint was measured to be 1.3mm. No new cracks were observed in the beam. As shown in Fig.7.14, the horizontal load strength was not increased in the positive loading cycles greater than DF of 1. Bond splitting cracks also initiated along the outer column bar at this loading stage.

In the loading to DF of 2, joint diagonal tension cracks were developed in the negative loading cycle(see Fig.7.15(c)). Those cracks opened wide and extended to the column flexural compression zone of the bottom column in conjunction with bond splitting cracks along the outer column bars. The maximum width of the joint diagonal tension cracks was 5mm for the positive loading cycle and 1.8mm for the negative loading cycle, respectively. In the negative loading cycles, the maximum horizontal load strength attained was 37kN, which was 88% of the ideal horizontal load strength. In the second loading cycle, some strength degradation was observed in the hysteresis loops(see Fig.7.14).

In the loading to DF of 4, joint diagonal tension cracks extended into the beam and opened wide to a maximum crack width of 11mm for the positive loading cycle and 7mm for the negative loading cycle, respectively. Bond splitting cracks along the column bars connected with the joint diagonal cracks which also extended and opened wide. The diagonal

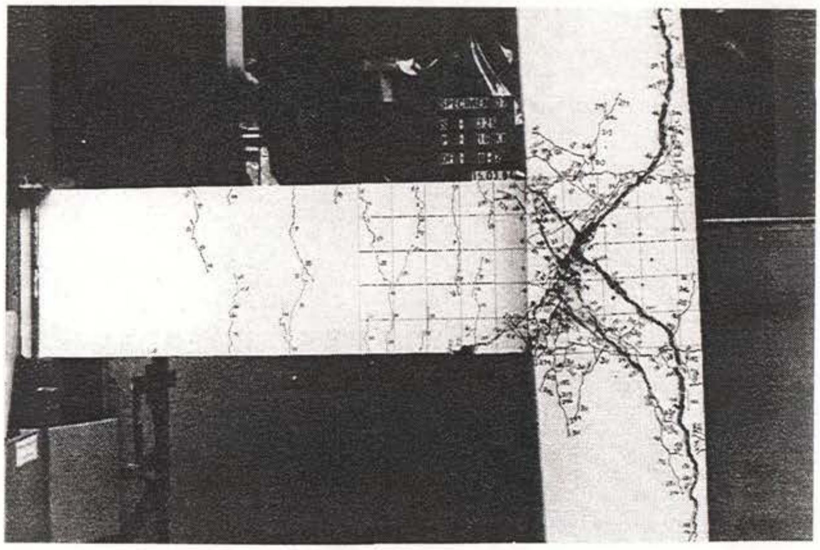

Fig.7.13 Observed Cracking of Specimen O7
at first cycle of DF=-8

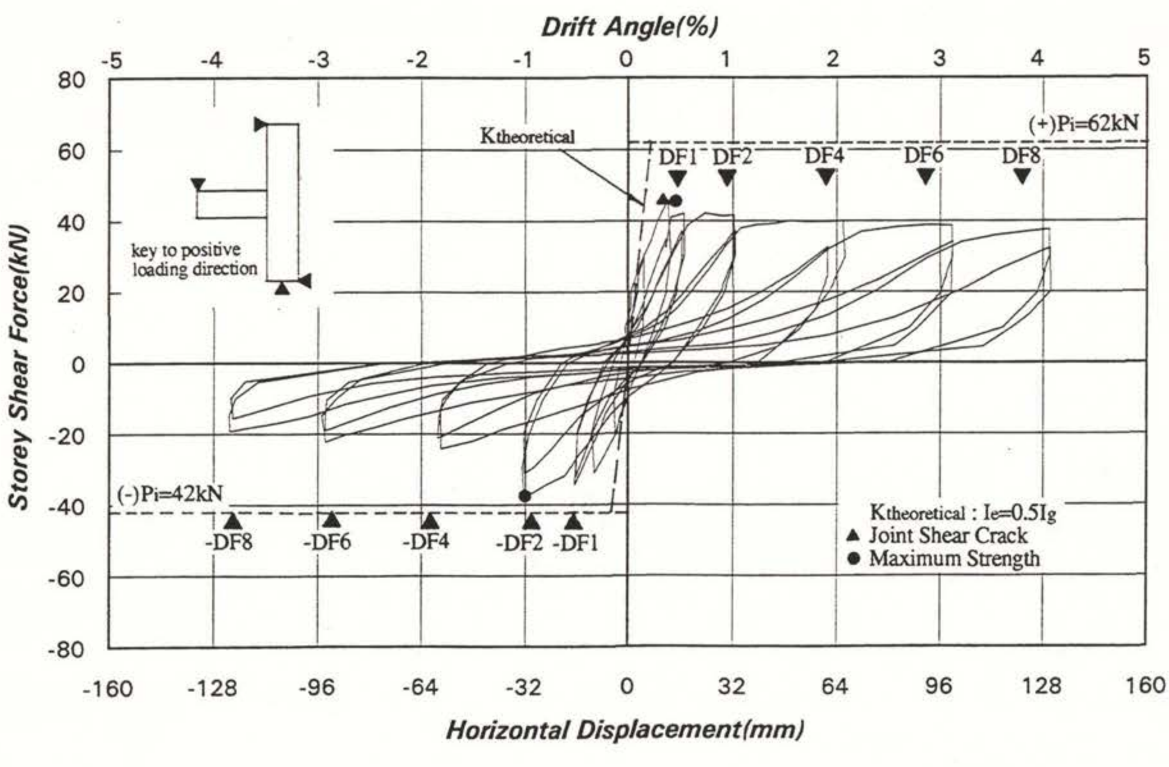

Fig.7.14 Storey Shear Force versus Horizontal Displacement Relationship
for Specimen O7

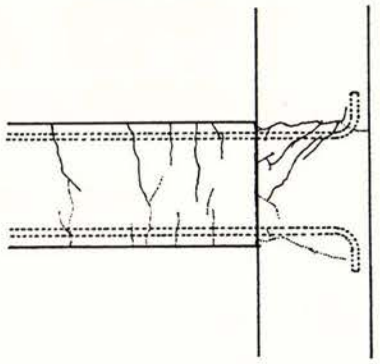

(a) at the peak of 0.75Pi
(R=0.36%)

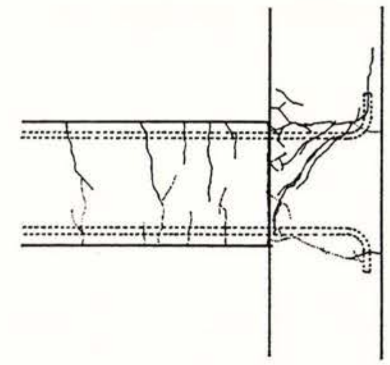

(b) at the peak of second cycle, DF=1
(R=0.48%)

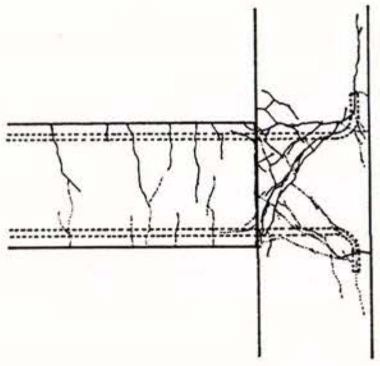

(c) at the peak of second cycle, DF=2
(R=0.96%)

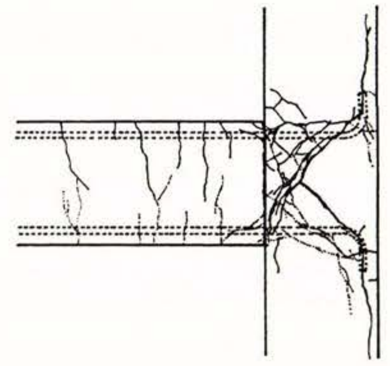

(d) at the peak of second cycle, DF=4
(R=1.92%)

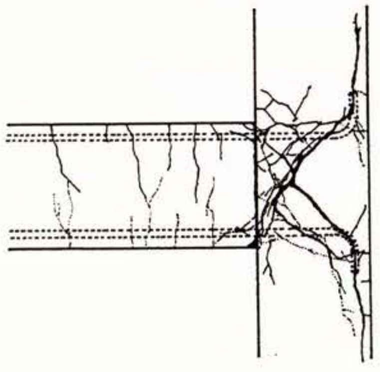

(e) at the peak of second cycle, DF=6
(R=2.88%)

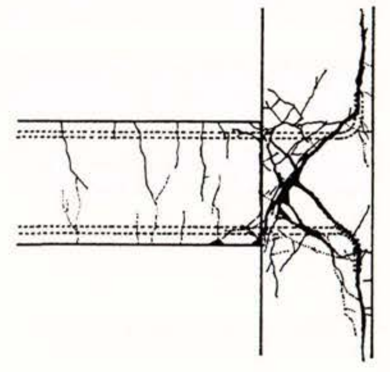

(f) at the peak of second cycle, DF=8
(R=3.84%)

Fig.7.15 Observed Cracking of the Joint(Specimen O7)

tension cracks opened in the horizontal direction rather than the perpendicular to the crack, indicating that the beam was being pulled out from the cracks. In the beam, only the flexural cracks along the column face tended to open. Severe strength degradation was observed for the negative loading cycle as shown in Fig.7.14.

In the loading to DF of 6, the maximum width of joint diagonal tension cracks was measured to be 18mm for the positive loading cycle and 11mm for the negative loading cycle. The joint deteriorated severely due to diagonal tension cracking(see Fig.7.15(e)). The bond splitting cracks along the column bar were also serious. The flexural crack of the top column opened wide in the positive loading cycle while that of the bottom column opened in the negative loading cycle. The damage in the beam was very slight.

In the loading to DF of 8, the maximum width of larger than 25mm was measured for the joint diagonal tension cracks. Concrete started to spall off in the joint. The joint suffered severe diagonal tension cracking. For the negative loading cycle, shear failure of the bottom column initiated in this loading cycle(see Fig.7.15(f)).

It was evident that for Specimen O7 in which the beam bars were not bent into the joint core, the response was governed by the joint shear failure. The test specimen could not reach the ideal horizontal load strength when the beam plastic hinge mechanism was developed. The maximum horizontal load strength of the specimen was determined by the development of the initial diagonal tension cracking in the joint for both loading directions.

7.3.3 Initial Stiffness

The theoretical initial stiffness was calculated for Specimen O7 as follows:

$$K_{theoretical}=8.5kN/mm$$

The theoretical stiffness $K_{theoretical}$ is shown in Fig.7.14. The measured stiffness at 75% of the theoretical ideal storey horizontal load strength of the test specimen was 3.8kN/mm for the positive loading cycle and 3.0kN/mm for the negative loading cycle. The average value of the stiffnesses estimated for the positive and negative loading cycles was comparable to that estimated for Specimen O6. However, the average value was only 40% of the theoretical stiffness. The effect of the configuration of the hooks at the ends of the beam bars on the initial stiffness of the test specimen was found to be insignificant.

The yield displacement of the test specimen was obtained to be 15.2mm which could be converted to 0.48% in terms of the storey drift angle. As observed for Specimen O6, the test specimen was rather flexible according to the current code requirements[SANZ 1992].

7.3.4 Beam Behaviour

7.3.4.1 Longitudinal Beam Bar Strains

Strains profiles measured along the longitudinal beam bars are shown in Figs.7.16 and 7.17. Fig.7.16 illustrates the strain profiles obtained from the wire strain gauge readings while Fig.7.17 shows those measured from the linear potentiometers attached to the steel rods welded to the beam bars.

In the elastic loading cycles, the gradual increase in tensile strains along the beam bars was observed. In the subsequent loading cycles, however, the strains measured in the beam were fairly constant as shown in Figs.7.16 and 7.17. Yield strain was not reached in the beam plastic hinge region. In the loading to DF of 2, however, the top beam bar in the joint reached the yield strain. In the loading to DF of 6, the bottom beam bar also yielded in tension in the joint core. The tensile strains along the beam bars measured in the joint core increased as the test progressed.

It could be concluded that the beam remained essentially in the elastic range during the test. However, the beam bars in the joint core were subjected to large tensile strains due to the joint diagonal tension cracking.

7.3.4.2 Slip of Beam Bars

The slip of the top and bottom beam bars in the joint are shown in Fig.7.18. The clear distance between two adjacent ribs of the beam bar was 11mm. The extension of the hook beyond the bend was four times bar diameter. The slip was estimated from the concrete at the column centre line as mentioned in Section 3.7.4.

As could be expected, the beam bars tended to be pulled out when subjected to tensile force. When subjected to compressive force, however, the bars did not push in. In the late loading stage, the bars tended to be pulled out even when subjected to compressive force as shown in Fig.7.18. The slip of top beam bar was small and relatively constant during the test. On the other hand, the slip of bottom beam bar increased gradually from the loading to DF of 2. The maximum slip was measured to 4.4mm for bottom beam bar.

In spite of the fact that the extension of the hook was only four times bar diameter, the slip measured from the column centre line was not so significant during the test.

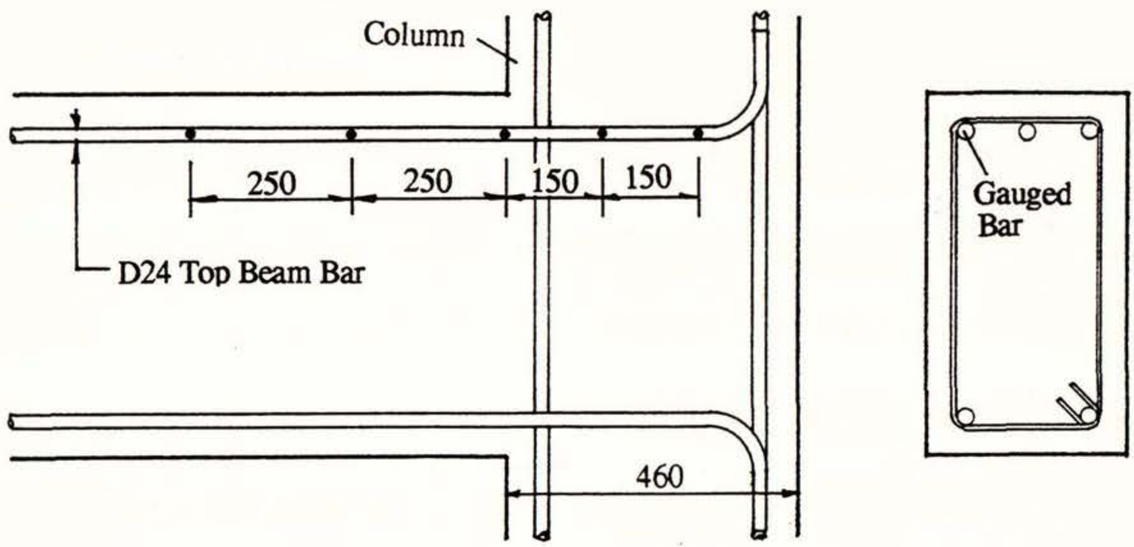

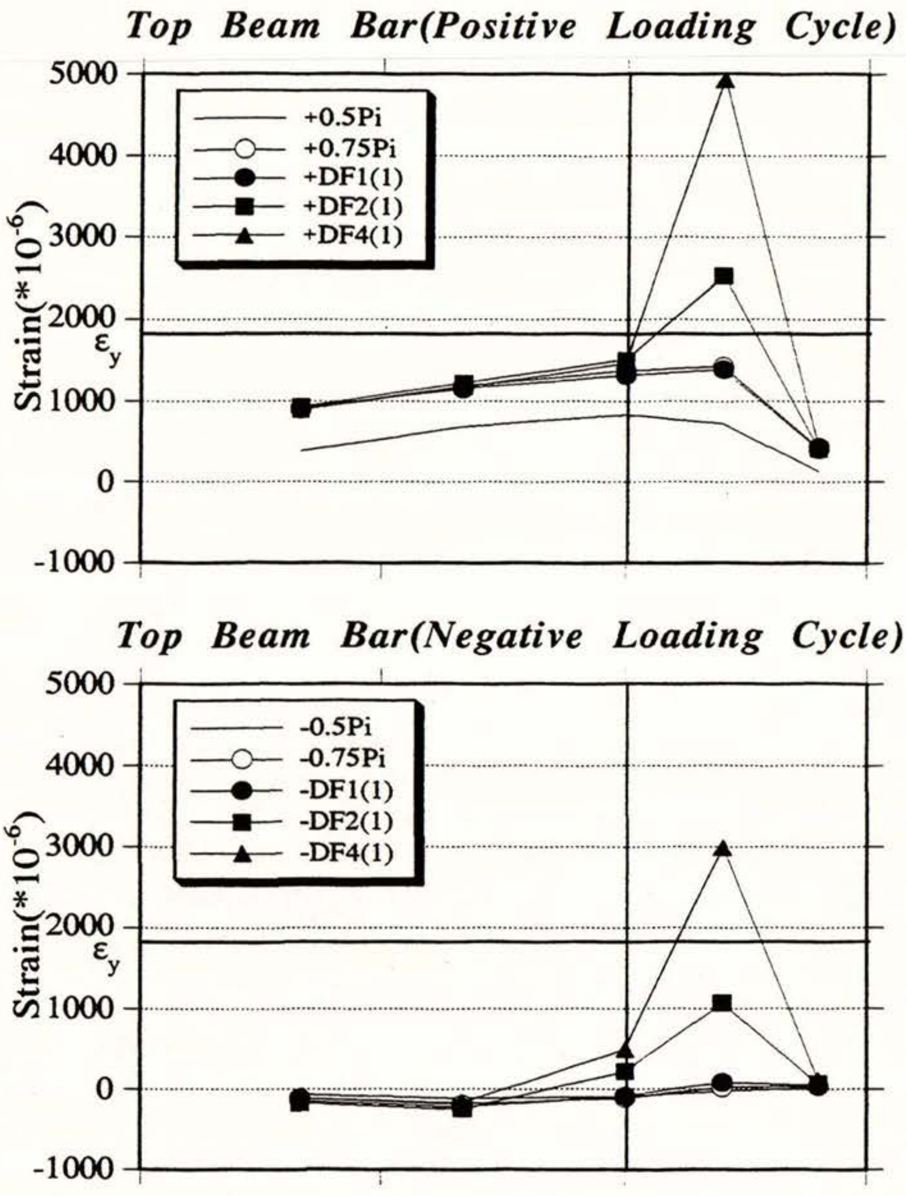

Fig.7.16(a) Strain Profiles of Top Beam Bar Measured by Wire Strain Gauges of Specimen O7

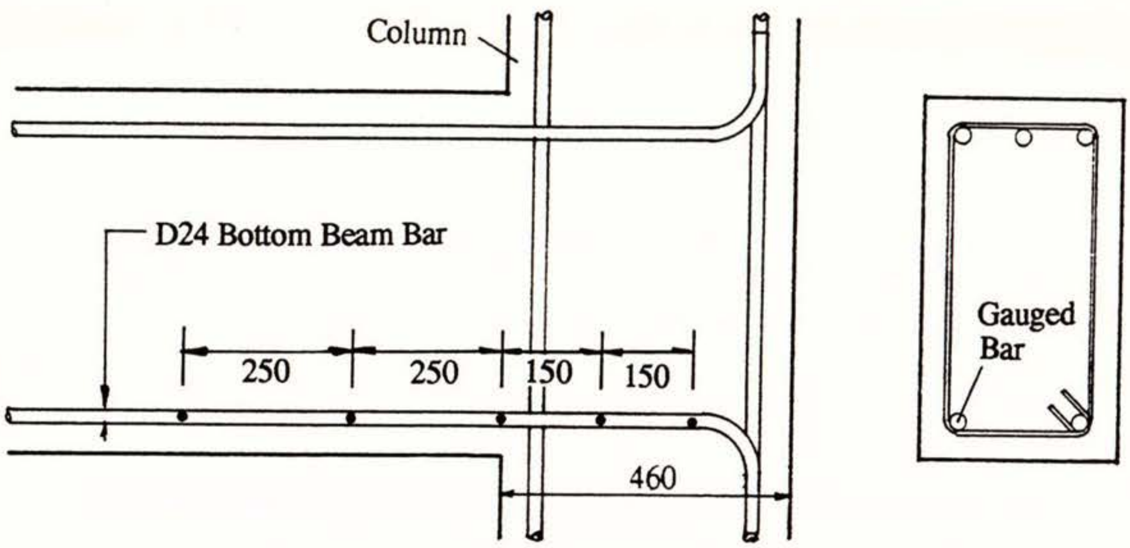

Bottom Beam Bar(Positive Loading Cycle)

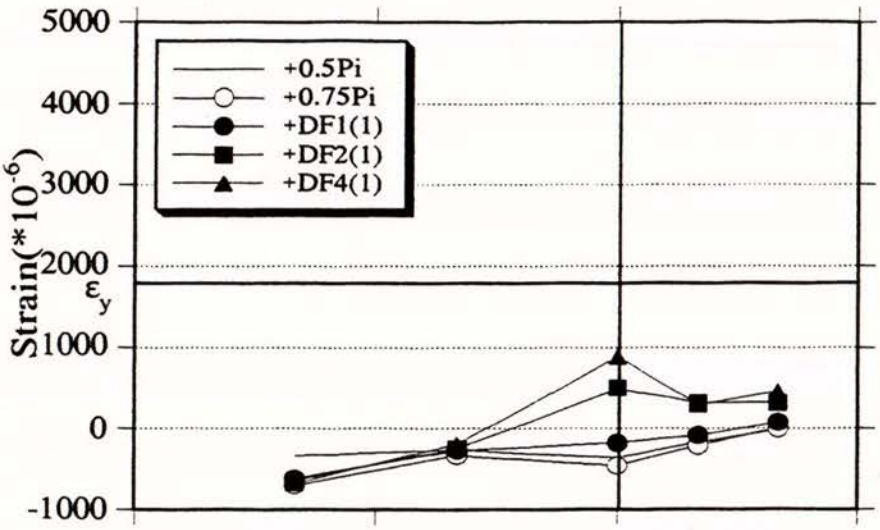

Bottom Beam Bar(Negative Loading Cycle)

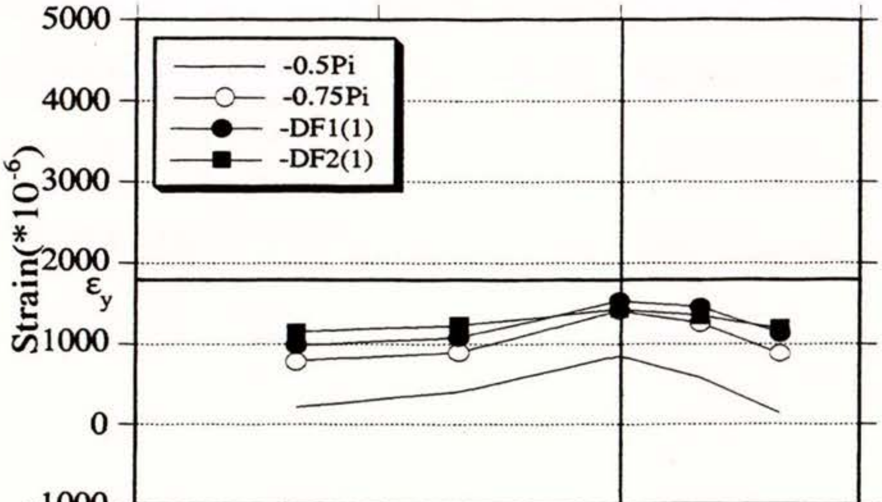

Fig.7.16(b) Strain Profiles of Bottom Beam Bar by Wire Strain Gauges
of Specimen O7

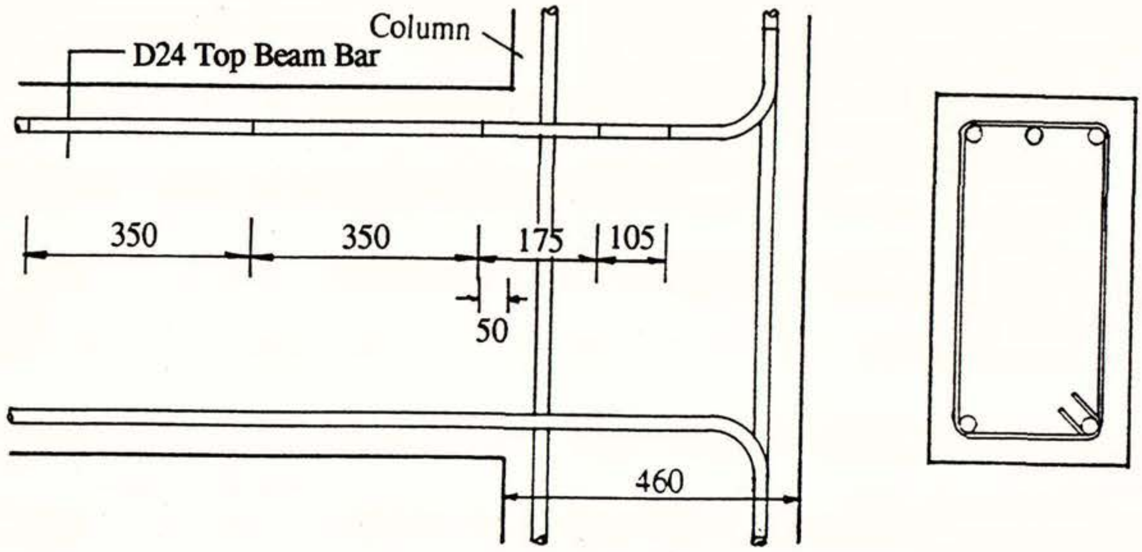

Top Beam Bar(Positive Loading Cycle)

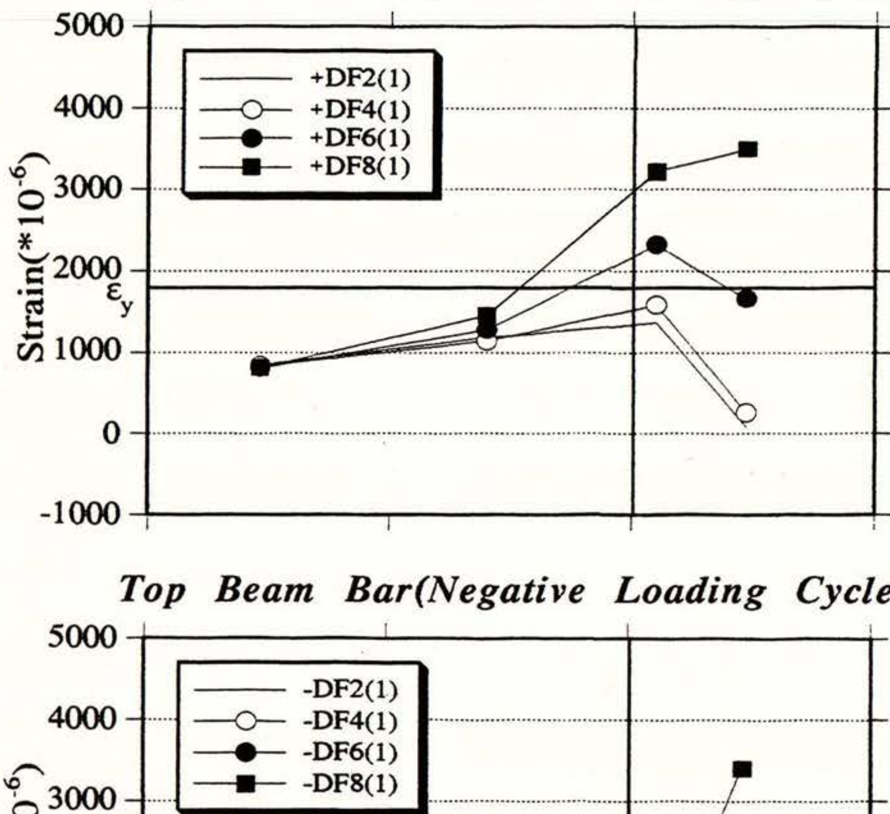

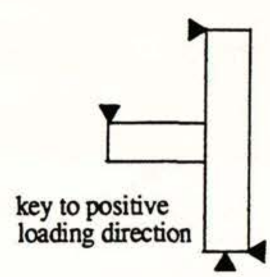

Top Beam Bar(Negative Loading Cycle)

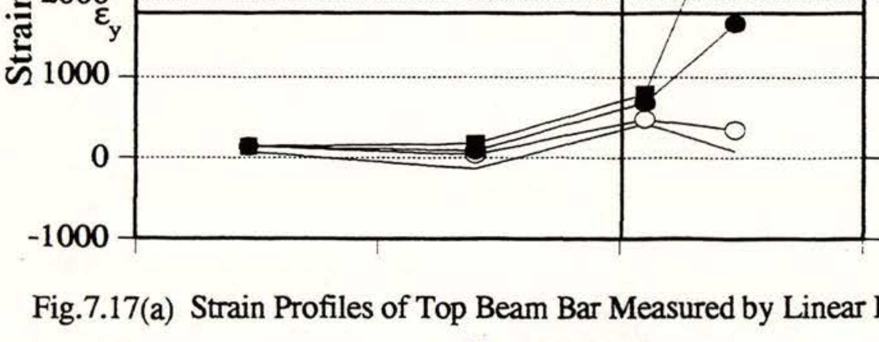

Fig.7.17(a) Strain Profiles of Top Beam Bar Measured by Linear Potensiometers of Specimen O7

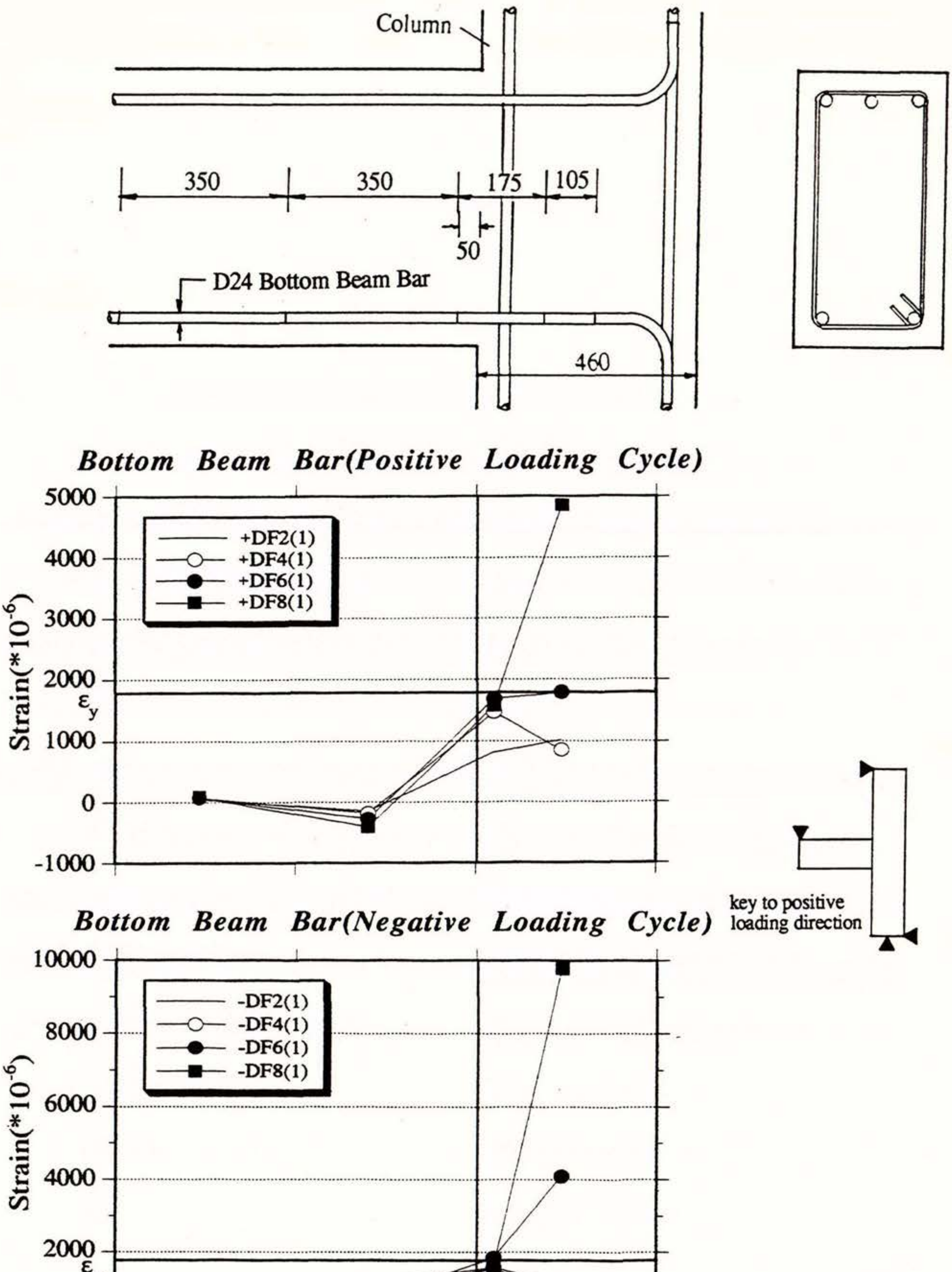

Fig.7.17(b) Strain Profiles of Bottom Beam Bar Measured by Linear Potensiometers of Specimen O7

Top Beam Bar

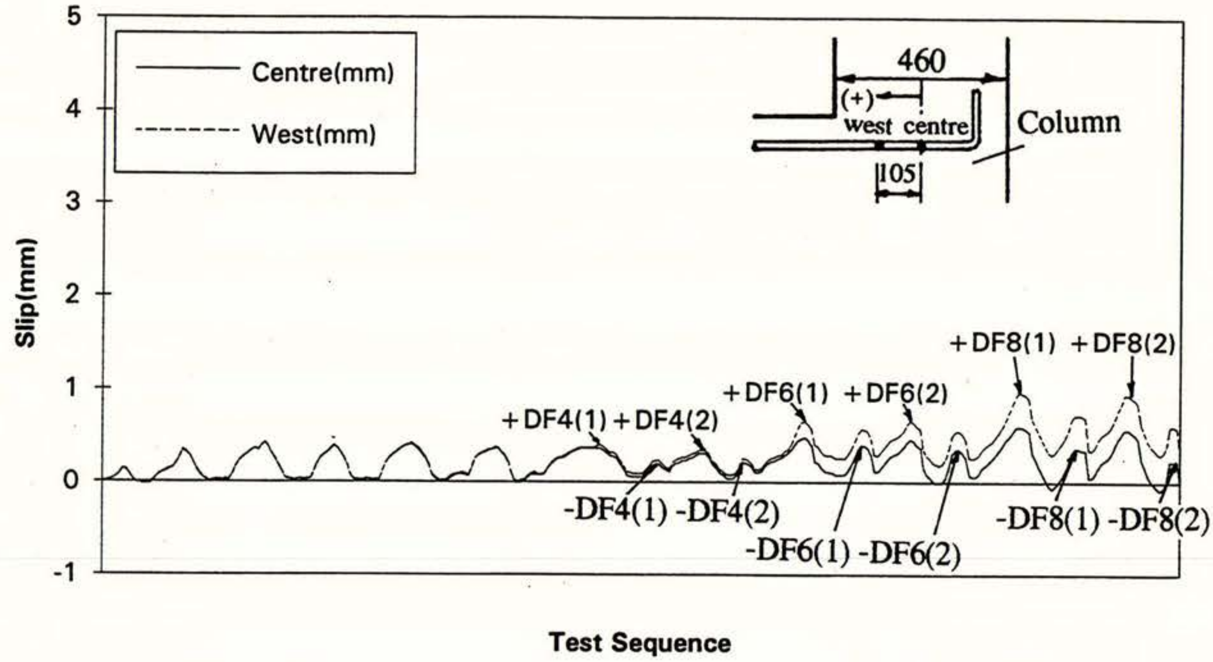

(a) Slip of Top Beam Bar

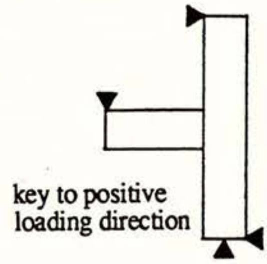

Bottom Beam Bar

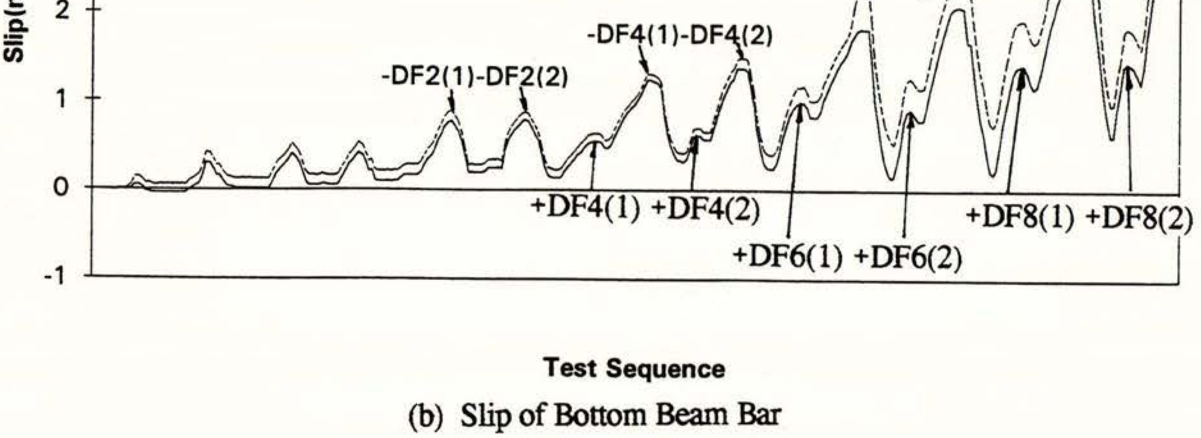

(b) Slip of Bottom Beam Bar

Fig.7.18 Measured Slip of Beam Bars of Specimen O7

7.3.4.3 Beam Shear Stress and Curvature

During the test, the maximum nominal shear stress in the beam was obtained to $0.10\sqrt{f'_c}$ during beam negative moment and $0.09\sqrt{f'_c}$ during beam positive moment, respectively, where f'_c is the measured concrete compressive strength. Those shear stresses were low enough not to result in diagonal tension cracks in the beam(see Fig.7.15(f)).

The maximum curvature obtained from the second set of the linear potentiometers from the column face was 0.003304(1/m) during beam positive moment and 0.004885(1/m) during beam negative moment. Those curvatures were far below the yield curvature calculated from the section analysis, which were 0.004925(1/m) during beam positive moment and 0.005768(1/m) during beam negative moment, respectively.

It was again shown that the beam of Specimen O7 was essentially elastic during testing.

7.3.5 Column Behaviour

7.3.5.1 Introduction

In the loading to DF of 1, bond splitting cracks along the outer column bar initiated. Those cracks were connected to the joint diagonal tension cracks and opened wide as the test progressed.

7.3.5.2 Longitudinal Column Bar Strains

Fig.7.19 shows the strains measured along the longitudinal column bars in the joint. Those strains were obtained from the wire strain gauges. For the outer column bar, small compressive or tensile strains were measured in the column flexural compression zone until loading to DF of 1. In the loading to DF of 2, the tensile strains measured at the column flexural compression zone gradually increased. However, the strains measured on the outer column bar were relatively small as shown in Fig.7.19(a).

For the inner column bar, the strain measured at the centre of the joint increased rapidly in the loading to $+0.75P_i$ in which diagonal tension cracks initiated. In the subsequent loading cycles, the tensile strains increased consistently along the column bars through the joint as shown in Fig.7.19(b). In the loading to DF of 2, the inner column bar at the beam face reached the yield strain. It could be expected that the bond forces of the inner column bars were reduced over the flexural tension zone.

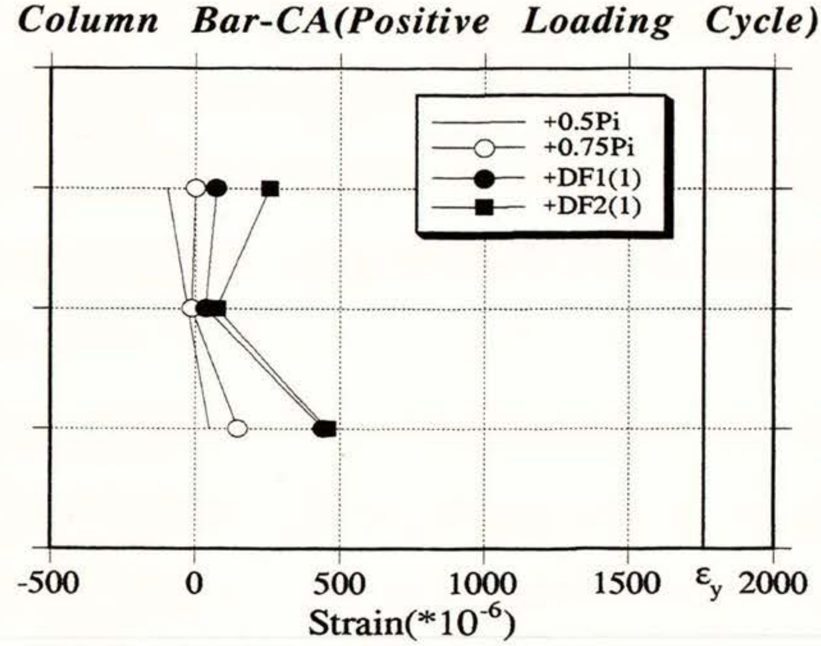

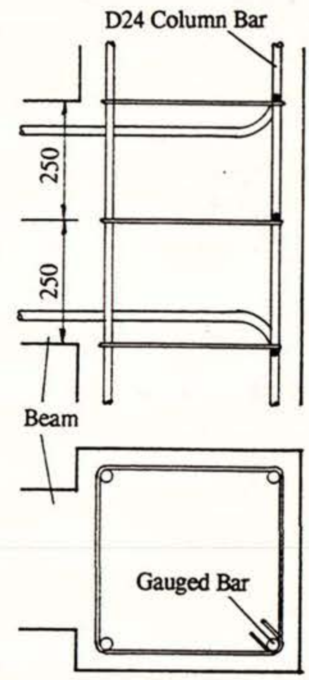

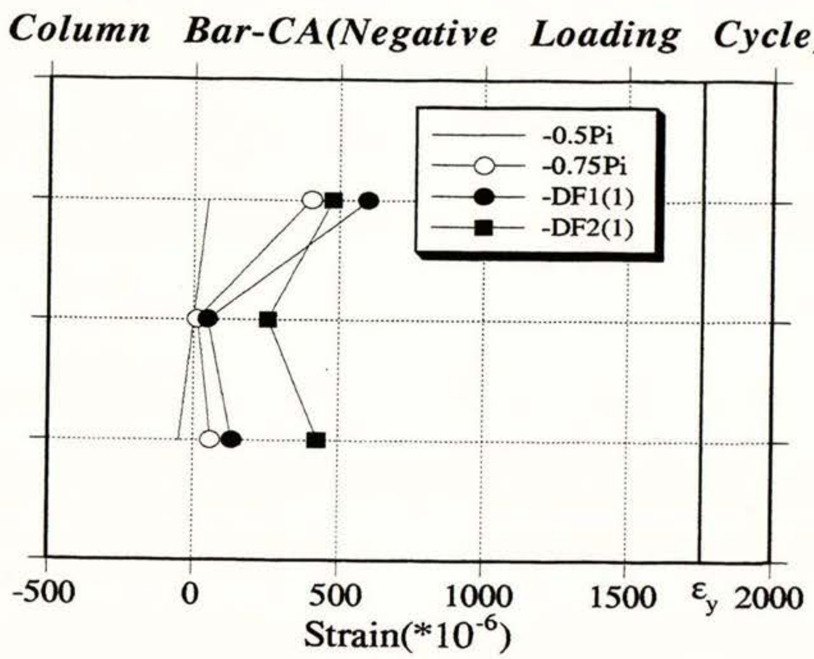

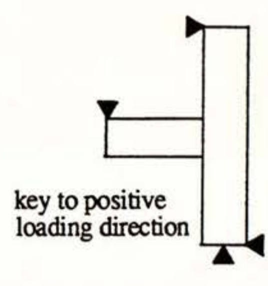

Fig.7.19(a) Strain Profiles of Column Bar of Specimen O7

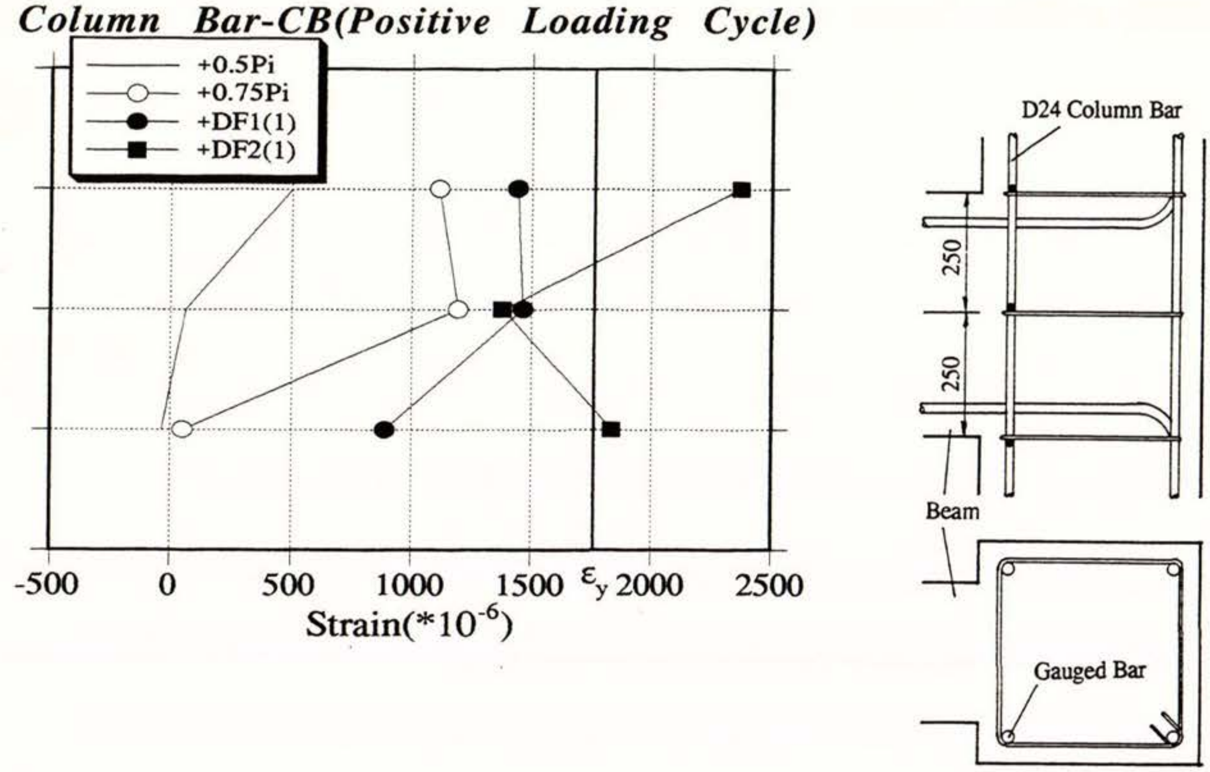

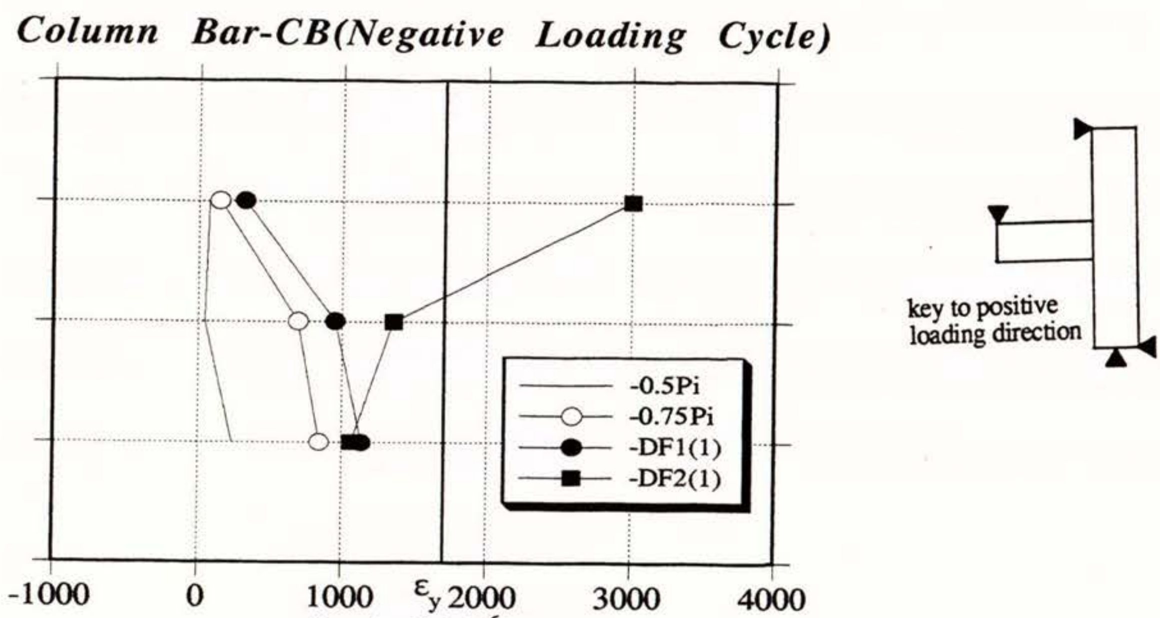

Fig.7.19(b) Strain Profiles of Column Bar of Specimen O7

As was observed for Specimen O6, the inner column bar was more stressed than the outer column bar. This is mainly due to the effect of the forces applied from the beam. Typical feature of the column bar strain profiles observed for Specimens O6 and O7 with small amount of transverse reinforcement in the joint core was that the strains measured along the column bars in the joint were relatively large after diagonal tension cracking. When compared with the column bar strain profiles in the joint measured for Specimen O6, the column bars at the flexural compression zone were more stressed in tension for Specimen O7 with the beam bars not bent into the joint core.

7.3.6 Joint Behaviour

7.3.6.1 Introduction

Joint diagonal tension cracks initiated at the nominal horizontal joint shear stress of $0.25\sqrt{f'_c}$ in the loading to $+0.75P_i$, where f'_c is the measured concrete compressive strength. In the subsequent loading cycles, joint diagonal tension cracks extended and opened wide. The maximum horizontal load strength of the test specimen was determined by the initial diagonal tension cracking. Maximum nominal horizontal joint shear stress was calculated to $0.25\sqrt{f'_c}$ for the positive loading cycle and $0.21\sqrt{f'_c}$ for the negative loading cycle, respectively.

7.3.6.2 Joint Hoop Strains

The strains of three hoops located in the joint region are shown in Fig.7.20 at the peak of the selected loading cycles.

After the diagonal tension cracks formed in the joint, the joint hoop strains increased gradually as the test progressed. This trend became more evident in the loading to DF of 1 for the positive loading cycle and DF of 2 for the negative loading cycle. In the loading to DF of 2, the hoops located at the beam face yielded.

When compared with the strain profiles measured for Specimen O6 shown in Fig.7.10, the hoops located at the beam face were more stressed than that at the centre of the joint. When top beam bars were in tension, the strain of the hoop measured near the top beam bars became large. It is likely that the hoops outside of, but close to, the joint core have an important role for the seismic performance of the joint with beam bars not bent into the joint core. This will be discussed later in this chapter.

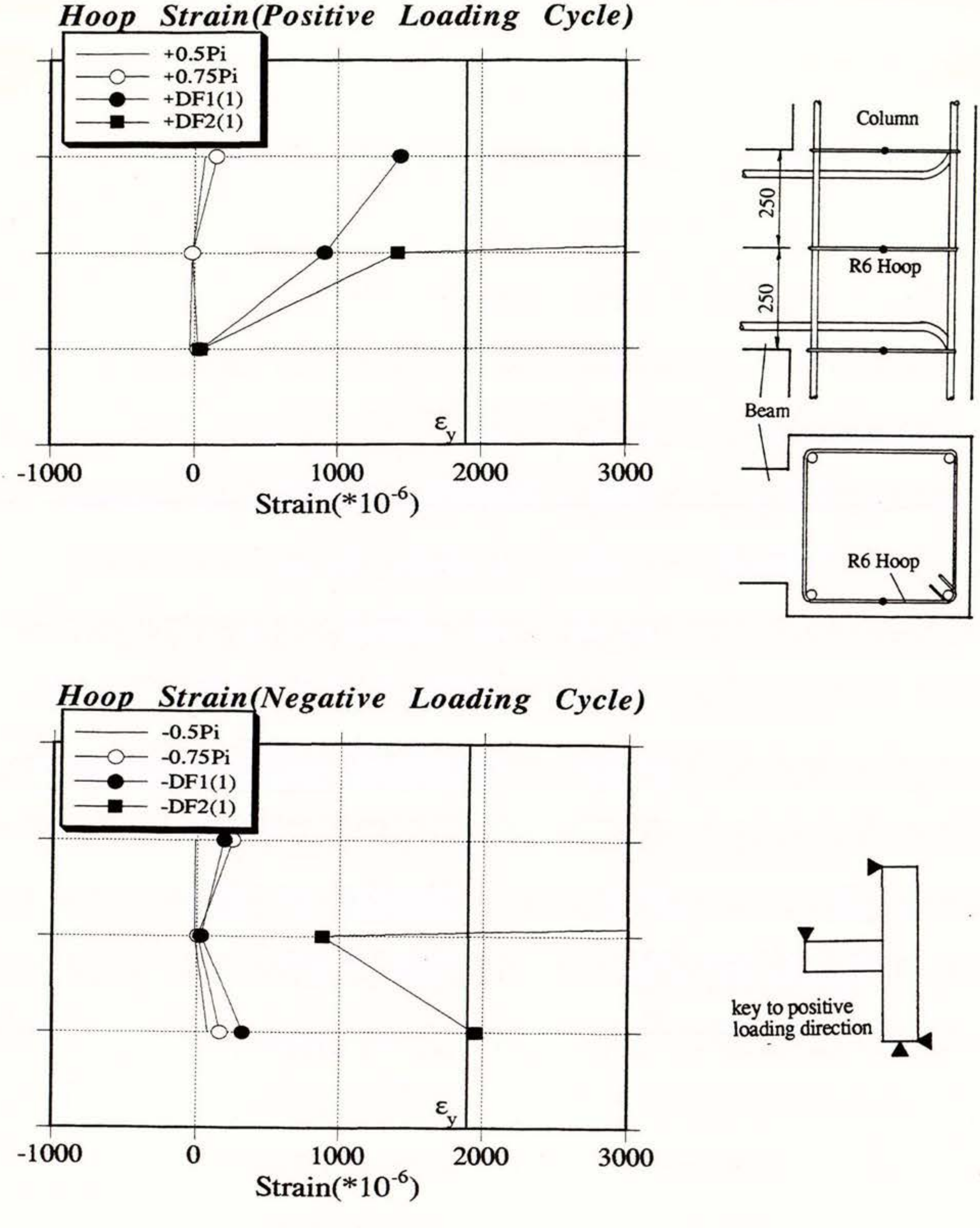

Fig.7.20 Hoop Strain Profiles of Specimen O7

7.3.6.3 Joint Shear Distortion and Expansion

Fig.7.21 shows the joint shear distortion and expansion. The joint shear distortion gradually increased after the loading to $+0.75P_i$ for the positive loading cycle and in the loading to DF of 2 for the negative loading cycle. In those loading cycles, diagonal tension cracks were observed in the joint. From the loading to DF of 4, joint shear distortion together with joint expansion increased rapidly. The maximum joint shear distortion was measured to approximately 3.5% in the loading to DF of 8. The maximum joint shear distortion and expansion measured for both the positive and negative loading cycle became comparable in the late loading stage. The maximum joint shear distortion and expansion obtained from Specimen O7 were much larger than those for Specimen O6.

7.3.7 Decomposition of Horizontal Displacement

The components of the horizontal displacement at the peak of the selected loading cycles are expressed as a percentage of the storey drift angle in Fig.7.22. No measurements were made for the column displacement.

In the loading to $\pm 0.75P_i$, the beam flexural displacement accounted for 35 to 50% of the storey drift. This value was somewhat smaller than that calculated for Specimen O6. Subsequent loading cycles resulted in the reduction of the contribution of beam flexure. In the loading to DF of 8, its contribution was only 6% for the positive loading cycle and 1% for the negative loading cycle. The contribution of beam shear displacement was negligible during the test.

The contribution of joint shear distortion increased rapidly from the loading to DF of 1 for the positive loading cycles and DF of 2 for the negative loading cycles. A significantly large contribution due to joint shear to the storey drift is clearly shown in Fig.7.22. The maximum contribution of joint shear distortion was 66% for the positive loading cycle and 68% for the negative loading cycle.

When compared with the test results for Specimen O6, it was evident that the joint shear behaviour governed the overall response of Specimen O7. Hence the beam-exterior column joint with beam bar anchorages typical of older reinforced concrete building frames, in which the beam bars were not bent into the joint core was identified to be possibly the weak link of the frame when subjected to severe seismic loading.

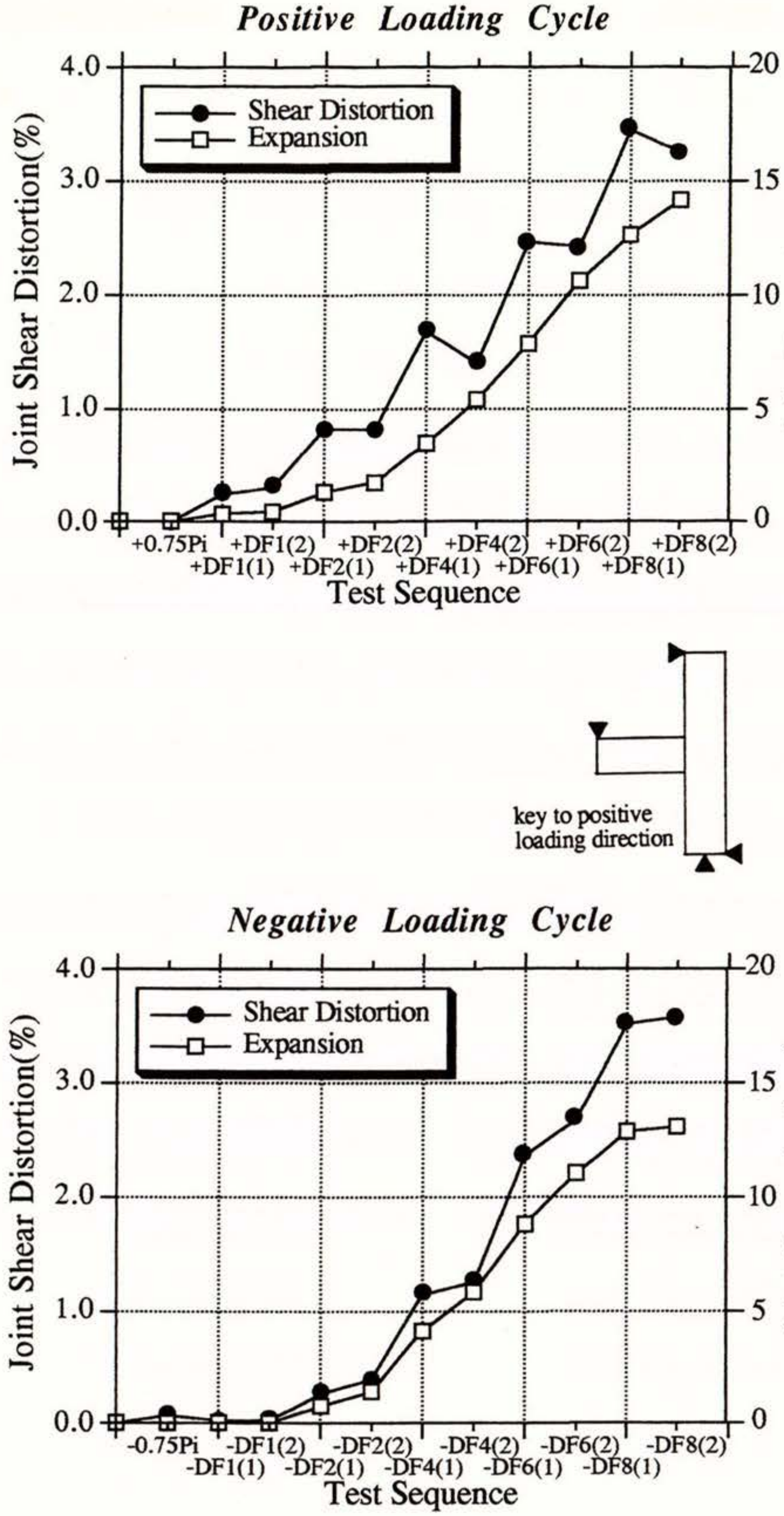

Fig.7.21 Joint Shear Distortion and Expansion of Specimen O7

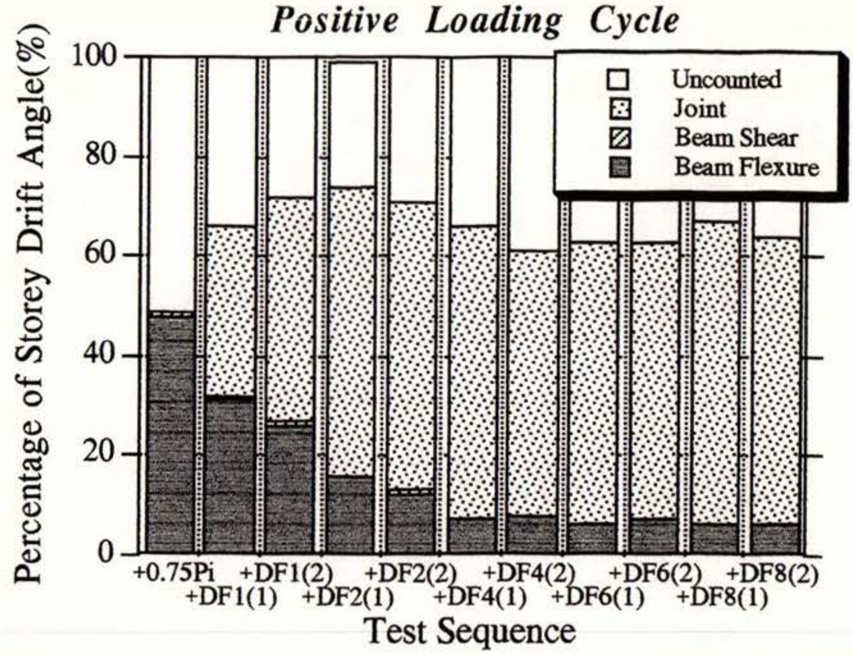

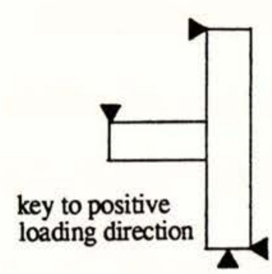

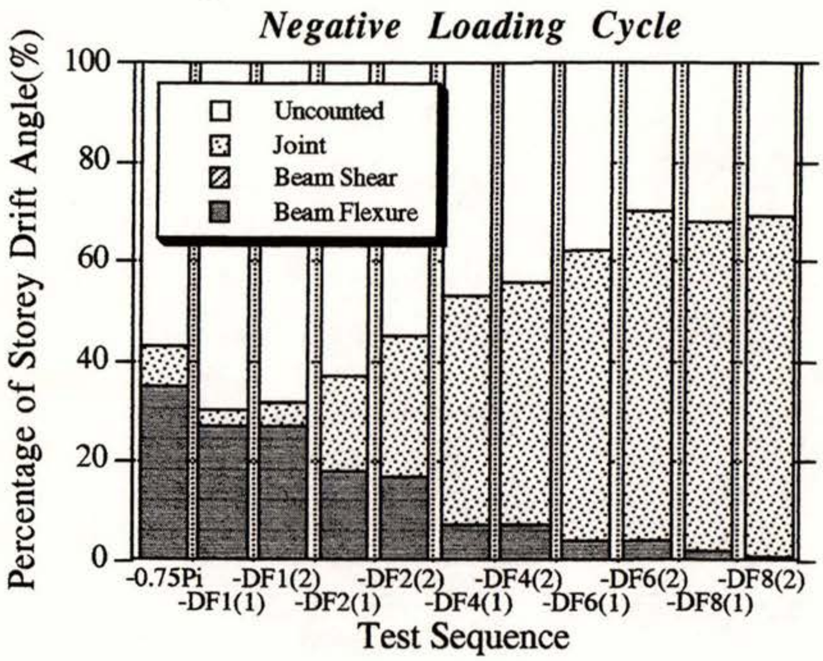

Fig.7.22 Component of Storey Drift Angle of Specimen O7

7.4 DISCUSSION OF THE TEST RESULTS

The test results clearly demonstrated that the anchorage details of the longitudinal beam reinforcement in beam-exterior column joints have a profound effect on their seismic behaviour. This section describes possible stress paths in the exterior joint under seismic loading, depending on the configuration of the beam bar anchorage in the exterior column.

The external actions and corresponding internal forces generated around the exterior joint, in which the beam bars are bent into the joint core are shown in Figs.7.23 and 7.24. At an exterior joint, reliance for beam bar anchorage is placed primarily on a standard hook rather than the straight portion of the beam bars between the inner column face and the hook. This results in a force introduced into the joint core concrete by means of bearing and bond stresses within the bend. The reinforcement detail shown in Fig.7.24 is arranged in such a way that a diagonal compression strut, which is the main shear resisting mechanism in a beam-exterior joint, can develop between the bend of the top beam bars and the lower right-hand corner of the joint, where compression forces in both the horizontal and vertical directions are introduced. The tensile stresses are generated at right angle to this compression strut which is responsible for the diagonal tension cracking in the joint core(see Fig.7.23).

A lightly reinforced beam-exterior joint with such beam bar anchorage in the exterior column, as is Specimen O6, can have a ductile response under simulated seismic loading when the maximum nominal horizontal joint shear stress was approximately $0.31\sqrt{f'_c}$, where f'_c is the measured concrete compressive strength.

The internal forces in the exterior joint, in which the beam bars are not bent into the joint core is illustrated in Fig.7.25. This anchorage detail of the beam bars in joints commonly used in older building frames is not sufficient to develop the diagonal compression strut mechanism within the joint along a corner to corner diagonal. This is because the diagonal compression strut cannot be locked into the bend of the beam bars in the joint core as shown in Fig.7.24. Instead, the outer column bars are pushed outward. The diagonal tension crack pattern observed for Specimen O7 with beam bars not bent into the joint core was less inclined to the column axis than that for Specimen O6, indicating the difficulty of developing the diagonal compression strut mechanism illustrated in Fig.7.24. In addition, the beam bar anchorage shown in Fig.7.25 does not act to restrain the opening of the joint diagonal tension cracks.

For the configuration of the beam bar anchorage typical of older building frames, an alternative stress path may be possible, in which the angle of the strut, beginning at the lower right-hand corner of the joint, is less inclined as is illustrated in Fig.7.25. This is possible only when adequate column hoops are placed close to the joint core to provide the necessary

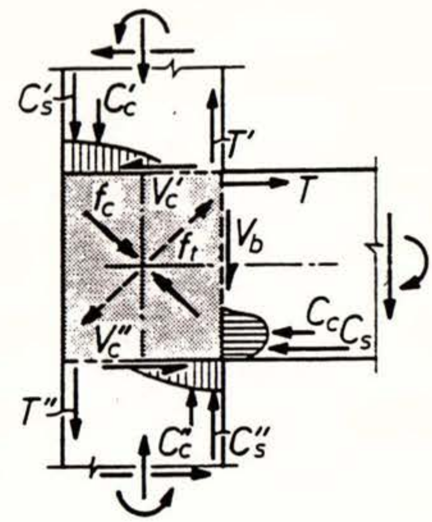

Fig.7.23 Forces Acting on a Beam-Exterior Column Joint

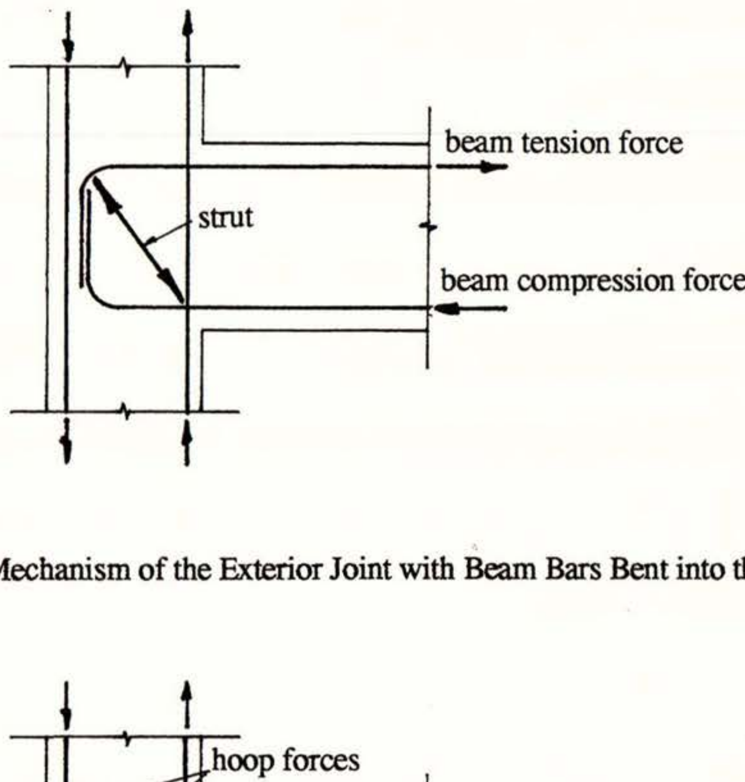

Fig.7.24 Diagonal Strut Mechanism of the Exterior Joint with Beam Bars Bent into the Joint

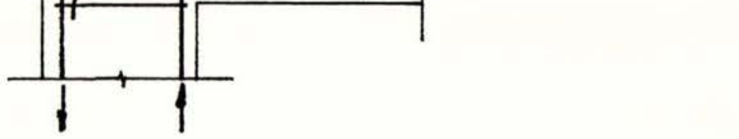

Fig.7.25 An Alternative Shear Mechanism of the Exterior Joint
with Beam Bars not Bent into the Joint

horizontal tie forces for the diagonal compression strut. The hoop forces at the inner face of the column will balance another strut which is much more inclined to the column axis from the bend of the top beam bar as shown in Fig.7.25. The hoop strain profiles observed for Specimen O7 during the test support this alternative stress path. For Specimen O7, however, the amount of column hoops close to the joint core was not large enough to sustain this mechanism since only one set of 6mm diameter hoops could participate in this mechanism, resulting in the joint shear failure.

The beam-exterior column joint with beam reinforcement details shown in Fig.7.25 failed in shear shortly after the diagonal tension cracking in the joint[Taylor 1974, Nilsson and Losberg 1976 and Scott et al 1994]. Therefore, the cracking strength of the joint can be used to assess the shear strength of joints with such reinforcing details.

7.5 CONCLUSIONS

The following conclusions are reached on the basis of the test results from Specimens O6 and O7.

(1) It was identified that the seismic response of beam-exterior column joints was significantly influenced by the reinforcement details of the beam bars in the joint core.

(2) Specimen O7 was a beam-exterior column joint subassemblage with the longitudinal reinforcement details commonly used in older reinforced concrete building frames, that is the beam bars were not bent into the joint core. The test conducted on Specimen O7 demonstrated that the seismic performance of the joint would be unsatisfactory in terms of stiffness, strength and ductility capacity of the structure. This is mainly due to the inadequate configuration of the beam bar anchorage and the inadequate amount of shear reinforcement in the joint region.

(3) Specimen O7 failed in shear shortly after the commencement of diagonal tension cracking in the joint. The maximum measured horizontal load strength of the test specimen was only 75 to 88% of the ideal horizontal load strength calculated based on the measured material strengths. The cracking strength can be used to estimate the shear strength of exterior joints with such beam anchorage details.

(4) Specimen O6 was detailed in the same manner as Specimen O7 except that the beam bars were bent into the joint core. The test on Specimen O6 showed a stable and ductile response with plastic hinge forming in the beam. Although only a small amount of shear reinforcement was provided in the joint core, the joint shear stress level of approximately

$0.31\sqrt{f'_c}$ was small enough not to result in severe reduction of the horizontal load strength of the specimen under severe seismic loading.

(5) Beam bars not bent into the joint core do not efficiently develop the diagonal compression strut within the joint along a corner to corner diagonal. For an exterior joint with such reinforcing details, however, a diagonal compression strut mechanism may develop with the strut less inclined to the column axis when column hoops are adequately placed close to the joint core. If the column hoops had been adequately placed in the vicinity of the joint core of the test specimen, a better seismic performance might have been obtained. Further research is necessary in this aspect.

CHAPTER 8

ANALYSIS OF THE TEST DATA AND RECOMMENDATIONS FOR SEISMIC ASSESSMENT METHODS

8.1 INTRODUCTION

In this chapter, the seismic behaviour of beam-column joints is discussed with the support of the experimental data obtained from this study as well as from other research. Emphasis is placed on the behaviour of joints without shear reinforcement. Bond mechanisms along the beam and column bars in the joint are first examined and then the shear resisting mechanisms of the joint without shear reinforcement are discussed. Methods to assess the seismic response of such joints are suggested. The seismic behaviour of beams with small quantities of transverse reinforcement is also described in terms of the curvature ductility factor and shear strength.

8.2 SEISMIC BEHAVIOUR OF INTERIOR JOINTS WITHOUT SHEAR REINFORCEMENT BEFORE DIAGONAL TENSION CRACKING

8.2.1 Forces and Crack Pattern

Fig.8.1 shows forces acting on a joint and internal stresses in a joint core induced under seismic action . Crack pattern for a joint before diagonal tension cracking occurs is shown in Fig.8.2(a). Within a joint core, internal diagonal tensile and compressive stresses denoted by f_t and f_c in Fig.8.1 are generated. When column cross sections are very large and/or when beams with very small amounts of flexural reinforcement are used, the diagonal tensile stresses in the beam-column joint core may be small enough not to develop diagonal tension cracks in the joint core. Such joints were demonstrated by the retrofitted Specimen R3 in which the joint shear stress was reduced by enlarging the column cross section(see Fig.8.3).

8.2.2 Bond Behaviour in Joints

Under severe earthquake loading, the bond stresses along the bars passing through the beam-interior column joints of early building frames investigated can be large, because high d_b/h_c ratios are often used for the joints, where d_b is beam bar diameter and h_c is the column depth. Generally these bond stresses considerably exceed the allowable bond stresses associated with the code requirements for development length. In such cases, premature bond deterioration and slip of bars within the joint may initiate under seismic loading. This results in loss of the stiffness of the frame due to the fixed-end rotation of members adjacent to

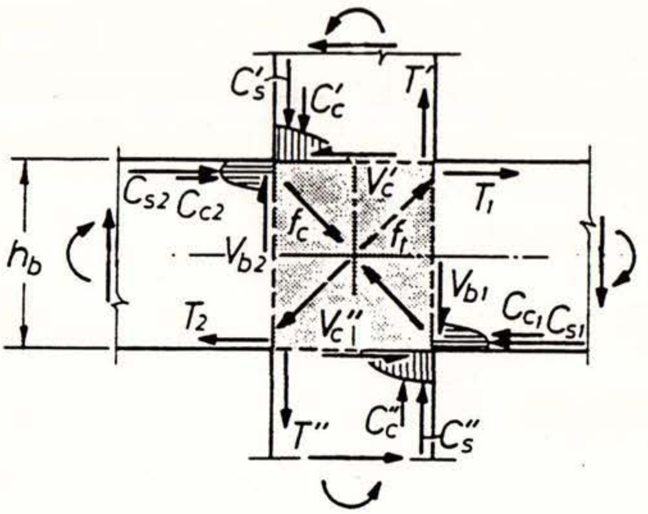

Fig.8.1 Forces Acting on a Beam-Interior Column Joint

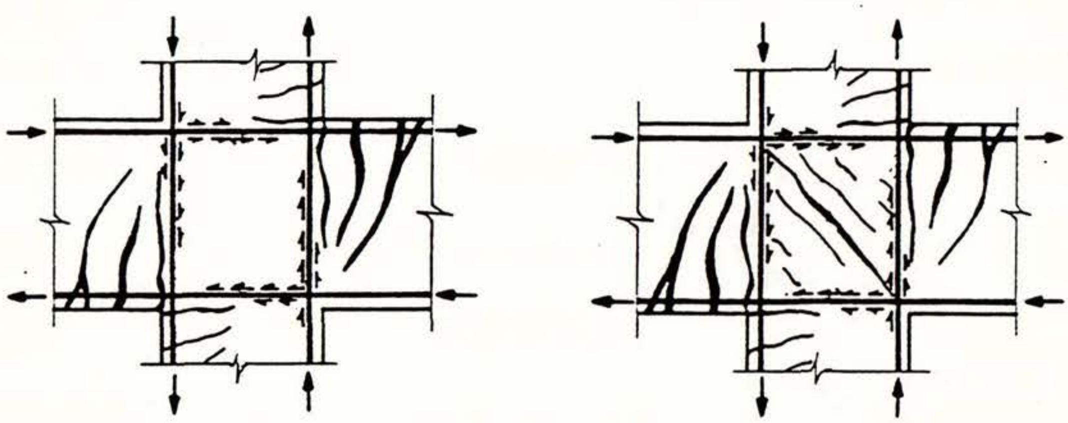

(a) Before Joint Diagonal Tension Cracking (b) After Joint Diagonal Tension Cracking

Fig.8.2 Crack Pattern for a Joint without Shear Reinforcement

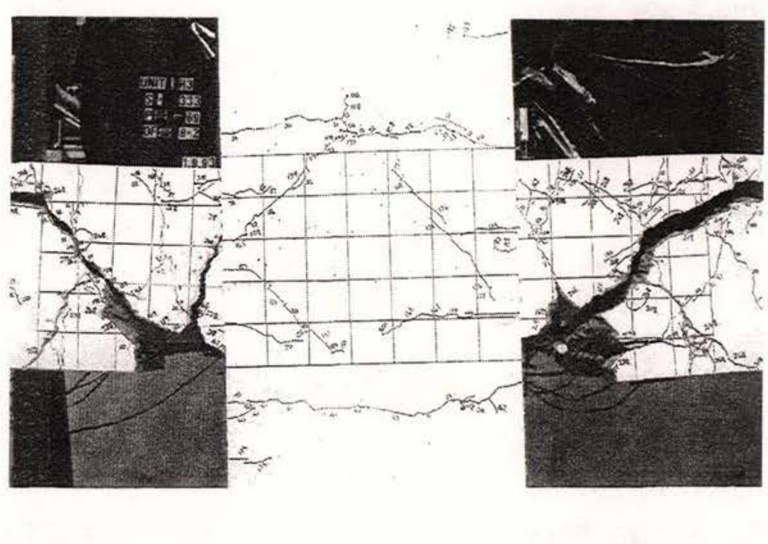

Fig.8.3 Observed Cracking of the Joint without Shear Reinforcement for Specimen R3

the joint[Popov 1984]. The bond response of longitudinal bars, both in beams and columns, plays a very important role in the shear behaviour of a beam-column joint. Therefore, the bond mechanisms along the bars within the beam-interior column joint are first examined. Only the bond of deformed bars is dealt with in this study.

Bond is made up of three components:

(1) Chemical adhesion
(2) Friction
(3) Mechanical interlocking between concrete and steel.

Bond of deformed bars depends primarily on mechanical interlocking. The other two components are of secondary importance[Lutz and Gergely 1967]. Various factors that affect the bond strength, and bond stress and slip relationship for the bars subjected to high-intensity reversed cyclic forces have been identified by several researchers[Eligehausen et al 1983, Ismail and Jirsa 1972(a) and (b)].

Flexural cracks along the beam and column face, which are inevitably formed even during the elastic response of a structure to an earthquake, affect the bond conditions along the bars near the cracks in the joint. Under such condition, some separation of the bar and concrete occurs in the vicinity of the cracks. Internal inclined cracks, which are referred to as "bond cracks", initiate shortly after flexural cracks form due to the tensile stresses in the concrete around the bars caused by the high bearing pressure on the concrete in front of the lugs[Luzs and Gergely 1967]. After the initiation of bond cracks, the bond transfer from steel to the surrounding concrete is mainly achieved by the mechanical interlocking between concrete and steel which induces inclined compressive forces spreading from the deformation lugs into concrete. Circumferential tensile stresses are also generated, which causes splitting cracks[Goto 1971]. The bond stress at a splitting crack in unconfined concrete may be as low as $0.36\sqrt{f'_c}$ MPa [Eligehausen et al 1983]. This value reveals that even under elastic loading cycles, bond splitting cracks may be formed in a beam-column joint.

In pullout tests specially designed not to restrain the concrete near the loading end, the bond behaviour in the vicinity of a crack running perpendicular to the bar was investigated by Hayashi et al 1985. The local bond stress and slip relationship obtained from such tests indicates that the maximum bond stress and bond stiffness were significantly lower near the crack than at some distance from the crack. No bond deterioration was observed at the distance of four or more times bar diameters from the crack. It can be expected that even in elastic loading cycles, bond deterioration along the beam and column bars in a beam-column joint initiates in the vicinity of the flexural cracks at the column and beam faces.

Formation of bond splitting cracks can be suppressed if the concrete surrounding the bars is effectively confined. That is, the bond performance can be significantly improved by confinement[Eligehausen et al 1983]. In a beam-column joint region, such confinement may be achieved by lateral pressure from the compressive stresses in beams and columns adjacent to the joint and also from the transverse reinforcement orthogonally placed in the joint, when available. The compression force transverse to the direction of the embedded bars in the beam-column joint is normally available from flexural compression force induced in the adjacent members during earthquake loading. Joint transverse reinforcement, in the form of intermediate column bars and joint hoops, can prevent a failure along a potential splitting crack. They cannot prevent the initiation of splitting cracks, but they enable bond action to be maintained along the cracks. This results in a more ductile local bond stress versus slip relationship[Eligehausen et al 1983].

The bond performance of bars passing through beam-column joints is not only influenced by the factors mentioned above. Bar diameter, concrete strength, clear distance between bars, casting direction of concrete and position of bars(top bar effect) also affect the bond behaviour along the bars in the joint.

For longitudinal beam bars passing through a joint, the least bond resistance is found in the region where the bars are in tension in the joint because of the early formation of splitting cracks caused by high circumferential tensile stresses and because of the flexural cracks at the column face. The vertical column bars there in tension also cause adverse effects. The best bond performance is achieved in the region of the longitudinal beam bars near the end of the joint where the bars are in compression. This is because at this end, confinement is provided by the flexural compression force of the columns acting on the joint. The expansion of the compressed bar due to the Poisson effect also causes compressive stresses in the concrete surrounding the bar.

A transition region between the tension and compression regions of the bar exists in a beam-column joint[Eligehausen et al 1983]. It should be noted that bond performance in the transition region of the joint without vertical and horizontal reinforcement crossing the interior of the joint will be significantly inferior to that of a well designed joint, since no confinement is provided in that region. Therefore, a more severe bond condition can be expected along beam and column bars in a joint without intermediate vertical bars and without horizontal transverse reinforcement.

8.2.3 Shear Mechanisms in Joints

As mentioned in Section 8.2.1, diagonal tensile and compressive stresses develop in the joint core concrete of a beam-column joint when subjected to seismic loading. The diagonal compressive stresses are introduced into the joint core mainly by beam and column concrete compressive forces due to flexure. On the other hand, bond forces along the main beam and column bars transmitted into the joint core induce the diagonal tensile stresses in the joint core concrete. When bond stresses are high enough to cause significant bond deterioration, the "compression" reinforcement of the beams and columns may actually be in tension at or near the face of the joint. In that case, beam or column concrete compressive forces due to flexure will need to be increased to compensate for the reduction of the compression force in the "compression" reinforcement, resulting in an increase in the diagonal compressive stresses in the joint core concrete and a reduction in the diagonal tensile stresses introduced into the joint core by bond forces.

When the nominal horizontal joint shear stress v_{jh} is small, diagonal tension cracks may not initiate in the joint core. Then the shear force transmitted into the uncracked joint core will be resisted by means of diagonal tensile and compressive stresses in the core concrete, irrespective of whether joint shear reinforcement is present or not.

The joint shear stress for the case when diagonal tension cracks initiates in the joint core is examined in the following sections, where the joint shear stress at cracking is expressed in terms of the nominal horizontal shear stress of the joint.

8.3 JOINT SHEAR STRENGTH AT THE STAGE OF DEVELOPING DIAGONAL TENSION CRACKING

8.3.1 Introduction

To assess the seismic performance of early building frames studied in this research, it is very important to investigate the shear strengths of the joints without shear reinforcement. As described in Chapter 2, one approach to the assessment of the shear strengths of such joints is to assume that the shear strength is reached at the stage of initial diagonal tension cracking in the joint core. When the concrete jacketing technique is used to retrofit an existing building frame, the placement of new horizontal joint shear reinforcement can be eliminated if the nominal joint shear stress can be reduced to a level at which diagonal tension cracking does not occur. The joint shear stress can be reduced by enlarging the column cross section. According to the test results in this study, the joint failure can be prevented by simply enlarging the joint section, without placing new hoops in the joint core. For example, the retrofitted Specimen R2 without new joint hoops in which the nominal joint shear stress v_{jh} was reduced to approximately $0.3\sqrt{f'_c}$ demonstrated almost the same behaviour as the retrofitted Specimen R1 with new joint hoops. The stress level $v_{jh}=0.3\sqrt{f'_c}$ corresponded approximately to the joint shear stress level at which diagonal tension cracks initiated in the joint core.

It is obviously of importance to determine the nominal joint shear stress at cracking for a wide range of variables, so as to assist designers with the assessment of likely joint behaviour. With this in mind the experimental data obtained from the eighty beam-interior column joints without transverse beams tested in Japan[Bessho et al 1986, Ohtsuki et al 1986, Goto et al 1987, Teraoka et al 1987, Kamimura and Nagatsuka 1988, Bessho et al 1989, Yamauchi et al 1990, Fujii and Morita 1990, Jinno et al 1991, and Kashiwazaki and Noguchi 1991] were used to investigate the nominal joint shear stress at cracking.

8.3.2 The Test Specimens Studied

The conditions of the specimens tested in Japan, from which the data were collected, were as follows:

(1) Normal weight concrete was used for the joint region
(2) Deformed steel bars were used for the longitudinal column and beam reinforcement
(3) Both the column depth h_c and the beam depth h_b were larger than 160mm
(4) The joint core was reinforced with either joint hoops and/or column intermediate bars
(5) Longitudinal beam and column bars passed through the joint core without special anchorage details or devices

The dimensions of the selected test specimens were 160×200mm to 500×500mm for the beam cross sections and 220×220mm to 570×570mm for the column cross sections. The aspect ratio of the joint h_c/h_b was 0.86 to 1.60. Most specimens were designed to develop beam plastic hinging.

The measured compressive cylinder strength f'_c of the concrete ranged from 23.3MPa to 92.6MPa while the yield strength f_y of the beam bar ranged from 345MPa to 1,069MPa.

8.3.3 Analysis of Test Data

The following factors can be considered to affect the joint shear stress at the stage when the joint diagonal tension cracks form:

(1) Compressive strength of concrete
(2) Axial load acting on the column
(3) Bond condition of the longitudinal beam bars passing through the joint

Horizontal joint shear forces V_{jh} were obtained from the beam face moments M_b and column shear forces V_c acting on the joint as illustrated in Fig.2.24. The nominal horizontal joint shear stress $v_{j,cr}$ at the onset of diagonal cracking was calculated from the effective joint area shown in Fig.2.25[SANZ 1982(a)] and is

$$v_{j,cr}=V_{jh.cr}/b_jh_j \tag{8.1}$$

where $V_{jh.cr}$ is the horizontal joint shear force at cracking, b_j is the effective joint width defined as shown in Fig.2.25 and h_j is the effective joint depth($=h_c$), where h_c is the overall column depth.

First, the effect of the concrete compressive strength on the joint shear stress at cracking was examined based on the measured concrete cylinder strengths. The results are plotted in Fig.8.4, with data points for the axial load levels $P_u/(A_g f'_c)$ of 0.12 and 0.18, where P_u is the axial load on column, A_g is the gross area of column cross section and f'_c is the measured compressive strength of concrete cylinder. From each group of the test data where the applied axial load levels are the same, it can be said that the nominal horizontal joint shear stress at first diagonal cracking increased with an increase in concrete compressive strength approximately linearly.

Also, when the same concrete compressive strength was used, the nominal joint shear stress at cracking increased with an increase in the axial load level. Fig.8.5 compares the nominal horizontal joint shear stresses at cracking for various axial compressive stresses on the column, P_u/A_g. Test units with different concrete compressive strengths are identified by different symbols. Again it is evident that the cracking stress was significantly affected by the level of axial compressive stress on the column. The increase in the cracking stress was approximately linear with an increase in the axial compressive stress and the rate of the increase was not affected by the concrete compressive strength significantly.

The effect of the bond condition along beam bars passing through the joint on the cracking stress was also examined. If the bond strength is assumed to be proportional to the square root of the concrete compressive strength f'_c, a bond index BI suggested by Kitayama et al 1987 can be used to gauge the severity of bond condition along beam bars passing through the joint. The beam bar bond index BI is defined as the total bar force to be transferred through the joint divided by the bar surface area and $\sqrt{f'_c}$, and is given by

$$BI = \frac{2f_y\frac{\pi d_b^2}{4}}{\pi d_b h_c\sqrt{f'_c}}$$

$$=\frac{f_y d_b}{2h_c\sqrt{f'_c}} \tag{8.2}$$

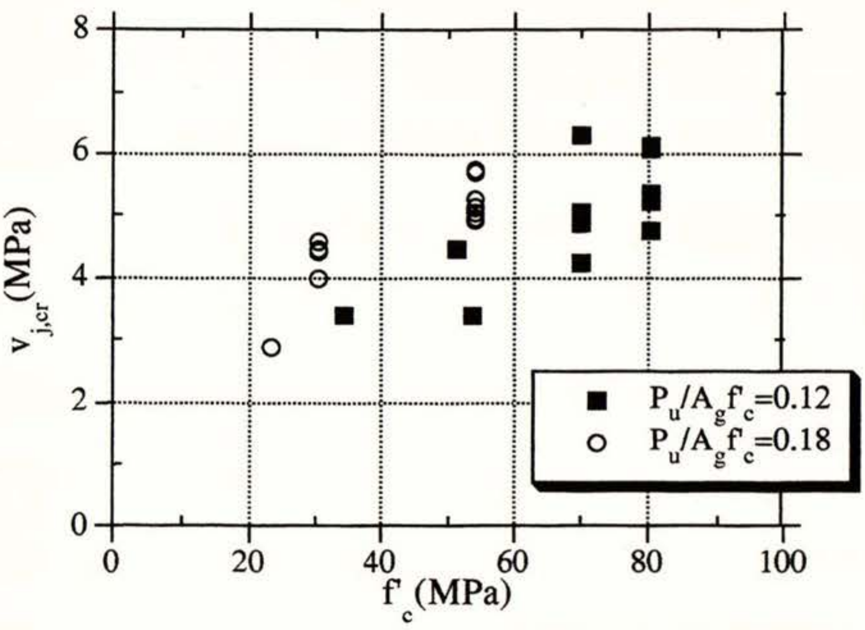

Fig.8.4 Concrete Compressive Cylinder Strength versus Joint Shear Stress at Cracking

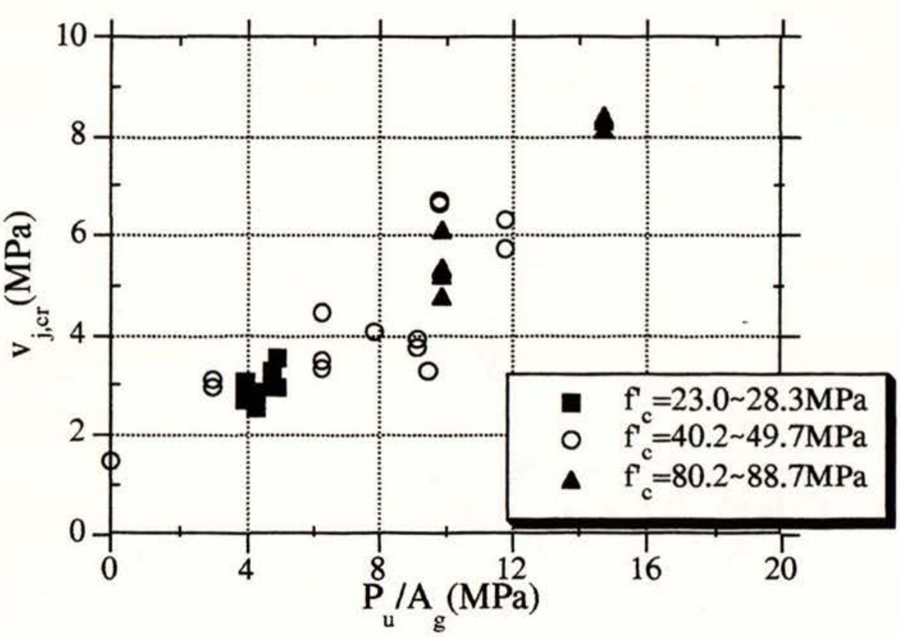

Fig.8.5 Axial Compression Stress on Column versus Joint Shear Stress at Cracking

where f_y : measured yield strength of beam bar, d_b : diameter of beam bar and h_c : column overall depth.

The nominal horizontal joint shear stress at cracking is plotted versus the beam bar bond index BI in Fig.8.6. No relationship can be seen between the cracking stress and the beam bar bond index from this figure. As mentioned in Section 8.2.3, however, good bond condition of beam bars(low BI values) in the joint results in larger diagonal tensile stresses in the joint core concrete when compared with poor bond condition(high BI value). In other words, poor bond condition of beam bars may increase the joint shear stress at cracking due to the reduction of diagonal tensile stress induced by beam bars. This was demonstrated by the test on a specimen conducted by Goto et al 1987. Beam bars in the joint of the specimen was set in vinyl tubes so that no steel bar forces could be transferred to the joint core concrete by means of bond. During the test, no joint diagonal tension cracks could be observed in spite of the maximum joint shear stress of $0.6\sqrt{f'_c}$ MPa calculated for the specimen. The bond condition of the specimen was extremely bad and is unlikely to occur in real beam-column joints. Therefore it may be concluded from the data plotted in Fig.8.6 that for the beam bar bond index in the investigated range of 1.25 to 2.75, the bond condition of beam bars in the joint core does not affect the joint shear stress at cracking significantly. Further research is required in this aspect.

8.3.4 Principal Tensile Stress at Cracking

As mentioned in Chapter 2, one approach to predict the joint shear stress at cracking is to assume that initial joint diagonal tension cracking occurs when the principal tensile stress of the joint core, f_{ct}, indicated by Mohr's circle for stress, reaches the diagonal tensile strength of the concrete, f_t. The principal tensile stress at joint diagonal tension cracking f'_{cr} can be found from the following equation.

$$f'_{cr} = -\frac{P_u}{2A_g} + \sqrt{\left(\frac{P_u}{2A_g}\right)^2 + (v_{j,cr})^2} \tag{8.3}$$

where P_u is axial load on column, A_g is gross area of column cross section and $v_{j,cr}$ is the nominal joint shear stress at cracking. Note that f'_{cr} is positive in tension and that P_u is positive in compression in the above Eq.8.3. There are approximations in Eq.8.3. For example, the concrete compressive stress at the centre of the joint may not be P_u/A_g since the flow of forces through the joint is more complex. However, the results obtained from the eighty test data are plotted against the concrete compressive strength in Fig.8.7. Assuming that the concrete cracking stress varies in proportion to $f'_c{}^{2/3}$ rather than $\sqrt{f'_c}$ [Raphael 1984], the mean value of f'_{cr} is $0.17f'_c{}^{2/3}$ MPa for the test data. Hence, although the test data scattered widely, at the onset of joint diagonal tension cracking it can be assumed that

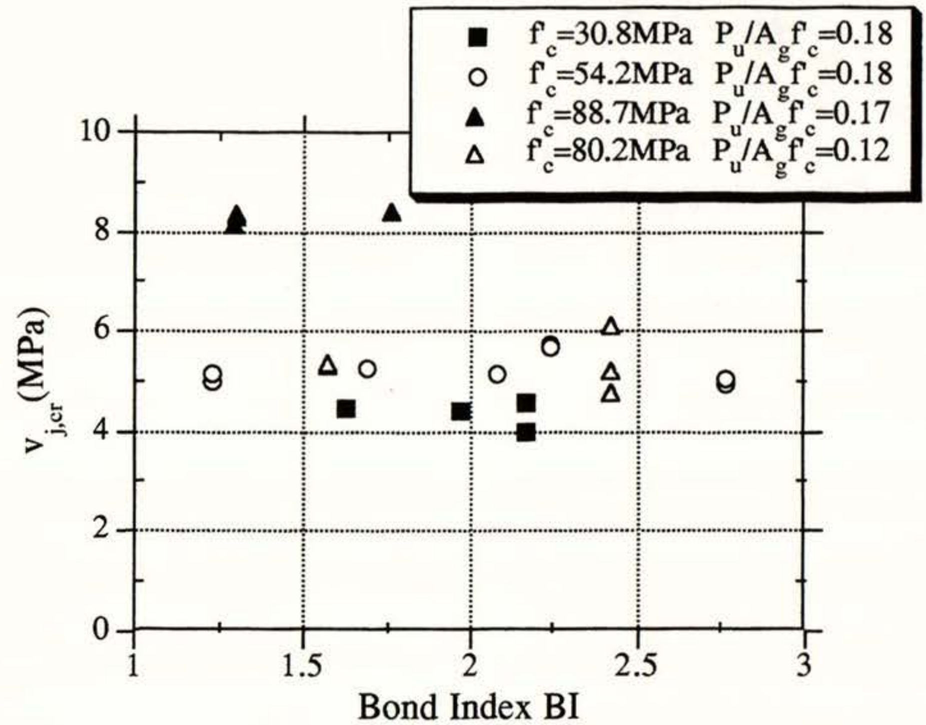

Fig.8.6 Beam Bar Bond Index versus Joint Shear Stress at Cracking

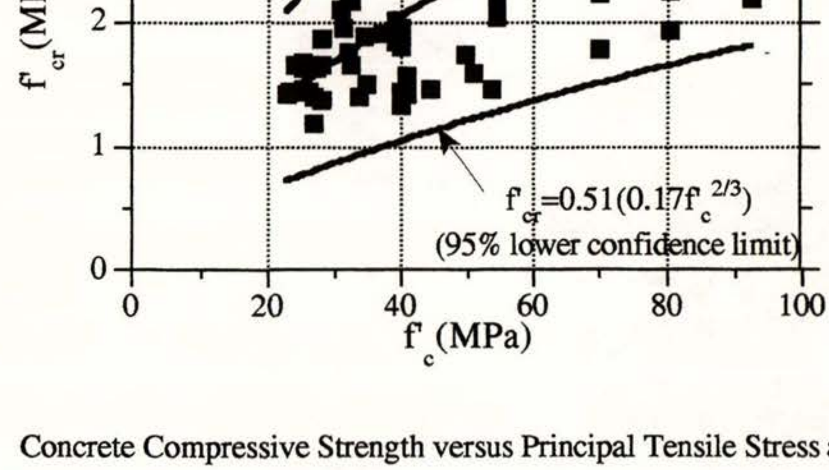

Fig.8.7 Concrete Compressive Strength versus Principal Tensile Stress at Cracking

$$f'_{cr}=0.17f'_c{}^{2/3} \tag{8.4}$$

with a coefficient of variation of 23.3%. For design purposes, the following equation with the 95% lower confidence limit can be used for the concrete compressive strength in the range of 20 to 100MPa :

$$f'_{cr}=0.51(0.17f'_c{}^{2/3}) \tag{8.5}$$

This expression is shown in Fig.8.7.

8.4 SEISMIC BEHAVIOUR OF INTERIOR JOINTS WITHOUT SHEAR REINFORCEMENT AFTER DIAGONAL TENSION CRACKING

8.4.1 Forces and Crack Pattern

Figs.8.1 and 8.2(b) show forces acting and a crack pattern for a beam-interior column joint without shear reinforcement after diagonal tension cracking, respectively. Under seismic actions, large shear and bond stresses may be introduced into the joints by these forces, irrespective of whether plastic hinges develop at column faces or beam faces. These forces may cause a failure of the joint core due to the breakdown of the diagonal tension or diagonal compression mechanisms. As mentioned in Chapter 2, it was found that the joints of reinforced concrete building frames designed prior to about 1970 may have such deficiencies since in the joint core typically no shear reinforcement is provided and also longitudinal beam bars of large diameter pass through the joint with relatively small depth, causing high bond stresses.

8.4.2 Shear Mechanisms in Joints with Good Bond Condition along the Beam Bars

Fig.8.8 illustrates the actions on a beam-interior column joint subjected to horizontal seismic loading. For the sake of simplicity, it is assumed that the bending moments introduced are the same at all four sides of the joint. The tensile resultant force is denoted by T, and the compressive resultant forces in the concrete and steel are shown by the symbols C_c and C_s, respectively. Axial load on the column is not considered. The horizontal joint shear force V_{jh} in the joint core can be expressed from Fig.8.8 as follows:

$$V_{jh}=T+(C_s+C_c)-V_c \tag{8.6}$$

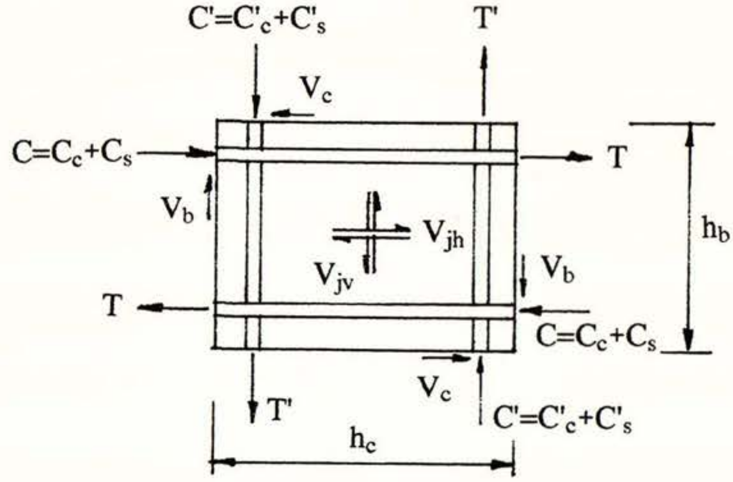

Fig.8.8 Forces Acting on a Beam-Interior Column Joint

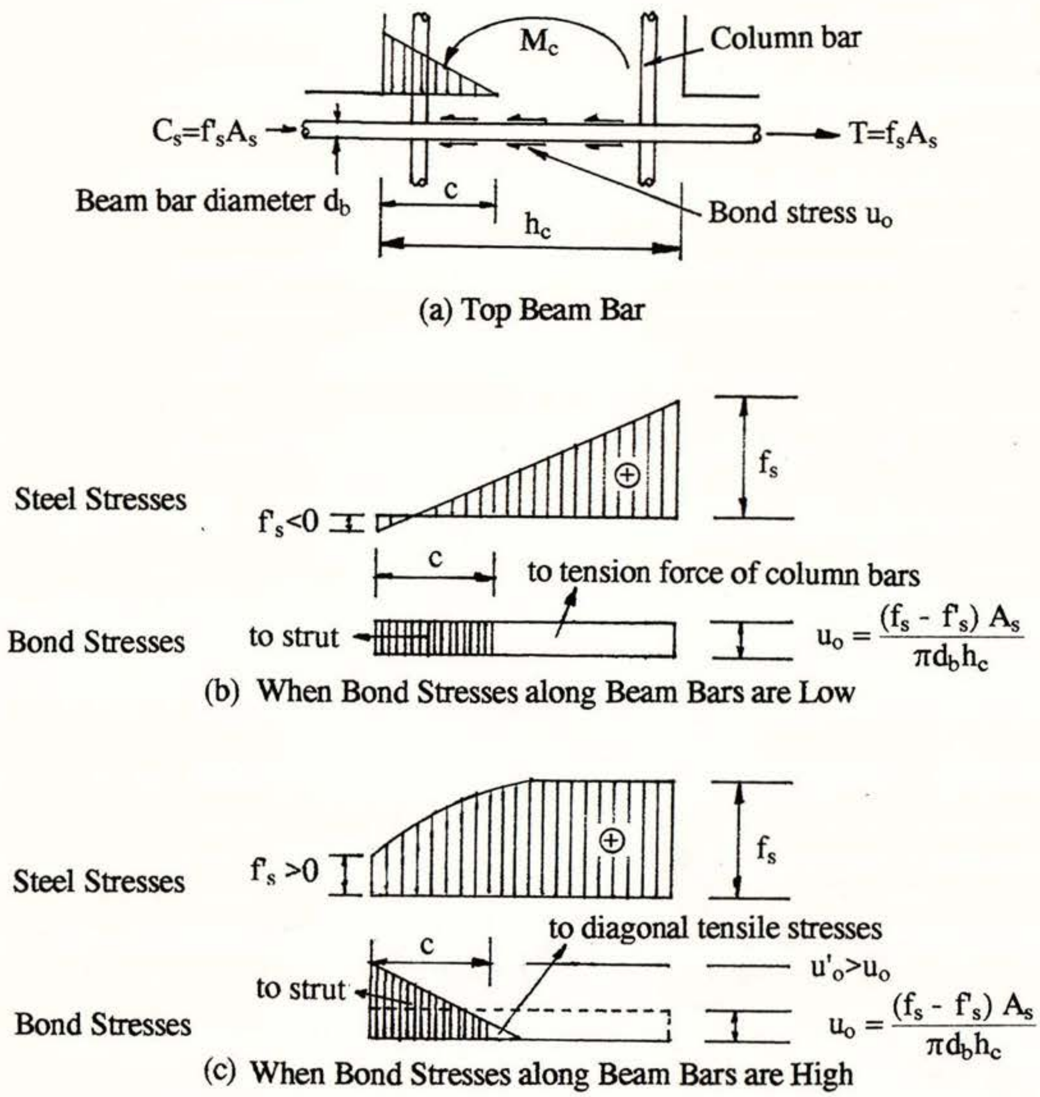

Fig.8.9 Bond Stress Distributions along the Top Beam Bar in a Joint

Similarly the vertical joint shear force, V_{jv} can also be obtained from the internal column forces, T', C_s' and C_c' and the beam shear force, V_b. Assuming that the bond stresses along the bars passing through the joint vary linearly, approximate distributions of steel stresses, when the bond stresses are low and high, are shown in Fig.8.9.

Two mechanisms of joint core shear resistance which occur after diagonal tension cracking, namely a diagonal compression strut mechanism and a truss mechanism, have been postulated by Park and Paulay[Park and Paulay 1975]. The diagonal compression strut mechanism shown in Fig.8.10(a) transfers mainly the forces from the concrete compression zones of the adjacent beams and columns across the joint core. After the development of flexural cracks at the beam or column face, it is appropriate to assume that the shear force in each of the adjoining members is introduced to the joint core mainly through the concrete compression zones in the beams and columns, respectively. Then the internal compression forces C_c and C_c' and shearing forces V_b and V_c are transferred to the diagonal concrete strut. Steel forces are transferred by bond predominantly to the joint core concrete that surrounds the bars. The bond force ΔT_c from the beam bars over the length of the neutral axis depth of the column c is assumed to be transmitted to the concrete strut. A similar force $\Delta T_c'$ from the longitudinal column bars is also transferred to the diagonal concrete strut. The concrete compression forces together with shearing forces and bond forces transmitted within the compression zone balance each other by means of the diagonal compression force D_c without the aid of any shear reinforcement in the joint core, apart from the role of confinement for the diagonal concrete strut.

The remaining steel bond forces ΔT_s and $\Delta T_s'$ should be also in equilibrium by means of a diagonal compression field with a capacity of D_s, where $\Delta T_s=C_s+T-\Delta T_c$ and $\Delta T_s'=C_s'+T'-\Delta T_c'$. When no bond deteriorations initiate along the beam and column bars in the joint, those bond forces ΔT_s and $\Delta T_s'$ may be large. The stress distribution of the beam bar in the joint under such condition is shown in Fig.8.9(b), in which uniformly distributed bond stresses are assumed. Prior to diagonal tension cracking of the joint, the joint shear force is transferred through the joint, causing diagonal compressive stress f_c and tensile stresses f_t in the core concrete(see Fig.8.1), as described in Section 8.2.3. After diagonal tension cracks form in the joint, the ability of the concrete to transmit the tensile stresses is severely reduced. Unless appropriate reinforcement is provided, shear failure may occur in the joint. When the reinforcement is present, tension forces are induced in the reinforcement due to the loss of tension capacity of the diagonally cracked concrete in the joint. This may enable the joint to carry the necessary shear force after diagonal tension cracking. Fig.8.10(b) illustrates the upper half of the joint without intermediate column bars. Assuming no tension capacity in the cracked concrete, vertical tension force $\sum T_c$ is required in the main column bars to balance the necessary horizontal shear force ΔT_s and a diagonal compression force D_s. From consideration of the equilibrium shown in Fig.8.10(b), the required vertical tension force is

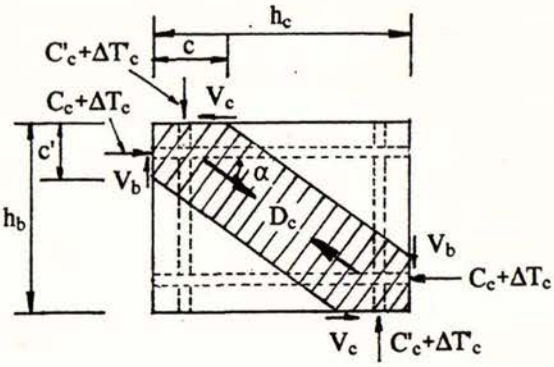

(a) Shear Carried by Diagonal Strut

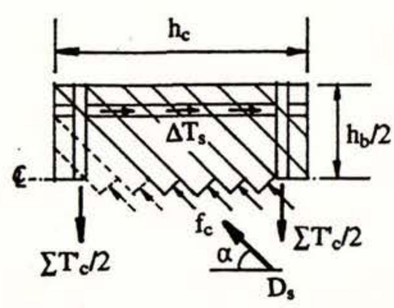

(b) Shear Carried by Tension Force of Column Bars

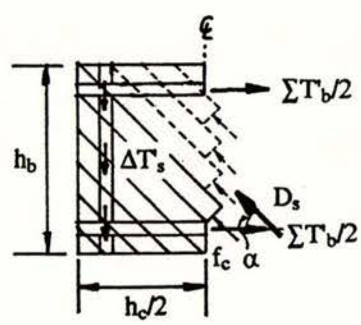

(c) Shear Carried by Tension Force of Beam Bars

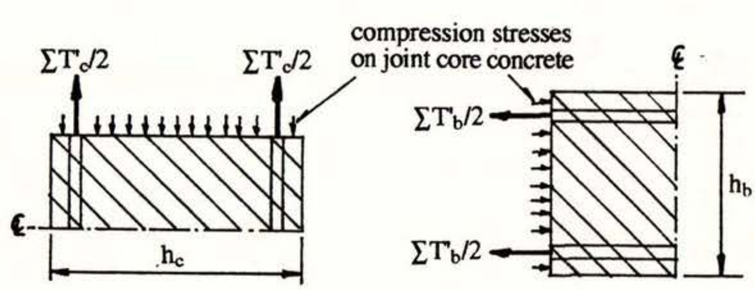

(d) Compression Stresses at the Boundaries of the Joint Core

Fig.8.10 Shear Transfer in a Joint without Shear Reinforcement
When Bond Stresses along Beam Bars are Low

$$\sum T'_c = \Delta T_s \tan\alpha \tag{8.7}$$

where α is the inclination of the diagonal compression force with respect to the horizontal centre axis. Tanα may be approximated by

$$\tan\alpha = h_b / h_c \tag{8.8}$$

where h_b is the overall depth of column and h_c is the overall depth of beam. Therefore additional tension forces are introduced in the column bars in the joint core.

The left half of the joint without hoops is shown in Fig.8.10(c). The column bar bond force $\Delta T'_s$ could also resolve itself into a diagonal compression force and the horizontal tension force supplied by main beam bars $\sum T'_b$ as shown in this figure. The additional tension force of the beam bars is then

$$\sum T'_b = \Delta T'_s / \tan\alpha \tag{8.9}$$

The additional tension forces expressed by Eqs. 8.7 and 8.9 are assumed to be generated in the longitudinal beam and column reinforcement within the joint core only. It is also assumed that these longitudinal reinforcement in tension within the joint core are well anchored in the adjacent beams and columns so that vertical and horizontal compression stresses are developed at the boundaries of the joint core concrete by means of bond stresses for anchorage, as shown in Fig.8.10(d). These compression stresses enable the core concrete to transfer the necessary shear stresses at the boundaries of the joint core by means of a diagonal compression field after joint diagonal tension cracking.

The additional tension forces mentioned above may result in significantly large tensile stresses in the column and beam bars in the joint core when no bond deterioration initiates along those bars in the joint.

8.4.3 Shear Mechanisms in Joints with Severe Bond Condition along the Beam Bars

In this section, the shear mechanisms in a joint without shear reinforcement is explained for the case when severe bond deterioration occurs along the longitudinal beam and column bars in the joint. When premature bond deterioration occurs along the beam bars in the joint, the compression forces of the beam bars may be completely lost at the column face where beam flexural compression force is applied. In such cases, the neutral axis depth from the compression side of the beam section, c will become larger. The stress distribution along the top beam bar, for this case is illustrated in Fig.8.9(c). As shown in this figure, the major part of the horizontal bond forces along the beam bars can be transmitted to the diagonal compression strut in the shaded region. Similarly, most of the vertical forces developed in the column bars $\Delta T_c'$ will be transmitted to the same region of the joint. The concrete compression, shear and bond forces at the lower right-hand corner of the joint will be combined into an equal and opposing diagonal compression force D_c as shown in Fig.8.11(a).

It is evident that bond forces along the beam and column bars can be disposed of more easily within a wider diagonal compression strut. In such case, the remaining steel bond forces ΔT_s and $\Delta T'_s$ will be small, as shown in Fig.8.11(b). Those bond forces are resisted by means of diagonal tensile stresses in the concrete f_t and additional tension forces in the beam and column bars T'_{b1} and T'_{c1} at a section between the two adjacent diagonal tension cracks(see Fig.8.11(c)). At a crack, the tensile stress in the concrete goes to zero and additional tension force T'_{c2} is required in the main column bars to balance the beam bar bond forces ΔT_s and a diagonal compression force. Similarly, additional tension force T'_{b2} is also required in the main beam bars to balance the column bar bond force $\Delta T'_s$ and a diagonal compression force, as illustrated in Fig.8.11(d). However, the magnitude of the additional tension forces both at a crack and at a section between the cracks will be small. It should be noted that local shear stresses on the crack surface are not shown in Fig.8.11(d).

8.4.4 Shear Mechanisms in the Joints of the Test Specimens

8.4.4.1 Introduction

The shear mechanisms in the joint without shear reinforcement have been described in the previous sections. As mentioned in Section 8.4.2, additional tension forces may be generated in the longitudinal beam and column bars in the joint core. To obtain the additional tensile stresses, it is necessary to determine realistic bond stress distributions of the longitudinal beam and column bars within the joint. As described in Chapters 4 and 6, however, the bond forces in terms of the average bond stresses change along the beam and column bars passing through the joint, depending on the stress conditions of the adjacent members acting on the joint. The estimated bond stress distributions also change as the tensile stresses induced at the tension side of the beam bars increase. In this section, the bond stress distributions along the beam bars in the joint without shear reinforcement are first examined, based on the test observations, and then a bond stress distribution along the beam bars is proposed to obtain the additional tension forces in the beam and column bars in the joint core. Finally, based on the joint shear mechanisms postulated in this study, the stress distributions along the beam and column bars in the joint are estimated for the specimens tested for this study and compared with the test results.

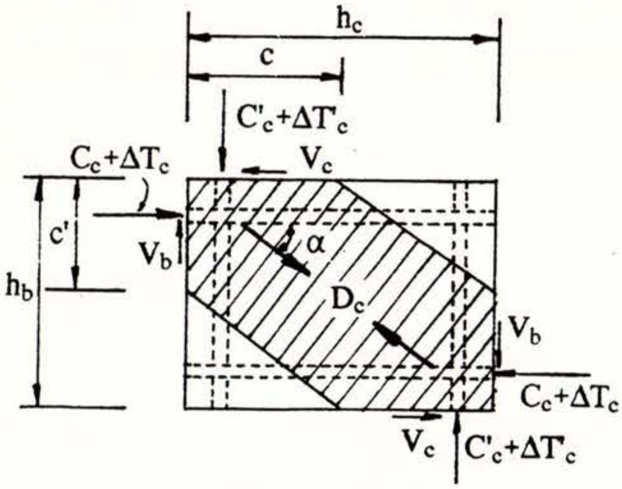

(a) Shear Carried by Diagonal Strut

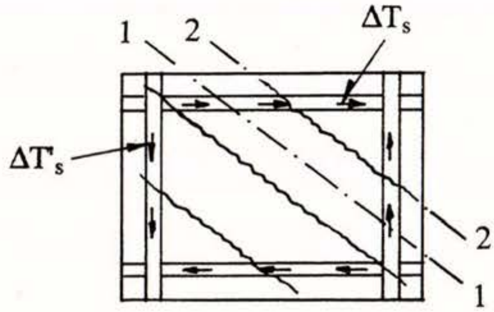

(b) Cracked Joint Core

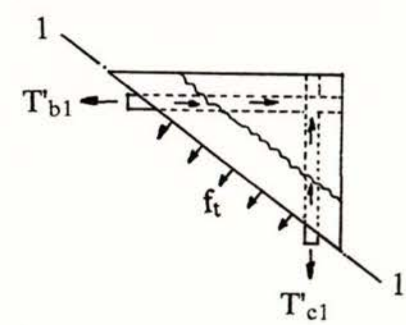

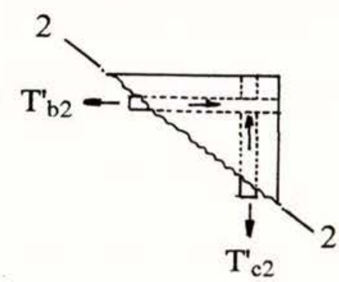

(c) Forces Transmitted Between Cracks (d) Forces Transmitted Across a Crack

Fig.8.11 Shear Transfer in a Joint without Shear Reinforcement When Bond Stresses along Beam Bars are High

8.4.4.2 Bond Stress Distributions in the Joints of the Test Specimens

According to the test observations, the bond stress distributions along the beam bars in the joint without shear reinforcement could be expressed at several stress levels of the beam bar at the tension side, as shown in Fig.8.12. A notable feature of the bond behaviour in such a joint is that bond deterioration initiates even in the early loading stages.

When beam bar stresses approach about 50% of the yield strength, bond resistance is significantly reduced and no bond stresses can develop over the region of approximately six bar diameter from the column face where beam flexural tension force is applied(see Fig.8.12(b)). A maximum bond stress of about $0.6\sqrt{f'_c}$ MPa was estimated in the transition region at this stage. At bar stress of about 75% of the yield strength, the location of the maximum bond stress moves somewhat towards the compression side of the beam bar in the transition region(see Fig.8.12(c)). Fig.8.12(d) illustrates the bond stress distribution when the yield strength is reached in the loading to a displacement ductility factor DF of 1 or 2. The bond stresses increase almost linearly towards compression side of the beam, in proportion to the flexural compression force of the column acting on the joint. It was observed that the stresses in the beam bars turned to be in tension along the whole length of the joint at this stage. The maximum bond stress was estimated from the measurements to be about $1.0\sqrt{f'_c}$ MPa. No measurements were made after the loading to DF of 2. However, it is likely that the bond stress distributions did not basically change further since only the flexural compression forces of the column offer confinement of the concrete surrounding the beam bars in the joint without shear reinforcement. It can be also expected that the bond resistance of the beam bar will be reduced over the region subjected to the column flexural compression force due to the effect of the high-intensity reversed cyclic forces and many diagonal tension cracks formed crossing the beam bars.

Fig.8.13 illustrates the assumed steel stress distribution of the beam bar in a joint without shear reinforcement. Also shown is the corresponding bond stress distribution which expresses the premature bond deterioration along the beam bars where the bars are in tension. The bond stresses increase linearly over the region subjected to column flexural tension forces and uniformly distributed bond stresses are assumed over the region subjected to column flexural compression forces. The bond force ΔT_s causing the additional tension forces in the longitudinal column bars in the joint core can be derived using the neutral axis depth of the column c as shown in Fig.8.13.

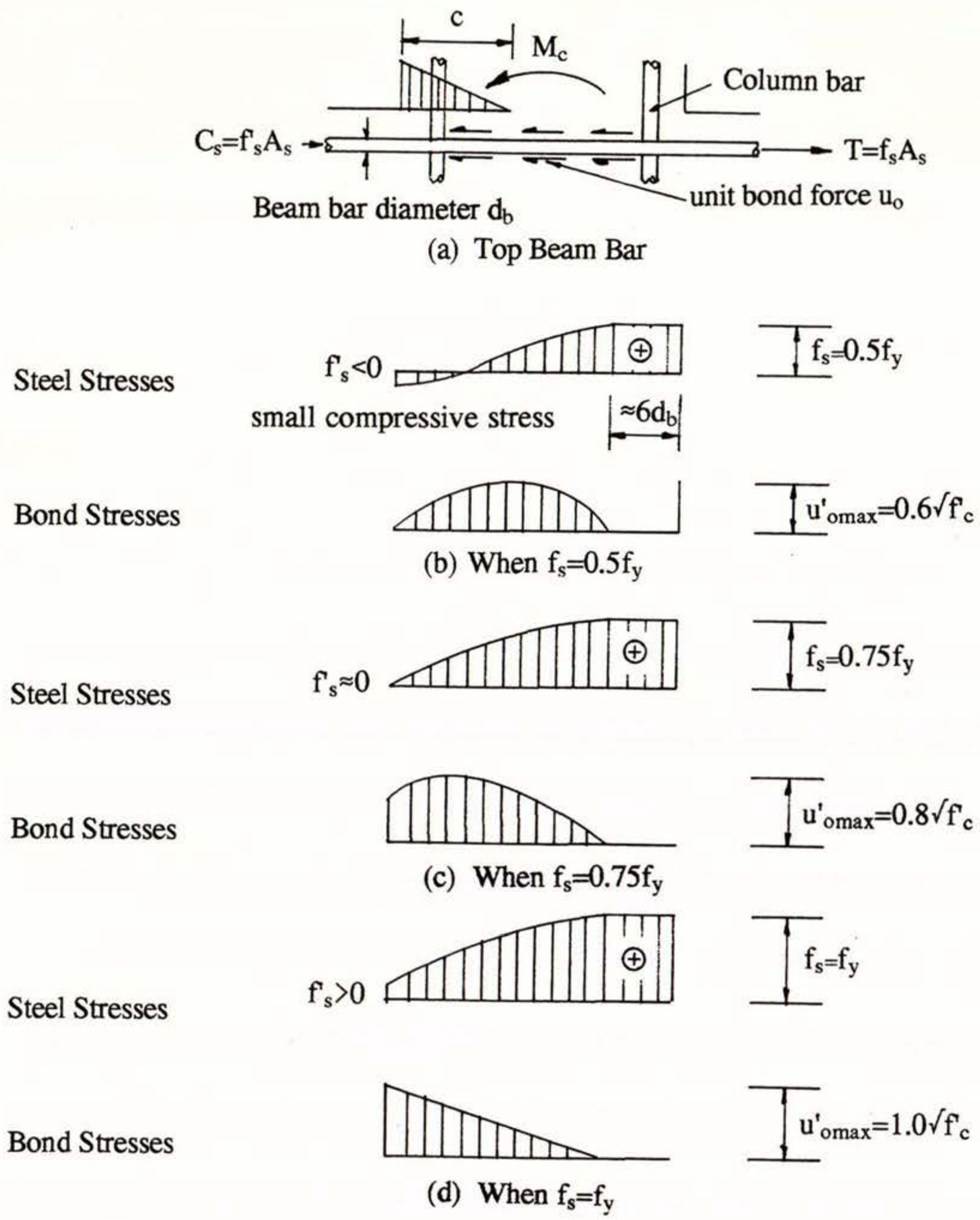

Fig.8.12 Bond Stress Distributions along the Beam Bars in the Joint without Shear Reinforcement

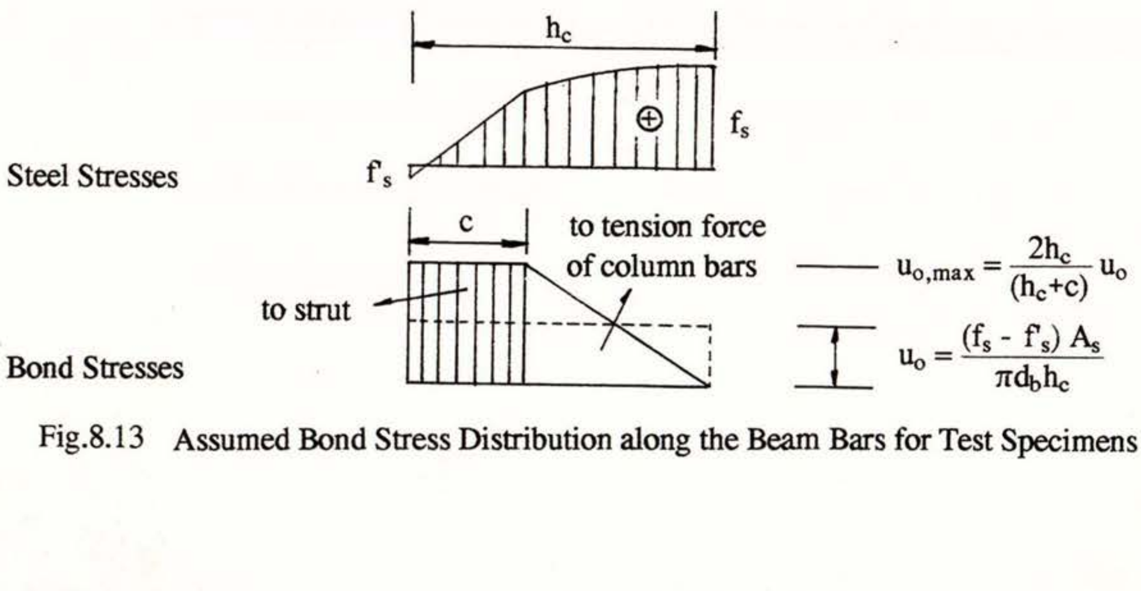

Fig.8.13 Assumed Bond Stress Distribution along the Beam Bars for Test Specimens

8.4.4.3 Stress Distributions along the Beam and Column Bars in the Joints of the Test Specimens

Fig.8.14 shows the method which can be used to calculate the main beam bar steel stresses within the joint, which takes into account the effect of the joint shear force on the beam bar forces in the joint core. The beam bar stresses at the column face, f_s and f'_s can be obtained from section analysis. The theoretical stress distribution caused by flexure alone within the joint can be estimated using the assumed bond stress distribution mentioned in the previous section (shown in Fig.8.13 or Fig.8.14(b)) and is illustrated in Fig.8.14(c). The beam bar stresses are distributed linearly over the region subjected to column flexural compression forces and parabolically over the region subjected to column flexural tension forces, as shown in Fig.8.14(c). The additional tension stresses may be induced in the main beam bars in the joint core to balance the column bond force $\Delta T'_s$ and a diagonal compression force(see Fig.8.10(c)). The column bar bond force $\Delta T'_s$ can be calculated assuming the similar bond stress distribution along the column bars to that along the beam bars as shown in Fig.8.14(b). The additional tension stresses so obtained are shown in Fig.8.14(d), indicating larger tensile stresses along the beam bars in the joint core when compared with those by flexure alone.

The measured strains along the column and beam bars in the joint of the test specimens were converted to bar stresses, namely the measured stresses. The results of the bar stress distributions are shown in Fig.8.15. Only the bar stresses, when the maximum strengths of the test specimens were attained, are plotted. Also plotted are the theoretical stress distributions caused by flexure alone, and those predicted by the method which takes into account the effect of the joint shear force on the column and beam bar forces in the joint core mentioned in Section 8.4.2, referred to as "predicted stresses". For the predicted stresses, the additional tensile stresses due to the bond force ΔT_s or $\Delta T'_s$ were assumed to be the same in all beam or column bars.

As shown in Fig.8.15, the stresses calculated from the readings of the strain gauges were significantly larger than those calculated as due to flexure alone. Even when bond deterioration along the main beam bars is assumed over the region subjected to column flexural tension forces, the large tensile stresses measured in the joint core cannot be explained by flexure alone. On the other hand, the predicted stress profiles, which took into account the additional tensile stresses induced by the joint shear forces ΔT_s or $\Delta T'_s$, approached the measured values. The main difference between the measured and predicted stress profiles can be found at the beam or column faces where the bars are to be in compression due to flexure alone. For Specimen O1, the predicted column bar stresses reached the yield stress in the joint core as well as at the beam face. For the predicted beam bar stresses obtained for Specimens O4 and O5, the yield stress was reached both in the joint core and at the column

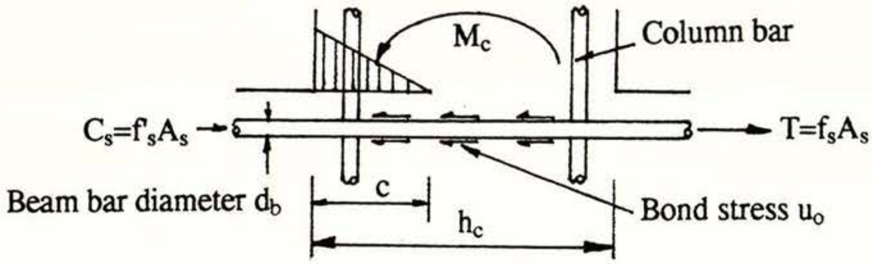

(a) Top Beam Bar

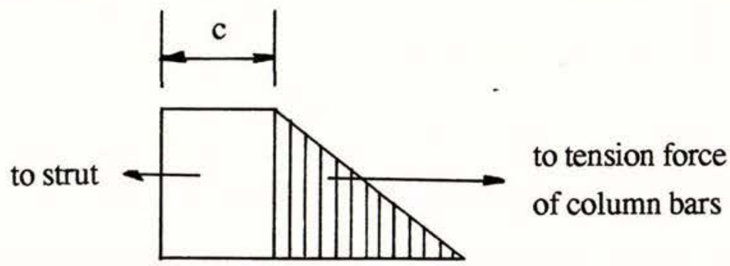

(b) Assumed Bond Stress Distribution

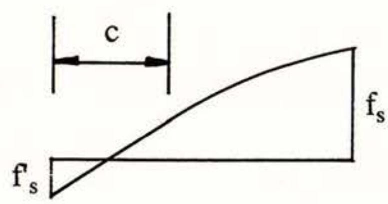

(c) Beam Bar Stress Distribution by Flexure Alone

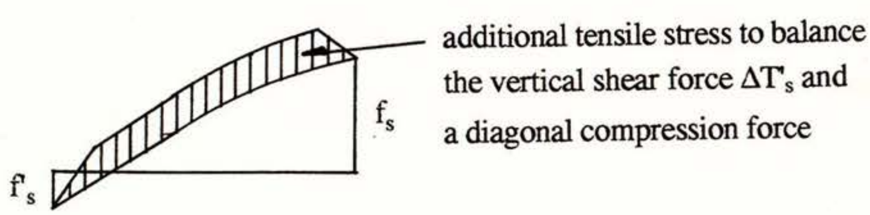

(d) Beam Bar Stress Distribution by Flexure and Column Bar Bond Forces

Fig.8.14 Method to Calculate the Beam Bar Stresses in a Joint

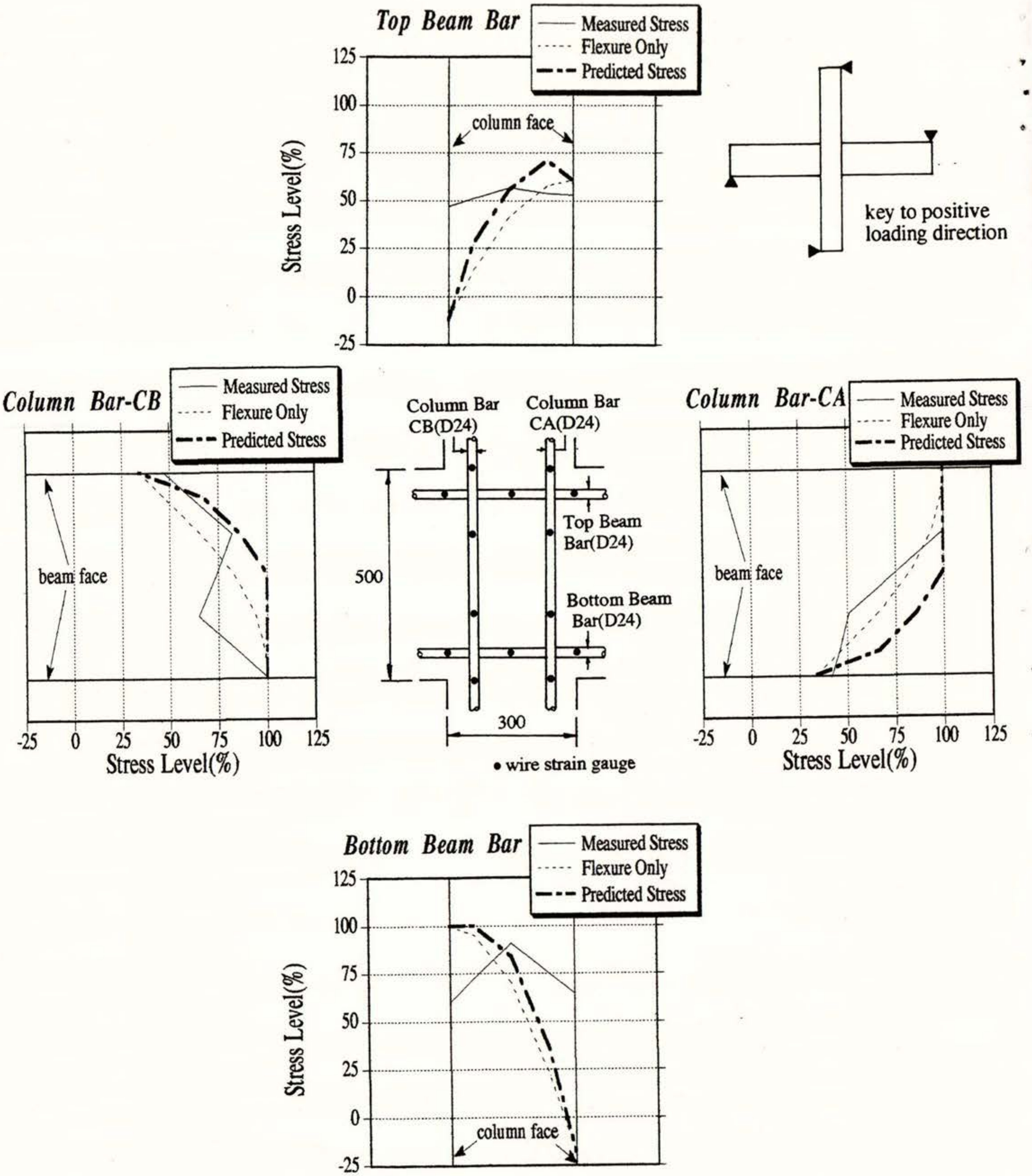

Fig.8.15(a) Stress Distributions along Beam and Column Bars in the Joint for Specimen O1

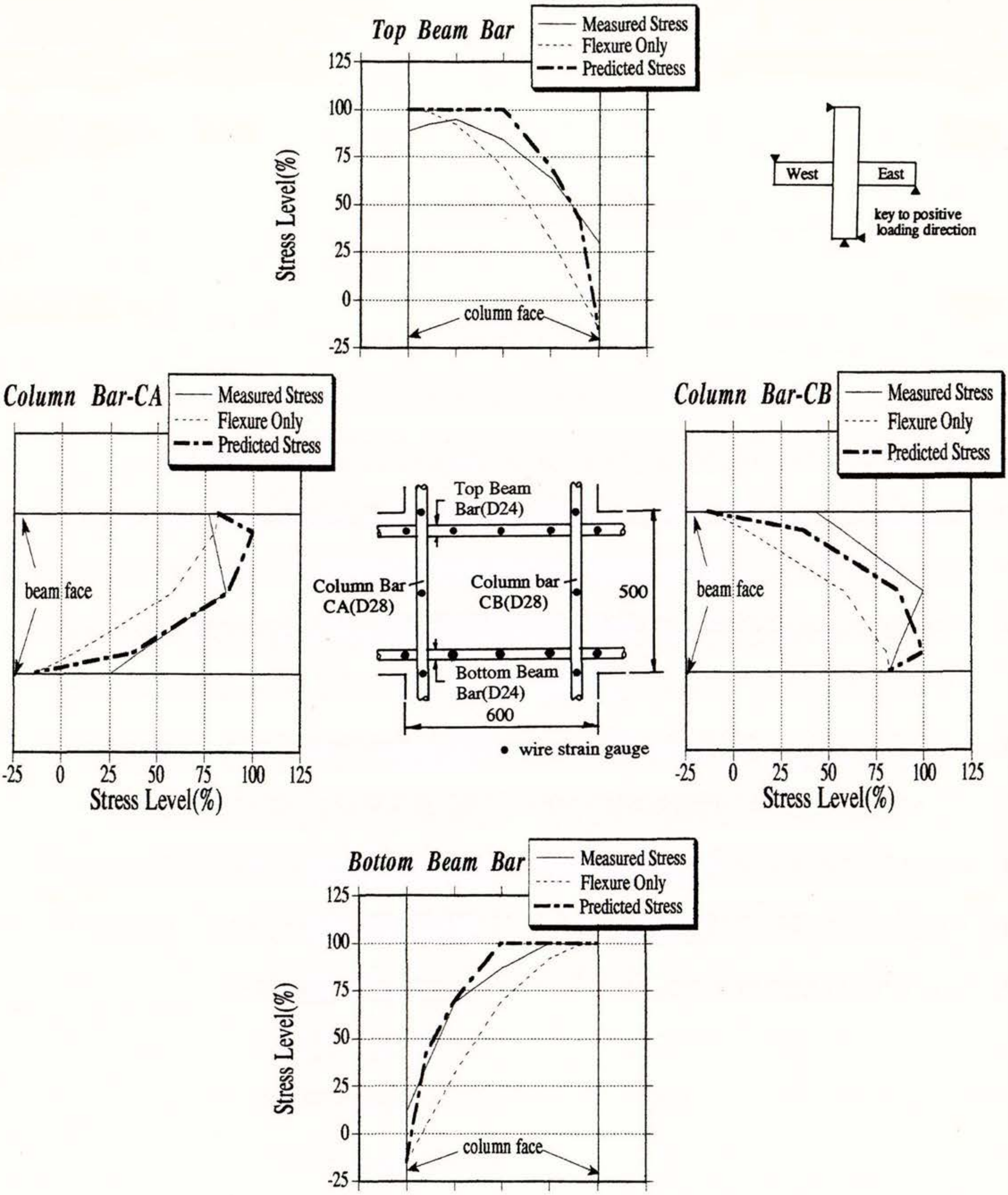

Fig.8.15(b) Stress Distributions along Beam and Column Bars in the Joint for Specimen O4

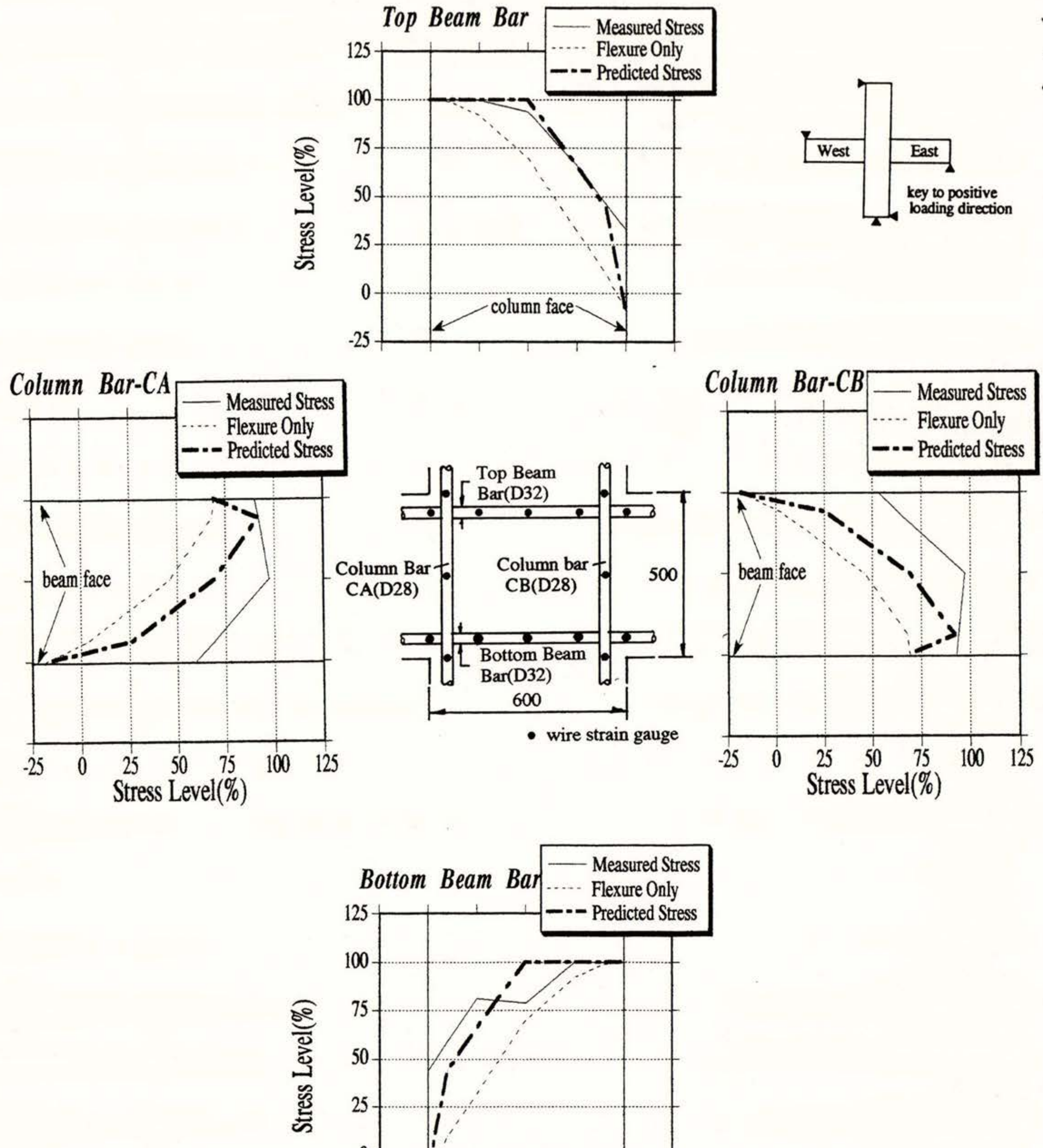

Fig.8.15(c) Stress Distributions along Beam and Column Bars in the Joint for Specimen O5

face. It should be noted that in order to develop the ideal strengths of the test specimens, the maximum value of the predicted steel stresses in the joint core is approximately 125% of the yield stress although it is shown as 100% of the yield stress in Fig.8.15. This means that the column or beam bars in the joint core yield in tension before developing the column or beam plastic hinges. However, if the steel forces transmitted into the joint core had been assumed to be smaller, the additional tensile stresses induced by the joint shear might have been reduced. As mentioned earlier, the predicted stresses at the beam or column faces were given by section analysis. When assuming the bond force distribution as illustrated in Fig.8.13, large bond forces must be generated in the regions subjected to flexural compression force of the column. For example, the bond stress along the beam bar over that region for Specimen O1 can be estimated to be $2.0\sqrt{f'_c}$ MPa, where f'_c is the measured compressive cylinder strength of concrete. If such large bond stresses can not be developed, the "compression" reinforcement may be in tension at the column face. This may result in a reduction of the steel forces transmitted into the joint, reducing the additional tensile stresses in the column and beam bars in the joint core.

For the test specimens, the horizontal joint core shear stresses v_{jh} was approximately $0.6\sqrt{f'_c}$ MPa when the ideal storey horizontal load strengths were reached. If the joint shear force had been much larger than that developed in the test specimens, the column or beam bars might have yielded in the joint core before developing the ideal flexural strength of the column or beam. This phenomenon was found in the test on the specimen conducted by Blaikie 1988. Blaikie's test results showed that the test specimen without horizontal joint shear reinforcement developed only 70% of the beam flexural strength due to the beam bar yielding not at the column face but in the joint core. The maximum nominal horizontal shear stress in the joint core of the test specimen was $1.0\sqrt{f'_c}$ MPa. It may be expected that the effect of the joint shear force on the stresses induced in the steel bars in the joint core was quite large for Blaikie's specimen when compared with the specimens tested for this study. This may result in significantly large tensile stresses in the beam bars in the joint core.

It has been shown from the predicted stress profiles along the longitudinal beam and column bars in the joint that the shear strength of the joint without shear reinforcement may be governed by the column or beam bar yielding in the joint core and that the large bond stresses are developed in the flexural compression zones of the joint after diagonal tension cracking occurs.

8.4.5 Joint Shear Strength

8.4.5.1 Joint Shear Strength When Governed by Diagonal Compression Failure

It is evident that when significant bond deterioration initiates, the joint shear forces are transmitted mainly by means of the diagonal compression strut mechanism. In that case, diagonal compression failure will control the strength of the joint. Also, when bond stresses are low and significant shear is transferred by a diagonal compression field acting with a large quantity of joint shear reinforcement, diagonal compression may control the strength of the joint.

It has been widely recognized that the presence of tensile strains in the horizontal and/or vertical directions in the joint reduce the diagonal compressive strength of the concrete[Stevens et al 1991]. When the joint shear force is large, significant diagonal tension cracking in both direction will occur in the joint core(see Fig.8.16), particularly when shear reinforcement is not present in the joint core. Under reversed cyclic loading in the inelastic range, as a consequence of earthquake forces, the diagonal tension cracks become large and disintegration of the concrete begins because of the repeated opening and closing of the cracks along which shear sliding movements occur. This is associated with drastic volumetric increase in the joint core concrete unless adequate confinement is provided. This phenomenon is likely to further reduce the diagonal compressive strength of the concrete.

8.4.5.2 Maximum Joint Shear Strength When Governed by Diagonal Compression

A rational approach to predict the shear behaviour of members, using the compression field theory was developed by Collins and Mitchell 1980. This theory has been applied in Canada to the design of beams and columns for shear and torsion[CSA 1984]. With the aim of preventing the crushing of concrete due to diagonal compression before the yield of the transverse and longitudinal bars, some useful design charts were derived from the work of Collins and Mitchell to define the limits of the angle of the diagonal compressive stresses in the concrete α for a given level of nominal transverse shear stress and for given tensile strains[Collins and Mitchell 1980]. In a somewhat simplified form the derivation gives

$$10° + \frac{35\,(v'_{jh} / f'_c)}{0.42 - 50\varepsilon_l} < (90° - \alpha) < 80° - \frac{35\,(v'_{jh} / f'_c)}{0.42 - 65\varepsilon_t} \qquad (8.10)$$

where ε_t and ε_l are tensile strains in column transverse and longitudinal directions, $90°$-α is angle of inclination of the diagonal compressive stresses to the longitudinal axis of the column

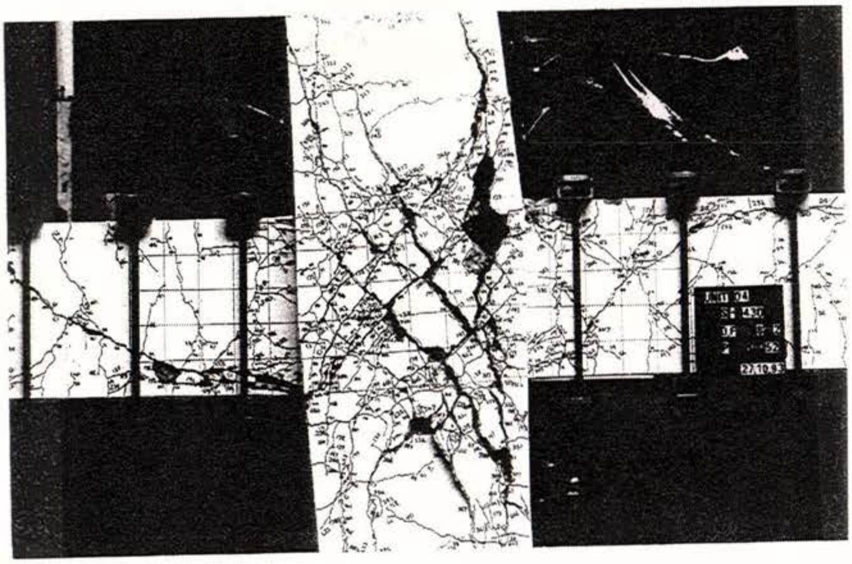

Fig.8.16 Observed Cracking of the Joint without Shear Reinforcement, Specimen O4

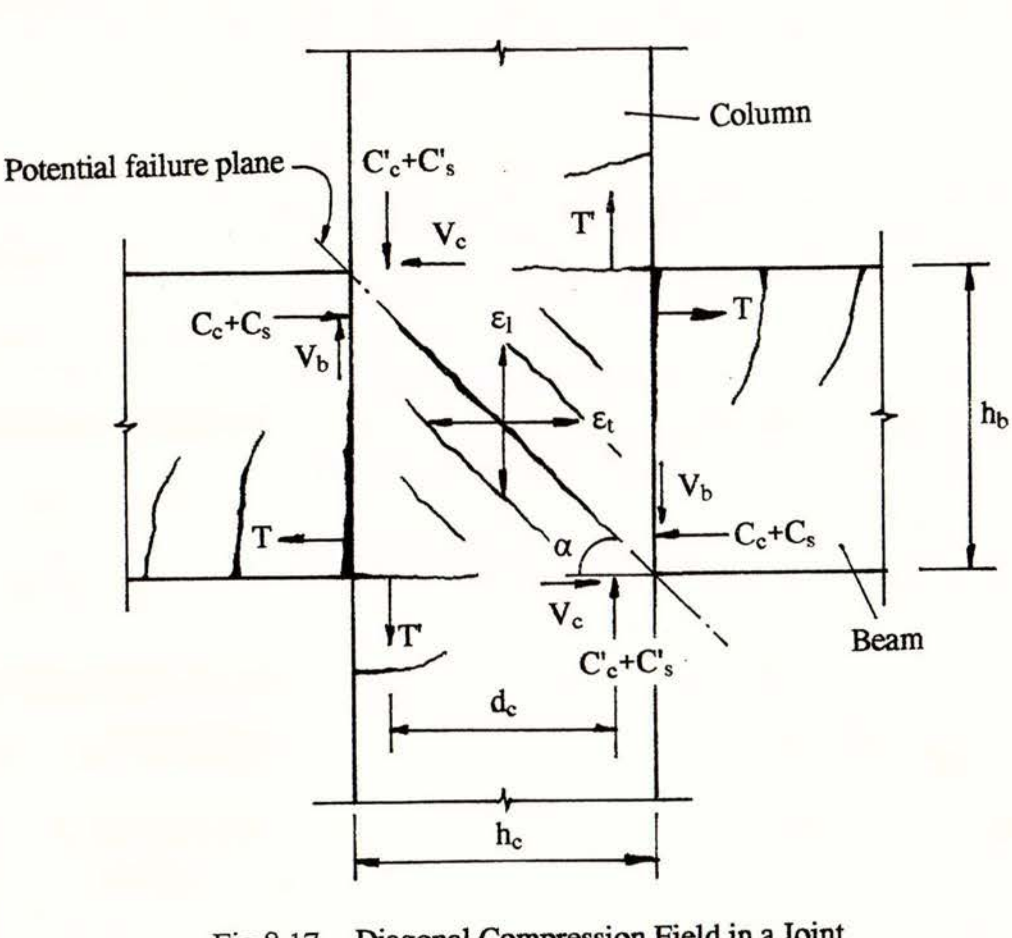

Fig.8.17 Diagonal Compression Field in a Joint

in degrees, α is the angle of inclination of potential failure plane in the joint to horizontal(see Fig.8.17), v'_{jh} is nominal transverse shear stress and f'_c is compressive strength of concrete.

The value of ε_t, ε_l and α need to be estimated in order to determine from Eq.8.10 the nominal horizontal joint shear stress at the stage of diagonal compression failure of the joint core concrete. When columns are expected to remain in the elastic range, the right hand side of Eq.8.10 will govern since $\varepsilon_t > \varepsilon_l$. When the aspect ratio of the joint is close to one, that is, $h_c \approx h_b$, and no axial compression load is applied to the column, the value of the angle of α will be close to 45 degree(see Fig.8.17), where h_c is overall depth of column and h_b is overall depth of beam. When the joint has little or no shear reinforcement, the tensile strain in the transverse direction of the diagonal compression strut at the stage of joint shear failure will be much larger than that for a well-designed joint.

Fig.8.18 plots the relationship between the maximum nominal horizontal joint shear stress v'_{jh} and the compressive strength of the concrete cylinder measured for the six beam-interior column joint specimens without shear reinforcement tested by other researchers[Hanson and Corner 1972, Bessho et al 1986, Blaikie 1988, Pessiki et al 1990 and Kawachi et al 1992]. The nominal horizontal joint shear stress v'_{jh} was defined as $v'_{jh} = V_{jh}/(b_j d_c)$, where V_{jh} is the horizontal joint shear force, b_j is the effective width of the joint and d_c is the effective depth of the column. The maximum joint shear stresses of all the specimens were reached before the theoretical flexural strengths of the beams were attained, except for the specimen of Hanson and Corner 1972. Although the available test data is limited, the maximum nominal joint shear stress increases almost in proportion to the measured compressive strength of concrete. This indicates that for these specimens the maximum joint shear stress was strongly affected by the diagonal compression failure of the joint core concrete[Stevens et al 1991]. Based on this limited test data, the following equation could be derived to give the lower bound for the test results.

$$v'_{jh}=0.19f'_c \tag{8.11}$$

When the above Eq.8.11 is used to estimate the nominal joint shear stress at diagonal compression failure, it is found from Eq.8.10 that the transverse tensile strain ε_t in the joint without shear reinforcement is approximately 0.35%.

In Eq.8.11, the nominal shear stress v'_{jh} was calculated using the effective depth of the column d_c, in stead of its full depth h_c. Assuming $d_c=7/8(0.9h_c)$ as a typical value for d_c, it is found as shown in Fig.8.19, that the limiting value for v_{jh} expressed by $v_{jh} = V_{jh}/(b_j h_c)$, where V_{jh} is the horizontal joint shear force, b_j is the effective width of the joint, h_c is the overall column depth, is

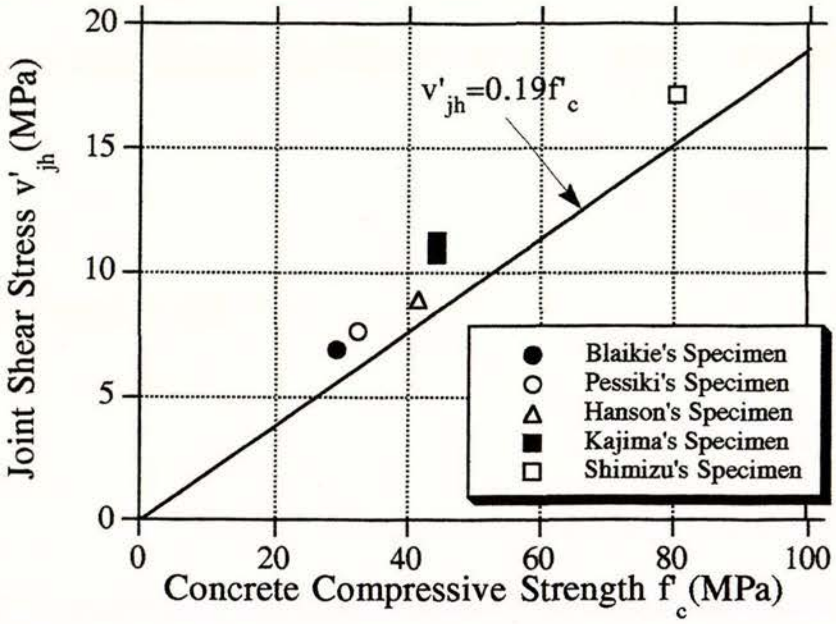

Fig.8.18 Joint Shear Stress v'_{jh} versus Concrete Compressive Strength Relationship

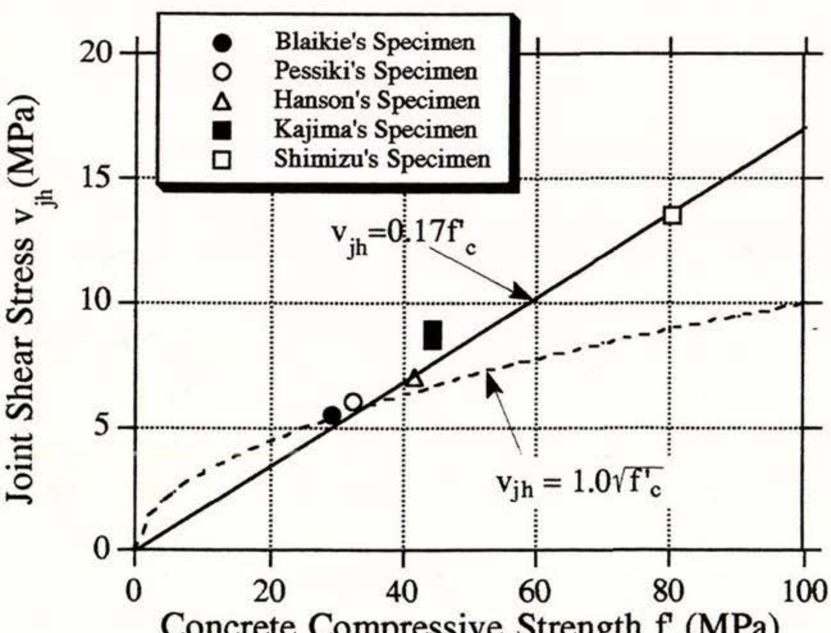

Fig.8.19 Joint Shear Stress v_{jh} versus Concrete Compressive Strength Relationship

$$v_{jh}=0.17f'_c \quad (8.12)$$

When the maximum joint shear stress is traditionally assumed to be in proportion to $\sqrt{f'_c}$, Eq.8.12 can be replaced by the following more conservative equation for when the concrete compressive strength is greater than 30MPa(see Fig.8.19).

$$v_{jh}=1.0\sqrt{f'_c} \quad (8.13)$$

8.4.5.3 Degradation of Joint Shear Strength When Governed by Diagonal Compression

As mentioned before, the upper limit of joint shear strength depends on the diagonal compressive strength of the joint core concrete. Of particular interest is the deterioration of joint shear strength under seismic forces. Diagonal tension cracking of the joint core in alternating directions due to seismic loading will reduce the diagonal compressive strength of the concrete. Therefore joint shear strengths may degrade as the imposed displacement ductility factor of the structure increases.

It has been quantified by Vecchio and Collins 1986 that the reduction of the compressive strength of the concrete in the direction of the principal compressive stress in the concrete is a function not only of the principal compressive strain, but also of the coexisting principal tensile strains, in which the strains are defined in terms of average values over the distances large enough to include several cracks. This reduction will be significant in a joint without shear reinforcement under earthquake loading because reversed cyclic loading will cause the principal tensile strain in the joint core to continue to increase with each cycle. This means that the diagonal compressive strength of the joint core concrete will decrease with each cycle until eventually failure may occur by concrete crushing.

The effect of the principal tensile strain in the joint core concrete on the joint shear strength can be assessed using the test results obtained from the specimens. The principal tensile strains were determined from the joint diagonal deformations measured during the test. For the four specimens, the joint aspect ratio was approximately 1.0 and no axial load existed on the columns, so that the directions of the joint diagonals were almost perpendicular to each other and each direction of the joint diagonals approximately coincided with the critical diagonal tension cracks in the joint. The measurements along the joint diagonals will give the principal tensile strains only when the direction of the critical crack is normal to principal tensile strain direction.

Fig.8.20 shows the relationship between joint shear stress expressed in terms of f'_c and principal tensile strains obtained from the measurements of the diagonal deformation of the

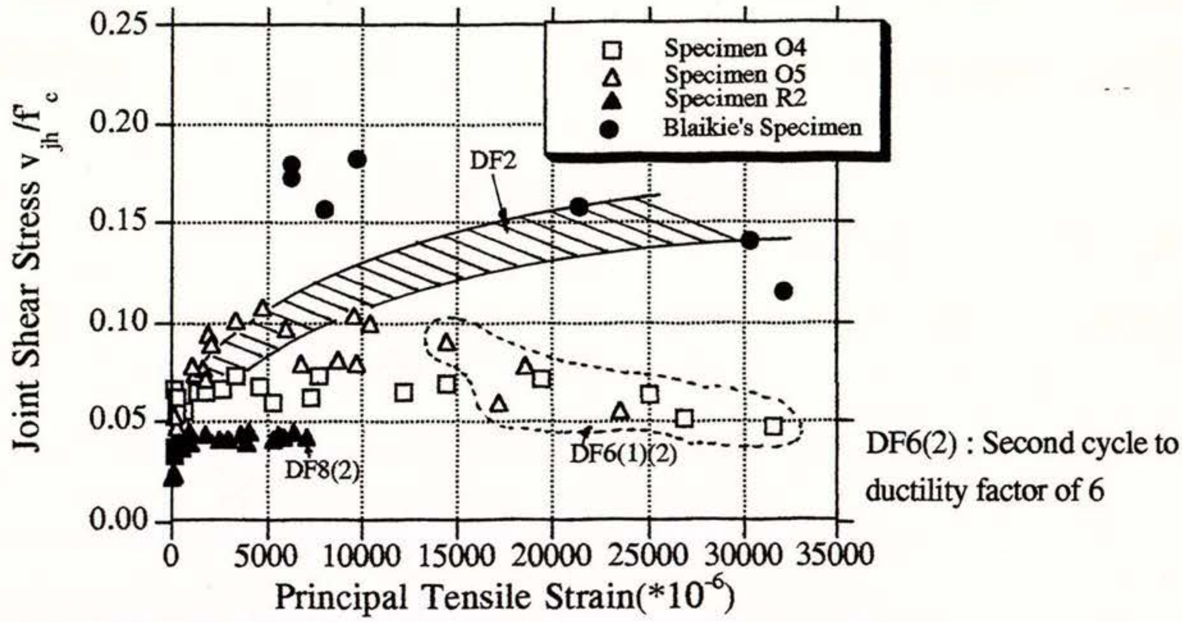

Fig.8.20 Joint Shear Stress versus Principal Tensile Strain Relationship

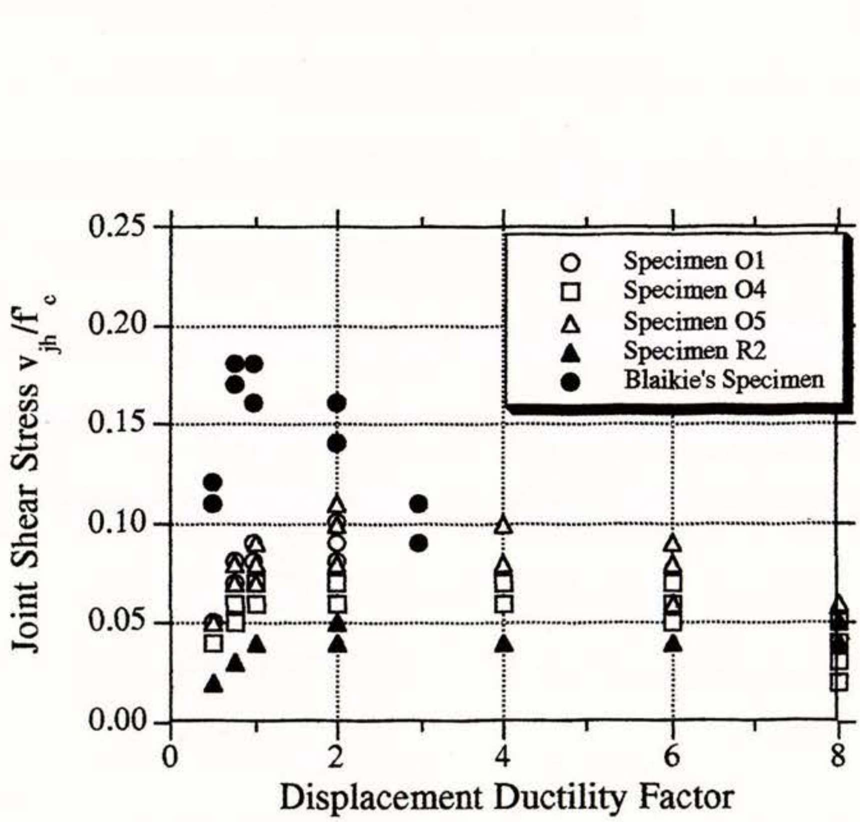

Fig.8.21 Joint Shear Stress versus Displacement Ductility Factor Relationship

joint. The principal tensile strains continued to increase with an increase in the displacement ductility factor DF, irrespective of the joint shear stresses. A maximum principal tensile strain of up to 0.7% was measured for Specimen R2 with a maximum joint shear stress of $0.05f'_c$ without strength degradation being observed up to a DF of 8. On the other hand, the other specimens with a larger joint shear stress showed degradation of joint shear strength with increasing DF as shown in Fig.8.20. Strength degradation began at a principal tensile strain of about 1%, independent of the joint shear stress. The maximum principal tensile strain measured for Specimen R2 was not large enough to cause strength degradation. It is likely that the degradation of the joint shear strengths is indicated by an increase in the principal tensile strains.

It can be clearly seen in Fig.8.20 that the larger the joint shear stress, the larger the increase in principal tensile strain with constant DF. The values measured in the loading to DF of 2 are shown by the shaded area. The principal tensile strains obtained in that loading stage became significantly larger as the joint shear stress increased. This will result in more rapid strength degradation for the specimens with the larger shear stress induced in the joint core. The critical principal tensile strain of approximately 1% was reached in the loading to DF of 1 for the specimen with the maximum joint shear stress of $0.18f'_c$ and to DF of 4 for the specimens with the joint shear stresses of $0.07f'_c$ to $0.11f'_c$.

Fig.8.21 plots the relationship between the joint shear stress and the displacement ductility factor DF for the test specimens studied. The seismic behaviour of these specimens without shear reinforcement are classified into the following three categories. When the maximum joint shear stress v_{jh} is less than $0.05f'_c$, the joint did not fail in shear up to a displacement ductility factor DF of 8, and the joint behaviour did not affect the ductility of the adjacent members in which a flexural plastic hinge was developed. At a joint shear stress v_{jh} of $0.17f'_c$, joint shear failure initiated at a displacement ductility factor DF of 1, followed by rapid strength degradation as shown in Fig.8.21. When the joint shear stress v_{jh} was $0.07f'_c$ to $0.11f'_c$, joint shear failure initiated during the loading to DF of 4 or 6 and the joint shear strength degraded moderately.

Based on the test data mentioned above, a model shown in Fig.8.22 is proposed for shear strength degradation of the joints without shear reinforcement. The test data is shown by solid circles and linear interpolation was used between the test data. As mentioned before, the maximum attainable shear stress of the joint without shear reinforcement is estimated to be $0.17f'_c$ in terms of nominal horizontal joint shear stress. The proposed model indicates that the larger the joint shear stress v_{jh}, the more rapid the strength degradation. The available displacement ductility factor is 1 at a joint shear stress v_{jh} of $0.17f'_c$, while at a joint shear stress v_{jh} of less than $0.05f'_c$ the available displacement ductility factor is at least 8. The proposed model is based on the results from beam-column joint specimens tested without

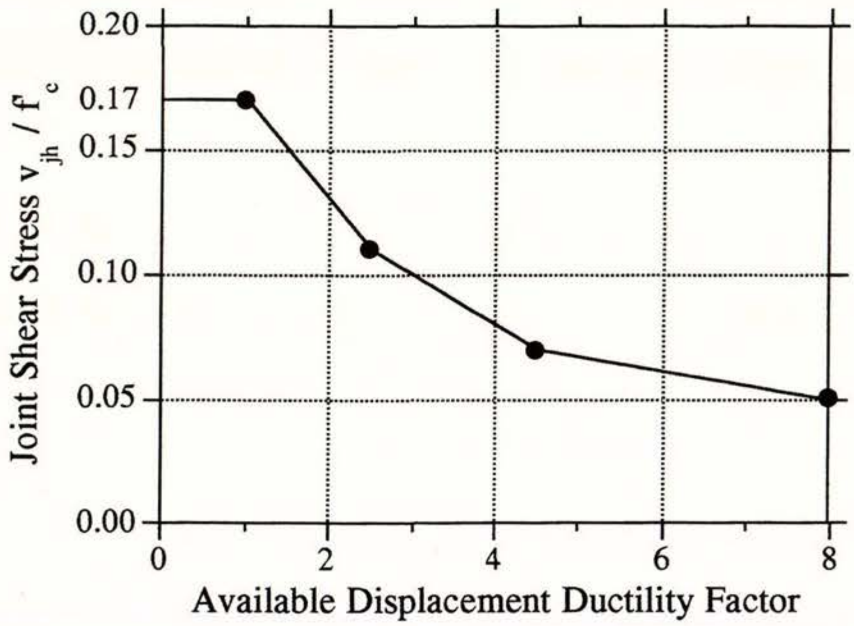

Fig.8.22 Degradation Model for the Joint Shear Stress

axial load acting on the columns. The effect of the axial load on the degradation of the joint shear strength needs to be investigated in future research.

The presence of joint hoops will restrict the increase in principal tensile strains in the joint core, resulting in delay in the strength degradation. However, when the quantity of joint hoops is not sufficient for the hoops to remain in the elastic range during seismic loading, the joint shear strength may degrade in the fashion shown in Fig.8.22.

8.5 SEISMIC BEHAVIOUR OF BEAMS WITH SMALL QUANTITIES OF TRANSVERSE REINFORCEMENT

8.5.1 Introduction

Transverse reinforcement is required in members to provide confinement of compressed concrete, restraint against buckling of longitudinal compression reinforcement and shear resistance. Inadequate quantities and detailing of transverse reinforcement are often found in the members of early reinforced concrete building frames. This may result in a reduction in the flexural ductility and shear failure of the members. This section examines the seismic behaviour of the beams with small quantities of transverse reinforcement in terms of curvature ductility and shear strength.

8.5.2 Curvature Ductility of Beam Sections

8.5.2.1 General

In spite of the poor ductile detailing in the plastic hinge region, the available curvature ductility factors of the beams obtained from conventional section analysis can be relatively large. As mentioned in Chapter 2, a section analysis showed that the curvature ductility factor of larger than 10 can be achieved for the typical beam section of the building frame being currently investigated. In this analysis, the maximum compressive strain of concrete was assumed to be ε_{cu}=0.004. Experimental evidence obtained from Specimens R3 and O6 also demonstrated the large curvature ductility capacities of the beams, provided that beam shear failure could be avoided.

It was found that in early building frames beam bars of large diameter often pass through columns of relatively small depth. Hence the anchorage of the beam bars in the joint cores may be poor. During severe earthquake loading, the plastic hinges in beams normally form near the beam-column joints. In such case, the beam bars may be in tension through the joint and the "compression" reinforcement of the beam on one side of the column may be actually in tension. Hence that steel will not act as "compression" reinforcement. This has been demonstrated by the results obtained from the tests on the beam-interior column joints without shear reinforcement conducted in this study. When the "compression" reinforcement is in tension, the available curvature ductility factor may be reduced. This section examines the effect of the stress conditions of the "compression" reinforcement on the curvature ductility capacity of the beam. The available curvature ductility capacities of the beams, taking into account the possible stress conditions of the "compression" reinforcement, are presented.

8.5.2.2 Calculation of Curvature Ductility Factors

The curvature ductility factor is expressed as ϕ_u / ϕ_y, where ϕ_y is the curvature when the tension reinforcement reaches the yield strain f_y / E_s, ϕ_u is the ultimate curvature when the concrete compressive strain in the extreme fibre reaches a specified limiting value, f_y is the yield strength of steel and E_s is modulus of elasticity of steel. The compressed concrete in the beam was treated as unconfined since typically only a small amount of transverse reinforcement was placed in the plastic hinge regions of the members of old building frames. The value for limiting concrete compressive strain was conservatively assumed to be ε_{cu}=0.004[Scott et al 1982].

Fig.8.23 shows the strain and stress diagrams of a beam section at stages corresponding to the first yield and ultimate curvatures. It is assumed in Fig.8.23 that plane sections remain plane after bending except that the strain in the "compression" reinforcement is not governed

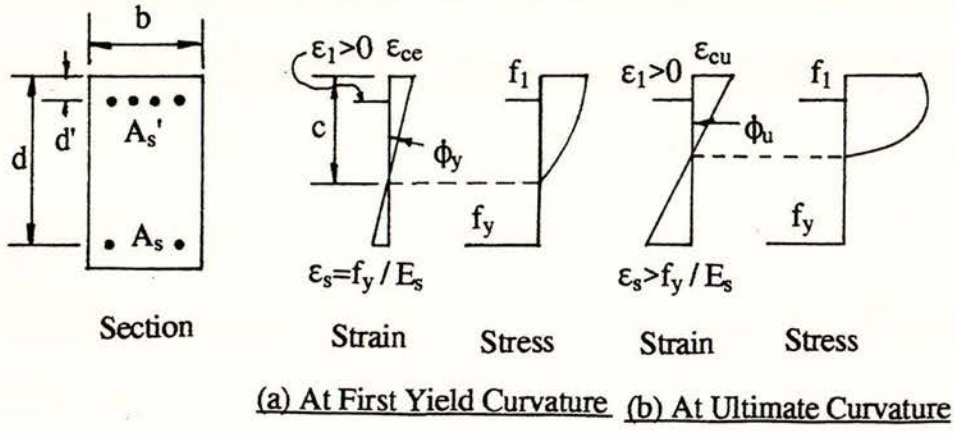

Fig.8.23 A beam Section with Flexure in Which Both the Top and Bottom Reinforcement are in tension

by that section behaviour. For a given neutral axis depth c, the curvature at first yield ϕ_y and the curvature at ultimate ϕ_u are calculated by(see Fig.8.23)

$$\text{Curvature at first yield} : \phi_y = \frac{f_y / E_s}{d - c} \tag{8.14}$$

$$\text{Curvature at ultimate} : \phi_u = \frac{\varepsilon_{cu}}{c} \tag{8.15}$$

where d is the depth from extreme compression fibre to the centroid of the tension reinforcement. The neutral axis depths at first yield and at ultimate can be found from analysis by satisfying the conditions of equilibrium for internal forces in the section and the compatibility of strains for a given strain of "compression" reinforcement. The concrete compression force for a given concrete strain in the extreme compression fibre can be obtained from the stress-strain relationship of the concrete. For chosen strains in the top and bottom reinforcement, the steel tensile forces can also be determined from the stress-strain relationship of the reinforcement. The stress-strain curve for unconfined concrete was expressed by the Kent and Park model[Kent and Park 1971], taking into account the nonlinear behaviour of the unconfined compressed concrete before and after yielding of the tension reinforcement. The stress-strain curve for longitudinal reinforcement was expressed by a bi-linear relation and did not take into account the strain hardening.

8.5.2.3 The Effect of the Stress Level of Compression Reinforcement

The effect of the stress level in the "compression" reinforcement on the neutral axis depths, curvatures, moment capacities and curvature ductility capacities was investigated for a typical beam cross section of the building frame investigated.

Fig.8.24 shows the typical beam cross section. The bottom and top reinforcement ratio ρ and ρ' was 0.67% and 1.34%, respectively. The steel yield strength f_y was assumed to be 300MPa while the concrete compressive strength was assumed to be 30MPa.

The relationship between the neutral axis depth expressed as c/d and level of stress in the "compression" reinforcement f_1/f_y is illustrated in Fig.8.24, where c is the depth of the neutral axis from the extreme compression fibre, d is the distance from the extreme compression fibre to the centroid of the tension reinforcement, f_1 is the stress in the "compression" reinforcement and f_y is the steel yield strength(see Fig.8.23). The stress in the "compression" reinforcement is positive if in tension and negative if in compression. This means that the stress in the "compression" reinforcement f_1/f_y becomes more tensile as the bond along the main beam bars in the joint deteriorates. It should be noted that for the given beam section the neutral axis depth at ultimate calculated for positive moment is small so that the neutral axis lies above the "compression" reinforcement. Therefore, the "compression" reinforcement was in tension even when the perfect bond was assumed along the beam bars in the joint.

As could be expected, the neutral axis depths at yield and ultimate increased as the tensile stress in the "compression" reinforcement was increased. This trend became more obvious for positive moment in which the amount of the "compression" reinforcement was larger. When the tensile stress in the "compression" reinforcement approached the steel yield strength, that was f_1/f_y=1.0, the neutral axis depth during positive and negative moment became almost the same. When the tensile stress in the "compression" reinforcement reached the yield strength, the neutral axis depth was increased by 30 to 90% at yield and 100 to 170% at ultimate, respectively, when compared with those obtained for the perfect bond condition along the main beam bars.

Fig.8.25 shows the relationship between yield and ultimate moment and stress level in the "compression" reinforcement. The yield and ultimate moments decreased as the tensile stress in the "compression" reinforcement was increased. However, the effect of the stress level in the "compression" reinforcement on the ultimate moment was not so significant. When the tensile stress level in the "compression" reinforcement f_1/f_y was 1.0, the decrease in the ultimate moment was 10% for positive moment and 5% for negative moment, respectively, when compared with those with the perfect bond condition along the beam bars.

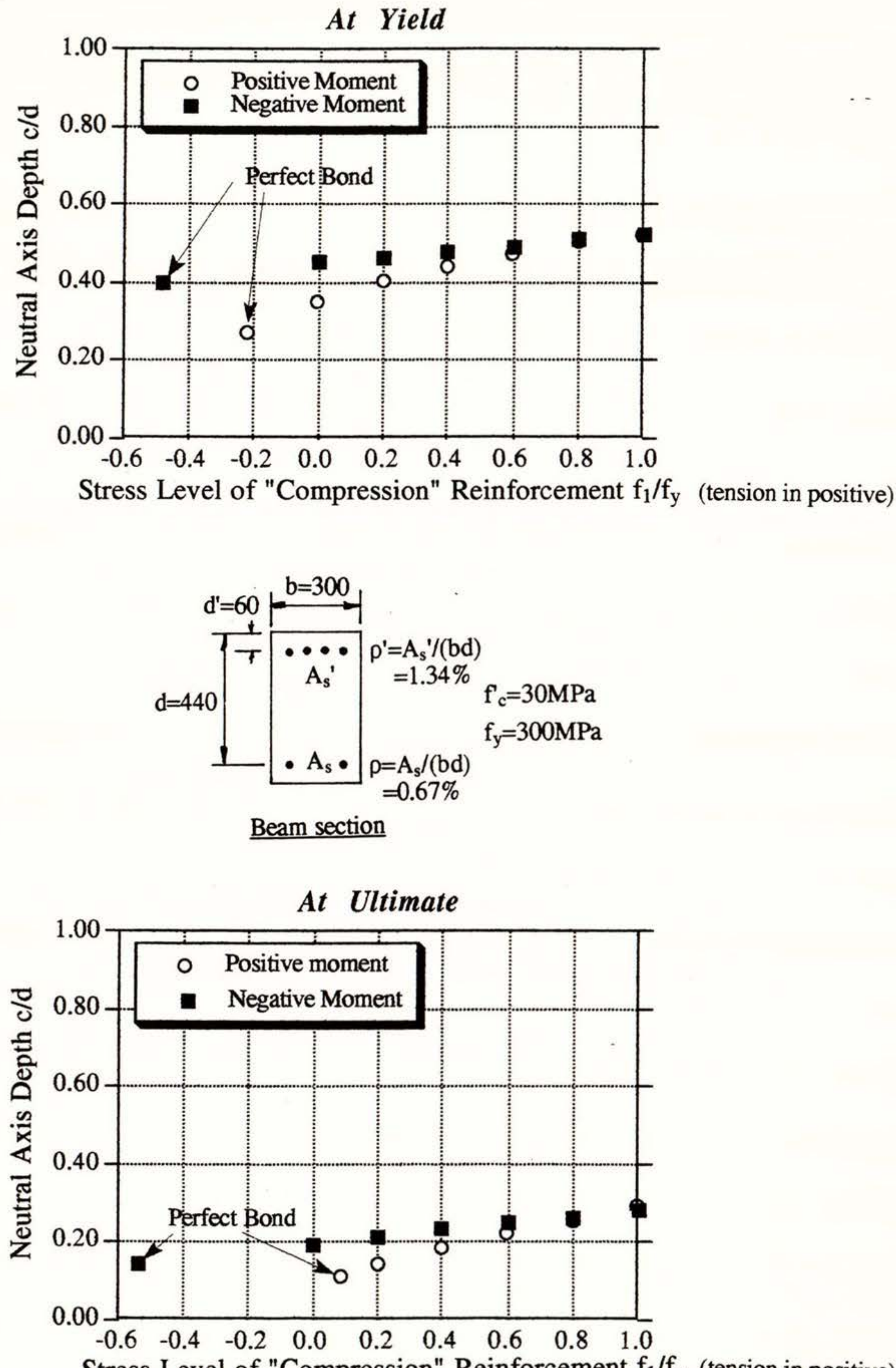

Fig.8.24 Neutral Axis Depth Related to Stress Level in the "Compression" Reinforcement

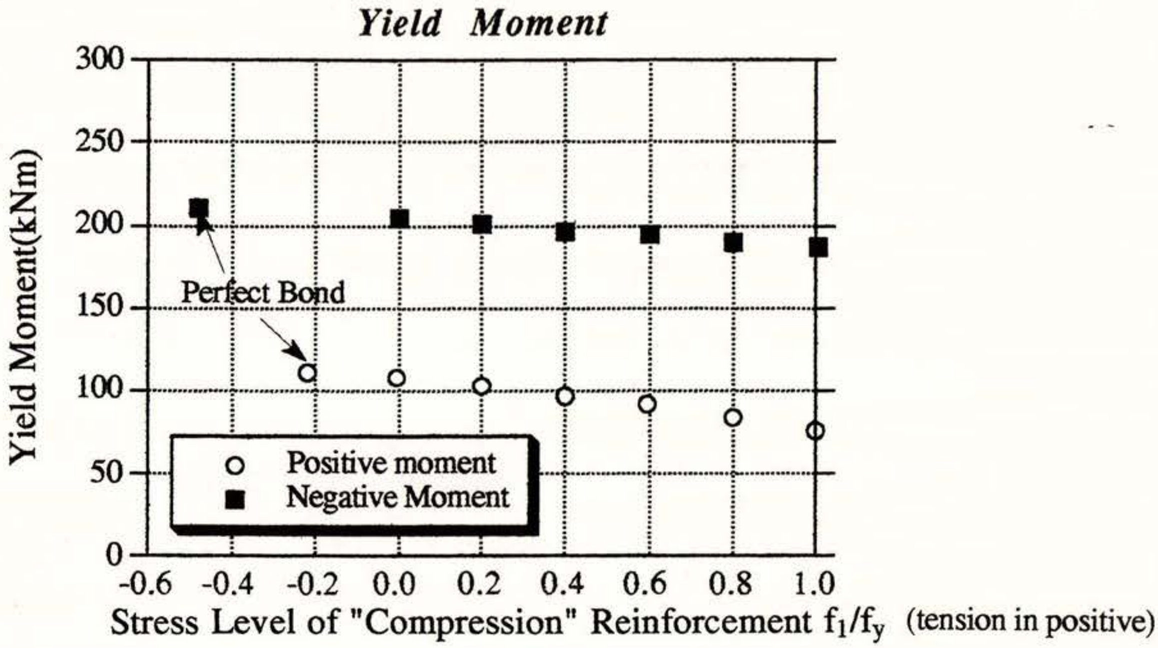

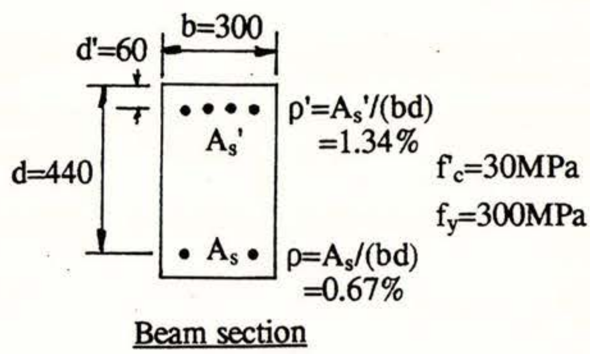

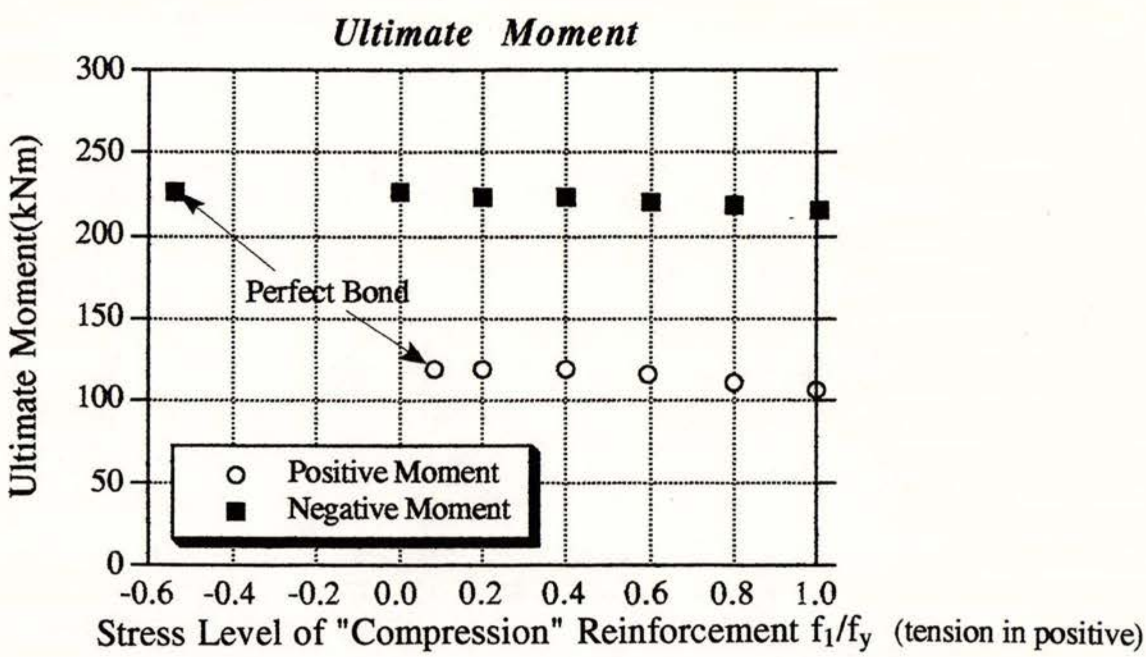

Fig.8.25 Moment Capacities Related to Stress Level in the "Compression" Reinforcement

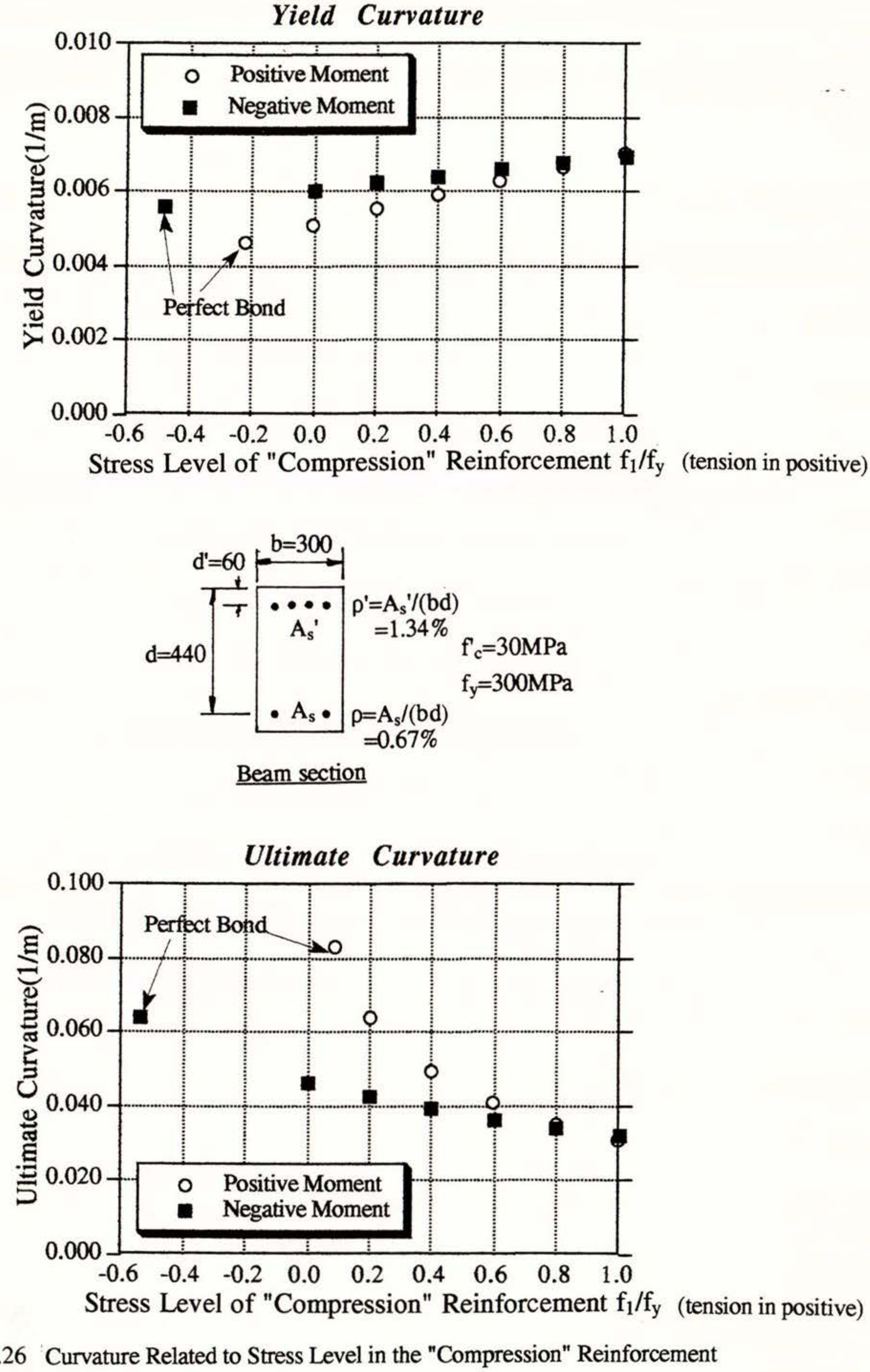

Fig.8.26 Curvature Related to Stress Level in the "Compression" Reinforcement

Fig.8.26 illustrates the effect of the stress level in the "compression" reinforcement on the yield and ultimate curvatures. As the tensile stress level in the "compression" reinforcement was increased, the yield curvature increased. In contrast, the value of the ultimate curvature decreased. This is because of the increase in the neutral axis depth, caused by the tensile stress induced in the "compression" reinforcement. The effect of the stress level in the "compression" reinforcement was more obvious when the "compression" reinforcement ratio was increased, as during positive moment. When the bond along the main beam bars in the joint was completely destroyed, which was the case when the stress level in the "compression" reinforcement was $f_1/f_y=1.0$, the yield curvature increased by 25 to 50% and the ultimate curvature decreased by 40 to 50% for the given beam cross section. When the stress in the "compression" reinforcement approached the yield strength, the yield and ultimate curvatures obtained during positive moment became close to the values obtained during negative moment.

The relationship between the curvature ductility factor and the stress level in the "compression" reinforcement is shown in Fig.8.27. As shown in this figure, the curvature

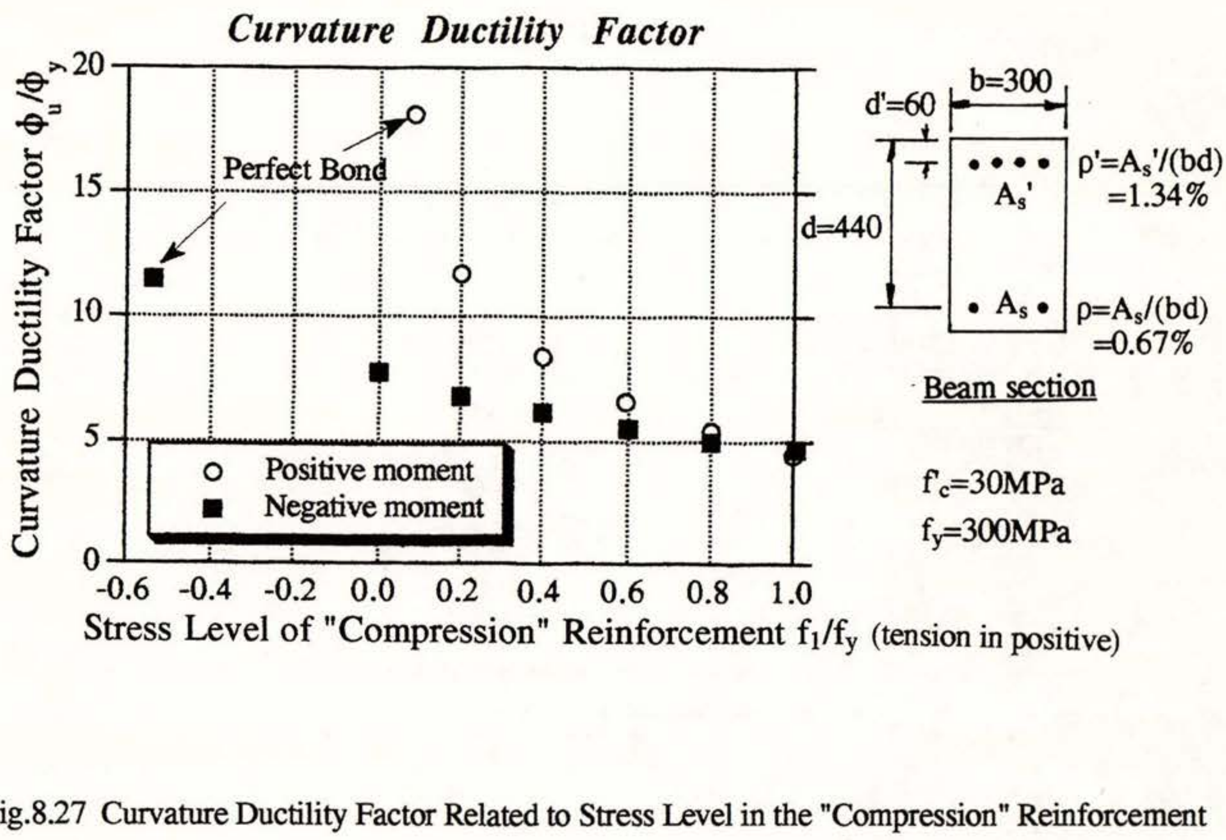

Fig.8.27 Curvature Ductility Factor Related to Stress Level in the "Compression" Reinforcement

ductility factor was significantly reduced when the tensile stress in the "compression" reinforcement was increased, especially during positive moment. This trend is a result of changes in the neutral axis depth at yield and ultimate as described before. An available curvature ductility factor of larger than 10 obtained for the perfect bond condition of the "compression" reinforcement approached approximately 5 for the given beam section as the tensile stress in the "compression" reinforcement was increased. When the tensile stress in the "compression" reinforcement was 40% of the yield strength, the curvature ductility factor was reduced to approximately one half of that for when the perfect bond was assumed for the main beam bars.

8.5.2.4 Curvature Ductility Factors of Beam Sections Taking into Account the Bond Conditions along the Main Beam Bars in the Beam-Interior Column Joints

In order to obtain a realistic estimate of the available curvature ductility capacity of a beam section, it is necessary to estimate the stress level in the "compression" reinforcement of the beam adjacent to the joint. The stress level in the "compression" reinforcement depends on the ratio of the column depth to the beam bar diameter, the stress level in the tension reinforcement and the bond stress conditions along the longitudinal reinforcement in the joint. As mentioned before, the bond stress distribution along the main beam bars in the joint without shear reinforcement was expressed as shown in Fig.8.28, when the axial load acting on the column was zero, after the tension reinforcement reached the yield strength and diagonal tension cracking was initiated. The bond stress distribution so obtained was based mainly on the experimental results in this study. By using the bond stress distribution along the longitudinal reinforcement in the joint without shear reinforcement illustrated in Fig.8.28, the tensile stress in the "compression" reinforcement can be calculated for the given strengths of the concrete and longitudinal reinforcement. Fig.8.28 shows the tensile stress in the "compression" reinforcement plotted against the ratio of the column depth to the beam bar diameter h_c/d_b when the concrete compressive strength and the steel yield strength were assumed to be 30MPa and 300MPa, respectively, where h_c is the column overall depth and d_b is the beam bar diameter. When the ratio of the column depth to beam bar diameter is small, large tensile stress can be expected to be generated in the "compression" reinforcement.

Figs.8.29(a), (b) and (c) illustrate the curvature ductility factors of beam sections, plotted against the tension reinforcement ratio ρ for a practical range of ratio of column depth to beam bar diameter h_c/d_b and ratio of top reinforcement area to bottom reinforcement area ρ'/ρ. The beams have a concrete compressive strength of 30MPa and a steel yield strength of 300MPa. The available curvature ductility factors decreased when the tension reinforcement ratio ρ was increased. When ρ was larger than 1.5%, the available curvature ductility factor was reduced to be less than 5 for the range of the ratio h_c/d_b of 12.5 to 25. When ρ was

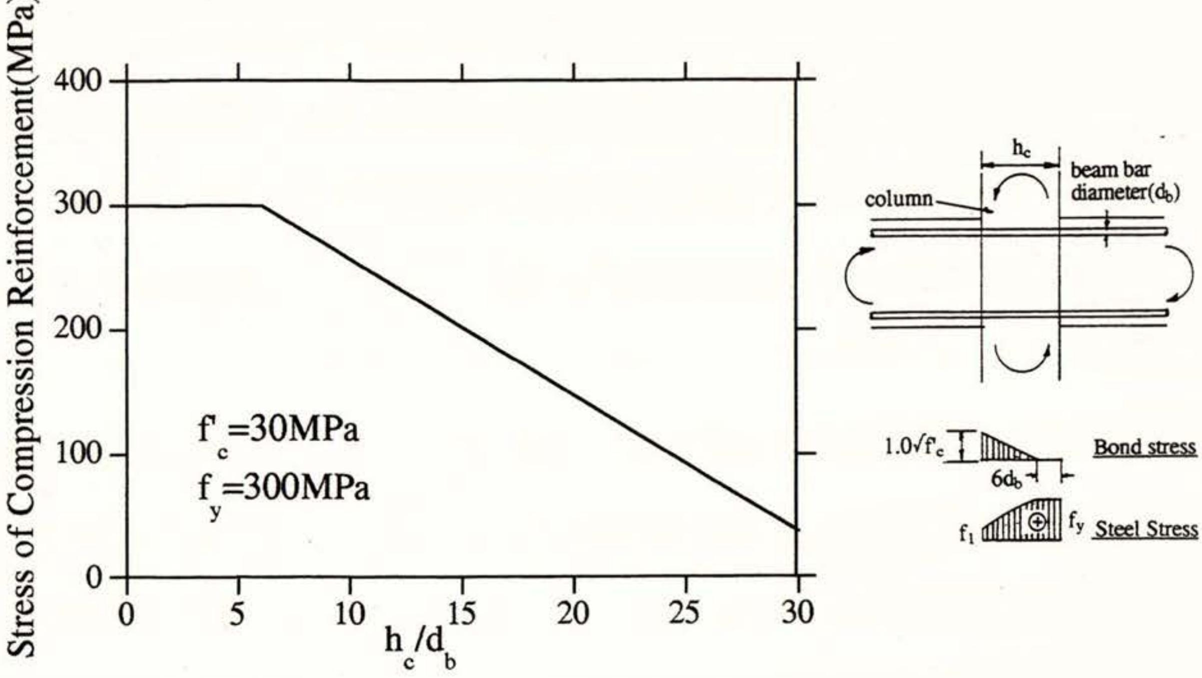

Fig.8.28 Tensile Stress in the "Compression" Reinforcement Related to h_c/d_b

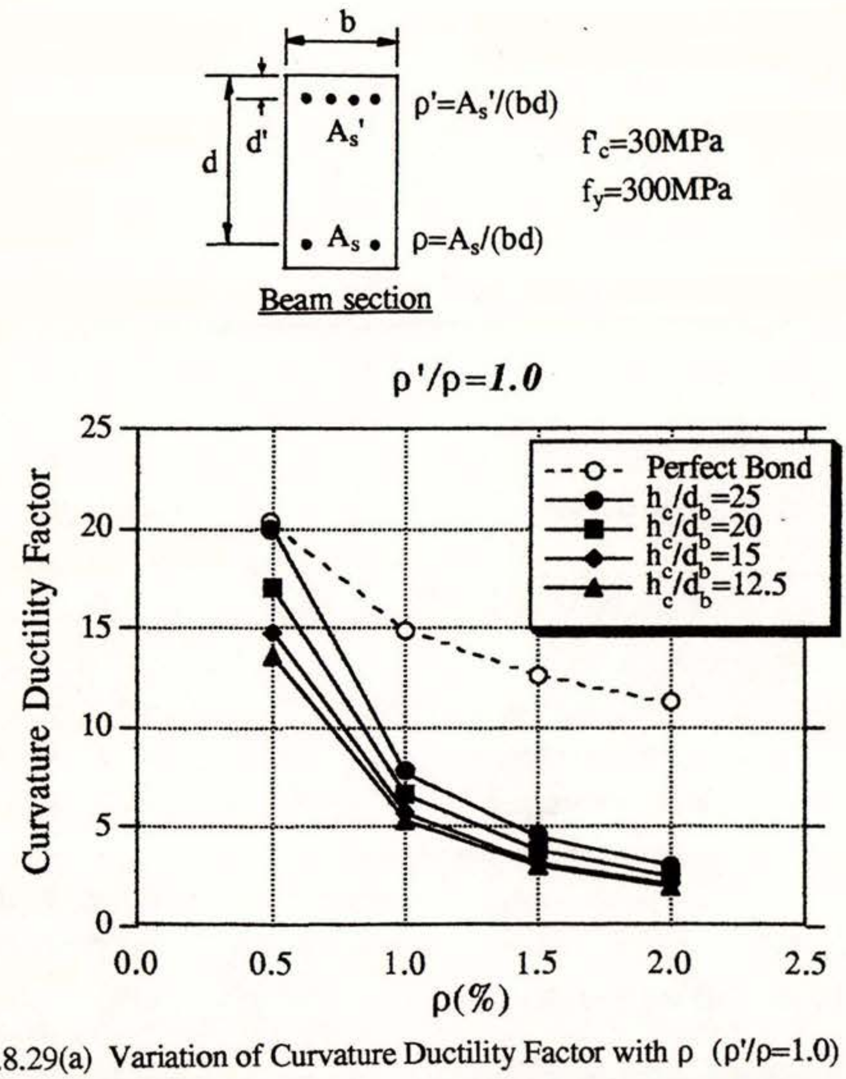

Fig.8.29(a) Variation of Curvature Ductility Factor with ρ (ρ'/ρ=1.0)

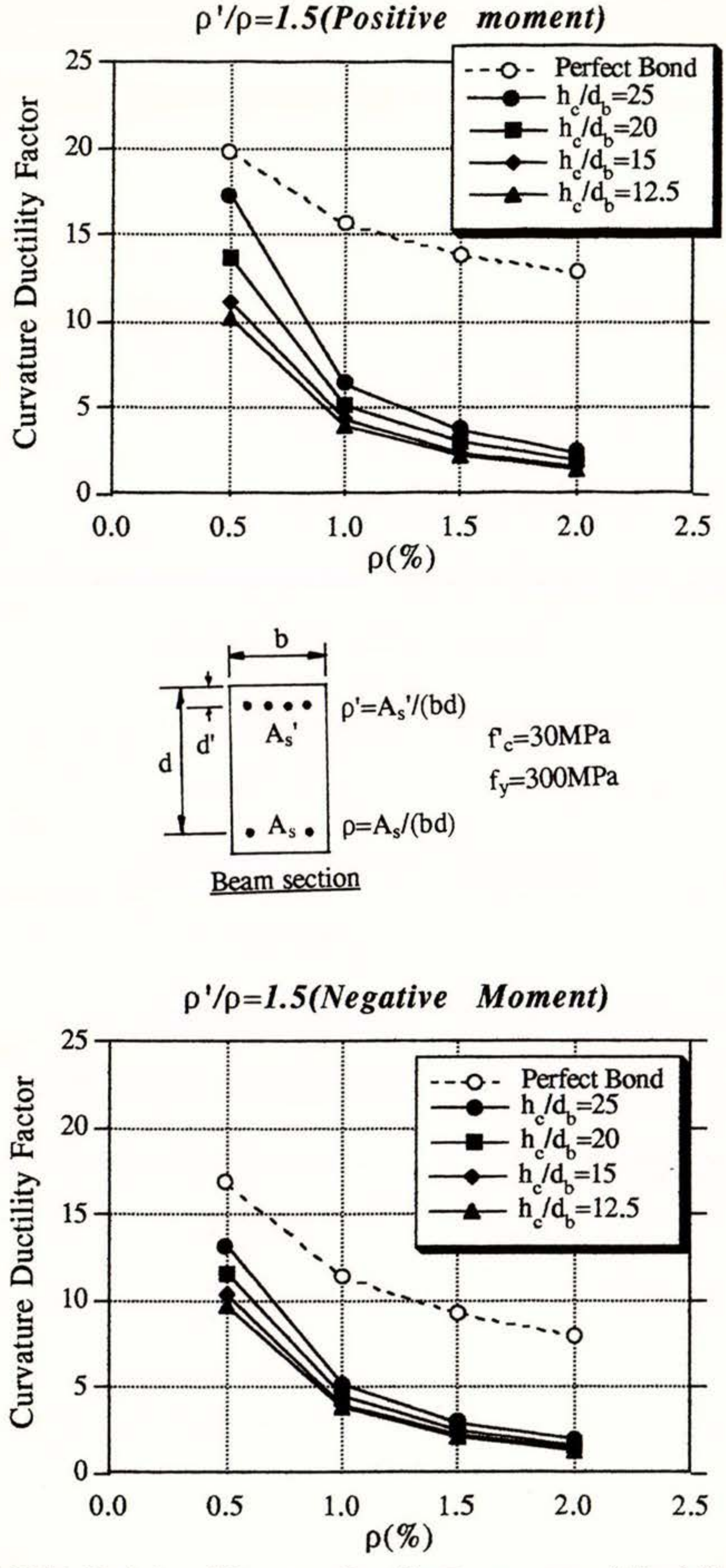

Fig.8.29(b) Variation of Curvature Ductility Factor with ρ (ρ'/ρ=1.5)

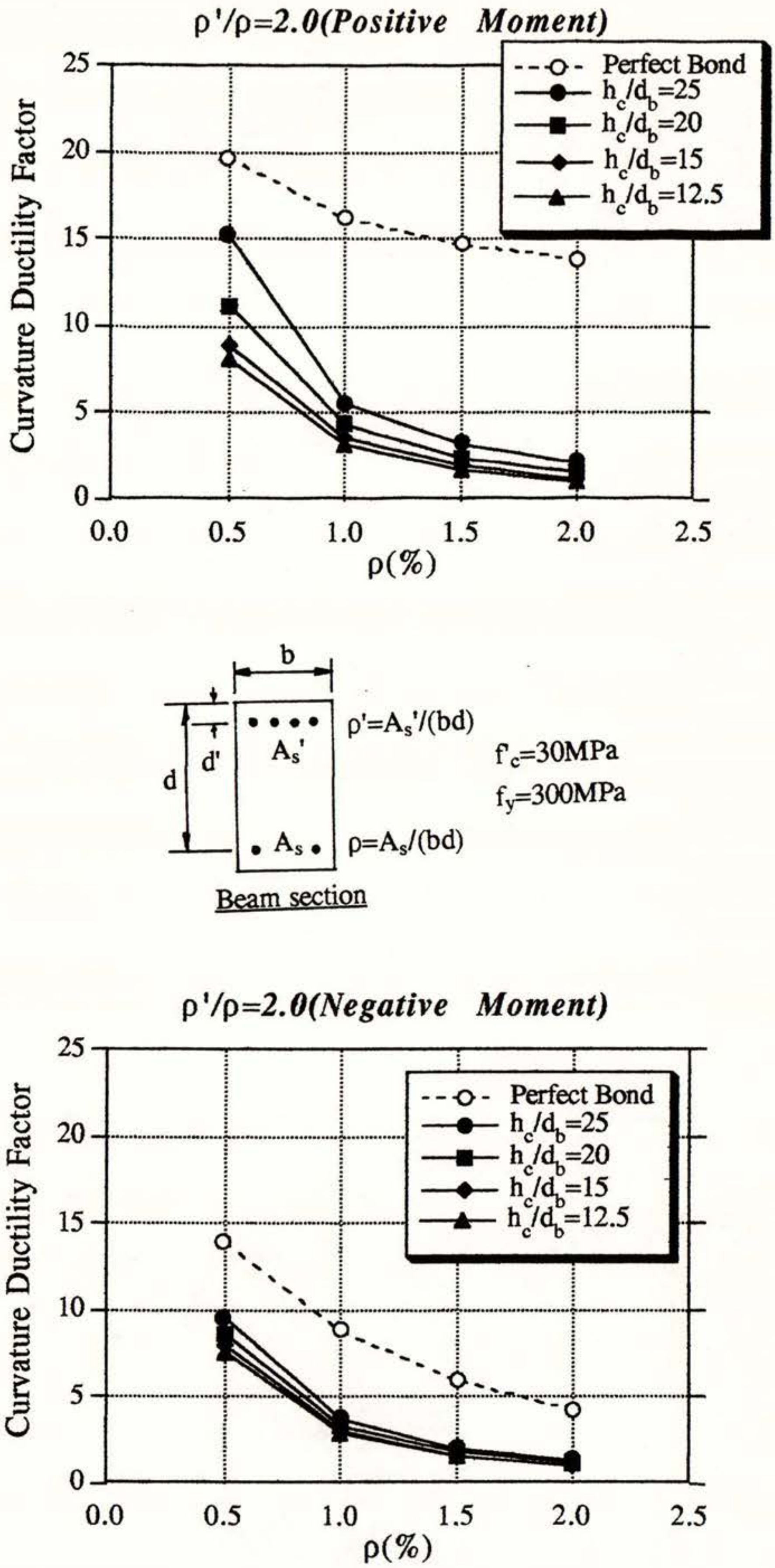

Fig.8.29(c) Variation of Curvature Ductility Factor with ρ (ρ'/ρ=2.0)

0.5% and ρ'/ρ was less than 1.5, an available curvature ductility factor larger than 10 was attained, irrespective of the column depth to beam bar diameter ratio. When the ratio of the the column depth to beam bar diameter was decreased and ρ=0.5%, the curvature ductility factor significantly decreased, especially during positive moment, indicating that the larger the "compression" reinforcement ratio, the larger the reduction of the available curvature ductility factors of the beam sections. When ρ was larger than 1.0%, the effect of the ratio h_c/d_b on the curvature ductility factor became insignificant in the range of h_c/d_b of 12.5 to 25. As Fig.8.29 indicates, the available curvature ductility factors were about 10 for beam sections with ρ=0.5% and about 5 for those with ρ=1.0%. Much smaller available curvature ductility factors were found for beam sections with ρ larger than 1.0%.

It was found from the dynamic analysis of the building frames designed in the late 1950's discussed in Chapter 2 that the maximum curvature ductility demand of the beams was about 10 under the severe earthquake motion. The ratio of the column depth to beam bar diameter h_c/d_b is typically in the range of 12.5 to 19 for the building frames. In such case, only a beam with tension reinforcement ratio ρ less than 0.5% can survive the earthquake. The effect of the tensile stress in the "compression" reinforcement due to bond deterioration along the beam bars in the joint on the available curvature ductility factor of the beam section will be critical during positive moment since "compression" reinforcement ratio is larger.

It should be mentioned that the bond stress distribution along the beam bars in the joint shown in Fig.8.28 was obtained from the results of tests on the beam-interior joint specimens without axial load on the columns. Usually the columns in the building frame are subjected to axial compression load. In such case, much better bond condition can be expected for the beam bars through the joint due to the transverse compression force acting on the beam bars in the joint[Taylor and Clarke 1976 and Eligehausen et al 1983]. Therefore, the "compression" reinforcement may not be stressed in tension as significantly as indicated above, resulting in the available curvature ductility factors of the beam sections being larger than those calculated above. It should also be mentioned that the value assumed for the limiting concrete compressive strain in the extreme fibre at ultimate, ε_{cu}=0.004, is a lower bound for the strain at crushing of the unconfined concrete[Scott et al 1982]. If a value higher than 0.004 is used in the ultimate curvature calculation, a greater flexural ductility will be obtained since the ultimate curvature depends very much on the value of the extreme fibre strain. Further research is necessary into these aspects.

8.5.3 Seismic Shear Strength of the Beam

8.5.3.1 Previous Models

The available curvature ductility factors described in Section 8.5.2 are applicable only if buckling of compression reinforcement in the beams and shear failure of the beams, columns and joints can be prevented under seismic loading. Shear strength in plastic hinge regions degrades as the ductility demand increases, due to reduced shear carried by the concrete shear resisting mechanisms. Extensive research has been conducted to establish a shear design procedure which enables the relationships between shear strength and displacement ductility factor to be obtained for columns[Ang et al 1988, Priestley and Calvi 1991, Aschheim and Moehle 1992, Wong et al 1993, and Priestley et al 1993]. Those relationships may be used to evaluate the potential shear failure and the available displacement ductility factor in conjunction with the shear demand of the member. This section briefly reviews the proposed models for shear strength. Predictions of the shear strength from those models are compared with the results of tests on Specimen R3, in which the beams failed in shear during beam negative moment. A modification to the concrete shear resisting mechanisms of an existing model[Priestley and Calvi 1991] is recommended for estimating the beam shear strength.

8.5.3.2 Current Design Code Equations for Shear Strength

Current design codes[ACI 318 1989 and SANZ 1982(a)] assume that all the shear reinforcement across a shear failure plane with an angle of 45 deg to the member axis reaches the yield strength, and the shear carried by the shear reinforcement V_s can be expressed by

$$V_s = \frac{A_v f_{yv} d}{s} \tag{8.16}$$

where A_v is the area of shear reinforcement at spacing s, f_{yv} is the yield strength of shear reinforcement and d is the effective depth of the member.

The prediction of the shear resisted by the 45 degree truss model is usually conservative, particularly for beams with a small amount of shear reinforcement. Consequently, it has become accepted design practice to add an empirical correction term to the 45 deg truss equation. The correction term is commonly referred to the "concrete contribution" V_c and is taken as the shear at the commencement of diagonal tension cracking.

For members without axial load, the ACI and the New Zealand Standards Association express the " concrete contribution" as follows:

ACI simplified equation $V_c=0.17\sqrt{f'_c}bd$ (MPa) (8.17)

NZ equation $V_c=(0.07+10\rho_w)\sqrt{f'_c}bd<0.2\sqrt{f'_c}bd$ (MPa) (8.18)

where f'_c is the concrete compressive strength, b is the member width, d is the effective depth of the member and ρ_w is the longitudinal tension steel ratio.

The nominal shear strength V_n is then given by an additive equation as follows:

$$V_n=V_c+V_s \tag{8.19}$$

It should be noted that Eqs. 8.17 to 8.19 refer to regions of members outside plastic hinge regions. For within plastic hinge regions, both the ACI and NZ codes define reduced values for the concrete components V_c.

Recently several design codes[CSA 1984, CEB-FIP Code 1990, and AIJ 1990] have adopted a more rational approach, using "diagonal compression field theory"[Collins and Mitchell 1980] or "plastic theory"[Nielsen 1984] for predicting the shear strength, allowing a wide range of values for the permissible angle of inclination of the principal compressive stress to the axis of the member. However, it has not yet been considered qualitatively by those design codes, except for the AIJ approach, that shear strength at plastic hinges degrades as the displacement ductility demand increases[AIJ 1990].

8.5.3.3 Proposed Models for Predicting the Seismic Shear Strength

Current design code equations cannot predict the real shear strength of a member since they are intended to provide a conservative estimate of the shear strength for safety. Besides, they do not clearly indicate the influence of the displacement ductility factor on the shear strength of the member. Considerable experimental and analytical research[Ang et al 1988, Priestley and Calvi 1991, Aschheim and Moehle 1992, Wong et al 1993, and Priestley et al 1993] has been carried out to propose more realistic shear strength equations which are related to the displacement ductility factor. Most of the proposed models express the degradation of shear strength as a reduced shear carried by the concrete mechanisms V_c due to reversal cyclic loading at the plastic hinges.

Model by Ang et al

Ang, Priestley and Paulay 1988 reviewed the existing U.S. and New Zealand design expressions for the shear strength of circular columns and compared them with the results from a comprehensive test programme involving 25 circular columns. It was identified by their work that current U.S. and New Zealand design equations for the concrete contribution are very conservative. Based on the experimental results, new design equations were suggested for the initial shear strength V_i as follows:

$$V_i=V_{ci}+V_{si} \tag{8.20}$$

$$V_{ci} = 0.37\,\alpha\,(1+\frac{3P}{f'_c A_g})\,\sqrt{f'_c}\,A_e \text{ (MPa)} \tag{8.21}$$

where $\alpha=2/(M/VD)>1.0$

$$V_{si} = \frac{\pi}{2} A_v\, f_{yv} \frac{D'}{s} \tag{8.22}$$

where V_{ci} is the initial shear strength carried by concrete, V_{si} is the initial shear strength carried by shear reinforcement, f'_c is the concrete compressive strength, M/VD is the column aspect ratio, D is the gross column diameter, D' is the diameter of confined core, A_g is the gross cross sectional area, A_e is the effective shear area=$0.8A_g$, A_v is the area of shear reinforcement, f_{yv} is the yield strength of the shear reinforcement and s is the spacing of shear reinforcement.

For the final shear strength after degradation, the concrete contribution of the initial shear strength was reduced. For the shear carried by shear reinforcement, a lower bound plastic theory solution was used to estimate the angle of the diagonal compression strut of the analogous truss mechanism while a 45 degree analogous truss mechanism was used for the initial shear strength. The following equations were suggested for the final shear strength V_f.

$$V_f=V_{cf}+V_{sf} \tag{8.23}$$

$$V_{cf}=18.5\rho_s\sqrt{f'_c}A_e<0.185\sqrt{f'_c}A_e \text{ (MPa)} \tag{8.24}$$

$$V_{sf}=\frac{\pi\, A_v\, f_{yv}D'}{2\,s}\sqrt{\frac{1-\varphi}{\varphi}} \leq \frac{2.15\,\pi\, A_v\, f_{yv}D'}{2\,s} \tag{8.25}$$

where V_{cf} is the final shear strength carried by concrete, V_{sf} is the final shear strength carried by shear reinforcement, ρ_s is the ratio of hoop or spiral reinforcement volumetric to the concrete core volume and φ is the mechanical reinforcement ratio(=$\rho_s f_{yv}/(\nu f'_c)$), ν is a factor for the reduced effective compressive concrete strength of the diagonal strut, D' is the diameter of confined core, A_e is the effective shear area, A_v is the area of shear reinforcement, f_{yv} is the yield strength of shear reinforcement and s is the spacing of shear reinforcement.

Maximum contributions of the concrete and shear reinforcement to the final shear strength were obtained when ρ_s is 0.01 and the angle of diagonal struts is 25 deg to the horizontal axis. A model for shear strength degradation with increasing displacement ductility has been suggested, which was similar to one proposed by the Applied Technology Council for retrofitting highway bridges[ATC 6-2 1983]. The initial shear strength V_i was assumed to apply for displacement ductility factors of up to 2. At higher ductilities, the shear strength degrades until a final value V_f was attained when the flexural ductility capacity was reached. Methods for estimating the flexural ductility capacities are presented elsewhere[Priestley and Park 1987].

Recent work by Wong et al 1993 proposed more general form of Ang et al's equations, including the effect of displacement history. It was shown that the reduction of shear strength with displacement ductility was more severe under biaxial seismic attack.

Model for Columns by Priestley et al

On the basis of the work of Ang et al 1988 and Wong et al 1993, the model proposed by Ang et al was modified. The strength enhancement provided by axial compression was separated from the "concrete contribution" of the shear strength and considered to result from arch action[Priestley et al 1993]. The shear strength of a column was considered to consist of three independent components: the concrete component V_c, the axial load component V_p and the shear reinforcement component V_s. Thus

$$V_n=V_c+V_p+V_s \tag{8.26}$$

The concrete component was given by

$$V_c=k\sqrt{f'_c}A_e \tag{8.27}$$

where k depends on the imposed displacement ductility factor, varying between 0.29 for the initial shear strength(MPa) and 0.1 for the final shear strength(MPa). The concrete component for the initial shear strength was applied to displacement ductility factor of up to 2 and degraded linearly to a displacement ductility factor of 4 for the final shear strength when the column is expected to be subjected to uniaxial displacement ductility demand.

The axial load component was obtained from

$$\begin{aligned} V_p &= P\tan\theta_{st} \\ &= \frac{(D-c)}{2a}P \end{aligned} \tag{8.28}$$

where P is the axial load on column, θ_{st} is the inclination of the strut by arch action, D is the overall section depth, c is the depth of the compression zone and either a=L for a cantilever column or a=L/2 for a column in double bending, where L is the column height. Note that V_p does not degrade with increasing displacement ductility factor.

The shear reinforcement component was based on a truss mechanism with an angle of 30 deg to the vertical axis rather than 45 deg, based on the visual observation of diagonal tension cracking during the tests. The shear carried by the shear reinforcement V_s is then given by

$$\text{For circular column} \quad : V_s = \frac{\pi}{2}\frac{A_v f_{yv} D'}{s}\cot(30\text{ deg}) \tag{8.29}$$

$$\text{For rectangular colum} \quad : V_s = \frac{A_v f_{yv} D'}{s}\cot(30\text{ deg}) \tag{8.30}$$

where A_v is the area of shear reinforcement, f_{yv} is the yield strength of shear reinforcement and D' is the distance between centres of hoop or spiral.

Model by Aschheim et al

Aschheim and Moehle 1992 reviewed the columns damaged in previous Californian earthquakes and laboratory data to determine the coefficient k in the concrete contribution for shear resistance $V_c=k\sqrt{f'_c}A_e$, where f'_c is the concrete compressive cylinder strength and A_e is the effective cross section area. The estimate of k obtained was as follows:

$$\text{For spirally reinforced columns} \quad : k = \frac{0.03\rho_s f_{yv}}{\mu}\ (\text{psi}) \tag{8.31}$$

$$\text{For rectangular reinforced columns} \quad : k = \frac{0.06 p_w f_{yv}}{\mu}\ (\text{psi}) \tag{8.32}$$

where ρ_s is the spiral reinforcement ratio, p_w is the web reinforcement ratio, f_{yv} is the yield strength of hoop or spiral reinforcement and μ is the displacement ductility factor.

It was assumed that the shear carried by shear reinforcement was defined by a 45 deg truss mechanism and did not change with increasing displacement ductility.

AIJ Approach

In Japan, a theoretical shear design method has been proposed and adopted in the recommendations of the Architectural Institute of Japan[AIJ 1990]. The method was based on the superposition of the truss and the arch mechanisms, and limiting the diagonal compressive stress in the concrete resulting from combined truss and the arch action. The angle of the truss mechanism was estimated using a lower bound plastic theory solution with the limited value of 22.5 deg to the axis of the member. For the initial shear strength, the effectiveness factor of diagonally compressed concrete ν_o was obtained using the equation by Nielsen 1984 as follows:

$$\nu_o = 0.7 - f'_c/200 \text{ (MPa)} \tag{8.33}$$

The shear carried by truss mechanism was given by

$$V_s = \frac{A_v f_{yv} j_t}{s} \cot(\theta_t) \tag{8.34}$$

$$\cot(\theta_t) = \min\left(\sqrt{\frac{(1-\varphi)}{\varphi}},\ 2,\ \frac{j_t}{h \tan\theta_{st}}\right) \tag{8.35}$$

where j_t is the distance between the upper and lower stringers and for a beam with multi-layered longitudinal reinforcement it is taken as the distance between the plastic centroids of the tension and compression longitudinal reinforcement, s is the spacing of the shear reinforcement, θ_t is the angle of the compression strut to member axis in truss mechanism, φ is the mechanical reinforcement ratio($=p_w f_{yv}/(\nu_o f'_c)$), p_w is the shear reinforcement ratio($=A_v/bs$), A_v is the area of shear reinforcement, b is the width of the section, f_{yv} is the yield strength of shear reinforcement(when $f_{yv} > 25f'_c$, $f_{yv} = 25f'_c$), h is the section depth and θ_{st} is the angle of the compression strut to the member axis in arch action.

The shear force carried by the arch mechanism V_c was given by

$$V_c = 0.5bh(1-\beta)\nu_o f'_c \tan\theta_{st} \tag{8.36}$$

where $\tan\theta_{st} = \sqrt{(L/h)^2+1} - L/h$, $\beta = [(1+\cot^2\theta_t)p_w f_{yv}]/(\nu_o f'_c)$, f'_c is the concrete compressive cylinder strength, and L is the clear span of a member.

The AIJ Approach assumes that the shear carried by arch action decreases with increase in the amount of shear reinforcement.

In order to allow for the degradation of diagonally compressed concrete due to diagonal cracking in two directions under reversed cyclic loading, the effective compressive strength of concrete in a plastic hinge region was reduced in proportion to the inelastic hinge rotation angle R_p as follows:

$$\nu f'_c=(1.0\text{-}15R_p)\nu_o f'_c \qquad 0<R_p<0.05 \qquad (8.37)$$

$$=0.25\nu_o f'_c \qquad 0.05<R_p \qquad (8.38)$$

where ν is an effectiveness factor for hinge region and R_p is an inelastic hinge rotation angle in radians. For practical purposes R_p can be taken as the total hinge rotation angle or member rotation angle. The maximum allowable value of $\cot\theta_t$ in truss action was reduced, taking into account the loss of interlocking action along the cracked surfaces in the plastic hinge region. The following equations were derived based on the experimental data:

$$\cot\theta_t=2.0\text{-}50R_p \qquad 0<R_p<0.02 \qquad (8.39)$$

$$=1 \qquad 0.02<R_p \qquad (8.40)$$

Model for Beams by Priestley

Priestley and Calvi 1991 proposed a simple model for the concrete contribution of the beam. The concrete contribution for the initial shear strength was calculated using the New Zealand code equations[SANZ 1982(a)]. After a displacement ductility factor of 2 is imposed, the concrete contribution was reduced linearly to a displacement ductility factor of 4 where the concrete contribution was totally ignored. The shear carried by the shear reinforcement was defined using a 45 deg truss mechanism for both the initial and final shear strength calculations.

8.5.3.4 Nominal Shear Stress in the Beam

Fig.8.30 shows observed cracking of Specimens R3 and O6, in which the beams suffered severe diagonal tension cracking. The relationships between the nominal shear stress and displacement ductility factor obtained for the beams of Specimens R3 and O6 are illustrated in Fig.8.31.

For Specimen R3, shear failure in the beams commenced with negative moment applied when the maximum nominal shear stress in the beams reached about $0.18\sqrt{f'_c}$, where f'_c is the measured concrete compressive cylinder strength. At a beam displacement ductility factor of approximately 2, the shear strength degraded rapidly with increasing displacement ductility as shown in Fig.8.31(a). It is clearly shown in Figs.8.30(a) and 8.31(a) that the concrete contribution to the shear resistance of the beam with inadequate quantities of transverse reinforcement, namely aggregate interlock[Fenwick and Paulay 1968], across the flexural compression zone and dowel action, were significantly reduced at a displacement ductility of

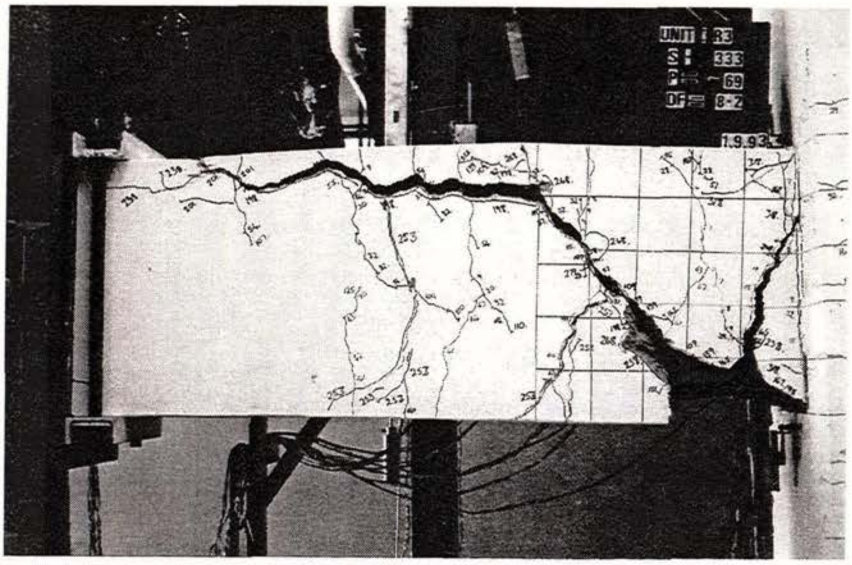

(a) Specimen R3

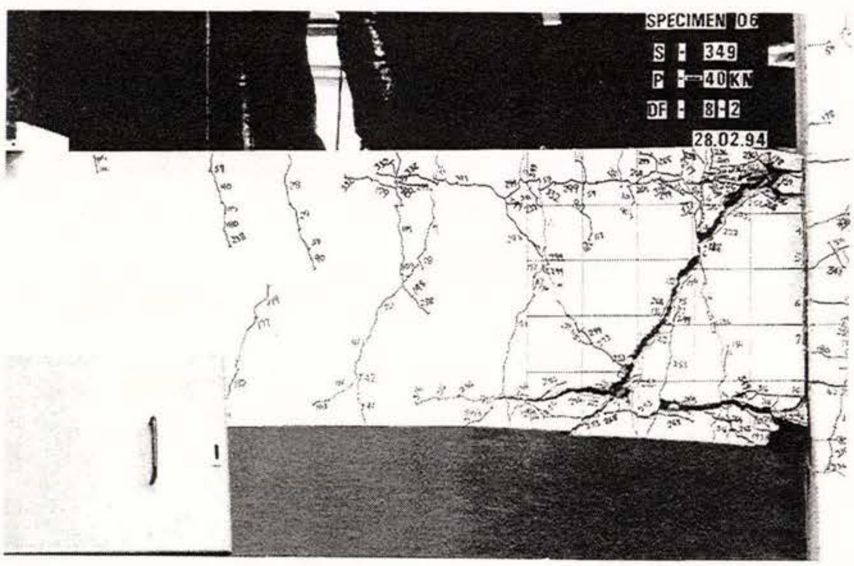

(b) Specimen O6

Fig.8.30 Observed Cracking at the Second Cycle to DF of -8

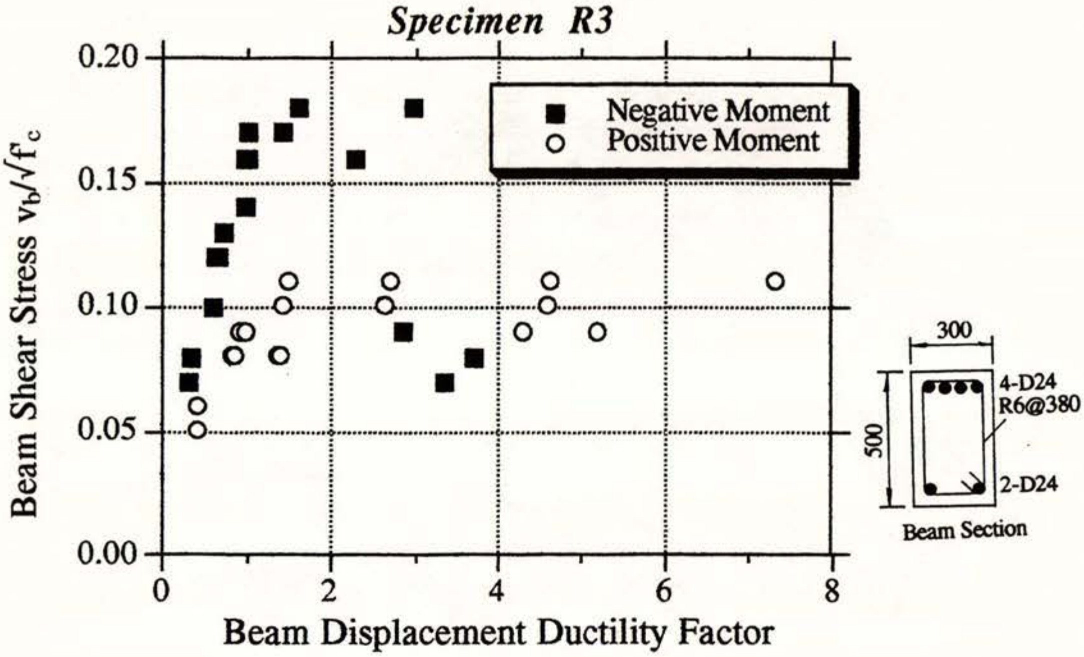

(a) Specimen R3

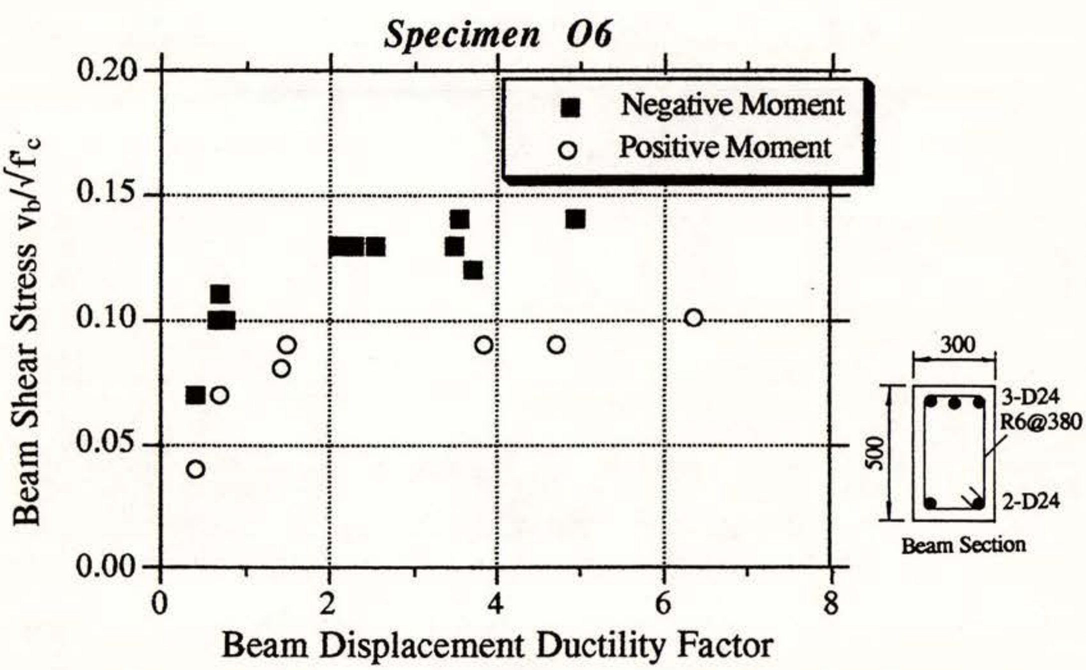

(b) Specimen O6

Fig.8.31 Beam Shear Stress versus Displacement Ductility Factor Relationship about 4. With positive moment applied, the maximum nominal shear stress in the beams was $0.11\sqrt{f'_c}$. Shear failure did not occur with positive moment applied and a ductile response was attained for that direction of shear force as shown in Fig.8.31(a).

For Specimen O6, the maximum nominal shear stress in the beam was $0.14\sqrt{f'_c}$ with negative moment applied and $0.11\sqrt{f'_c}$ with positive moment applied. Only a small reduction in shear strength of the beam was observed for both directions of shear force as illustrated in Fig.8.31(b). Although severe diagonal tension cracking was observed during positive moment applied(see Fig.8.30(b)), the concrete contribution to shear resistance did not degrade significantly. Based on the limited test data obtained in this study, it was found that it was not until the maximum nominal shear stress in the beam reached approximately $0.18\sqrt{f'_c}$ that the shear strength was reduced due to the degradation in the concrete shear resisting mechanisms. It should be mentioned that this nominal shear stress of $0.18\sqrt{f'_c}$ is almost identical to the diagonal tension cracking stress recommended by ACI 318 1989.

8.5.3.5 Comparison of the Proposed Models with Test Data

The relationship between the shear strength and the displacement ductility factor of the beam of Specimen R3 during negative moment, in which shear failure in the beams commenced, was estimated using the proposed models described in Section 8.5.3.3 and compared with the test results in Fig.8.32. Also shown is the shear force corresponding to the ideal flexural strength V_{if} of the beam. The predicted shear strengths were calculated using the measured material strengths.

It is shown in Fig.8.32 that the models proposed for columns by Ang et al and Priestley et al overestimate the test results. On the other hand, Ashheim et al's model generally gives a conservative estimate, especially at low displacement ductility levels. The AIJ approach and Priestley et al's model for beams predict the available displacement ductility factor with good accuracy as shown in Fig.8.32, where the available displacement ductility factor is defined as when shear failure commenced. However, the AIJ approach underestimates the effect of the displacement ductility on the shear strength after the beam failed in shear. The model proposed for the beams by Priestley et al gives a good estimate for the influence of the displacement ductility factor on the shear strength.

In summary, a comparison of experimental results in this study with the proposed shear strength models indicated that only the model proposed for beams by Priestley and Calvi 1991 could provide a good estimate for the shear behaviour of the beams of the test specimen, which failed in shear during negative moment.

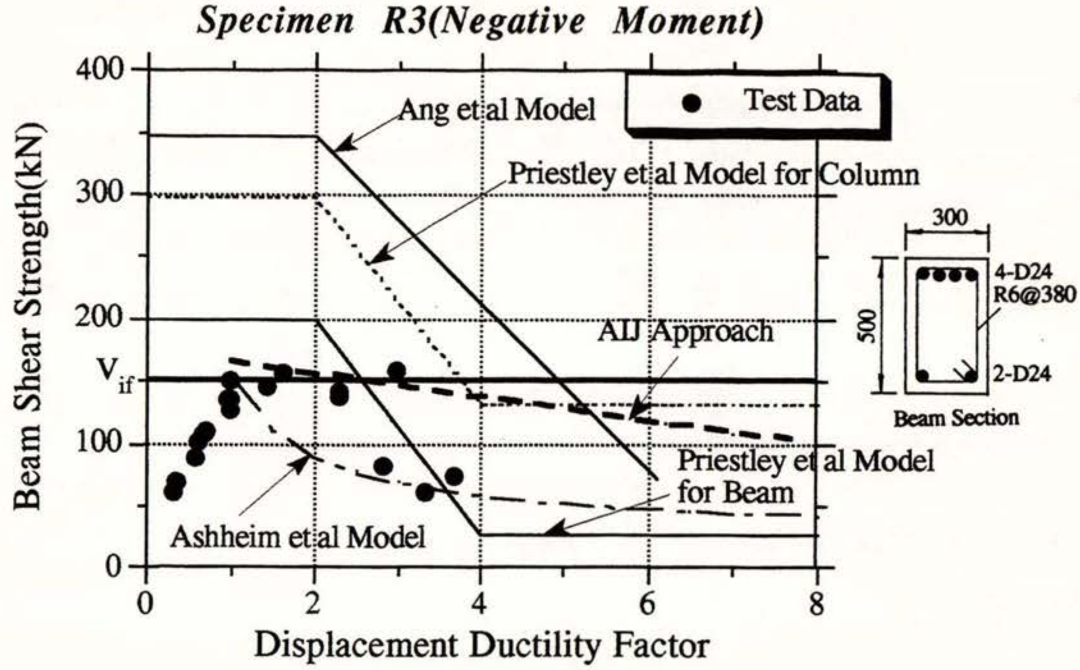

Fig.8.32 Comparison of the Proposed Models with Test Data

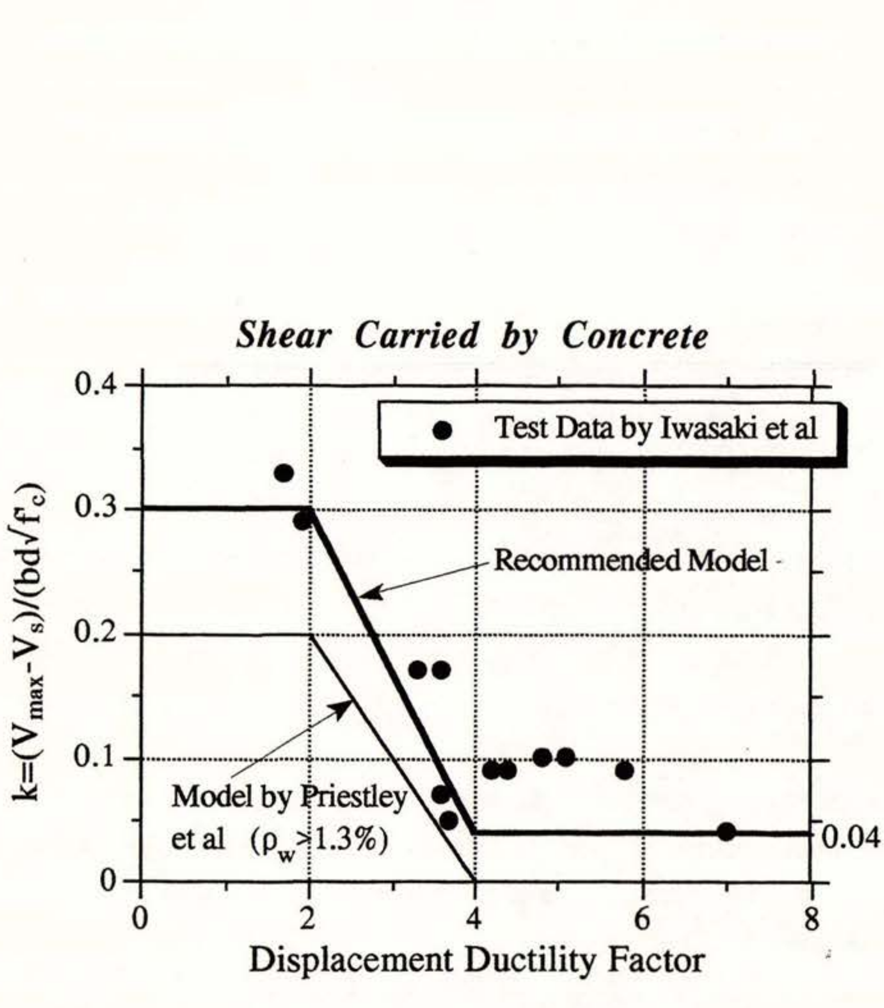

Fig.8.33 Degradation of the Concrete Contribution of Shear Strength

8.5.3.6 Concrete Contribution for Shear Strength of the Beam

As mentioned before, the concrete contribution for the initial shear strength in the model of Priestley and Calvi 1991 was based on the New Zealand Code equations[SANZ 1982(a)]. However, it has been shown that existing design equations are very conservative for the initial shear strength[Ang et al 1988, and Mattock and Wang 1984]. Therefore, a more realistic estimate is necessary for the concrete contribution to the initial shear strength.

The experimental results obtained by Iwasaki et al 1985 were reviewed to assess the shear carried by the concrete V_c. Only test data obtained from columns which failed in shear with rectangular cross section and without axial load acting were used to investigate V_c for beams. The dimensions, reinforcement ratio and measured material strengths for the selected test specimens were as follows:

column aspect ratio	$2.0 < M/VD < 6.0$
shear reinforcement ratio	$0.08\% < p_w < 0.51\%$
tension reinforcement ratio	$0.88\% < \rho_w < 2.12\%$
measured concrete compressive strength	$25.2\text{MPa} < f'_c < 33.3\text{MPa}$

The shear carried by concrete V_c may be expressed by

$$V_c = k\sqrt{f'_c}bd \tag{8.41}$$

The maximum shear strength V_{max} obtained from the selected test specimens, when the axial load is zero, was defined as the sum of the contributions from the concrete V_c and from the shear reinforcement V_s. Thus

$$V_{max} = V_c + V_s \tag{8.42}$$

The angle of the truss mechanism needs to be estimated to define the term V_s. When it is assumed that the angle of the truss mechanism coincides with the angle of diagonal tension cracking, a 45 degree truss mechanism is a good estimate for beams without axial load. Visual observation of diagonal tension cracks supported the assumption of an approximately 45 deg strut angle for beams(see Fig.8.30) and for columns without axial load[Ang et al 1988]. Hence the term V_s was defined as

$$V_s = \frac{A_v f_{yv} d}{s} \tag{8.43}$$

where A_v is the area of shear reinforcement at spacing s, f_{yv} is the yield strength of shear reinforcement, and d is the effective depth of the member.

The coefficient k in the concrete contribution V_c is then calculated as

$$k = \frac{V_{max} - V_s}{\sqrt{f'_c}\, bd} \tag{8.44}$$

Fig.8.33 shows the relationship between the displacement ductility factor and the value k so calculated. Also shown is the shear carried by the concrete according to the model of Priestley and Calvi 1991.

Two significant trends are apparent in the scattered data of Fig.8.33. The first is that the concrete contribution represented by the value for k decreases considerably when the displacement ductility factor approaches 4. The second is that the shear carried by the concrete does not go to zero even when the displacement ductility factor is larger than 4.

It was identified in Fig.8.33 that the concrete contribution of the beam for the initial shear strength in the model proposed by Priestley and Calvi 1991 was very conservative. This is because the model uses the code equation which gives a conservative prediction of the initial shear strength. Although the available test data is limited, Fig.8.33 suggests that the concrete term V_c for the initial shear strength used in Priestley et al's equation could be replaced by $0.3\sqrt{f'_c}bd$. It was also found that the V_c for the final shear strength could be larger than $0.04\sqrt{f'_c}bd$, as shown in Fig.8.33.

8.6 CONCLUSIONS

One approach to the assessment of the shear strength of beam-column joints without shear reinforcement is to assume that the shear strength is reached at the stage of initial diagonal tension cracking in the joint core. Based on the test results from eighty beam-interior column joint specimens tested by other researchers, the joint shear strengths at diagonal tension cracking were investigated in terms of the principal tensile stresses in the joint. It was found that Eq.8.5 can be used as one method to assess the shear strength of the joint without shear reinforcement.

The shear mechanisms of beam-column joints without shear reinforcement after diagonal tension cracking were developed and examined using the test results. In the model developed, it was assumed that for a joint without shear reinforcement the longitudinal beam and column bars passing through the joint core act as both flexural reinforcement and joint shear reinforcement. As a consequence, large tensile stresses were developed in these bars in the joint core, which are compared with the test results obtained from this study in Fig.8.15. The results of this phenomenon are :

1. That the horizontal and vertical expansion of the joint core may be significantly large.

2. That as can be expected from the behaviour illustrated in Fig.8.15, the bond condition in the joint core may be quite different from that in a well designed joint. It is likely that only small steel forces in the flexural tension zones can be transmitted to the core concrete by means of bond while the large bond forces must be developed in the flexural compression zones.

3. That the flexural compression reinforcement in the beams and columns adjacent to the joint may be in tension. The loss of compression force in the steel may impair the ductility of the members.

The maximum shear strength of a beam-column joint with no shear reinforcement depends on the available steel bar forces to carry the joint shear forces. The additional forces, which are induced in the longitudinal beam and column bars due to the joint shear mechanisms postulated in this study, could limit the development of the maximum flexural strengths of the members adjacent to the joint. Therefore, when assessing an existing moment resisting frame with no joint shear reinforcement, the effect of the joint shear force on the longitudinal steel bars in the joint core should be investigated.

When diagonal compression failure governs the joint strength, the maximum shear strength of the joint can be estimated using Eq.8.12. The shear strength degradation model shown in Fig.8.22 is proposed for joints without shear reinforcement and can be used to estimate the available displacement ductility factor of an existing structure when joint shear failure occurs.

The seismic behaviour of beams with inadequate quantities of transverse reinforcement was examined in terms of the curvature ductility capacity and the shear strength.

When beam bars of large diameter pass through a column with relatively small depth, as is found in early building frames, the "compression" reinforcement of the beam on one side of the column may actually be in tension. The curvature analysis of the beams, taking into account the effect of the actual stress in the "compression" reinforcement showed that the available curvature ductility factors may be significantly reduced as a result of increasing tensile stress in the "compression" reinforcement. The available curvature ductility factors were calculated to be about 10 for the beam sections with ρ of 0.5% and about 5 for those with ρ of 1.0%. Much smaller curvature ductility factors were available for beam sections with ρ larger than 1.0%.

Those curvature ductility factor values were obtained when the extreme fibre concrete compressive strain of the concrete was taken as ε_{cu}=0.004 and the bond stress distribution along the beam bars passing through the joint was assumed to be the same as that obtained from the results of tests on the beam-interior column joint specimens without axial load acting on the columns. Those assumptions may result in a conservative estimate of the available curvature ductility factors when columns do carry axial compression load.

A comparison of the experimental results in this study with previously proposed shear strength models indicates that a modification to the concrete shear resisting mechanisms is required for the model to give a realistic prediction of the shear strengths of beams. The experimental results obtained by other researchers were reviewed to assess the shear carried by the concrete V_c of the beams. It was identified that the concrete contribution of the beam for the initial shear strength in a previously proposed model was very conservative. It is suggested that the concrete term V_c for the initial shear strength be $0.3\sqrt{f'_c}bd$. The concrete term V_c decreases as the displacement ductility factor of the beam increases. The shear carried by the concrete mechanisms of the beams did not become zero even when the displacement ductility factors were larger than 4. It was found that V_c for the final shear strength is larger than $0.04\sqrt{f'_c}bd$.

CHAPTER 9

CONCLUSIONS AND RECOMMENDATIONS

9.1 GENERAL

This study investigated the seismic behaviour of early reinforced concrete building frames constructed prior to 1970 in New Zealand. The emphasis was placed on the behaviour of the beam-column joint regions which are typical of moment resisting perimeter frames of a reinforced concrete building designed and constructed in Christchurch in the late 1950's. It was also attempted to develop concrete jacketing techniques for retrofitting early building frames, including the beam-column joint regions.

9.2 SEISMIC ASSESSMENT OF AN EXISTING REINFORCED CONCRETE BUILDING DESIGNED IN THE LATE 1950'S IN NEW ZEALAND

The seismic performance of a typical reinforced concrete building frame designed and constructed in Christchurch in the late 1950's was assessed.

The results of the seismic assessment indicated that the available lateral load strength of the frame was very close to the design seismic force assuming elastic response obtained from NZS 4203 : 1984 and was larger than that from NZS 4203 : 1992. The inelastic mechanism of the frame was a mixture of flexural and shear failures in the beams and columns. A critical aspect with respect to shear was found in the behaviour of the beam-column joints with little or no shear reinforcement. The relatively large joint shear input during severe earthquakes indicated that the joints of the early concrete frame was likely to be governed by joint shear failure. It was also found that anchorage of the longitudinal beam bars in the joint core of exterior and interior columns of the typical frame would be poor under a severe earthquake.

9.3 EXPERIMENTAL INVESTIGATIONS

9.3.1 The Seismic Behaviour of the Beam-Interior Column Joints without Shear Reinforcement

Three full-scale beam-interior column joints, Specimens O1, O4 and O5, were constructed and tested under simulated seismic loading to investigate the seismic behaviour of joints without shear reinforcement.

Specimen O1 represented a critical joint region of the perimeter frame of the building investigated. The diameter of longitudinal beam bars to column depth ratio was 1/12.5 which did not satisfy the current New Zealand code for ductile frames. The maximum nominal horizontal shear stress in the beam-column joint was $0.61\sqrt{f'_c}$ MPa, where f'_c is the measured compressive strength of concrete cylinder. The test on Specimen O1 demonstrated that the performance of the beam-interior column joint region of the frame would be poor in a major earthquake in terms of the stiffness, strength and ductility. This is mainly due to the lack of shear reinforcement and inadequate anchorage of longitudinal beam bars in the joint core.

Specimens O4 and O5 had the same dimensions and reinforcing details except that the beam bar diameter used was 24mm for Specimen O4 and 32mm for Specimen O5, respectively. The main aim of this test was to investigate the effect of the bond condition along the longitudinal beam reinforcement in the joint on the behaviour of the joint without shear reinforcement. The diameter of longitudinal beam bar to column depth ratio was 1/25 for Specimen O4, which is the maximum value allowed by the current New Zealand code and 1/18.75 for Specimen O5, respectively. The maximum nominal horizontal joint shear stress was $0.47\sqrt{f'_c}$ MPa for Specimen O4 and $0.61\sqrt{f'_c}$ MPa for Specimen O5. The specimens showed a limited ductile response during the test. The horizontal load strengths of both specimens degraded quickly due to severe joint diagonal tension cracking. The effect of the two different bond conditions along the beam bars in the joint on the seismic behaviour of the joints without shear reinforcement was found not to be significant.

After diagonal tension cracking occurred in the joint core without shear reinforcement, large tensile strains were measured along the beam and column bars in the joint core, indicating significant joint expansion. Bond stresses along the beam and column bars in the joint were mainly generated over the regions where flexural compression forces of the adjacent members acted. The initial stiffnesses of all beam-interior column joint specimens without shear reinforcement were significantly low when compared with the theoretical values, mainly due to the fixed-end rotation of the members adjacent to the joint, in which large tensile strains along the beam and column bars initiated.

9.3.2 The Seismic Behaviour of the Beam-Exterior Column Joints with Beam Bar End Hooks Not Bent into the Joint Core

Two full-scale beam-exterior column joints, Specimens O6 and O7, were constructed, in which only a small amount of shear reinforcement was placed in the beam, the columns and the joint core. The hooks of the longitudinal beam reinforcement of Specimen O7 were not bent into the joint core, which is typical of early building frames, while those of Specimen O6 were bent into the joint core. The test specimens were tested under simulated seismic loading and their behaviour was compared.

The beam-column joint of Specimen O7 failed in shear shortly after diagonal tension cracking in the joint before reaching the ideal horizontal load strength. By comparison, Specimen O6 showed a stable and ductile response with a plastic hinge forming in the beam during the test. It was identified that the seismic performance of the beam-exterior column joint was significantly influenced by the configuration, particularly the direction of the hooks at the ends of the beam bars anchored inside or outside in the joint core. The beam bar hooks when not bent into the joint core, were not able to develop the diagonal compression strut mechanism within the joint along a corner to corner diagonal.

It is noted that, in case of Specimen O6, the seismic performance of the joint was satisfactory although only a small amount of shear reinforcement was provided in the joint core. This is because the maximum nominal horizontal joint shear stress of $0.31\sqrt{f'_c}$ MPa obtained for Specimen O6 was small enough not to result in the severe reduction of its horizontal load strength and also the configuration of the beam bar hooks, bent into the joint core, was adequate to develop the diagonal compression strut mechanism in the joint under severe seismic loading.

9.3.3 <u>The Seismic Behaviour of the Beams with Small Quantities of Transverse Reinforcement</u>

Based on the results tested on Specimens R3 and O6, two limiting conditions were identified for the seismic behaviour of the beams with small quantities of shear reinforcement. At a maximum nominal beam shear stress of less than $0.14\sqrt{f'_c}$ MPa, the beams did not fail in shear. When the maximum beam shear stress approached $0.18\sqrt{f'_c}$ MPa, beam shear failure commenced. At this stage, the hysteresis loops showed a rapid strength degradation, mainly due to the reduced shear carried by the concrete shear resisting mechanism, particularly aggregate interlock.

When beam shear failure was avoided, the beam even if the amount of transverse reinforcement is small, showed a ductile response until the end of testing. The curvature ductility factors of at least 14 and 9 were obtained for the beam sections of Specimen R3 and Specimen O6, respectively, during the test.

9.3.4 <u>The Seismic Behaviour of the Beam-Interior Column Joints Retrofitted Using Concrete Jacketing</u>

Three full-scale beam-interior column joint regions with reinforcement details typical of the building frame designed in the late 1950's were retrofitted by jacketing with new reinforced concrete. Specimen R1 was a specimen retrofitted by jacketing both the beams and columns of the as-built Specimen O1, which was previously damaged under simulated seismic loading. New hoops were also placed in the joint core. Specimen R2 was a specimen retrofitted by jacketing the beams and columns of another as-built specimen, without any previous damage, in the same manner except that new joint hoops were not placed. Specimen R3 was a specimen retrofitted by jacketing the columns of the other non-damaged as-built specimen. New joint hoops were not placed.

Results of the simulated seismic load tests showed that jacketing of columns, beams and joint with new reinforced concrete was a useful technique for enhancing the stiffness, strength and ductility of poorly detailed as-built beam-column joint regions. The tests also showed that the effect of previous damage to the as-built specimen had no significant influence on the overall seismic response of the retrofitted specimen.

It was also found that even when no joint core hoops are present in the existing beam-column joints, no new joint core hoops are required if the existing column is enlarged by jacketing so that the horizontal nominal shear stress in the joint core is reduced to less than $0.3\sqrt{f'_c}$ MPa. This finding was for joints with no axial load on the columns. When axial compression load is present on columns, a greater horizontal joint shear stress would be tolerable.

The overall response of Specimen R3, which was retrofitted by jacketing the columns alone, was governed by the beam shear failure after developing the theoretical ideal flexural strength of the beam. Limited ductility response, that is available displacement ductility factor of 2.5, was attained for the specimen.

9.4 THEORETICAL CONSIDERATIONS

9.4.1 The Seismic Behaviour of the Beam-Interior Column Joints without Shear Reinforcement

One approach to the assessment of the shear strength of the joint without shear reinforcement is to assume that the shear strength is reached at the stage of initial diagonal tension cracking in the joint core. Based on the results from the eighty beam-interior column joint specimens tested by other researchers, the joint shear strength at diagonal tension cracking was investigated in terms of the principal tensile stresses in the joint. It was found that Eq.8.5 can be used as one method to assess the shear strength of the joint without shear reinforcement.

The shear resisting mechanisms of a joint without shear reinforcement after diagonal tension cracking were developed and examined using the test results. In the model developed it was assumed that the longitudinal beam and column bars passing through the joint core act as both flexural reinforcement and joint shear reinforcement. As a consequence, large tensile stresses are developed in these bars in the joint core. These tensile stresses were compared with the test results obtained from this study in Fig.8.15.

It was found that the maximum shear strength of a joint with no shear reinforcement depends on the forces in the longitudinal reinforcement available to carry the joint shear forces. The additional forces which are induced in these longitudinal bars due to the joint shear mechanisms postulated in this study, could limit the development of the maximum flexural strength of the members adjacent to the joint. Therefore, when assessing an existing moment resisting frame with no joint shear reinforcement, the effect of the joint shear force on the longitudinal steel bar forces in the joint core should be investigated.

When diagonal compression failure governs the joint strength, the maximum shear strength of the joint can be estimated by Eq.8.12. The shear strength degradation model shown in Fig.8.22 is proposed for joints without shear reinforcement and can be used to estimate the available displacement ductility factor of an existing structure when joint shear failure occurs.

9.4.2 The Seismic Behaviour of Beams with Small Quantities of Transverse Reinforcement

The seismic behaviour of the beams with small quantities of transverse reinforcement was examined in terms of the curvature ductility capacity and shear strength.

When beam bars of large diameter pass through column with relatively small depth, as is often found in early building frames, the "compression" reinforcement in the beam on one side of the column may actually be in tension. This is due to bond slip through the joint and also, if the tension steel area is small, due to the neutral axis depth being small enough for the "compression steel" to be in tension. The curvature analysis of the beams, taking into account the effect of the stress conditions of the "compression" reinforcement, showed that the available curvature ductility capacities were significantly reduced as a result of increasing tensile stress in the "compression" reinforcement. The available curvature ductility factors were calculated to be about 10 for the beam sections with ρ of 0.5% and about 5 for those with ρ of 1.0%, where ρ is tension reinforcement ratio. Much smaller curvature ductility factors were available for beam sections with ρ larger than 1.0%.

A comparison of the experimental results in this study with the shear strength models proposed for columns and beams indicates that a modification to the concrete shear resisting mechanisms is necessary for the model to predict realistically the shear strength of the beams.

Experimental results obtained by other researchers were reviewed to assess the shear carried by the concrete V_c of the beam. It was identified that the concrete contribution of the beam for the initial shear strength in the proposed model was very conservative. It was suggested that the concrete term V_c for the initial shear strength be $0.3\sqrt{f'_c}bd$. The concrete term V_c decreased as the displacement ductility factor imposed on the beam increased. The shear carried by the concrete mechanisms of the beam was found not to go to zero even when the imposed displacement ductility factor is larger than 4. It was found that V_c for the final shear strength after degradation is larger than $0.04\sqrt{f'_c}bd$.

9.5 RECOMMENDATIONS FOR FUTURE RESEARCH

The following research is recommended to obtain a better understanding of the seismic behaviour of older reinforced concrete buildings.

Further experimental research is necessary to investigate the seismic performance of members and subassemblages with dimensions and reinforcing details typical of early reinforced concrete buildings, such as lap splices of beam bars in plastic hinge region.

In particular, the present study involved deformed longitudinal reinforcement. Plain round longitudinal bars were used in New Zealand before the mid-1960's. Tests on beam-column joints involving plain round longitudinal bars are needed.

In this study, the test was carried out on the beam-column joint regions without axial load acting on the columns. Therefore, a next stage of the study should investigate the seismic performance of beam-column joint regions when axial loads are applied to the columns. The following aspects should be examined when axial load is present on the column.

(1) Bond performance of the beam bars passing through the joint
(2) Maximum joint shear strength
(3) Degradation of the joint shear strength

The degradation models for the shear strength of the joints and beams proposed in this study need to be further refined to obtain a more realistic assessment of the behaviour of early building frames under severe earthquakes.

More analytical research is required to examine the overall seismic performance of the retrofitted buildings as well as of the original buildings, providing information regarding effectiveness of the retrofit techniques used. In particular, an analysis of the performance of the retrofitted 1950's building studied in this thesis would provide useful comparison of various retrofit methods

The initial stiffnesses obtained from beam-column joints without shear reinforcement tested in this study were significantly low when compared with theoretical values, mainly due to the large tensile strains along the beam and column bars in the joint core. A method to give a more realistic estimate for the initial stiffness of the frame with dimensions and reinforcing details typical of older building frames is required.

The hooks of longitudinal beam bars entering external columns not bent into the joint core do not efficiently develop the diagonal compression strut within the joint along a corner to corner diagonal. For the exterior joint with this configuration of hooks, however, a diagonal compression strut mechanism may develop at an angle less than 45 degree to the column axis when column hoops are adequately placed close to the joint core. If the column hoops had been adequately placed in the vicinity of the joint core of the test specimen, a better seismic performance might have been obtained. Further research is necessary in this aspect.

Retrofitting of reinforced concrete frames involves alternative procedures of infill walls, steel bracing and jacketing techniques. These techniques were found to be effective and constructible for many existing structures. However, the cost performance of such retrofit techniques is still uncertain since the retrofit procedures often include a complicated construction process. Retrofit methods which make the construction process simpler and more economical are required. These methods may involve the precast elements and new materials.

REFERENCES

ACI Committee 318, 1993, "Building Code Requirements for Reinforced Concrete and Commentary(ACI 318RM-89)", American Concrete Institute, Detroit, 353 pp.

ACI-ASCE Committee 426, 1973, "Shear Strength of Reinforced Concrete Members", Journal of Structural Engineering, American Society of Civil Engineers, Vol.99, No.6, pp.1091-1187.

Adin, M.A., Yankelevesky, D.Z. and Farhey, D.N., 1993, "Cyclic Behaviour of Epoxy-Repaired Reinforced Concrete Beam-Column Joints", Structural Journal, American Concrete Institute, Vol.90, No.1, pp.170-179.

Aguilar, J., Juarez, H., Ortega, R. and Igresias, J., 1989, "The Mexico Earthquake of 19 September 1985 - Statistics of Damage and of Retrofitting Techniques in Reinforced Concrete Buildings Affected by the 1985 Earthquake", Earthquake Spectra, EERI, Vol.5, No.1, pp.145-151.

AIJ, 1990, "Design for Earthquake Resistant Reinforced Concrete Buildings Based on Ultimate Strength Concept", Architectural Institute of Japan.

Alcocer, S. M. and Jirsa, J. O., 1990, "Assessment of the Response of Reinforced Concrete Frame Connections Redesigned by Jacketing", Proceedings of 4th U.S. National Conference on Earthquake Engineering, Vol.3, Palm Springs, pp.295-304.

Altin, S. , Ersoy, U. and Tankut, T., 1990, "Seismic Strengthening of Reinforced Concrete Frames With Reinforced Concrete Infills", Report No.METU/SML-90/01, Middle East Technical University, Ankara, 81 pp.

Anderson, D.R., Sweeney, D.J. and Williams, T.A., 1981, "Introduction to Statistics(An Applications Approach)", West Publishing Company, 602 pp.

Ang, B. G., Priestley, M. J. N. and Paulay, T., 1988, "Seismic Shear Strength of Circular Concrete Bridge Columns", Structural Journal, American Concrete Institute, Vol.86, No.1, pp.45-59.

Aoyama, H., 1980, "A Method for the Evaluation of the Seismic Capacity of Existing Reinforced Concrete Buildings in Japan", Bulletin of the New Zealand National Society for Earthquake Engineering, Vol.14, No.3, pp.105-130.

Aoyama, H., Kato, D., Katsumata, H. and Hosokawa, Y., 1984, "Strength and Behaviour of Postcast Shear Walls for Strengthening of Existing Reinforced Concrete Buildings", Proceedings of 8th World Conference on Earthquake Engineering, San Fransisco, pp.485-492.

Arakawa, T., 1980, "Effect of Welded Band Plates on Aseismic Characteristics of Reinforced Concrete Columns", Proceedings of 7th World Conference on Earthquake Engineering, Istanbul, pp.283-240.

Aschheim, M. and Moehle, J. P., 1992, "Shear Strength and Deformability of RC Bridge Columns Subjected to Inelastic Cyclic Displacements", Report UNB/EERC-92/04, Earthquake Engineering Research Center, University of California at Berkeley, 93 pp.

ATC, 1983, "Seismic Retrofitting Guidelines for Highway Bridges ATC-6-2", Applied Technology Council, Palo Alto, California, 205 pp.

ATC, 1987, "Evaluating the Seismic Resistance of Existing Buildings ATC-14", Applied Technology Council, Redwood City, California, 370 pp.

ATC, 1989, "A Handbook for Seismic Evaluation of Existing Buildings ATC-22", Applied Technology Council, Redwood City, California, 169 pp.

Badoux, M. and Jirsa, J.O., 1990, "Steel Bracing of RC Frames for Seismic Retrofitting", Journal of Structural Engineering, American Society of Civil Engineers, Vol.116, No.1, pp.55-74.

Bass, R.A., Carrasquillo, R. L. and Jirsa, J. O., 1989, "Shear Transfer Across New and Existing Concrete Interface", Structural Journal, American Concrete Institute, Vol.86, No.4, pp.383-393.

Beckingsale, C.W., 1980, "Post Elastic Behaviour of Reinforced Concrete Beam-Column Joints", PhD Thesis, Department of Civil Engineering, University of Canterbury, Christchurch, 359 pp.

Benuska, L., 1990, "Loma Prieta Earthquake Reconnaissance Report" Earthquake Spectra, EERI, Supplement to Vol.6, No.1, pp.151-187.

Bessho, S., Fukushima, M. and Hatamoto, H, 1986, "Columns and Beam-Column Joints of a 30 Story Reinforced Concrete High-Rise Building (in Japanese)", Kajima Technical Research Report, Vol.34, pp.107-114.

Bessho, S., Okamoto, K. and Hatamoto, H., 1989, "Lateral Loading Behaviour of Reinforced Concrete Wide Beam to Column Subassemblages (in Japanese)", Transactions of Architectural Institute of Japan, pp.481-482.

Bett, B.J., Klingner, R.E. and Jirsa, J.O., 1988, "Lateral Load Response of Strengthened and Repaired Reinforced Concrete Columns", Structural Journal, American Concrete Institute, Vol.85, No.5, pp.499-508.

Blaikie, E. L., 1988, "Behaviour of Unreinforced and Lightly Reinforced Concrete Beam-Column Joints", Proceedings of Pacific Concrete Conference, Vol.1, Auckland, pp.181-193.

Brunsdon, D. R. and Priestley, M. J. N., 1984, "Assessment of Seismic Performance Characteristics of Reinforced Concrete Buildings Constructed Between 1936 and 1975", Bulletin of the New Zealand National Society for Earthquake Engineering, Vol.17, No.3, pp.163-181.

Bush, T.D., Roach, C.E., Jones, E.A. and Jirsa, J.O., 1986, "Behaviour of a Strengthened Reinforced Concrete Frame", Proceedings of 3rd U.S. National Conference on Earthquake Engineering, Charleston, pp.1203-1214.

Carr, A. and Moss, P. J., 1980, "The Effects of Large Displacements on the Earthquake Response of Tall Concrete Frame Structures", Bulletin of the New Zealand National Society for Earthquake Engineering, Vol.13, No.4, pp.317-328.

CEB-FIP Model Code, 1990, (First Draft), Chapter 6-14 and Appendices, Bulletin D'Information No.196.

Chai, Y.H., Priestley, M.J.N. and Seible, F., 1991, "Seismic Retrofit of Circular Bridge Columns for Enhanced Seismic Performance", Structural Journal, American Concrete Institute, Vol.88, No.5, pp.572-584.

Cheung, P. C., 1991, "Seismic Design of Reinforced Concrete Beam-Column Joints With Floor Slab", Research Report 91-4, Department of Civil Engineering, University of Canterbury, Christchurch, 328 pp.

Collins, M. P. and Mitchell, D., 1980, "Shear and Torsion Design of Prestressed and Non-Prestressed Concrete Beams", Journal of the Prestressed Concrete Institute, Vol.25, No.5, pp.32-101.

Corazao, M. and Durrani, A.J., 1989, "Repair and strengthening of Beam-Column Connections Subjected to Earthquake Loadings", Technical Report NCEER-89-0013, Rice University.

CSA, 1984, "Design of Concrete Structures for Buildings With Explanatory Notes, CAN3-A23.3-M84", Canadian Standards Association, Rexdale, Ontario.

Eligehausen, R., Popov, E. P. and Bertero, V. V., 1983, "Local Bond Stress-Slip Relationships of Deformed Bars Under Generalized Excitations", Report UNB/EERC-83/23, Earthquake Engineering Research Center, University of California at Berkeley, 179 pp.

Endo, T., Okifuji, A., Sugano, S. Hayashi, T., Shimizu, T., Takahara, K., Saito, H. and Yoneyama, Y., 1984, "Practices of Seismic Retrofit of Existing Concrete Structures in Japan", Proceedings of 8th World Conference on Earthquake Engineering, San Fransisco, pp.469-476.

Erläuterungen et al 1961, Erläuterungen zur Verwendung von Rippen-Torstahl, 2nd Edit, Istegstahl Gesellschaft, Köln, Nov.1961

Fenwick, R. C. and Paulay, T., 1968, "Mechanisms of Shear Resistance of Concrete Beams", Journal of the Structural Division, American Concrete of Civil Engineers, Vol.94, No.10, pp.2235-2350.

Foutch, D.A., Hjelmstad, K.D., Calderon, E.D.V., Gutierrez, E.F. and Downs, R.E., 1989, "The Mexico Earthquake of 19 September 1985 - Case Studies of Seismic Strengthening for Two Buildings in Mexico City", Earthquake Spectra, EERI, Vol.5, No.1, pp.153-173.

French, C.W., Thorp, G.A. and Tsai, W., 1990, "Epoxy Repair Techniques for Moderate Earthquake Damage", Structural Journal, American Concrete Institute, Vol.87, No.4, pp.416-424.

Fujii, S. and Morita, S., 1990, "Behaviour of Exterior and Interior Reinforced Concrete Beam-Column Joints (in Japanese)", Proceedings of Japan Concrete Institute, Vol.12, No.2, pp.691-696.

Fuse, T., Okuta, K., Hiramatsu, K. and Hara, N., 1992, "Cyclic loading Tests of Reinforced Concrete Columns Strengthened With Steel Tube", Proceedings of 10th World Conference on Earthquake Engineering, Vol.9, Madrid, pp.5227-5233.

Gates, J., Mellon, S. and Klein, G., 1988, "The Whittier Narrows, California Earthquake of October 1, 1987 - Damage to State Highway Bridges", Earthquake Spectra, EERI, Vol.4, No.2, pp.377-388.

Gates, W.E., Nester, M.R. and Whitby T.R., 1992, "Managing Seismic Risk : A Case History of Seismic Retrofit for a Non-Ductile Reinforced Concrete Frame High Rise Office Building", Proceedings of 10th World Conference on Earthquake Engineering, Vol.9, Madrid, pp.5261-5266.

Giberson, M. F., 1969, "Two Nonlinear Beams With Definition of Ductility", Journal of the Structural Division, American Society of Civil Engineers, Vol.95, No.2, pp.137-157.

Glogau, O. A., 1980, "Low Rise Reinforced Concrete Buildings of Limited Ductility - Some Lessons from Recent Earthquake Damage", Bulletin of the New Zealand National Society for Earthquake Engineering, Vol.13, No.2, pp.182-193.

Goel, S.C. and Lee, H., 1990, "Seismic Strengthening of RC Structures by Ductile Steel Bracing System", Proceedings of 4th U.S. National Conference on Earthquake Engineering, Vol.3, Palm Springs, pp.323-331.

Goto, Y., 1971, "Cracks Formed in Concrete Around Deformed Tension Bars", Structural Journal, American Concrete Institute, Vol.68, No.4, pp.244-251.

Goto, Y., Joh, O. and Shibata, T., 1987, "Effect of Joint reinforcement on the Shear Resistance of R/C Interior Beam-Column Joints (in Japanese)", Proceedings of Japan Concrete Institute, Vol.9, No.2, pp.187-192.

Gulkan, P., 1977, "The Inelastic Response of Repaired Reinforced Concrete Beam-Column Connections", Proceedings of 6th World Conference on Earthquake Engineering, New Delhi, pp.2473-2478.

Gyoten, Y., Mizuhata, K. and Fukusumi, T., 1977, "An Investigation of Mechanical Reliability of Shear Wall Repaired With Epoxy Mortar", Proceedings of 6th World Conference on Earthquake Engineering, New Delhi, pp.2526-2531.

Hanson, N. H. and Conner, H. W., 1972, "Tests of Reinforced Concrete Beam-Column Joints Under Simulated Seismic Loading", Portland Cement Association Research and Development, Bulletin RD 012, 11 pp.

Hayashi, T., Niwa, H. and Fukuhara, M., 1980, "The Strengthening Method of the Existing Reinforced Concrete Buildings", Proceedings of 7th World Conference on Earthquake Engineering, Istanbul, pp.89-96.

Hayashi, S., Kokusho, S. and Yoshida, H., 1985, "Experiments of Bond Behaviour Between Deformed Bars and Concrete in the Neighborhood of the Cracks", Transactions of Architectural Institute of Japan, No.348, pp.86-97.

Higashi, Y., Ohkubo, M. and Fujimata, K., 1977, "Behaviour of Reinforced Concrete Columns and Frames Strengthened by Adding Precast Concrete Walls", Proceedings of 6th World Conference on Earthquake Engineering, New Delhi, pp.2505-2510.

Higashi, Y., Endo, T., Ohkubo, M. and Shimizu, Y., 1980, "Experimental Study on Strengthening Reinforced Concrete Structure by Adding Shear Wall", Proceedings of 7th World Conference on Earthquake Engineering, Istanbul, pp.173-180.

Higashi, Y., Endo, T. and Shimizu, Y., 1984, "Experimental Studies on Retrofitting of Reinforced Concrete Building Frames", Proceedings of 8th World Conference on Earthquake Engineering, San Fransisco, pp.477-484.

Hiraishi, H., 1984, "Evaluation of Shear and Flexural Deformations of Flexural Type Shear Walls", Bulletin of the New Zealand National Society for Earthquake Engineering, Vol.17, No.2, pp.135-144.

Ismail, H. A. F. and Jirsa, J. O., 1972(a), "Bond Deterioration in Reinforced Concrete Subjected to Low Cycle Loads", Structural Journal, American Concrete Institute, Vol.69, No.6, pp.335-343.

Ismail, H. A. F. and Jirsa, J. O., 1972(b), "Behaviour of Anchored Bars Under Low Cycle Overloads Producing Inelastic Strains", Structural Journal, American Concrete Institute, Vol.69, No.7, pp.433-438.

Iwasaki, T., Kawashima, K., Hagiwara, R., Hasegawa, K., Koyama, T. and Yoshida, T., 1985, "Experimental Investigation on Hysteretic Behaviour of Reinforced Concrete Bridge Pier Columns", Proceedings of Second Joint US-Japan Workshop on Performance and Strengthening of Bridge Structures and Research Needs, San Fransisco, California.

JABDP, 1977, "Standard for Seismic Capacity Evaluation of Existing Reinforced Concrete Buildings in Japan (in Japanese)", Japan Association for Building Disaster Prevention, 131 pp.(Revised in 1990)

Jara, M., Hernandez, C., Garcia, R. and Robles, F., 1989, "The Mexico Earthquake of 19 September 1985 - Typical Cases of Repair and Strengthening of Concrete Buildings", Earthquake Spectra, EERI, Vol.5, No.1, pp.175-193.

Jinno, Y., Kohuchi, T. and Kumagai, T., 1991, "An Experimental Study on Behaviour of Reinforced Concrete Interior Beam-Column Joints using High-Strength Materials (in Japanese)", Transactions of Architectural Institute of Japan, pp.591-592.

Jirsa, J. O., 1987, "Repair of Damaged Buildings - Mexico City", Proceedings of Pacific Conference on Earthquake Engineering, Vol.3, Wairakei, pp.25-34.

Jirsa, J.O. and Badoux, M., 1990, "Strategies for Seismic Redesign of Buildings", Proceedings of 4th U.S. National Conference on Earthquake Engineering, Vol.3, Palm Springs, pp.343-351.

Kamimura, T. and Nagatsuka, N., 1988, "Experimental Study for the Failure of Reinforced Concrete Interior Beam-Column Joints (in Japanese)", Transactions of Architectural Institute of Japan, pp.419-420.

Kashiwazaki, T. and Noguchi, H., 1991, "Experimental Study on the Shear Performance of Reinforced Concrete Interior Joints With Ultra High-Strength Materials (in Japanese)", Proceedings of Japan Concrete Institute, Vol.13, No.2, pp.187-192.

Katsumata, H., Kobatake, Y. and Takeda, T., 1988, "A Study of Strengthening With Carbon Fiber for Earthquake-Resistant Capacity of Existing Reinforced Concrete Columns", Proceedings of 9th World Conference of Earthquake Engineering, Vol.7, Tokyo/Kyoto, pp.517-522.

Kawachi, T., Jinno, Y., Kadoriku, J. and Kumagai, H., 1992, "An Experimental Study on Behaviour of Reinforced Concrete Interior Beam-Column Joints Using High-Strength Materials (in Japanese)", Shimizu Technical Research Report, Vol.55, pp.41-50.

Kawamata, S. and Ohnuma, M., 1980, "Strengthening Effect of Eccentric Steel Braces to Existing Reinforced Concrete Frames", Proceedings of 7th World Conference on Earthquake Engineering, Istanbul, pp.513-520.

Kent, D. C. and Park, R., 1971, "Flexural Members With Confined Concrete", Journal of Structural Engineering, American Society of Civil Engineers, Vol.97, No.7, pp.1969-1989.

Kitayama, K., Otani, S. and Aoyama, H., 1987, "Earthquake Resistant Design Criteria for Reinforced Concrete Interior Beam-Column Joints", Proceedings of Pacific Conference on Earthquake Engineering, Vol.1, Wairakei, pp.315-326.

Lee, D.L.N., Wright, J.K. and Hanson, R.D., 1977, "Repair of Damaged Reinforced Concrete Frame Structures", Proceedings of 6th World Conference on Earthquake Engineering, New Delhi, pp.2486-2491.

Lutz, L. A. and Gergely, P., 1967, "Mechanics of Bond and Slip of Deformed Bars in Concrete", Structural Journal, American Concrete Institute, Vol.64, No.11, pp.711-721.

MacGregor, J.G., 1989, "Free Body Diagrams, Mechanical Models, and Experimental Evidence", Concrete International : Design and Construction, American Concrete Institute, Vol.11, No.6, pp.72-78.

Mander, J. B., Priestley, M. J. N. and Park, R., 1988, "Theoretical Stress-Strain Model for Confined Concrete", Journal of Structural Engineering, American Society of Civil Engineers, Vol.114, No.8. pp.1804-1026.

Mattock, A. H. and Wang, Z., 1984, "Shear Strength of Reinforced Concrete Members Subjected to High Axial Compressive Stress", Structural Journal, American Concrete Institute, Vol.81, No.3, pp.287-298.

McCafferty, R.M. and Moody M.L., 1973, "An Example of Epoxy Mortar Repair of A Reinforced Concrete Beam-Column Joint", Proceedings of 5th World Conference on Earthquake Engineering, Rome, pp.868-871.

Migliacci, A., Antonucci, R., Maio, N.A., Napoli, P., Ferretti, A.S. and Via, G., 1983, "Repair Techniques of Reinforced Concrete Beam-Column Joints", Final Report, International Association of Bridge and Structural Engineering Symposium on Strengthening of Building Structures-Diagnosis and Therapy, Venice, pp.335-362.

Miki, T., Homma, T. and Hirosawa, M., 1973, "Evaluation of Earthquake Resistant Properties and Strengthening of Existing Building", Proceedings of 5th World Conference on Earthquake Engineering, Rome, pp.911-918.

Miranda, E. and Bertero, V.V., 1990, "Post-Tensioning Technique for Seismic Upgrading of Existing Low-Rise Buildings", Proceedings of 4th U.S. National Conference on Earthquake Engineering, Vol.3, Palm Springs, pp.393-402.

Mitchell, D., Dandurand, A. and Paultre, P., 1988, "Repair and Upgrading of Concrete Structures in Mexico City After the 1985 Earthquake", Canadian Journal of Civil Engineering, Vol.15, No.6. pp.1052-1066.

Moehle, J. P., 1992, "Displacement-Based Design of RC Structures Subjected to Earthquake", Earthquake Spectra, EERI, Vol.8, No.3, pp.403-428.

Moehle, J.P., 1994, "Preliminary Report on the Seismological and Engineering Aspects of the January 17, 1994 Northridge Earthquake", Report UCB/EERC-94-01, Earthquake Engineering Research Center, University of California at Berkeley.

Nielsen, M. P., 1984, "Limit Analysis and Concrete Plasticity", Prentice-Hall, Englewood Cliffs, N.J., 420 pp.

Nilsson, I. H. E. and Losberg A., 1976, "Reinforced Concrete Corners and Joints Subjected to Bending Moment", Journal of Structural Engineering, American Society of Civil Engineers, Vol.102, No.6, pp.1229-1254.

Nishimura, Y and Minami, K, 1986 ,"Effects of Reinforcing Bars of Bent Bar Anchorages in Exterior Joints(in Japanese)", Proceedings of Japan Concrete Institute, Vol.8, pp.645-648.

Ohtsuka, H., Saitoh, K., Yasuda, Y. and Okuri, K, 1986, "Experimental Study on Beam-Column Joints of Tall Reinforced Concrete Buildings (in Japanese)", Transactions of Architectural Institute of Japan, pp.89-90.

Okada, T., Murakami, M., Seki, M. and Ando, A., 1983, "Repair and Strengthening of Reinforced Concrete Buildings", Final Report, International Association of Bridge and Structural Engineering Symposium on Strengthening of Building Structures-Diagnosis and Therapy, Venice, pp.379-386.

Otani, S., 1980, "Nonlinear Dynamic Analysis of Reinforced Concrete Building Structures", Canadian Journal of Civil Engineering, Vol.7, No.2, pp.333-344.

Owen, G.N., Scholl, R.E. and Egbunye, I.O., 1984, "Vibration Testing of an Epoxy-Repaired Full Scale Reinforced Concrete Structure", Proceedings of 8th World Conference on Earthquake Engineering, San Fransisco, pp.517-523.

Park, R. and Paulay, T, 1975, "Reinforced Concrete Structures", John Willey & Sons, New York.

Park, R., 1986, "Ductility Design Approach for Reinforced Concrete Frames", Earthquake Spectra, EERI, Vol.2, No.2, pp.565-619.

Park, R. and Ruitong, D., 1988, "Ductility of Doubly Reinforced Concrete Beam Sections", Structural Journal, American Concrete Institute, Vol.85, No.2, pp.217-225.

Park, R., 1989, "Evaluation of Ductility of Structures and Structural Assemblages from Laboratory Testing", Bulletin of the New Zealand National Society for Earthquake Engineering, Vol.22, No.3, pp.155-166.

Park, R., 1992, "Seismic Assessment and Retrofit of Concrete Structures - United States and New Zealand Developments", Proceedings of Technical Conference of New Zealand Concrete Society, Wairakei, pp.18-25.

Paulay, T. and Scarpas, A., 1981, "The Behaviour of Exterior Beam-Column Joints", Bulletin of the New Zealand National Society for Earthquake Engineering, Vol.14, No.3, pp.131-144.

Paulay, T., 1989, "Equilibrium Criteria for Reinforced Concrete Beam-Column Joints", Structural Journal, American Concrete Institute, Vol.86, No.6, pp.635-643.

Paulay, T. and Priestley, M.J.N., 1992, "Seismic Design of Reinforced Concrete and Masonry Buildings", John Wiley & Sons, New York.

Paultre, P. and Mitchell, D., 1990, "Some Considerations for Achieving Ductility in Reinforced Concrete Frame Structures", European Earthquake Engineering, Vol.4, No.2, pp.27-37.

Pessiki, S. P., Conley, C. H., Gergely, P. and White, R. N., 1990, "Seismic Behaviour of Lightly-Reinforced Concrete Column and Beam-Column Joint Details", Technical Report NCEER-90-0014, National Center for Earthquake Engineering Research, State University of New York at Buffalo, New York.

Pincheira, J. A., 1993, "Design Strategies for the Seismic Retrofit of Reinforced Concrete Frames", Earthquake Spectra, EERI, Vol.9, No.4, pp.817-842.

Pincheira, J.A. and Jirsa, J.O., 1992, "Post-Tensioned Bracing for Seismic Retrofit of RC Frames", Proceedings of 10th World Conference on Earthquake Engineering, Madrid, pp.5199-5204.

Popov, E. P., 1984, "Bond and Anchorage of Reinforcing Bars Under Cyclic Loading". Structural Journal, American Concrete Institute, Vol.81, No.4, pp.21-25.

Popov, E.P. and Bertero, V.V., 1975, "Repaired R/C Members Under Cyclic Loading", Earthquake Engineering and Structural Dynamics, Vol.4, pp.129-144.

Priestley, M. J. N. and Park, R., 1987, "Strength and Ductility of Concrete Bridge Columns Under Seismic Loading", Structural Journal, American Concrete Institute, Vol.84, No.1, pp.61-77.

Priestley, M. J. N., 1988, "The Whittier Narrows, California Earthquake of 1 October 1987 - Damage to the I-5/I-605 Separator", Earthquake Spectra, EERI, Vol.4, No.2, pp.389-405.

Priestley, M. J. N. and Calvi, G. M., 1991, "Toward a Capacity-Design Assessment Procedure for Reinforced Concrete Frames", Earthquake Spectra, EERI, Vol.7, No.3, pp.413-437.

Priestley, M.J.N. and Seible, F., 1991, "Seismic Assessment and Retrofit of Bridges", Report No.SSRP-91/03, University of California at San Diego, 426 pp.

Priestley, M.J.N., Fyfe, E. and Seible, F., 1991, "Column Retrofit Using Fibreglass-Epoxy Jackets", Proceedings of the First Annual Seismic Research Workshop, California Department of Transportation, Sacramento, pp.217-224.

Priestley, M. J. N., 1992, "Seismic Assessment of Bridge Structures", Proceedings of an International Symposium on Earthquake Disaster Prevention, Mexico City.

Priestley, M. J. N. , Seible, F. , Verma, R. and Xiao, Y., 1993, "Seismic Shear Strength of Reinforced Concrete Columns", Report No.SSPR-93/06, University of California at San Diego, 120 pp.

Raphael, J. M., 1984, "Tensile Strength of Concrete", Structural Journal, American Concrete Institute, Vol.81, No.2, pp.158-165.

Rodriguez, M. and Park, R., 1989, "Repair and Strengthening of Reinforced Concrete Columns", Proceedings of Silver Jubilee Conference, New Zealand Concrete Society, Wairakei, pp.26-33.

Rodriguez, M. and Park, R., 1991, "Repair and Strengthening of Reinforced Concrete Buildings for Seismic Resistance", Earthquake Spectra, EERI, Vol.7, No.3, pp.439-459.

Rodriguez, M. and Park, R., 1994, "Seismic Load Tests of Reinforced Concrete Columns Strengthened by Jacketing", Structural Journal, American Concrete Institute, Vol.91, No.2, pp.150-159.

Rosenblueth, E. and Meli, R., 1986, "The 1985 Earthquake : Causes and Effects in Mexico City", Concrete International, Vol.8, No.5, pp.23-34.

SANZ, 1982(a), "Code of Practice for the Design of Concrete Structures NZS 3101:1982", Parts 1 and 2, Standards Association of New Zealand, Wellington.

SANZ, 1982(b), "Metal-Arc Welding of Grade 275 Reinforcing Bar NZS 4702:1982", Standards Association of New Zealand, Wellington.

SANZ, 1984, "Code of Practice for General Structural Design and Design Loadings for Buildings NZS 4203:1984", Standards Association of New Zealand, Wellington.

SANZ, 1992, "Code of Practice for General Structural Design and Design Loadings for Buildings NZS 4203:1992", Parts 1 and 2, Standards Association of New Zealand, Wellington.

Saiidi, M. and Sozen, M. A., 1979, "Simple and Complex Models for Nonlinear Seismic Response of Reinforced Concrete Structures", Report UILU-ENG-79-2013, Department of Civil Engineering, University of Illinois.

Schlaich, J., Schäfer, K. and Jennewein, M., 1987, "Toward a Consistent Design of Reinforced Concrete Structures", Journal of the Prestressed Concrete Institute, Vol.32, No.3, pp.74-150.

Scott, B. D., Park, R. and Priestley, M. J. N., 1982, "Stress-Strain Behaviour of Concrete Confined by Overlapping Hoops at Low and High Strain Rates", Structural Journal, American Concrete Institute, Vol.79, No.1, pp.13-27.

Scott, R. H., Feltham, I. and Whittle, R. T., 1994, "Reinforced Concrete Beam-Column Connections and BS 8110", The Structural Engineer, Vol.72, No.4, pp.55-60.

Shiga, T., 1977, "Earthquake Damage and the Amount of Walls in Reinforced Concrete Buildings", Proceedings of 6th World Conference on Earthquake Engineering, New Delhi, pp.2467-2472.

Soesianawati, M. T., Park R. and Priestley, M. J. N., 1987, "Flexural Ductility of Reinforced Concrete Columns With Low Axial Load and Limited Transverse Reinforcement", Proceedings of Pacific Conference on Earthquake Engineering, Vol.1, Wairakei, pp.201-212.

Stevens, N. B., Uzumeri, S. M. and Collins, M. P., 1991, "Reinforced Concrete Subjected to Reversed Cyclic Shear - Experiments and Constitutive Model", Structural Journal, American Concrete Institute, Vol.88, No.2, pp.135-146.

Stoppenhagen, D. R. and Jirsa, J. O., 1987, "Seismic Repair of A Reinforced Concrete Frame Using Encased Columns", PMFSEL Report No.87-2, Department of Civil Engineering, University of Texas at Austin, 169 pp.

Sugano, S. and Fujimura, M., 1980, "Aseismic Strengthening of the Existing Reinforced Concrete Buildings", Proceedings of 7th World Conference on Earthquake Engineering, Istanbul, pp.449-457.

Sugano, S., 1981, "Seismic Strengthening of Existing Reinforced Concrete Building in Japan", Bulletin of the New Zealand National Society for Earthquake Engineering, Vol.14, No.4, pp.209-222.

Sugano, S. and Endo, T., 1983, "Seismic Strengthening of Reinforced Concrete Building in Japan", Final Report, International Association of Bridge and Structural Engineering Symposium on Strengthening of Building Structures-Diagnosis and Therapy, Venice, pp.371-379.

Suleiman, R. E., Ersoy, U. and Tankut, T., 1991, "Behaviour of Jacketed Reinforced Concrete Columns Subjected to Combined Axial Load and Bending", Report No. METU/SML-91/04, Middle East Technical University, Ankara, 62 pp.

Tanaka, H. and Park, R., 1987, "Effectiveness of Transverse Reinforcement With Alternative Anchorage Details in Reinforced Concrete Columns", Proceedings of Pacific Conference on Earthquake Engineering, Vol.1, Wairakei, pp.225-235.

Tasai, A., 1992, "Effective Repair With Resin for Bond Failure of RC Members", Proceedings of 10th World Conference on Earthquake Engineering, Vol.9, Madrid, pp.5211-5216.

Taylor, H. P. J., 1974, "The Behaviour of In Situ Concrete Beam-Column Joints", Technical Report 42.492, Cement and Concrete Association, London, 32 pp.

Taylor, H. P. J. and Clarke, J. L., 1976, "Some Detailing Problems in Concrete Frame Structures", The Structural Engineer, Vol.54, No.1, pp.19-32.

Teraoka, M., Munemura, Y., Satoh, K., Fuziwara, T., Kobayashi, K. and Hayashi, K., 1987, "Study on the Mechanical Properties of Reinforced Concrete Cross Type Beam-Column Joints (in Japanese)", Fujita Kogyo Technical Research Report, No.23, pp.7-12.

Tsai, W.J. and French, C.E., 1988, "Repaired Reinforced Concrete Interior Joints Under Cyclic Loadings", Structural Engineering Report No.88-04, Department of Civil and Mineral Engineering, University of Minnesota, 246 pp.

Umemura, H., 1980, "A Guideline to Evaluate Seismic Performance of Existing Medium- and Low-Rise Reinforced Concrete Buildings and its Application" Proceedings of 7th World Conference on Earthquake Engineering, Istanbul, pp.505-512.

UNIDO, 1983, "Repair and Strengthening of Reinforced Concrete, Stone and Brick-Masonry Buildings", Building Construction Under Seismic Conditions in the Balkan Regions, PROJECT PER/79/015, United Nations Industrial Development Organisation, Vienna, 231 pp.

Vecchio, F. J. and Collins, M. P., 1986, "The Modified Compression-Field Theory for Reinforced Concrete Elements Subjected to Shear", Structural Journal, American Concrete Institute, Vol.83, No.2, pp.219-231.

Velkov, M. and Gavrilovic, P.M., 1980, "Repaired Reinforced Concrete Members and Joints Under Cyclic Loading" Proceedings of 7th World Conference on Earthquake Engineering, Istanbul, pp.297-304.

Wong. Y.L., Paulay, T. and Priestley, M. J. N., 1993, "Response of Circular Reinforced Concrete Columns to Multi-Directional Seismic Attack", Structural Journal, American Concrete Institute, Vol.90, No.2, pp.180-191.

Wyllie, L. A. Jr., 1983, "Seismic Strengthening Procedures for Existing Structures", Final Report, International Association of Bridge and Structural Engineering Symposium on Strengthening of Building Structures-Diagnosis and Therapy, Venice, pp.363-370.

Yamamoto, T., 1992, "FRP Strengthening of RC Columns for Seismic Retrofitting", Proceedings of 10th World Conference on Earthquake Engineering, Vol.9, Madrid, pp.5205-5210.

Yamauchi, S., Chiba, O., Yanagishita, K. and Kikuta, S., 1990, "Experimental Study on Subassemblages of Reinforced Concrete High-Rise Building(Part 1) (in Japanese)", Transactions of Architectural Institute of Japan, pp.365-366.

Zahn, F. A., Park, R., Priestley, M. J. N. and Chapman, H. E., 1986, "Development of Design Procedures for the Flexural Strength and Ductility of Reinforced Concrete Bridge Columns", Bulletin of the New Zealand National Society for Earthquake Engineering, Vol.19, No.3, pp.200-212.